



Journal of
*Cardiovascular
Development and Disease*

Leaders in Cardiovascular Research

A special issue dedicated to
Professor Robert Anderson

Edited by

Deborah Henderson and Nigel Brown

Printed Edition of the Special Issue Published in
Journal of Cardiovascular Development and Disease

**Leaders in Cardiovascular Research: A
special issue dedicated to Professor
Robert Anderson**

Leaders in Cardiovascular Research: A special issue dedicated to Professor Robert Anderson

Editors

Deborah Henderson

Nigel Brown

MDPI • Basel • Beijing • Wuhan • Barcelona • Belgrade • Manchester • Tokyo • Cluj • Tianjin



Editors

Deborah Henderson
Biosciences Institute
Newcastle University
Newcastle
United Kingdom

Nigel Brown
Molecular and Clinical
Sciences Research Institute
St George's
Univeristy of London
London
United Kingdom

Editorial Office

MDPI
St. Alban-Anlage 66
4052 Basel, Switzerland

This is a reprint of articles from the Special Issue published online in the open access journal *Journal of Cardiovascular Development and Disease* (ISSN 2308-3425) (available at: www.mdpi.com/journal/jcdd/special_issues/Professor-Robert-Anderson).

For citation purposes, cite each article independently as indicated on the article page online and as indicated below:

LastName, A.A.; LastName, B.B.; LastName, C.C. Article Title. <i>Journal Name</i> Year , Volume Number, Page Range.
--

ISBN 978-3-0365-6026-7 (Hbk)

ISBN 978-3-0365-6025-0 (PDF)

Cover image courtesy of Robert Anderson

© 2022 by the authors. Articles in this book are Open Access and distributed under the Creative Commons Attribution (CC BY) license, which allows users to download, copy and build upon published articles, as long as the author and publisher are properly credited, which ensures maximum dissemination and a wider impact of our publications.

The book as a whole is distributed by MDPI under the terms and conditions of the Creative Commons license CC BY-NC-ND.

Contents

About the Editors	vii
Preface to "Leaders in Cardiovascular Research: A special issue dedicated to Professor Robert Anderson"	ix
Nigel A. Brown and Deborah J. Henderson The Editors' Personal Biography of Professor Robert Anderson Reprinted from: <i>J. Cardiovasc. Dev. Dis.</i> 2021 , <i>8</i> , 6, doi:10.3390/jcdd8010006	1
Rohit S. Loomba, Justin T. Tretter, Timothy J. Mohun, Robert H. Anderson, Scott Kramer and Diane E. Spicer Identification and Morphogenesis of Vestibular Atrial Septal Defects Reprinted from: <i>J. Cardiovasc. Dev. Dis.</i> 2020 , <i>7</i> , 35, doi:10.3390/jcdd7030035	5
Catherine A. Stothard, Silvia Mazzotta, Arjun Vyas, Jurgen E. Schneider, Timothy J. Mohun and Deborah J. Henderson et al. <i>Pax9</i> and <i>Gbx2</i> Interact in the Pharyngeal Endoderm to Control Cardiovascular Development Reprinted from: <i>J. Cardiovasc. Dev. Dis.</i> 2020 , <i>7</i> , 20, doi:10.3390/jcdd7020020	17
Laís Costa Marques, Gabriel Romero Liguori, Ana Carolina Amarante Souza and Vera Demarchi Aiello Left Ventricular Noncompaction Is More Prevalent in Ventricular Septal Defect than Other Congenital Heart Defects: A Morphological Study Reprinted from: <i>J. Cardiovasc. Dev. Dis.</i> 2020 , <i>7</i> , 39, doi:10.3390/jcdd7040039	41
Justin T. Tretter, Saurabh Kumar Gupta, Yu Izawa, Tatsuya Nishii and Shumpei Mori Virtual Dissection: Emerging as the Gold Standard of Analyzing Living Heart Anatomy Reprinted from: <i>J. Cardiovasc. Dev. Dis.</i> 2020 , <i>7</i> , 30, doi:10.3390/jcdd7030030	57
Peter Agger and Robert S. Stephenson Assessing Myocardial Architecture: The Challenges and Controversies Reprinted from: <i>J. Cardiovasc. Dev. Dis.</i> 2020 , <i>7</i> , 47, doi:10.3390/jcdd7040047	77
Bjarke Jensen, Vincent M. Christoffels and Antoon F. M. Moorman An Appreciation of Anatomy in the Molecular World Reprinted from: <i>J. Cardiovasc. Dev. Dis.</i> 2020 , <i>7</i> , 44, doi:10.3390/jcdd7040044	95
Laura Fedele and Thomas Brand The Intrinsic Cardiac Nervous System and Its Role in Cardiac Pacemaking and Conduction Reprinted from: <i>J. Cardiovasc. Dev. Dis.</i> 2020 , <i>7</i> , 54, doi:10.3390/jcdd7040054	111
Eduardo Back Sternick and Damián Sánchez-Quintana Critical Assessment of the Concepts and Misconceptions of the Cardiac Conduction System over the Last 100 Years: The Personal Quest of Robert H. Anderson Reprinted from: <i>J. Cardiovasc. Dev. Dis.</i> 2021 , <i>8</i> , 5, doi:10.3390/jcdd8010005	145
Ray Deepe, Emily Fitzgerald, Renélynn Wolters, Jenna Drummond, Karen De Guzman and Maurice J.B. van den Hoff et al. The Mesenchymal Cap of the Atrial Septum and Atrial and Atrioventricular Septation Reprinted from: <i>J. Cardiovasc. Dev. Dis.</i> 2020 , <i>7</i> , 50, doi:10.3390/jcdd7040050	157

Maurice J. B. van den Hoff and Andy Wessels Muscularization of the Mesenchymal Outlet Septum during Cardiac Development Reprinted from: <i>J. Cardiovasc. Dev. Dis.</i> 2020 , 7, 51, doi:10.3390/jcdd7040051	179
Deborah J. Henderson, Lorraine Eley and Bill Chaudhry New Concepts in the Development and Malformation of the Arterial Valves Reprinted from: <i>J. Cardiovasc. Dev. Dis.</i> 2020 , 7, 38, doi:10.3390/jcdd7040038	193
Diane E. Spicer and Thora S. Steffensen A Rare Presentation of Common Arterial Trunk with Intact Ventricular Septum Reprinted from: <i>J. Cardiovasc. Dev. Dis.</i> 2020 , 7, 43, doi:10.3390/jcdd7040043	221
Michael Rigby Atrioventricular Septal Defect: What Is in a Name? Reprinted from: <i>J. Cardiovasc. Dev. Dis.</i> 2021 , 8, 19, doi:10.3390/jcdd8020019	231
Catherine C. Pickin, James Castle, Vibha Shaji, Adeolu Banjoko, Aimee-Louise Chambault and Anna N. Seale et al. Congenitally Malformed Hearts: Aspects of Teaching and Research Involving Medical Students Reprinted from: <i>J. Cardiovasc. Dev. Dis.</i> 2021 , 8, 34, doi:10.3390/jcdd8040034	247
Mary N. Sheppard Sudden Death in Congenital Heart Disease: The Role of the Autopsy in Determining the Actual Cause Reprinted from: <i>J. Cardiovasc. Dev. Dis.</i> 2020 , 7, 58, doi:10.3390/jcdd7040058	259

About the Editors

Deborah Henderson

Deborah Henderson is a cardiac developmental biologist who focuses on understanding the morphogenetic mechanisms that underpin formation of the heart and great vessels and that are disrupted to result in congenital heart defects (CHD). She trained as a developmental biologist at the Institute of Child Health, UCL, before moving to Newcastle University in 2002 to establish an independent research team. Since then she has led a research team using a range of model systems and approaches in mouse and zebrafish to investigate how and why specific malformations arise—a particular interest in this respect is bicuspid aortic valve.

Deborah is also the Newcastle Director of the Human Developmental Biology Resource (hdbr.org), a human embryonic and fetal biobank that supports research projects around the world.

Nigel Brown

Professor Nigel Brown was Vice-Principal of St George's, University of London, and also Foundation Director of the Institute of Medical and Biomedical Education, on his recent retirement. Previous senior roles included being Dean of the Faculty of Medicine and Biomedical Sciences and Dean of Research. Professor Brown's research area is embryonic development, including interests in mechanisms of congenital heart defects, left–right asymmetry and adverse effects of drugs and chemicals on the unborn. He continues research as an Emeritus Professor. Professor Brown has been at St George's since 1989, initially as Head of Teratology in the MRC Experimental Embryology and Teratology Unit, before joining the University staff. He qualified in the 1970s, including a studentship at the University of Mainz, Germany, progressing to an NIH post-doctoral fellowship then an Assistant Professor at George Washington University Medical School, DC, before returning to the UK with the MRC.

Preface to “Leaders in Cardiovascular Research: A special issue dedicated to Professor Robert Anderson”

In 2019, the *Journal of Cardiovascular Development and Disease* began a series of Special Issues entitled “Leaders in Cardiovascular Research” which highlight the work and achievements of outstanding and unique researchers that have made major and often paradigm-shifting contributions to the field.

This publication focuses on the many accomplishments of Prof Robert H Anderson, who is acknowledged world-wide as the current leading cardiac anatomist and foremost expert on embryonic heart developmental morphology. Over a career of more than 50 years, Bob has collaborated widely and productively, and has been the person to whom researchers have turned to help unravel the mysteries of heart morphogenesis. These collaborations have spanned the spectrum, from clinical cardiac surgery and pathology, to molecular investigations of embryonic cardiovascular development in human and many other species.

This book contains a set of commissioned scientific papers, case studies and reviews on topics to which Prof Anderson has made consistent and essential contributions over his long and on-going career.

Deborah Henderson and Nigel Brown

Editors



Editorial

The Editors' Personal Biography of Professor Robert Anderson

Nigel A. Brown ^{1,*}  and Deborah J. Henderson ²

¹ Molecular and Clinical Sciences Research Institute, St. George's, University of London, London SW17 0RE, UK

² Bioscience Institute, Centre for Life, Newcastle University, Newcastle-upon-Tyne NE1 3BZ, UK; deborah.henderson@newcastle.ac.uk

* Correspondence: nbrown@sgul.ac.uk

Citation: Brown, N.A.; Henderson, D.J. The Editors' Personal Biography of Professor Robert Anderson. *J. Cardiovasc. Dev. Dis.* **2021**, *8*, 6. <https://doi.org/10.3390/jcdd8010006>

Received: 12 January 2021

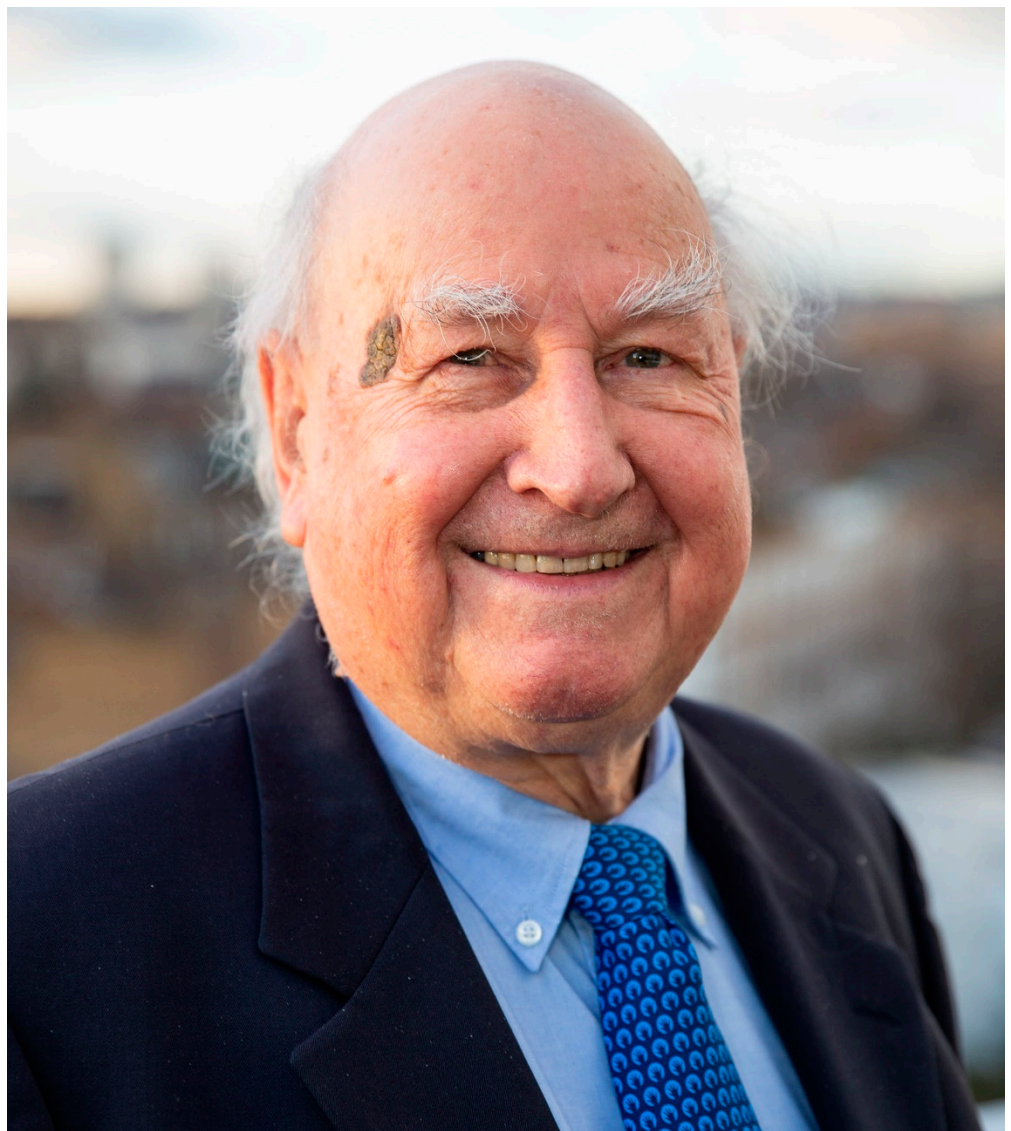
Accepted: 13 January 2021

Published: 19 January 2021

Publisher's Note: MDPI stays neutral with regard to jurisdictional claims in published maps and institutional affiliations.



Copyright: © 2021 by the authors. Licensee MDPI, Basel, Switzerland. This article is an open access article distributed under the terms and conditions of the Creative Commons Attribution (CC BY) license (<https://creativecommons.org/licenses/by/4.0/>).



Robert (Bob) Henry Anderson was born in Wellington, Shropshire, UK, in 1942 and he completed his medical training in Manchester (UK) in 1966. In that same year, he married Christine, without whose constant support Bob would surely not have become the legendary figure he is today. Within 5 or 6 years, Bob had already published research in

many of the areas that would define his career (Christine also had two children), and by 1979, he was rapidly and deservedly Professor of Paediatric Cardiac Morphology at the UK National Heart and Lung Institute in London.

Those first publications covered cardiac nerves (*Experientia*, 1971) [1]; the conduction system (*J. Anat.*, 1971) [2]; embryonic heart development (*Br. Heart J.*, 1972) [3]; situs inversus (*Circulation*, 1972) [4] and congenital heart malformation (*Br. Heart J.*, 1972) [5]. One feature of these papers, which has continued ever since, is Bob's acknowledgement of prescient contributions from the early researchers (and, of course, to correct them whenever necessary). In his first publication on the development of the heart, in 1972 [3], he cited papers from 1893, 1906, 1910, 1912 and 1914. He also started as he meant to continue, by naturally citing five of his own papers. Bob has never been afraid to commit his current understanding to paper and is always very willing to change that, in another publication, when new evidence arrives.

Over the following 50 years, Bob published more than 1000 peer-reviewed papers, making significant advances in these and in many other areas, establishing his reputation as a world-leading researcher. His seminal studies are cited by many of the contributions in this Special Issue—just a tiny reflection of Bob's enduring influence on heart research. This would be sufficient for a major career, but there is much more to Bob's contributions than just his substantial research record. He worked tirelessly to ensure a consistent and logical terminology for heart structures and their congenital abnormalities and to make this congruent with their developmental origins. Bob knows the correct identity and name of everything in and connected with the heart. Woe betide anyone who strays from this correctness, in print or in presentations.

In many ways, the most impactful aspect of Bob's legacy is his education of and positive influence on several generations of clinicians and scientists, all across the wide field of heart research and practice. Again, many of those protégées appear as authors within this Special Issue and, indeed, functioned as Reviewers and Editors. From the beginning, in 1967, as an anatomy lecturer to medical students, Bob has been an enthusiastic and inspiring educator. Bob's passion for the topic and his unfailing support for the learner are given freely, regardless of level, whether to the undergraduate in their first experiences, or to the expert in one of Bob's masterclasses. Bob has toured the world throughout his career, lecturing in his inimitable pulpit style, and he continues to do so with regular visits to the USA (Chicago, Cincinnati, Denver, Milwaukee and Pittsburgh), Canada and India. Bob's huge and infectious enthusiasm for the subject, and indeed, for life, is one aspect of his ability to make dear (in some cases, life-long) friends of his colleagues all over the world.

Those continuing regular visits illustrate Bob's impressive longevity, not only in education but also research. Bob nominally retired in 2007, but it was difficult for many of us to discern any change. He now has Professorial and/or Consultant appointments in London, Newcastle, Manchester, Birmingham and Southampton in the UK, and in Charleston and Houston in the USA. Bob remains, as has always been the case, a prolific research collaborator. Over the past few decades of cellular and molecular technical advances, numerous developmental labs have sought out Bob as the go-to person to help them interpret their studies in the context of the intricate morphogenesis of the heart. He has a remarkable 4D model of embryonic heart anatomy in his brain, and these collaborations continue to be highly productive. Just as in his educational activities, Bob freely shares everything he knows in the research lab (which is worth bearing in mind when discussing your own work with Bob).

Bob is one of those enviable people who is good at everything they do, and he also has a wide-ranging store of deep knowledge. For example, he was a talented sportsman, so an impressive awareness of current UK sports (especially Manchester City) is not a surprise, but his encyclopaedic knowledge of US baseball is unexpected. Of course, Bob still plays a very creditable game of golf, on at least a weekly basis. Bob is also an accomplished pianist, a more-than-capable member of a classical duo or trio. Perhaps his greatest love is wine, for which he has impeccable taste and understanding. Bob has a very fine collection at

home, and warehoused, and he is always generous in sharing this with the very many colleagues he and Christine have entertained and accommodated at their home in London.

During these more than 50 years of service to clinical practice, research and education, Bob has been honoured in many ways. Suffice to mention here just two recent awards: in 2017, he was elected as an honorary fellow of the European Congenital Heart Surgeon's Association, and in 2019, he was accorded honorary membership of the Congenital Heart Surgeon's Society of North America. We hope that this Special Issue is a fitting addition to these honours and that he knows that this reflects the high regard and affection that all of us involved in this collection have for the unique person that is Bob Anderson.

Funding: This research received no external funding.

Conflicts of Interest: The authors declare no conflict of interest.

References

1. Anderson, R.H. Fluorescing valvular nerves in the guinea-pig heart. *Experientia* **1971**, *27*, 1063–1064. [CrossRef] [PubMed]
2. Anderson, R.H.; Latham, R.A. The cellular architecture of the human atrioventricular node, with a note on its morphology in the presence of a left superior vena cava. *J. Anat.* **1971**, *109*, 443–455. [PubMed]
3. Anderson, R.H.; Taylor, I.M. Development of atrioventricular specialized tissue in human heart. *Br. Heart. J.* **1972**, *34*, 1205–1214. [CrossRef] [PubMed]
4. Anderson, R.H.; Arnold, R.; Jones, R.S. D-bulboventricular loop with L-transposition in situs inversus. *Circulation* **1972**, *46*, 173–179. [CrossRef] [PubMed]
5. Latham, R.A.; Anderson, R.H. Anatomical variations in atrioventricular conduction system with reference to ventricular septal defects. *Br. Heart J.* **1972**, *34*, 185–189. [CrossRef] [PubMed]



Article

Identification and Morphogenesis of Vestibular Atrial Septal Defects

Rohit S. Loomba ^{1,*}, Justin T. Tretter ², Timothy J. Mohun ³, Robert H. Anderson ⁴,
Scott Kramer ⁵ and Diane E. Spicer ⁵

¹ Division of Cardiology, Advocate Children's Hospital, Chicago, IL 60453, USA

² Heart Institute, Cincinnati Children's Hospital Medical Center, Cincinnati, OH 45229, USA;
justin.tretter@cchmc.org

³ Francis Crick Institute, London NW1 1AT, UK; tim.mohun@gmail.com

⁴ Cardiovascular Research Centre, Institute of Genetic Medicine, Newcastle University,
Newcastle upon Tyne NE1 3BZ, UK; sejiran@ucl.ac.uk

⁵ Division of Pediatric Cardiology, University of Florida, Gainesville, FL 32611, USA;
scott.kramer888@gmail.com (S.K.); spicerpath@hotmail.com (D.E.S.)

* Correspondence: loomba.rohit@gmail.com

Received: 2 May 2020; Accepted: 10 August 2020; Published: 10 September 2020

Abstract: *Background:* The vestibular atrial septal defect is an interatrial communication located in the antero-inferior portion of the atrial septum. Reflecting either inadequate muscularization of the vestibular spine and mesenchymal cap during development, or excessive apoptosis within the developing antero-inferior septal component, the vestibular defect represents an infrequently recognized true deficiency of the atrial septum. We reviewed necropsy specimens from three separate archives to establish the frequency of such vestibular defects and their associated cardiac findings, providing additional analysis from developing mouse hearts to illustrate their potential morphogenesis. *Materials and methods:* We analyzed the hearts in the Farouk S. Idriss Cardiac Registry at Ann and Robert H. Lurie Children's Hospital in Chicago, IL, the Van Mierop Archive at the University of Florida in Gainesville, Florida, and the archive at Johns Hopkins All Children's Heart Institute in St. Petersburg, Florida, identifying all those exhibiting a vestibular atrial septal defect, along with the associated intracardiac malformations. We then assessed potential mechanisms for the existence of such defects, based on the assessment of 450 datasets of developing mouse hearts prepared using the technique of episcopic microscopy. *Results:* We analyzed a total of 2100 specimens. Of these, 68 (3%) were found to have a vestibular atrial septal defect. Comparable defects were identified in 10 developing mouse embryos sacrificed at embryonic data 15.5, by which stage the antero-inferior component of the atrial septum is usually normally formed. *Conclusion:* The vestibular defect is a true septal defect located in the muscular antero-inferior rim of the oval fossa. Our retrospective review of autopsied hearts suggests that the defect may be more common than previously thought. Increased awareness of the location of the defect should optimize its future clinical identification. We suggest that the defect exists because of failure, during embryonic development, of union of the components that bind the leading edge of the primary atrial septum to the atrioventricular junctions, either because of inadequate muscularisation or excessive apoptosis.

Keywords: vestibular atrial septal defect; atrial septal defect; cardiac development; atrial septum

1. Introduction

The vestibular defect is a true septal defect located in the antero-inferior muscular rim of the oval fossa [1]. Initially noted and described as a solitary finding, a formal investigation of its frequency,

as far as we are aware, has yet to be completed using large series of autopsied hearts [2,3]. We describe here the findings from our review of necropsy specimens from three separate archives. We also provide evidence from examination of developing murine hearts, which offer an explanation for the morphogenesis of the lesion.

2. Methods

We analyzed all hearts in the Farouk S. Idriss Cardiac Registry at Ann and Robert H. Lurie Children’s Hospital in Chicago, IL, the Van Mierop Archive at the University of Florida in Gainesville, Florida, and the archive at Johns Hopkins All Children’s Heart Institute in St. Petersburg, Florida, paying particular attention to the integrity or otherwise of the antero-inferior margin of the oval fossa. In hearts where there had been surgical intervention, we also took note of the findings as described in the original autopsy reports so as to ensure that any unexpected communications observed were not the results of the prior surgery. The findings are summarized in Table 1. We then assessed the formation and closure of the atrial septum in mouse embryos as revealed using the technique of episcopic microscopy, the mechanisms of septal development known to be comparable in mice and humans [1,4]. Parkes mice were used for these investigations. Over 400 datasets were examined, providing evidence of the temporal changes occurring during septation of the atrial chambers in the mouse heart. The datasets covered the period from the eleventh day of intrauterine development to term, which in the mouse usually occurs on the nineteenth day of development.

Table 1. Characteristics of the specimens noted to have vestibular atrial septal defects.

Right-Sided Superior Caval Vein	68 (100)
Drainage of right-sided superior caval vein	
Right-sided atrium	68 (100)
Left-sided superior caval vein	4 (6)
Drainage of left-sided superior caval vein	
Coronary sinus	4 (100)
Pulmonary vein drainage	
Left-sided atrium	68 (100)
Right-sided atrium	
Normal	26 (38)
Dilated	42 (62)
Left-sided atrium	
Normal	46 (68)
Dilated	20 (29)
Hypoplastic	2 (3)
Oval fossa-type atrial septal defect	53 (78)
Coronary sinus defect	3 (4)
Common atrioventricular junction	10 (15)
Ventricular topology	
Right	67 (98)
Left	1 (2)
Atrioventricular connections	
Concordant	65 (94)
Discordant	1 (2)
Absent left-sided atrioventricular valve	1 (2)
Absent right-sided atrioventricular valve	1 (2)
Right-sided atrioventricular valve abnormality	40 (59)
Left-sided atrioventricular valve abnormality	19 (28)
Pulmonary atresia	17 (25)

Table 1. *Cont.*

Aortic atresia	1 (2)
Ventriculoarterial connections	
Concordant	60 (89)
Discordant	5 (7)
Double outlet right ventricle	3 (4)
Right-sided ventricle morphology	
Tripartite	51 (75)
Bipartite	12 (18)
Unipartite	5 (7)
Left-sided ventricle morphology	
Tripartite	66 (96)
Bipartite	1 (2)
Unipartite	1 (2)
Right outflow tract obstruction	
None	31 (46)
Infundibular	3 (5)
Valvar	6 (9)
Infundibular and valvar	11 (15)
Valvar atresia	17 (25)
Position of aorta relative to the pulmonary trunk	
Anterior	1 (2)
Anterior, rightward	7 (10)
Posterior, rightward	58 (84)
Side by side, rightward	1 (2)
Common arterial trunk	1 (2)
Left ventricular outflow tract obstruction	
None	54 (79)
Subvalvar	4 (6)
Valvar	7 (10)
Subvalvar and valvar	2 (3)
Valvar atresia	1 (2)
Interventricular communication	31 (46)
Aortic arch sidedness	
Left	66 (98)
Right	1 (2)
Coarctation of the aorta	4 (6)
Interruption of the aortic arch	2 (3)
Abnormal coronary artery origins or course	3 (6)
Arterial duct	
Absent	27 (40)
Present	33 (49)
Ligated	8 (11)
Cardiac apex	
Leftward	67 (98)
Pointing to middle	1 (2)
Trisomy 21	5 (7)
22 q deletion	1 (2)

3. Results

3.1. Human Necroscopy Specimens

We analyzed a total of 2100 specimens, with 68 (3%) found to have a vestibular atrial septal defect. We use this denominator of 68 hearts with vestibular atrial septal defects for our subsequent descriptions. All the defects were found in the antero-inferior muscular rim of the oval fossa, typically

in the area antero-superior to the mouth of the coronary sinus (Figure 1). This area, which provides the antero-inferior muscular buttress of the oval fossa, includes the narrow vestibule of the right atrium that lies between the antero-inferior rim and the hinge of the septal leaflet of the tricuspid valve. A slight variation was observed in the position of the defect, with its size also varying (Figure 2). Some of the defects were slit-like and tiny, but large defects were also found, as in one of the hearts examined from an adult patient (Figure 2). The defects opened to the left atrium adjacent to the hinges of the leaflets of the mitral valve, with retention of the normal off-setting of the hinges of the atrioventricular valvar leaflets in the hearts having separate atrioventricular junctions (Figure 3).

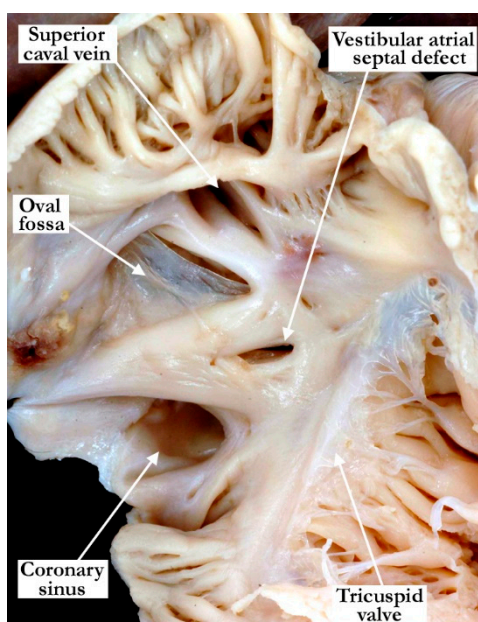


Figure 1. The vestibular atrial septal defect seen in this image is midway between the antero-inferior rim of the oval fossa and the hinge point of the tricuspid valve. This is the most common position for the defect. There is a dilated coronary sinus secondary to a persistent left superior caval vein.

In terms of associated lesions, all hearts had a usual atrial arrangement, with right-sided superior caval veins that drained into the roof of the right-sided atrium. A left-sided superior caval vein was present in four (6%) of the hearts, in all instances draining into the coronary sinus. The pulmonary veins returned to the left atrium in a normal fashion in all of the specimens. The morphologically right atrium was dilated in 42 hearts (62%), with the morphologically left atrium being dilated in 20 (29%), and hypoplastic in two (3%). An additional defect was present in the oval fossa in 53 hearts (78%), with an additional coronary sinus interatrial communication found in three (4%). A common atrioventricular junction was present in 10 (15%), accompanied by the anticipated “ostium primum” atrial component of the associated atrioventricular septal defect. In these hearts, the atrial septum itself was well-formed, with a recognizable oval fossa. The vestibular defect itself was in the leading edge of the septum, adjacent to the “ostium primum” defect (Figure 4). The atrioventricular connections were concordant in 65 (94%), discordant in one (2%), solitary and right-sided in one (2%), and solitary and left-sided in one (2%). An abnormality of the right-sided atrioventricular valve was noted in 40 hearts (59%), with a left-sided atrioventricular valvar abnormality noted in 19 (28%). Abnormalities of the atrioventricular valves included both stenosis and dysplasia. Ventricular topology was right-handed in all the hearts except for the one with discordant atrioventricular connections (98%). The ventriculo-arterial connections were concordant in 60 (89%), discordant in five (7%), and double outlet right ventricle in three (4%). Pulmonary atresia was present in 17 hearts (25%), while aortic atresia was present in one (2%). The aorta was most commonly posterior and rightward (58, 84%). Right ventricular outflow tract obstruction was present in 37, (58%) most commonly at the level of the

arterial valve. An interventricular communication was present in 31 (46%). The aortic arch coursed over the left-sided pulmonary artery and bronchus in 66 (98%). Coarctation of the aorta was present in four (6%), with interruption of the aortic arch present in two (3%). The coronary arterial origins were abnormal in three (6%). An arterial duct was present in 33 (49%), ligated in eight (11%), and absent in 27 (40%). The cardiac apex was leftward in all but one heart, which had an apex that was pointed towards the midline. A history of trisomy 21 was documented in five patients (7%), with a history of 22 q deletion documented in one (2%).

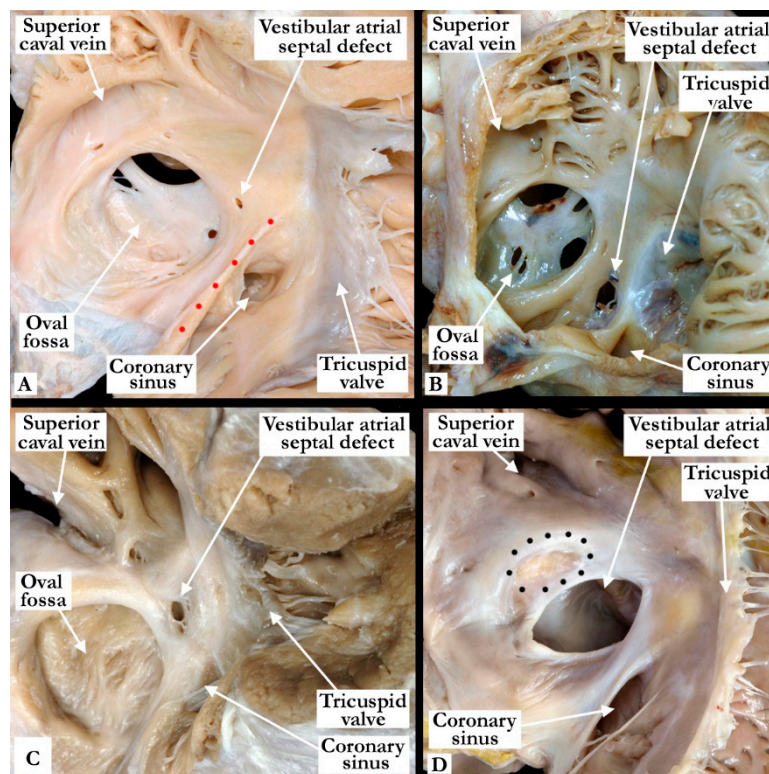


Figure 2. The images show the variations in size and position of vestibular atrial septal defects. In (Panel A), we show a small defect within the antero-inferior rim of the oval fossa. There is also a fenestrated flap valve at the floor of the oval fossa. The Eustachian valve (red dots) is prominent in this specimen. In (Panels B,C), the defects are larger and focally fenestrated with the defect shown in (Panel B) in a more inferior position, while the defect seen in (Panel C) is toward the most superior extent of the margins of the true atrial septum. There is an intact flap valve in the heart shown in (Panel C), and a fenestrated flap valve at the floor of the oval fossa in the heart seen in (Panel B). In (Panel D), we show an exceedingly large vestibular defect. This was an incidental finding at autopsy in a 46-year-old patient who died secondary to a stroke. It was approximately 2 cm in diameter. The borders of the oval fossa are marked with black dots and the foramen was closed.

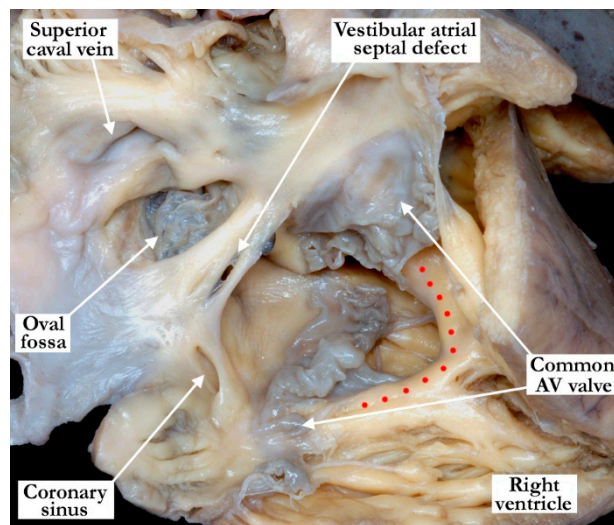


Figure 3. This heart with a common atrioventricular junction guarded by a common valve is viewed from the right ventricle, with the ventricular septum marked with red dots. There is a competent flap valve at the floor of the oval fossa, and a vestibular septal defect in the antero-inferior muscular rim, directly adjacent to the atrial component of the atrioventricular septal defect.

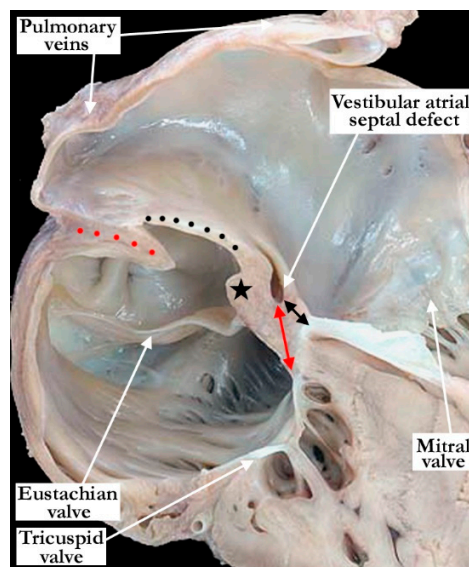


Figure 4. The heart is sectioned in a four-chamber plane to demonstrate the position of a vestibular atrial septal defect in the inferior muscular buttress. The defect occurs between the vestibules of the right and left atrium. When there is normal offsetting of the atrioventricular valves, as in the heart shown, the defect is typically closer to the mitral valve (double-headed black arrow) and farther from the tricuspid valve (double-headed red arrow). The antero-inferior rim of the oval fossa is marked with a black star. In this image, the opening of the defect to the right atrium is not seen. The flap valve (black dots) at the floor of the oval fossa was well-formed and overlaps the superior interatrial fold (red dots). Note the imperforate tricuspid valve in this heart which also had pulmonary atresia with an intact ventricular septum.

3.2. Developmental Considerations

Since the defects observed in the autopsied hearts were all found either within the antero-inferior buttress of the oval fossa, or at the site of anchorage of the floor of the fossa to the buttress, we reasoned that knowledge of normal development of the atrial septum might permit us better to understand the morphology and location of the defects. We studied, therefore, the temporal changes occurring

during septation of the atrial chambers in the mouse heart, taking advantage of our access to over 400 datasets prepared from developing mouse embryos which cover the period from the eleventh day of intrauterine development to term, which in the mouse usually occurs on the nineteenth day of development. The key stages take place during embryonic day (E) 10.5, with the initial appearance of the primary atrial septum, and continue through E13.5, when it is possible to recognise the margins of the oval fossa, along with the formation of the oval foramen (foramen ovale). Persistent patency of the oval foramen, of course, continues until term. The foramen, nonetheless, is capable of being closed from E13.5 until term in the developing murine heart. The floor of the fossa, derived from the primary atrial septum, is itself usually intact from E13.5 onwards to term. The period from E10.5 through E13.5 corresponds to the sixth through the eighth week of human intrauterine development.

At E10.5, the primary atrial septum can be recognised as a muscular ridge growing from the roof of the atrial component of the heart tube, which is a common structure at this stage of development. By this stage, the borders of the confluence of the systemic venous tributaries with the common atrial cavity are already marked by the venous valves, with the opening of the systemic venous sinus already committed to the right side of the developing atrial chamber (Figure 5A). The atrioventricular canal at this early stage is committed exclusively to the cavity of the developing left ventricle, although the parietal wall of the right atrium is already in continuity with the wall of the developing right ventricle in the roof of the embryonic interventricular communication. The primary septum itself carries a mesenchymal cap on its leading edge, with the space between the cap and the atrioventricular cushions representing the primary atrial foramen. Dorsally at this stage, the atrial walls are continuous with the pharyngeal mesenchyme through the persisting mesocardial connection. Growth from the mesenchyme into the right margin of the mesocardium has already produced inequality in size of its rims, which now protrude into the atrial cavity as the pulmonary ridges (Figure 5B). As yet, there is no formation of the pulmonary veins, but the floor of the dorsal mesocardial connection, known as the pulmonary pit, will eventually provide the site of connection between the developing pulmonary veins and the atrial cavity.

By the next day of intrauterine development (E11.5—Figure 5C), the primary atrial septum has grown towards the cushions developed within the atrioventricular canal. The canal itself has now expanded rightwards so as to bring the cavity of the right atrium into direct connection with that of the right ventricle. The upper margin of the primary foramen has now broken away from the atrial roof to form the secondary atrial foramen, while the size of the primary foramen is much reduced. By now, the growth of mesenchymal tissue into the rightward margin of the dorsal mesocardial connection has produced an intraluminal swelling that overlaps the rightward and dorsal extent of the leading edge of the primary atrial septum. This is the vestibular spine, also known as the dorsal mesenchymal protrusion. The pulmonary vein by this stage has canalised within the pharyngeal mesenchyme, opening to the atrium through the pulmonary pit. The growth of the vestibular spine ensures that the pulmonary venous orifice is committed to the developing left atrium. By E13.5, the mesenchymal cap on the atrial septum has fused with the atrial margins of the atrioventricular cushions, which themselves have fused together to separate the atrioventricular canal into the developing tricuspid and mitral valvar orifices (Figure 5D—Lower right-hand panel). The rightward margin of the cap is now itself overlapped by the vestibular spine, with an obvious seam noted between these structures. The two entities together form the caudal rim of the developing oval fossa. Both by now are losing their mesenchymal characteristics and are attaining the same texture of the walls of the cardiac chambers, which we interpret as indicating their muscularisation. The cranial margin of the fossa can now be recognised as a small ridge formed to the right side of the cranial attachment of the primary atrial septum.

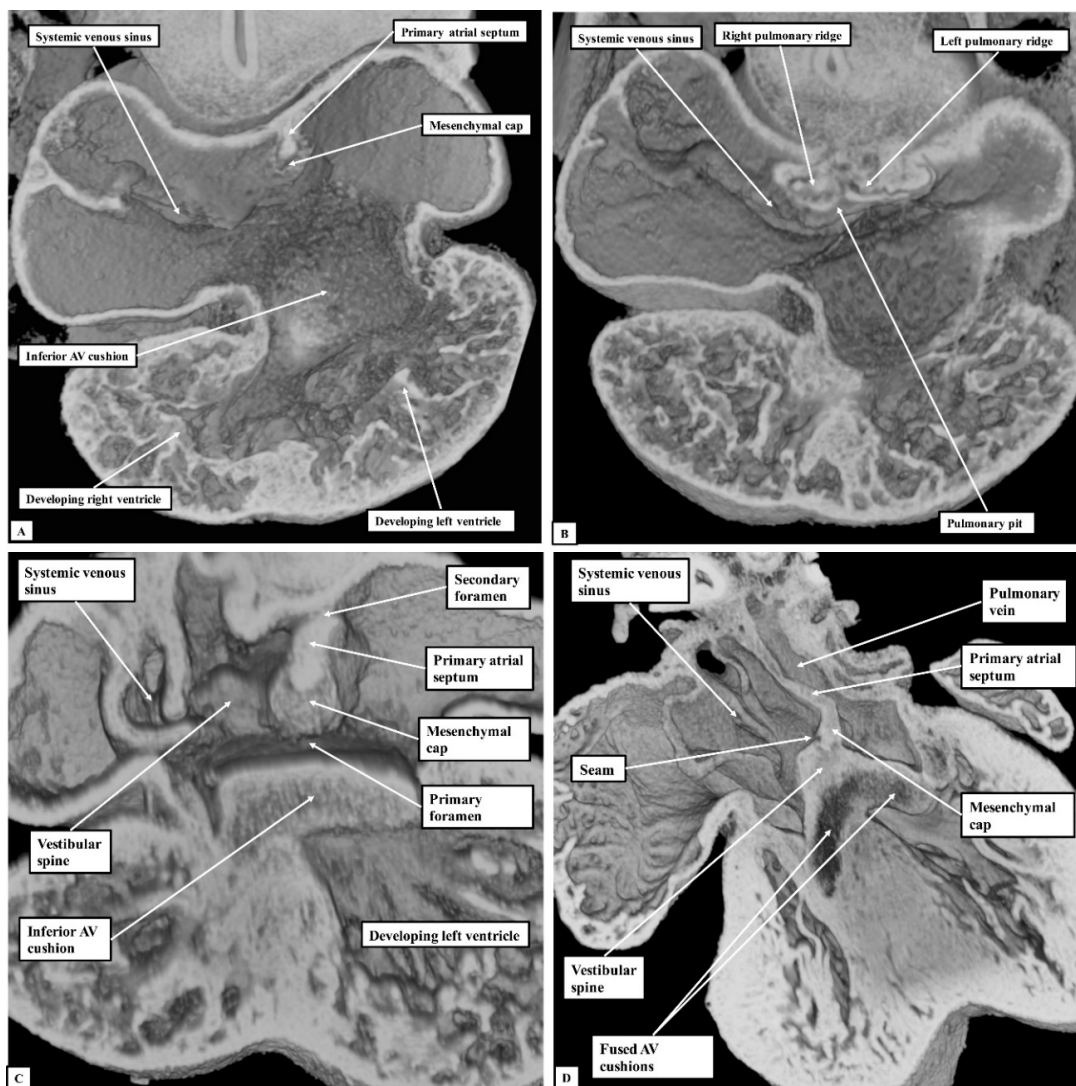


Figure 5. The images show ventral (Panel A) and more dorsal (Panel B) sections taken from the same episodic dataset prepared from a developing mouse embryo sacrificed on the eleventh day of intrauterine development (E10.5). The lower panels show similar four-chamber sections at the stages of embryonic days 11.5 (Panel C) and 13.5 (Panel D) Abbreviation: AV—Atrioventricular.

If development proceeds in a normal fashion, the margins of the oval fossa are intact by E15.5. We examined episodic datasets prepared from 48 mouse embryos at this stage. In 38 of the mice, the findings show the normal arrangement, with the primary septum folded on itself cranially, its length being considerably greater than the length of the fossa (Figure 6A). In these 38 datasets, the vestibular spine and mesenchymal cap fused together to form the caudal rim of the fossa, with obliteration of the seam initially seen between the two components during E13.5 (Figure 5D). The primary septum now forms the floor of the oval fossa, with the space between its cranial margin and the atrial roof forming the oval foramen, or secondary atrial foramen. The excessive length of the septum relative to the dimensions of the fossa provides the mechanism that permits closure of the foramen subsequent to birth. In 10 of the datasets prepared from mice sacrificed at E15.5, however, we found deficiencies of either the inferior rim of the oval fossa, or the attachment of the leading edge of the primary septum. In two, the findings could be attributed to the failure of formation of the vestibular spine (Figure 6B), with additional failure of growth of the primary septum in one of the two. In both, the lack of growth of the spine was associated with persistence of a common atrioventricular junction, with the atrioventricular cushions fused to each other, and also to the crest of the muscular ventricular septum,

in other words producing an “ostium primum” defect. In four further datasets, although the vestibular spine had protruded in anticipated fashion to form the caudal margin of the oval fossa, thus separating the right and left atrioventricular junctions and forming the caudal rim of the fossa, the primary septum itself was deficient adjacent to the caudal rim, thus producing a hole in the floor of the fossa adjacent to its antero-inferior buttress, in other words, an “ostium secundum” defect (Figure 6C) The defect was large in two of the datasets but smaller in the remaining two. In the remaining four datasets, the mesenchymal cap had failed to fuse with the vestibular spine. The spaces in the floor of the oval fossa in these four hearts (Figure 7), therefore, are directly comparable to the vestibular defects found in our autopsied hearts.

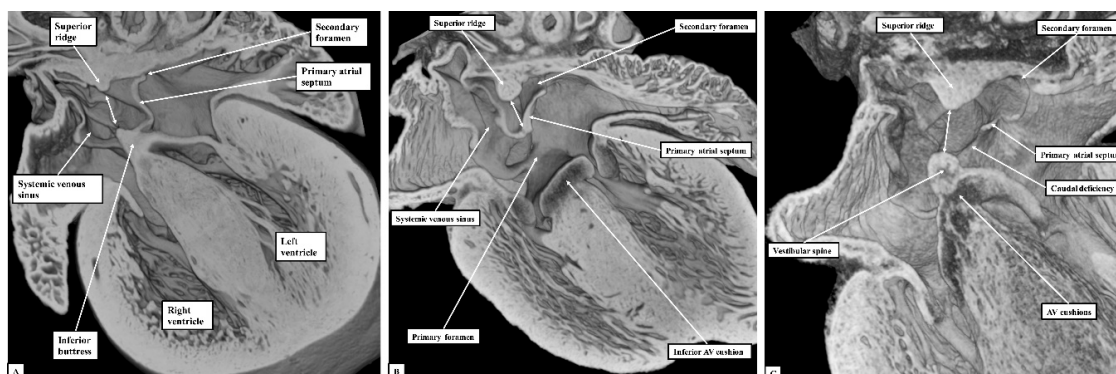


Figure 6. The images show sections prepared in the four-chamber plane from mouse embryos sacrificed at the sixteenth day of development (E15.5). (Panel A) shows the normal arrangement, with the primary atrial septum forming the floor of the oval fossa (double-headed white arrow). (Panel B) shows an “ostium primum” defect, with common atrioventricular junction due to failure of formation of the vestibular spine. (Panel C) shows a large defect in the primary septum adjacent to the vestibular spine, thus producing a caudal defect within the oval fossa. The double-headed white arrow shows the margins of the oval fossa. AV—Atrioventricular.

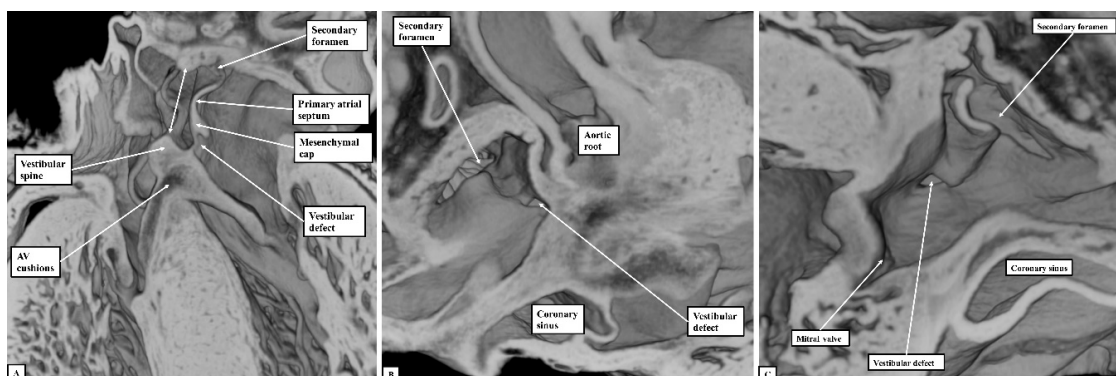


Figure 7. The images show the features of the vestibular defect, as was found in four of the datasets. The dataset used to prepare the figure is sectioned so as to show the appearance of the defect in the four-chamber plane (Panel A), and as seen from the right (Panel B) and left (Panel C) sides. The double-headed white arrow in the left-hand panel shows the margins of the oval fossa. AV—Atrioventricular.

4. Discussion

The majority of interatrial communications can be divided anatomically into two groups: those located within the rims of the oval fossa, and those located outside the oval fossa [5]. The latter lesions include the sinus venosus, coronary sinus, and “ostium primum” defects. The true defects of the atrial septum are those confined within the rims of the oval fossa. Additionally known as “ostium secundum” defects, they exist because of deficiencies of the floor of the fossa, which is derived from the primary

atrial septum [1]. Some time ago, another form of true atrial septal defect was described by Sharratt and colleagues. It was located within the anterior-inferior rim of the fossa [3]. This defect, called a vestibular defect, produced a communication between the vestibules of the mitral and tricuspid valves. As we now show, such defects can also be found in the setting of a common atrioventricular junction.

These defects are a result of either inadequate muscularization of the vestibular spine and mesenchymal cap during development, or excessive apoptosis within the developing antero-inferior septal component, the vestibular defect represents an infrequently recognized true deficiency of the atrial septum. The detailed morphogenesis of the atrial septum is described at length in the results.

The initial account of such a vestibular defect was followed by a description by Fukuda and colleagues following surgical correction [2]. As we now confirm, this part of the atrial septum is produced by the fusion of the vestibular spine, or dorsal mesenchymal protrusion, with the mesenchymal cap carried on the leading edge of the primary atrial septum. Webb and colleagues had emphasised the significance of the vestibular spine in completing atrial septation, although the spine itself was first described by His in the 19th century [6]. The importance of the spine was then endorsed by Blom and colleagues, who described the process of atrioventricular septation as requiring not only the fusion of the endocardial AV cushions and downward growth of the muscular primary atrial septum, but also the ventral proliferation of the spine [7]. The latter investigators found a reduced amount of extracardiac mesenchyme in the vestibular spine of human embryos with Down's syndrome, leading to a lack of ventral protrusion of this mesenchymal mass in the setting of a common atrioventricular junction. The role of the spine was then reinforced by Snarr and colleagues, who chose to describe it as the dorsal mesenchymal protrusion. They demonstrated, in an elegant fashion, its relationship to the newly discovered second heart field [8]. As we have now shown using episcopic microscopy, this non-endocardially derived mesenchymal component, along with the mesenchymal cap carried on the leading edge of the primary atrial septum, eventually fuse to form the definitive antero-inferior buttress of the oval fossa. As we also show, it is improper fusion of the spine with the remaining components of the developing septum that is the essence of the vestibular defect.

All of the defects that we found are comparable to the lesion initially reported by Sharratt and colleagues [3]. Recognition of the presence of the vestibular defect is important since percutaneous closure of isolated or multifenestrated defects within the fossa could still leave residual shunting through the vestibular defect [9,10]. Our retrospective review of autopsied hearts now suggests that the defect may be more common than previously thought. It is also perhaps pertinent that none of the original autopsy reports prepared for the hearts we investigated described the presence of the vestibular defects. It could well be, therefore, that the defects could go unnoticed during autopsy examination unless specifically sought. It is also possible that the right atrial entrance to the defect could be mistaken for a Thebesian vein. In all of our specimens, we excluded this possibility by probing the defect, confirming that it represented a true interatrial communication. Diagnosis also represents an echocardiographic challenge. When the vestibular defect is present concomitant with an oval fossa defect, its location can suggest the presence of multiple defects within the floor of the oval fossa. Increased awareness of the defect should optimize its future clinical identification.

5. Conclusions

The vestibular defect is a true atrial septal defect located in the muscular antero-inferior rim of the oval fossa. The other type of true atrial septal defect occurs when there is a deficiency of the primary atrial septum or the flap valve at the floor of the oval fossa. Review of the episcopic data sets suggest that the defect exists because of failure, during embryonic development, of union of the components that bind the leading edge of the primary atrial septum to the atrioventricular junctions, either because of inadequate muscularisation or excessive apoptosis. The retrospective review of a large cohort of autopsied hearts suggests that the defect may be more common than previously thought. Increased awareness of the location of the defect should optimize its future clinical identification.

Author Contributions: Conceptualization and methodology for this retrospective review was initiated by R.H.A. and D.E.S. The retrospective investigation and data curation of the 2.100 specimens was carried out by D.E.S. and S.K. at the University of Florida-Congenital Heart Center, D.E.S. and R.S.L. at the Lurie Children’s Hospital in Chicago and by D.E.S. at Johns Hopkins All Children’s Hospital in Florida. The formal analysis and original draft was done by R.S.L. The episcopic mouse data was performed and provided by R.H.A. and T.J.M. Critical review, editing and data review was done by all authors (R.S.L., J.T.T., T.J.M., R.H.A., S.K., D.E.S.). All specimen images were produced and labeled by D.E.S. with the episcopic images prepared by R.H.A. and T.J.M. Project supervision was done by R.H.A. and D.E.S. All authors have read and agreed to the published version of the manuscript.

Funding: This research received no external funding.

Conflicts of Interest: The authors declare no conflict of interest.

References

1. Jensen, B.; Spicer, D.E.; Sheppard, M.N.; Anderson, R.H. Development of the atrial septum in relation to postnatal anatomy and interatrial communications. *Heart* **2017**, *103*, 456–462. [CrossRef] [PubMed]
2. Fukuda, T.; Kashima, I.; Yoshiba, S. Surgical treatment of an unusual atrial septal defect: The vestibular defect. *Cardiol. Young* **2004**, *14*, 212–214. [CrossRef]
3. Sharratt, G.P.; Webb, S.; Anderson, R.H. The vestibular defect: An interatrial communication due to a deficiency in the atrial septal component derived from the vestibular spine. *Cardiol. Young* **2003**, *13*, 184–190. [CrossRef]
4. Mohun, T.J.; Weninger, W.J. Imaging heart development using high-resolution episcopic microscopy. *Curr. Opin. Genet. Dev.* **2011**, *21*, 573–578. [CrossRef]
5. Ezon, D.; Goldberg, J.; Kyle, W. *Atlas of Congenital Heart Disease Nomenclature*; Ezon Educational Services: Kentucky, KY, USA, 2015.
6. Webb, S.; Brown, N.A.; Anderson, R.H. Formation of the atrioventricular septal structures in the normal mouse. *Circ. Res.* **1998**, *82*, 645–656. [CrossRef] [PubMed]
7. Blom, N.A.; Ottenkamp, J.; Wenink, A.G.; Gittenberger-de Groot, A.C. Deficiency of the vestibular spine in atrioventricular septal defects in human fetuses with down syndrome. *Am. J. Cardiol.* **2002**, *91*, 180–184. [CrossRef]
8. Snarr, B.S.; Wirrig, E.E.; Phelps, A.L.; Trusk, T.C.; Wessels, A. A spatiotemporal evaluation of the contribution of the dorsal mesenchymal protrusion to cardiac development. *Dev. Dyn.* **2007**, *236*, 1287–1294. [CrossRef] [PubMed]
9. Martins, J.D.F.; Anderson, R.H. The anatomy of interatrial communications—What does the interventionist need to know? *Cardiol. Young* **2000**, *10*, 464–473. [CrossRef] [PubMed]
10. Wahl, A.; Windecker, S.; Meier, B. Evaluation and treatment of abnormalities of the interatrial septum. *Catheter. Cardiovasc. Interv.* **2004**, *63*, 94–103. [CrossRef]



© 2020 by the authors. Licensee MDPI, Basel, Switzerland. This article is an open access article distributed under the terms and conditions of the Creative Commons Attribution (CC BY) license (<http://creativecommons.org/licenses/by/4.0/>).

Article

Pax9 and *Gbx2* Interact in the Pharyngeal Endoderm to Control Cardiovascular Development

Catherine A. Stothard¹, Silvia Mazzotta¹, Arjun Vyas¹, Jurgen E. Schneider² , Timothy J. Mohun³, Deborah J. Henderson¹, Helen M. Phillips¹ and Simon D. Bamforth^{1,*} 

¹ Newcastle University Biosciences Institute, Centre for Life, Newcastle-upon-Tyne NE1 3BZ, UK; catherinestothard@gmail.com (C.A.S.); silvia.mazzotta@abdn.ac.uk (S.M.); A.Vyas1@newcastle.ac.uk (A.V.); deborah.henderson@newcastle.ac.uk (D.J.H.); helen.phillips@newcastle.ac.uk (H.M.P.)

² Biomedical Imaging, University of Leeds, Leeds LS2 9JT, UK; J.E.Schneider@leeds.ac.uk

³ The Francis Crick Institute, London NW1 1AT, UK; tim.mohun@gmail.com

* Correspondence: simon.bamforth@newcastle.ac.uk; Tel.: +44-191-241-8764

Received: 25 March 2020; Accepted: 19 May 2020; Published: 25 May 2020

Abstract: The correct formation of the aortic arch arteries depends on a coordinated and regulated gene expression profile within the tissues of the pharyngeal arches. Perturbation of the gene regulatory networks in these tissues results in congenital heart defects affecting the arch arteries and the outflow tract of the heart. Aberrant development of these structures leads to interruption of the aortic arch and double outlet right ventricle, abnormalities that are a leading cause of morbidity in 22q11 Deletion Syndrome (DS) patients. We have recently shown that *Pax9* functionally interacts with the 22q11DS gene *Tbx1* in the pharyngeal endoderm for 4th pharyngeal arch artery morphogenesis, with double heterozygous mice dying at birth with interrupted aortic arch. Mice lacking *Pax9* die perinatally with complex cardiovascular defects and in this study we sought to validate further potential genetic interacting partners of *Pax9*, focussing on *Gbx2* which is down-regulated in the pharyngeal endoderm of *Pax9*-null embryos. Here, we describe the *Gbx2*-null cardiovascular phenotype and demonstrate a genetic interaction between *Gbx2* and *Pax9* in the pharyngeal endoderm during cardiovascular development.

Keywords: *Pax9*; *Gbx2*; *Tbx1*; pharyngeal endoderm; arch arteries

1. Introduction

Normal morphogenesis of the mammalian heart and aortic arch arteries is controlled by a complex interaction of tissues and gene expression. Genetic mutations that alter heart development result in congenital heart defects which affect nearly 1% of the population, and result in structural defects to the heart and its associated great vessels [1]. Conotruncal defects affecting the outflow tract (OFT) of the heart and the aortic arch arteries are a major feature in 22q11 deletion syndrome (DS) [2], and of the 45 genes haploinsufficient in these patients, *TBX1* is thought to be the most important for cardiovascular development [3–5]. The OFT is formed from cells of the second heart field (SHF), a group of progenitor cells located in the splanchnic mesoderm that migrate to the heart and subsequently continue to provide progenitors to the heart throughout embryogenesis [6]. Initially formed as a common vessel, the OFT divides into the aorta and pulmonary trunk, and these two vessels separate and rotate around each other as the aorticopulmonary septal complex spirals caudally. Septation is completed by the fusion of the interventricular septum with the OFT endocardial cushions of the atrioventricular canal [7] and requires a contribution from neural crest cells [8]. Failure in the fusion of the OFT cushions, or if the OFT rotates aberrantly, can result in common arterial trunk (CAT) and transposition of the great arteries (TGA), respectively [9]. An atrioventricular septal defect (AVSD) can occur if there is an abnormal fusion of the superior and inferior endocardial cushions [10]. The aortic arch arteries

are derived from the pharyngeal arch arteries (PAAs) that form within the pharyngeal arches from SHF-derived endothelial cells [11]. The pharyngeal arches are a transient series of protrusions that develop in a cranial to caudal sequence along the lateral surface of the head [12] and are comprised of endoderm, mesoderm, ectoderm, and neural crest cell-derived mesenchyme [13]. The pharyngeal arches develop by forming pouches from the endoderm that meet clefts from the ectoderm to define the boundaries of each arch [14] and the endoderm is considered vital for providing cues for this patterning event in a range of species [15–17]. Disruption to pharyngeal segmentation is seen when pharyngeal endoderm gene expression is perturbed [15,18–20]. There are five bilaterally symmetrical pairs of PAAs that connect the aortic sac to the dorsal aorta. The PAAs then asymmetrically remodel to form the left-sided aortic arch and double circulatory system [21] and this process is conserved between mice and humans [22]. Aberrant PAA formation and remodelling can result in defects such as interruption of the aortic arch type B (IAA-B) [23].

The 22q11DS gene *Tbx1* is known to interact with many genes in cardiovascular development, including *Pax9* [24,25] and *Gbx2* [24]. *Pax9* is specifically expressed in the pharyngeal endoderm at embryonic day (E) 9.5 [26], although it is later expressed in the craniofacial region and skeleton. Mice deficient for *Pax9* die perinatally with a cleft palate, absent pharyngeal-derived glands, skeletal abnormalities and have complex heart and aortic arch artery defects [25,27]. *Pax9* has been shown to functionally interact with *Tbx1* in the pharyngeal endoderm for 4th PAA morphogenesis, as double-heterozygous mice develop IAA-B [25]. *Gbx2* has also been implicated in cardiovascular development [28,29] and is normally expressed in all three germ layers of the mouse at the early head fold stage (E7.5) in a domain that extends rostrally from the posterior end of the embryo, encompassing the node, into the prospective hindbrain [30]. In the pharynx, *Gbx2* is expressed in the pharyngeal arch endoderm and ectoderm at E8.5 [31] but restricted to the pharyngeal endoderm by E9.5 [28]. *Gbx2* is downregulated in the pharyngeal endoderm of *Pax9*-null embryos [25] and in the pharyngeal endoderm and ectoderm of *Tbx1*-null embryos [28].

In this study, we have examined the cardiovascular phenotype in *Gbx2*-null mice and identified a genetic interaction for cardiovascular development between *Gbx2* and *Pax9* in complex mutants in the pharyngeal endoderm. We also explored a potential genetic interaction between *Tbx1*, *Pax9* and *Gbx2* for aortic arch artery morphogenesis.

2. Materials and Methods

2.1. Mice

The mice used in this study have previously been described: *Gbx2*^{fllox} [32], *Pax9*^{+/-} [27], *Pax9*^{Cre} [25], *Sox2*^{Cre} [33], *Tbx1*^{+/-} [34], and *R26R*^{eYFP} [35]. All mice were maintained on a C57Bl/6J genetic background. All studies involving animals were performed in accordance with the UK Home Office Animals (Scientific Procedures) Act 1986.

2.2. Breeding

Male and female mice were mated and the detection of a vaginal plug the next morning considered to be embryonic day (E) 0.5. Pregnant females were culled on the required day and embryos collected. Embryos at E9.5–E11.5 were staged by somite counting. PCR genotyping primers are available on request.

2.3. Imaging

Magnetic resonance imaging (MRI), High Resolution Episcopic Microscopy (HREM) and micro-computed tomography (μ CT) techniques were performed as previously described [25,36–39]. Volume data sets were segmented using Amira software (ThermoFisher Scientific, Waltham, MA, USA) to create 3-dimensional (3-D) images. Structures were manually outlined using the label field function of Amira and surface rendered to produce the 3-D images. Intra-cardiac ink injections were performed

as described [28]. Haematoxylin and eosin staining, immunohistochemistry, and whole-mount in situ hybridisation, were performed using standard techniques. mRNA expression on sections was examined by in situ hybridisation using RNAscope® Multiplex Fluorescent v2 Assay (Advanced Cell Diagnostics, Newark, CA, USA) following the manufacturer's instructions. Probe and antibody details are given in Table S5.

2.4. Identifying Conserved Binding Sites in the *GBX2* Locus

Human and mouse genomic *GBX2* sequences were aligned in Geneious 10.2.6 (<https://www.geneious.com>) using the Align feature, identifying a highly conserved region ~2kb downstream from the 2nd and final *GBX2* coding exon. This region was scanned for TBX1/5 and PAX5/9 consensus binding sequences using the rVista (<https://rvista.dcode.org/>) and JASPAR (<http://jaspar.genereg.net/>) databases. One TBX5 and three PAX5/9 sites were identified with the following sequences: TBX-BE-1, CAGCACCTCA; PAX-BE-1, AGGCAGCCCTTGATG; PAX-BE-2, GTCTCAGCTGGCTGATTAA; and PAX-BE-3, TTAATCCAAGGTTGGGTTTTG.

2.5. Luciferase Assay

The 500 bp *Gbx2* conserved region was amplified from mouse genomic DNA by PCR and sub-cloned into the pGL3-Promoter plasmid (Promega, Madison, WI, USA) downstream of luciferase. The cDNAs for *PAX9* and *TBX1* were cloned into pcDNA3.1. JEG3 cells were seeded at a density of 1×10^5 cells per well in 24-well plates and transfections were performed in triplicate with jetPRIME (Polyplus-transfection, Illkirch, France) using a total of 0.5 μ g DNA in a reaction volume of 300 μ L. Positive control reporter constructs were 2xTkGl2, containing synthetic TBX binding sites [5], and p2.4BMP4-luc which binds PAX9 [40]. A renilla luciferase vector (5 ng) was included as a transfection control. Wells without DNA or with the empty pcDNA3.1 vector served as negative controls. All wells received an equal quantity of DNA per transfection. A dual-luciferase assay (Promega) was performed 24 h after transfection.

2.6. Flow Cytometry

The pharyngeal arch region of E9.5 *Pax9Cre;eYFP* control embryos ($n = 5$; 23–27 somites) was dissected from the rest of the embryo and dissociated to single cells with Accumax (ThermoFisher Scientific) by incubating at 37 °C for 30 min. The reaction was stopped by the addition of 10% fetal calf serum (FCS), the cells washed in PBS, and resuspended in 10% FCS. Cells were stained with propidium iodide. Fluorescence-activated cell sorting was performed on a Becton Dickinson FACS Aria II using a 100 μ m nozzle and a sheath pressure of 20 psi. Single cells were gated using FSC-A vs SSC-A followed by FSC-A vs. FSC-H and FSC-A vs SSC-W to remove any doublets. Live single cells were gated using propidium iodide vs. FSC-A, and this population finally gated on eYFP-positive and -negative cells and sorted into collection tubes.

2.7. Quantitative Real-Time RT-PCR (qPCR)

RNA from flow-sorted cells was extracted using Trizol reagent (ThermoFisher Scientific) combined with a Purelink RNA Mini Kit (ThermoFisher Scientific) and on-column DNase1 treatment. RNA was eluted with 30 μ L RNase-free water. Total RNA was converted to cDNA using a High-Capacity cDNA Reverse transcription kit (Applied Biosystems) and random hexamers. qPCR was performed using SYBR Green JumpStart Taq ReadyMix (Sigma, St. Louis, MO, USA) using previously described *Gbx2* and *Gapdh* primers [25]. All qPCR reactions were performed in triplicate on a QuantStudio 7 Real-Time PCR System (ThermoFisher Scientific). Data were analysed using the comparative Ct method.

2.8. Statistical Analysis

A chi-squared test was used to compare genotype frequencies of litters. Fisher's exact test and Pearson chi-squared test for associations were used to compare defect frequencies between the

different genotypes (SPSS). qPCR data were tested for variance using the Shapiro–Wilk test (Prism 8.01 software, GraphPad) and a two-tailed unpaired t-test performed. Luciferase data were analysed using one-way ANOVA with Tukey’s multiple comparison test (Prism 8.01 software, GraphPad). Groups were considered significantly different when $p < 0.05$.

3. Results

3.1. *Gbx2* Expression in the Pharyngeal Endoderm

Coordinated gene expression in the pharyngeal arches is a prerequisite for the correct development of the PAA. We confirmed the expression of *Gbx2*, *Pax9* and *Tbx1* in mid-embryogenesis mouse embryos. At E8.5, *Gbx2* and *Pax9* are expressed in the pharyngeal region of the mouse embryo, with *Gbx2* also expressed at the mid-hindbrain boundary (Figure 1A,B) [27,28,41]. At E9.5, *Gbx2* and *Pax9* are co-expressed in the pharyngeal endoderm (Figure 1C), as are *Pax9* and *Tbx1* (Figure 1D) [25]. *Gbx2*, *Pax9* and *Tbx1* expression are maintained in the pharyngeal endoderm at E10.5 (Figure 1E,F). Analysis of *Pax9Cre* activated eYFP positive cells [25] by qPCR from E9.5 embryos confirmed that *Gbx2* expression is enriched in the pharyngeal endoderm compared to the remaining pharyngeal arch tissues (Figure 1G). *Gbx2* expression is bilaterally reduced in the pharyngeal endoderm of *Pax9*-null embryos at E9.5 as shown by whole-mount in situ hybridisation (Figure 1H–K) [25].

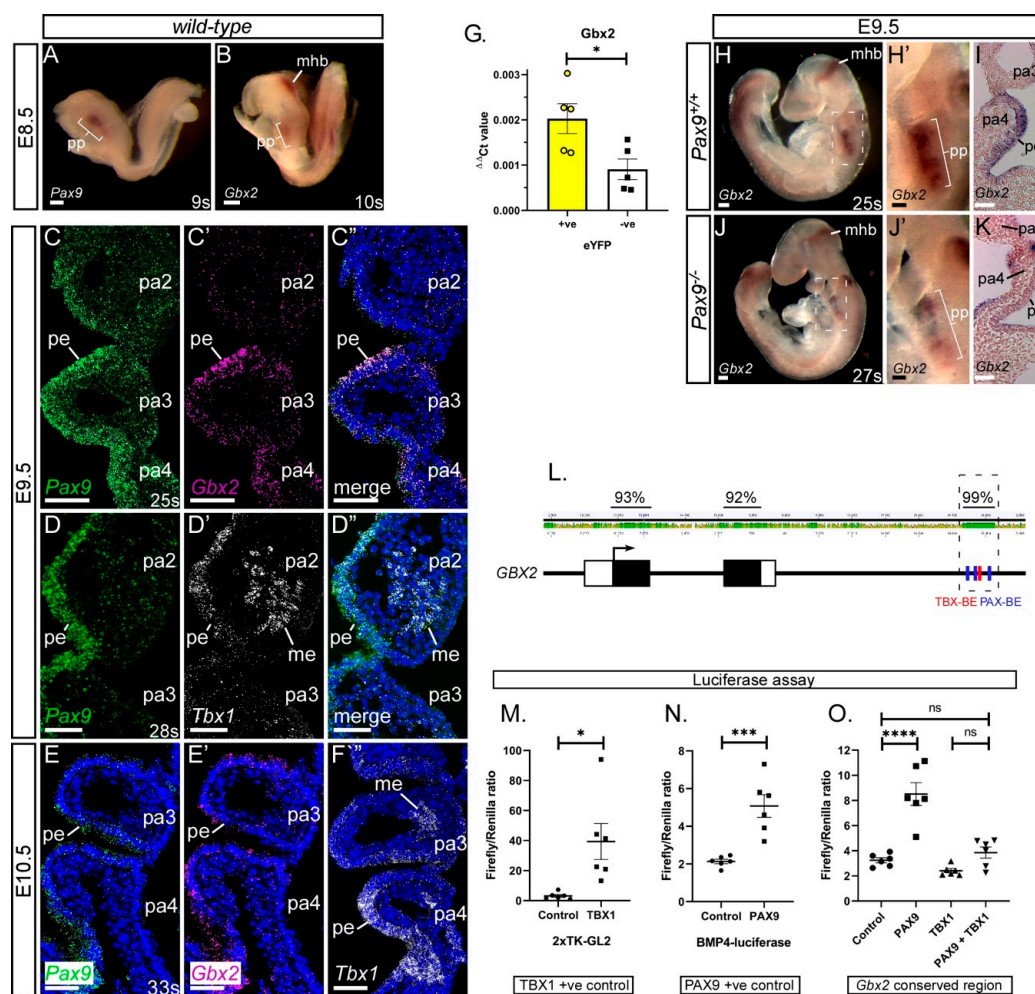


Figure 1. *Gbx2* and *Pax9* expression in the pharyngeal endoderm. (A–F) RNA in situ hybridisation was used to visualise transcripts in the normal developing embryo. At E8.5 whole embryo in situ hybridisation reveals *Pax9* (A) and *Gbx2* (B) expression in the pharyngeal pouch (pp) region. *Gbx2* is

also expressed in the mid-hindbrain (mhb) (n = 3 embryos per probe, 9–11 somites). (C–F) RNAScope probes were used on sections at E9.5 (n = 3, 24–28 somites) and E10.5 (n = 3, 33 somites). At E9.5 *Pax9* and *Gbx2* (C), and *Pax9* and *Tbx1* (D) co-localise to the pharyngeal endoderm. At E10.5 *Pax9* (E), *Gbx2* (E') and *Tbx1* (F), are all expressed in the pharyngeal endoderm. (G) qPCR on flow-sorted cells from *Pax9Cre;eYFP* E9.5 embryos (n = 5, 23–27 somites) shows a significant enrichment for *Gbx2* in the eYFP-positive cells compared to eYFP-negative. * $p < 0.05$; two-tailed unpaired t-test. (H,J) Whole embryo in situ hybridisation at E9.5 in wild-type (H; n = 3, 24–26 somites) and *Pax9*^{-/-} (J; n = 6, 23–27 somites) embryos. *Gbx2* expression is reduced in the pharyngeal pouch in *Pax9*^{-/-} embryos. (I,K) Sections of stained embryos revealed reduced *Gbx2* staining in the pharyngeal endoderm in *Pax9*^{-/-} embryos (K) compared to controls (I). (L) Diagram of the *GBX2* locus showing the degree of conservation (%) between human and mouse *GBX2* sequences. A 500 bp region, ~2kb down from the second, and final, *GBX2* coding exon is 99% conserved and contains PAX (blue) and TBX (red) binding elements (BE). (M–O) Luciferase assays show that *Pax9* activates the *Gbx2* conserved region but *Tbx1* does not (O). Controls for *Tbx1* (M) and *Pax9* (N) show significant activation of luciferase. Data presented as the mean ± s.e.m. of 6 individual experiments, each performed in triplicate. * $p < 0.05$, *** $p < 0.01$, **** $p < 0.001$. Scale bars: 100 μm in (A,B,H,J); 50 μm in (C–F),(H', I, J',K). Abbreviations: me, mesoderm; pa, pharyngeal arch; pe, pharyngeal endoderm; s, somites. The somite numbers given in the legend reflect the range analysed for the whole study. The figure contains representative images only.

We have previously identified *Gbx2* as a potential target gene of *Pax9* [25]. To examine the *Gbx2* locus for potential regulatory elements we aligned the mouse and human sequences and found a 500 bp region with 99% homology (Figure 1L). This region, located ~2kb downstream of the second and final *Gbx2* coding exon, contains a previously reported TBX binding site [42]. Scanning this region identified the known TBX site as well as three potential PAX binding sites. This 500 bp conserved region was sub-cloned into a luciferase plasmid and transfected into JEG3 cells with PAX9 and TBX1 expression plasmids. Dual-luciferase assays showed a significant upregulation of luciferase in the presence of the PAX9 expression plasmid, but no effect was seen with TBX1 (Figure 1O). Co-transfection of PAX9 with TBX1 resulted in no increase in luciferase compared to the control suggesting that TBX1 might be repressing the effect of PAX9 on the *Gbx2* conserved region. This data implies that PAX9 and TBX1 may interact with a potential *GBX2* enhancer to regulate the expression of *GBX2*, and this interaction is likely to occur in the pharyngeal endoderm where all three genes are expressed from E9.5.

3.2. *Gbx2*-Null Cardiovascular Defects

As *Gbx2* was significantly down-regulated in *Pax9*^{-/-} embryos [25], and PAX9 was able to activate a conserved region of the *Gbx2* locus, we asked whether these two genes genetically interacted in vivo. *Gbx2*^{-/-} mice have previously been shown to have cardiovascular defects at foetal and embryonic stages [28,29]. To confirm these observations we created a null allele of *Gbx2* by crossing *Gbx2*^{fllox} mice [32] with *Sox2Cre* mice [33], which drives Cre-mediated recombination in all embryonic tissues by gastrulation. *Gbx2*^{fllox};*Sox2Cre* mice, carrying the recombined *Gbx2*-null allele, hereafter referred to as the *Gbx2*⁻ allele, were subsequently crossed with wild-type mice to breed out the *Sox2Cre* allele and to propagate the *Gbx2*⁻ allele through the germline. Heterozygous *Gbx2*^{+/-} mice were intercrossed to generate *Gbx2*^{-/-} embryos for analysis of cardiovascular developmental defects. Slide in situ hybridisation on E9.5 embryo sections demonstrated complete loss of *Gbx2* RNA in *Gbx2*^{-/-} embryos (Figure S1). Genotype analysis of embryos and neonates (E8.5 to P0) indicated there was a statistically significant reduction in the expected number of *Gbx2*^{-/-} offspring observed (Table S1) despite no evidence of an excessive number of resorptions.

Analysis of *Gbx2*^{-/-} embryos at E15.5 by magnetic resonance imaging (MRI) revealed that 64% (n = 16/25) had some form of cardiovascular developmental defect including aberrant right subclavian artery (A-RSA), right-sided aortic arch (RAA), right-sided arterial duct (RAD) and double-outlet

right ventricle (DORV) (Figure 2A–C; Table 1), although interruption of the aortic arch (IAA) was not observed. Of these *Gbx2*^{-/-} embryos with cardiovascular defects, 56% (n = 9/16) displayed additional overt left-right patterning defects such as right pulmonary isomerism, bilateral superior caval veins draining into a common right atrium (i.e., right atrial isomerism), and mirror-image aortic arch arteries (Figure 2D–H; Table 1). An enlargement of the right dorsal aorta, compared to the left, was also noted in two *Gbx2*^{-/-} embryos analysed by high-resolution episcopic microscopy (HREM), indicating that these embryos would have developed an aberrant right-sided dorsal aorta by the foetal stage (Figure 2O,P). A left-right patterning phenotype in *Gbx2*^{-/-} mice has not previously been reported. Left-right patterning is established via a *Nodal-Pitx2c* gene regulated pathway [43] and to investigate whether the left-right patterning defect was due to altered *Pitx2c* expression, whole-mount in situ hybridisation was performed on *Gbx2*^{-/-} embryos at E8.5 (n = 6). No obvious change in *Pitx2c* expression, however, was observed in the left lateral plate mesoderm (Figure 2I,J).

Table 1. Number of cardiovascular defects observed in *Gbx2*;*Pax9* mutant mice.

Genotype	n	Abnormal	VSD	AVSD	DORV + IVC	CAT	RAA/RAD +/or A-SA ^a	IAA-B +/- A-RSA	Absent CC ^b	L-R Defect ^c
<i>Gbx2</i> ^{-/-}	25	16 (64%)	2 (8%)	0	10 (40%)	0	13 (52%)	0	0	9 (36%)
<i>Gbx2</i> ^{+/-} ; <i>Pax9</i> ^{+/-}	28	6 (21%)	0	0	0	0	4 (14%)	2 (7%)	0	0
<i>Gbx2</i> ^{+/-} ; <i>Pax9</i> ^{+/-}	14	14 (100%)*	3 (21%)	0	7 (50%)	1 (7%)	8 (57%)	5** (36%)	2 (16%)	6 (43%)
<i>Pax9</i> ^{-/-}	9	9 (100%)	2 (22%)	0	3 (44%)	0	0	8 (89%)	5 (56%)	0
<i>Gbx2</i> ^{+/-} ; <i>Pax9</i> ^{-/-}	9	9 (100%)	2 (22%)	0	5 (56%)	2 (22%)	1 (11%)	8 (89%)	6 (67%)	0
<i>Gbx2</i> ^{-/-} ; <i>Pax9</i> ^{-/-}	2	2 (100%)	0	1 (50%)	0	1 (50%)	1 (50%)	1 (50%)	1 (50%)	0
<i>Gbx2</i> ^{-flox} ; <i>Pax9</i> ^{Cre}	14	3 (21%)	0	0	0	0	3 (21%)	0	1 (7%)	0

Embryos and neonates were collected from *Gbx2*^{+/-};*Pax9*^{+/-} and *Gbx2*^{flox};*Pax9*^{Cre} crosses. All embryos were analysed at E13.5–E15.5 by MRI, μ CT and histology. Neonates were analysed by dissection at P0: *Gbx2*^{+/-};*Pax9*^{+/-} (n = 12), *Gbx2*^{-/-};*Pax9*^{+/-} (n = 1), *Pax9*^{-/-} (n = 2), *Gbx2*^{+/-};*Pax9*^{-/-} (n = 2), and *Gbx2*^{-/-};*Pax9*^{-/-} (n = 1). Results for embryos and neonates are combined. The outflow tract phenotype was not assessed in neonates. All wild-type (n = 12), *Pax9*^{+/-} (n = 8), *Gbx2*^{+/-} (n = 22), *Gbx2*^{flox} (n = 6), *Gbx2*^{-flox} (n = 9) and *Pax9*^{Cre} (n = 12) control embryos and neonates assessed were normal. There was a statistically significant increase in the incidence of cardiovascular defects in total, and IAA-B specifically, in *Gbx2*^{-/-};*Pax9*^{+/-} embryos compared to the *Gbx2*^{-/-} embryos. * *p* < 0.05, ** *p* = 0.01 (Fisher’s exact test). ^a A-SA refers to a right or left retro-esophageal subclavian artery, cervical origin of the RSA, or an isolated RSA. One *Pax9*^{-/-}, three *Gbx2*^{-/-} and both *Gbx2*^{-/-};*Pax9*^{-/-} embryos had isolated RSA. ^b Absent common carotid artery (CC), resulting in the internal and external carotid arteries arising directly from the main aortic vessels, unilaterally or bilaterally. ^c L-R defect refers to an overt left-right patterning defect where embryos show either right pulmonary isomerism, right atrial isomerism or mirror image branching of the aortic arch arteries. Abbreviations: AoA, aortic arch; A-RSA, aberrant right subclavian artery; A-SA, aberrant subclavian artery (left or right); AVSD, atrioventricular septal defect; DORV + IVC, double outlet right ventricle with interventricular communication; IAA-B, interruption of the aortic arch, type B; RAA, right-sided aortic arch; RAD, right-sided arterial duct; RSA, right subclavian artery; VSD, perimembranous ventricular septal defect.

Analysis of *Gbx2*^{-/-} embryos at E10.5 by intracardiac ink injection and HREM demonstrated that the 4th PAA was affected in 71% (n = 12/17) of embryos, being either absent or hypoplastic (Figure 2K–P; Table 2). Ink injection of *Gbx2*^{+/-} embryos at E10.5 revealed a low level of unilateral 4th PAA defects (Table 2). Embryos at E11.5 also showed PAA defects by HREM including absent and hypoplastic 4th PAAs as well as delayed septation of the OFT compared to stage-matched controls (Figure 2Q–S). Immunohistochemical staining for ERG1 showed that the endothelium within the 3rd and 4th pharyngeal arches had formed lumenised PAAs at E10.5 in control embryos (Figure 2T), but in *Gbx2*^{-/-} embryos a visibly reduced number of endothelial cells around the 4th PAA, or only isolated endothelial cells present within the 4th pharyngeal arch, were observed (Figure 2U,V).

Table 2. Number of pharyngeal arch artery defects observed in *Gbx2*;*Pax9* mutant embryos.

Genotype	n	PAA	Abnormal (%)	Unilateral Defect	Bilateral Defect	Bilateral Defects		
						Present	Hypo/Int/Abs	Absent
<i>Gbx2</i> ^{+/-}	44	4	3 (7%)	3 (7%)	0	-	-	-
<i>Gbx2</i> ^{+/-} ; <i>Pax9</i> ^{+/-}	63	4	20 (32%)	13 (21%)	7 (11%)	-	3	4
<i>Gbx2</i> ^{-/-}	17	4	12 (71%)	7 (41%)	5 (29%)	-	3	2
<i>Gbx2</i> ^{-/-} ; <i>Pax9</i> ^{+/-}	7	4	7 (100%)	1 (14%)	6 (86%) *	-	2	4
<i>Pax9</i> ^{-/- a}	22	1	13 (59%)	1 (5%)	12 (55%)	11	1	-
		2	8 (36%)	3 (14%)	5 (23%)	4	1	-
		3	17 (77%)	3 (14%)	14 (64%)	-	10	4
		4	22 (100%)	1 (5%)	21 (95%)	-	3	18
<i>Gbx2</i> ^{+/-} ; <i>Pax9</i> ^{-/-}	6	1	6 (100%)	0	6 (100%)	6	-	-
		2	2 (33%)	2 (33%)	0	-	-	-
		3	6 (100%)	0	6 (100%)	-	1	5
		4	6 (100%)	0	6 (100%)	-	-	6
<i>Gbx2</i> ^{-/-} ; <i>Pax9</i> ^{-/-}	1	4	1 (100%)	0	1 (100%)	-	-	1
<i>Gbx2</i> ^{+floX} ; <i>Pax9Cre</i>	19	4	2 (10%)	1 (5%)	1 (5%)	-	-	1
<i>Gbx2</i> ^{-floX} ; <i>Pax9Cre</i>	14	4	7 (50%) *	5 (36%)	2 (14%)	-	1	1

Embryos were collected from *Gbx2*^{+/-};*Pax9*^{+/-} and *Gbx2*^{flox};*Pax9Cre* crosses and assessed for PAA defects by intracardiac ink injections. *Gbx2*^{-/-} embryos were also imaged using HREM (E10.5, n = 3 and E11.5, n = 5) to visualise the PAA. Data are combined. For *Pax9*^{-/-} and *Gbx2*^{+/-};*Pax9*^{-/-} genotypes each left and right PAA 1–4 was scored as having a unilateral or bilateral defect, and the bilateral defects categorised as either present, a combination of hypoplastic, interrupted and/or absent (Hypo/Int/Abs), and bilaterally absent. For all other genotypes ink injection was performed at E10.5 and only the 4th PAA was scored. All control embryos, *Pax9*^{+/-} (n = 18), *Gbx2*^{+floX} (n = 22) and *Gbx2*^{-floX} (n = 15) were normal. There was a significantly increased incidence of bilateral 4th PAA defects in *Gbx2*^{-/-};*Pax9*^{+/-} embryos compared to *Gbx2*^{-/-} embryos, and abnormal 4th PAA defects in *Gbx2*^{-floX};*Pax9Cre* embryos compared to *Gbx2*^{+floX};*Pax9Cre* embryos. * *p* < 0.05 (Pearson’s Chi-square test for associations). ^a New data (n = 2) combined with published data (n = 20) [25].

All mice deficient for *Gbx2* die perinatally, and a high proportion of these are with cardiovascular abnormalities affecting the outflow tract and/or the 4th PAA-derived arteries. In contrast to previously published data, where 50% of *Gbx2*-null embryos had a PAA phenotype and 39% of foetuses had a cardiovascular defect [28,29], we observed a higher penetrance of cardiovascular abnormalities at embryonic (71%) and foetal (64%) stages. Our *Gbx2*-null embryos did not present with IAA as previously described [29]. *Gbx2* has been postulated to be a downstream target of *Pax9* [25], and here we also demonstrate that a conserved region in the *Gbx2* locus is activated by PAX9.

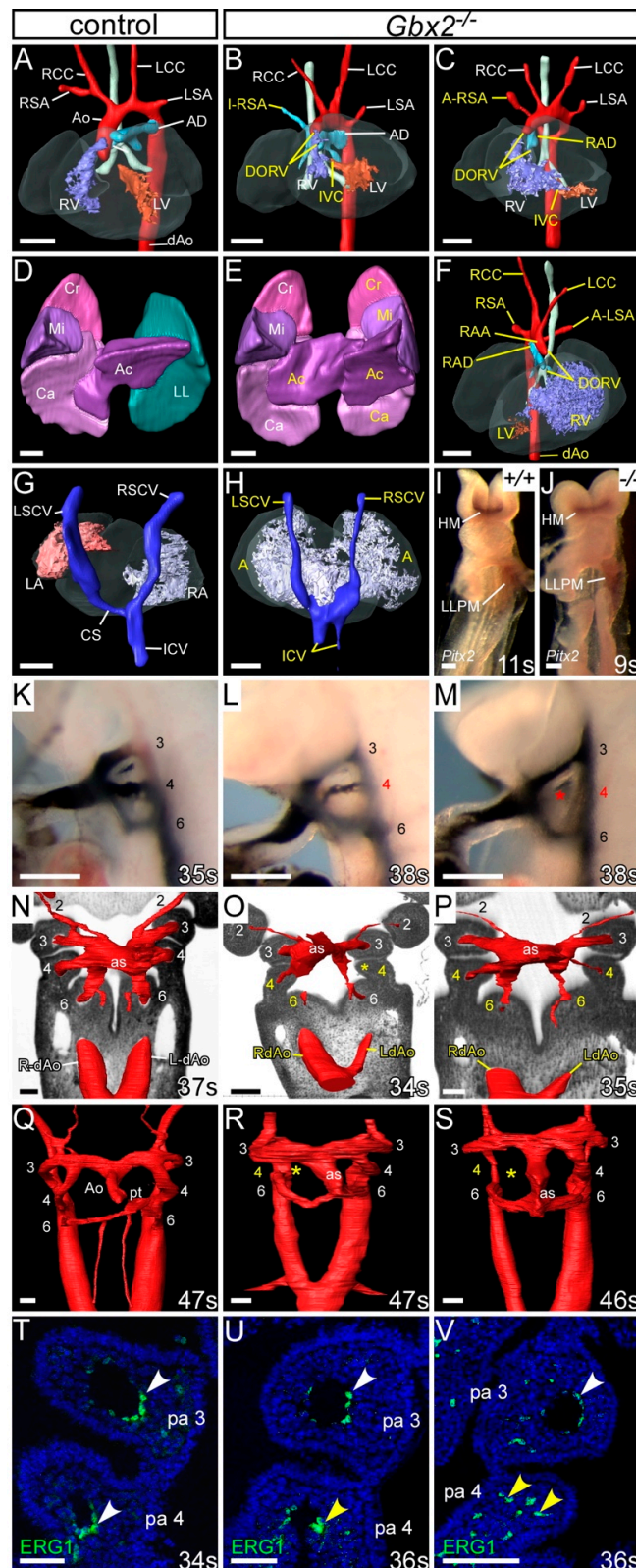


Figure 2. Cardiovascular defects in *Gbx2*^{-/-} embryos. (A–H) 3D reconstructions from MRI datasets of E15.5 embryos. (A) *Gbx2*^{+/+} control embryo with normal heart and aortic arch arteries. (B,C) In *Gbx2*^{-/-} embryos (n = 25), defects seen include double outlet right ventricle (DORV) with interventricular communication (IVC), retro-oesophageal aberrant right subclavian artery (A-RSA), isolated RSA (I-RSA)

and right-sided arterial duct (RAD). (D–H) Left-right patterning defects were observed in a subset of *Gbx2*^{-/-} embryos (n = 9/25). (D) Normal lungs from a control embryo showing cranial (Cr), middle (Mi), caudal (Ca) and accessory (Ac) lobes of the right lung, and a single lobed left lung (LL). (E) *Gbx2*^{-/-} embryo with right pulmonary isomerism. (F) *Gbx2*^{-/-} embryo heart with mirror image arrangement of the arch arteries and the ventricles, DORV and an aberrant left subclavian artery (A-LSA). (G,H) Dorsal view of the heart and the caval veins. (G) Control embryo showing the right superior caval vein (RSCV) and inferior caval vein (ICV) draining directly into the right atrium (RA) and the left SCV (LSVC) draining into the RA via the coronary sinus (CS). (H) *Gbx2*^{-/-} embryo with the right and left SCVs, and the paired ICV, draining directly into a common atrium (right atrial isomerism). (I,J) Whole-mount in situ hybridisation with a *Pitx2* riboprobe. *Pitx2* isoforms were seen in the head mesoderm (HM) and left lateral plate mesoderm (LLPM) of control (n = 3) and *Gbx2*^{-/-} (n = 6) embryos. All embryos were between 9–11 somites. (K–M) Intracardiac ink injection into E10.5 embryos (34–38 somites). (K) In control embryos (n = 18), PAAs 3–6 are patent to ink, are of equivalent diameter and are bilaterally symmetrical. (L,M) In *Gbx2*^{-/-} embryos (n = 17), the 4th PAAs are frequently hypoplastic (L) or non-patent to ink (M; asterisk). (N–S) Embryos were examined by high-resolution episcopic microscopy at E10.5 (34–35 somites; N–P) and E11.5 (45–47 somites; Q–S). Coronal views are shown. (N) In control E10.5 embryos (n = 5), the 3rd, 4th, and 6th PAAs, and the left and right dorsal aortae (L/RdAo), are of equal size and bilaterally symmetrical. (O,P) In *Gbx2*^{-/-} embryos (n = 3), the 4th PAAs were either absent (O; asterisk), or hypoplastic (O,P). The left dorsal aorta was seen to be abnormally thinner than the right (O,P). (Q) In control embryos at E11.5 (n = 3), the outflow tract is septated into the aorta (A) and pulmonary trunk (pt), and the right 6th PAA has thinned. (R,S) In *Gbx2*^{-/-} embryos (n = 5), the 4th PAAs are frequently unilaterally absent (asterisk). Septation of the aortic sac (as) is delayed. (T–V) Immunostaining using anti-ERG1 antibody at E10.5 (34–36 somites). (T) Control embryos (n = 3) have a ring of ERG1-positive endothelium lining the 3rd and 4th PAAs (white arrowheads). (U,V) In *Gbx2*^{-/-} embryos (n = 4), the 4th PAAs appeared to have abnormal endothelial cells (U), or disorganized endothelial cells within the 4th pharyngeal arch in the absence of a PAA (V; yellow arrowheads). Scale bars: 500 μm in (A–H); 100 μm in (I–S); 50 μm in (T–V). Abbreviations: Ao, aorta; AD, arterial duct; LCC, left common carotid artery; LSA, left subclavian artery; LV, left ventricle; pa, pharyngeal arch; RCC, right common carotid artery; RSA, right subclavian artery; RV, right ventricle; s, somites. The somite numbers given in the legend reflect the range analysed for the whole study. The figure contains representative images only.

3.3. Genetic Interaction between *Gbx2* and *Pax9*

To investigate a genetic interaction in vivo, mice heterozygous for *Pax9* and *Gbx2*, which are viable and fertile with no observed developmental defects, were intercrossed to produce *Gbx2*^{+/-};*Pax9*^{+/-} mice and embryos for analysis. *Gbx2*^{+/-};*Pax9*^{+/-} mice were observed to survive to weaning albeit at a significantly lower than expected number ($p < 0.05$; Table S2). To investigate any perinatal lethality to explain the loss of *Gbx2*^{+/-};*Pax9*^{+/-} mice, neonates were observed from the day of birth. Four pups were recovered which had died on the first post-natal day, all of which were *Gbx2*^{+/-};*Pax9*^{+/-}, and showed a cardiovascular defect when dissected including RAA, IAA-B and A-RSA (Figure 3A–C; Table 1). Surviving littermates were culled and a further eight *Gbx2*^{+/-};*Pax9*^{+/-} neonates were identified which showed no cardiovascular defects. All wild type (n = 8), *Gbx2*^{+/-} (n = 10) and *Pax9*^{+/-} (n = 9) littermates were normal. To further investigate the *Gbx2*^{+/-};*Pax9*^{+/-} cardiovascular phenotype, embryos were collected at E15.5 and analysed by histology. From 16 *Gbx2*^{+/-};*Pax9*^{+/-} embryos collected, two had a defect affecting the arch arteries including RAA and A-RSA (Figure 3D–I) and RAD (Table 1). Embryos were collected at E10.5 to analyse the forming PAA by ink injection. This revealed that 30% (n = 19/63) of *Gbx2*^{+/-};*Pax9*^{+/-} mutants had a defect where the 4th PAA was either hypoplastic or absent in affected embryos (Figure 3J–L; Table 2).

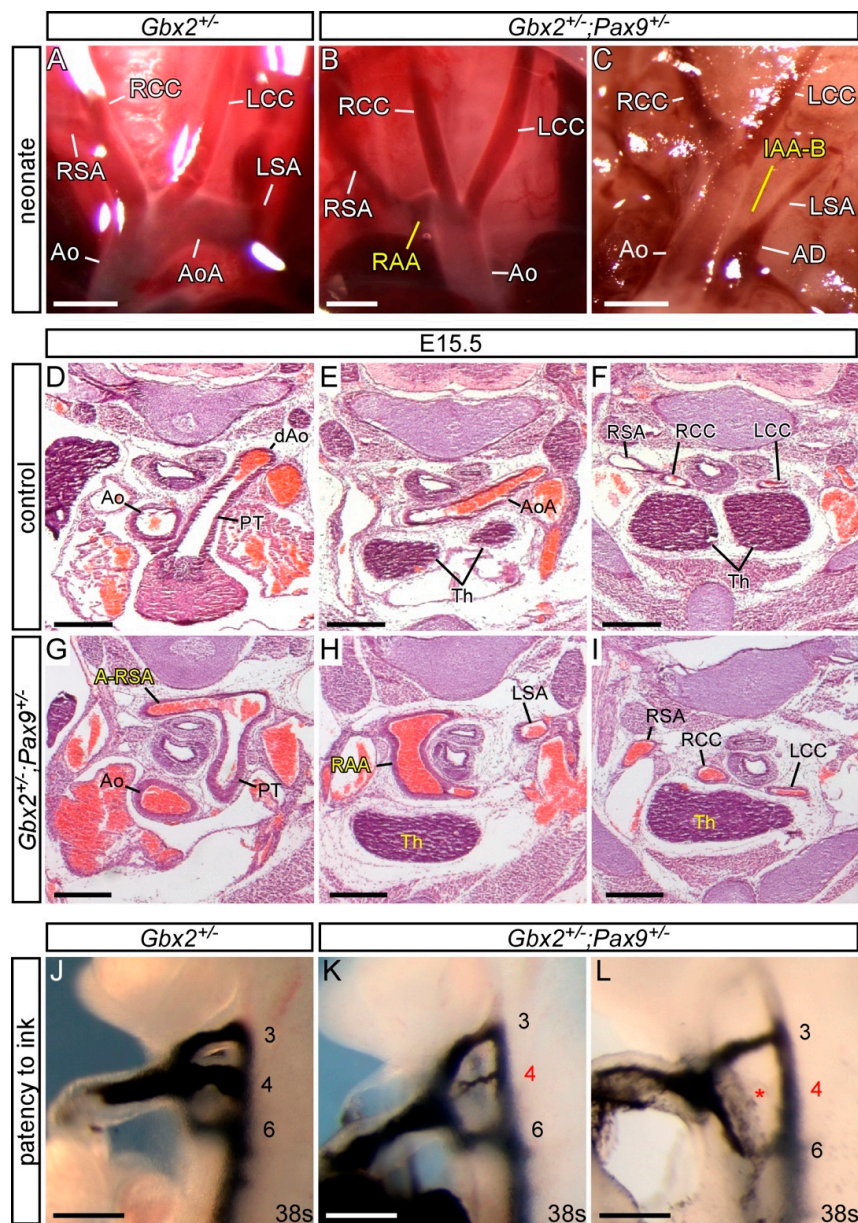


Figure 3. Cardiovascular defects in *Gbx2*^{+/-};*Pax9*^{+/-} mice. (A–C) Neonates were dissected on the day of birth. (A) Arch arteries of control neonates were normal. (B) A subset of *Gbx2*^{+/-};*Pax9*^{+/-} neonates (4/12) displayed right-sided aortic arch (RAA; B) or IAA-B (C). (D–I) H&E stained transverse sections of E15.5 embryos. (D–F) Normal outflow tract (D), aortic arch arteries and thymus (Th; E,F) in a control embryo. (G–I) A *Gbx2*^{+/-};*Pax9*^{+/-} embryo (from n = 16) with aberrant right subclavian artery (A-RSA; G), a right-sided aortic arch (RAA; H) and abnormal thymus (H,I). (J–L) Intracardiac ink injection into E10.5 embryos (34–41 somites). (J) In control embryos, PAAs 3–6 are patent to ink, are of equivalent diameter and are bilaterally symmetrical. (K,L) In *Gbx2*^{+/-};*Pax9*^{+/-} embryos (n = 63), 32% had hypoplastic (K) or non-patent to ink (L; asterisk) 4th PAAs. Scale bars: 1 mm in (A–C); 500 μm in (D–L). Abbreviations: AD, arterial duct; Ao, aorta; AoA, aortic arch; LCC, left common carotid artery; LSA, left subclavian artery; PT, pulmonary trunk; RCC, right common carotid artery; RSA, right subclavian artery; s, somites. The somite numbers given in the legend reflect the range analysed for the whole study. The figure contains representative images only.

Our data therefore indicates that there is a genetic interaction occurring between *Gbx2* and *Pax9*, albeit at a low incidence, where biallelic expression of both genes is required for cardiovascular

development to proceed normally. There was a loss in the expected number of double heterozygous mice at weaning and an observable aortic arch artery phenotype in a subset of embryos and neonates, including IAA-B which was not seen in *Gbx2*^{-/-} mice in this study (Table 1).

To see if a further reduction in *Gbx2* and *Pax9* alleles would result in a more penetrant cardiovascular phenotype, *Gbx2*^{+/-};*Pax9*^{+/-} mice were intercrossed and embryos and neonates collected for analysis. Genotyping revealed that all mice null for *Gbx2* were under-represented ($p = 1.12 \times 10^{-4}$; Table S3). We first analysed mutant mice null for *Gbx2* and simultaneously heterozygous for *Pax9* (i.e., *Gbx2*^{-/-};*Pax9*^{+/-}). One *Gbx2*^{-/-};*Pax9*^{+/-} neonate was recovered that died on the day of birth with IAA-B, A-RSA, and an absent left common carotid artery resulting in the left internal and external carotid arteries arising from the aortic arch and dorsal aorta as previously described in *Pax9*^{-/-} embryos [25] (Figure 4A,B). *Gbx2*^{-/-};*Pax9*^{+/-} embryos at E13.5 and E15.5 were examined for cardiovascular defects by histology and MRI respectively, which showed a significantly increased penetrance of OFT and arch artery defects compared to those observed in *Gbx2*^{-/-} mice (100% versus 64%, $p < 0.05$; Figure 4C–M; Table 1). There was also a significant increase in the presentation of IAA-B in *Gbx2*^{-/-};*Pax9*^{+/-} mice compared to *Gbx2*^{-/-} mice (36% versus 0, $p < 0.01$; Figure 4B,E; Table 1), a defect not observed in our *Gbx2*^{-/-} or *Pax9*^{+/-} mice. We also observed a partial CAT (type A4 where the common trunk is associated with IAA [44]) in one *Gbx2*^{-/-};*Pax9*^{+/-} embryo (Figure 4G), a phenotype not previously described in *Gbx2*-null and *Pax9*-null embryos [25,28,29]. Analysis of the PAA at E10.5 by ink injection revealed that all *Gbx2*^{-/-};*Pax9*^{+/-} embryos had an affected 4th PAA, with a significantly higher incidence of bilateral 4th PAA defects compared to *Gbx2*^{-/-} embryos ($p < 0.05$; Figure 4N–Q; Table 2).

As *Pax9* heterozygosity modified the *Gbx2*^{-/-} phenotype we next looked to see if *Gbx2* heterozygosity modified the *Pax9*^{-/-} phenotype. *Gbx2*^{+/-};*Pax9*^{-/-} embryos examined at E15.5 and E10.5 presented with the typical *Pax9*-null cardiovascular phenotype (Figure 5) and no left-right patterning defects were seen. Two cases of type A4 partial CAT, however, were observed (Figure 5I; Table 1). At E10.5 there was an insignificant increase in the penetrance of 1st and 3rd PAA defects in the *Gbx2*^{+/-};*Pax9*^{-/-} embryos (Figure 5L; Table 2).

From the *Gbx2*^{+/-};*Pax9*^{+/-} intercross only three *Gbx2*^{-/-};*Pax9*^{-/-} mice were recovered from a total of 172 offspring, one each at P0, E15.5 and E10.5, and these mice displayed the typical *Pax9*^{-/-} phenotypes, as well as AVSD and full CAT (with an isolated right subclavian artery), both of which are defects not previously seen in either *Gbx2*^{-/-} or *Pax9*^{-/-} embryos (Figure 6; Tables 1 and 2).

The thymus is always absent in *Pax9*^{-/-} embryos [25], yet usually unaffected in *Gbx2*^{-/-} embryos (Figure S2; Table S4). In 70% of *Gbx2*^{-/-};*Pax9*^{+/-} embryos the thymus was abnormal or absent. The palate, however, was only affected in mice with *Pax9*^{-/-} genotypes (Figure S2).

It appears, therefore, that creating complex alleles of *Gbx2* and *Pax9* reveals evidence of a genetic interaction occurring between these two genes as cardiovascular defects are seen in double heterozygous embryos. Furthermore, by creating more complex *Gbx2*;*Pax9* alleles such as *Pax9* heterozygosity with the *Gbx2*^{-/-} genotype and *Gbx2* heterozygosity with the *Pax9*^{-/-} genotype, not only are *Pax9*-null type defects such as IAA-B and absent common carotid arteries introduced, but also a CAT phenotype not seen in either single *Gbx2*^{-/-} or *Pax9*^{-/-} embryos is observed.

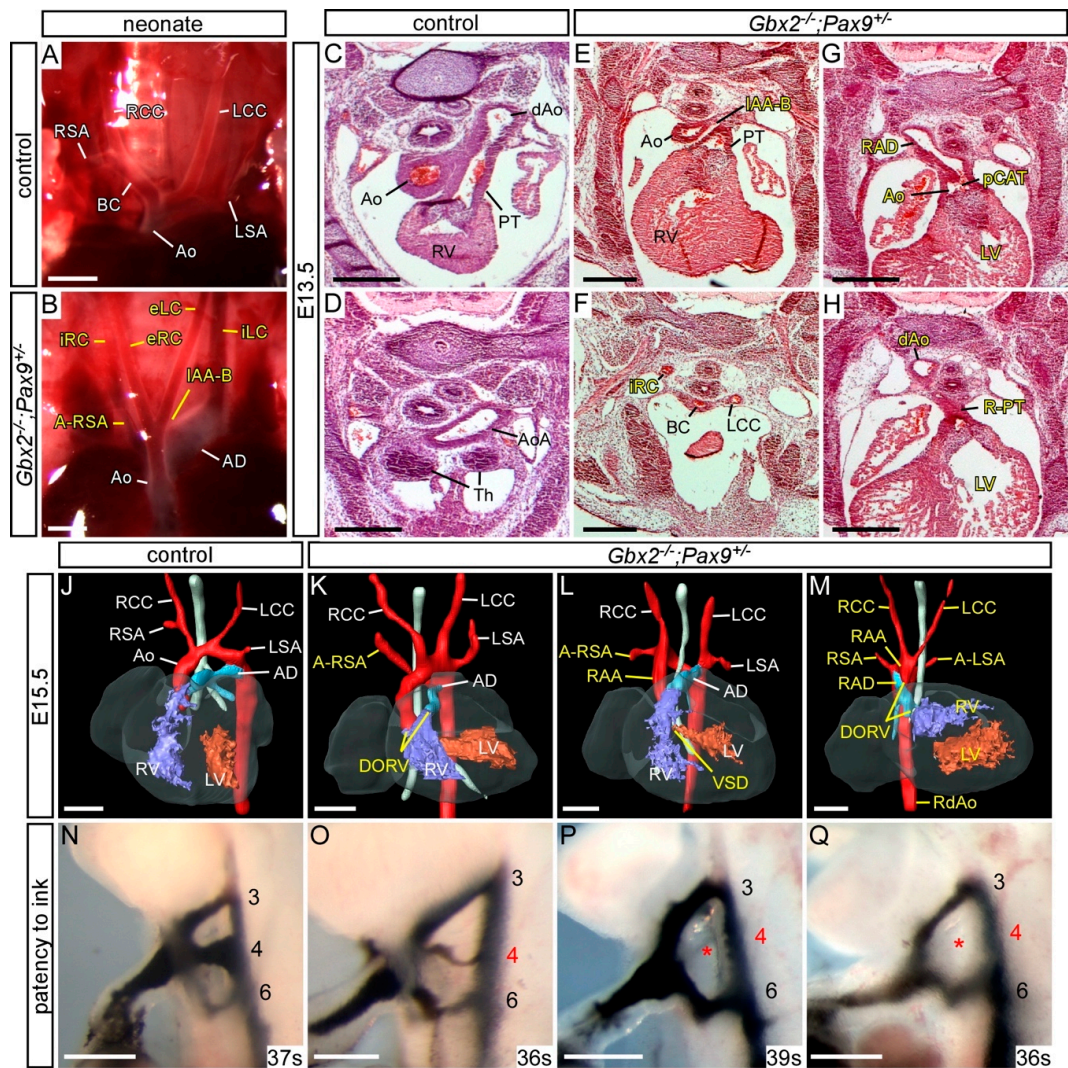


Figure 4. Cardiovascular defects in *Gbx2*^{-/-};*Pax9*^{+/-} mice. (A–B) Neonates were dissected on the day of birth. (A) Arch arteries of control neonates were normal. (B) One *Gbx2*^{-/-};*Pax9*^{+/-} neonate found dead on the day of birth displayed IAA-B and an aberrant left and right internal and external carotid artery (iLC, eLC, iRC, eRC). (C–H) H&E stained transverse sections of E13.5 embryos (n = 5). A normal outflow tract (C), aortic arch (Ao) and thymus (Th; D) are seen in control embryos. In two *Gbx2*^{-/-};*Pax9*^{+/-} mutant embryos (E–H) the defects include IAA-B (E), an aberrant right internal carotid artery (iRC; F), and a partial common arterial trunk (pCAT) emerging from the left ventricle (G). The pulmonary trunk is right-sided (R-PT; H) and the aorta was interrupted (not shown). The thymus is absent in both mutants (F,H). (J–M) 3D reconstructions of MRI datasets of hearts from a normal control embryo (J) and *Gbx2*^{-/-};*Pax9*^{+/-} mutant embryos (n = 8). Defects include aberrant right subclavian artery (A-RSA; K,L), double outlet right ventricle (DORV; K,M), right-sided aortic arch (RAA; L,M). Situs patterning defects were also observed, including mirror image aortic arch arteries (RAA, RAD, RdAo) with aberrant left subclavian artery (A-LSA) and aberrantly positioned ventricles (M). (N–Q) Intracardiac ink injection into E10.5 embryos (35–39 somites). (N) In control embryos, PAAs 3–6 are patent to ink. (K,L) In *Gbx2*^{+/-};*Pax9*^{+/-} embryos (n = 7), all had an aberrant 4th PAA including hypoplastic (O) or non-patent to ink (P,Q; asterisk) vessels. Scale bars: 1 mm in (A–B); 500 μm in (C–Q). Abbreviations: Ao, aorta; AD, arterial duct; dAo, dorsal aorta; LCC, left common carotid artery; LSA, left subclavian artery; LV, left ventricle; PT, pulmonary trunk; RCC, right common carotid artery; RSA, right subclavian artery; RV, right ventricle; s, somites. The somite numbers given in the legend reflect the range analysed for the whole study. The figure contains representative images only.

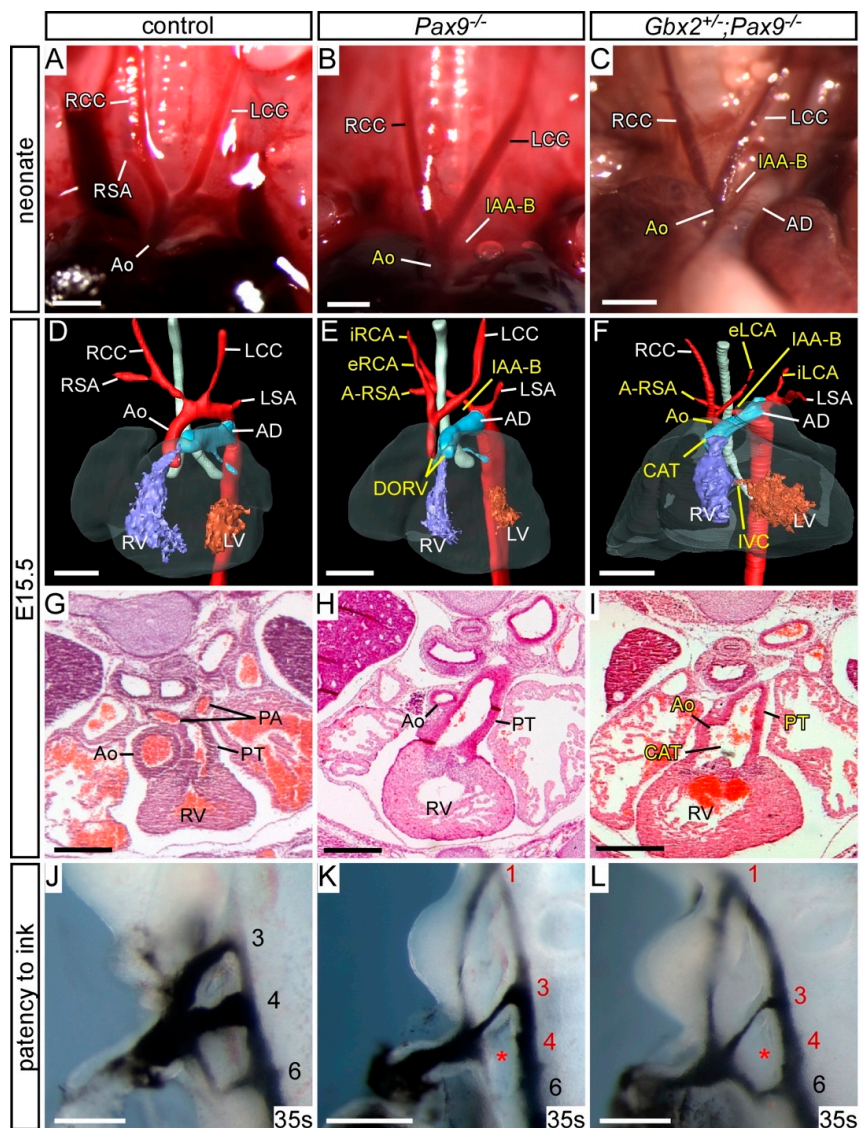


Figure 5. Cardiovascular defects in *Gbx2*^{+/-};*Pax9*^{-/-} mice. (A–C) Neonates were dissected on the day of birth. (A) Arch arteries of control neonates were normal. (B) *Pax9*^{-/-} (n = 2) and (C) *Gbx2*^{+/-};*Pax9*^{+/-} (n = 2) neonates found dead on the day of birth displayed interruption of the aortic arch (IAA-B) and presumed aberrant right subclavian artery. (D–F) 3D reconstructions of E15.5 hearts from MRI datasets. (D) *Gbx2*^{+/-} control embryo with normal heart and aortic arch arteries. (E) *Pax9*^{-/-} embryos (n = 7) presented with defects such as IAA-B, A-RSA, double outlet right ventricle (DORV), hypoplastic aorta and aberrant carotid arteries (eRCA, iRCA). (F) *Gbx2*^{+/-};*Pax9*^{-/-} embryos (n = 7) showed typical *Pax9*^{-/-} cardiovascular defects including IAA-B and absent common carotid artery, but also common arterial trunk (CAT). (G–I) E15.5 embryos were sectioned and stained with H&E. (G) Control embryos had a normal outflow tract. (H) *Pax9*^{-/-} embryos had DORV (not shown) and hypoplastic aorta. (I) *Gbx2*^{+/-};*Pax9*^{-/-} embryo with CAT. (J–L) Embryos at E10.5 were analysed by intracardiac ink injection (35–38 somites). (J) Control embryos had normal PAAs patent to ink. (K) *Pax9*^{-/-} embryos showed typical defects such as persistent 1st, hypoplastic 3rd and absent 4th PAAs (asterisk), as did *Gbx2*^{+/-};*Pax9*^{-/-} embryos (n = 6; L). Scale bars: 1 mm in (A–C); 500 μm in (D–L). Abbreviations: Ao, aorta; AD, arterial duct; LCC, left common carotid artery; LSA, left subclavian artery; LV, left ventricle; PA, pulmonary artery; PT, pulmonary trunk; RCC, right common carotid artery; RSA, right subclavian artery; RV, right ventricle; s, somites. The somite numbers given in the legend reflect the range analysed for the whole study. The figure contains representative images only.

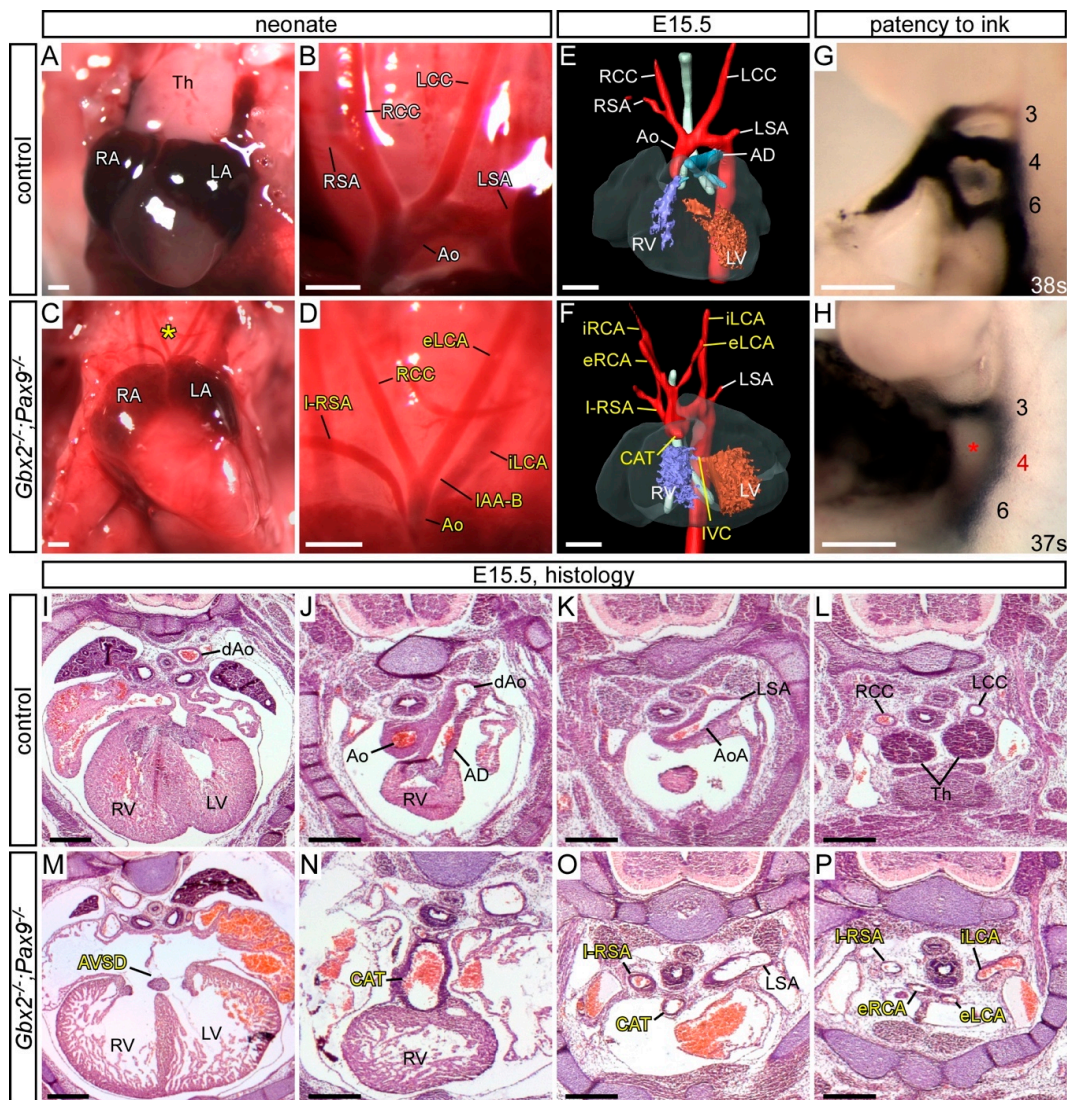


Figure 6. Cardiovascular defects in the three *Gbx2*^{-/-};*Pax9*^{-/-} mutants recovered. (A–D) Neonates were dissected on the day of birth. The thymus (A) and arch arteries (B) were normal in controls, but in a *Gbx2*^{-/-};*Pax9*^{-/-} neonate the thymus was absent (asterisk; C) and the arch arteries were abnormal (D) displaying interrupted aortic arch type B (IAA-B), isolated right subclavian artery (I-RSA) and abnormal left carotid arteries (eLCA, iLCA). (E,F) 3D reconstructions of E15.5 hearts from MRI datasets. (E) Control embryo with normal heart and aortic arch arteries. (F) *Gbx2*^{-/-};*Pax9*^{-/-} embryo with IAA-B, I-RSA, common arterial trunk (CAT) with interventricular communication (IVC), and aberrant carotid arteries (eLCA, iLCA, eRCA, iRCA). (G,H) Embryos at E10.5 were analysed by intracardiac ink injection. (G) Control embryos had normal PAAs patent to ink. (H) *Gbx2*^{-/-};*Pax9*^{-/-} embryo with a non-patent 4th PAA (asterisk). (I–P) H&E stained transverse sections of E15.5 embryos. (I–L) Control embryo with normal heart (I), outflow tract (J), aortic arch arteries (K,L) and thymus (Th; L). (M–P) Sections from the *Gbx2*^{-/-};*Pax9*^{-/-} embryo depicted in F. (M) An atrioventricular septal defect (AVSD) is seen, as well as the CAT (N) with associated I-RSA (O) and aberrant carotid arteries (P). Scale bars: 500 μm. Abbreviations: AD, arterial duct; Ao, aorta; AoA, aortic arch; dAo, dorsal aorta; LA, left atrium; LCC, left common carotid artery; LSA, left subclavian artery; LV, left ventricle; RA, right atrium; RCC, right common carotid artery; RSA, right subclavian artery; RV, right ventricle.

3.4. *Gbx2* and *Pax9* Interact in the Pharyngeal Endoderm for Cardiovascular Development

To further investigate the site of this genetic interaction we utilised our *Pax9Cre* mouse line, where the *Pax9Cre* allele corresponds to a *Pax9*-null allele [25], to conditionally recombine the *Gbx2^{flox}* allele specifically in the pharyngeal endoderm (Figure S3). Embryos conditionally deleted for *Gbx2* using *Pax9Cre* (i.e., *Gbx2^{-flox};Pax9Cre*) lost the majority of *Gbx2* mRNA expression from the pharyngeal endoderm at E9.5 (Figure 7B). Embryos at E10.5 were examined by ink injection to assess the PAAs. Whereas only 10% (2/19) of embryos double heterozygous for *Gbx2* in the pharyngeal endoderm (i.e., *Gbx2^{+flox};Pax9Cre*) had an abnormal 4th PAA (Table 2), there was a significant increase in the penetrance of 4th PAA defects (7/14; $p < 0.05$) in the embryos null for *Gbx2* in the pharyngeal endoderm (i.e., *Gbx2^{-flox};Pax9Cre*) (Figure 7D; Table 2). Examining *Gbx2^{-flox};Pax9Cre* mutant mice at E15.5 by MRI revealed cardiovascular defects including RAA, A-RSA and absent common carotid arteries in 3/14 embryos analysed (Figure 7F; Table 1). Despite a relatively low incidence of cardiovascular defects in embryos with a conditional *Pax9Cre* driven deletion of *Gbx2*, this data collectively demonstrates that a genetic interaction between *Gbx2* and *Pax9* is taking place in the pharyngeal endoderm.

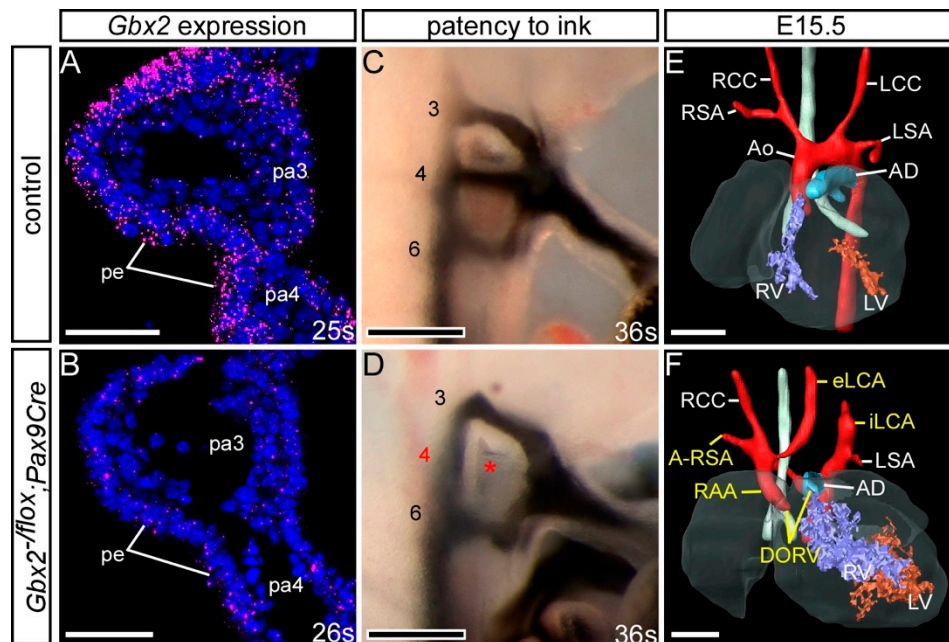


Figure 7. Conditional deletion of *Gbx2* from the pharyngeal endoderm. Embryos with one *Gbx2*-null allele and a heterozygous conditional deletion of *Gbx2* using *Pax9Cre* (*Gbx2^{-flox};Pax9Cre*) were analysed. (A,B) RNAscope in situ hybridisation for *Gbx2* at E9.5 (n = 5 per genotype; 24–29 somites). (A) In control embryos *Gbx2* expression was observed in the pharyngeal endoderm (pe) of the pharyngeal arches (pa). (B) *Gbx2* expression was reduced in the pharyngeal endoderm of *Gbx2^{-flox};Pax9Cre* mutants. (C,D) Embryos at E10.5 were analysed by intracardiac ink injection (36–38 somites). (C) Control embryos had normal PAAs patent to ink. (D) *Gbx2^{-flox};Pax9Cre* embryos (n = 14) showed PAA defects such as absent 4th PAAs (asterisk). (E,F) 3D reconstructions of E15.5 hearts from MRI datasets. (E) Control embryo with normal heart and aortic arch arteries. (F) A *Gbx2^{-flox};Pax9Cre* embryo (from n = 14 analysed) with double-outlet right ventricle (DORV), right-sided aortic arch (RAA), aberrant right subclavian artery (A-RSA) and abnormal left external and internal carotid arteries (eLCA, iLCA). Scale bars: 50 μ m in (A,B); 100 μ m in (C,D); 500 μ m in (E,F). Abbreviations: Ao, aorta; AD, arterial duct; LCC, left common carotid artery; LSA, left subclavian artery; LV, left ventricle; RCC, right common carotid artery; RSA, right subclavian artery; RV, right ventricle; s, somite. The somite numbers given in the legend reflect the range analysed for the whole study. The figure contains representative images only.

3.5. Exploring a Genetic Interaction between *Gbx2*, *Pax9* and *Tbx1*

Tbx1 has been shown to genetically interact with *Gbx2* and *Pax9* in the pharyngeal ectoderm and endoderm respectively [25,28]. Our and published data [42] also show that *Pax9* and *Tbx1* occupy the same conserved region in the *Gbx2* locus (Figure 1) and *Tbx1*, *Pax9* and *Gbx2* are co-expressed in the pharyngeal endoderm at E9.5 and E10.5 (Figure 1C–F) [25,28]. *Pax9* and *Gbx2*, and *Tbx1* and *Gbx2*, are downregulated in the pharyngeal endoderm of *Tbx1*^{-/-} and *Pax9*^{-/-} mice respectively (Figure 8A–L) [24,25] but *Pax9* and *Tbx1* expression were maintained in the pharyngeal endoderm of *Gbx2*^{-/-} embryos at E9.5 (Figure 8D,H). We nevertheless speculated that a gene regulatory network may be occurring in the pharyngeal endoderm involving *Gbx2*, *Pax9* and *Tbx1*. To investigate this we analysed *Gbx2*^{+/-};*Pax9*^{+/-};*Tbx1*^{+/-} triple heterozygous embryos at E15.5–E16.5 by μCT imaging and compared the observed cardiovascular defects with double heterozygous *Tbx1*^{+/-};*Pax9*^{+/-} and *Tbx1*^{+/-};*Gbx2*^{+/-} embryos (Figure 8M–R; Table 3). Although a non-significant reduction in the penetrance of 4th PAA derived defects was seen in *Tbx1*^{+/-};*Gbx2*^{+/-} embryos compared to *Tbx1*^{+/-} embryos, a similar number and type of cardiovascular defect was observed between *Tbx1*^{+/-};*Pax9*^{+/-} double heterozygous and *Tbx1*^{+/-};*Gbx2*^{+/-};*Pax9*^{+/-} triple heterozygous embryos (Figure 8S,T). This suggests that there was no change to the *Tbx1*^{+/-};*Pax9*^{+/-} 4th PAA-derived phenotype caused by haploinsufficiency of *Gbx2*.

Table 3. Number of cardiovascular defects observed in *Tbx1*;*Gbx2*;*Pax9* mutant mice.

Genotype	<i>n</i>	VSD	RAA +/- A-RSA	IAA-B +/- A-RSA	4th PAA Defect
<i>Tbx1</i> ^{+/-} ^a	21	2 (10%)	13 (62%)	1 (5%)	14 (67%)
<i>Tbx1</i> ^{+/-} ; <i>Pax9</i> ^{+/-} ^b	24	5 (21%)	9 (38%)	15 (63%) **	24 (100%)
<i>Tbx1</i> ^{+/-} ; <i>Gbx2</i> ^{+/-}	10	3(30%)	2(20%)	1(10%)	3(30%)
<i>Tbx1</i> ^{+/-} ; <i>Gbx2</i> ^{+/-} ; <i>Pax9</i> ^{+/-}	8	3 (38%)	4 (50%)	4 (50%)	8 (100%)

Embryos were collected from *Tbx1*^{+/-};*Gbx2*^{+/-} and *Pax9*^{+/-} crosses. Embryos were analysed by μCT at E13.5–E16.5. There was a statistically significant increase in the incidence of IAA-B in the *Tbx1*^{+/-};*Pax9*^{+/-} embryos compared with the *Tbx1*^{+/-} embryos. ** *p* < 0.0001 (Pearson’s chi-squared test for associations with continuity correction). ^a New data (*n* = 3) combined with published MRI data (*n* = 19) [25]. ^b New data (*n* = 4) combined with published MRI data (*n* = 20) [25]. Abbreviations: A-RSA, aberrant right subclavian artery; IAA-B, interruption of the aortic arch, type B; RAA, right-sided aortic arch; VSD, perimembranous ventricular septal defect.

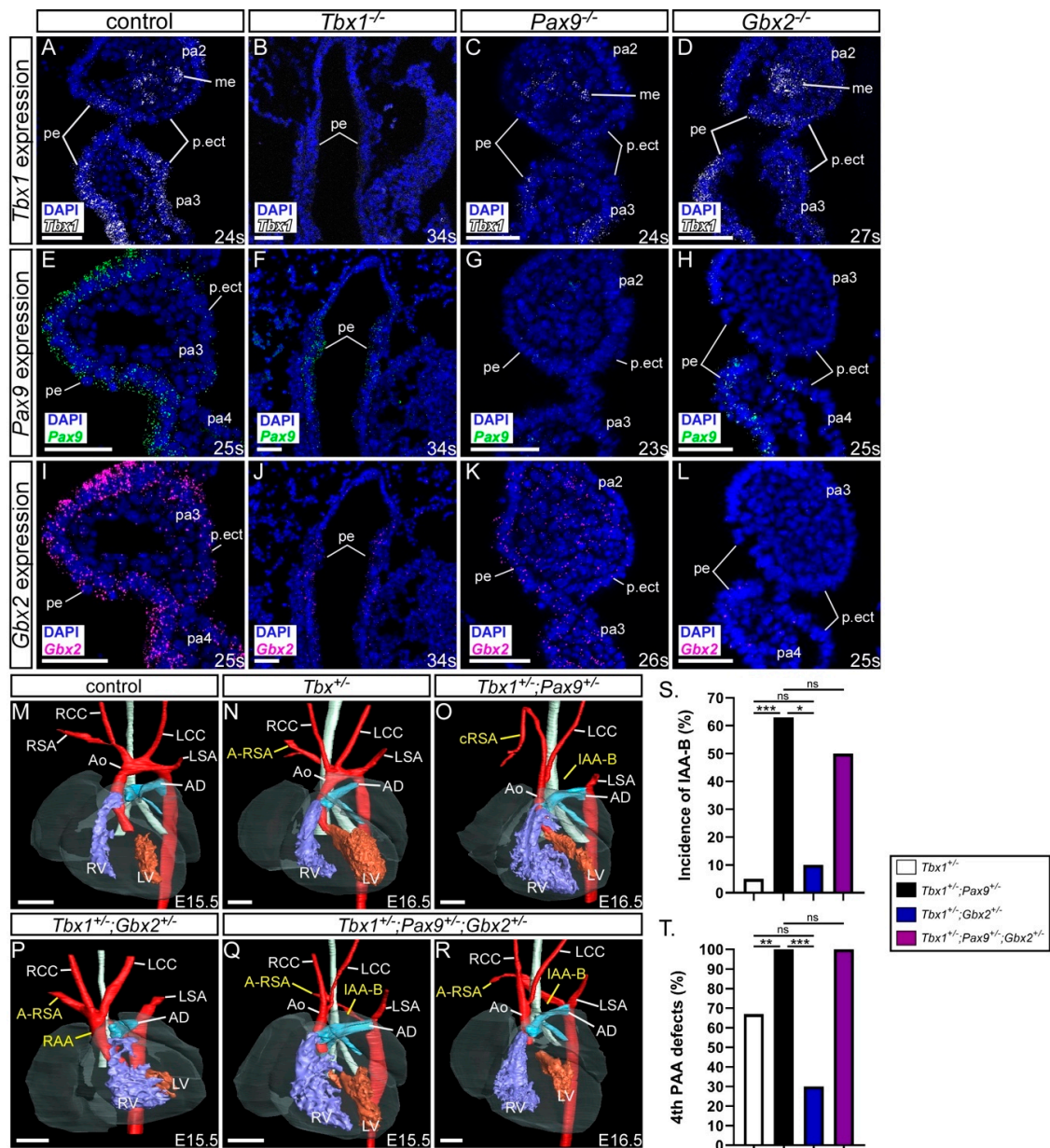


Figure 8. *Gbx2* heterozygosity does not modify the *Tbx1*;*Pax9* double heterozygous phenotype. (A–L) *Tbx1*, *Pax9* and *Gbx2* expression in E9.5–E10.5 control and *Tbx1*^{-/-}, *Pax9*^{-/-} and *Gbx2*^{-/-} embryos (n ≥ 3 embryos per probe; 23–34 somites). (A) *Tbx1* is expressed in the pharyngeal endoderm, mesoderm and ectoderm in control embryos. *Tbx1* expression is absent in *Tbx1*^{-/-} embryos (B), reduced in *Pax9*^{-/-} embryos (C), and normal in *Gbx2*^{-/-} embryos (D). (E) *Pax9* is expressed in the pharyngeal endoderm in control embryos. *Pax9* expression is reduced in *Tbx1*^{-/-} embryos (F), absent in *Pax9*^{-/-} embryos (G), and present in *Gbx2*^{-/-} embryos (H). (I) *Gbx2* is expressed in the pharyngeal endoderm in control embryos. *Gbx2* expression is reduced in *Tbx1*^{-/-} embryos (J), reduced in *Pax9*^{-/-} embryos (K), and absent in *Gbx2*^{-/-} embryos (L). (M–R) 3D reconstructions of E15.5–16.5 hearts from μ CT datasets. (M) Control embryo with normal heart and aortic arch arteries. (N) *Tbx1*^{+/-} embryo with aberrant right subclavian artery (A-RSA). (O) *Tbx1*^{+/-}; *Pax9*^{+/-} embryo with interrupted aortic arch type B (IAA-B) and cervical origin of the right subclavian artery (cRSA). (P) *Tbx1*^{+/-}; *Gbx2*^{+/-} embryo with a right-sided aortic arch (RAA) and A-RSA. (Q,R) *Tbx1*^{+/-}; *Pax9*^{+/-}; *Gbx2*^{+/-} embryos with IAA-B and A-RSA. (S,T) Graphical representation of IAA-B incidence (S) and 4th pharyngeal arch artery (PAA) incidence (T) in *Tbx1*;*Pax9*;*Gbx2* embryos. * *p* < 0.05; ** *p* < 0.001; *** *p* < 0.0001; Pearson chi-squared test for associations

with continuity correction. Scale bars: 500 μm in M-R; 50 μm in (A-L). Abbreviations: Ao, aorta; AD, arterial duct; LCC, left common carotid artery; LSA, left subclavian artery; LV, left ventricle; me, mesoderm; pa, pharyngeal arch; pe, pharyngeal endoderm; p.ect, pharyngeal ectoderm; RCC, right common carotid artery; RSA, right subclavian artery; RV, right ventricle; s, somite. The somite numbers given in the legend reflect the range analysed for the whole study. The figure contains representative images only.

4. Discussion

In this study, we have employed imaging and gene interaction methodologies to provide an in-depth analysis of the *Gbx2* mutant cardiovascular phenotype throughout embryogenesis and demonstrate a genetic interaction with *Pax9* in the pharyngeal endoderm.

4.1. *Gbx2*-Null Mice

Our analysis of the *Gbx2*-null cardiovascular phenotype revealed differences from two previously published papers. At mid-embryogenesis we found 71% of mutants had an abnormal 4th PAA, compared to 50% previously reported [28], and at foetal stages, we identified 64% of mutants had a cardiovascular defect, although none displayed IAA, compared to 39% previously reported where IAA was included [29]. One explanation for the cardiovascular phenotype discrepancy between studies is the *Gbx2*-null allele used. In the previously published studies, the neomycin selection cassette was retained in the first intron of *Gbx2* [32,41], whereas it was removed from the allele used in our study. It is possible that the presence or absence of the neomycin cassette, which has been described to alter mutant mouse phenotypes [45], may have influenced the presentation of the cardiovascular phenotype. Alternatively, some cardiovascular defects may have been overlooked in the previous reports, or a subtle change in genetic background may influence the presentation of phenotypes.

The cardiovascular structures predominantly affected in *Gbx2*-null embryos were the OFT, with DORV seen in 40% of mutants, and the 4th PAA-derived vessels, with 50% of mutants having an aberrant subclavian artery which was either retro-oesophageal or isolated. Although the formation of the 4th PAA was more frequently observed to be affected at mid-embryogenesis in *Gbx2*-null embryos, with this vessel seen to be absent or hypoplastic in 71% of mutants, this did not translate into an IAA-B phenotype at the foetal stage as would be expected if the left 4th PAA had failed to form. Immunolabelling of *Gbx2*^{-/-} embryos showed a disorganisation of the endothelial cells within the 4th pharyngeal arch indicating that the 4th PAA fails to lumenise. This has also been previously described in *Gbx2*^{-/-} embryos [29], as well as in other mouse models where the failure of the 4th PAA is a feature, for example, in *Pax9*^{-/-} [25] and *Tbx1* mutant [28] embryos. The discrepancy in 4th PAA defects observed at an earlier developmental stage, yet not manifesting into a defect at a later stage, is a well-known phenomenon observed in *Tbx1*^{+/-} embryos [25,28,46–49]. The recovery of the left 4th PAA may explain why we did not observe IAA-B in the *Gbx2*-null embryos.

Patients that present with an incomplete reversal of the internal organs are diagnosed with heterotaxy which refers to any defect of left-right patterning and arrangement of the visceral organs. We identified previously unreported left-right patterning defects in a third of all *Gbx2*-null mutants examined. We did not find any change in *Pitx2c* expression in the left lateral plate mesoderm in *Gbx2*-null embryos at E8.5, although we did not pre-select embryos for in situ hybridisation analysis based on any morphological abnormalities such as the orientation of the OFT. *Gbx2* may function in left-right patterning independently of *Pitx2c*. Left-right patterning defects are largely a result of abnormalities at the node of the primitive streak from E7.0 [50] and *Gbx2* is expressed in all three germ layers at gastrulation in the posterior epiblast [30], a region encompassing the node. Overall, the number of *Gbx2*^{-/-} embryos obtained was significantly lower than expected showing that more than half of *Gbx2*^{-/-} embryos are lost prior to E8.5 in early embryogenesis, regardless of the accompanying *Pax9* genotype. Early *Gbx2* expression could, therefore, be critical for gastrulation and some embryos lacking *Gbx2* may not proceed through development at this stage. The surviving embryos may then go on to develop left-right patterning and cardiovascular defects. Alternatively, *Gbx2* may function

downstream of *Pitx2c* to regulate the asymmetric development of the internal organs. *Pitx2* is a regulator of gene expression [51] and the *Pitx2c* isoform plays an important role in the final stages of organ asymmetry [52] including aortic arch and outflow tract development [53,54]. *Pitx2c* mutant mice have OFT defects due to abnormal proliferation within the OFT myocardium [55]. *Gbx2* may, therefore, be a downstream target of *Pitx2c* and further work is required to investigate this possibility.

4.2. Genetic Interaction with *Pax9*

Mice double heterozygous for *Gbx2* and *Pax9* were under-represented at weaning, and some were found to die at birth with cardiovascular defects. These data indicate there is a genetic interaction between *Pax9* and *Gbx2* in cardiovascular development. Interestingly, the RAA and IAA-B phenotypes observed in *Gbx2*^{+/-};*Pax9*^{+/-} neonates are commonly seen in *Gbx2*^{-/-} and *Pax9*^{-/-} mice respectively [25,29] but not in single heterozygous mice for these genes. When *Gbx2*^{-/-} mice were also heterozygous for *Pax9* (i.e., *Gbx2*^{-/-};*Pax9*^{+/-}), 100% of embryos and neonates presented with a cardiovascular defect (significantly increased when compared to 64% of *Gbx2*^{-/-} mice), including left-right patterning defects, and there was a significantly increased incidence of IAA-B. Moreover, CAT was observed, a phenotype not previously identified in *Gbx2*^{-/-} or *Pax9*^{-/-} mice [25,29]. When we produced embryos null for *Pax9* and heterozygous for *Gbx2* (i.e., *Gbx2*^{+/-};*Pax9*^{-/-}), or double knockouts, they all presented with typical *Pax9*-null defects but also additionally displayed CAT or AVSD. Embryos with a *Pax9*^{-/-} genotype, however, did not display a left-right patterning defect as seen in the *Gbx2*^{-/-} mice. Our data suggest that a reduction in bi-allelic *Gbx2* and *Pax9* expression leads to a modification of the phenotypes typically seen in the single-gene knockout mice.

The cardiovascular defects observed in the *Gbx2*;*Pax9* mutant mice such as AVSD, CAT and DORV are reminiscent of abnormal SHF development. Two-thirds of patients with heterotaxy have AVSD [56] and this defect arises from the failure of the SHF-derived dorsal mesenchymal protrusion to complete atrioventricular septation [57]. Patients with 22q11DS, where hemizygous expression of *TBX1* underlies the observed cardiovascular defects, may present with CAT [58], and this phenotype is fully penetrant in *Tbx1*-null mice [34,59]. *Tbx1* is expressed in the SHF [60], which overlaps with the pharyngeal endoderm [61], where *Pax9* and *Gbx2* are also expressed. It is therefore feasible that the pharyngeal endoderm expression of *Pax9* and *Gbx2* are influencing the formation of SHF-derived cardiovascular structures. There could also be a defective contribution in the *Gbx2*;*Pax9* mutant mice from neural crest cells (NCC) migrating through the pharyngeal arches and into the OFT where they participate in septation [8]. Mouse models with NCC defects often present with CAT [62,63]. It has been reported that a reduced number of NCC are present within the caudal pharyngeal arches in *Pax9*-null embryos at E10.5 [25] and *Gbx2*-null mice show aberrant migration of NCC [28,29]. A NCC defect, combined with deficiencies in the pharyngeal endoderm component of the SHF, could, therefore, become more penetrant on a *Gbx2*;*Pax9* mutant background resulting in a higher incidence of the CAT and IAA-B phenotypes [64].

4.3. *Gbx2* and *Pax9* Interact in the Pharyngeal Endoderm

Cardiovascular defects were observed when *Gbx2* was conditionally deleted from the developing embryo using the *Pax9Cre* allele, and these were at a comparable level to that observed in the constitutive double heterozygous embryos, although the IAA-B phenotype was not seen. A higher incidence of 4th PAA defects, however, was seen in the conditional mutants at E10.5 when analysed by ink injection compared to those observed at foetal stages. As discussed above, it is well recognised that the 4th PAA can recover during development and there is not always a direct correlation to defects that are subsequently seen at the foetal stages. At the E10.5 stage, half the conditional *Gbx2*^{-fllox};*Pax9Cre* embryos presented with 4th PAA defects, whereas 100% of the constitutive *Gbx2*^{-/-};*Pax9*^{+/-} embryos did, suggesting that either 4th PAA morphogenesis is only partly controlled from the pharyngeal endoderm or the Cre-mediated recombination of the *Gbx2*-floxed allele is not 100% efficient. Residual expression of *Gbx2* RNA was observed in the pharyngeal endoderm of *Gbx2*^{-fllox};*Pax9Cre* embryos

(Figure 7B), which may be due to the concomitant onset of *Pax9Cre* and *Gbx2* expression at E8.5 resulting in a slight delay in Cre activity on the *Gbx2*-floxed allele. It has previously been shown that the deletion of *Gbx2* from the pharyngeal ectoderm using *AP2αCre* mice resulted in a 47% penetrance of 4th PAA defects at E10.5 with the distribution of unilateral and bilateral 4th PAA defects in conditional endoderm and ectoderm mutants being very similar [28]. It is therefore tempting to speculate that *Gbx2* expression from both pharyngeal epithelial tissues is required for correct 4th PAA morphogenesis. The incidence of defects seen at foetal and embryonic stages in the constitutive *Gbx2*^{-/-}, *Pax9*^{-/-} and *Gbx2*;*Pax9* complex mutants was fairly concordant indicating that 4th PAA defects observed at E10.5 in these genotypes did proceed directly to arch artery defects at foetal stages.

4.4. The *Tbx1*;*Pax9* Double Heterozygous Phenotype is not Modulated by *Gbx2* Haploinsufficiency

Mice heterozygous for *Tbx1* typically have defects affecting the 4th PAA such as IAA and A-RSA [65], but have also been shown to present with further cardiac defects such as VSD [59,66]. *Tbx1* has been shown to genetically interact with *Pax9* and *Gbx2* in the pharyngeal endoderm and ectoderm, respectively [25,28]. We identified three PAX binding sites in a highly conserved region of the *GBX2* locus, as well as a previously validated TBX binding site [42]. In luciferase assays, PAX9 was able to activate the *Gbx2* conserved region although TBX1 did not, and when PAX9 and TBX1 were co-expressed, PAX9 was not able to activate the reporter. This suggests that PAX9 can activate *Gbx2* through binding to the conserved region, whereas TBX1 acts as a repressor. However, to fully provide conclusive evidence for a molecular interaction for *Gbx2* expression to be driven by *Pax9* or *Tbx1*, further experiments would need to be performed such as an electromobility shift assay or chromatin immunoprecipitation experiments. Mutating the putative binding sites in the luciferase assay would also determine specificity. Gene expression is highly dynamic during cardiovascular development with constant switching between gene activation and suppression [67]. For example, *Tbx1* acts as a poised enhancer to bind and keep DNA in the open state to then recruit other transcription or regulatory factors. It has been shown that *Tbx1* recruits P53 to *Gbx2* to modulate *Gbx2* expression through histone methylation [42]. As *Tbx1* also regulates histone modification [68] it could have a potential role in controlling the timely activation of *Gbx2* by *Pax9* during cardiovascular development.

Tbx1, *Pax9* and *Gbx2* are all expressed in the pharyngeal endoderm at E9.5 and E10.5, and could, therefore, function together in the endoderm which is acting as a signalling centre to interact with other tissue types required in PAA morphogenesis. *Pax9* and *Tbx1* were each downregulated in *Tbx1*^{-/-} and *Pax9*^{-/-} embryos respectively, which suggests that *Tbx1* and *Pax9* act in a non-hierarchical pathway [25]. *Tbx1* and *Pax9* expression in *Gbx2*^{-/-} embryos, however, were unaffected indicating that these genes function hierarchically upstream of *Gbx2*. This is reflected in our phenotyping data where we did not identify any difference in the incidence of 4th PAA-derived defects at foetal stages in *Tbx1*^{+/-}; *Pax9*^{+/-}; *Gbx2*^{+/-} triple heterozygous mutants compared to *Tbx1*^{+/-}; *Pax9*^{+/-} double heterozygous mutants. Of note, however, in our study we only identified a low penetrance of 4th PAA-derived defects in *Tbx1*^{+/-}; *Gbx2*^{+/-} mutants, and only one incidence (10%) of IAA-B. This is in contrast to that previously shown for embryos of the same genotype where 27% of mutants (6 out of 22) had IAA-B [28]. This could possibly be attributed to the use of a different *Gbx2* targeted allele as discussed above.

5. Conclusions

In summary, a genetic regulatory network comprising of *Tbx1*, *Pax9* and *Gbx2* is required to control morphogenesis of the arch arteries and the outflow tract of the developing cardiovascular system, and this interaction occurs, in part, within the pharyngeal epithelia at mid-embryogenesis in the mouse. An earlier role for *Gbx2* in establishing left-right patterning requires further investigation.

Supplementary Materials: The following are available online at <http://www.mdpi.com/2308-3425/7/2/20/s1>. Figure S1. No *Gbx2* mRNA is detected in *Gbx2*^{-/-} embryos created by recombining the *Gbx2*^{lox} allele with *Sox2Cre* at E9.5; Figure S2. Thymus and palate abnormalities seen in *Gbx2*;*Pax9* mutant embryos and neonates; Figure

S3. *Pax9Cre* activity in the pharyngeal endoderm in E9.5 embryos. Table S1. Expected and observed genotypes of embryos and foetuses collected from a *Gbx2*^{+/-} intercross; Table S2. Expected and observed genotypes of weaned pups from a *Gbx2*^{+/-} × *Pax9*^{+/-} cross; Table S3. Expected and observed genotypes of embryos and foetuses collected from a *Gbx2*^{+/-}; *Pax9*^{+/-} intercross; Table S4. Summary of thymus phenotypes observed in *Gbx2* and *Gbx2*; *Pax9* mutant embryos at E15.5 and neonates at P0; Table S5. Antibodies and probes used for immunostaining and in situ hybridisation.

Author Contributions: Conceptualization, S.D.B.; methodology, J.E.S. and T.J.M.; formal analysis, C.A.S. and S.D.B.; investigation, C.A.S, S.M. and A.V.; Writing—original draft preparation, S.D.B.; writing—review and editing, C.A.S., D.J.H. and H.M.P.; visualization, C.A.S. and S.D.B.; supervision, D.J.H., H.M.P. and S.D.B.; project administration, S.D.B.; funding acquisition, S.D.B. All authors have read and agreed to the published version of the manuscript.

Funding: This research was funded by a British Heart Foundation project grant (PG/16/39/32115; to SDB) and a British Heart Foundation Non-Clinical PhD Studentship (FS/16/8/31984; to SDB). JES would like to acknowledge infrastructure funding from the British Heart Foundation, UK (SI/14/1/30718).

Acknowledgments: The 2xTk-GL2 and BMP4-luc control plasmids were gifts from Anita Rauch and Rena D'Souza. The *Gbx2* and *Pitx2* probes were gifts from Alexandra Joyner and Dominic Norris. We acknowledge the Newcastle University Flow Cytometry Core Facility (FCCF) for assistance with the generation of the flow cytometry data.

Conflicts of Interest: The authors declare no conflict of interest.

References

1. Andersen, T.A.; Troelsen Kde, L.; Larsen, L.A. Of mice and men: Molecular genetics of congenital heart disease. *Cell. Mol. Life Sci.* **2014**, *71*, 1327–1352. [CrossRef] [PubMed]
2. Boudjemline, Y.; Fermont, L.; Le Bidois, J.; Lyonnet, S.; Sidi, D.; Bonnet, D. Prevalence of 22q11 deletion in fetuses with conotruncal cardiac defects: A 6-year prospective study. *J. Pediatr.* **2001**, *138*, 520–524. [CrossRef]
3. Papangelis, I.; Scambler, P. The 22q11 deletion: DiGeorge and velocardiofacial syndromes and the role of TBX1. *Wiley Interdiscip. Rev. Dev. Biol.* **2013**, *2*, 393–403. [CrossRef] [PubMed]
4. Yagi, H.; Furutani, Y.; Hamada, H.; Sasaki, T.; Asakawa, S.; Minoshima, S.; Ichida, F.; Joo, K.; Kimura, M.; Imamura, S.; et al. Role of TBX1 in human del22q11.2 syndrome. *Lancet* **2003**, *362*, 1366–1373. [CrossRef]
5. Zweier, C.; Sticht, H.; Aydin-Yaylagul, I.; Campbell, C.E.; Rauch, A. Human TBX1 missense mutations cause gain of function resulting in the same phenotype as 22q11.2 deletions. *Am. J. Hum. Genet.* **2007**, *80*, 510–517. [CrossRef] [PubMed]
6. Kelly, R.G. The second heart field. *Curr. Top. Dev. Biol.* **2012**, *100*, 33–65. [CrossRef] [PubMed]
7. Anderson, R.H.; Moorman, A.F.; Brown, N.A.; Bamforth, S.D.; Chaudhry, B.; Henderson, D.J.; Mohun, T.J. Normal and abnormal development of the heart. In *Pediatric and Congenital Cardiology, Cardiac Surgery and Intensive Care*; da Cruz, E., Ivy, D., Jagers, J., Eds.; Springer: London, UK, 2014; pp. 151–177.
8. Waldo, K.; Miyagawa-Tomita, S.; Kumiski, D.; Kirby, M.L. Cardiac neural crest cells provide new insight into septation of the cardiac outflow tract: Aortic sac to ventricular septal closure. *Dev. Biol.* **1998**, *196*, 129–144. [CrossRef]
9. Bajolle, F.; Zaffran, S.; Kelly, R.G.; Hadchouel, J.; Bonnet, D.; Brown, N.A.; Buckingham, M.E. Rotation of the myocardial wall of the outflow tract is implicated in the normal positioning of the great arteries. *Circ. Res.* **2006**, *98*, 421–428. [CrossRef]
10. Anderson, R.H.; Wessels, A.; Vettukattil, J.J. Morphology and Morphogenesis of Atrioventricular Septal Defect With Common Atrioventricular Junction. *World J. Pediatr. Congenit. Heart Surg.* **2010**, *1*, 59–67. [CrossRef]
11. Wang, X.; Chen, D.; Chen, K.; Jubran, A.; Ramirez, A.; Astrof, S. Endothelium in the pharyngeal arches 3, 4 and 6 is derived from the second heart field. *Dev. Biol.* **2017**, *421*, 108–117. [CrossRef]
12. Graham, A.; Smith, A. Patterning the pharyngeal arches. *Bioessays* **2001**, *23*, 54–61. [CrossRef]
13. Chapman, D.L.; Garvey, N.; Hancock, S.; Alexiou, M.; Agulnik, S.I.; Gibson-Brown, J.J.; Cebra-Thomas, J.; Bollag, R.J.; Silver, L.M.; Papaioannou, V.E. Expression of the T-box family genes, *Tbx1-Tbx5*, during early mouse development. *Dev. Dyn.* **1996**, *206*, 379–390. [CrossRef]
14. Veitch, E.; Begbie, J.; Schilling, T.F.; Smith, M.M.; Graham, A. Pharyngeal arch patterning in the absence of neural crest. *Curr. Biol.* **1999**, *9*, 1481–1484. [CrossRef]

15. Piotrowski, T.; Nusslein-Volhard, C. The endoderm plays an important role in patterning the segmented pharyngeal region in zebrafish (*Danio rerio*). *Dev. Biol.* **2000**, *225*, 339–356. [CrossRef]
16. McCauley, D.W.; Bronner-Fraser, M. Neural crest contributions to the lamprey head. *Development* **2003**, *130*, 2317–2327. [CrossRef]
17. Graham, A.; Okabe, M.; Quinlan, R. The role of the endoderm in the development and evolution of the pharyngeal arches. *J. Anat.* **2005**, *207*, 479–487. [CrossRef]
18. Edlund, R.K.; Ohyama, T.; Kantarci, H.; Riley, B.B.; Groves, A.K. Foxi transcription factors promote pharyngeal arch development by regulating formation of FGF signaling centers. *Dev. Biol.* **2014**, *390*, 1–13. [CrossRef]
19. Hasten, E.; Morrow, B.E. Tbx1 and Foxi3 genetically interact in the pharyngeal pouch endoderm in a mouse model for 22q11.2 deletion syndrome. *PLoS Genet.* **2019**, *15*, e1008301. [CrossRef]
20. Jackson, A.; Kasah, S.; Mansour, S.L.; Morrow, B.; Basson, M.A. Endoderm-specific deletion of Tbx1 reveals an FGF-independent role for Tbx1 in pharyngeal apparatus morphogenesis. *Dev. Dyn.* **2014**, *243*, 1143–1151. [CrossRef]
21. Hiruma, T.; Nakajima, Y.; Nakamura, H. Development of pharyngeal arch arteries in early mouse embryo. *J. Anat.* **2002**, *201*, 15–29. [CrossRef]
22. Bamforth, S.D.; Chaudhry, B.; Bennett, M.; Wilson, R.; Mohun, T.J.; Van Mierop, L.H.; Henderson, D.J.; Anderson, R.H. Clarification of the identity of the mammalian fifth pharyngeal arch artery. *Clin. Anat.* **2013**, *26*, 173–182. [CrossRef] [PubMed]
23. Suntratonpipat, S.; Bamforth, S.D.; Johnson, A.L.; Noga, M.; Anderson, R.H.; Smallhorn, J.; Tham, E. Childhood presentation of interrupted aortic arch with persistent carotid ducts. *World J. Pediatr. Congenit. Heart Surg.* **2015**, *6*, 335–338. [CrossRef] [PubMed]
24. Ivins, S.; van Lammerts Beuren, K.; Roberts, C.; James, C.; Lindsay, E.; Baldini, A.; Ataliotis, P.; Scambler, P.J. Microarray analysis detects differentially expressed genes in the pharyngeal region of mice lacking Tbx1. *Dev. Biol.* **2005**, *285*, 554–569. [CrossRef] [PubMed]
25. Phillips, H.M.; Stothard, C.A.; Shaikh Qureshi, W.M.; Kousa, A.I.; Briones-Leon, J.A.; Khasawneh, R.R.; O’Loughlin, C.; Sanders, R.; Mazzotta, S.; Dodds, R.; et al. Pax9 is required for cardiovascular development and interacts with Tbx1 in the pharyngeal endoderm to control 4th pharyngeal arch artery morphogenesis. *Development* **2019**, *146*. [CrossRef]
26. Neubuser, A.; Koseki, H.; Balling, R. Characterization and developmental expression of Pax9, a paired-box-containing gene related to Pax1. *Dev. Biol.* **1995**, *170*, 701–716. [CrossRef]
27. Peters, H.; Neubuser, A.; Kratochwil, K.; Balling, R. Pax9-deficient mice lack pharyngeal pouch derivatives and teeth and exhibit craniofacial and limb abnormalities. *Genes Dev.* **1998**, *12*, 2735–2747. [CrossRef]
28. Calmont, A.; Ivins, S.; Van Bueren, K.L.; Papangelis, I.; Kyriakopoulou, V.; Andrews, W.D.; Martin, J.F.; Moon, A.M.; Illingworth, E.A.; Basson, M.A.; et al. Tbx1 controls cardiac neural crest cell migration during arch artery development by regulating Gbx2 expression in the pharyngeal ectoderm. *Development* **2009**, *136*, 3173–3183. [CrossRef]
29. Byrd, N.A.; Meyers, E.N. Loss of Gbx2 results in neural crest cell patterning and pharyngeal arch artery defects in the mouse embryo. *Dev. Biol.* **2005**, *284*, 233–245. [CrossRef]
30. Li, J.Y.H.; Joyner, A.L. *Otx2* and *Gbx2* are required for refinement and not induction of mid-hindbrain gene expression. *Development* **2001**, *128*, 4979–4991.
31. Bouillet, P.; Chazaud, C.; Oulad-Abdelghani, M.; Dollé, P.; Chambon, P. Sequence and expression pattern of the *Stra7* (*Gbx-2*) homeobox-containing gene induced by retinoic acid in P19 embryonal carcinoma cells. *Dev. Dyn.* **1995**, *204*, 372–382. [CrossRef]
32. Li, J.Y.; Lao, Z.; Joyner, A.L. Changing requirements for Gbx2 in development of the cerebellum and maintenance of the mid/hindbrain organizer. *Neuron* **2002**, *36*, 31–43. [CrossRef]
33. Hayashi, S.; Lewis, P.; Pevny, L.; McMahon, A.P. Efficient gene modulation in mouse epiblast using a Sox2Cre transgenic mouse strain. *Mech. Dev.* **2002**, *119*, S97–S101. [CrossRef]
34. Jerome, L.A.; Papaioannou, V.E. DiGeorge syndrome phenotype in mice mutant for the T-box gene, Tbx1. *Nat. Genet.* **2001**, *27*, 286–291. [CrossRef] [PubMed]
35. Srinivas, S.; Watanabe, T.; Lin, C.S.; William, C.M.; Tanabe, Y.; Jessell, T.M.; Costantini, F. Cre reporter strains produced by targeted insertion of EYFP and ECFP into the ROSA26 locus. *BMC Dev. Biol.* **2001**, *1*, 4. [CrossRef]

36. Geyer, S.H.; Mohun, T.J.; Weninger, W.J. Visualizing Vertebrate Embryos with Episcopic 3D Imaging Techniques. *Sci. World J.* **2009**, *9*, 1423–1437. [CrossRef]
37. Degenhardt, K.; Wright, A.C.; Horng, D.; Padmanabhan, A.; Epstein, J.A. Rapid 3D phenotyping of cardiovascular development in mouse embryos by micro-CT with iodine staining. *Circ. Cardiovasc. Imaging* **2010**, *3*, 314–322. [CrossRef]
38. Bamforth, S.D.; Schneider, J.E.; Bhattacharya, S. High-throughput analysis of mouse embryos by magnetic resonance imaging. *Cold Spring Harb. Protoc.* **2012**, *2012*, 93–101. [CrossRef]
39. Schneider, J.E.; Bose, J.; Bamforth, S.D.; Gruber, A.D.; Broadbent, C.; Clarke, K.; Neubauer, S.; Lengeling, A.; Bhattacharya, S. Identification of cardiac malformations in mice lacking Ptdsr using a novel high-throughput magnetic resonance imaging technique. *BMC Dev. Biol.* **2004**, *4*, 16. [CrossRef]
40. Ogawa, T.; Kapadia, H.; Feng, J.Q.; Raghov, R.; Peters, H.; D'Souza, R.N. Functional Consequences of Interactions between Pax9 and Msx1 Genes in Normal and Abnormal Tooth Development. *J. Biol. Chem.* **2006**, *281*, 18363–18369. [CrossRef]
41. Wassarman, K.M.; Lewandoski, M.; Campbell, K.; Joyner, A.L.; Rubenstein, J.L.; Martinez, S.; Martin, G.R. Specification of the anterior hindbrain and establishment of a normal mid/hindbrain organizer is dependent on Gbx2 gene function. *Development* **1997**, *124*, 2923–2934.
42. Caprio, C.; Baldini, A. p53 suppression partially rescues the mutant phenotype in mouse models of DiGeorge syndrome. *Proc. Natl. Acad. Sci. USA* **2014**, *111*, 13385–13390. [CrossRef] [PubMed]
43. Brennan, J.; Norris, D.P.; Robertson, E.J. Nodal activity in the node governs left-right asymmetry. *Genes Dev.* **2002**, *16*, 2339–2344. [CrossRef] [PubMed]
44. Van Praagh, R.; Van Praagh, S. The anatomy of common aortopulmonary trunk (truncus arteriosus communis) and its embryologic implications. A study of 57 necropsy cases. *Am. J. Cardiol.* **1965**, *16*, 406–425. [CrossRef]
45. Olson, E.N.; Arnold, H.H.; Rigby, P.W.J.; Wold, B.J. Know Your Neighbors: Three Phenotypes in Null Mutants of the Myogenic bHLH Gene MRF4. *Cell* **1996**, *85*, 1–4. [CrossRef]
46. Lindsay, E.A.; Baldini, A. Recovery from arterial growth delay reduces penetrance of cardiovascular defects in mice deleted for the DiGeorge syndrome region. *Hum. Mol. Genet.* **2001**, *10*, 997–1002. [CrossRef]
47. Guris, D.L.; Duester, G.; Papaioannou, V.E.; Imamoto, A. Dose-dependent interaction of Tbx1 and Crkl and locally aberrant RA signaling in a model of del22q11 syndrome. *Dev. Cell.* **2006**, *10*, 81–92. [CrossRef]
48. Randall, V.; McCue, K.; Roberts, C.; Kyriakopoulou, V.; Beddow, S.; Barrett, A.N.; Vitelli, F.; Prescott, K.; Shaw-Smith, C.; Devriendt, K.; et al. Great vessel development requires biallelic expression of Chd7 and Tbx1 in pharyngeal ectoderm in mice. *J. Clin. Invest.* **2009**, *119*, 3301–3310. [CrossRef]
49. Ryckebusch, L.; Bertrand, N.; Mesbah, K.; Bajolle, F.; Niederreither, K.; Kelly, R.G.; Zaffran, S. Decreased Levels of Embryonic Retinoic Acid Synthesis Accelerate Recovery From Arterial Growth Delay in a Mouse Model of DiGeorge Syndrome. *Circ. Res.* **2010**, *106*, 686–694. [CrossRef]
50. Shiratori, H.; Hamada, H. The left-right axis in the mouse: From origin to morphology. *Development* **2006**, *133*, 2095–2104. [CrossRef]
51. Cox, C.J.; Espinoza, H.M.; McWilliams, B.; Chappell, K.; Morton, L.; Hjalt, T.A.; Semina, E.V.; Amendt, B.A. Differential regulation of gene expression by PITX2 isoforms. *J. Biol. Chem.* **2002**, *277*, 25001–25010. [CrossRef]
52. Liu, C.; Liu, W.; Lu, M.F.; Brown, N.A.; Martin, J.F. Regulation of left-right asymmetry by thresholds of Pitx2c activity. *Development* **2001**, *128*, 2039–2048. [PubMed]
53. Franco, D.; Campione, M. The role of Pitx2 during cardiac development. Linking left-right signaling and congenital heart diseases. *Trends Cardiovasc. Med.* **2003**, *13*, 157–163. [CrossRef]
54. Liu, C.; Liu, W.; Palie, J.; Lu, M.F.; Brown, N.A.; Martin, J.F. Pitx2c patterns anterior myocardium and aortic arch vessels and is required for local cell movement into atrioventricular cushions. *Development* **2002**, *129*, 5081–5091. [PubMed]
55. Ai, D.; Liu, W.; Ma, L.; Dong, F.; Lu, M.F.; Wang, D.; Verzi, M.P.; Cai, C.; Gage, P.J.; Evans, S.; et al. Pitx2 regulates cardiac left-right asymmetry by patterning second cardiac lineage-derived myocardium. *Dev. Biol.* **2006**, *296*, 437–449. [CrossRef]
56. Burns, T.; Yang, Y.; Hiriart, E.; Wessels, A. The Dorsal Mesenchymal Protrusion and the Pathogenesis of Atrioventricular Septal Defects. *J. Cardiovasc. Dev. Dis.* **2016**, *3*, 29. [CrossRef]


57. Snarr, B.S.; O'Neal, J.L.; Chintalapudi, M.R.; Wirrig, E.E.; Phelps, A.L.; Kubalak, S.W.; Wessels, A. Isl1 expression at the venous pole identifies a novel role for the second heart field in cardiac development. *Circ. Res.* **2007**, *101*, 971–974. [CrossRef]
58. Unolt, M.; Versacci, P.; Anaclerio, S.; Lambiase, C.; Calcagni, G.; Trezzi, M.; Carotti, A.; Crowley, T.B.; Zackai, E.H.; Goldmuntz, E.; et al. Congenital heart diseases and cardiovascular abnormalities in 22q11.2 deletion syndrome: From well-established knowledge to new frontiers. *Am. J. Med. Genet. Part A* **2018**, *176*, 2087–2098. [CrossRef]
59. Merscher, S.; Funke, B.; Epstein, J.A.; Heyer, J.; Puech, A.; Lu, M.M.; Xavier, R.J.; Demay, M.B.; Russell, R.G.; Factor, S.; et al. TBX1 is responsible for cardiovascular defects in velo-cardio-facial/DiGeorge syndrome. *Cell* **2001**, *104*, 619–629. [CrossRef]
60. Xu, H.; Morishima, M.; Wylie, J.N.; Schwartz, R.J.; Bruneau, B.G.; Lindsay, E.A.; Baldini, A. Tbx1 has a dual role in the morphogenesis of the cardiac outflow tract. *Development* **2004**, *131*, 3217–3227. [CrossRef]
61. Park, E.J.; Ogden, L.A.; Talbot, A.; Evans, S.; Cai, C.L.; Black, B.L.; Frank, D.U.; Moon, A.M. Required, tissue-specific roles for Fgf8 in outflow tract formation and remodeling. *Development* **2006**, *133*, 2419–2433. [CrossRef]
62. Conway, S.J.; Henderson, D.J.; Copp, A.J. Pax3 is required for cardiac neural crest migration in the mouse: Evidence from the splotch (Sp2H) mutant. *Development* **1997**, *124*, 505–514. [PubMed]
63. Keyte, A.; Hutson, M.R. The neural crest in cardiac congenital anomalies. *Differentiation* **2012**, *84*, 25–40. [CrossRef] [PubMed]
64. Bradshaw, L.; Chaudhry, B.; Hildreth, V.; Webb, S.; Henderson, D.J. Dual role for neural crest cells during outflow tract septation in the neural crest-deficient mutant Splotch(2H). *J. Anat.* **2009**, *214*, 245–257. [CrossRef] [PubMed]
65. Lindsay, E.A.; Vitelli, F.; Su, H.; Morishima, M.; Huynh, T.; Prampero, T.; Jurecic, V.; Ogunrinu, G.; Sutherland, H.F.; Scambler, P.J.; et al. Tbx1 haploinsufficiency in the DiGeorge syndrome region causes aortic arch defects in mice. *Nature* **2001**, *410*, 97–101. [CrossRef] [PubMed]
66. Zhang, Z.; Baldini, A. In vivo response to high-resolution variation of Tbx1 mRNA dosage. *Hum. Mol. Genet.* **2008**, *17*, 150–157. [CrossRef]
67. Dupays, L.; Mohun, T. Spatiotemporal regulation of enhancers during cardiogenesis. *Cell. Mol. Life Sci. CMLS* **2017**, *74*, 257–265. [CrossRef]
68. Fulcoli, F.G.; Franzese, M.; Liu, X.; Zhang, Z.; Angelini, C.; Baldini, A. Rebalancing gene haploinsufficiency in vivo by targeting chromatin. *Nat. Commun.* **2016**, *7*. [CrossRef]



© 2020 by the authors. Licensee MDPI, Basel, Switzerland. This article is an open access article distributed under the terms and conditions of the Creative Commons Attribution (CC BY) license (<http://creativecommons.org/licenses/by/4.0/>).

Article

Left Ventricular Noncompaction Is More Prevalent in Ventricular Septal Defect than Other Congenital Heart Defects: A Morphological Study

Laís Costa Marques ¹, Gabriel Romero Liguori ^{1,2}, Ana Carolina Amarante Souza ¹ and Vera Demarchi Aiello ^{1,*} 

¹ Laboratory of Pathology, Heart Institute (InCor), Hospital das Clinicas HCFMUSP, Faculdade de Medicina, Universidade de Sao Paulo, Sao Paulo 05403-000, Brazil; laiscostamarques@gmail.com (L.C.M.); gabriel.liguori@usp.br (G.R.L.); anacarol.amarante@gmail.com (A.C.A.S.)

² Laboratory for Tissue Engineering and Organ Fabrication (LTEOF), Heart Institute (InCor), Hospital das Clinicas HCFMUSP, Faculdade de Medicina, Universidade de Sao Paulo, Sao Paulo 05403-000, Brazil

* Correspondence: vera.aiello@incor.usp.br; Tel.: +55-11-2661-5252

Received: 30 August 2020; Accepted: 24 September 2020; Published: 25 September 2020

Abstract: Left ventricular noncompaction (LVNC) is a condition characterized by prominent ventricular trabeculae and deep intertrabecular recesses and has been described as a possible substrate for arrhythmias, thromboembolism, and heart failure. Herein, we explored the prevalence of LVNC morphology among hearts with congenital heart defects (CHD). We examined 259 postnatal hearts with one of the following CHD: isolated ventricular septal defect (VSD); isolated atrial septal defect (ASD); atrioventricular septal defect (AVSD); transposition of the great arteries (TGA); isomerism of the atrial appendages (ISOM); Ebstein’s malformation (EB); Tetralogy of Fallot (TF). Eleven hearts from children who died of non-cardiovascular causes were used as controls. The thickness of the compacted and non-compacted left ventricular myocardial wall was determined and the specimens classified as presenting or not LVNC morphology according to three criteria, as proposed by Chin, Jenni, and Petersen. Normal hearts did not present LVNC, but the CHD group presented different percentages of LVNC in at least one diagnostic criterium. The prevalence of LVNC was respectively, according to Chin’s, Jenni’s and Petersen’s methods: for VSD—54.2%, 35.4%, and 12.5%; ASD—8.3%, 8.3%, and 8.3%; AVSD—2.9%, 2.9%, and 0.0%; TGA—22.6%, 17%, and 5.7%; ISOM—7.1%, 7.1%, and 7.1%; EB—28.6%, 9.5%, and 0.0%; TF—5.9%, 2.9%, and 2.9%. VSD hearts showed a significantly greater risk of presenting LVNC when compared to controls (Chin and Jenni criteria). No other CHD presented similar risk. Current results show some agreement with previous studies, such as LVNC morphology being more prevalent in VSDs. Nonetheless, this is a morphological study and cannot be correlated with symptoms or severity of the CHD.

Keywords: congenital heart defects; left ventricular noncompaction; ventricular septal defects

1. Introduction

Left ventricular noncompaction (LVNC) is a condition first described in the late 1980s [1]. It is defined as a heart morphologically characterized by excessively prominent ventricular trabeculations and deep intertrabecular recesses that communicate with the ventricular cavity [2]. Diagnostic criteria vary according to different authors [3]. There are two-dimensional echocardiography criteria, such as those described by Chin [4], Jenni [5], and Stöllberger [6], as well as criteria based on cardiac magnetic resonance, as proposed by Petersen [7] and Jacquier [8]. Usually, echocardiography is the first line diagnostic modality [3].

During the last 30 years, LVNC has gained increasing recognition and a great number of authors focused on investigating and describing this anatomic abnormality and its relationship with clinical and pathological findings. Some reports associated the presence of LVNC with the occurrence of heart failure, malignant arrhythmias, and thromboembolic events [9–11]. These symptoms became considered as the tripod of LVNC [4,12]. In children with congenital heart disease (CHD) undergoing heart surgery, LVNC is known to be associated with longer hospital length of stay and higher perioperative complications compared to CHD-only patients without myocardial abnormalities [13].

One of the relevant discussions regarding LVNC is how the disease develops. While some authors believe LVNC is a failure of compaction of the preexisting trabecular formation of the heart [14], others say that the compacted component of the heart is well formed and the excessive trabeculations are a proliferation defect [15]. Although the most commonly accepted hypothesis states that the compacted component of the heart derives from initial trabeculations undergoing compaction, Anderson et al. showed that, in the early stages of ventricular formation (Carnegie stages 15 and 16), a well formed compacted ventricle is already present, despite the existence of a thick layer of persisting trabecular myocardium [15].

Given that congenital heart defects (CHD) are also established during heart development, there might be possible associations between CHD and LVNC derived from common genetic abnormalities. Understanding this association could guide both clinical practice, as well as anatomy, embryology and genetic studies aiming to understand the development of LVNC. Although many authors reported cases of patients presenting concomitant CHD and LVNC [16–24], to date, only four studies sought to establish epidemiological associations between the two entities. All of them, however, selected first patients known to have LVNC and looked for the prevalence of CHD among them. The data from these studies are summarized in Table 1 and Figure 1.

Herein, we hypothesize that the presence of CHD is a major finding and the concomitant occurrence of LVNC is a complicator, not the opposite. Thus, we investigated the prevalence of LVNC in heart specimens of patients with CHD.

Table 1. Summary of the current studies available in literature about prevalence of congenital heart defects among cases of noncompaction.

Reference	Sample Size	Criteria	Total of CHD	Congenital Heart Defect (n)
Stähli (2013) [25]	202	Jenni	40 (19.8%)	Uni-or bicuspid aortic valves (7) Ebstein Anomaly (6) Tetralogy of Fallot (3) Aortic Coarctation (2)
Zuckerman (2010) [26]	50	Jenni	13 (26.0%)	VSD (7) ASD (4) PAPVC (1) Pulmonary atresia with intact ventricular septum (1)
Punn (2010) [27]	44	Jenni	13 (29.5%)	Ebstein Anomaly (7) AVSD (3) VSD (3) Tetralogy of Fallot (2) Pulmonary valve stenosis (2)
Tsai (2009) [28]	46	Chin	38 (82.6%)	VSD (17) ASD (16) PDA (14) Ebstein Anomaly (5)

CHD, congenital heart disease; VSD, ventricular septal defect; ASD, atrial septal defect; PAPVC, partial anomalous pulmonary venous connection; AVSD, atrioventricular septal defect; PDA, patent ductus arteriosus.

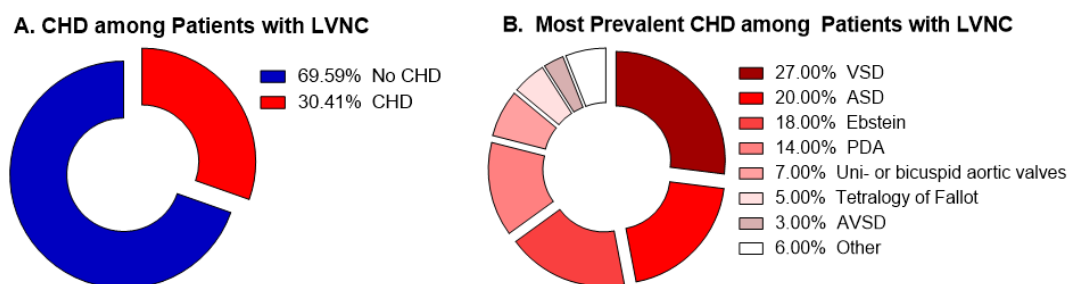


Figure 1. Summary of the current studies available in literature. (A) Percentage of patients with CHD among all the patients presenting LVNC. (B) Percentage of each CHD among all the patients presenting concomitant CHD/LVNC.

2. Materials and Methods

From the anatomical archives of the Laboratory of Pathology of the Heart Institute (InCor), University of Sao Paulo Medical School, Brazil, we identified 279 postnatal hearts with one of the following congenital heart defects: (1) isolated ventricular septal defect (VSD); (2) isolated atrial septal defect (ASD); (3) atrioventricular septal defect (AVSD); (4) transposition of the great arteries (TGA); (5) isomerism of the atrial appendages; (6) Ebstein anomaly; and (7) tetralogy of Fallot. In 20 hearts, the analysis was not possible, either because of previous dissection or previous surgery; the remaining 259 hearts were examined.

The myocardial thickness of the compacted and non-compacted regions in each heart were determined for the left ventricular inlet, apex and outlet muscular walls. Measurements were performed in the long axis. The points of measurements were: at the inlet wall, in a point immediately proximal to the insertion of the anterolateral papillary muscle of the left ventricle; at the apical wall; at the left ventricular free wall, along the surface of myocardial section, at the distal third of the length between the apex and the line of aortic valve insertion, considered as the measurement of the ventricular outlet.

According to the 17-segmental model as described by Partridge and Anderson [29], the inlet measurement was taken perpendicular to the compacted myocardium at segment #7, with the anatomical section corresponding to the vertical long axis image; the apical measurement at segment #17 of the same axis and the outlet measurement at the median point of segment #8 of the echocardiographic parasternal long axis view. The papillary muscles were not included in the measurements.

According to the values found for the apex, specimens were classified as presenting or not LVNC according to three categorization criteria, as proposed by Chin, Jenni, and Petersen (Table 2).

Table 2. Criteria for detection of LVNC in the clinical practice.

Criterion	Method	Acquisition	Moment	LVNC Threshold
Chin et al.	Echocardiography	Short axis	End-diastolic	C/T < 0.5
Jenni et al.	Echocardiography	Short axis	End-systolic	NC/C > 1.4 (or >2.0 in adults)
Petersen et al.	CMR	Long axis	End-diastolic	NC/C > 2.3

C: compacted; NC: non-compacted; T: total (compacted + non-compacted); CMR: cardiovascular magnetic resonance.

This study was conducted in accordance with the Declaration of Helsinki, and the protocol was approved by the “Comissão de Ética para análise de projetos de pesquisa, Hospital das Clínicas da Faculdade de Medicina da Universidade de São Paulo”, protocol #534.621 (19/02/2014).

Statistical Analysis

Data were expressed as the median and interquartile ranges (IQR). Comparisons for the quantitative variables were made through Kruskal–Wallis one-way analysis of variance with post-hoc Holm–Sidak test, or through Mann–Whitney test. To assess qualitative associations, Chi-square or Fisher’s exact test were conducted and odds ratio (OR) was determined. All statistical analyses were performed using GraphPad Prism 6.0 (Graphpad Software Inc., La Jolla, CA, USA).

3. Results

3.1. Sample Characteristics

A total of 259 patients were included in the present study. Briefly, 87.3% of the patients were children, i.e., age below 18-year-old and 51.0% were female. Fifty-one (19.7%) patients presented ventricular septal defect (VSD), 16 (6.2%) atrial septal defect, 41 (15.8%) atrioventricular septal defect, 54 (20.8%) transposition of the great arteries, 29 (11.2%) atrial isomerism, 23 (8.9%) Ebstein’s anomaly, and 34 (13.1%) tetralogy of Fallot. Regarding the VSD types, 74.5% were isolated perimembranous, 5.8% were isolated muscular, 11.7% were subarterial, and in 7.8% there was more than one defect (two cases with more than one muscular defect and two with one perimembranous and one muscular). The atrioventricular septal defects were divided in: complete form (one orifice, interatrial and interventricular communications)—72%; partial form (two orifices, communication at the atrial level only)—28%. Cases of transposition of the great arteries (TGA) comprised: intact ventricular septum, interatrial communication only—52.2%; interatrial communication associated with subpulmonary stenosis—2.1%; ventricular septal defect—45.6%. Hearts with isomerism of the atrial appendages had right isomerism—54.2% and left isomerism—45.8%.

Eleven (4.9%) patients without congenital heart disease were included as healthy controls. The overview of the demographic data stratified for type of congenital heart defect is described in Table 3.

Table 3. Sample Characteristics.

CHD	Sex			Age		
	Male	Female	NA	Children	Adult	NA
normal	4 (36.4%)	6 (54.5%)	1 (9.1%)	11 (100.0%)	0 (0.0%)	0 (0.0%)
VSD	25 (49.0%)	24 (47.0%)	2 (4.0%)	43 (84.3%)	7 (13.7%)	1 (2.0%)
ASD	5 (31.3%)	8 (50%)	3 (18.7%)	11 (68.8%)	2 (12.5%)	3 (18.7%)
AVSD	17 (41.5%)	24 (58.6%)	0 (0.0%)	33 (80.5%)	8 (19.5%)	0 (0.0%)
TGA	33 (61.1%)	20 (37.0%)	1 (1.9%)	51 (94.5%)	3 (5.5%)	0 (0%)
Isomerism	10 (34.5%)	18 (62.1%)	1 (3.4%)	26 (89.7%)	1 (3.4%)	2 (6.9%)
Ebstein	7 (30.4%)	16 (69.6%)	0 (0.0%)	21 (91.3%)	2 (8.7%)	0 (0.0%)
Fallot	18 (52.9%)	16 (47.1%)	0 (0.0%)	30 (88.2%)	4 (11.8%)	0 (0.0%)
TOTAL	119 (45.9%)	132 (51.0%)	8 (3.1%)	226 (87.3%)	27 (10.4%)	6 (2.3%)

VSD, ventricular septal defect; ASD, atrial septal defect; AVSD, atrioventricular septal defect; TGA, transposition of the great arteries; NA, not available.

3.2. Both Short and Long Axis of the Heart Can Be Used for Noncompaction Measurements

We first analyzed how the acquisition method influences the diagnostic results. We used the Bland-Altman test for analyzing the agreement between the measurements performed in the short versus the long axis of the heart. Results indicate there is no fixed bias resulting in statistically significant differences among the methods, thus, both may be used interchangeably (Figure 2).

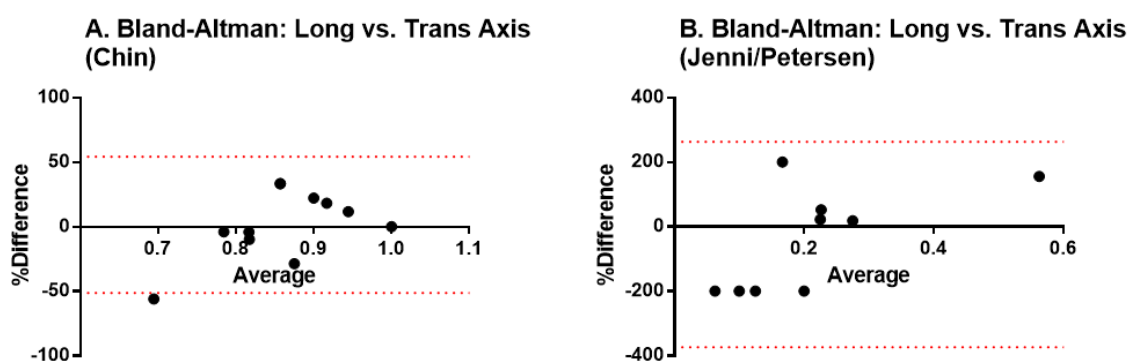


Figure 2. Bland-Altman tests to validate the agreement between measurements performed in the short versus the long axis of the heart. (A) transversal axis; (B) longitudinal axis

3.3. Different Ventricular Walls Present Different Degrees of LVNC

Ventricular trabeculation was evaluated in three left ventricle portions: the inlet, apex, and outlet. Then, the Chin, Jenni, and Petersen analysis were performed for each of these portions.

Using Chin’s method, it was possible to observe statistically significant differences among the specimens with VSD and TGA ($p < 0.0001$), VSD and isomerism ($p = 0.0031$), ASD and TGA ($p = 0.0031$), and ASD and isomerism ($p = 0.0397$) for the left ventricle inlet (Figure 3A). When analyzing the ventricular apex, there were differences among normal heart and hearts with VSD ($p < 0.0001$), TGA ($p = 0.0011$), and Ebstein ($p = 0.0002$) (Figure 3B). There were also differences among hearts with VSD and AVSD ($p < 0.0001$), isomerism ($p = 0.0021$), and Fallot ($p < 0.0001$), besides TGA vs. Fallot ($p = 0.0016$) and Ebstein vs. Fallot ($p = 0.0005$). Finally, the analysis of the left ventricle outlet showed statistically significant differences when comparing hearts with VSD and TGA ($p = 0.0034$) and TGA vs. Fallot ($p = 0.0059$) (Figure 3C). For all the three portions, the hearts with ventricular septal defect demonstrated an increased proportion of trabeculated ventricular wall (focal noncompaction), when compared to the normal heart or to other congenital heart defects.

Jenni’s method includes the stratification of patients between children and adults. Thus, due to the limited number of adult patients, the data for this group was plotted (Figure 3G–I), but could not be statistically analyzed. When analyzing the data for the pediatric group, however, some differences could also be found. In regard to the left ventricle inlet, differences were evidenced between hearts with VSD and TGA ($p = 0.0004$) and VSD and isomerism ($p = 0.0019$) (Figure 3D). The same was found when comparing hearts with ASD and hearts with TGA ($p = 0.0081$) or isomerism ($p = 0.0096$). When analyzing the heart apex, the normal hearts demonstrated less trabeculation than hearts with VSD ($p < 0.0001$), TGA ($p = 0.0024$), and Ebstein ($p = 0.0002$), while hearts with VSD showed more trabeculation than those with AVSD ($p = 0.0015$), isomerism ($p = 0.0019$), and Fallot ($p < 0.0001$) (Figure 3E). It was also possible to describe differences among hearts with TGA vs. Fallot ($p = 0.0241$) and Ebstein vs. Fallot ($p = 0.0019$). For the left ventricular outlet, there was only difference between hearts with VSD and TGA ($p = 0.0390$), so that the former were more trabeculated than the later (Figure 3F).

Petersen’s method, in turn, although performing data acquisition differently than Jenni’s method, uses the same calculation to define trabeculation. However, this method does not separate children and adults, so that the data from all the patients could be analyzed together. The findings showed differences between hearts with VSD and those with TGA ($p < 0.0001$) and isomerism ($p = 0.0031$), besides also between hearts with ASD and TGA ($p = 0.0031$) and isomerism ($p = 0.0399$), for the left ventricle inlet (Figure 3J). The analysis of the apex portion demonstrated statistically significant differences between the normal hearts and hearts with VSD ($p < 0.0001$), ASD ($p = 0.0360$), TGA ($p = 0.0012$), and Ebstein ($p = 0.0002$) (Figure 3K). There were also differences between the hearts with VSD and AVSD ($p < 0.0001$), isomerism ($p = 0.0050$), and Fallot ($p < 0.0001$). Differences among hearts

with TGA and Fallot ($p = 0.0016$), besides Ebstein and Fallot ($p = 0.0005$), could also be described. Finally, for the left ventricle outlet, Petersen’s analysis demonstrated differences between the hearts with VSD vs. TGA ($p = 0.0034$) and TGA vs. Fallot ($p = 0.0059$) (Figure 3L).

Figure 4 shows four examples of cases with LVNC.

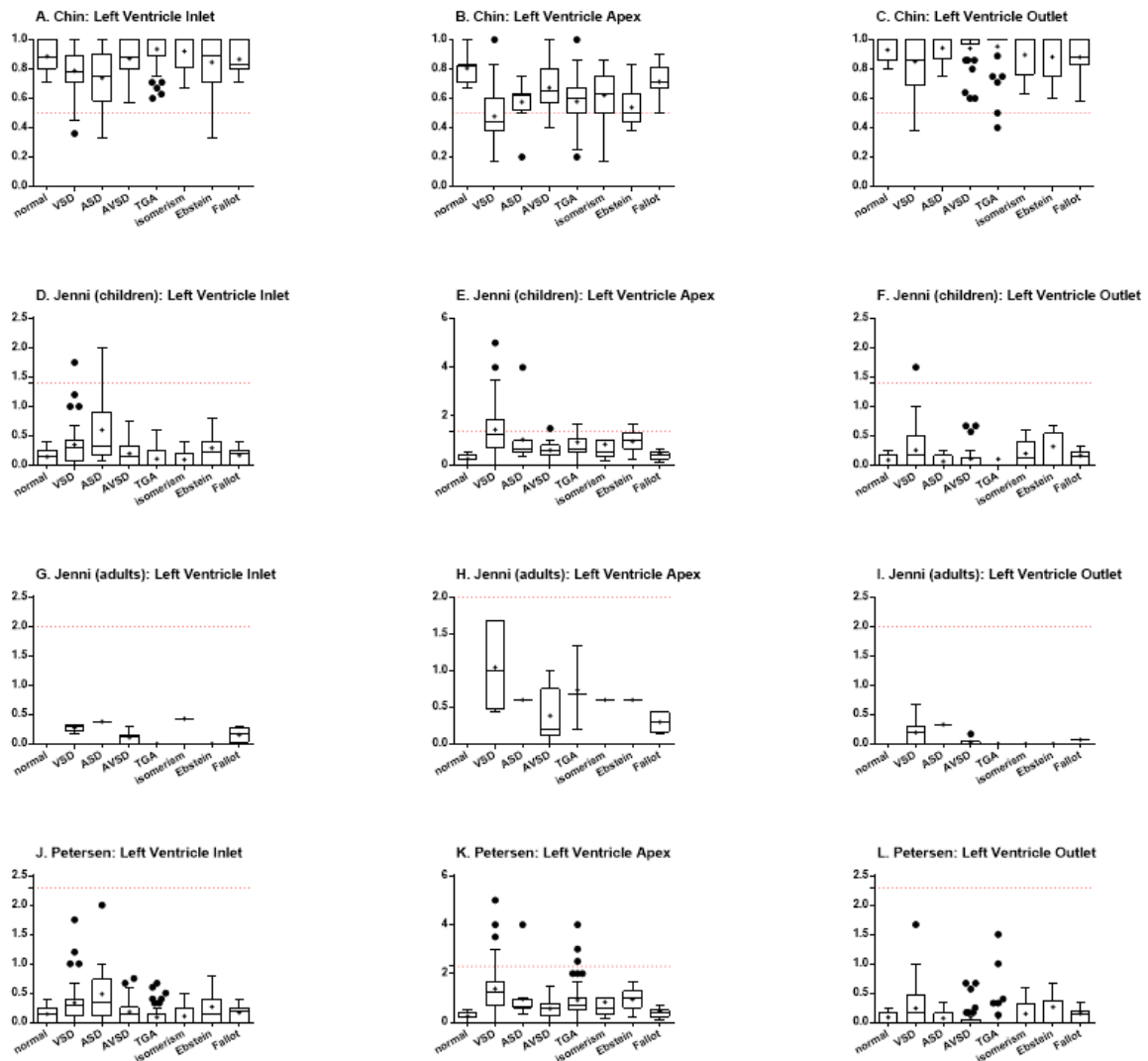


Figure 3. Indexes of ventricular trabeculation, as evaluated by Chin, Jenni, and Petersen methods, in the inlet, apex and outlet muscular walls of the left ventricle. The red dotted lines represent the threshold for LVNC for each criterium. (A) Chin, left ventricle inlet; (B) Chin, left ventricle apex; (C) Chin, left ventricle outlet; (D) Jenni, (children) left ventricle inlet; (E) Jenni, (children) left ventricle apex; (F) Jenni, (children) left ventricle outlet; (G) Jenni, (adults) left ventricle inlet; (H) Jenni, (adults) left ventricle apex; (I) Jenni, (adults) left ventricle outlet; (J) Petersen, left ventricle inlet; (K) Petersen, left ventricle apex; (L) Petersen, left ventricle outlet.

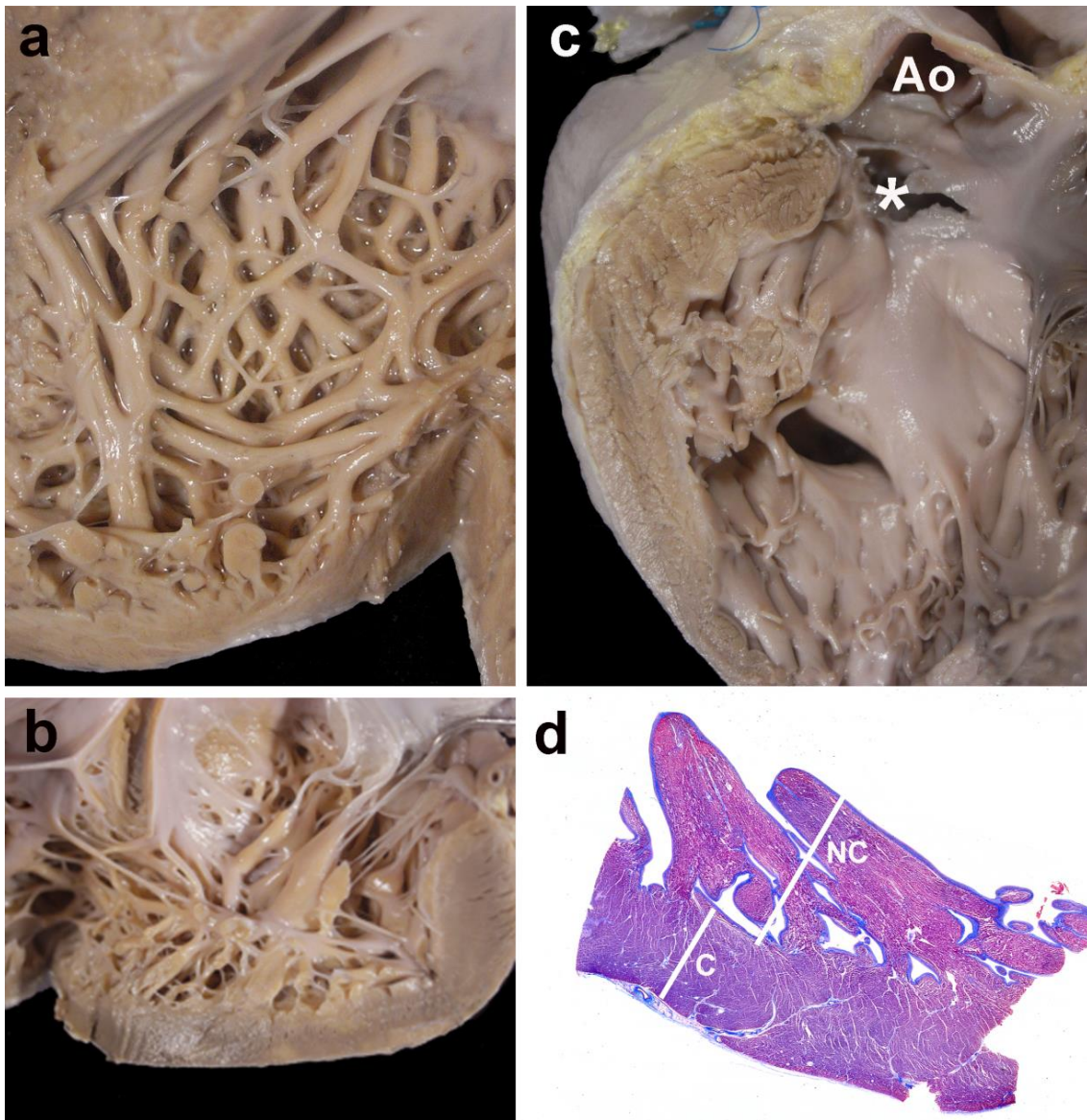


Figure 4. Gross and histological morphology. Four examples of cases showing focal non-compaction of the left ventricle. (a) and (b) Left ventricular wall of two cases with Ebstein’s anomaly of the tricuspid valve. The apical regions show a thick noncompacted layer when compared to the compacted myocardium. In (c), a case with a muscular trabecular ventricular septal defect shows a focal area of noncompaction at the left ventricular outlet free wall (* the membranous septum has been accidentally torn, but was originally intact); Ao—opened aorta. Panel (d) depicts the histological aspect of the apical region of a case with complete transposition of the great arteries, although histology was not used for measurements. The noncompacted layer (NC) is thicker than the compacted myocardium (C); Masson’s trichrome stain.

3.4. LVNC Is More Often Associated with Ventricular Septal Defect than Other Congenital Heart Diseases

The odds ratio for presenting left ventricular noncompaction (hyper-trabeculation) was calculated relative to the normal hearts. The findings were summarized in Table 4. Briefly, hearts presenting VSD showed a significantly increase in the risk of presenting LVNC when compared to normal hearts when using the Chin ($p = 0.0013$; OR 27.09; 95CI 1.51–486.10) and Jenni ($p = 0.0241$; OR 12.78; 95CI 0.71–230.3) criteria. As also demonstrated by the quantitative analysis (Figure 3), the Petersen method was the most conservative and did not evidence any differences among the groups.

Table 4. Percentage of hearts presenting LVNC according to Chin, Jenni, and Petersen (apex).

	Chin			Jenni			Petersen		
	% (n)	OR* (95% CI)	p-Value	% (n)	OR* (95% CI)	p-Value	% (n)	OR* (95% CI)	p-Value
normal	0.0% (0/11)	-	-	0.0% (0/11)	-	-	0.0% (0/11)	-	-
VSD	54.2% (26/48)	27.09 (1.51–486.10)	0.0013	35.4% (17/48)	12.78 (0.71–230.3)	0.0241	12.5% (6/48)	3.52 (0.18–67.21)	0.5820
ASD	8.3% (1/12)	3.00 (0.11–81.68)	1.0000	8.3% (1/12)	3.00 (0.11–81.68)	1.0000	8.3% (1/12)	3.00 (0.11–81.68)	1.0000
AVSD	2.9% (1/34)	1.03 (0.04–27.12)	1.0000	2.9% (1/34)	1.03 (0.04–27.12)	1.0000	0.0% (0/34)	0.33 (0.01–17.79)	1.0000
TGA	22.6% (12/53)	6.93 (0.38–126.1)	0.1064	17.0% (9/53)	4.91 (0.27–90.81)	0.3382	5.7% (3/53)	1.59 (0.08–33.07)	1.0000
Isomerism	7.1% (2/28)	2.17 (0.96–48.89)	1.0000	7.1% (2/28)	2.17 (0.096–48.89)	1.0000	7.1% (2/28)	2.17 (0.096–48.89)	1.0000
Ebstein	28.6% (6/21)	9.65 (0.49–189.20)	0.0711	9.5% (2/21)	2.95 (0.13–67.00)	0.5343	0.0% (0/21)	0.53 (0.01–28.79)	1.0000
Fallot	5.9% (2/34)	1.77 (0.08–39.70)	1.0000	2.9% (1/34)	1.030 (0.04–27.12)	1.0000	2.9% (1/34)	1.030 (0.04–27.12)	1.0000

* Odds ratio (OR) versus normal hearts.

When considering the types of VSDs, no significant difference was detected both in the quantitative indexes (Chin, $p = 0.1680$; Jenni/Petersen, $p = 0.2357$) and in the proportion of cases of LVNC (Chin, $p = 0.0876$; Jenni, $p = 0.4128$; Petersen, $p = 0.3361$) (Figure 5).

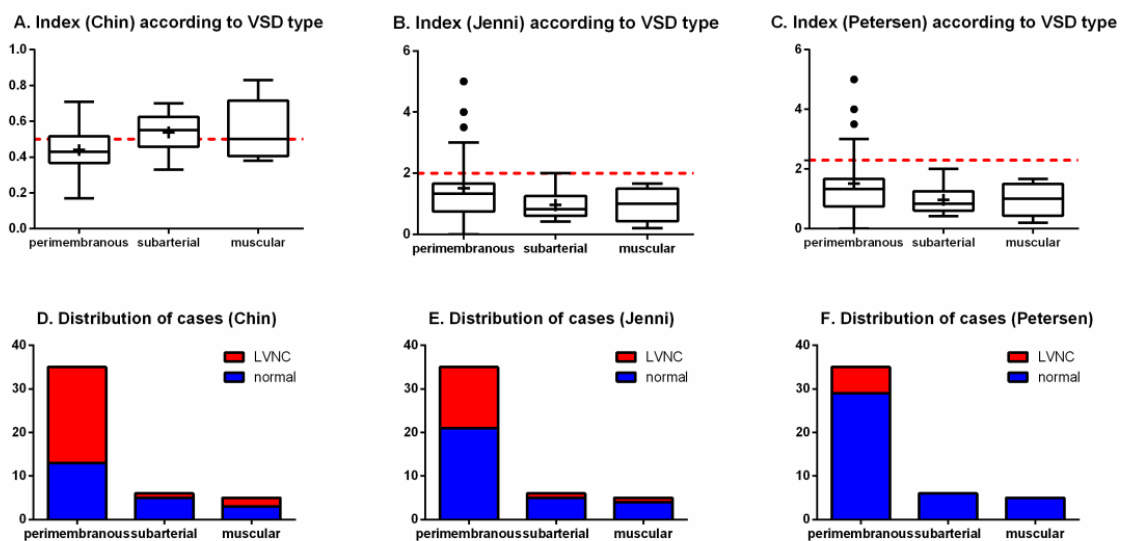


Figure 5. Indexes of left ventricular trabeculation according to VSD type (superior panels) and distribution of cases (inferior panels), as evaluated by Chin, Jenni, and Petersen methods, in. The red dotted lines represent the threshold for LVNC for each criterium. (A) index (Chin) according to VSD type; (B) index (Jenni) according to VSD type; (C) index (Petersen) according to VSD type; (D) distribution of cases (Chin); (E) distribution of cases (Jenni); (F) distribution of cases (Petersen).

Two of the four specimens with more than one VSD (2 with 1 perimembranous + 1 muscular and 2 with more than one muscular) were positive for the LVNC phenotype at the apical measurement, but the statistical comparison did not find differences in prevalence in this group, possibly due to the small number of cases.

Hearts with TGA and Ebstein, although not reaching statistical significance, showed a trend to an increased risk of LVNC (TGA: $p = 0.1064$; OR 6.93; 95CI 0.38–126.1; Ebstein: $p = 0.0711$; OR 27.09; 95CI 0.49–189.2) when analyzed by Chin’s method.

3.5. Different LVNC Diagnostic Criteria Lead to Important Differences in Outcomes

When the prevalence of LVNC was ranked for the congenital heart diseases according to the three different diagnostic methods, differences could be evidenced among them (Table 5). Still, for all the methods, hearts with VSD were those presenting the higher prevalence of LVNC. Oppositely, also for all the methods, hearts with AVSD were those with the lower prevalence of LVNC. For the other diseases, there were differences among the methods.

Table 5. Rank of LVNC prevalence among congenital heart diseases according to Chin, Jenni, and Petersen (apex).

	Chin	Jenni	Petersen
1	VSD	VSD	VSD
2	Ebstein	TGA	ASD
3	TGA	Ebstein	Isomerism
4	ASD	ASD	TGA
5	Isomerism	Isomerism	Fallot
6	Fallot	AVSD/Fallot	AVSD/Ebstein
7	AVSD	-	-

For the hearts with TGA and atrial isomerism, samples were stratified according to the associated defects. Hearts with TGA were stratified among isolated TGA, TGA with ASD, TGA with ASD plus VSD, and TGA with VSD (Table 6). Hearts with atrial isomerism were stratified among isolated isomerism, isomerism with ASD, isomerism with ASD and VSD, and isomerism with AVSD, and other combinations (Table 7). All combinations were compared to hearts presenting the isolated defect, either TGA or isomerism. Although hearts with TGA and isomerism combined with ASD plus VSD showed the higher prevalence of LVNC for all the three diagnostic criteria, the only statistically significant difference was found for hearts with TGA combined with ASD plus VSD when using Jenni’s method ($p = 0.0324$; OR 10.67; 95CI 1.30–86.98).

Table 6. Percentage of hearts presenting LVNC in TGA according to Chin, Jenni, and Petersen (apex).

CHD	% (n)	Chin		Jenni			Petersen		
		OR* (95% CI)	p-Value	% (n)	OR* (95% CI)	p-Value	% (n)	OR* (95% CI)	p-Value
isolated TGA	22.2% (4/18)	-	-	11.1% (2/18)	-	-	5.6% (1/18)	-	-
TGA + ASD	6.7% (1/15)	0.25 (0.02–2.53)	0.3457	6.7% (1/15)	0.57 (0.05–7.0)	1.000	0.0% (0/15)	0.38 (0.01–9.94)	1.0000
TGA + ASD + VSD	57.1% (4/7)	4.67 (0.72–30.12)	0.1563	57.1% (4/7)	10.67 (1.30–86.98)	0.0324	28.6% (2/7)	6.8 (0.51–91.55)	0.1796
TGA + VSD	23.1% (3/13)	1.05 (0.19–5.77)	1.0000	15.4% (2/13)	1.46 (0.18–11.94)	1.0000	0.0% (0/13)	0.43 (0.02–11.47)	1.0000

* Odds ratio (OR) versus isolated TGA.

Table 7. Percentage of hearts presenting LVNC in isomerism according to Chin, Jenni, and Petersen (apex).

CHD	Chin			Jenni			Petersen		
	% (n)	OR * (95% CI)	p-Value	% (n)	OR * (95% CI)	p-Value	% (n)	OR * (95% CI)	p-Value
isolated isomerism	0.0% (0/3)	-	-	0.0% (0/3)	-	-	0.0% (0/3)	-	-
isomerism + ASD	0.0% (0/4)	0.78 (0.01–49.95)	1.0000	0.0% (0/4)	0.78 (0.01–49.95)	1.0000	0.0% (0/4)	0.78 (0.01–49.95)	1.0000
isomerism + ASD + VSD	20.0% (1/5)	2.33 (0.70–76.73)	1.0000	20.0% (1/5)	2.33 (0.70–76.73)	1.0000	20.0% (1/5)	2.33 (0.70–76.73)	1.0000
isomerism + AVSD	0.0% (0/8)	0.41 (0.01–25.19)	1.0000	0.0% (0/8)	0.41 (0.01–25.19)	1.0000	0.0% (0/8)	0.41 (0.01–25.19)	1.0000
other combinations	11.1% (1/9)	1.23 (0.04–38.33)	1.0000	11.1% (1/9)	1.23 (0.04–38.33)	1.0000	11.1% (1/9)	1.23 (0.04–38.33)	1.0000

* Odds ratio (OR) versus isolated isomerism.

3.6. Prevalence of LVCN According to Age

The prevalence of LVNC was stratified for each disease between children and adults, and reported for the three diagnostic criteria. The summary of the findings is described in Table 8. In general, the prevalence of the disease was higher in children than in adults.

Table 8. Percentage of hearts presenting LVNC according to Chin, Jenni, and Petersen when stratified by age in years (y) at the apex.

CHD	Chin		Jenni		Petersen	
	Children (≤18 y)	Adults (>18 y)	Children (≤18 y)	Adults (>18 y)	Children (≤18 y)	Adults (>18 y)
VSD	57.1% (24/42)	40% (2/5)	40.5% (17/42)	0.0% (0/5)	14.3% (6/42)	0.0% (0/5)
ASD	11.1% (1/9)	0.0% (0/1)	11.1% (1/9)	0.0% (0/1)	11.1% (1/9)	0.0% (0/1)
AVSD	3.6% (1/28)	0.0% (0/6)	3.6% (1/28)	0.0% (0/6)	0.0% (0/28)	0.0% (0/6)
TGA	22% (11/50)	33.3% (1/3)	18% (9/50)	0.0% (0/3)	6% (3/50)	0.0% (0/3)
Isomerism	8% (2/25)	0.0% (0/2)	8% (2/25)	0.0% (0/2)	8% (2/25)	0.0% (0/2)
Ebstein	31.6% (6/19)	0.0% (0/2)	10.5% (2/19)	0.0% (0/2)	0.0% (0/19)	0.0% (0/2)
Fallot	6.7% (2/30)	0.0% (0/4)	3.3% (1/30)	0.0% (0/4)	3.3% (1/30)	0.0% (0/4)
TOTAL	23.2% (47/203)	13.0% (3/23)	16.3% (33/203)	0.0% (0/23)	6.4% (13/203)	0.0% (0/23)

Not applicable for normal hearts.

3.7. Sex Influence on the Prevalence of LVCN

We investigated the influence of sex in the prevalence of LVNC. For this purpose, data were stratified, for each congenital heart disease and diagnostic method, between males and females. The results are summarized in Table 9. Briefly, the prevalence of LVNC in males and females varied according to the disease and was increased to either strata depending on the disease. The statistical analysis, however, could only evidence an increased risk for females to present LVNC among patients with VSD, when using the Petersen criteria ($p = 0.0192$; OR 15.40; 95CI 0.80–297.2). In these patients, while 22.7% of the female presented LVNC, no male patient had the disease. For all the other congenital heart defects and diagnostic criteria, no statistically significant differences could be found.

Table 9. Percentage of hearts presenting LVNC according to Chin, Jenni, and Petersen when stratified by sex (apex).

CHD	Chin				Jenni				Petersen			
	Male	Female	OR (95% CI)	p-Value	Male	Female	OR (95% CI)	p-Value	Male	Female	OR (95% CI)	p-Value
VSD	41.7% (10/24)	68.2% (15/22)	3.00 (0.89–10.06)	0.0852	25.0% (6/24)	45.5% (10/22)	2.50 (0.72–8.71)	0.2167	0.0% (0/24)	22.7% (5/22)	15.40 (0.80–297.2)	0.0192
ASD	25.0% (1/4)	0.0% (0/6)	0.17 (0.01–5.68)	0.4000	25.0% (1/4)	0.0% (0/6)	0.18 (0.01–5.68)	0.4000	25.0% (1/4)	0.0% (0/6)	0.18 (0.01–5.68)	0.4000
AVSD	7.1% (1/14)	0.0% (0/20)	0.22 (0.01–5.80)	0.4118	7.1% (1/14)	0.0% (0/20)	0.22 (0.01–5.80)	0.4118	0.0% (0/14)	0.0% (0/20)	0.70 (0.01–37.79)	1.0000
TGA	18.8% (6/32)	25.0% (5/20)	1.44 (0.38–5.55)	0.7300	15.6% (5/32)	15% (3/20)	0.95 (0.20–4.51)	1.0000	3.1% (1/32)	10% (2/20)	3.44 (0.29–40.74)	0.5511
Isomerism	10.0% (1/10)	5.9% (1/17)	0.56 (0.03–10.12)	1.0000	10.0% (1/10)	5.9% (1/17)	0.56 (0.03–10.12)	1.0000	10.0% (1/10)	5.9% (1/17)	0.56 (0.03–10.12)	1.0000
Ebstein	14.3% (1/7)	35.7% (5/14)	3.33 (0.31–36.13)	0.6126	0.0% (0/7)	14.3% (2/14)	3.00 (0.13–71.37)	0.5333	0.0% (0/7)	0.0% (0/14)	0.52 (0.01–28.78)	1.0000
Fallot	11.1% (2/18)	0.0% (0/16)	0.20 (0.01–4.50)	0.8889	15.6% (1/18)	0.0% (0/16)	0.35 (0.01–9.31)	1.0000	15.6% (1/18)	0.0% (0/16)	0.35 (0.01–9.31)	1.0000
TOTAL	20.2% (22/109)	22.6% (26/115)	1.06 (0.90–1.24)	0.7551	13.8% (15/109)	13.9% (16/115)	1.01 (0.47–2.16)	1.0000	3.7% (4/109)	7.0% (8/115)	1.963 (0.57–6.71)	0.3766

Not applicable for normal hearts.

4. Discussion

Herein, we aimed to describe the prevalence of the noncompaction ventricular pattern among hearts with different types of congenital heart disease. We examined 259 specimens with seven different congenital heart defects (VSD, ASD, AVSD, TGA, isomerism, Ebstein malformation and tetralogy of Fallot) according to three classification criteria (Jenni, Chin, and Petersen). To the best of our knowledge, this is the largest sample describing associations between LVNC and CHD. We found that (1) the prevalence of LVNC varies when using different diagnostic criteria; and (2) VSD was the CHD with greater prevalence of LVNC for all the three criteria, followed by Ebstein and TGA—when using Chin or Jenni criteria—or ASD and isomerism—when using Petersen criteria.

Many authors reported cases of patients presenting concomitant CHD and LVNC, including Ebstein [16,18,20,22], congenital atresia of the left main coronary artery [19], VSD [24], double-chambered left ventricle [23], patent ductus arteriosus [21], and also a complex congenital defect formed by *cor-triatriatum*, VSD, persistent left superior caval vein and an anomalous extracardiac vessel [17]. To date, however, only four studies sought to establish epidemiological associations between the two entities. In these studies, authors selected first patients known to have LVNC and looked for the prevalence of CHD among them. Taken together, they showed that, among patients with LVNC, 30.4% presented a CHD (range 19.1–78.0%). Of these patients, most of them had VSD, followed by ASD, Ebstein, PDA, uni- or bicuspid aortic valve, tetralogy of Fallot, and AVSD, respectively. While the three studies using Jenni criteria found CHD prevalence between 19.1% and 29.5%, one study using Chin criteria found 78.0% prevalence of CHD among patients with LVNC.

The prevalence of each CHD found by these four studies matches with the expected prevalence for CHD in the general population. Literature describes the most prevalent CHD as being VSD, ASD, PDA, pulmonary stenosis, and TOF [30]. Among these diseases, only pulmonary stenosis was not described as a major CHD among patients with LVNC. Interestingly, however, authors showed Ebstein malformation as one of the major CHD among patients with LVNC. This is in accordance with our findings, in which we demonstrated a high prevalence of LVNC among Ebstein patients. Thus, even with the disease not being a prevalent CHD, its prevalence among LVNC specimens is high. However, the same was not true for TGA, which was also shown to have a high prevalence of LVNC in our sample, but did not stand out in the other studies.

An important limitation, both in our study as in the rest of literature, is the classification criteria for LVNC. As previously mentioned, several of them exist, Chin, Jenni, and Petersen being the most relevant of them. Each of these criteria uses different methodologies, not only the ratio threshold, but also the reference axis (short vs. long), the moment of acquisition (end-systolic vs. end-diastolic), and also the imaging technique (echocardiography vs. MRI). In the present study, we performed the gross analysis of heart specimens, thus, neither an echocardiography nor MRI. We analyzed the specimens sectioned in the long axis (as in Petersen) because they were already dissected on this axis, as this is the standard for necropsy studies in our institution. In order to analyze if the chosen axis would result in diagnostic bias, we performed the Bland-Altman test, which showed that there was no difference between the short and long-axis measurements; thus, both could be used interchangeably. Still, the classification criteria seem to be a major issue when stratifying patients with or without LVNC. While some criteria, such as Chin, are very permissive, resulting in high sensitivity and low specificity, others, like Petersen, are more restrictive, resulting in high specificity. In their original study, Petersen et al. [7] claim an 86% sensitivity and a 99% specificity, pointing out also that the sensitivity of cardiovascular magnetic resonance is increased as compared to the other methods of cardiac imaging.

Another limitation of the study involving heart specimens is the lack of information about the contraction status of the myocardium. We admit that this uncertainty could be a bias in our study, but believe that it would not be important in determining the ratio between compacted and non-compacted layers, because contraction status would apply to both layers.

Unfortunately, because we used necropsy hearts, we could not perform hemodynamic studies—as measuring ejection fraction, shortening fraction, etc.—and thus, we could not correlate our findings

with the clinical status of the patient. Furthermore, in the majority of our cases such data were not available in the electronic health record. Several authors argue that hypertrabeculation of the left ventricle does not mean debilitated heart [15,31]. They defend that excessive trabeculation alone is not clinically relevant and there must be other modifications, such as reduced ejection fraction, fibrosis, and dilated left ventricle, in order to consider LVNC as a disease. These parameters, however, are already known hallmarks of cardiomyopathy. Thus, it is still difficult to define patients affected by LVNC, either by genetic or imaging diagnostic tools, with absolute certainty. Although for the general population the LVNC diagnosis might not necessarily lead to poor prognosis, this might not be true for children with CHD, which already have a diseased heart and, thus, may be more susceptible to the detrimental effect of hypertrabeculation. Hence, particularly in the case of patients with VSD (and maybe also Ebstein and TGA), diseases which we demonstrated to be a risk factor for LVNC, the screening could be beneficial for the management of the disease and possibly a feature to affect late follow-up after surgery. The recent description of LVNC as a trait in the MOGE(S) nosology system allows to recognize that the LVNC finding may possibly contribute to left ventricular dysfunction in coexisting morphofunctional disorders, such as the congenital heart defects [32].

Another point deserving discussion is that the diagnosis of LVNC was made in our series whenever a single region of the left ventricular wall was positive. Therefore, it would be better to describe “focal LVNC”, while in cases with dilated cardiomyopathy phenotype of the disease, the non-compacted pattern is usually diffuse.

5. Conclusions

The prevalence of focal LVNC phenotype among CHD patients varies widely according to the criteria being used. In the present study, we showed that the Chin criteria are more permissive, while Petersen’s are more restrictive. According to both Chin and Jenni classification methods, VSD is a risk factor for LVNC. This is not true when using Petersen classification but, still, VSD was also the CHD with higher LVNC prevalence when using this classification method. Ebstein and TGA demonstrated trends towards representing a risk factor for LVNC, but could not be confirmed in the present study. Follow-up studies should be performed in large cohorts of living patients, children and adults, and include clinical data such as symptoms and exam results.

Author Contributions: L.C.M.: conceptualization; data collection; data analysis; writing—original draft preparation; G.R.L.: Data analysis; writing—original draft preparation; writing—review and editing; A.C.A.S.: Data collection; V.D.A.: Conceptualization; methodology; data analysis; writing—review and editing; project supervision. All authors have read and agreed to the published version of the manuscript.

Funding: This project was supported by the São Paulo Research Foundation (FAPESP research grants 2013/25059-8 and 2010/16811-0).

Conflicts of Interest: The authors declare no conflict of interest.

References

1. Engberding, R.; Bender, F. Identification of a rare congenital anomaly of the myocardium by twodimensional echocardiography: Persistence of isolated myocardial sinusoids. *Am. J. Cardiol.* **1984**, *53*, 1733–1734. [CrossRef]
2. Lofiego, C.; Biagini, E.; Pasquale, F.; Ferlito, M.; Rocchi, G.; Perugini, E.; Bacchi-Reggiani, M.L.; Boriani, G.; Leone, O.; Caliskan, K.; et al. Wide spectrum of presentation and variable outcomes of isolated left ventricular non-compaction. *Heart* **2007**, *93*, 65–71. [CrossRef] [PubMed]
3. Almeida, A.G.; Pinto, F. Non-compaction cardiomyopathy. *Heart* **2013**, *99*, 1535–1542. [CrossRef]
4. Chin, T.K.; Perloff, J.K.; Williams, R.G.; Jue, K.; Mohrmann, R. Isolated noncompaction of left ventricular myocardium. A study of eight cases. *Circulation* **1990**, *82*, 507–513. [CrossRef] [PubMed]
5. Jenni, R.; Oechslin, E.; Schneider, J.; Attenhofer, C.; Kaufmann, P.A. Echocardiographic and pathoanatomical characteristics of isolated left ventricular non-compaction: A step towards classification as a distinct cardiomyopathy. *Heart* **2001**, *86*, 666–671. [CrossRef] [PubMed]

6. Stöllberger, C.; Finsterer, J.; Blazek, G. Left ventricular hypertrabeculation/noncompaction and association with additional cardiac abnormalities and neuromuscular disorders. *Am. J. Cardiol.* **2002**, *90*, 899–902. [CrossRef]
7. Petersen, S.E.; Selvanayagam, J.B.; Wiesmann, F.; Robson, M.D.; Francis, J.M.; Anderson, R.H.; Watkins, H.; Neubauer, S. Left Ventricular Non-Compaction. *J. Am. Coll. Cardiol.* **2005**, *46*, 101–105. [CrossRef]
8. Jacquier, A.; Thuny, F.; Jop, B.; Giorgi, R.; Cohen, F.; Gaubert, J.-Y.; Vidal, V.; Bartoli, J.M.; Habib, G.; Moulin, G. Measurement of trabeculated left ventricular mass using cardiac magnetic resonance imaging in the diagnosis of left ventricular non-compaction. *Eur. Hear. J.* **2010**, *31*, 1098–1104. [CrossRef]
9. Ritter, M.; Oechslin, E.; Sütsch, G.; Attenhofer, C.; Schneider, J.; Jenni, R. Isolated Noncompaction of the Myocardium in Adults. *Mayo Clin. Proc.* **1997**, *72*, 26–31. [CrossRef]
10. Xu, L.; Yang, J.; Yang, Y. Acute Kidney Infarction Due to Left Ventricular Thrombus Embolization In Patient with Isolated Left Ventricular Noncompaction: A Case Report. *Hear. Surg. Forum.* **2017**, *20*, 252–255. [CrossRef]
11. Papadopoulos, K.; Petrou, P.M.; Michaelides, D. Left Ventricular Noncompaction Cardiomyopathy Presenting with Heart Failure in a 35-Year-Old Man. *Tex. Hear. Inst. J.* **2017**, *44*, 260–263. [CrossRef]
12. Oechslin, E.N.; Jost, C.H.A.; Rojas, J.R.; A Kaufmann, P.; Jenni, R. Long-term follow-up of 34 adults with isolated left ventricular noncompaction: A distinct cardiomyopathy with poor prognosis. *J. Am. Coll. Cardiol.* **2000**, *36*, 493–500. [CrossRef]
13. Ramachandran, P.; Woo, J.G.; Ryan, T.D.; Bryant, R.; Heydarian, H.C.; Jefferies, J.L.; Towbin, J.A.; Lorts, A. The Impact of Concomitant Left Ventricular Non-compaction with Congenital Heart Disease on Perioperative Outcomes. *Pediatr. Cardiol.* **2016**, *37*, 1307–1312. [CrossRef]
14. Sedmera, D.; Pexieder, T.; Vuillemin, M.; Thompson, R.P.; Anderson, R.H. Developmental patterning of the myocardium. *Anat. Rec.* **2000**, *258*, 319–337. [CrossRef]
15. Anderson, R.H.; Jensen, B.; Mohun, T.J.; Petersen, S.E.; Aung, N.; Zemrak, F.; Planken, R.N.; Maciver, D.H. Key Questions Relating to Left Ventricular Noncompaction Cardiomyopathy: Is the Emperor Still Wearing Any Clothes? *Can. J. Cardiol.* **2017**, *33*, 747–757. [CrossRef] [PubMed]
16. Attenhofer Jost, C.H.; Connolly, H.M.; O’Leary, P.W.; Warnes, C.A.; Tajik, A.J.; Seward, J.B. Left heart lesions in patients with Ebstein anomaly. *Mayo Clin. Proc.* **2005**, *80*, 361–368. [CrossRef] [PubMed]
17. Singh, N.; Aga, P.; Singh, R.; Tiwari, B. Non-compaction of the left ventricular myocardium with Cor-triatriatum and associated anomalies. *BMJ Case Rep.* **2013**, *2013*, bcr2012008104. [CrossRef] [PubMed]
18. Fazio, G.; Visconti, C.; D’Angelo, L.; Grassedonio, E.; Re, G.L.; D’Amico, T.; Suter, L.; Novo, G.; Ferrara, F.; Midiri, M.; et al. Diagnosis and definition of biventricular non-compaction associated to Ebstein’s anomaly. *Int. J. Cardiol.* **2011**, *150*, e20–e24. [CrossRef] [PubMed]
19. Zheng, J.; Song, H.; Jiang, S.; Li, T. Congenital Atresia of the Left Main Coronary Artery with Noncompaction of the Ventricular Myocardium in an Asymptomatic Young Child. *Pediatr. Cardiol.* **2012**, *34*, 1998–2002. [CrossRef] [PubMed]
20. Nimeri, N.A.; Nahia, F.F.A.; Ibrahim, A.S.; Khella, A.Y. The first reported case of non-compacted cardiomyopathy in a preterm infant with Ebstein’s anomaly. *BMJ Case Rep.* **2012**, *2012*, bcr0220125861. [CrossRef] [PubMed]
21. Calzolari, M.; Gaddi, O.; Ilari, B.; Iotti, R.; Tortorella, G.; Muià, N.; Guiducci, U. Association of non-compacted myocardium and patent ductus arteriosus in a young asymptomatic male patient: Findings in screening for contact sport eligibility. *Ital. Hear. J. Suppl. Off. J. Ital. Fed. Cardiol.* **2002**, *3*, 659–664.
22. Vermeer, A.M.C.; Van Engelen, K.; Postma, A.V.; Baars, M.J.; Christiaans, I.; De Haij, S.; Klaassen, S.; Mulder, B.J.; Keavney, B. Ebstein anomaly associated with left ventricular noncompaction: An autosomal dominant condition that can be caused by mutations in MYH7. *Am. J. Med. Genet. Part C Semin. Med. Genet.* **2013**, *163*, 178–184. [CrossRef] [PubMed]
23. Correia, A.S.; Madureira, A.J.; Almeida, P.B.; Goncalves, A.; Araújo, V. Double-chambered left ventricle plus left ventricular non-compaction: Report of an abnormal association. *Eur. Hear. J. Cardiovasc. Imaging* **2012**, *14*, 127. [CrossRef] [PubMed]
24. Laghari, A.H.; Tai, J.M.; Saleem, S. Non-compaction of the left ventricle and associated ventricular septal defect. *BMJ Case Rep.* **2012**, bcr2012006614. [CrossRef] [PubMed]

25. Stähli, B.E.; Gebhard, C.; Biaggi, P.; Klaassen, S.; Buechel, E.V.; Jost, C.H.A.; Jenni, R.; Tanner, F.; Greutmann, M. Left ventricular non-compaction: Prevalence in congenital heart disease. *Int. J. Cardiol.* **2013**, *167*, 2477–2481. [CrossRef]
26. Zuckerman, W.A.; Richmond, M.E.; Singh, R.K.; Carroll, S.J.; Starc, T.J.; Addonizio, L.J. Left-ventricular noncompaction in a pediatric population: Predictors of survival. *Pediatr. Cardiol.* **2011**, *32*, 406–412. [CrossRef]
27. Punn, R.; Silverman, N.H. Cardiac Segmental Analysis in Left Ventricular Noncompaction: Experience in a Pediatric Population. *J. Am. Soc. Echocardiogr.* **2010**, *23*, 46–53. [CrossRef]
28. Tsai, S.F.; Ebenroth, E.S.; Hurwitz, R.A.; Cordes, T.M.; Schamberger, M.S.; Batra, A.S. Is Left Ventricular Noncompaction in Children Truly an Isolated Lesion? *Pediatr. Cardiol.* **2009**, *30*, 597–602. [CrossRef]
29. Partridge, J.B.; Anderson, R.H. Left ventricular anatomy: Its nomenclature, segmentation, and planes of imaging. *Clin. Anat.* **2009**, *22*, 77–84. [CrossRef]
30. Van Der Linde, D.; Konings, E.E.; Slager, M.A.; Witsenburg, M.; A Helbing, W.; Takkenberg, J.J.M.; Roos-Hesselink, J.W. Birth Prevalence of Congenital Heart Disease Worldwide. *J. Am. Coll. Cardiol.* **2011**, *58*, 2241–2247. [CrossRef]
31. Zemrak, F.; Ahlman, M.A.; Captur, G.; Mohiddin, S.A.; Kawel-Boehm, N.; Prince, M.R.; Moon, J.C.; Hundley, W.G.; Lima, J.A.; Bluemke, D.A.; et al. The relationship of left ventricular trabeculation to ventricular function and structure over a 9.5-year follow-up: The MESA study. *J. Am. Coll. Cardiol.* **2014**, *64*, 1971–1980. [CrossRef] [PubMed]
32. Arbustini, E.; Favalli, V.; Narula, N.; Serio, A.; Grasso, M. Left Ventricular Noncompaction. *J. Am. Coll. Cardiol.* **2016**, *68*, 949–966. [CrossRef] [PubMed]



© 2020 by the authors. Licensee MDPI, Basel, Switzerland. This article is an open access article distributed under the terms and conditions of the Creative Commons Attribution (CC BY) license (<http://creativecommons.org/licenses/by/4.0/>).



Review

Virtual Dissection: Emerging as the Gold Standard of Analyzing Living Heart Anatomy

Justin T. Tretter ^{1,2}, Saurabh Kumar Gupta ³, Yu Izawa ⁴, Tatsuya Nishii ⁵ and Shumpei Mori ^{6,*}

¹ Heart Institute, Cincinnati Children's Hospital Medical Center, Cincinnati, OH 45229, USA; justin.tretter@cchmc.org

² Department of Pediatrics, University of Cincinnati College of Medicine, Cincinnati, OH 45229, USA

³ Department of Cardiology, All India Institute of Medical Sciences, New Delhi 110029, India; drsaurabhmd@gmail.com

⁴ Division of Cardiovascular Medicine, Department of Internal Medicine, Kobe University Graduate School of Medicine, Kobe, Hyogo 650-0017, Japan; u.izawa@gmail.com

⁵ Department of Radiology, National Cerebral and Cardiovascular Center, Suita, Osaka 564-8565, Japan; ttsynishii@ncvc.go.jp

⁶ UCLA Cardiac Arrhythmia Center, UCLA Health System, David Geffen School of Medicine at UCLA, Los Angeles, CA 90095, USA

* Correspondence: shumpei@g.ucla.edu; Tel.: +310-794-1717; Fax: +310-794-6492

Academic Editors: Deborah Henderson and Nigel Brown

Received: 14 July 2020; Accepted: 10 August 2020; Published: 12 August 2020

Abstract: Traditionally, gross cardiac anatomy has been described mainly based on the findings in the dissection suite. Analyses of heart specimens have contributed immensely towards building a fundamental knowledge of cardiac anatomy. However, there are limitations in analyzing the autopsied heart removed from the thorax. Three-dimensional imaging allows visualization of the blood-filled heart in vivo in attitudinally appropriate fashion. This is of paramount importance for not only demonstration of cardiac anatomy for educational purposes, but also for the detailed anatomical evaluation in patients with acquired and congenital heart disease. In this review, we discuss the advantages of three-dimensional imaging, specifically focusing on virtual dissection, a volume rendering-based reconstruction technique using computed tomographic data. We highlight examples of three-dimensional imaging in both education and guiding patient management.

Keywords: cardiac anatomy; computed tomography; congenital heart disease; three-dimensional imaging; virtual dissection; volume rendering

1. Introduction

The modern understanding of cardiac anatomy is incomplete without referencing the works of Professor Robert H. Anderson. He continues to be a pillar to which our knowledge of cardiac anatomy in both normal as well as malformed hearts is supported. During his long illustrious career, he has enriched the field of cardiac development and anatomy, the latter of which has largely depended on analysis of heart specimens. The autopsy-based analyses, however, have inherent disadvantages of loss of in vivo blood-filled shape and attitudinally appropriate relationship to surrounding structures. Besides, delineation of cardiac anatomy mandates dissection, which results in deformation and permanent loss of its original state.

Modern computed tomography scanners acquire high-resolution datasets. Simultaneous improvement in computational capabilities now permits high-quality three-dimensional reconstruction of computed tomographic datasets. The three-dimensional reconstructions, particularly when achieved

by volume rendering, permit visualization of cardiac anatomy equivalent to the dissection of heart specimens with the additional benefit of viewing in attitudinally appropriate orientation. Such dissection performed virtually has an added advantage of evaluating cardiac anatomy *in vivo*. Furthermore, the feasibility of reconstructing in any plane relevant to the cardiologist, radiologist or surgeon makes virtual dissection an ideal tool for education and clinical decision making. The ease and accuracy of cardiac anatomy using virtual dissection has prompted Professor Anderson to consider it as the gold standard for analysis of cardiac anatomy in living patients [1–3]. We are honored to contribute to this special issue of the journal, recognizing the monumental contributions that Professor Anderson has made to the field of cardiovascular medicine. In this review, we discuss the advantages and applications of volume-rendered images, specifically focusing on virtual dissection, in understanding patient-specific cardiac anatomy.

2. The Concept of Three-Dimensional Imaging Using the Volume-Rendering Method

Recent advances in visualization have permitted much needed three-dimensional reconstruction of datasets obtained from computed tomography and magnetic resonance imaging. Although commonly performed using commercial software packages, three-dimensional reconstruction can also be achieved using free open-source software [4–8]. These software are being increasingly used in clinical practice for diagnosis as well as to guide transcatheter and surgical intervention [9–13]. Some of these software have additional capability for creating and modifying the three-dimensional data to provide the appropriate file format for three-dimensional printing and various forms of extended reality [14,15]. Irrespective of the software and the visualization technique (virtual model on a monitor, printed model, or augmented/virtual reality), the general concept of three-dimensional imaging is the same in the regard that all three-dimensional visualization techniques rely on differential visualization of each iso- or anisotropic image voxel based on its attenuation density (computed tomography), signal intensity (magnetic resonance imaging), or intensity of echocardiographic signal (three-dimensional ultrasound). If a phasic dataset is obtained, four-dimensional images with time-dependent change in the cardiac anatomy can also be demonstrated (Supplementary Movies 1 and 2).

Commonly, contrast enhancement is used for detailed cardiac evaluation to visualize the chambers, vessels, and/or coronary arteries. When the contrast agent is used, it is the enhanced chamber and/or the lumen of these vessels that are usually the focus of reconstruction (Figures 1 and 2). We call this volume-rendering blood pool imaging as endocast images [1,16,17]. This is analogous to conventional die casting used for the dissected heart to create molds [18].

In this material, we mainly focused on the computed tomographic images as the spatial resolution of clinical datasets is commonly superior to that obtained from cardiac magnetic resonance imaging. However, three- or four-dimensional analysis is also feasible for datasets obtained from magnetic resonance imaging, which have advantages in its non-invasiveness, temporal resolution, tissue characterization, perfusion analysis, and flow analysis [19,20].

Virtual dissection is nothing but a modification of the volume-rendering technique wherein the focus is shifted to the walls of the cardiac chambers and vessels. While endocast images can be extremely useful, especially when visualizing the great vessels and their relationships to the other intrathoracic structures or relating to angiographic imaging, they become less informative when aiming to understand the detailed intracardiac anatomy and how this relates to the proximal great vessels. It is often the walls, septums, and valves of the chambers and/or vessels which are targeted for transcatheter or surgical intervention [17], information which can be demonstrated in exquisite detail by virtual dissection [21–25]. In this technique, the enhanced chamber is virtually removed from the original datasets by the process of manual thresholding. The non-enhanced walls, septums, and valves are then visualized to produce images similar to real dissection.

Depending on the interest of visualization, reconstruction using the volume-rendering method requires a combination of various concepts of imaging (Figures 1 and 2).

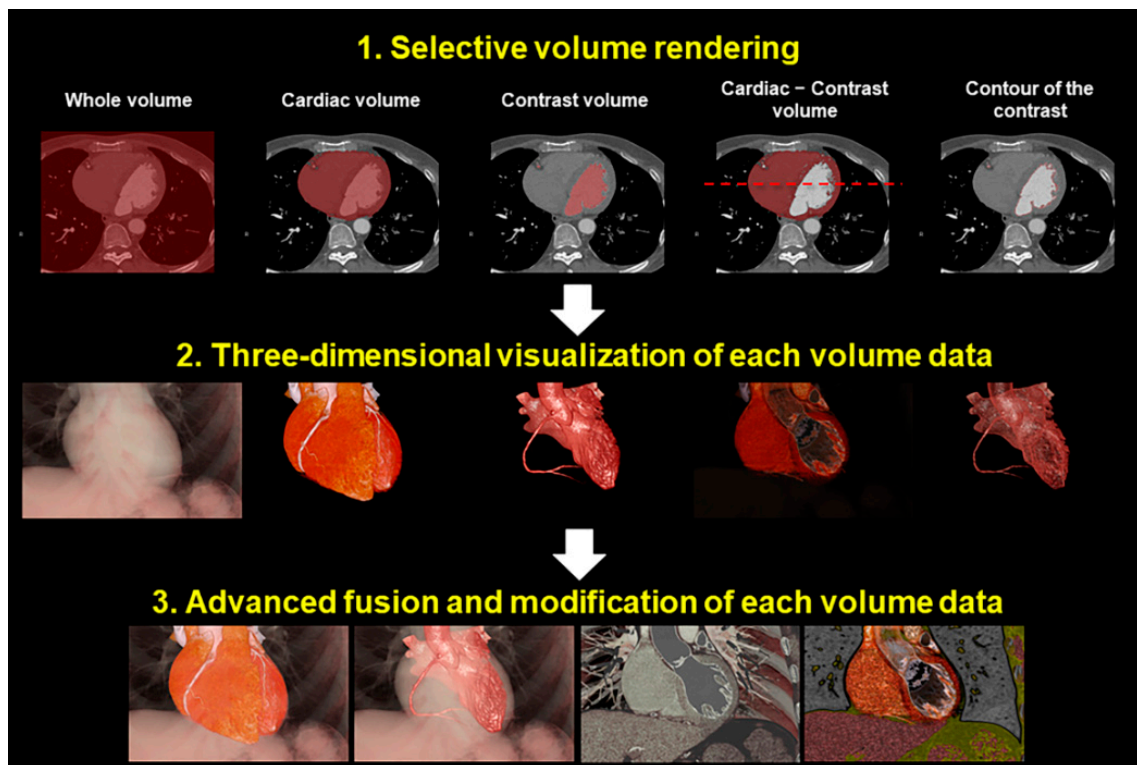


Figure 1. Concept of the image reconstruction. Each volume of interest can be reconstructed separately and can be merged at the reconstructors' disposal.

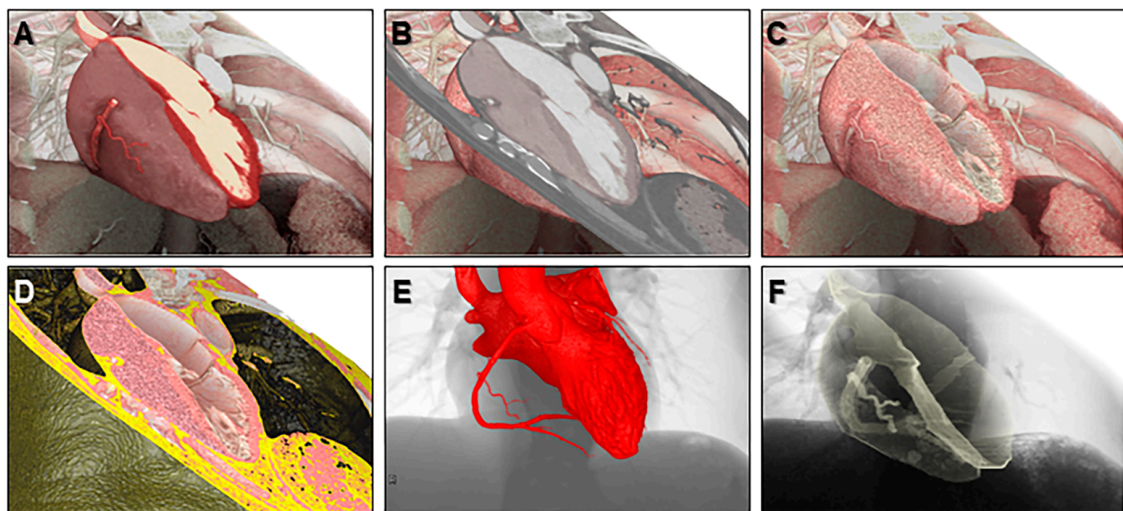


Figure 2. Representative various volume-rendered images reconstructed from a single dataset. We call these volume-rendering techniques 2.5-dimensional imaging (A,B), virtual dissection imaging (C,D), endocast imaging (E), and shell imaging (F).

3. The Advantage of the Virtual Dissection Compared to Conventional Real Dissection

The main advantage of virtual dissection from computed tomographic datasets is that it can provide a high-resolution image of the blood-filled heart without removing it from the thorax (Figure 3). Unlike dissection of the heart specimens, the cut planes during virtual dissection are not fixed and are practically unlimited. Almost any view can be recreated for optimal visualization of the structures of interest as per the need. Each voxel retains its three-dimensional spatial coordinate, allowing the reconstructed image to show the details of living heart anatomy in attitudinally appropriated

fashion [1]. In other words, the right, left, superior, inferior, anterior, and posterior directions are precisely demonstrated, allowing for accurate anatomical education and understanding. This is particularly important in providing relative orientation of cardiac structures with surrounding structures, including the esophagus, trachea and bronchi, lungs, diaphragm, nerves, vertebral column, and thorax itself [1]. Historically, the nomenclature of cardiac anatomy was based on describing the heart in the Valentine position, with the autopsied heart removed from the chest and placed on its apex. While much of this attitudinally incorrect nomenclature has been engrained in the cardiovascular fields, this creates misunderstanding and ambiguity when assessing various cardiovascular structures from common imaging modalities (i.e., angiography, cardiac magnetic resonance and computed tomography, etc.) or by intraoperative assessment with the heart *in vivo* [1,26,27]. Virtual dissection, on the other hand, by permitting constant guidance about relative orientation of the heart enables a similar attitudinally correct understanding of the *in vivo* cardiac anatomy by all members of the medical team. Virtual dissection also avoids the risk of being exposed by the potentially toxic fixatives used for specimen preservation, such as formalin. For these reasons, we believe the technique of virtual dissection from computed tomographic datasets has in many ways surpassed analysis of the autopsied heart as the gold standard for understanding detailed cardiac anatomy.

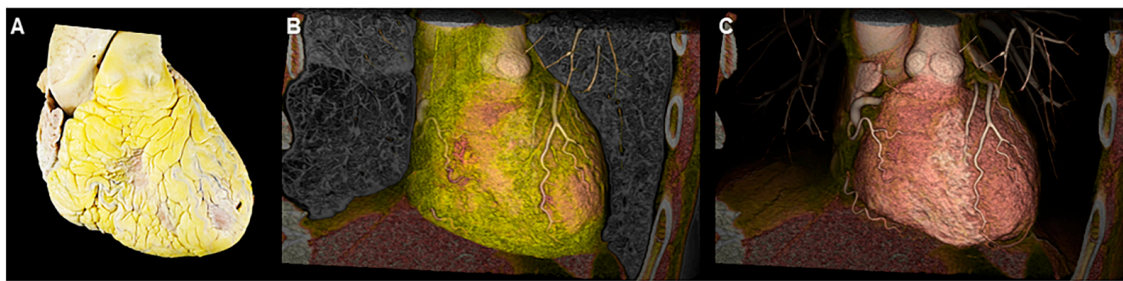


Figure 3. Real dissection (A) and virtual dissection images (B,C). When using virtual dissection images, attitudinal relationships with surrounding structures are maintained with easy modification on images to effectively show the structural anatomy of interest.

4. Educational Implication of the Three-Dimensional Living Heart Anatomy

It is well understood that “form begets function”. Therefore, it is not surprising that the foundation of medical education often begins with instruction in anatomy followed by (patho)physiology. While medical students are taught cardiac anatomy in their first years of medical education, supplemented by cadaveric dissection and inspection, the cardiology and cardiothoracic surgery trainees are often starved of such experiences. This relates to several factors, including the scarcity of preserved heart archives, competing educational requirements in a relatively limited time, and demanding clinical schedules [28–30]. So as to keep and improve the quality of anatomical knowledge, dissection-based teaching alone during medical school has to be complemented with newer teaching/learning methods, based on clinical imaging including computed tomography and magnetic resonance imaging [31–33]. Many cardiology trainees expand upon their knowledge in basic cardiac anatomy by interpretation of two-dimensional imaging modalities, primarily echocardiography. Assessing such a complex three-dimensional organ by two-dimensional means with a narrow field of view is fraught with error [34]. Education in cardiac anatomy using three-dimensional reconstructions has many advantages. There has been interest in using three-dimensional printed models for education albeit with the limitations of availability and costs. On most occasions, the assessment using printed models is also restricted to a singular plane of dissection [35]. Furthermore, similar to the heart specimens, freedom of moving the printed model extracted out of the chest cavity makes the assessment prone to errors. An unnatural tactile feeling of printed models also falls short of the real heart.

While three-dimensional imaging lacks the tactile advantage of the printed model of the heart, an excellent demonstration of cardiac anatomy in attitudinally appropriate orientation makes up for this deficiency to a large extent. Three-dimensional imaging has the potential to serve as the mainstay of imparting knowledge of cardiac anatomy in the absence of heart specimens [1]. Even at centers with a well-maintained archive of heart specimens, virtual dissection has a complementary role in educating students and health professionals. The ease of storing computed tomographic datasets in electronic format with the feasibility of creating endocast and/or virtual dissection images at any time practically immortalizes the anatomic details of any patient (Figures 4–7) [35]. The electronic format also eliminates problems related to sharing of knowledge across institutions which is severely restricted with the use of heart specimens. Figure 8 shows the representative volume-rendered images usually used during routine educational lectures to show the three-dimensional relationship of each anatomical structure in the thorax.

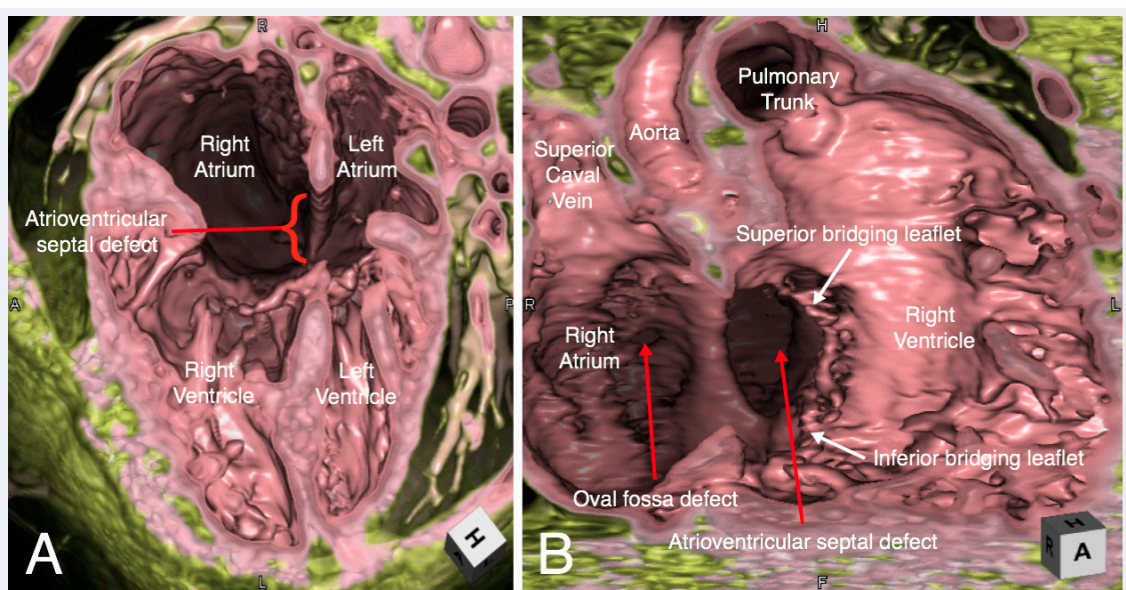


Figure 4. Virtual dissection of an atrioventricular septal defect in four-chamber (Panel A) and right anterior oblique (Panel B) planes. In the right anterior oblique plane (Panel B) the superior and inferior bridging leaflets are seen to have chordal attachments to the crest of the muscular interventricular septum, with small ventricular level shunting between the chordae. There is a large atrial component to the defect. There is additionally a small oval fossa defect.

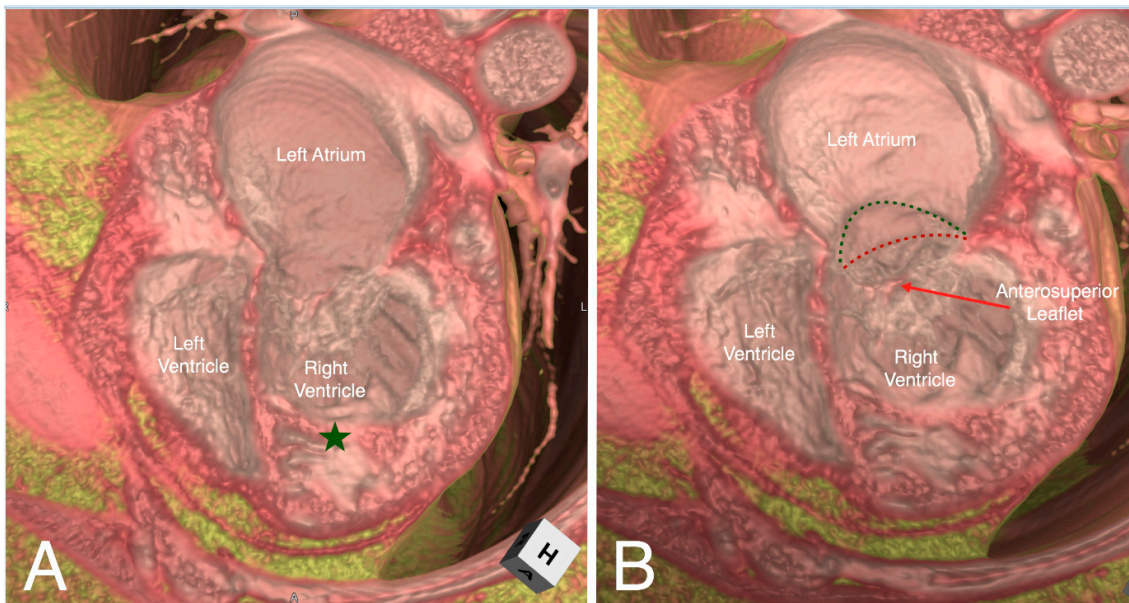


Figure 5. Virtual dissection of a patient with congenitally corrected transposition in a four-chamber plane demonstrating discordant atrioventricular connections with left-hand ventricular topology (Panel A). The moderator band (green star) and septal attachments of the left-sided atrioventricular valve identifies the left-sided ventricle as the morphological right ventricle. Tilting the dissected heart anteriorly and superiorly (Panel B), the hinge points of the septal and inferior tricuspid leaflets (red dashed line) are displaced inferiorly (the green dashed line represents its normal attachment points).

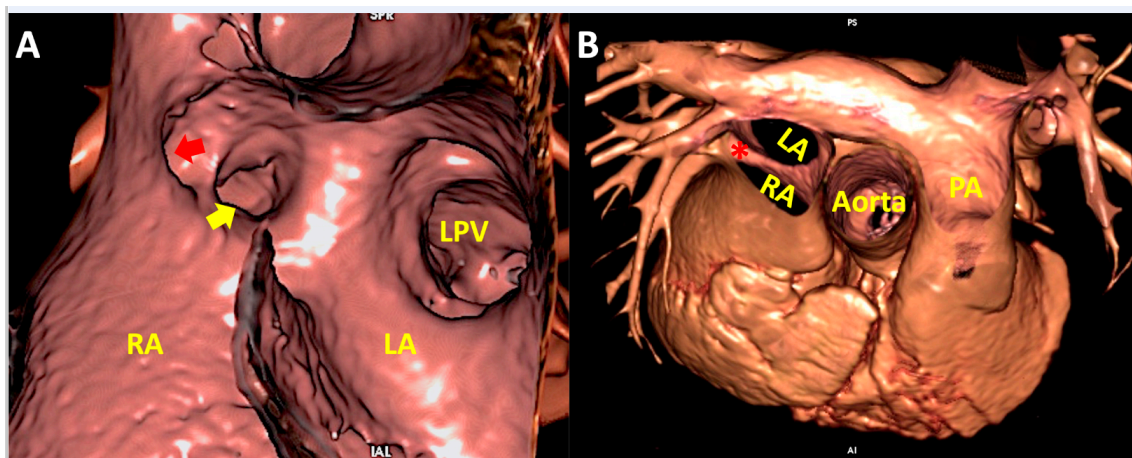


Figure 6. Virtual dissection of a superior sinus venosus interatrial communication in left anterior oblique projection (Panel A) and as viewed from the superior direction (Panel B). Panel A shows extrasseptal location of the defect with anomalous connection of right superior pulmonary vein (red arrow) having retained connection to the left atrium. The right inferior pulmonary vein (yellow arrow) and left pulmonary veins connect normally to the left atrium. Panel B shows overriding of the superior caval vein on the atrial septum (*) when viewed from above. LA—left atrium; LPV—left pulmonary veins; PA—pulmonary artery; RA—right atrium.

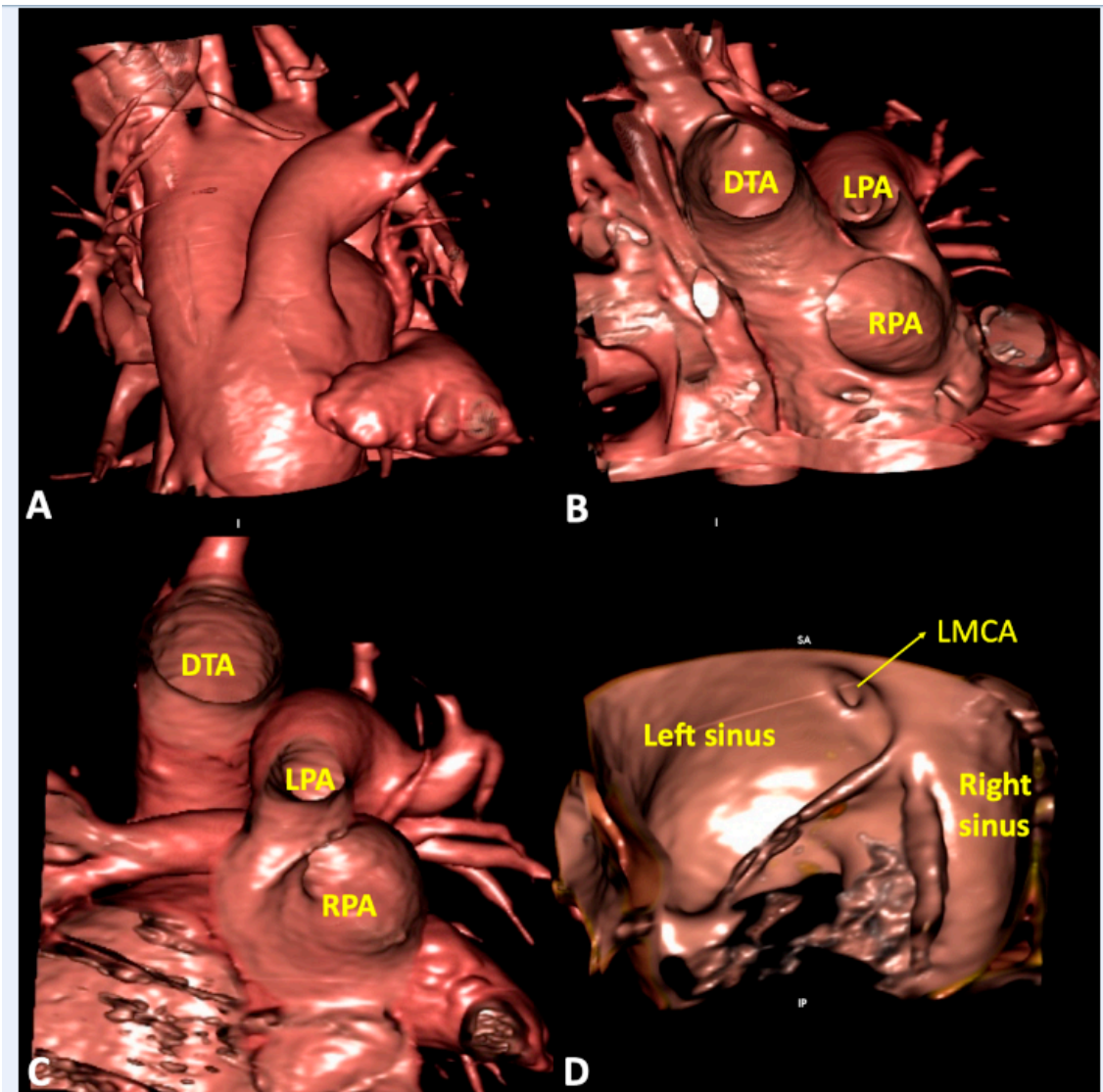


Figure 7. Virtual dissection of patients with common arterial trunk. (Panel A and B) from the same patient shows how it is difficult to clarify common versus separate origin of left and right pulmonary artery based on the external appearance (Panel A). The internal virtual dissection view (Panel B), on the other hand, clearly demonstrates separate origin of the pulmonary arteries. (Panel C) demonstrates crossed pulmonary arteries with the origin of the right pulmonary artery positioned to the left of the left pulmonary artery. (Panel D) shows juxtacommissural origin of left main coronary artery in a patient with bisinusate truncal valve. DTA—descending thoracic aorta; LMCA—left main coronary artery; LPA—left pulmonary artery; RPA—right pulmonary artery.

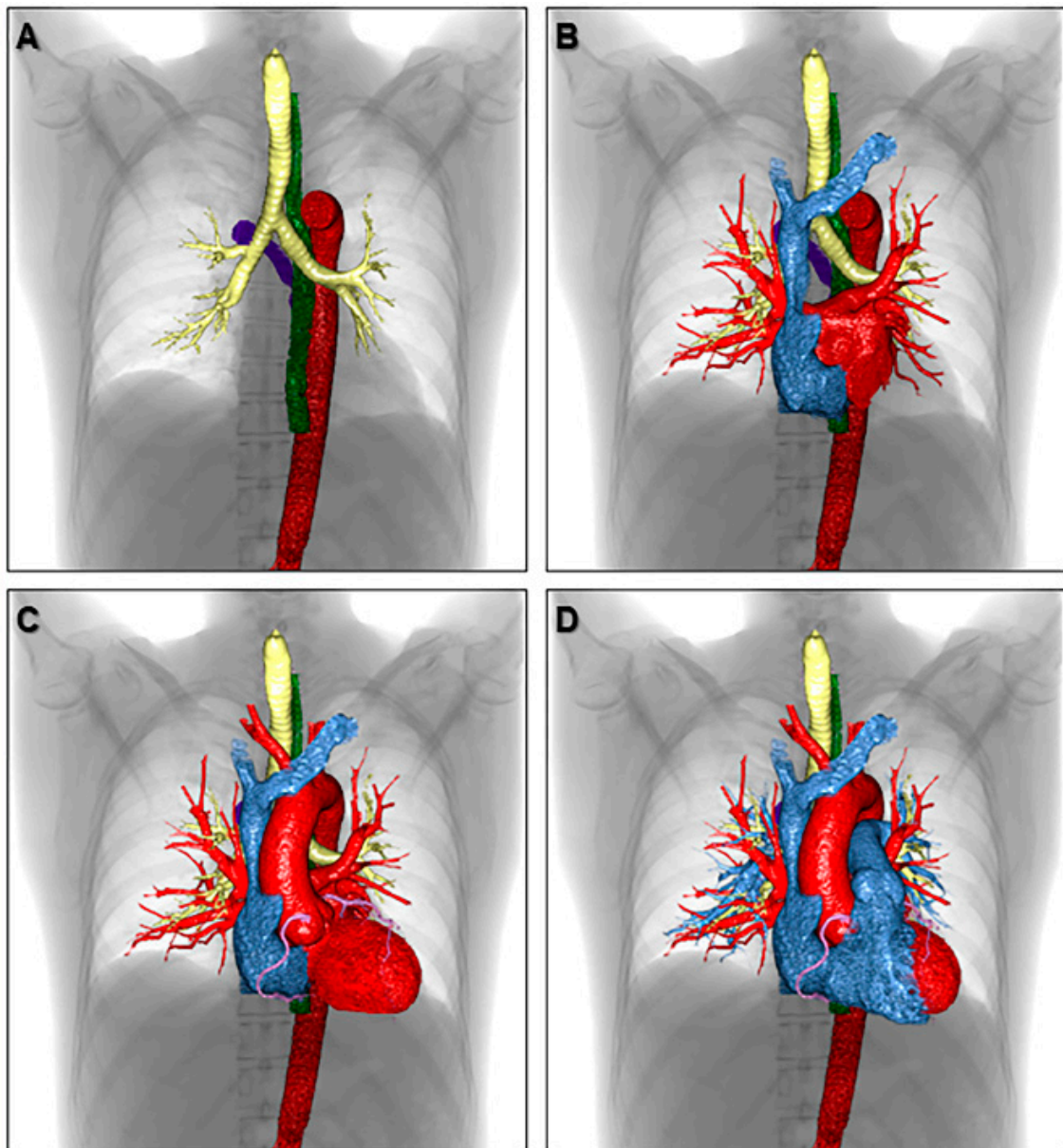


Figure 8. Volume-rendered images showing the three-dimensional relationship of each anatomical structure in the thorax. The azygos vein (purple), descending aorta (red), esophagus (green), trachea, and bronchi (yellow) are shown in panel (A). Both atria are added in panel (B). The left ventricle, aortic root, ascending aorta, aortic arch, and coronary artery are added in panel (C). The right ventricle, pulmonary root, pulmonary trunk, and pulmonary arteries are reconstructed in panel (D) to finalize the components of cardiac silhouette.

5. Clinical Implication in Acquired Heart Disease with Representative Cases

For educational and diagnostic purposes related to the heart, it is not always sufficient to understand only the cardiac anatomy. Often, it is more important to clarify relationships with the adjacent structures in the thoracic cavity [36–38]. Volume-rendered images are useful to relate to abnormal findings in chest radiography in individual cases (Figure 9).

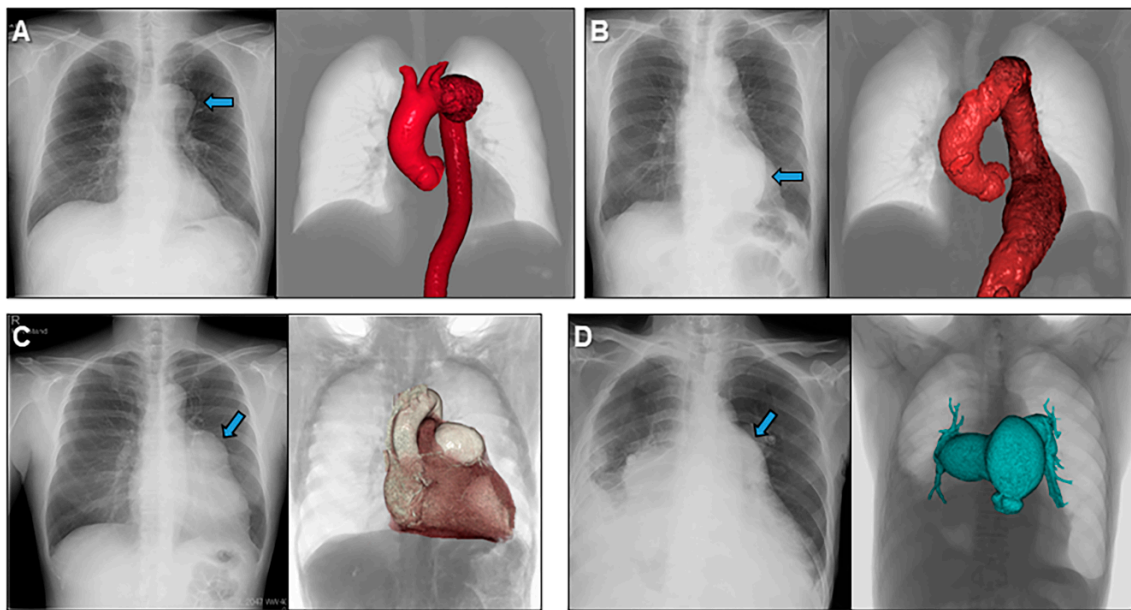


Figure 9. Volume-rendered images to understand abnormal chest radiographies showing a case with aneurysms of the aortic arch (A), descending aorta (B), left coronary artery (C), and pulmonary trunk and pulmonary arteries (D).

For more specific purposes, volume-rendered images, involving both endocast and virtual dissection images, can be also used to educate fluoroscopic anatomy to cardiac interventionists and electrophysiologists as their procedures are commonly performed under fluoroscopic guidance and with angiography (Figure 10). Virtual simulation of the invasive procedure, including electrophysiological study (Figure 11), biventricular pacing [39], radiofrequency catheter ablation, and His-bundle pacing are also feasible. Image demonstration from the surgeon’s view, as well as virtual simulation of the cardiac surgery in preoperative fashion is also feasible with stereoscopic presentation (Figure 12) [40].

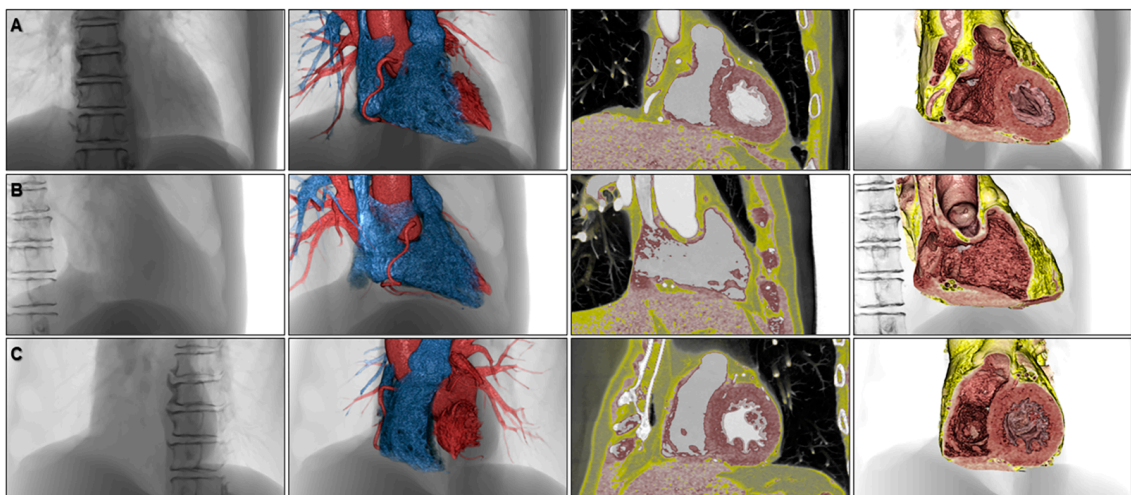


Figure 10. Volume-rendered images to appreciate fluoroscopic anatomy viewed from the frontal (A), right anterior oblique (B), and left anterior oblique (C) directions. The left panels, second left panels, second right panels, and right panels show fluoroscopy-like volume-rendered images, endocast images, 2.5-dimensional images, and virtual dissection images, respectively.

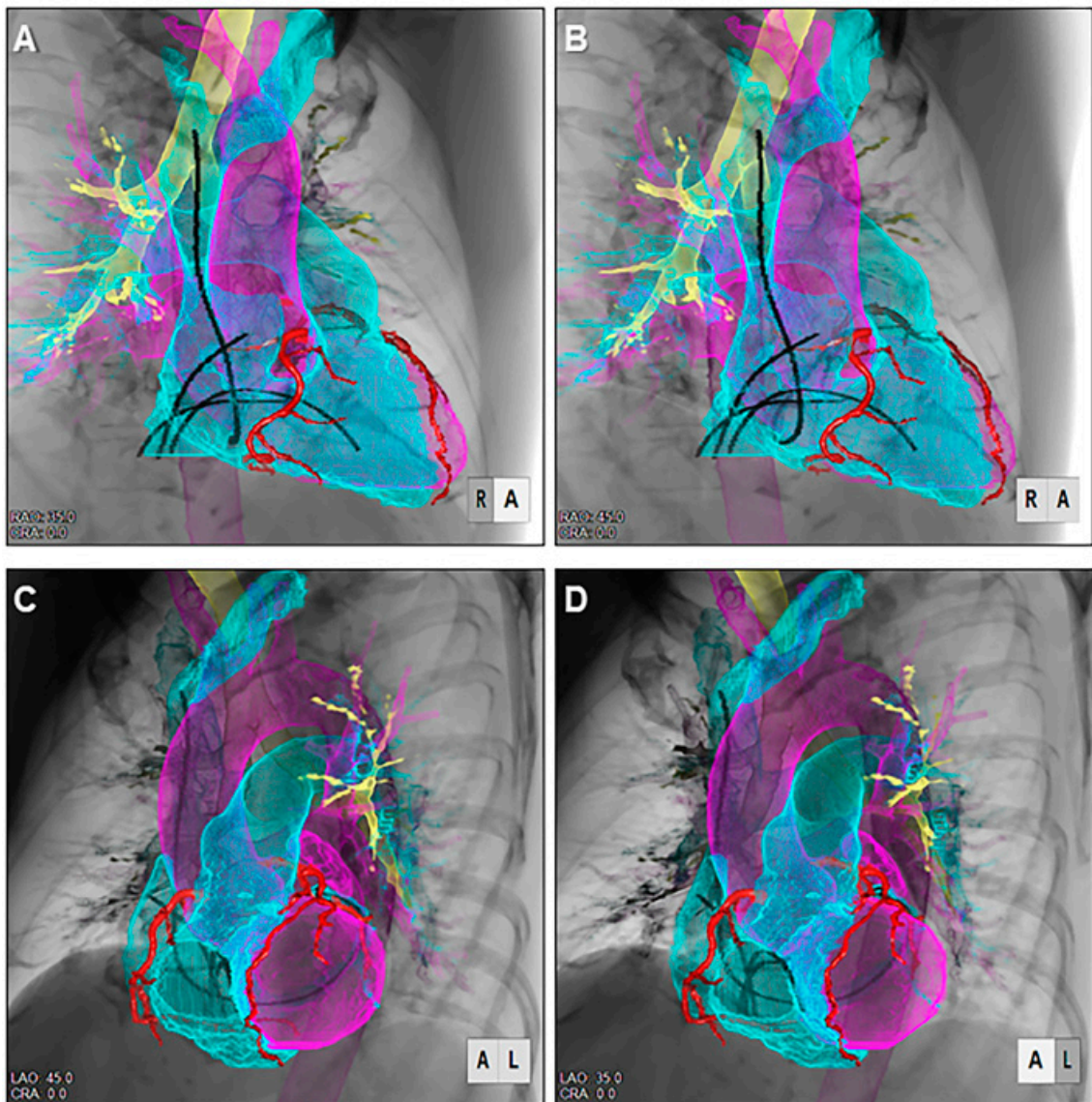


Figure 11. Stereoscopic displays (cross-eyed method) of virtual electrophysiologic catheters placed within the heart reconstructed using shell-imaging technique viewed from the right anterior oblique (A,B) and left anterior oblique (C,D) directions.

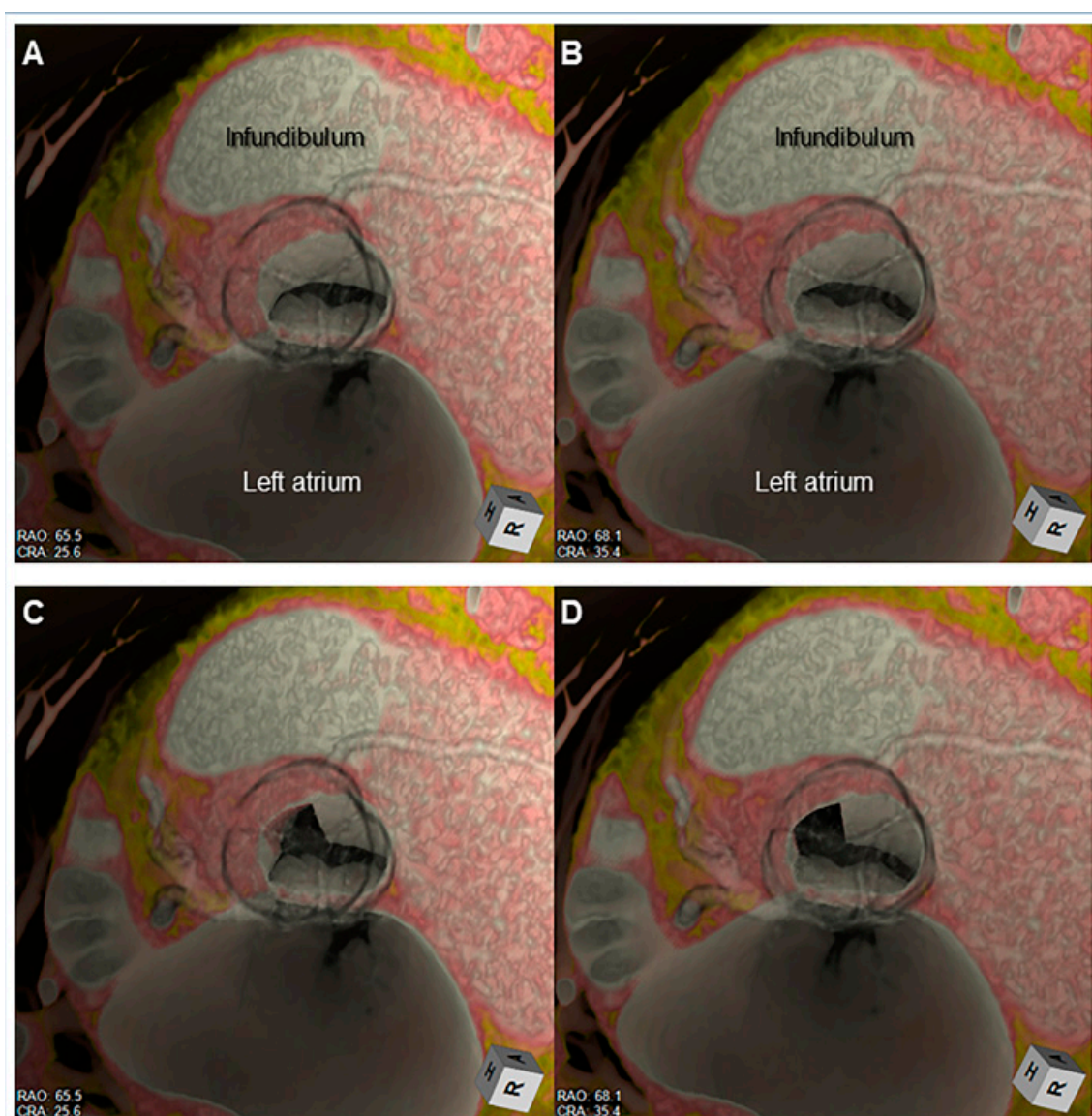


Figure 12. Stereoscopic displays (cross-eyed method) of virtual dissection images demonstrated from the surgeon's view show presurgical virtual simulation of the Morrow's septal myectomy. The hypertrophied septal myocardium located apical to the bottom of the right coronary aortic sinus (A,B) is virtually resected at its left half (C,D).

6. Clinical Implication in Congenital Heart Disease with Representative Cases

Similar applications of three-dimensional reconstructions can be applied towards congenital heart disease. This includes not only in the evaluation of unrepaired congenital heart disease which may involve complex abnormal three-dimensional relationships of chambers and vessels, deficiencies in septation, or abnormalities of atrioventricular or semilunar valves but also in the evaluation of their repaired and palliated forms. A combination of both endocast and virtual dissection images is often beneficial to provide a comprehensive three-dimensional understanding. There is increasing application towards the adult congenital population, given the complexity of evaluating many of their repaired and palliated lesions as well as the common scenario of poor acoustic windows limiting complete echocardiographic evaluation [41].

In addition to cases demonstrated in Figures 4–7, examples of three-dimensional images to guide interventional and surgical management in the congenital heart disease population are illustrated in the following:

- Relationship of the great arteries to an interventricular communication in the setting of double outlet right ventricle for surgical planning (Figure 13);
- Unicuspid aortic valve for surgical repair planning (Figure 14, Supplementary Movie 2);
- Obstruction in surgically constructed pulmonary venous baffles for surgical planning (Figure 15) [16];
- Right ventricular outflow tract obstruction in repaired tetralogy of Fallot to guide transcatheter pulmonary valve replacement (Figure 16).

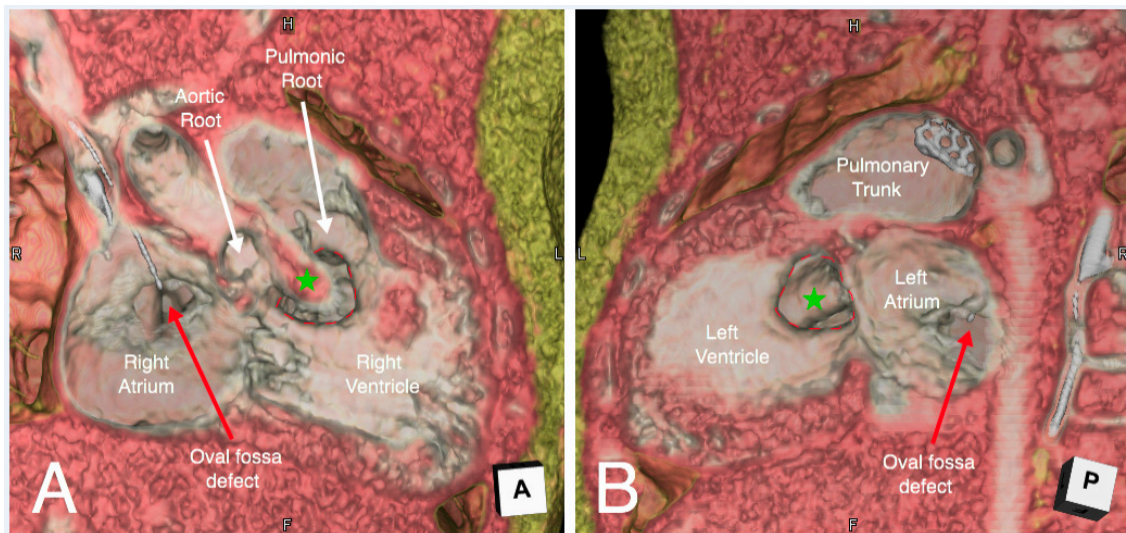


Figure 13. Virtual dissection of a patient with double outlet right ventricle with the interventricular communication (red dashed line) viewed from the right (Panel A) and left side (Panel B). The interventricular communication is doubly committed, bisected by the prominent outlet septum (green star). However, the potential pathway to the relatively larger pulmonary root is larger than that to the small aortic root with subaortic narrowing. There is a stent within the patent arterial duct seen entering the distal pulmonary trunk in this patient with a hypoplastic transverse aortic arch, coarctation of the aorta and ductal-dependent systemic arterial blood flow.

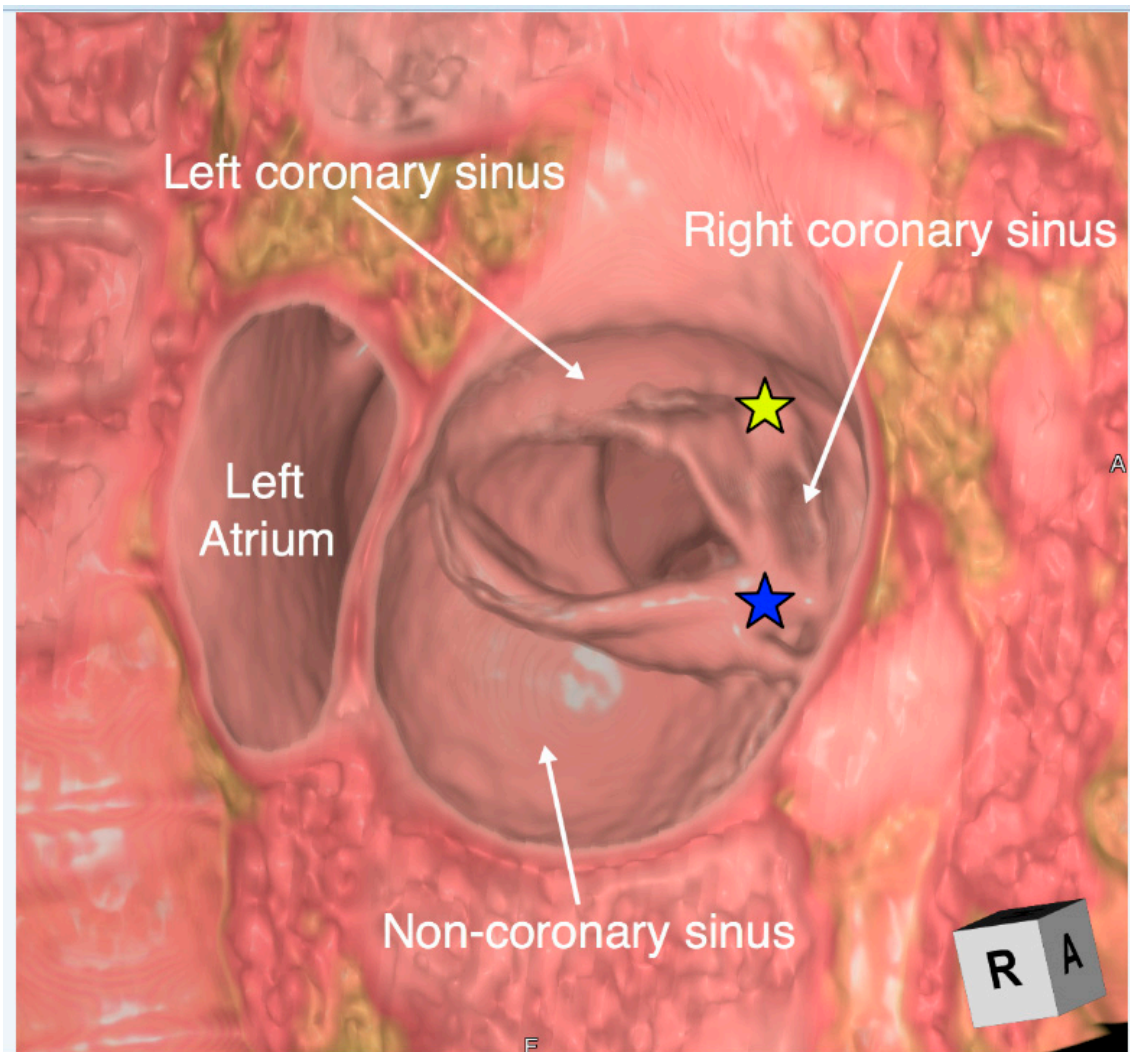


Figure 14. Virtual dissection of a unicuspid and unicommissural aortic valve viewed from the aorta. There is fusion with a raphe between both the right and left coronary leaflets (yellow star) and the right and non-coronary leaflets (blue star). A four-dimensional video is displayed in Supplemental Movie 2.

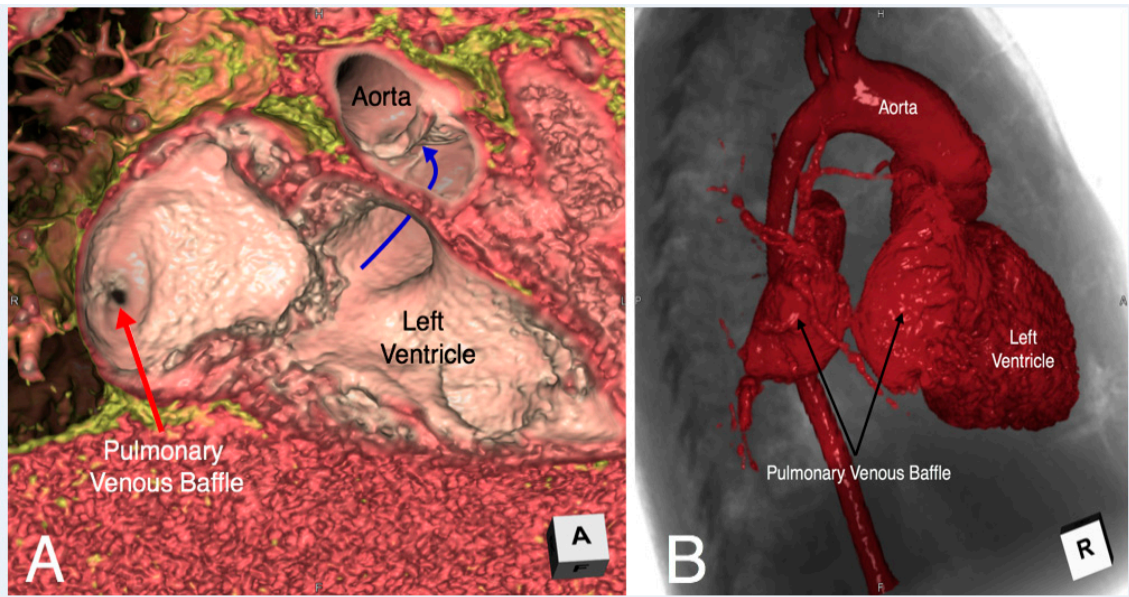


Figure 15. Virtual dissection (Panel A) and endocast reconstruction (Panel B) of a patient with congenitally corrected transposition status post double switch who developed severe obstruction of the pulmonary venous baffle. While the endocast image (Panel B) demonstrates the severe obstruction, it is the virtual dissection image (Panel A) which adds additional insight that the mechanism of obstruction is related to a membrane which has formed obstructing the pulmonary venous baffle.

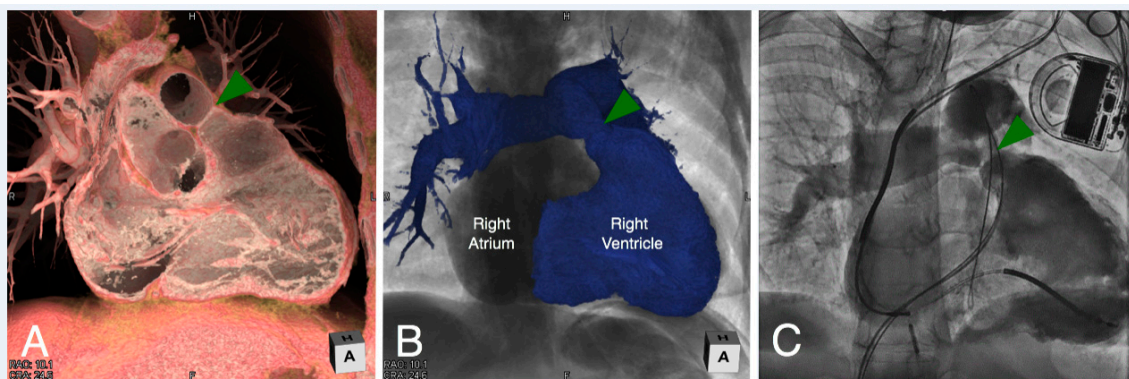


Figure 16. Virtual dissection (Panel A) and endocast reconstruction (Panel B) of a patient with repaired tetralogy of Fallot with moderate right ventricular outflow tract obstruction. Both images are viewed in a right anterior oblique plane. The virtual dissection image (Panel A) demonstrates a discrete ridge at the pulmonary sinutubular junction (green arrowhead). An angiogram was obtained in similar plane (Panel C) during cardiac catheterization confirming the anatomy, prior to placing a transcatheter pulmonary valve to relieve the obstruction.

7. Advanced Application of the Three-Dimensional Imaging

Three-dimensional imaging is currently used to create files for converting the image into three-dimensional printing [42] and virtual reality [33]. The printed model is useful for education as discussed above (Figure 17). Furthermore, it is also useful for surgeons for preoperational recognition of the complex anatomy, especially with the application of procedural simulation [12,43–45], as well as surgical training of the complicated procedures [46]. For this purpose, both endocast and virtual dissection images are used. Virtual reality supports the interactive sharing of the three-dimensional images during the simulated operation and also can guide the invasive procedures and operations, especially in such fields of orthopedics and neurosurgery [47,48]. As the heart is a highly moving

structure, the application of virtual reality into the clinical cardiovascular fields can be challenging. However, many groups are exploring this application [15,45]. Three-dimensional images, when combined with some software which has extended application equivalent to computer aided design, allow customization of the device by virtually simulating its shape and course (Figure 18) [49].

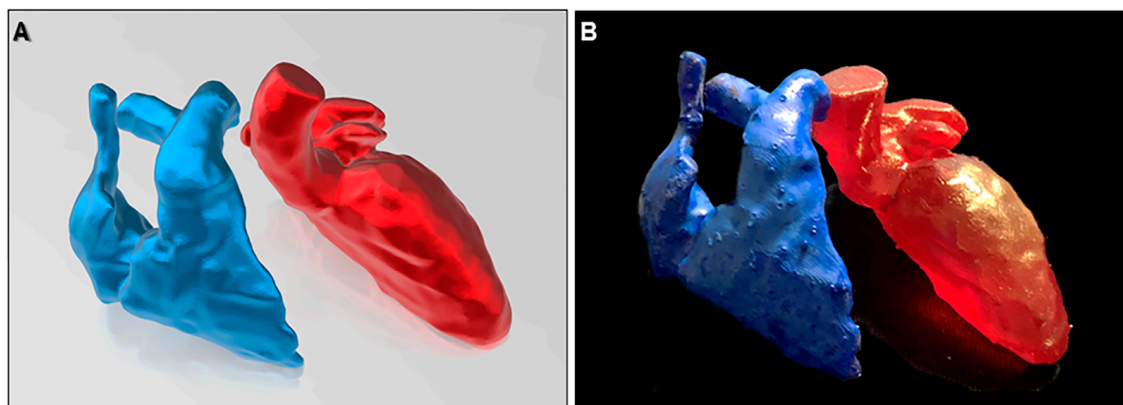


Figure 17. Virtual (A) and real (B) images of three-dimensional printing model of the right and left heart.

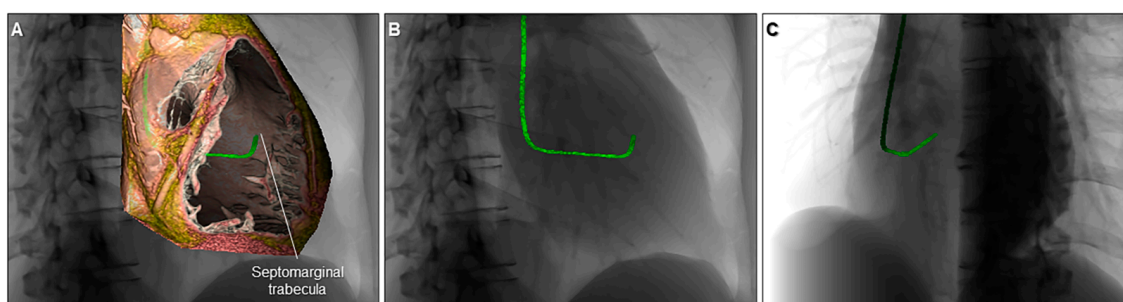


Figure 18. Virtual simulation of the catheter shape appropriate for right ventricular septal pacing visualized within the cardiac silhouette. The right ventricle is cut to show the septomarginal trabecula (A). The three-dimensional shape of the catheter is visualized in relation to the cardiac silhouette viewed from the right anterior oblique (B) and left anterior oblique (C) directions.

There is no doubt three-dimensional printed models and the increasing use of augmented and virtual reality can be extremely useful for education, procedural simulation and planning [12,43–45]. However, in our experience, utilizing the endocast and virtual dissection images on a monitor is often the most optimal strategy in clinical practice to provide a detailed evaluation of three-dimensional cardiac anatomy to support transcatheter and surgical planning while balancing costs and time efficiency [4,11,12,16,50,51]. Three-dimensional images in this paper were reconstructed using commercially available software/workstation (Horos, Pixmeo, Geneva, Switzerland; Ziostation2; Ziosoft, Tokyo, Japan; 3D Builder, Microsoft, Redmond, WA, USA).

Furthermore, for the analysis of cadaveric hearts, three-dimensional imaging plays an important role to clarify three-dimensional arrangement of the myocardial mesh and conduction system using diffusion tensor magnetic resonance imaging and microcomputed tomography [52,53].

8. Limitations of Three-Dimensional Imaging and Importance of Basic Anatomical Knowledge and Multidisciplinary Relationship

When creating three-dimensional images based on the volume-rendering method, it should be always kept in mind that the quality of the final image depends on the quality of the raw data. In this regard, the collaboration of radiologists and radiological technologists is an important prerequisite to

optimize image acquisition with appropriate radiation dose and contrast material [54]. While radiation exposure is a risk that must be weighed when considering alternative imaging options, with improving technology and the ability for minimal radiation exposure with modern scanners, the afforded spatial resolution has prompted increasing use of cardiac computed tomography [55].

The volume-rendered image might not precisely reflect the real anatomy. For example, the visualized anatomy can be enlarged or contracted from the real thing, depending on the software and window level/width applied. Thin or moving structures, such as the floor of the oval fossa (primary septum), membranous septum, and valvar leaflets are sometimes difficult to reconstruct, and can easily be mistaken for a defect. Some software can virtually create structures that are not present, such as vessels, as if it were a part of the real anatomy. Smoothing is commonly applied to some extent, which may distort the original information in the raw data. Therefore, measurements should not be performed on the volume-rendered image but should be measured using two-dimensional multiplanar reconstruction images. This can then be overlaid on the three-dimensional image for an improved understanding of these measurements related to the three-dimensional structure (Figure 19). Thus, to avoid creating images that can potentially mislead clinical judgement, it is paramount for the reconstructor to accurately interpret the anatomy based on the two-dimensional axial data [56]. It is the responsibility of the image creator to firmly visualize what can be seen in the raw data, and to acknowledge any structures which may be inaccurately demonstrated due to poor imaging quality. For this purpose, the most important basis for image reconstruction is the fundamental knowledge based on the real dissection-based anatomy, as we cannot visualize what we did not know [57]. Therefore, even if virtual dissection is considered the gold standard for anatomical analysis, as proposed by Professor Anderson [2], it is his achievements based on dissection-based cardiac anatomy that enables appropriate virtual dissection. Thus, virtual dissection can never completely replace the real dissection, but can surely provide complementary information relevant to educational and clinical management of patients with heart disease. Keeping good communication with radiologists, anatomists, clinical cardiologists, interventionalists, and surgeons is fundamental as these several departments are usually involved in the patient's care. These means of continuous multidisciplinary communication not only positively impact those performing procedures, but with constructive feedback to the imager relating the intraoperative findings to the provided reconstructions, also improve the quality and accuracy of reconstructions.

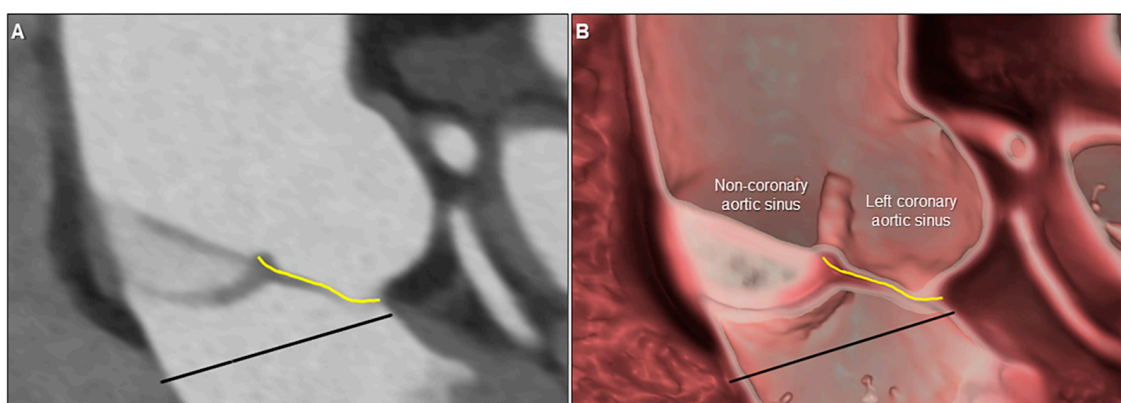


Figure 19. Two-dimensional multiplanar reconstruction (A) and three-dimensional virtual dissection (B) images showing the complicated anatomy of the aortic root. Yellow line and black line indicate geometric height and virtual basal ring plane, respectively. Measurement performed on the two-dimensional image can be projected on the three-dimensional image to secure the accuracy of the virtual dissection images.

9. Conclusions

The obtained three-dimensional data from each patient should be fully utilized to create images to show comprehensible clinical cardiac anatomy critical to the clinical diagnosis and treatment. In this

regard, virtual dissection, a three-dimensional volume-rendering imaging technique, is emerging as the gold standard for understanding detailed cardiac anatomy in the living patient. This technique is useful for both medical education as well as a detailed clinical evaluation of the complex three-dimensional heart, whether demonstrating normal anatomy for educational purposes or evaluating the patient with acquired or congenital heart disease. Any reconstruction depends both on the source imaging data as well as the anatomical understanding of the reconstructor. It is a requirement for radiologists, anatomists, cardiologists, interventionalists and surgeons to keep abreast of the benefits and limitations of these techniques and to fully utilize the three-dimensional anatomical data obtained to optimize patient management and outcomes.

Supplementary Materials: The following are available online at <http://www.mdpi.com/2308-3425/7/3/30/s1>, Supplementary Movie 1. Four-dimensional virtual dissection demonstrating the dynamic motion of the normal mitral valve throughout the cardiac cycle as viewed from the left atrium, Supplementary Movie 2. Four-dimensional virtual dissection demonstrating the dynamic motion of a unicuspid and unicommissural aortic valve. There is fusion with a raphe between both the right and left coronary leaflets and the right and non-coronary leaflets. The labeled image is displayed in Figure 14.

Author Contributions: Conceptualization, J.T.T., S.K.G., and S.M.; data acquisition and reconstruction of pediatric hearts, J.T.T. and S.K.G.; data acquisition and reconstruction of adult hearts, Y.I., T.N., and S.M.; validation, J.T.T., S.K.G., and S.M.; resources, J.T.T., S.K.G., Y.I., T.N., and S.M.; writing—original draft preparation, J.T.T. and S.M.; writing—review and editing, J.T.T., S.K.G., Y.I., T.N., and S.M.; radiological supervision, T.N.; overall supervision, S.M.; final revision and project administration, J.T.T. and S.M. All authors have read and agreed to the published version of the manuscript.

Funding: This research received no external funding.

Conflicts of Interest: The authors declare no conflict of interest.

References

1. Mori, S.; Tretter, J.T.; Spicer, D.E.; Bolender, D.L.; Anderson, R.H. What is the real cardiac anatomy? *Clin. Anat.* **2019**, *32*, 288–309. [CrossRef]
2. Anderson, R.H. Re-Setting the Gold Standard. *J. Cardiovasc. Electrophysiol.* **2015**, *26*, 713–714. [CrossRef]
3. Lin, E.; Alessio, A. What are the basic concepts of temporal, contrast, and spatial resolution in cardiac CT? *J. Cardiovasc. Comput. Tomogr.* **2009**, *3*, 403–408. [CrossRef]
4. Gupta, S.K.; Spicer, D.E.; Anderson, R.H. A new low-cost method of virtual cardiac dissection of computed tomographic datasets. *Ann. Pediatr. Cardiol.* **2019**, *12*, 110–116. [CrossRef]
5. Nagata, K.; Endo, S.; Honda, T.; Yasuda, T.; Hirayama, M.; Takahashi, S.; Kato, T.; Horita, S.; Furuya, K.; Kasai, K.; et al. Accuracy of CT Colonography for Detection of Polypoid and Nonpolypoid Neoplasia by Gastroenterologists and Radiologists: A Nationwide Multicenter Study in Japan. *Am. J. Gastroenterol.* **2017**, *112*, 163–171. [CrossRef]
6. Matsumoto, Y.; Izumo, T.; Sasada, S.; Tsuchida, T.; Ohe, Y. Diagnostic utility of endobronchial ultrasound with a guide sheath under the computed tomography workstation (ziostation) for small peripheral pulmonary lesions. *Clin. Respir. J.* **2017**, *11*, 185–192. [CrossRef]
7. Xu, X.; Zheng, Y.; Yao, S.; Sun, G.; Xu, B.; Chen, X. A low-cost multimodal head-mounted display system for neuroendoscopic surgery. *Brain Behav.* **2018**, *8*. [CrossRef] [PubMed]
8. Clifton, W.; Damon, A.; Valero-Moreno, F.; Nottmeier, E.; Pichelmann, M. The SpineBox: A Freely Available, Open-access, 3D-printed Simulator Design for Lumbar Pedicle Screw Placement. *Cureus* **2020**, *12*. [CrossRef]
9. Wada, K.; Arimoto, H.; Ohkawa, H.; Shirotani, T.; Matsushita, Y.; Takahara, T. Usefulness of preoperative three-dimensional computed tomographic angiography with two-dimensional computed tomographic imaging for rupture point detection of middle cerebral artery aneurysms. *Neurosurgery* **2008**, *62*, 126–132. [CrossRef] [PubMed]
10. Fukuzawa, K.; Nagamatsu, Y.; Mori, S.; Kiuchi, K.; Takami, M.; Izawa, Y.; Konishi, H.; Ichibori, H.; Imada, H.; Hyogo, K.; et al. Percutaneous Pericardiocentesis With the Anterior Approach: Demonstration of the Precise Course with Computed Tomography. *JACC Clin. Electrophysiol.* **2019**, *5*, 730–741. [CrossRef]

11. Steele, J.; Alsaied, T.; Crotty, E.J.; Tretter, J.T. Computed Tomographic 3-Dimensional Virtual Dissection Aiding Surgical Planning in a Rare Pediatric Case of Bicuspid Aortic Valve with Ascending Aorta Pseudoaneurysm. *Circ. Cardiovasc. Imaging* **2020**, *13*. [CrossRef] [PubMed]
12. McGovern, E.M.; Tretter, J.T.; Moore, R.A.; Goldstein, B.H. Simulation to Success: Treatment of a 3D printed heart before complex systemic venous baffle intervention. *JACC Case Rep.* **2020**, *2*, 486–487. [CrossRef]
13. Nishimori, M.; Kiuchi, K.; Mori, S.; Kurose, J.; Izawa, Y.; Kouno, S.; Nakagawa, H.; Shimoyama, S.; Fukuzawa, K.; Hirata, K.I. Atypical inferoseptal accessory pathway connection associated with an aneurysm of the coronary sinus: Insight from a three-dimensional combined image of electroanatomic mapping and computed tomography. *HeartRhythm Case Rep.* **2018**, *4*, 389–392. [CrossRef] [PubMed]
14. Vukicevic, M.; Mosadegh, B.; Min, J.K.; Little, S.H. Cardiac 3D Printing and its Future Directions. *JACC Cardiovasc. Imaging* **2017**, *10*, 171–184. [CrossRef] [PubMed]
15. Silva, J.N.A.; Southworth, M.; Raptis, C.; Silva, J. Emerging Applications of Virtual Reality in Cardiovascular Medicine. *JACC Basic Transl. Sci.* **2018**, *3*, 420–430. [CrossRef] [PubMed]
16. Schneider, K.; Ghaleb, S.; Morales, D.L.S.; Tretter, J.T. Virtual dissection and endocast three-dimensional reconstructions: Maximizing computed tomographic data for procedural planning of an obstructed pulmonary venous baffle. *Cardiol. Young* **2019**, *29*, 1104–1106. [CrossRef]
17. Mori, S.; Spicer, D.E.; Anderson, R.H. Revisiting the Anatomy of the Living Heart. *Circ. J.* **2016**, *80*, 24–33. [CrossRef]
18. Anderson, R.H.; Razavi, R.; Taylor, A.M. Cardiac anatomy revisited. *J. Anat.* **2004**, *205*, 159–177. [CrossRef]
19. Codreanu, A.; Odille, F.; Aliot, E.; Marie, P.Y.; Magnin-Poull, I.; Andronache, M.; Mandry, D.; Djaballah, W.; Régent, D.; Felblinger, J.; et al. Electroanatomic characterization of post-infarct scars comparison with 3-dimensional myocardial scar reconstruction based on magnetic resonance imaging. *J. Am. Coll. Cardiol.* **2008**, *52*, 839–842. [CrossRef]
20. Cochet, H.; Komatsu, Y.; Sacher, F.; Jadidi, A.S.; Scherr, D.; Riffaud, M.; Derval, N.; Shah, A.; Roten, L.; Pascale, P.; et al. Integration of merged delayed-enhanced magnetic resonance imaging and multidetector computed tomography for the guidance of ventricular tachycardia ablation: A pilot study. *J. Cardiovasc. Electrophysiol.* **2013**, *24*, 419–426. [CrossRef]
21. Mori, S.; Nishii, T.; Takaya, T.; Kashio, K.; Kasamatsu, A.; Takamine, S.; Ito, T.; Fujiwara, S.; Kono, A.K.; Hirata, K. Clinical structural anatomy of the inferior pyramidal space reconstructed from the living heart: Three-dimensional visualization using multidetector-row computed tomography. *Clin. Anat.* **2015**, *28*, 878–887. [CrossRef] [PubMed]
22. Mori, S.; Fukuzawa, K.; Takaya, T.; Takamine, S.; Ito, T.; Fujiwara, S.; Nishii, T.; Kono, A.K.; Yoshida, A.; Hirata, K. Clinical Structural Anatomy of the Inferior Pyramidal Space Reconstructed Within the Cardiac Contour Using Multidetector-Row Computed Tomography. *J. Cardiovasc. Electrophysiol.* **2015**, *26*, 705–712. [CrossRef] [PubMed]
23. Mori, S.; Fukuzawa, K.; Takaya, T.; Takamine, S.; Ito, T.; Fujiwara, S.; Nishii, T.; Kono, A.K.; Yoshida, A.; Hirata, K. Clinical cardiac structural anatomy reconstructed within the cardiac contour using multidetector-row computed tomography: Left ventricular outflow tract. *Clin. Anat.* **2016**, *29*, 353–363. [CrossRef] [PubMed]
24. Mori, S.; Fukuzawa, K.; Takaya, T.; Takamine, S.; Ito, T.; Fujiwara, S.; Nishii, T.; Kono, A.K.; Yoshida, A.; Hirata, K. Clinical cardiac structural anatomy reconstructed within the cardiac contour using multidetector-row computed tomography: Atrial septum and ventricular septum. *Clin. Anat.* **2016**, *29*, 342–352. [CrossRef]
25. Mori, S.; Fukuzawa, K.; Takaya, T.; Takamine, S.; Ito, T.; Fujiwara, S.; Nishii, T.; Kono, A.K.; Yoshida, A.; Hirata, K. Clinical cardiac structural anatomy reconstructed within the cardiac contour using multidetector-row computed tomography: The arrangement and location of the cardiac valves. *Clin. Anat.* **2016**, *29*, 364–370. [CrossRef]
26. Anderson, R.H.; Loukas, M. The importance of attitudinally appropriate description of cardiac anatomy. *Clin. Anat.* **2009**, *22*, 47–51. [CrossRef]
27. De Almeida, M.C.; Spicer, D.E.; Anderson, R.H. Why do we break one of the first rules of anatomy when describing the components of the heart? *Clin. Anat.* **2019**, *32*, 585–596. [CrossRef]
28. Ghosh, S.K. Cadaveric dissection as an educational tool for anatomical sciences in the 21st century. *Anat. Sci. Educ.* **2017**, *10*, 286–299. [CrossRef]

29. Ruzyccki, S.M.; Desy, J.R.; Lachman, N.; Wolanskyj-Spinner, A.P. Medical education for millennials: How anatomists are doing it right. *Clin. Anat.* **2019**, *32*, 20–25. [CrossRef]
30. Hołda, M.K.; Stefura, T.; Koziej, M.; Skomarowska, O.; Jasińska, K.A.; Sałabun, W.; Klimek-Piotrowska, W. Alarming decline in recognition of anatomical structures amongst medical students and physicians. *Ann. Anat.* **2019**, *221*, 48–56. [CrossRef]
31. Spitzer, V.M.; Scherzinger, A.L. Virtual anatomy: An anatomist's playground. *Clin. Anat.* **2006**, *19*, 192–203. [CrossRef] [PubMed]
32. Fonseca, C.G.; Backhaus, M.; Bluemke, D.A.; Britten, R.D.; Chung, J.D.; Cowan, B.R.; Dinov, I.D.; Finn, J.P.; Hunter, P.J.; Kadish, A.H.; et al. The Cardiac Atlas Project—An imaging database for computational modeling and statistical atlases of the heart. *Bioinformatics* **2011**, *27*, 2288–2295. [CrossRef] [PubMed]
33. Maresky, H.S.; Oikonomou, A.; Ali, I.; Ditzkofsky, N.; Pakkal, M.; Ballyk, B. Virtual reality and cardiac anatomy: Exploring immersive three-dimensional cardiac imaging, a pilot study in undergraduate medical anatomy education. *Clin. Anat.* **2019**, *32*, 238–243. [CrossRef] [PubMed]
34. Tretter, J.T.; Mori, S. Two-Dimensional Imaging of a Complex Three-Dimensional Structure: Measurements of Aortic Root Dimensions. *J. Am. Soc. Echocardiogr.* **2019**, *32*, 792–794. [CrossRef] [PubMed]
35. Baskar, S.; Gray, S.B.; Del Grippo, E.L.; Osakwe, O.; Powell, A.W.; Tretter, J.T. Cardiac morphology for the millennial cardiology fellow: Nomenclature and advances in morphologic imaging. *Congenit. Heart Dis.* **2018**, *13*, 808–810. [CrossRef]
36. Hasegawa, K.; Takaya, T.; Mori, S.; Ito, T.; Fujiwara, S.; Nishii, T.; Kono, A.K.; Shimoura, H.; Tanaka, H.; Hirata, K.I. Compression of the Right Ventricular Outflow Tract due to Straight Back Syndrome Clarified by Low-dose Dual-source Computed Tomography. *Intern. Med.* **2016**, *55*, 3279–3283. [CrossRef]
37. Ichibori, H.; Mori, S.; Takaya, T.; Kiuchi, K.; Ito, T.; Fujiwara, S.; Fukuzawa, K.; Tatsumi, K.; Tanaka, H.; Nishii, T.; et al. Slit-Like Deformation of the Coronary Sinus Orifice due to Compression of the Inferior Pyramidal Space by the Severely Dilated Left Ventricle. *Pacing Clin. Electrophysiol.* **2016**, *39*, 1026–1029. [CrossRef]
38. Konishi, H.; Mori, S.; Nishii, T.; Izawa, Y.; Tamada, N.; Tanaka, H.; Kiuchi, K.; Fukuzawa, K.; Hirata, K.I. Extracardiac compression of the inferolateral branch of the coronary vein by the descending aorta in a patient with dilated cardiomyopathy. *J. Arrhythm.* **2017**, *33*, 646–648. [CrossRef]
39. Izawa, Y.; Mori, S.; Nishii, T.; Matsuzoe, H.; Imada, H.; Suehiro, H.; Nakayama, K.; Matsumoto, K.; Tanaka, H.; Fujiwara, S.; et al. Optimal image reconstruction using multidetector-row computed tomography to facilitate cardiac resynchronization therapy. *Echocardiography* **2017**, *34*, 1073–1076. [CrossRef]
40. Toh, H.; Mori, S.; Shimoyama, S.; Izawa, Y.; Yokota, S.; Shinkura, Y.; Takeshige, R.; Nagasawa, A.; Soga, F.; Tanaka, H.; et al. Optimal reconstruction of left ventricular outflow tract obstruction before surgical myectomy in a case with hypertrophic obstructive cardiomyopathy. *Echocardiography* **2018**, *35*, 537–540. [CrossRef]
41. Burchill, L.J.; Huang, J.; Tretter, J.T.; Khan, A.M.; Crean, A.M.; Veldtman, G.R.; Kaul, S.; Broberg, C.S. Noninvasive Imaging in Adult Congenital Heart Disease. *Circ. Res.* **2017**, *120*, 995–1014. [CrossRef] [PubMed]
42. Costello, J.P.; Olivieri, L.J.; Krieger, A.; Thabit, O.; Marshall, M.B.; Yoo, S.J.; Kim, P.C.; Jonas, R.A.; Nath, D.S. Utilizing Three-Dimensional Printing Technology to Assess the Feasibility of High-Fidelity Synthetic Ventricular Septal Defect Models for Simulation in Medical Education. *World J. Pediatr. Congenit. Heart Surg.* **2014**, *5*, 421–426. [CrossRef] [PubMed]
43. Bhatla, P.; Tretter, J.T.; Ludomirsky, A.; Argilla, M.; Latson, L.A.; Chakravarti, S., Jr.; Barker, P.C.; Yoo, S.J.; McElhinney, D.B.; Wake, N.; et al. Utility and Scope of Rapid Prototyping in Patients with Complex Muscular Ventricular Septal Defects or Double-Outlet Right Ventricle: Does it Alter Management Decisions? *Pediatr. Cardiol.* **2017**, *38*, 103–114. [CrossRef] [PubMed]
44. Bhatla, P.; Tretter, J.T.; Chikkabyrappa, S.; Chakravarti, S.; Mosca, R.S. Surgical planning for a complex double-outlet right ventricle using 3D printing. *Echocardiography* **2017**, *34*, 802–804. [CrossRef]
45. Moore, R.A.; Riggs, K.W.; Kourtidou, S.; Schneider, K.; Szugye, N.; Troja, W.; D'Souza, G.; Rattan, M.; Bryant, R.; Taylor, M.D., III; et al. Three-dimensional printing and virtual surgery for congenital heart procedural planning. *Birth Defects Res.* **2018**, *110*, 1082–1090. [CrossRef]
46. Yoo, S.J.; Spray, T.; Austin, E.H.; Yun, T.J., III; van Arsdell, G.S. Hands-on surgical training of congenital heart surgery using 3-dimensional print models. *J. Thorac. Cardiovasc. Surg.* **2017**, *153*, 1530–1540. [CrossRef]

47. Jud, L.; Fotouhi, J.; Andronic, O.; Aichmair, A.; Osgood, G.; Navab, N.; Farshad, M. Applicability of augmented reality in orthopedic surgery—A systematic review. *BMC Musculoskelet. Disord.* **2020**, *21*, 103. [CrossRef]
48. Elmi-Terander, A.; Burström, G.; Nachabé, R.; Fagerlund, M.; Ståhl, F.; Charalampidis, A.; Edström, E.; Gerdhem, P. Augmented reality navigation with intraoperative 3D imaging vs. fluoroscopy-assisted free-hand surgery for spine fixation surgery: A matched-control study comparing accuracy. *Sci. Rep.* **2020**, *10*, 707. [CrossRef]
49. Kasamatsu, A.; Takaya, T.; Mori, S.; Kashio, K.; Takahashi, H.; Ito, T.; Takamine, S.; Fujiwara, S.; Nishii, T.; Kono, A.K.; et al. Reconstruction of an extracardiac aortocoronary collateral and simulation of selective angiography with multidetector-row computed tomography. *Circulation* **2015**, *131*, 476–479. [CrossRef]
50. Gupta, S.K.; Anderson, R.H. Virtual dissection: An alternative to surface-rendered virtual three-dimensional cardiac model. *Ann. Pediatr. Cardiol.* **2020**, *13*, 102–103. [CrossRef]
51. Sachdeva, S.; Gupta, S.K. Imaging Modalities in Congenital Heart Disease. *Indian J. Pediatr.* **2020**, *87*, 385–397. [CrossRef] [PubMed]
52. Stephenson, R.S.; Agger, P.; Omann, C.; Sanchez-Quintana, D.; Jarvis, J.C.; Anderson, R.H. Resolving the True Ventricular Mural Architecture. *J. Cardiovasc. Dev. Dis.* **2018**, *5*, 34. [CrossRef] [PubMed]
53. Stephenson, R.S.; Atkinson, A.; Kottas, P.; Perde, F.; Jafarzadeh, F.; Bateman, M.; Iaizzo, P.A.; Zhao, J.; Zhang, H.; Anderson, R.H.; et al. High resolution 3-Dimensional imaging of the human cardiac conduction system from microanatomy to mathematical modeling. *Sci. Rep.* **2017**, *7*, 7188. [CrossRef] [PubMed]
54. Nishii, T.; Watanabe, Y.; Shimoyama, S.; Kono, A.K.; Sofue, K.; Mori, S.; Takahashi, S.; Sugimura, K. Tailored Duration of Contrast Material Injection in High-Pitch Computed Tomographic Aortography With a Double-Level Test Bolus Method. *Invest. Radiol.* **2017**, *52*, 274–280. [CrossRef]
55. Han, B.K.; Rigsby, C.K.; Hlavacek, A.; Leipsic, J.; Nicol, E.D.; Siegel, M.J.; Bardo, D.; Abbara, S.; Ghoshhajra, B.; Lesser, J.R.; et al. Computed Tomography Imaging in Patients with Congenital Heart Disease Part I: Rationale and Utility. An Expert Consensus Document of the Society of Cardiovascular Computed Tomography (SCCT): Endorsed by the Society of Pediatric Radiology (SPR) and the North American Society of Cardiac Imaging (NASCI). *J. Cardiovasc. Comput. Tomogr.* **2015**, *9*, 475–492.
56. Anderson, R.H.; Bolender, D.; Mori, S.; Tretter, J.T. Virtual Reality Perhaps, but Is this Real Cardiac Anatomy? *Clin. Anat.* **2019**, *32*, 468. [CrossRef]
57. Bradfield, J.S.; Fujimura, O.; Boyle, N.G.; Shivkumar, K. Catheter ablation in the vicinity of the proximal conduction system: Your eyes cannot see what your mind does not know. *Heart Rhythm* **2019**, *16*, 378–379. [CrossRef]



© 2020 by the authors. Licensee MDPI, Basel, Switzerland. This article is an open access article distributed under the terms and conditions of the Creative Commons Attribution (CC BY) license (<http://creativecommons.org/licenses/by/4.0/>).

Review

Assessing Myocardial Architecture: The Challenges and Controversies

Peter Agger^{1,2,*†} and Robert S. Stephenson^{3,†} 

¹ Comparative Medicine Lab, Department of Clinical Medicine, Aarhus University, 8220 Aarhus N, Denmark

² Department of Pediatrics, Randers Regional Hospital, Skovlyvej 15, 8930 Randers NE, Denmark

³ Institute of Clinical Sciences, College of Medical and Dental Sciences, University of Birmingham, Birmingham B15 2TT, UK; r.s.stephenson@bham.ac.uk

* Correspondence: peter.agger@clin.au.dk

† These authors contributed equally to this work.

Received: 31 August 2020; Accepted: 8 October 2020; Published: 29 October 2020

Abstract: In recent decades, investigators have strived to describe and quantify the orientation of the cardiac myocytes in an attempt to classify their arrangement in healthy and diseased hearts. There are, however, striking differences between the investigations from both a technical and methodological standpoint, thus limiting their comparability and impeding the drawing of appropriate physiological conclusions from the structural assessments. This review aims to elucidate these differences, and to propose guidance to establish methodological consensus in the field. The review outlines the theory behind myocyte orientation analysis, and importantly has identified pronounced differences in the definitions of otherwise widely accepted concepts of myocytic orientation. Based on the findings, recommendations are made for the future design of studies in the field of myocardial morphology. It is emphasised that projection of myocyte orientations, before quantification of their angulation, introduces considerable bias, and that angles should be assessed relative to the epicardial curvature. The transmural orientation of the cardiomyocytes should also not be neglected, as it is an important determinant of cardiac function. Finally, there is considerable disagreement in the literature as to how the orientation of myocardial aggregates should be assessed, but to do so in a mathematically meaningful way, the normal vector of the aggregate plane should be utilised.

Keywords: review; diffusion tensor imaging; micro computed tomography; heart; methodology; myocyte orientation; myocardial aggregation

1. Background

Myocardial architecture and cardiac function are closely linked [1–7]. Hence, the anatomy of the heart and the cellular construction of the myocardium has been the focus of research for centuries [8]. Traditionally, histology has been the method of choice [9–11], but owing to its two-dimensional nature, this technique fails to visualise the myocardial mass in its entirety. It has long been recognised that the myocardium is a highly complex three-dimensional syncytium [12,13], thus it is preferable to investigate its architecture using tools capable of representing this three-dimensionality. Such tools have been provided in the shape of diffusion tensor imaging [14,15], computed tomography [16–18], confocal microscopy [19] and ultrasound [20], with diffusion tensor imaging and computed tomography being the most prevalent and valid methods for quantifying myocardial architecture in three dimensions.

Since the beginning of the 1990s, diffusion tensor magnetic resonance imaging has been extensively used in the experimental setting to characterise myocardial architecture in both autopsied [21] and beating hearts [22]. Even though several independent groups have used this imaging technique for more than 20 years, there is still no consensus on the appearance of the myocardial microstructure, the way

in which we quantify the orientation of the cells, nor on interpretations relative to physiology and pathology [7]. The main principle behind quantification of myocardial architecture is the measurement of cardiomyocyte orientation. The cardiomyocytes are elongated cells measuring approximately 100 by 20 by 20 microns, and the overall goal is to assess the orientation of their long axis, as this is the main direction of force transmission. Diffusion tensor imaging achieves this by quantifying the direction and magnitude of Brownian motion of water molecules, that is the spontaneous diffusion occurring in both viable and fixed tissues [15]. In short, the result is presented as a three-dimensional mathematical construct called a tensor, the dimensions of which reflect the likely pattern of diffusion, itself a validated surrogate of the myocyte orientation (Figure 1). Likewise, computed tomography describes the myocardial morphology by the use of a tensor, but in this case the tensor is calculated by variations in x-ray attenuation within the tissue, where the direction of least difference is deemed to represent the longitudinal course of the myocyte chains. Consequently, this is referred to as a “structure tensor” rather than a “diffusion tensor” [18,23].

In general, a tensor is described using its three orthogonal axes. These are called eigenvectors, which are designated as being primary (e_1), secondary (e_2), and tertiary (e_3). A complete mathematical description of a tensor is beyond the scope of this paper, but the interested reader is advised to consult specific literature dedicated to this matter [24]. To avoid confusion, it is important to note that owing to the underlying mathematical principles of tensor calculation, the long axis of the cardiomyocytes corresponds with the primary eigenvector in the diffusion tensor. Whilst in the structure tensor, the tertiary eigenvector aligns with the cardiomyocytes’ long axes [25,26]. The subsequent mathematical determination of myocyte orientation is identical for the two techniques. It has been rightfully argued that the main drawback of diffusion tensor imaging is its inability to assess the anatomy directly, instead using the spontaneous diffusion of water as a surrogate measure of the myocyte orientation [27]. Conversely, computed tomography, together with high-resolution conventional magnetic resonance imaging, provides the opportunity to evaluate the myocardial architecture based on tracking of actual anatomical features or “structures” [17,18]. This is an obvious advantage of computed tomography, but diffusion tensor imaging also holds important advantages. First of all, it is the only technique that currently holds potential as a clinical tool [28], and secondly it is the only validated and widely used methodology for assessing the orientation of the myocardial aggregates [7,17,29,30].

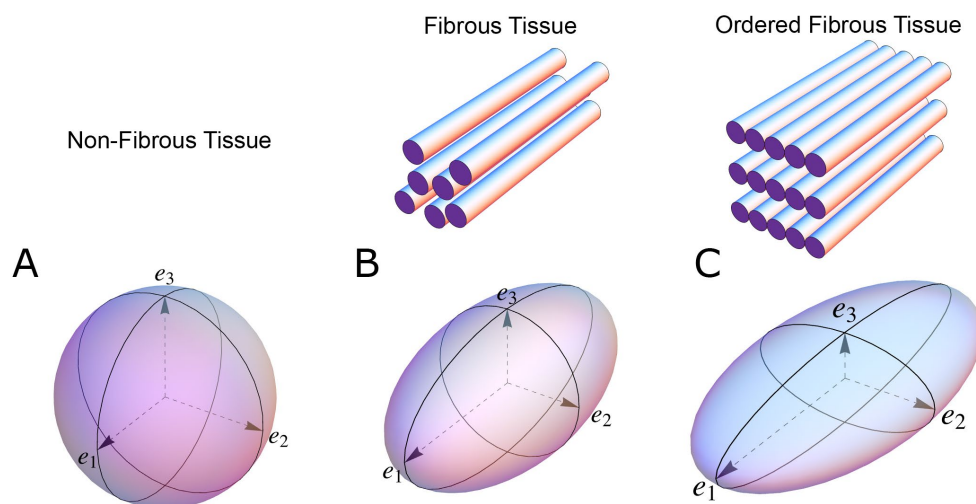


Figure 1. The shape of the diffusion tensor in different tissue environments. (A) Showing that all eigenvectors have equal magnitude in non-fibrous tissue resulting in a spherical shaped diffusion tensor. (B) Showing how, in fibrous tissue, the diffusion tensor takes on an ellipsoid shape when the magnitude of the primary eigenvector (e_1) increases relative to the secondary eigenvector (e_2) and tertiary eigenvector (e_3). (C) In ordered tissue, the diffusion tensor can take on a flattened ellipsoid shape whereby the secondary eigenvector (e_2) has a larger magnitude than the tertiary eigenvector (e_3).

To understand why this is the case, we need to dig a little deeper into the concepts of tissue diffusion. In an environment without cell membranes and other diffusion boundaries, the water molecules are equally likely to diffuse in all directions, thus the diffusion tensor assumes the shape of a sphere (Figure 1A). In biological tissues, whether within a cell or in the surrounding extracellular matrix, diffusion will be hindered mainly by the hydrophobic cell membranes. In tissues consisting of non-isotropic cells, such as in the brain or in muscles, the water diffuses most easily along the long axis of the cells. If the cells are grouped in common directional alignment, the tensor becomes an ellipsoid, with its long axis in the same direction as the common cellular long axis (Figure 1B). This configuration is typified by skeletal muscle, and by the long axonal tracts of the nervous system, particularly the spinal cord [31]. If the cells are also grouped into secondary substructures of reasonably regular shape, the signal from the extracellular water might cause differences in the magnitude of the secondary and tertiary eigenvectors. This is particularly the case when the cells are arranged so as to compartmentalise themselves in laminar fashion. As the myocytes in the laminar structure are aggregated tightly together, the water molecules are more likely to diffuse across this structure than through it. Thus, the secondary eigenvector will align with the plane of the laminar substructure, as this is the direction of greatest diffusion magnitude orthogonal to the primary eigenvector. Consequently, the diffusion tensor will assume a more flattened ellipsoid shape (Figure 1C). It is now well established that, in the myocardium, the primary eigenvector of the diffusion tensor follows the orientation of the chains of cardiomyocytes [21,32–35]. It has then been suggested that the secondary eigenvector follows the surface of the flattened groupings of cardiomyocytes, often described as myocardial sheets [32], laminae [9], sheetlets [36], lamellae [37], lamellar units [7,38] or aggregated units of cardiomyocytes [30]. This disagreement in nomenclature can be attributed to the current lack of a suitable three-dimensional anatomical description of these sub-structures. It is inherently difficult to assign a suitable name to a structure whose anatomical extent is unknown. Given our knowledge of their structural heterogeneity in size and thickness, we believe “myocardial aggregates”, as a name, currently provides the most suitable denomination. It was LeGrice and co-workers [39] who originally posited the existence of myocardial aggregates using electron microscopy. Computed tomography [8], confocal microscopy [19], ultrasound [40], and even photographically based methods [41], have also been used to evaluate the micro-anatomical features of the myocardial aggregates. None of these methods, however, can assess the aggregate normal vector, which we believe is key to calculating the precise orientation of the myocardial aggregates. To date, the normal of the myocardial aggregations has been assessed using diffusion tensor imaging [4], structure tensor calculation [42] and conventional histology [11]. Despite this, the most prominent approach is to assess myocardial aggregate orientation using the in-plane secondary eigenvector, which we claim is not founded in mathematical theory.

Many investigators are now exploring the remodelling of myocyte orientation in disease, with results now emerging characterising changes in hypertrophic and dilated cardiomyopathies, and congenital malformations [16,26,43–45]. This has led to the desire to explore the prognostic and diagnostic potential of myocyte orientation analysis [28], thus knowledge of its technical limitations and methodological inconsistencies is paramount. This review will discuss the variability and validity of current practices in the field and propose guidance to establish methodological consensus in the field.

2. Assessing Myocardial Architecture

2.1. Establishing Reference Points

In order to describe the orientation of the chains of cardiomyocytes, it is agreed that unique points of reference are needed. There is general agreement in the published literature that, in the first instance, the global orientation of the heart itself should be described using the left ventricular long axis. This is usually achieved by placing a line between the apex and the fibrous continuity between the leaflets of the aortic and mitral valves [39,45–47]. An alternative approach is to interpolate a line between the centres of the ventricular cavity in a series of short axis images [25,48–51]. The left ventricular long axis,

along with two orthogonal radial vectors (e_{R1} and e_{R2}), then provides the global geometric coordinate system for defining the position of the heart (Figure 2A). In some studies, these are the only points of reference used when assessing myocytic orientation [51–53]. Systolic mural thickening, however, which is the main rearrangement of the myocardium through the cardiac cycle, predominantly occurs relative to a radial axis at right angles to the epicardium [54]. Hence, it makes sense physiologically that angles be assessed relative to the epicardial tangential plane (Figure 3), as this provides the most relevant information concerning cardiodynamics [17,25]. Therefore, once the orientation of the left ventricle is established using the left ventricular long axis (e_{ax}), a second local coordinate system should be introduced, which can be positioned relative to the individual region of interest in the heart (Figure 2B). On this basis, one can propose three orthogonal vectors, which can be considered as being longitudinal (e_l), circumferential (e_c), and radial (e_r). The circumferential vector is orthogonal to the left ventricular long axis, and tangential to the epicardium. The longitudinal vector is orthogonal to the circumferential vector, and again tangential to the epicardium. The radial vector is orthogonal to both the longitudinal and circumferential vectors. It is also normal to the epicardium, or more accurately normal to the epicardial tangential plane [55] (Figure 2B). For the sake of ease of analyses, these three vectors of the local coordinate system are translated into three planes of reference (Figure 4). In Figure 4 the epicardial tangential plane (A) is defined by the longitudinal and the circumferential vectors (e_l and e_c), while the circumferential and radial vectors (e_c and e_r) define the local horizontal plane (C). The radial and the longitudinal vectors (e_r and e_l) define the local sagittal plane (B).

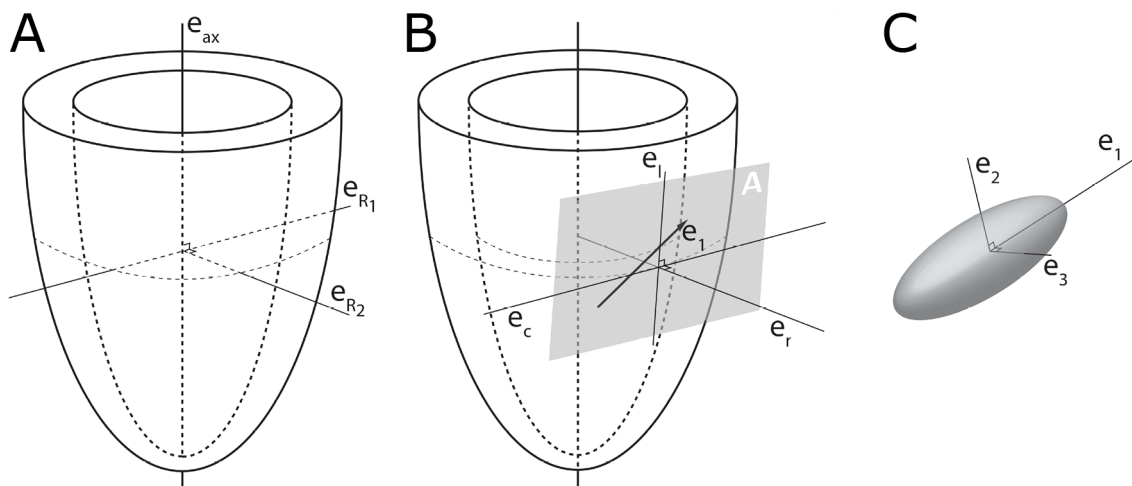


Figure 2. Establishment of the reference planes. (A) Illustrates the global geometric coordinate system defining the position of the left ventricle. It is defined by the orthonormal basis $[\vec{e}_{ax}, \vec{e}_{R1}, \vec{e}_{R2}]$ where \vec{e}_{ax} is the left ventricular long axis and \vec{e}_{R1} and \vec{e}_{R2} being orthogonal radial vectors, which are not used in the determination of myocyte orientations. (B) Subsequently, the local wall coordinate system is defined based on the orthonormal basis $[\vec{e}_r, \vec{e}_c, \vec{e}_l]$, where \vec{e}_r is the local radial vector, i.e., the normal of the epicardial tangential plane A, \vec{e}_l is the local longitudinal vector, i.e., the normal of the local horizontal plane, and lastly \vec{e}_c is the local circumferential vector. (C) Finally, the diffusion tensor is defined by a sub-local coordinate system based on the orthonormal bases $[\vec{e}_1, \vec{e}_2, \vec{e}_3]$, which are the three eigenvectors. Modified from [25].

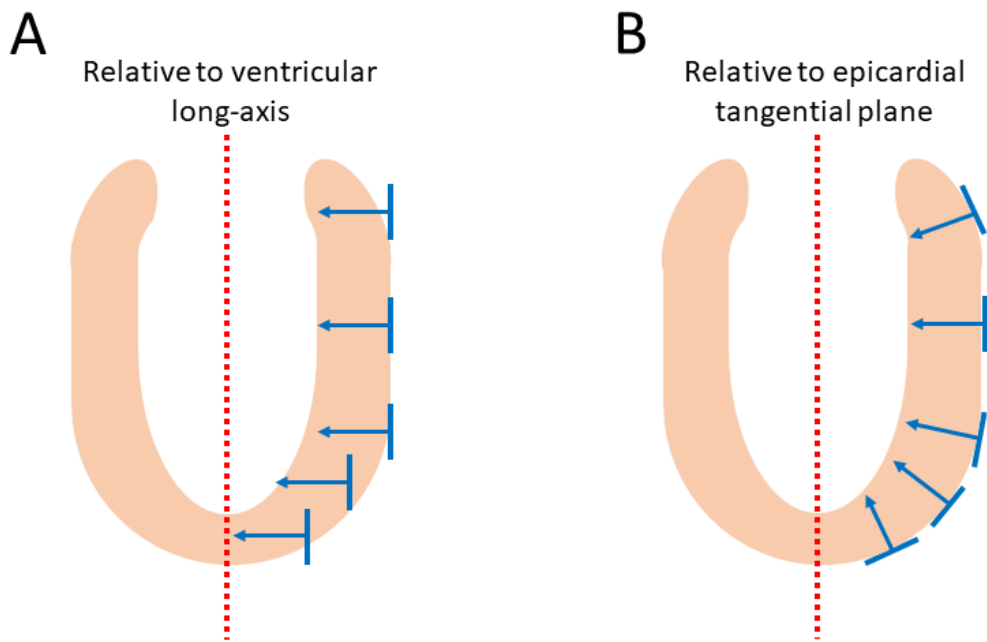


Figure 3. Epicardial wall normalisation. Schematic illustration of the influence of epicardial curvature on the quantification of myocyte orientation. The figure shows how myocyte orientation can be assessed either relative of the left ventricular long axis (A) or the epicardial tangential plane (B). Owing to the rounded shape of the ventricular cavities, the myocardial contractile forces work perpendicular to the epicardial surface. Therefore, to measure myocyte orientation accurately throughout the entire myocardium, we should quantify relative to the epicardial curvature (B). If we assess myocytes orientation relative to the left ventricular long axis (A), we do not compensate for the epicardial curvature, thus myocyte orientation will not correlate with wall deformation.

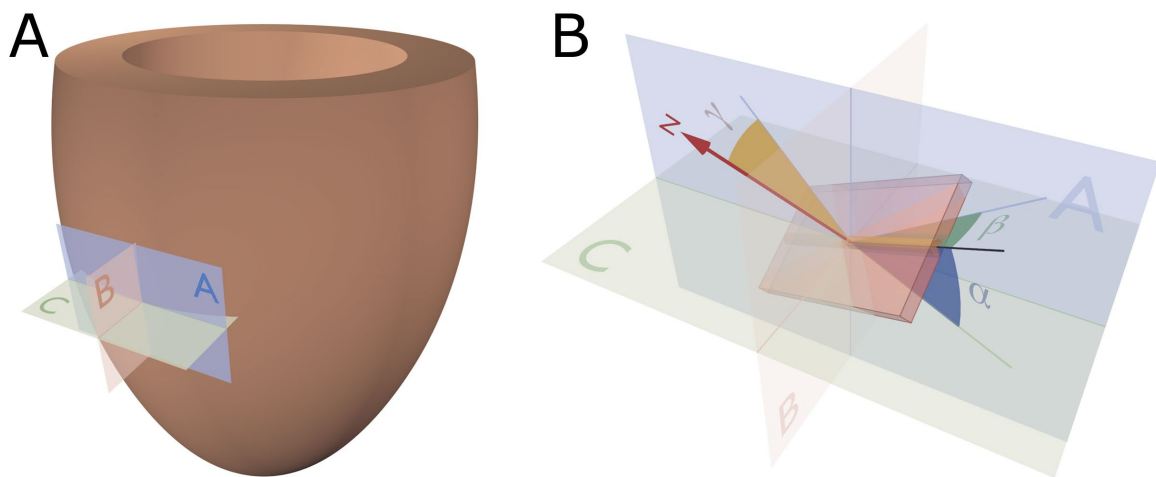


Figure 4. Reference planes and angle definitions. (A) showing a schematic of the left ventricle with the local orthogonal reference planes aligned with the epicardium. Plane A is parallel to the epicardial tangential plane, while the orthogonal plane B is parallel to the left ventricular long axis. Consequently, plane C is orthogonal to both planes A and B and is often referred to as the local “horizontal” plane. (B) Outlines our recommended angle definitions. The helical angle α is the angle between the primary eigenvector (black line) and plane C. The intrusion angle β is the angle between the primary eigenvector and plane A. Lastly, the aggregate angle is measured using the aggregate plane normal (N) assessed against the epicardial tangential plane A. The unit of aggregated cardiomyocytes is depicted as the yellow box, which is a schematic oversimplification.

It serves to mention that using only the left ventricular long axis as a reference point, and thus presuming that the left ventricle can be contemplated as cylindrical in shape for analytical purposes, will render skewed results when investigating the myocardial architecture at the base and apex of the ventricular cone. In these areas, the epicardium is in reality far from parallel with the long axis. Ideally, therefore, a subset of reference points is needed for each region of interest as described above. These reference vector definitions have already been used by different groups [27,34,56,57], but are far from universally employed. This so-called epicardial normalisation must be adopted to account for the inherent epicardial curvature, and to provide the most physiologically meaningful estimate of myocyte and aggregate orientation (Figure 3) [25].

2.2. The Helical Angle

By using “standard” planes of reference based on “unique” reference points (Figures 2 and 4), it becomes possible to quantify myocyte orientation by analysing the eigenvector corresponding to the myocyte chain’s long axis. In order to completely describe the orientation of a vector in a three-dimensional space, one needs to assess its orientation relative to two of the three reference planes discussed above [58]. It is Streeter and his colleagues who are usually credited with introducing the notion of the helical angle, which assesses myocyte orientation relative to the equatorial/horizontal plane of the ventricular cone [59,60]. However, this notion of change in myocyte angle relative to transmural position goes further back in time [61]. The idea that such angulation could be assessed relative to the horizontal plane was originally introduced by Feneis [62]. The notion was later endorsed by Hort [63] when the latter performed his extensive investigations of myocardial structure. Such helical angles are considered positive in the sub-endocardium, approximately zero in the mid-wall, and negative in the sub-epicardium.

The assessments by Streeter and his colleagues, along with those performed by his predecessors, were conducted manually, either by dissection, histology or both. Such methods were then used by others examining human [64] and animal specimens [65]. In 1992, Bovendeerd and colleagues investigated the mechanics of myocardial architecture with a Finite Element model [66]. They sought to replicate the assessments of Streeter by projecting the paths of the myocyte chains onto the epicardial tangential plane before measuring the helical angle (Figure 5). Apart from a few notable exceptions [34,52,67,68], this “projection method” has become the standard approach for assessing helical angles [28,69]. Of the alternative strategies, the one used by Geerts and co-workers is of interest, since they assessed the helical angle as the angle between the primary eigenvector and the local horizontal short axis plane, and thus avoided the need for projection [52] (Figure 5).

It has long been suspected that the ventricular cardiomyocytes change their orientation through the cardiac cycle to accommodate the dynamic wall deformation required to eject blood. Streeter and colleagues investigated this in dogs, they found no changes in the helical orientation of the myocytes in systole versus diastole [60]. While Streeter’s assessments were based on histologic evaluation, Dou and co-workers investigated the same phenomenon more than three decades later in humans using diffusion tensor imaging [70]. Contrary to the findings of Streeter and colleagues, they found the helical orientation to change through the cardiac cycle, going from a more circumferential orientation in diastole towards a more longitudinal orientation in systole. This finding has subsequently been confirmed in humans [36] and in rats [48,50], all using diffusion tensor imaging. In a recent and more detailed study of the entire heart by Omann and colleagues, the helical angle was found to only change significantly in the left ventricle and the septum, whereas no significant change was found in the right ventricle [4]. In the midwall and endocardial third of the left ventricle, the helical angle increased 15 to 20 degrees during contraction. This is comparable to the results of Chen and associates. According to their analyses the helical angle changes from approximately ± 50 degrees in diastole to ± 65 degrees in systole [48]. Comparing these data to those obtained in humans shows good agreement in some studies [67,71,72], while others find completely different extremes [73,74]. These inconsistencies are likely caused by differences in resolution, differences in the definition of the angle itself, and the use

of projected angle calculations. This is a pertinent issue in the field. Owing to a lack of consensus regarding angle definitions and the associated quantification, many research teams would produce varying results even when analysing the same heart.

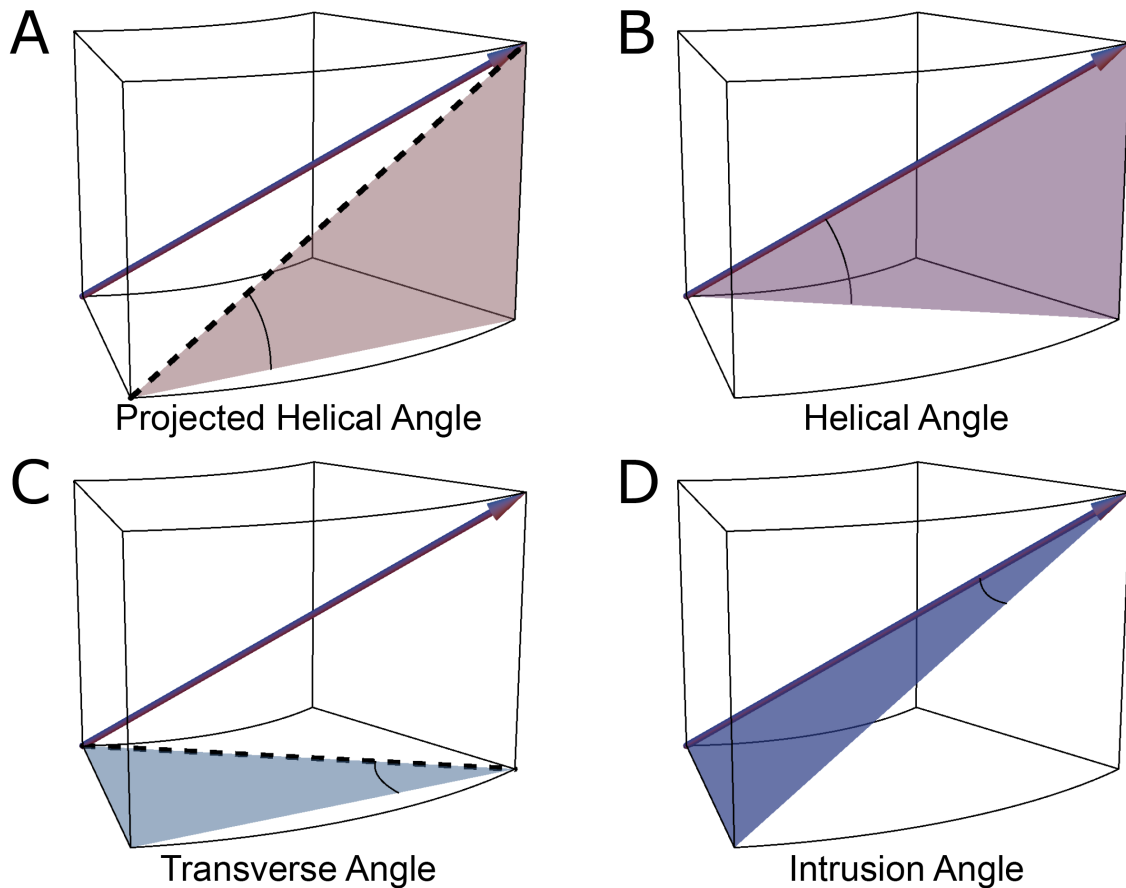


Figure 5. Commonly used angles in analysis of myocardial architecture. This figure illustrates the most commonly used definitions of helical and ‘transmural’ angulations with projection (A,C) and without projection (B,D). In this schematic illustration, the principal orientation of the cardiomyocytes, that is the primary eigenvector (arrow in all images), is depicted within a block of myocardium with the epicardium facing out of the page. (A) The projected helical angle is defined as the angle between the local horizontal plane and the projection of the primary eigenvector onto the epicardial tangential plane. (B) The helical angle is the angle between the primary eigenvector and the local horizontal plane. (C) The transverse angle is defined as the angle between the epicardial tangential plane and the projection of the primary eigenvector onto the local horizontal plane. (D) The intrusion angle is defined as the angle between the primary eigenvector and the epicardial tangential plane.

2.3. Transmural Orientation

Irrespective of the precise angle definition, once the helical orientation of the cardiomyocytes is determined relative to the local horizontal plane of the left ventricle, it also becomes necessary to consider any change in transmural orientation relative to the epicardial tangential plane (Figure 5). Once these two angles are defined, one has established the precise orientation of the cardiomyocytes. Thus, it is the combination of the helical and transmural orientations that provides the complete anatomical description of the orientation of the cardiomyocyte chains [25]. The notion of transmural angulation (i.e., across the wall) was also investigated by Streeter and his colleagues, and consequently named by them: the angle of imbrication [75]. This term, however, has not survived the passage of time. A significant number of morphological studies, nonetheless, have

explicitly denied the existence of populations of cardiomyocytes aggregated together with transmural orientation [10,34,36,51,66–68,76–78]. Evidence now confirms that transmural angulations do indeed exist [4,13,55,79], and it is suggested they play a key role in cardiac function [54,56,80]. The notion of mural antagonism and its functional significance [2,80] is yet to gain field-wide acclaim; this may be due, in part, to the historical dogma attached to the existence of transmurally arranged cardiomyocytes.

In various investigations, transmural angulation of the cardiomyocytes chains has been assessed either as the angle of intrusion, or the transverse angle (Figure 5). These two angles differ one from the other, with the transverse angle projected onto the local horizontal plane before it is then assessed relative to the epicardial tangential plane, while the angle of intrusion is measured without projection. The angle of intrusion has been used sparingly [55,56,79,81], while the transverse angle has been more commonly assessed [32,33,48,50,52,53,71,73,82,83]. We have previously discussed the limitations inherent to projection-based quantification [25]. Although it is argued that projected angles may be informative in a functional context, for example, when compared with measurements of strain [56,84], they actually act to mask the true anatomical arrangement of the myocyte chains. The concept of projection error is discussed further in Section 2.5.

2.4. Myocardial Aggregate Orientation

Anatomists have long discussed the existence of anatomical subgroupings or aggregations of cardiomyocytes within the myocardium [12,85,86]. The extent of such myocardial aggregations and their role in both the compartmentalisation and deformation of the ventricular walls remain two of the most significant controversies in cardiac morphology. These aggregations are of major importance in the continuous rearrangement of the myocardium through the cardiac cycle [4,28]. Studies of the supporting fibrous matrix have shown that the cardiomyocytes are packed together in functional subunits [87]. This notion of packing led LeGrice and colleagues to propose that the ventricular walls are organised in anatomical subunits of a laminar nature [9]. They stated that the individual myocardial aggregates were arranged in relatively uniform fashion, with a thickness of four to six myocytes. This notion was then endorsed by Scollan and colleagues [32]. As can be seen from Figure 6, the arrangement of the myocardial aggregates is more of a complex heterogenous mesh of interconnected aggregations. The sub-organisation of the myocardium into myocardial aggregates, in our opinion, is an indisputable fact. However, the exact anatomical dimensions of the aggregations, and their alignment within the ventricular walls, are less easily elucidated. Although this conundrum remains unresolved, it has been speculated that the units are joined together in an infinite heterogeneous branching continuum, with no discernible beginning or end [8,17,30,37,88]. It is hypothesised that this so-called cardiac mesh allows the aggregations of myocytes to slide one against the other during systolic mural thickening [6,10,39,65,89]. Evidence also suggests that the organisation into structural subunits determines the properties of electric conduction through the myocardium [90,91]. Even though the precise micro-anatomical organisation of such aggregations of cardiomyocytes is far from clarified, much emphasis has been placed on their three-dimensional orientation.

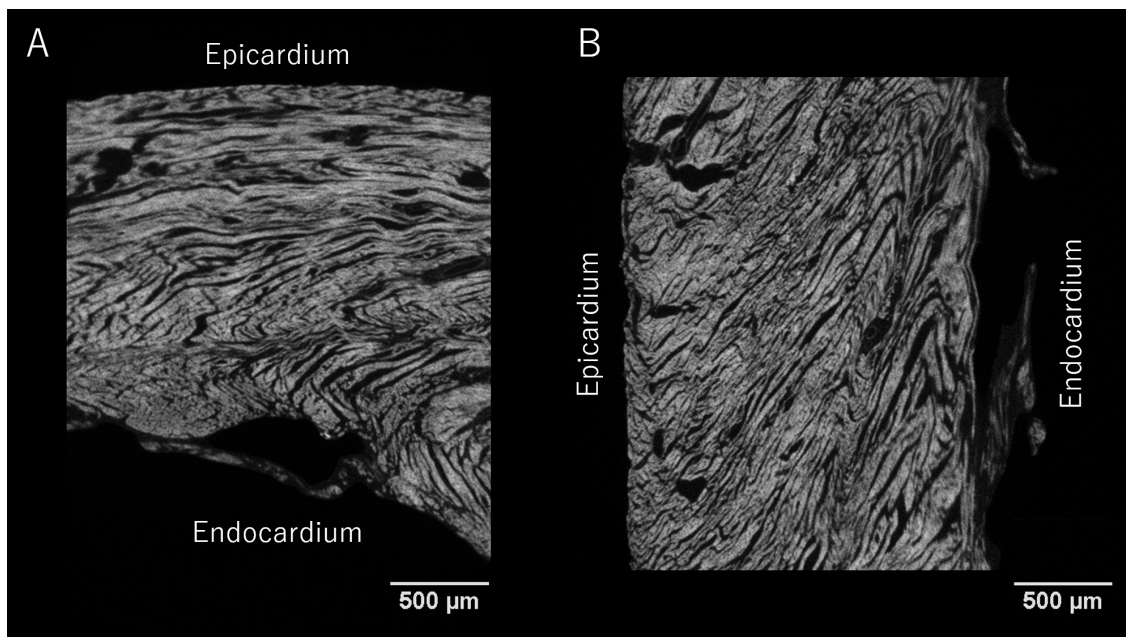


Figure 6. Micro-computed tomography of the myocardium. Contrast enhanced micro-computed tomography images of a sample preparation taken from the posterior-basal region of a rabbit left ventricle showcasing the aggregations of cardiomyocytes. Panel (A) shows the sample in short axis view, panel (B) shows the corresponding four-chamber view. Scale bars represent 500 μm . The isotropic spatial resolution is approximately 4 μm .

Before function can be attributed in a meaningful fashion to the myocardial aggregates, it is necessary to appreciate both their extent and their orientation. The so-called “sheet angle” was introduced allegedly to provide such information. Early studies had used histological techniques in an attempt to characterise the orientation of the myocardial aggregates [9–11,77,92,93], even though their extent had not been established in three dimensions. It was in 1998 that Scollan and his associates pointed towards the non-random orientation of the secondary and tertiary eigenvectors in diffusion tensor imaging and hypothesised that this feature may be linked to the orientation of the myocardial aggregates [32]. There is absolutely no consensus in the literature regarding the definition of this angle [25]. Several investigators have again made use of projection when calculating the so-called sheet angles [32,36,50,57,70,81,94,95]; this introduces a “projection error” as described in Section 2.5. Only the works of Chen and colleagues [48], Kung and associates [34], and the work from our own group [4,25,43,44] have assessed the orientation of the myocardial aggregates without the use of projections. As when assessing all other types of myocytic angulations, eigenvector projection serves no relevant purpose in assessment of the orientation of the aggregates [25]. It is the tertiary eigenvector, being the normal of the aggregate plane (Figure 7), which should be used when adopting the diffusion tensor approach [25]. Conversely, when using the structure tensor approach, it is the primary eigenvector, being the normal of the aggregate plane, which should be adopted [96]. Myocardial aggregates are of a planar nature. The only mathematically correct way of describing the orientation of a plane in space is to use its normal vector (Figure 7). We encourage researchers in the field of myocardial morphology to adopt this mathematical logic. In further support of this ideology, it is a generally accepted notion that changes in the orientation of the myocardial aggregates aid in radial thickening of the ventricular walls [39]. It is therefore reasonable to conclude that the orientation of the aggregations should be assessed relative to the local epicardial tangential plane (Figures 3 and 4). Thus, the most intuitive way of assessing the orientation of a myocardial aggregate, is to assess the angle between the normal vector of the aggregate and the epicardial tangential plane itself. This angle is depicted in Figure 4 as γ .

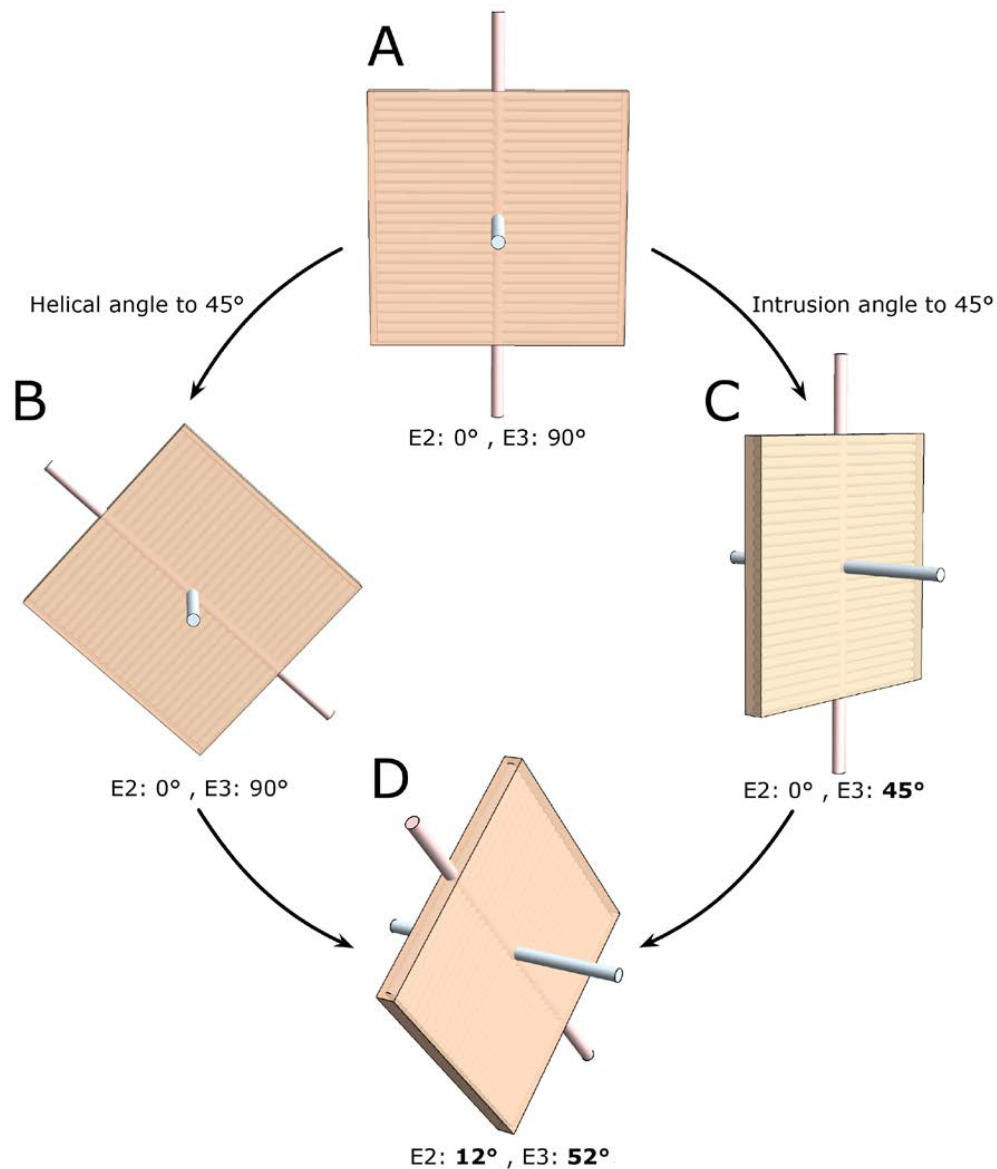


Figure 7. Differences in the quantification of myocardial aggregate orientation. In the literature, myocardial aggregate orientation is assessed using either the eigenvector situated within the aggregate plane, in diffusion tensor imaging referred to as the secondary eigenvector (E2) i.e., the pink shaded rod, or it is assessed using the aggregate plane normal, in diffusion tensor imaging referred to as the tertiary eigenvector (E3) i.e., the light blue shaded rod. This schematic shows a myocardial aggregate (beige box) made up of cardiomyocyte chains (depicted as lines running across the box). In panel (A) the aggregate is orientated parallel to the myocardial surface, with the helical and intrusion angle at 0 degrees. When adopting the most widely used E2-angle definition [36] this configuration results in an E2 angle of 0 degrees, conversely when using the E3-angle definition [25] the E3 angle is 90 degrees. Assigning a helical angle of 45 degrees to the cardiomyocyte chains, as shown in panel (B), changes neither the E2 nor the E3 angle. However, when we assign an intrusion angle to the myocyte chains, as shown in panel (C), the aggregate now angles towards the endocardium as is the case during myocardial thickening. This crucial reorientation is detected by the E3 angle, which changes to 45 degrees, the change is not detected by the E2 angle, which remains 0 degrees. If we assign both a 45 degree helical and a 45 degree intrusion angle to the cardiomyocyte chains, as shown in panel (D), despite this marked reorientation the E2 angle increases by only 12 degrees whereas the associated E3 angle is 52 degrees. This figure illustrates why the E3 angle more accurately measures aggregate transmuralty and reorientation during wall thickening, and emphasises why the two cannot be readily compared.

2.5. Consequences of Projected Angles

As we have already discussed, it is frequent to find studies where vectors have been projected onto reference planes prior to assessing their angulations [25]. If we now accept the fact that not all cardiomyocytes are arranged in surface parallel fashion, or in other words that myocyte chains exhibit a transmural orientation, we must also accept that projected angles are prone to bias or anatomically inaccurate results. Previously we assessed the consequences of projection when calculating helical, intrusion, and aggregate angle [25]. We showed the larger the intrusion angulation, the more the corresponding projected helical angle deviates away from its true value. The transmural orientation of cardiomyocytes in particular is very sensitive to projection, with the larger the helical angle, the greater the deviation of the projected transverse angle away from the non-projected intrusion angle. It was to circumvent such issues that Lunkenheimer and co-workers elegantly used circular knives to remove blocks of ventricular wall, thereby removing the influence of the helical angle when calculating the intrusion angle [13]. The artefact attributed to projection, is undisputable and a phenomenon we can easily recreate with everyday objects (Figure 8). It is surprising, therefore, that projection error has received so little attention in the existing literature [42].

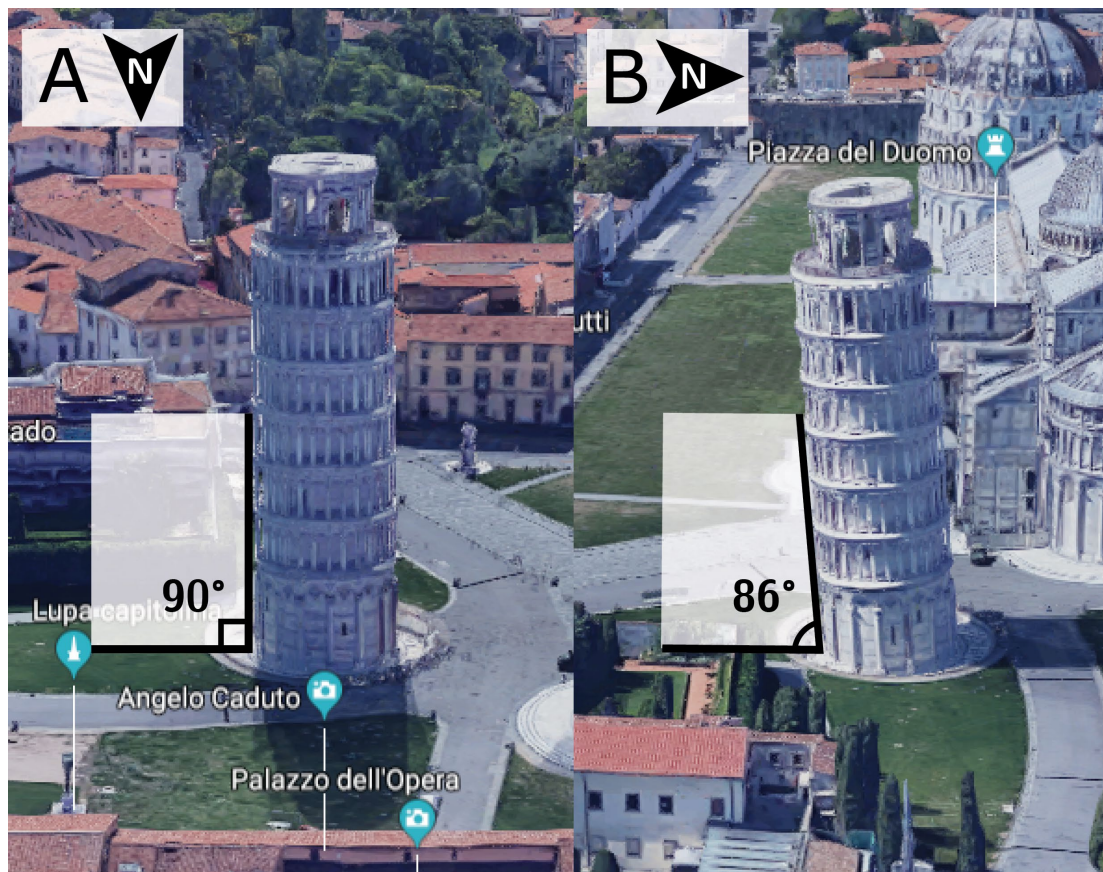


Figure 8. Projection artefact. The leaning tower of Pisa taken as an everyday example of projection artefact. The tower leans in a southward direction. Thus, when viewed from the north, the tower appears to be standing straight (A). When viewed from the east, however, the tower is obviously leaning (B). The straight appearance of the tower in panel A is an artefact brought upon by the projection of the tower into the camera lens. It would be inappropriate to use two-dimensional photography in an attempt to quantify the inclination of the tower. All projected angles in the setting of myocardial morphology are subject to projection artefact. ©2018 Google, Data SIO, NOAA, U.S. Navy, NGA, GEBCO, Landsat/Copernicus.

The leaning tower of Pisa taken as an everyday example of projection artefact. The tower leans in a southward direction. Thus, when viewed from the north, the tower appears to be standing straight (A). When viewed from the east, however, the tower is obviously leaning (B). The straight appearance of the tower in panel A is an artefact brought upon by the projection of the tower into the camera lens. It would be inappropriate to use two-dimensional photography in an attempt to quantify the inclination of the tower. All projected angles in the setting of myocardial morphology are subject to projection artefact. ©2018 Google, Data SIO, NOAA, U.S. Navy, NGA, GEBCO, Landsat/Copernicus.

3. Conclusions

This review points towards several controversies in the field of myocardial architecture. Data obtained by high-resolution imaging can be analysed, displayed, and mathematically modified in myriads of ways. We can learn much that is novel from studies of myocardial micro-architecture, but currently there is little consensus in the literature as to how myocyte orientation is defined and quantified. For as long as disagreements prevail, we will remain unable to compare studies and draw valid anatomical, physiological, and clinical conclusions. Based on this review we suggest the following points be considered in future studies of myocardial architecture. Firstly, as myocardial thickening occurs perpendicular to the epicardium, its curvature should be taken into account when assessing myocyte orientations. Second, there is no need to project myocyte orientations prior to quantification. In fact, projection introduces considerable bias. Third, the transmural component of myocyte orientation should be assessed, as it is a major determinant of cardiac function. Fourth and last, the normal vector of the myocardial aggregates should be used when quantifying aggregate orientation.

Funding: Robert S. Stephenson was supported in part by the European Union's Horizon 2020 research and innovation programme under the Marie Skłodowska-Curie grant agreement No 707663.

Acknowledgments: Along with Robert Stephenson (University of Birmingham), Stephen Hall and Rajmund Mokso (Lund University, Sweden), and Jonathan Jarvis (Liverpool John Moore's University, U.K.) were involved in the acquisition of the data used in Figure 6.

Conflicts of Interest: The authors have no conflict of interest.

References

1. Ingels, N.B., Jr. Myocardial fiber architecture and left ventricular function. *Technol. Health Care* **1997**, *5*, 45–52. [CrossRef] [PubMed]
2. Lunkenheimer, P.P.; Niederer, P.; Stephenson, R.S.; Redmann, K.; Batista, R.V.; Smerup, M.; Anderson, R.H. What is the clinical significance of ventricular mural antagonism? *Eur. J. Cardio Thorac. Surg.* **2017**, *53*, 714–723. [CrossRef] [PubMed]
3. Lunkenheimer, P.P.; Redmann, K.; Florek, J.; Fassnacht, U.; Cryer, C.W.; Wubbeling, F.; Niederer, P.; Anderson, R.H. The forces generated within the musculature of the left ventricular wall. *Heart* **2004**, *90*, 200–207. [CrossRef] [PubMed]
4. Omann, C.; Agger, P.; Bøgh, N.; Laustsen, C.; Ringgaard, S.; Stephenson, R.S.; Anderson, R.H.; Hjortdal, V.; Smerup, M. Resolving the natural myocardial remodelling brought upon by cardiac contraction; a porcine ex-vivo cardiovascular magnetic resonance study of the left and right ventricle. *J. Cardiovasc. Magn. Reson.* **2019**, *21*, 1–19. [CrossRef]
5. Spotnitz, H.M. Macro design, structure, and mechanics of the left ventricle. *J. Thorac. Cardiovasc. Surg.* **2000**, *119*, 1053–1077. [CrossRef]
6. Maciver, D.H.; Partridge, J.B.; Agger, P.; Stephenson, R.S.; Boukens, B.J.D.; Omann, C.; Jarvis, J.C.; Zhang, H. The end of the unique myocardial band: Part II. Clinical and functional considerations. *Eur. J. Cardio Thorac. Surg.* **2017**, *53*, 120–128. [CrossRef]
7. Stephenson, R.S.; Agger, P.; Lunkenheimer, P.P.; Zhao, J.; Smerup, M.; Niederer, P.; Anderson, R.H.; Jarvis, J.C. The functional architecture of skeletal compared to cardiac musculature: Myocyte orientation, lamellar unit morphology, and the helical ventricular myocardial band. *Clin. Anat.* **2015**, *29*, 316–332. [CrossRef] [PubMed]

8. Anderson, R.H.; Niederer, P.F.; Sanchez-Quintana, D.; Stephenson, R.S.; Agger, P. How are the cardiomyocytes aggregated together within the walls of the left ventricular cone? *J. Anat.* **2019**, *235*, 697–705. [CrossRef]
9. LeGrice, I.J.; Smaill, B.H.; Chai, L.Z.; Edgar, S.G.; Gavin, J.B.; Hunter, P.J. Laminar structure of the heart: Ventricular myocyte arrangement and connective tissue architecture in the dog. *Am. J. Physiol. Circ. Physiol.* **1995**, *269*, H571–H582. [CrossRef] [PubMed]
10. Li, R.A.; Takayama, Y.; McCulloch, A.; Covell, J.W. Laminar fiber architecture and three-dimensional systolic mechanics in canine ventricular myocardium. *Am. J. Physiol. Content* **1999**, *276*, H595–H607. [CrossRef]
11. Harrington, K.B.; Rodriguez, F.; Cheng, A.; Langer, F.; Ashikaga, H.; Daughters, G.T.; Criscione, J.C.; Ingels, N.B.; Miller, D.C. Direct measurement of transmural laminar architecture in the anterolateral wall of the ovine left ventricle: New implications for wall thickening mechanics. *Am. J. Physiol. Circ. Physiol.* **2004**, *288*, H1324–H1330. [CrossRef] [PubMed]
12. Mall, F.P. On the muscular architecture of the ventricles of the human heart. *Am. J. Anat.* **1911**, *11*, 211–266. [CrossRef]
13. Lunkenheimer, P.P.; Redmann, K.; Kling, N.; Jiang, X.; Rothaus, K.; Cryer, C.W.; Wübbeling, F.; Niederer, P.; Heitz, P.U.; Ho, S.Y.; et al. Three-dimensional architecture of the left ventricular myocardium. *Anat. Rec. Part A* **2006**, *288*, 565–578. [CrossRef]
14. Froeling, M.; Strijkers, G.J.; Nederveen, A.J.; A Chamuleau, S.; Luijten, P.R. Feasibility of in vivo whole heart DTI and IVIM with a 15 minute acquisition protocol. *J. Cardiovasc. Magn. Reson.* **2014**, *16*, O15. [CrossRef]
15. Agger, P.; Lass, T.; Smerup, M.; Frandsen, J.; Pedersen, M. Optimal preservation of cardiac tissue prior to dtmri. *J. Anat.* **2015**, *227*, 695–701. [CrossRef]
16. Stephenson, R.S.; Jones, C.B.; Guerrero, R.; Zhao, J.; Anderson, R.H.; Jarvis, J.C. High-Resolution Contrast-Enhanced Micro-Computed Tomography to Identify the Cardiac Conduction System in Congenitally Malformed Hearts. *JACC Cardiovasc. Imaging* **2018**, *11*, 1706–1712. [CrossRef] [PubMed]
17. Gilbert, S.H.; Benoist, D.; Benson, A.P.; White, E.; Tanner, S.F.; Holden, A.V.; Dobrzynski, H.; Bernus, O.; Radjenovic, A. Visualization and quantification of whole rat heart laminar structure using high-spatial resolution contrast-enhanced MRI. *Am. J. Physiol. Circ. Physiol.* **2011**, *302*, H287–H298. [CrossRef]
18. Ni, H.; Castro, S.J.; Stephenson, R.S.; Jarvis, J.C.; Lowe, T.; Hart, G.; Boyett, M.R.; Zhang, H. Extracting myofibre orientation from micro-ct images: An optimisation study. In Proceedings of the Computing in Cardiology, Zaragoza, Spain, 22–25 September 2013; pp. 823–826.
19. Young, A.A.; LeGrice, I.J.; Young, M.A.; Smaill, B.H. Extended confocal microscopy of myocardial laminae and collagen network. *J. Microsc.* **1998**, *192*, 139–150. [CrossRef]
20. Lee, W.-N.; Larrat, B.; Pernot, M.; Tanter, M. Ultrasound elastic tensor imaging: Comparison with MR diffusion tensor imaging in the myocardium. *Phys. Med. Biol.* **2012**, *57*, 5075–5095. [CrossRef]
21. Hsu, E.W.; Muzikant, A.; Matulevicius, S.A.; Penland, R.C.; Henriquez, C.S. Magnetic resonance myocardial fiber-orientation mapping with direct histological correlation. *Am. J. Physiol. Content* **1998**, *274*, H1627–H1634. [CrossRef]
22. Edelman, R.R.; Gaa, J.; Wedeen, V.J.; Loh, E.; Hare, J.M.; Prasad, P.V.; Li, W. In vivo measurement of water diffusion in the human heart. *Magn. Reson. Med.* **1994**, *32*, 423–428. [CrossRef]
23. Zhao, J.; Butters, T.D.; Zhang, H.; Pullan, A.J.; LeGrice, I.J.; Sands, G.B.; Smaill, B.H. An Image-Based Model of Atrial Muscular Architecture: Effects of structural anisotropy on electrical activation. *Circ. Arrhythmia Electrophysiol.* **2012**, *5*, 361–370. [CrossRef]
24. Mori, S. Mathematics of Diffusion Tensor Imaging. In *Introduction to Diffusion Tensor Imaging*; Academic Press: San Diego, CA, USA, 2014; pp. 33–37.
25. Agger, P.; Omann, C.; Laustsen, C.; Stephenson, R.S.; Anderson, R.H. Anatomically correct assessment of the orientation of the cardiomyocytes using diffusion tensor imaging. *NMR Biomed.* **2019**, *33*. [CrossRef] [PubMed]
26. Garcia-Cañadilla, P.; Cook, A.C.; Mohun, T.J.; Oji, O.; Schlossarek, S.; Carrier, L.; McKenna, W.J.; Moon, J.C.; Captur, G. Myoarchitectural disarray of hypertrophic cardiomyopathy begins pre-birth. *J. Anat.* **2019**, *235*, 962–976. [CrossRef]
27. Gilbert, S.H.; Sands, G.B.; LeGrice, I.J.; Smaill, B.H.; Bernus, O.; Trew, M.L. A framework for myoarchitecture analysis of high resolution cardiac MRI and comparison with diffusion Tensor MRI. In Proceedings of the 2012 Annual International Conference of the IEEE Engineering in Medicine and Biology Society, San Diego, CA, USA, 28 August–1 September 2012; pp. 4063–4066.

28. Nielles-Vallespin, S.; Khalique, Z.; Ferreira, P.F.; De Silva, R.; Scott, A.D.; Kilner, P.; McGill, L.-A.; Giannakidis, A.; Gatehouse, P.D.; Ennis, D.; et al. Assessment of Myocardial Microstructural Dynamics by In Vivo Diffusion Tensor Cardiac Magnetic Resonance. *J. Am. Coll. Cardiol.* **2017**, *69*, 661–676. [CrossRef] [PubMed]
29. Pope, A.J.; Sands, G.B.; Smaill, B.H.; LeGrice, I.J. Three-dimensional transmural organization of perimysial collagen in the heart. *Am. J. Physiol. Circ. Physiol.* **2008**, *295*, H1243–H1252. [CrossRef]
30. Stephenson, R.S.; Agger, P.; Omann, C.; Sanchez-Quintana, D.; Jarvis, J.C.; Anderson, R.H. Resolving the True Ventricular Mural Architecture. *J. Cardiovasc. Dev. Dis.* **2018**, *5*, 34. [CrossRef]
31. Alexander, A.L.; Lee, J.E.; Lazar, M.; Field, A.S. Diffusion tensor imaging of the brain. *Neurotherapeutics* **2007**, *4*, 316–329. [CrossRef]
32. Scollan, D.; Holmes, A.A.; Winslow, R.; Forder, J. Histological validation of myocardial microstructure obtained from diffusion tensor magnetic resonance imaging. *Am. J. Physiol. Content* **1998**, *275*, H2308–H2318. [CrossRef] [PubMed]
33. Holmes, A.A.; Scollan, D.; Winslow, R.L. Direct histological validation of diffusion tensor MRI in formaldehyde-fixed myocardium. *Magn. Reson. Med.* **2000**, *44*, 157–161. [CrossRef]
34. Kung, G.L.; Nguyen, T.C.; Itoh, A.; Skare, S.; Ingels, N.B.; Miller, D.C.; Ennis, D.B. The presence of two local myocardial sheet populations confirmed by diffusion tensor MRI and histological validation. *J. Magn. Reson. Imaging* **2011**, *34*, 1080–1091. [CrossRef] [PubMed]
35. Mekkaoui, C.; Huang, S.; Chen, H.H.; Dai, G.; Reese, T.; Kostis, W.J.; Thiagalingam, A.; Maurovich-Horvat, P.; Ruskin, J.N.; Hoffmann, U.; et al. Fiber architecture in remodeled myocardium revealed with a quantitative diffusion CMR tractography framework and histological validation. *J. Cardiovasc. Magn. Reson.* **2012**, *14*, 70. [CrossRef] [PubMed]
36. Ferreira, P.F.; Kilner, P.J.; McGill, L.-A.; Nielles-Vallespin, S.; Scott, A.D.; Ho, S.Y.; McCarthy, K.P.; Haba, M.M.; Ismail, T.F.; Gatehouse, P.D.; et al. In vivo cardiovascular magnetic resonance diffusion tensor imaging shows evidence of abnormal myocardial laminar orientations and mobility in hypertrophic cardiomyopathy. *J. Cardiovasc. Magn. Reson.* **2014**, *16*, 87. [CrossRef]
37. Lunkenheimer, P.P.; Niederer, P.F. Hierarchy and inhomogeneity in the systematic structure of the mammalian myocardium: Towards a comprehensive view of cardiodynamics. *Technol. Heal. Care* **2012**, *20*, 423–434. [CrossRef] [PubMed]
38. Agger, P.; Stephenson, R.S.; Dobrzynski, H.; Atkinson, A.; Iaizzo, P.A.; Anderson, R.H.; Jarvis, J.C.; Allan, S.L.; Partridge, J.B.; Zhao, J.; et al. Insights from echocardiography, magnetic resonance imaging, and microcomputed tomography relative to the mid-myocardial left ventricular echogenic zone. *Echocardiography* **2016**, *33*, 1546–1556. [CrossRef] [PubMed]
39. LeGrice, I.J.; Takayama, Y.; Covell, J.W. Transverse Shear Along Myocardial Cleavage Planes Provides a Mechanism for Normal Systolic Wall Thickening. *Circ. Res.* **1995**, *77*, 182–193. [CrossRef]
40. Lee, W.-N.; Pernot, M.; Couade, M.; Messas, E.; Bruneval, P.; Bel, A.; Hagege, A.A.; Fink, M.; Tanter, M. Mapping Myocardial Fiber Orientation Using Echocardiography-Based Shear Wave Imaging. *IEEE Trans. Med Imaging* **2011**, *31*, 554–562. [CrossRef]
41. Zhao, J.; Krueger, M.W.; Seemann, G.; Meng, S.; Zhang, H.; Dössel, O.; LeGrice, I.J.; Smaill, B.H. Myofiber orientation and electrical activation in human and sheep atrial models. In Proceedings of the 2012 Annual International Conference of the IEEE Engineering in Medicine and Biology Society, San Diego, CA, USA, 28 August–1 September 2012; pp. 6365–6368.
42. Teh, I.; McClymont, D.; Zdora, M.-C.; Whittington, H.J.; Davidoiu, V.; Lee, J.; Lygate, C.A.; Rau, C.; Zanette, I.; Schneider, J.E. Validation of diffusion tensor MRI measurements of cardiac microstructure with structure tensor synchrotron radiation imaging. *J. Cardiovasc. Magn. Reson.* **2017**, *19*, 31. [CrossRef]
43. Agger, P.; Lakshminrusimha, S.; Laustsen, C.; Gugino, S.; Frandsen, J.R.; Smerup, M.; Anderson, R.H.; Hjortdal, V.; Steinhorn, R.H. The Myocardial Architecture changes in Persistent Pulmonary Hypertension of the Newborn in an Ovine Animal Model. *Pediatr. Res.* **2016**, *79*, 565–574. [CrossRef]
44. Agger, P.; Ilkjær, C.; Laustsen, C.; Smerup, M.; Frandsen, J.R.; Ringgaard, S.; Pedersen, M.; Partridge, J.B.; Anderson, R.H.; Hjortdal, V. Changes in overall ventricular myocardial architecture in the setting of a porcine animal model of right ventricular dilation. *J. Cardiovasc. Magn. Reson.* **2017**, *19*, 93. [CrossRef]

45. Nielsen, E.A.; Smerup, M.; Agger, P.; Frandsen, J.; Ringgaard, S.; Pedersen, M.; Vestergaard, P.; Nyengaard, J.R.; Andersen, J.B.; Lunkenheimer, P.P.; et al. Normal right ventricular three-dimensional architecture, as assessed with diffusion tensor magnetic resonance imaging, is preserved during experimentally induced right ventricular hypertrophy. *Anat. Rec.* **2009**, *292*, 640–651. [CrossRef]
46. Smerup, M.; Nielsen, E.; Agger, P.; Frandsen, J.; Vestergaard-Poulsen, P.; Andersen, J.; Nyengaard, J.; Pedersen, M.; Ringgaard, S.; Hjortdal, V.; et al. The Three-Dimensional Arrangement of the Myocytes Aggregated Together Within the Mammalian Ventricular Myocardium. *Anat. Rec. Adv. Integr. Anat. Evol. Biol.* **2009**, *292*, 1–11. [CrossRef] [PubMed]
47. Healy, L.J.; Jiang, Y.; Hsu, E. Quantitative comparison of myocardial fiber structure between mice, rabbit, and sheep using diffusion tensor cardiovascular magnetic resonance. *J. Cardiovasc. Magn. Reson.* **2011**, *13*, 74. [CrossRef] [PubMed]
48. Chen, J.; Liu, W.; Zhang, H.; Lacy, L.; Yang, X.; Song, S.-K.; Wickline, S.A.; Yu, X. Regional ventricular wall thickening reflects changes in cardiac fiber and sheet structure during contraction: Quantification with diffusion tensor MRI. *Am. J. Physiol. Circ. Physiol.* **2005**, *289*, H1898–H1907. [CrossRef]
49. Benson, A.P.; Gilbert, S.H.; Li, P.; Newton, S.M.; Holden, A.V. Reconstruction and Quantification of Diffusion Tensor Imaging-Derived Cardiac Fibre and Sheet Structure in Ventricular Regions used in Studies of Excitation Propagation. *Math. Model. Nat. Phenom.* **2008**, *3*, 101–130. [CrossRef]
50. Hales, P.W.; Schneider, J.E.; Burton, R.A.; Wright, B.J.; Bollensdorff, C.; Kohl, P. Histo-anatomical structure of the living isolated rat heart in two contraction states assessed by diffusion tensor MRI. *Prog. Biophys. Mol. Biol.* **2012**, *110*, 319–330. [CrossRef]
51. Zhang, L.; Allen, J.; Hu, L.; Caruthers, S.D.; Wickline, S.A.; Chen, J. Cardiomyocyte architectural plasticity in fetal, neonatal, and adult pig hearts delineated with diffusion tensor MRI. *Am. J. Physiol. Circ. Physiol.* **2012**, *304*, H246–H252. [CrossRef] [PubMed]
52. Geerts, L.; Bovendeerd, P.; Nicolay, K.; Arts, T. Characterization of the normal cardiac myofiber field in goat measured with MR-diffusion tensor imaging. *Am. J. Physiol. Circ. Physiol.* **2002**, *283*, H139–H145. [CrossRef] [PubMed]
53. Pervolaraki, E.; Anderson, R.A.; Benson, A.P.; Hayes-Gill, B.; Holden, A.V.; Moore, B.J.R.; Paley, M.N.; Zhang, H. Antenatal architecture and activity of the human heart. *Interface Focus* **2013**, *3*, 20120065. [CrossRef] [PubMed]
54. Partridge, J.B.; Smerup, M.H.; E Petersen, S.; Niederer, P.F.; Anderson, R.H. Linking left ventricular function and mural architecture: What does the clinician need to know? *Heart* **2013**, *100*, 1289–1298. [CrossRef]
55. Smerup, M.; Agger, P.; Nielsen, E.A.; Ringgaard, S.; Pedersen, M.; Niederer, P.; Anderson, R.H.; Lunkenheimer, P.P. Regional and Epi- to Endocardial Differences in Transmural Angles of Left Ventricular Cardiomyocytes Measured in Ex Vivo Pig Hearts: Functional Implications. *Anat. Rec. Adv. Integr. Anat. Evol. Biol.* **2013**, *296*, 1724–1734. [CrossRef]
56. Smerup, M.; Partridge, J.; Agger, P.; Ringgaard, S.; Pedersen, M.; Petersen, S.; Hasenkam, J.; Niederer, P.; Lunkenheimer, P.; Anderson, R. A mathematical model of the mechanical link between shortening of the cardiomyocytes and systolic deformation of the left ventricular myocardium. *Technol. Heal. Care* **2013**, *21*, 63–79. [CrossRef]
57. Toussaint, N.; Stoeck, C.T.; Schaeffter, T.; Kozerke, S.; Sermesant, M.; Batchelor, P.G. In vivo human cardiac fibre architecture estimation using shape-based diffusion tensor processing. *Med. Image Anal.* **2013**, *17*, 1243–1255. [CrossRef]
58. Agger, P. Myocardial Remodelling in Right Ventricular Dilation. Ph.D. Thesis, Aarhus University, Aarhus, Denmark, 2016.
59. Streeter, D.D.; Bassett, D.L. An engineering analysis of myocardial fiber orientation in pig's left ventricle in systole. *Anat. Rec. Adv. Integr. Anat. Evol. Biol.* **1966**, *155*, 503–511. [CrossRef]
60. Streeter, D.D.; Spotnitz, H.M.; Patel, D.P.; Ross, J.; Sonnenblick, E.H. Fiber Orientation in the Canine Left Ventricle during Diastole and Systole. *Circ. Res.* **1969**, *24*, 339–347. [CrossRef] [PubMed]
61. Steensen, N. *De Musculis et Glandulis Observationum Specimen, Cum Epistolis Diabius Anatomicis*; Matthias Godiche: Copenhagen, Denmark, 1664.
62. Feneis, H. Das gefüge des herzmuskels bei systole und diastole. *Morphol. Jahrb.* **1943**, *89*, 371–406.

63. Hort, W. Makroskopische und mikrometrische untersuchungen am myokard verschieden stark gefüllter linker kammern. In *Virchows Archiv für Pathologische Anatomie und Physiologie und für Klinische Medizin*; Springer: Berlin/Heidelberg, Germany, 1960; Volume 333, pp. 523–564.
64. A Greenbaum, R.; Ho, S.Y.; Gibson, D.G.; E Becker, A.; Anderson, R.H. Left ventricular fibre architecture in man. *Heart* **1981**, *45*, 248–263. [CrossRef] [PubMed]
65. Waldman, L.K.; Nosan, D.; Villarreal, F.; Covell, J.W. Relation between transmural deformation and local myofiber direction in canine left ventricle. *Circ. Res.* **1988**, *63*, 550–562. [CrossRef]
66. Bovendeerd, P.; Arts, T.; Huyghe, J.M.; Van Campen, D.; Reneman, R. Dependence of local left ventricular wall mechanics on myocardial fiber orientation: A model study. *J. Biomech.* **1992**, *25*, 1129–1140. [CrossRef]
67. Reese, T.G.; Weisskoff, R.M.; Smith, R.N.; Rosen, B.R.; Dinsmore, R.E.; Wedeen, V.J. Imaging myocardial fiber architecture in vivo with magnetic resonance. *Magn. Reson. Med.* **1995**, *34*, 786–791. [CrossRef] [PubMed]
68. Wu, M.-T.; Tseng, W.-Y.I.; Su, M.-Y.M.; Liu, C.-P.; Chiou, K.-R.; Wedeen, V.J.; Reese, T.G.; Yang, C.-F. Diffusion Tensor Magnetic Resonance Imaging Mapping the Fiber Architecture Remodeling in Human Myocardium After Infarction. *Circulation* **2006**, *114*, 1036–1045. [CrossRef]
69. Teh, I.; McClymont, D.; Burton, R.A.B.; Maguire, M.L.; Whittington, H.J.; Lygate, C.A.; Kohl, P.; Schneider, J.E. Resolving Fine Cardiac Structures in Rats with High-Resolution Diffusion Tensor Imaging. *Sci. Rep.* **2016**, *6*, 30573. [CrossRef] [PubMed]
70. Dou, J.; Reese, T.G.; Tseng, W.-Y.I.; Wedeen, V.J. Cardiac diffusion MRI without motion effects. *Magn. Reson. Med.* **2002**, *48*, 105–114. [CrossRef] [PubMed]
71. Lombaert, H.; Peyrat, J.-M.; Croisille, P.; Rapacchi, S.; Fanton, L.; Cheriet, F.; Clarysse, P.; Magnin, I.; Delingette, H.; Ayache, N. Human Atlas of the Cardiac Fiber Architecture: Study on a Healthy Population. *IEEE Trans. Med Imaging* **2012**, *31*, 1436–1447. [CrossRef]
72. Eggen, M.D.; Swingen, C.M.; Iaizzo, P.A. Ex vivo diffusion tensor MRI of human hearts: Relative effects of specimen decomposition. *Magn. Reson. Med.* **2011**, *67*, 1703–1709. [CrossRef] [PubMed]
73. Nielles-Vallespin, S.; Mekkaoui, C.; Gatehouse, P.; Reese, T.G.; Keegan, J.; Ferreira, P.F.; Collins, S.; Speier, P.; Feiweier, T.; De Silva, R.; et al. In vivo diffusion tensor MRI of the human heart: Reproducibility of breath-hold and navigator-based approaches. *Magn. Reson. Med.* **2012**, *70*, 454–465. [CrossRef] [PubMed]
74. McGill, L.-A.; Ismail, T.F.; Nielles-Vallespin, S.; Ferreira, P.F.; Scott, A.D.; Roughton, M.; Kilner, P.J.; Ho, S.Y.; McCarthy, K.P.; Gatehouse, P.D.; et al. Reproducibility of in-vivo diffusion tensor cardiovascular magnetic resonance in hypertrophic cardiomyopathy. *J. Cardiovasc. Magn. Reson.* **2012**, *14*, 86. [CrossRef] [PubMed]
75. Streeter, D.D. Gross morphology and fiber geometry of the heart. In *Handbook of Physiology*; Section 2: The Cardiovascular System; American Physiological Society: Bethesda, MD, USA, 1979; pp. 61–112.
76. Tseng, W.-Y.I.; Reese, T.G.; Weisskoff, R.M.; Brady, T.J.; Wedeen, V.J. Myocardial Fiber Shortening in Humans: Initial Results of MR Imaging. *Radiology* **2000**, *216*, 128–139. [CrossRef]
77. Cheng, A.; Langer, F.; Rodriguez, F.; Criscione, J.C.; Daughters, G.T.; Miller, D.C.; Ingels, N.B. Transmural sheet strains in the lateral wall of the ovine left ventricle. *Am. J. Physiol. Circ. Physiol.* **2005**, *289*, H1234–H1241. [CrossRef]
78. Helm, P.A.; Younes, L.; Beg, M.F.; Ennis, D.B.; Leclercq, C.; Faris, O.P.; McVeigh, E.; Kass, D.; Miller, M.I.; Winslow, R.L. Evidence of Structural Remodeling in the Dyssynchronous Failing Heart. *Circ. Res.* **2006**, *98*, 125–132. [CrossRef]
79. Schmid, P.; Lunkenheimer, P.P.; Redmann, K.; Rothaus, K.; Jiang, X.; Cryer, C.W.; Jaermann, T.; Niederer, P.; Boesiger, P.; Anderson, R.H. Statistical Analysis of the Angle of Intrusion of Porcine Ventricular Myocytes from Epicardium to Endocardium Using Diffusion Tensor Magnetic Resonance Imaging. *Anat. Rec. Adv. Integr. Anat. Evol. Biol.* **2007**, *290*, 1413–1423. [CrossRef] [PubMed]
80. Lunkenheimer, P.P.; Redmann, K.; Niederer, P.; Schmid, P.; Smerup, M.; Stypmann, J.; Däbritz, S.; Rothaus, K.; Anderson, R.H. Models Versus Established Knowledge in Describing the Functional Morphology of the Ventricular Myocardium. *Heart Fail. Clin.* **2008**, *4*, 273–288. [CrossRef] [PubMed]
81. Jiang, Y.; Pandya, K.; Smithies, O.; Hsu, E.W. Three-dimensional diffusion tensor microscopy of fixed mouse hearts. *Magn. Reson. Med.* **2004**, *52*, 453–460. [CrossRef] [PubMed]
82. Chen, J.; Song, S.-K.; Liu, W.; McLean, M.; Allen, J.S.; Tan, J.; Wickline, S.A.; Yu, X. Remodeling of cardiac fiber structure after infarction in rats quantified with diffusion tensor MRI. *Am. J. Physiol. Circ. Physiol.* **2003**, *285*, H946–H954. [CrossRef]

83. Li, W.; Lu, M.; Banerjee, S.; Zhong, J.; Ye, A.; Molter, J.; Yu, X. Ex vivo diffusion tensor MRI reflects microscopic structural remodeling associated with aging and disease progression in normal and cardiomyopathic Syrian hamsters. *NMR Biomed.* **2009**, *22*, 819–825. [CrossRef]
84. Tseng, W.-Y.I.; Dou, J.; Reese, T.G.; Wedeen, V.J.; Tseng, W.I. Imaging myocardial fiber disarray and intramural strain hypokinesis in hypertrophic cardiomyopathy with MRI. *J. Magn. Reson. Imaging* **2005**, *23*, 1–8. [CrossRef]
85. Robb, J.S.; Robb, R.C. The normal heart: Anatomy and physiology of the structural units. *Am Heart J* **1942**, *23*, 455–467. [CrossRef]
86. Grimm, A.F.; Katele, K.V.; Lin, H.L. Fiber bundle direction in the mammalian heart. An extension of the “nested shells” model. *Basic Res Cardiol* **1976**, *71*, 381–388. [CrossRef]
87. Caulfield, J.B.; Borg, T.K. The collagen network of the heart. *Lab. Investig.* **1979**, *40*, 364–372.
88. Maciver, D.H.; Stephenson, R.S.; Jensen, B.; Agger, P.; Sanchez-Quintana, D.; Jarvis, J.C.; Partridge, J.B.; Anderson, R.H. The end of the unique myocardial band: Part I. Anatomical considerations. *Eur. J. Cardio Thorac. Surg.* **2017**, *53*, 112–119. [CrossRef]
89. Spotnitz, H.; Spotnitz, W.D.; Cottrell, T.S.; Spiro, D.; Sonnenblick, E.H. Cellular basis for volume related wall thickness changes in the rat left ventricle. *J. Mol. Cell. Cardiol.* **1974**, *6*, 317–322. [CrossRef]
90. Hooks, D.A.; Trew, M.L.; Caldwell, B.J.; Sands, G.B.; LeGrice, I.J.; Smaill, B.H. Laminar Arrangement of Ventricular Myocytes Influences Electrical Behavior of the Heart. *Circ. Res.* **2007**, *101*, e103–e112. [CrossRef] [PubMed]
91. Trew, M.L.; Caldwell, B.J.; Sands, G.B.; Hooks, D.A.; Tai, D.C.-S.; Austin, T.M.; LeGrice, I.J.; Pullan, A.J.; Smaill, B.H. Cardiac electrophysiology and tissue structure: Bridging the scale gap with a joint measurement and modelling paradigm. *Exp. Physiol.* **2006**, *91*, 355–370. [CrossRef] [PubMed]
92. Ashikaga, H.; Criscione, J.C.; Omens, J.H.; Covell, J.W.; Ingels, N.B. Transmural left ventricular mechanics underlying torsional recoil during relaxation. *Am. J. Physiol. Circ. Physiol.* **2004**, *286*, H640–H647. [CrossRef]
93. Ashikaga, H.; Omens, J.H.; Covell, J.W. Time-dependent remodeling of transmural architecture underlying abnormal ventricular geometry in chronic volume overload heart failure. *Am. J. Physiol. Circ. Physiol.* **2004**, *287*, H1994–H2002. [CrossRef] [PubMed]
94. Helm, P.; Beg, M.F.; Miller, M.I.; Winslow, R.L. Measuring and Mapping Cardiac Fiber and Laminar Architecture Using Diffusion Tensor MR Imaging. *Ann. N. Y. Acad. Sci.* **2005**, *1047*, 296–307. [CrossRef]
95. Gilbert, S.H.; Smaill, B.H.; Walton, R.D.; Trew, M.L.; Bernus, O. DT-MRI measurement of myolaminar structure: Accuracy and sensitivity to time post-fixation, b-value and number of directions. *Annu. Int. Conf. IEEE Eng. Med. Biol. Soc.* **2013**, *2013*, 699–702.
96. Gilbert, S.; Trew, M.; Smaill, B.; Radjenovic, A.; Bernus, O. Measurement of Myocardial Structure: 3D Structure Tensor Analysis of High Resolution MRI Quantitatively Compared to DT-MRI. In *Computer Vision*; Springer: Berlin/Heidelberg, Germany, 2013; pp. 207–214.

Publisher’s Note: MDPI stays neutral with regard to jurisdictional claims in published maps and institutional affiliations.



© 2020 by the authors. Licensee MDPI, Basel, Switzerland. This article is an open access article distributed under the terms and conditions of the Creative Commons Attribution (CC BY) license (<http://creativecommons.org/licenses/by/4.0/>).

Review

An Appreciation of Anatomy in the Molecular World

Bjarke Jensen *, Vincent M. Christoffels and Antoon F. M. Moorman

Department of Medical Biology, Amsterdam Cardiovascular Sciences, University of Amsterdam, Amsterdam UMC, Meibergdreef 15, 1105AZ Amsterdam, The Netherlands; v.m.christoffels@amsterdamumc.nl (V.M.C.); a.f.moorman@amsterdamumc.nl (A.F.M.M.)

* Correspondence: b.jensen@amsterdamumc.nl; Tel.: +31-20-566-4659 or +31-62-645-0696

Received: 25 September 2020; Accepted: 13 October 2020; Published: 15 October 2020

Abstract: Robert H. Anderson is one of the most important and accomplished cardiac anatomists of the last decades, having made major contributions to our understanding of the anatomy of normal hearts and the pathologies of acquired and congenital heart diseases. While cardiac anatomy as a research discipline has become largely subservient to molecular biology, anatomists like Professor Anderson demonstrate anatomy has much to offer. Here, we provide cases of early anatomical insights on the heart that were rediscovered, and expanded on, by molecular techniques: migration of neural crest cells to the heart was deduced from histological observations (1908) and independently shown again with experimental interventions; pharyngeal mesoderm is added to the embryonic heart (1973) in what is now defined as the molecularly distinguishable second heart field; chambers develop from the heart tube as regional pouches in what is now considered the ballooning model by the molecular identification of regional differentiation and proliferation. The anatomical discovery of the conduction system by Purkinje, His, Tawara, Keith, and Flack is a special case because the main findings were never neglected in later molecular studies. Professor Anderson has successfully demonstrated that sound knowledge of anatomy is indispensable for proper understanding of cardiac development.

Keywords: heart development; cardiac conduction system; cardiac structure

1. Introduction

Single cell sequencing of whole hearts of adults and embryos reveals a stunning complexity [1,2] that could not have been anticipated on the basis of the dominant disciplines of heart research of the 20th century, anatomy and electrophysiology. History shows that over time some techniques become obsolete and some disciplines, such as morphology, disappear [3]. Not everything, however, gets supplanted in the brave new world. Instead, problems in biology and medicine are addressed by an increasing diversity of tools and approaches as revealed by the interdisciplinarity of recent studies [4–6]. Concerning cardiac pathologies, the criteria for structural assessments of hypertrophy, wall thinning, excessive trabeculae, and much more have not changed much while imaging has undergone profound developments [7]. This testifies to the persistent role of anatomy in biomedical investigations of the heart.

Here, we provide examples of highly perceptive discoveries made within anatomy that were later rediscovered, and much elaborated on, using technological approaches developed in the fields of developmental and molecular biology. As we go back in time, the descriptions become fewer and less detailed and at some point, one can reasonably ask whether the original descriptions in fact concern the same matter as described in current research. Our primary aim is not to establish who made the original descriptions. Rather, we want to highlight a few cases to emphasize the importance of complementary approaches. The reason for the emphasis on anatomy is to celebrate our dear friend Bob Anderson.

2. Early and Highly Perceptive Insights

2.1. Neural Crest Cells

In 1908 the first of two large volumes appeared on the development of the Australian lungfish [8]. Exquisite illustrations of wax-model reconstructed embryos came with transparent overlay paper on which small ovals indicated the migration of “freien Mesodermzellen” (free mesoderm cells) from the neural tube and down the pharyngeal arches (Figure 1). It is only in hindsight, however, that we appreciate that Greil [8] was describing neural crest cells migrating to the major arteries and into the cardiac outflow tract [9]. That the neural crest cells play an important role in establishing separate channels for the pulmonary and systemic circulation has been described in a number of species thereafter [10,11]. To get to that insight, however, Greil’s descriptions were not considered. Instead, it was the use of quail-chick chimeras [12] that allowed Kirby and Stewart to understand that the neural tube (including premigratory neural crest) they had ablated contributes to the aorticopulmonary septum (which results from fusion of mesenchymal cushions) [13].

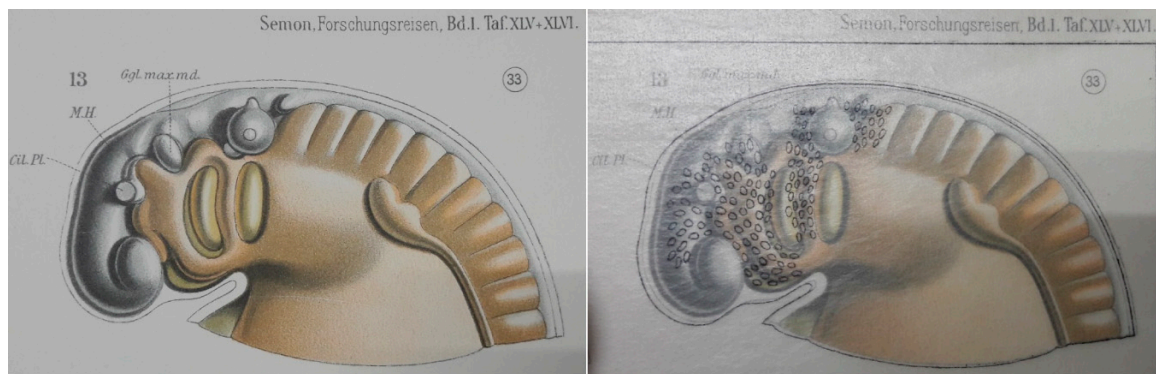


Figure 1. Neural crest cells migrating down the pharyngeal arches of a stage 33 embryonic Australian lungfish. Transparent overlay paper was used in this description from 1908 to show the migration (black ovals in right-hand image represent the positions of neural crest cells). Photographed from [8].

2.2. Cardio-Pharyngeal Mesoderm or Second Heart Field

Not only neural crest cells are migrating into the outflow tract. Early 20th century anatomists realized that the entire outflow tract in amniotic vertebrates is migrating towards the ventricle and Sir Arthur Keith found that “Dr. A. Greil, of Vienna, had published in the previous year (*Morph. Jahrb.*, 1903, Bd. xxxi., p. 123) [14] a splendid research on the development of the heart of reptiles in which he demonstrated that the bulbus cordis, while a separate chamber at an early stage, becomes at a later stage overwhelmed by the musculature of the ventricles, and is thus not obliterated but incorporated as an intrinsic part of the ventricular system” [15] (the reference [14] is inserted by us). This incorporation was deduced from static anatomy of different developmental stages and it was by labelling the outflow tract of developing chicken that Maria de la Cruz added experimental support [16].

It is not only that cardiomyocytes change position within the heart. Virágh and Challice published in 1973 that the morphology of the cells at the arterial and venous poles of the embryonic mouse heart seemed similar to that of the cells of the neighboring mesoderm, from which they deduced that “splanchnic mesoderm” is added to the heart [17]. This notion has been thoroughly validated by lineage tracing experiments [18]. The second heart field, as this part of the splanchnic mesoderm is now called, also gives rise to facial musculature and thus establishes the link between craniofacial and cardiac malformations in syndromes such as DiGeorge syndrome [19]. The current tally of molecularly identified heart fields is three [20], and maybe even four if we accept the division of the second heart field into anterior and posterior parts [21,22]. A common issue has then emerged of whether the

‘splitting’ has become excessive and ‘lumping’ should be encouraged [23,24]. In this regard anatomy and molecular biology has surely seen many instances of parallel evolution.

2.3. Chamber Formation: Bulges, Segments, and Finally Balloons

Already Gaskell deduced that the myocardium between chambers was more embryonic-like in character [25,26]: “The study of the development of the heart shows that it is originally a simple tube with muscular walls from end to end of which waves of contraction pass; a portion of this tube expands to form the auricles and another portion to form the ventricle; these two being connected by an unexpanded part called the canalis auricularis”. This was corroborated by detailed anatomical studies of early embryos that described a primitive heart tube in which “the ventricles are outgrowths; or bulgings from the primitive cardiac tube” [27]. In the South American lungfish [28], for example, the atrium and ventricle are also “localized bulgings” and the atriums “expand markedly over the dorsal curvature of the heart, while the comparatively much slighter degree of ventricular expansion occurs wholly along the ventral curvature”. These descriptions strongly resemble our current notion of chamber development by “ballooning” of chambers from the outer curvature of the looped primitive heart tube [29]. Accordingly, the harmonizing views on vertebrate heart anatomy and development that were developed a century ago are still valid [30] (Figure 2).

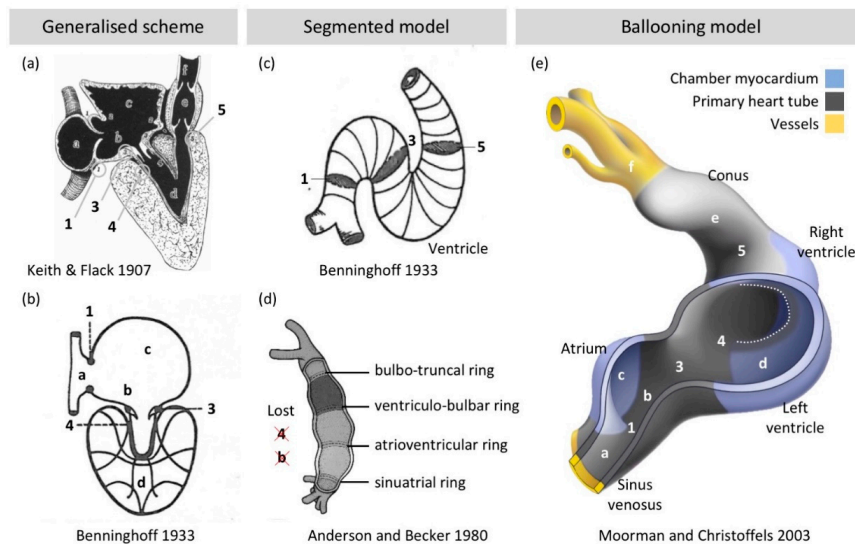


Figure 2. Building plan of the heart. (a) Keith and Flack [30] developed a “generalized” scheme of the vertebrate heart where the primitive parts (1,b,3,4,5) form a single domain (although their scheme is much inspired by the formed fish heart in which it is often the case that the atrioventricular part (3,4) is separated from the conal or bulbar valve area (5) by chamber myocardium). (b) The scheme of the cardiac conduction system by Benninghoff [31] is highly similar to that of (a) and while the labels a–d and 1,3,4 are inserted by us such that they correspond to (a), the primitive parts (1,b,3,4) still form a single domain. (c) Benninghoff [31], when conceptualizing the development of the conduction system from a comparative perspective (and maintaining that ectotherms do not have a conduction system comparable to that found in mammals and birds), emphasized the “Ostienringe” (1,3,5) as the precursors of future (“künftigen”) chamber junctions. Although this is still compatible with the ballooning model [29], the depiction of the junctions as entirely separate from each other (1,3,5) was perpetuated (d) to mean that everything between, for example, junctions 1 and 3 would be atrium, whereas Benninghoff’s model (c) does not exclude the presence of an “auricular canal” (label b in (a,b)), or remnant of the primary heart tube. (d) The segmented model presumes that parts b and 4 are lost and the precursors of all segments of the adult heart are present at the heart tube stage, which is therefore in conflict with the addition of cells from the second heart field, the “generalized” scheme (a) and the ballooning model (e) [29]. Image (a) is adapted from [30], (b,c) from [31], and (d) from [32].

It is then remarkable that the foundational descriptions were superseded by the notion that the primitive heart tube is made up of serially arranged primitive stages of the same segments that the adult heart has [33–35]. This ‘frame shift mutation’ in the understanding of the heart may have originated with Benninghoff [36], specifically in the schemes and simplifications he introduced for the earliest development of the conduction system [31]. Although his generalized scheme of the vertebrate heart (Figure 2b) is essentially the same as that of Keith and Flack [30] (Figure 2a), he presumed that junctions of the adult heart can be found back in the heart tube [31] (Figure 2c). Additionally, by illustrating the junctions as separate from each other (see the rings labelled 1, 3, 5 in Figure 2c), the single domain of primary heart tube myocardium, which is integral to the generalized model of the vertebrate heart, became segmented. This segmentation was taken very literal in later adaptations by Bob Anderson and others [33,34,37] in which the primary myocardium that makes up the entire heart tube was thought to be a tiny fraction of the tube only and organized in a series of rings (Figure 2d).

This segmented model (Figure 2d) is at odds with the anatomy of the heart tube (there is not a series of bulges), with the fact that a very substantial number of cells from the second heart field are added in later developmental stages (see Section 2.2) and that the heart tube comprises primary (non-chamber) myocardium only. It seems that ‘ventricle’ in the sense of a cavity was confused with the identity of the surrounding walls. Much of the ventricular (and atrial) cavity is indeed surrounded by ventricular (and atrial) wall, but a smaller part is surrounded by the primary heart tube (Figure 2e). In the case of Bob Anderson, it was the immunohistochemical detection of G1N2 and the remodeling of the atrioventricular junction it revealed [38] that caused him to discard the segmental model [39]. The ballooning model (or ‘bulging’ model in old parlance) is now extensively supported by data from human and model animal embryos [40–42].

3. Detailed Analyses of Ventricular Structure, But How Does It Relate to Function?

3.1. Myocyte Orientation of the Compact Wall

Pettigrew [43] documented in 1864 a surprisingly regular organization of the muscle of the left ventricle in various mammals, from a left-handed spiral in the subepicardial wall to a circumferential orientation in the mid-wall and a right-handed spiral in the sub-endocardial parts. In the mathematical analyses of Streeter [44], the spirals are geodesic lines, i.e., short routes around the cavity, and such a structure presumably would enable efficient pumping. Reptile hearts represent to some extent the ancestral condition of the mammalian heart [45,46] and Shaner [47] and Benninghoff [31,36] documented that reptile ventricles do not have the mammalian spiral organization of their compact wall. That allows for the conjecture that the spiraling configuration is related to some aspects of generating the greater cardiac output and higher systemic blood pressure that distinguishes mammals from reptiles.

From the observations of the spiral organization grew the notion that the left ventricular wall wrings like a towel in systole, which is supported by the tracking of fixed positions of the wall throughout the cardiac cycle. The ventricular wall is thick and for the ventricle to wring, layers closer to the cavity must move more than layers more to the outside. Consistently, sheets of aggregated muscle are found in much of the ventricular wall [48]. At least for the right ventricle, such sheets increase the risk of discontinuous electrical propagation, by which they can be a predisposing factor for arrhythmias [49]. Clonal analyses of ventricular cardiomyocytes of embryonic mice reveal that daughter cells are positioned much like pearls on a string [50,51]. Such configuration resembles geodesic lines. At early stages of development, the compact wall is only a few cells thick. Clonal analyses revealed a mostly circumferential orientation in the LV and a mostly longitudinal orientation in the RV. These analyses give much more detail than previous anatomical studies that suggested that the primitive fiber orientation is circumferential [52]. Recent X-ray-based tractography of fetal human hearts suggests the gradient of left-to-right handed orientation develop in the fetal period [53].

The spiral organization also spurred the notion that the entire ventricular mass is organized as a single band, as advocated by Torrent-Guasp, who famously cooked hearts and ‘unwound’ them [54,55]. The unwinding procedure starts with ripping the right ventricular free wall from the anterior interventricular sulcus and thus tearing naturally occurring bands of heart muscle. This attracted the ire of Bob Anderson who tried to impose nonsense-mediated decay of the concept [56]. Arguing against the single-banded ventricle may be one of the discourses he has spent the most words on. Evidence from developmental and comparative anatomy as well as functional studies has been amassed against the notion of a single-banded ventricle [57,58], but not everybody is convinced [59] and Bob Anderson will seemingly pick up the gauntlet every time [60].

Analyses of the spiraling organization is becoming quite sophisticated with the introduction of MRI and CT-based measurements enabling diffusion tensor imaging and tractography, respectively [53,61]. Nonetheless, one can reasonably posit that it is not obvious what the functional significance is of steeper or flatter helical angles, although experiments and case–control studies do show that hypertrophy of the ventricular walls associates with helical angles that deviate from normal [62,63]. The foundational analytic method that Streeter applied to the compact wall, did not apply well to the trabecular muscle on the luminal side of the ventricles. Later studies largely neglected the trabecular muscle. In clinical literature, however, the last three decades have seen a rapid increase in interest of the trabecular muscle as it has become associated with poor pump function [7,64–68].

3.2. Trabeculae, Compaction and Differential Growth as a Mechanism for Shape Change

The trabecular muscle of the left ventricle comprises only some 15% of the normal ventricular mass, the rest being compact wall [69]. While detailed analysis of the structure of the compact wall as geodesic lines can be made [61], the complex organization of the trabecular mass is more difficult to analyze [44]. Trabeculae are thought to increase wall stiffness [70] and negatively impact on the maximal stroke volume [71], in addition to facilitating thrombus formation like the trabecular muscle of the left atrial appendage [72] in atrial fibrillation [73]. The trabecular muscle component is proportionally greater than that of the compact wall in the hearts of embryos and in the cold-blooded vertebrates [74]. Subsequently, trabeculae have then been associated with immature [64,75] and primitive states [76,77]. A notion then formed of trabeculae being redundant at best and possibly even deleterious to pump function. In some individuals, the trabeculae are excessive and comprise more than 25% of the left ventricular mass [69]. These individuals can be diagnosed with left ventricular noncompaction [7,64–68]. The term noncompaction [64] relates to the hypothesis that the normal fetal ventricle is proportionally less trabeculated than the embryonic ventricle due to a putative process of compaction of the embryonic trabeculae into compact wall [78]. Noncompaction therefore assumes that compaction has failed [64]. It is therefore surprising that when thousands of individuals of the general population are surveyed, i.e., the study population has not been preselected on disease, a large fraction fulfills structural criteria for noncompaction while having normal pump function and no greater risk of severe outcomes [5,79–83]. Additionally, the evidence supporting the process of compaction taking place is surprisingly weak.

In the embryo, tissues and organs grow incredibly fast [84]. Volume measurements of trabeculae reveal an increase during development and not a decrease, as would be expected if compaction was an important process in the formation of the compact wall [85] (Figure 3). In the normal adult left ventricle, the trabecular component comprises approximately 5 g/m^2 [69], which equals a greater volume than the entire embryo at the end of the embryonic period (8 weeks of gestation) [84]. A normal Carnegie stage 23 embryo and a normal papillary muscle, which derives from the embryonic trabeculae [86], are roughly similar in size (Figure 3). Furthermore, recent studies in mouse show that the growth of the compact wall is much more affected by diminished proliferation in the compact wall than diminished proliferation in the trabeculae [87]. That the trabeculae exhibit growth throughout gestation does not necessarily negate the existence of compaction (and thus noncompaction) in a narrow time window, but it does illustrate the tremendous scope for shape change by differential growth rates.

Differential growth rates are evidently the driver of chamber formation and septation and, outside the heart, also the driver of morphogenesis of the limbs etc. [84,88]. Such “alternative splicing of information” has attracted the attention of Bob Anderson and while his erudition facilitated the notion of compaction [74,77], his quick pen now assigns only a minor role to compaction [89]. While the importance of compaction remains debated, the “mystery” of noncompaction [90] is being clarified because studies framed in the context of noncompaction have advanced our understanding of normal development of ventricular trabeculae [91–94] and their impact on health [5,79,80,95]. Thus, even if noncompaction turns out to be “the mitral valve prolapse of the 21st century” [68], i.e., excessively diagnosed, our knowledge of the biology of the trabeculae has increased in the process.

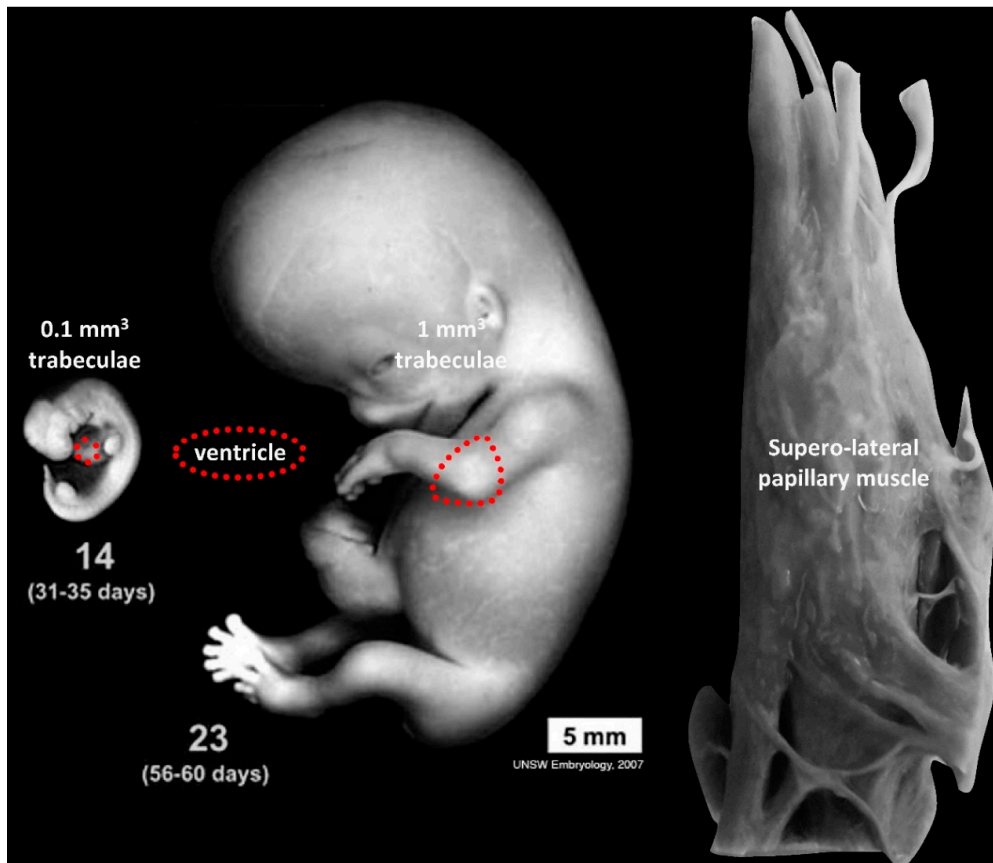


Figure 3. Growth of the cardiac ventricle (dashed red line) from a proportionally very trabeculated stage (14) to the end of embryonic development where compaction is presumed to have taken place (23) compared to the superior-lateral papillary muscle of the adult heart (which develops from embryonic trabeculae). From Carnegie stages 14 to 23, the volume of trabecular muscle increases approximately an order of magnitude [85] and then approximately five orders of magnitude to reach 10 g in the adult heart [69] (note that [85] included the ventricular septum in the volume of trabeculae and the numbers we show are a bit lower than in [85]). Images of embryos are adapted from Hill, M.A. (1 September 2020) Embryology Embryonic Development. Retrieved from https://embryology.med.unsw.edu.au/embryology/index.php/Embryonic_Development.

4. What Makes an Atrial Septum?

Already in the late 19th century, Röse observed that the atrial septum of placental mammals was different from that of other vertebrates by having a circular depression, the oval fossa [96,97]. The floor of the oval fossa was shown to derive from the primary atrial septum and the rim of the oval fossa, then, became known as the secondary septum [98]. Ironically, the developmental studies of the time, including the one by Odgers [98], were cognizant that the largest part of the secondary septum,

the posterior-superior part, was a folding-in of the atrial roof (Figure 4a,b). Therefore, this part was not a true septum as emphasized by Patten for example: “The walls of the right and left atria can then be separated from one another by merely dividing a little loose connective tissue, and the separation can be carried as far as practically to the margin of the limbus fossae ovalis. The whole of the dorsal and oral portion of the so-called septum secundum atriorum is therefore merely the result of the coaptation of adjacent portions of the walls of the two atria, and is not a true septum comparable to the septum primum” [99]. During the 20th century, the use of the term secondary septum persisted. In contrast, the original images were replaced with schematics that showed the fold as filled with heart muscle and the secondary septum now appeared like a septum [100,101] (Figure 4c,d).

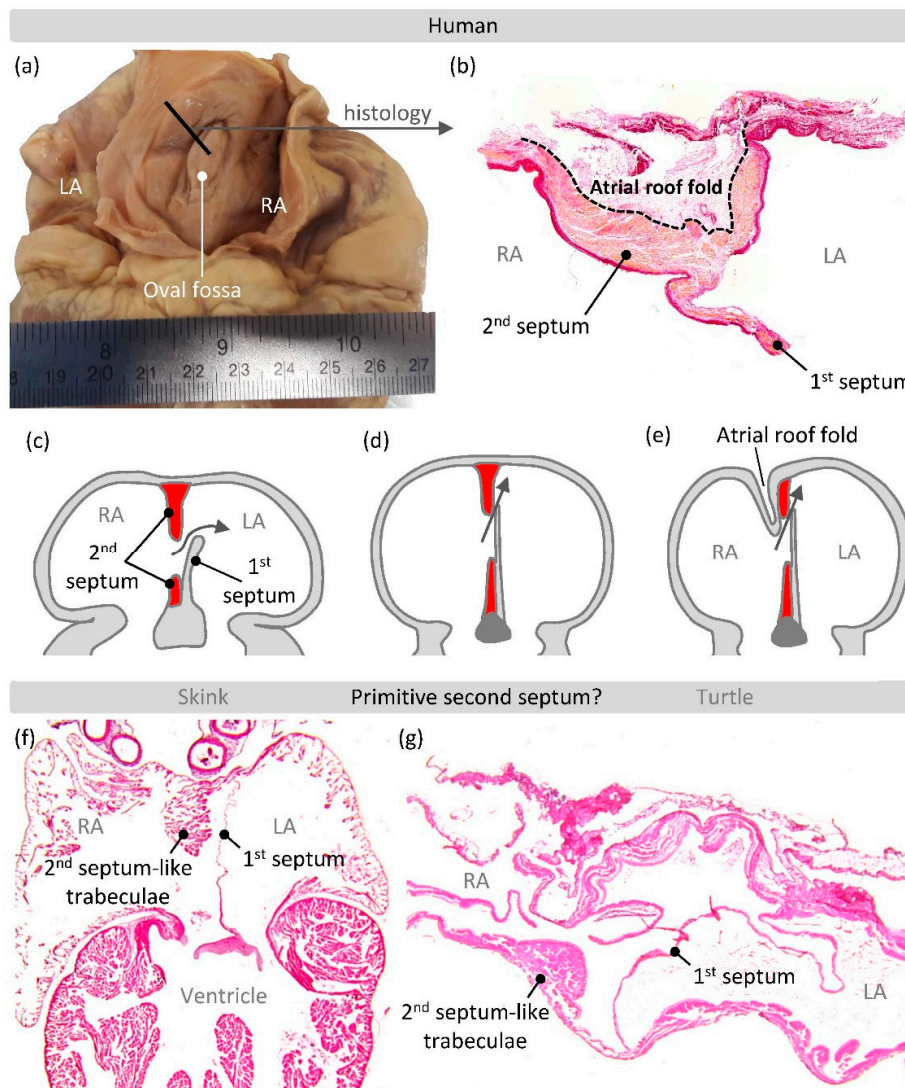


Figure 4. The atrial septum. (a) The atrial septum of the heart of an adult human exposed by a cut through the intercaval (sinus venarum) area. The thick black line indicates the part of the posterior-superior part of the septum that was sectioned with histology. (b) Histology showing the fold in the atrial roof (a very similar setting has been demonstrated in pig, for example [102,103]). (c,d) Schematic representations of the atrial septum of perinatal stages, with the secondary septum in red. Notice that the fold in the atrial roof is not cartooned. Adapted from [104,105]. (e) Example of schematic that makes a compromise between fold and septum, adapted from [106]. (f,g) Histology of reptiles showing a secondary septum-like aggregate of trabecular muscle in the right atrium of a skink ((f) horizontal section) and a turtle ((g) transverse section), adapted from [107].

Such anatomical “missense mutations” attracted the ire of Bob Anderson [108], who, after two decades of emphasizing fold over septum and knowing that the foundational descriptions were (largely) accurate, fumed that it “is difficult to explain why these facts did not make their way into standard accounts of cardiac development” [109]. Solace can be found in that recent accounts emphasize the folding in of the atrial roof [110] and even if they perpetuate the old erroneous view, the septum may become a fold in adaptations (see Figure 4c that appears to have inspired Figure 4d, which in turn got adapted such that the fold was included Figure 4e). It has been emphasized that in mouse there is more of a secondary septum (the fold is not very pronounced) [111] and many reptiles have a secondary septum-like structure suggesting that an actual septum rather than fold may be the evolutionary primitive condition [107] (Figure 4f,g).

Fold or septum, either is a barrier for blood flow and in this sense they are synonymous. The functional significance is that the dorsal rim is required for the closure of the foramen ovale after birth and the foramen ovale itself is likely an evolutionary adaptation to the long gestation that characterizes many placental mammals [112]. The evolutionary and developmental history of full atrial septation has recently been shown to have an additional component, namely a mesenchymal contribution called the vestibular spine or dorsal mesenchymal protrusion [112–115]. Accordingly, among the categories of atrial septal defects there is now a vestibular atrial defect and the prevalence of which seems underappreciated [116].

5. The Special Case of the Cardiac Conduction System

It is clearly so that more accurate knowledge is better, but at the same time it is certainly also true that the society of anatomical sciences has an epigenetic state predisposing it to spending many words on fine details. The cardiac conduction system, however, exemplifies a case where painstaking and tedious anatomical work led to insights of great clinical importance such as which parts of the heart can be operated on in corrective surgery [117–119] and which parts are most suitable for artificial pacing [120,121].

The cardiac conduction system comprises only a tiny fraction of the total myocardial mass of the heart and it took the advent of histology for Jan Purkinje to notice the large pale fibers with faint striations that we now call cardiac Purkinje fibers among the more readily identifiable chamber muscle [122]. Purkinje investigated the hearts of several species, but the fibers were most readily identifiable in sheep hearts [122]. Later, Wilhelm His junior described the bundle which penetrates the insulating plane and thus establishes communication between the atria and the ventricles [123]. Tawara expanded on this to show one system comprising the atrioventricular node, the His bundle, its bundle branches, and the Purkinje fibers it terminates in [124]. It is remarkable that the first descriptions of the conduction system with immunohistochemistry were firmly embedded in the foundational anatomical knowledge [125–129].

Regarding Tawara’s discoveries, it is interesting that Tawara was encouraged by his mentor Aschoff to investigate the atrioventricular bundle because of its perceived importance by “experimental physiologists” rather than anatomists [124]. Additionally, Tawara’s investigations into the connections between the bundle branches and the Purkinje fibers were essentially fruitless until Aschoff suggested he investigated sheep hearts (as Purkinje had) and “with this first sheep heart, I was able to completely solve the riddle” [124]. The efficacy of the sheep heart for making these discoveries, we now better understand, is that ungulates have extremely well-developed Purkinje systems [122,130]. That sheep are particularly suitable for the characterization of Purkinje fibers, exemplifies what is now called the Krogh principle, namely that for “a large number of problems, there will be some animal of choice or a few such animals on which it can be most conveniently studied” [131]. It is convenience, or relative ease of experimentation, that has drawn so much of molecular work to model systems such as fruit flies, zebrafish, and mice [132,133]. As more genomes are sequenced and molecular techniques become more broadly applicable [134], the number of species and biological problems that are investigated

may again radiate out and many disciplines will then be needed, including anatomy. Hopefully, there will be future Bob Andersons who then preach the important anatomical insights to the uninitiated.

Funding: This research received no external funding.

Conflicts of Interest: The authors declare no conflict of interest.

References

1. Gladka, M.M.; Molenaar, B.; De Ruiter, H.; Van Der Elst, S.; Tsui, H.; Versteeg, D.; Lacraz, G.P.A.; Huibers, M.M.H.; Van Oudenaarden, A.; Van Rooij, E. Single-cell sequencing of the healthy and diseased heart reveals cytoskeleton-associated protein 4 as a new modulator of fibroblasts activation. *Circulation* **2018**, *138*, 166–180. [CrossRef] [PubMed]
2. DeLaughter, D.M.; Bick, A.G.; Wakimoto, H.; Mckean, D.; Gorham, J.M.; Kathiriya, I.S.; Hinson, J.T.; Homsy, J.; Gray, J.; Pu, W.; et al. Single-Cell Resolution of Temporal Gene Expression during Heart Development. *Dev. Cell* **2016**, *39*, 480–490. [CrossRef] [PubMed]
3. Nyhart, L. The Disciplinary Breakdown of German Morphology, 1870–1900. *Isis* **1987**, *78*, 365–389. [CrossRef] [PubMed]
4. Gifford, C.A.; Ranade, S.S.; Samarakoon, R.; Salunga, H.T.; De Soysa, T.Y.; Huang, Y.; Zhou, P.; Elfenbein, A.; Wyman, S.K.; Bui, Y.K.; et al. Oligogenic inheritance of a human heart disease involving a genetic modifier. *Science* **2019**, *364*, 865–870. [CrossRef] [PubMed]
5. Meyer, H.V.; Dawes, T.J.W.; Serrani, M.; Bai, W.; Tokarczuk, P.; Cai, J.; De Marvao, A.; Henry, A.; Lumbers, T.; Gierten, J.; et al. Genetic and functional insights into the fractal structure of the heart. *Nature* **2020**, *584*, 589–594. [CrossRef] [PubMed]
6. Hulsmans, M.; Clauss, S.; Xiao, L.; Aguirre, A.D.; King, K.R.; Hanley, A.; Hucker, W.J.; Wülfers, E.M.; Seemann, G.; Courties, G.; et al. Macrophages Facilitate Electrical Conduction in the Heart. *Cell* **2017**, *169*, 510–522.e20. [CrossRef] [PubMed]
7. Hussein, A.; KarimianPour, A.; Collier, P.; Krasuski, R.A. Isolated Noncompaction of the Left Ventricle in Adults. *J. Am. Coll. Cardiol.* **2015**, *66*, 578–585. [CrossRef]
8. Greil, A. *Entwicklungsgeschichte des Kopfes und des Blutgefäßsystemes von Ceratodus forsteri. I. Gesammtentwicklung bis zum Beginn der Blutzirkulation. Denkschriften der Medizinisch-Naturwissenschaftlichen Gesellschaft zu Jena 4*; Fischer: Jena, Germany, 1908; pp. 661–934. (In German)
9. Ericsson, R.; Joss, J.; Olsson, L. The fate of cranial neural crest cells in the Australian lungfish, *Neoceratodus forsteri*. *J. Exp. Zool.* **2008**, *310*, 345–354. [CrossRef]
10. Lopez, D.; Durán, A.C.; De Andrés, A.V.; Guerrero, A.; Blasco, M.; Sans-Coma, V. Formation of cartilage in the heart of the Spanish terrapin, *Mauremys leprosa* (Reptilia, Chelonia). *J. Morphol.* **2003**, *258*, 97–105. [CrossRef]
11. Poelmann, R.E.; Groot, A.C.G.-D.; Biermans, M.W.M.; Dolfing, A.I.; Jagessar, A.; Van Hattum, S.; Hoogenboom, A.; Wisse, L.J.; Vicente-Steijn, R.; De Bakker, M.; et al. Outflow tract septation and the aortic arch system in reptiles: Lessons for understanding the mammalian heart. *EvoDevo* **2017**, *8*, 9. [CrossRef]
12. Le Douarin, N. A biological cell labeling technique and its use in experimental embryology. *Dev. Biol.* **1973**, *30*, 217–222. [CrossRef]
13. Kirby, M.L.; Gale, T.F.; E Stewart, D. Neural crest cells contribute to normal aorticopulmonary septation. *Science* **1983**, *220*, 1059–1061. [CrossRef] [PubMed]
14. Greil, A. Beiträge zur vergleichenden anatomie und entwicklungsgeschichte des herzens und des truncus arteriosus der wirbelthiere. *Morph. Jahrb.* **1903**, *31*, 123–310.
15. Keith, A. Schorstein lecture on the fate of the bulbus cordis in the human heart. *Lancet* **1924**, *204*, 1267–1273. [CrossRef]
16. De La Cruz, M.V.; Gómez, C.S.; Arteaga, M.M.; Argüello, C. Experimental study of the development of the truncus and the conus in the chick embryo. *J. Anat.* **1977**, *123*, 661–686.
17. Virágh, S.; Challice, C. Origin and differentiation of cardiac muscle cells in the mouse. *J. Ultrastruct. Res.* **1973**, *42*, 1–24. [CrossRef]

18. Kelly, R.G.; Brown, N.A.; Buckingham, M.E. The Arterial Pole of the Mouse Heart Forms from Fgf10-Expressing Cells in Pharyngeal Mesoderm. *Dev. Cell* **2001**, *1*, 435–440. [CrossRef]
19. Diogo, R.; Kelly, R.G.; Christiaen, L.; Levine, M.; Ziermann, J.M.; Molnar, J.L.; Noden, D.M.; Tzahor, E. A new heart for a new head in vertebrate cardiopharyngeal evolution. *Nat. Cell Biol.* **2015**, *520*, 466–473. [CrossRef]
20. Mommersteeg, M.T.; Domínguez, J.N.; Wiese, C.; Norden, J.; Vries, C.D.G.-D.; Burch, J.B.; Kispert, A.; Brown, N.A.; Moorman, A.F.M.; Christoffels, V.M. The sinus venosus progenitors separate and diversify from the first and second heart fields early in development. *Cardiovasc. Res.* **2010**, *87*, 92–101. [CrossRef]
21. Meilhac, S.M.; Lescroart, F.; Blanpain, C.; Buckingham, M. Cardiac Cell Lineages that Form the Heart. *Cold Spring Harb. Perspect. Med.* **2014**, *4*, a013888. [CrossRef]
22. Bressan, M.; Liu, G.; Mikawa, T. Early Mesodermal Cues Assign Avian Cardiac Pacemaker Fate Potential in a Tertiary Heart Field. *Science* **2013**, *340*, 744–748. [CrossRef] [PubMed]
23. Abu-Issa, R.; Waldo, K.; Kirby, M.L. Heart fields: One, two or more? *Dev. Biol.* **2004**, *272*, 281–285. [CrossRef]
24. Moorman, A.F.M.; Christoffels, V.M.; Anderson, R.H.; Hoff, M.J.V.D. The heart-forming fields: One or multiple? *Philos. Trans. R. Soc. B* **2007**, *362*, 1257–1265. [CrossRef]
25. Gaskell, W.H. On the Innervation of the Heart, with especial reference to the Heart of the Tortoise. *J. Physiol.* **1883**, *4*, 43–230. [CrossRef]
26. Bakker, M.L.; Christoffels, V.M.; Moorman, A.F.M. The Cardiac Pacemaker and Conduction System Develops From Embryonic Myocardium that Retains Its Primitive Phenotype. *J. Cardiovasc. Pharmacol.* **2010**, *56*, 6–15. [CrossRef]
27. Keith, A.; Flack, M. The auriculo-ventricular bundle of the human heart. *Lancet* **1906**, *168*, 359–364. [CrossRef]
28. Robertson, J.I. Memoirs: The development of the heart and vascular system of *Lepidosiren paradoxa*, in Quart. *J. Cell. Sci.* **1913**, *59*, 53–132.
29. Moorman, A.F.M.; Christoffels, V.M. Cardiac Chamber Formation: Development, Genes, and Evolution. *Physiol. Rev.* **2003**, *83*, 1223–1267. [CrossRef]
30. Keith, A.; Flack, M. The Form and Nature of the Muscular Connections between the Primary Divisions of the Vertebrate Heart. *J. Anat. Physiol.* **1907**, *41*, 172–189.
31. Benninghoff, A. Das Herz. In *Handbuch der vergleichende Anatomie der Wirbeltiere*; Bolk, L., Ed.; Urban & Schwarzenberg: Berlin, Germany, 1933; pp. 467–555.
32. Anderson, R.H.; Becker, A.E. *Cardiac Anatomy: Integrated Text and Colour Atlas*; Gower Medical Pub.: London, UK, 1980.
33. Anderson, R.H.; Becker, A.E.; Wenink, A.C.G.; Janse, M.J. The Development of the Cardiac Specialized Tissue. In *The Conduction System of the Heart: Structure, Function and Clinical Implications*; Wellens, H.J.J., Lie, K.I., Janse, M.J., Eds.; Springer: Dordrecht, The Netherlands, 1978; pp. 3–28.
34. Wenink, A.C.G. Development of the human cardiac conducting system. *J. Anat.* **1976**, *121*, 617–631.
35. Bettex, D.A.; Prêtre, R.; Chassot, P.-G. Is our heart a well-designed pump? The heart along animal evolution. *Eur. Hear. J.* **2014**, *35*, 2322–2332. [CrossRef] [PubMed]
36. Benninghoff, A. Über die Beziehungen des Reizleitungssystems und der papillarmuskeln zu den Konturfasern des Herzschauches. *Anat. Anz* **1923**, *57*, 185–208.
37. Srivastava, D.; Olson, E.N. A genetic blueprint for cardiac development. *Nat. Cell Biol.* **2000**, *407*, 221–226. [CrossRef]
38. Wessels, A.; Vermeulen, J.L.M.; Verbeek, F.J.; Virágh, S.Z.; Kálmán, F.; Lamers, W.H.; Moorman, A.F.M. Spatial distribution of “tissue-specific” antigens in the developing human heart and skeletal muscle III. An immunohistochemical analysis of the distribution of the neural tissue antigen G1N2 in the embryonic heart; implications for the development of the atrioventricular conduction system. *Anat. Rec. Adv. Integr. Anat. Evol. Biol.* **1992**, *232*, 97–111. [CrossRef]
39. Anderson, R.H. Simplifying the understanding of congenital malformations of the heart. *Int. J. Cardiol.* **1991**, *32*, 131–142. [CrossRef]
40. Ivanovitch, K.; Esteban, I.; Torres, M. Growth and Morphogenesis during Early Heart Development in Amniotes. *J. Cardiovasc. Dev. Dis.* **2017**, *4*, 20. [CrossRef] [PubMed]
41. Sizarov, A.; Ya, J.; De Boer, B.A.; Lamers, W.H.; Christoffels, V.M.; Moorman, A.F.M. Formation of the Building Plan of the Human Heart. *Circulation* **2011**, *123*, 1125–1135. [CrossRef]

42. Sizarov, A.; Devalla, H.D.; Anderson, R.H.; Passier, R.; Christoffels, V.M.; Moorman, A.F.M. Molecular Analysis of Patterning of Conduction Tissues in the Developing Human Heart. *Circ. Arrhythmia Electrophysiol.* **2011**, *4*, 532–542. [CrossRef]
43. Pettigrew, J.B. XIV. On the arrangement of the muscular fibres in the ventricles of the vertebrate heart, with physiological remarks. *Philos. Trans. R. Soc. Lond.* **1864**, *154*, 445–500. [CrossRef]
44. Streeter, D.D., Jr. Gross Morphology and Fiber Geometry of the Heart. *Handb. Physiol.* **1979**, 61–112.
45. Goodrich, E.S. Note on the Reptilian Heart. *J. Anat.* **1919**, *53*, 298–304. [PubMed]
46. Jensen, B.; Christoffels, V.M. Reptiles as a Model System to Study Heart Development. *Cold Spring Harb. Perspect. Biol.* **2019**, *12*, a037226. [CrossRef]
47. Shaner, R.F. On the Muscular Architecture of the Vertebrate Ventricle. *J. Anat.* **1923**, *58*, 59–70.
48. Lunkenheimer, P.P.; Niederer, P.; Sanchez-Quintana, D.; Murillo, M.; Smerup, M. Models of Ventricular Structure and Function Reviewed for Clinical Cardiologists. *J. Cardiovasc. Transl. Res.* **2012**, *6*, 176–186. [CrossRef]
49. Kelly, A.; Salerno, S.; Connolly, A.; Bishop, M.; Charpentier, F.; Stølen, T.; Smith, G.L. Normal interventricular differences in tissue architecture underlie right ventricular susceptibility to conduction abnormalities in a mouse model of Brugada syndrome. *Cardiovasc. Res.* **2017**, *114*, 724–736. [CrossRef]
50. Meilhac, S.M.; Esner, M.; Kelly, R.G.; Nicolas, J.-F.; Buckingham, M.E. The Clonal Origin of Myocardial Cells in Different Regions of the Embryonic Mouse Heart. *Dev. Cell* **2004**, *6*, 685–698. [CrossRef]
51. Meilhac, S.M.; Esner, M.; Kerszberg, M.; Moss, J.E.; Buckingham, M.E. Oriented clonal cell growth in the developing mouse myocardium underlies cardiac morphogenesis. *J. Cell Biol.* **2004**, *164*, 97–109. [CrossRef]
52. Shaner, R.F. The Development of the Muscular Arrangement in the Ventricles of the Heart. *Can. Med Assoc. J.* **1929**, *20*, 386–390. [PubMed]
53. Garcia-Cañadilla, P.; Dejea, H.; Bonnin, A.; Balicevic, V.; Loncaric, S.; Zhang, C.; Butakoff, C.; Aguado-Sierra, J.; Vázquez, M.; Jackson, L.H.; et al. Complex Congenital Heart Disease Associated with Disordered Myocardial Architecture in a Midtrimester Human Fetus. *Circ. Cardiovasc. Imaging* **2018**, *11*, 007753. [CrossRef]
54. Torrent-Guasp, F.; Buckberg, G.D.; Clemente, C.; Cox, J.L.; Coghlan, H.C.; Gharib, M. The Structure and Function of the Helical Heart and Its Buttress Wrapping. I. The Normal Macroscopic Structure of the Heart. *Semin. Thorac. Cardiovasc. Surg.* **2001**, *13*, 301–319. [CrossRef]
55. Buckberg, G.D.; Nanda, N.C.; Nguyen, C.; Kocica, M.J. What Is the Heart? Anatomy, Function, Pathophysiology, and Misconceptions. *J. Cardiovasc. Dev. Dis.* **2018**, *5*, 33. [CrossRef] [PubMed]
56. Anderson, R.H. Spatial orientation of the ventricular muscle band. *J. Thorac. Cardiovasc. Surg.* **2002**, *124*, 389–392. [CrossRef]
57. MacIver, D.H.; Partridge, J.B.; Agger, P.; Stephenson, R.S.; Boukens, B.J.D.; Omann, C.; Jarvis, J.C.; Zhang, H. The end of the unique myocardial band: Part. II. Clinical and functional considerations. *Eur. J. Cardiothorac. Surg.* **2018**, *53*, 120–128. [CrossRef] [PubMed]
58. MacIver, D.H.; Stephenson, R.S.; Jensen, B.; Damián Sánchez-Quintana, P.A.; Jarvis, J.C.; Partridge, J.B.; Anderson, R.H. The end of the unique myocardial band: Part. I. Anatomical considerations. *Eur. J. Cardiothorac. Surg.* **2018**, *53*, 112–119. [CrossRef] [PubMed]
59. Stephenson, A.; Adams, J.W.; Vaccarezza, M. The vertebrate heart: An evolutionary perspective. *J. Anat.* **2017**, *231*, 787–797. [CrossRef] [PubMed]
60. Anderson, R.H. Evolution of the vertebrate heart. *J. Anat.* **2018**, *232*, 886–887. [CrossRef]
61. Agger, P.; Omann, C.; Laustsen, C.; Stephenson, R.S.; Anderson, R.H. Anatomically correct assessment of the orientation of the cardiomyocytes using diffusion tensor imaging. *NMR Biomed.* **2019**, *33*, 4205. [CrossRef]
62. Agger, P.; Ilkjær, C.; Laustsen, C.; Smerup, M.; Frandsen, J.R.; Ringgaard, S.; Pedersen, M.; Partridge, J.B.; Anderson, R.H.; Hjortdal, V. Changes in overall ventricular myocardial architecture in the setting of a porcine animal model of right ventricular dilation. *J. Cardiovasc. Magn. Reson.* **2017**, *19*, 93. [CrossRef]
63. Ariga, R.; Tunnicliffe, E.M.; Manohar, S.G.; Mahmod, M.; Raman, B.; Piechnik, S.K.; Francis, J.M.; Robson, M.D.; Neubauer, S.; Watkins, H. Identification of Myocardial Disarray in Patients with Hypertrophic Cardiomyopathy and Ventricular Arrhythmias. *J. Am. Coll. Cardiol.* **2019**, *73*, 2493–2502. [CrossRef]
64. Chin, T.K.; Perloff, J.K.; Williams, R.G.; Jue, K.; Mohrmann, R. Isolated noncompaction of left ventricular myocardium. A study of eight cases. *Circulation* **1990**, *82*, 507–513. [CrossRef]

65. Jenni, R.; Oechslin, E.; Schneider, J.; Jost, C.A.; Kaufmann, P. Echocardiographic and pathoanatomical characteristics of isolated left ventricular non-compaction: A step towards classification as a distinct cardiomyopathy. *Heart* **2001**, *86*, 666–671. [CrossRef] [PubMed]
66. Jenni, R.; Rojas, J.; Oechslin, E. Isolated Noncompaction of the Myocardium. *N. Engl. J. Med.* **1999**, *340*, 966–967. [CrossRef] [PubMed]
67. Petersen, S.E.; Selvanayagam, J.B.; Wiesmann, F.; Robson, M.D.; Francis, J.M.; Anderson, R.H.; Watkins, H.; Neubauer, S. Left Ventricular Non-Compaction. *J. Am. Coll. Cardiol.* **2005**, *46*, 101–105. [CrossRef]
68. Captur, G.; Flett, A.S.; Jacoby, D.L.; Moon, J.R. Left ventricular non-compaction: The mitral valve prolapse of the 21st century? *Int. J. Cardiol.* **2013**, *164*, 3–6. [CrossRef] [PubMed]
69. Grothoff, M.; Pachowsky, M.; Hoffmann, J.; Posch, M.; Klaassen, S.; Lehmkuhl, L.; Gutberlet, M. Value of cardiovascular MR in diagnosing left ventricular non-compaction cardiomyopathy and in discriminating between other cardiomyopathies. *Eur. Radiol.* **2012**, *22*, 2699–2709. [CrossRef] [PubMed]
70. Halaney, D.L.; Sanyal, A.; Nafissi, N.A.; Escobedo, D.; Goros, M.; Michalek, J.E.; Acevedo, P.; Pérez, W.; Escobar, G.P.; Feldman, M.D.; et al. The Effect of Trabeculae Carneae on Left Ventricular Diastolic Compliance: Improvement in Compliance with Trabecular Cutting. *J. Biomech. Eng.* **2017**, *139*, 0310121–0310128. [CrossRef]
71. Shave, R.E.; Lieberman, D.E.; Drane, A.L.; Brown, M.G.; Batterham, A.M.; Worthington, S.; Atencia, R.; Feltrer, Y.; Neary, J.; Weiner, R.B.; et al. Selection of endurance capabilities and the trade-off between pressure and volume in the evolution of the human heart. *Proc. Natl. Acad. Sci. USA* **2019**, *116*, 19905–19910. [CrossRef] [PubMed]
72. Ho, S.Y.; Sanchez-Quintana, D.; A Cabrera, J.; Anderson, R.H. Anatomy of the left atrium: Implications for radiofrequency ablation of atrial fibrillation. *J. Cardiovasc. Electrophysiol.* **1999**, *10*, 1525–1533.
73. Rillig, A.; Tiltz, R.; Lin, T.; Fink, T.; Heeger, C.-H.; Arya, A.; Metzner, A.; Mathew, S.; Wissner, E.; Makimoto, H.; et al. Unexpectedly High Incidence of Stroke and Left Atrial Appendage Thrombus Formation After Electrical Isolation of the Left Atrial Appendage for the Treatment of Atrial Tachyarrhythmias. *Circ. Arrhythmia Electrophysiol.* **2016**, *9*, e003461. [CrossRef]
74. Sedmera, D.; Pexieder, T.; Vuillemin, M.; Thompson, R.P.; Anderson, R.H. Developmental patterning of the myocardium. *Anat. Rec.* **2000**, *258*, 319–337. [CrossRef]
75. Feldt, R.H.; Rahimtoola, S.H.; Davis, G.D.; Swan, H.; Titus, J.L. Anomalous ventricular myocardial patterns in a child with complex congenital heart disease. *Am. J. Cardiol.* **1969**, *23*, 732–734. [CrossRef]
76. Angelini, A.; Melacini, P.; Barbero, F.; Thiene, G. Evolutionary persistence of spongy myocardium in humans. *Circulation* **1999**, *99*, 2475. [CrossRef] [PubMed]
77. Freedom, R.M.; Yoo, S.-J.; Perrin, D.; Taylor, G.; Petersen, S.; Anderson, R.H. The morphological spectrum of ventricular noncompaction. *Cardiol. Young* **2005**, *15*, 345–364. [CrossRef] [PubMed]
78. Towbin, J.A.; Jefferies, J.L. Cardiomyopathies Due to Left Ventricular Noncompaction, Mitochondrial and Storage Diseases, and Inborn Errors of Metabolism. *Circ. Res.* **2017**, *121*, 838–854. [CrossRef] [PubMed]
79. Zemrak, F.; Ahlman, M.A.; Captur, G.; Mohiddin, S.A.; Kawel-Boehm, N.; Prince, M.R.; Moon, J.C.; Hundley, W.G.; Lima, J.A.; Bluemke, D.A.; et al. The Relationship of Left Ventricular Trabeculation to Ventricular Function and Structure Over a 9.5-Year Follow-Up. *J. Am. Coll. Cardiol.* **2014**, *64*, 1971–1980. [CrossRef]
80. Weir-McCall, J.R.; Yeap, P.M.; Papagiorcopulo, C.; Fitzgerald, K.; Gandy, S.J.; Lambert, M.; Belch, J.J.F.; Cavin, I.; Littleford, R.; Macfarlane, J.A.; et al. Left Ventricular Noncompaction. *J. Am. Coll. Cardiol.* **2016**, *68*, 2157–2165. [CrossRef]
81. Ivanov, A.; Dabiesingh, D.S.; Bhumireddy, G.P.; Mohamed, A.; Asfour, A.; Briggs, W.M.; Ho, J.; Khan, S.A.; Grossman, A.; Klem, I.; et al. Prevalence and Prognostic Significance of Left Ventricular Noncompaction in Patients Referred for Cardiac Magnetic Resonance Imaging. *Circ. Cardiovasc. Imaging* **2017**, *10*, e006174. [CrossRef]
82. Oechslin, E.N.; Jenni, R.; Klaassen, S. Left ventricular noncompaction is a myocardial phenotype: Cardiomyopathy—Yes or no? *Can. J. Cardiol.* **2020**, in press. [CrossRef]
83. Van Waning, J.I.; Caliskan, K.; Chelu, R.G.; Van Der Velde, N.; Pezzato, A.; Michels, M.; Van Slegtenhorst, M.A.; Boersma, E.; Nieman, K.; Majoor-Krakauer, D.; et al. Diagnostic CMR Imaging Criteria in Noncompaction Cardiomyopathy and the Yield of Genetic Testing. *Can. J. Cardiol.* **2020**, in press. [CrossRef]

84. De Bakker, B.S.; De Jong, K.H.; Hagoort, J.; De Bree, K.; Besselink, C.T.; De Kanter, F.E.C.; Veldhuis, T.; Bais, B.; Schildmeijer, R.; Ruijter, J.M.; et al. An interactive three-dimensional digital atlas and quantitative database of human development. *Science* **2016**, *354*, aag0053. [CrossRef]
85. E Blausen, B.; Johannes, R.S.; Hutchins, G.M. Computer-based reconstructions of the cardiac ventricles of human embryos. *Am. J. Cardiovasc. Pathol.* **1990**, *3*, 37–43.
86. Miquerol, L.; Moreno-Rascon, N.; Beyer, S.; Dupays, L.; Meilhac, S.M.; Buckingham, M.E.; Franco, D.; Kelly, R.G. Biphasic Development of the Mammalian Ventricular Conduction System. *Circ. Res.* **2010**, *107*, 153–161. [CrossRef]
87. Tian, X.; Li, Y.; He, L.; Zhang, H.; Huang, X.; Liu, Q.; Pu, W.; Zhang, L.; Li, Y.; Zhao, H.; et al. Identification of a hybrid myocardial zone in the mammalian heart after birth. *Nat. Commun.* **2017**, *8*, 87. [CrossRef]
88. Sissman, N.J. Developmental landmarks in cardiac morphogenesis: Comparative chronology. *Am. J. Cardiol.* **1970**, *25*, 141–148. [CrossRef]
89. Anderson, R.H.; Jensen, B.; Mohun, T.J.; Petersen, S.E.; Aung, N.; Zemrak, F.; Planken, R.N.; Maciver, D.H. Key Questions Relating to Left Ventricular Noncompaction Cardiomyopathy: Is the Emperor Still Wearing Any Clothes? *Can. J. Cardiol.* **2017**, *33*, 747–757. [CrossRef]
90. Oechslin, E.; Jenni, R. Left Ventricular Noncompaction. *J. Am. Coll. Cardiol.* **2018**, *71*, 723–726. [CrossRef]
91. Luxán, G.; Casanova, J.C.; Martínez-Poveda, B.; Prados, B.; D’Amato, G.; MacGrogan, D.; Gonzalez-Rajal, A.; Dobarro, D.; Torroja, C.; Martinez, F.; et al. Mutations in the NOTCH pathway regulator MIB1 cause left ventricular noncompaction cardiomyopathy. *Nat. Med.* **2013**, *19*, 193–201. [CrossRef]
92. D’Amato, G.; Luxán, G.; Del Monte-Nieto, G.; Martínez-Poveda, B.; Torroja, C.; Walter, W.; Bochter, M.S.; Benedito, R.; Cole, S.; Martinez, F.; et al. Sequential Notch activation regulates ventricular chamber development. *Nat. Cell Biol.* **2015**, *18*, 7–20. [CrossRef] [PubMed]
93. Del Monte-Nieto, G.; Ramialison, M.; Adam, A.A.S.; Wu, B.; Aharonov, A.; D’Uva, G.; Bourke, L.M.; Pitulescu, M.E.; Chen, H.; De La Pompa, J.L.; et al. Control of cardiac jelly dynamics by NOTCH1 and NRG1 defines the building plan for trabeculation. *Nat. Cell Biol.* **2018**, *557*, 439–445. [CrossRef] [PubMed]
94. Sandireddy, R.; Cibi, D.M.; Gupta, P.; Singh, A.; Tee, N.; Uemura, A.; Epstein, J.A.; Singh, M.K. Semaphorin 3E/PlexinD1 signaling is required for cardiac ventricular compaction. *JCI Insight* **2019**, *4*, e125908. [CrossRef] [PubMed]
95. E Sigvardsen, P.; Fuchs, A.; Kühl, J.T.; Afzal, S.; Køber, L.; Nordestgaard, B.G.; Kofoed, K.F. Left ventricular trabeculation and major adverse cardiovascular events: The Copenhagen General Population Study. *Eur. Hear. J. Cardiovasc. Imaging* **2020**, jeaa110. [CrossRef] [PubMed]
96. Röse, C. Beiträge zur vergleichenden Anatomie des Herzens der Wirbelthiere. *Morphol. Jahrb.* **1890**, *16*, 27–96.
97. Rowlatt, U. Comparative anatomy of the heart of mammals. *Zool. J. Linn. Soc.* **1990**, *98*, 73–110. [CrossRef]
98. Odgers, P.N.B. The Formation of the Venous Valves, the Foramen Secundum and the Septum Secundum in the Human Heart. *J. Anat.* **1935**, *69*, 412–422.5.
99. Waterston, D. XII.—The Development of the Heart in Man. *Trans. R. Soc. Edinb.* **1919**, *52*, 257–302. [CrossRef]
100. Patten, B.M. Developmental defects at the foramen ovale. *Am. J. Pathol.* **1938**, *14*, 135–162.9.
101. Patten, B.M. The changes in circulation following birth. *Am. Hear. J.* **1930**, *6*, 192–205. [CrossRef]
102. Crick, S.J.; Sheppard, M.N.; Ho, S.Y.; Gebstein, L.; Anderson, R.H. Anatomy of the pig heart: Comparisons with normal human cardiac structure. *J. Anat.* **1998**, *193*, 105–119. [CrossRef]
103. Hara, H.; Virmani, R.; Ladich, E.; Mackey-Bojack, S.; Titus, J.L.; Karnicki, K.; Stewart, M.; Pelzel, J.M.; Schwartz, R.S. Patent foramen ovale: Standards for a preclinical model of prevalence, structure, and histopathologic comparability to human hearts. *Catheter. Cardiovasc. Interv.* **2007**, *69*, 266–273. [CrossRef]
104. Hara, H.; Virmani, R.; Ladich, E.; Mackey-Bojack, S.; Titus, J.; Reisman, M.; Gray, W.; Nakamura, M.; Mooney, M.; Poulouse, A.; et al. Patent Foramen Ovale: Current Pathology, Pathophysiology, and Clinical Status. *J. Am. Coll. Cardiol.* **2005**, *46*, 1768–1776. [CrossRef]
105. Calvert, P.A.; Rana, B.S.; Kydd, A.C.; Shapiro, L.M. Patent foramen ovale: Anatomy, outcomes, and closure. *Nat. Rev. Cardiol.* **2011**, *8*, 148–160. [CrossRef] [PubMed]
106. Homma, S.; Messé, S.R.; Rundek, T.; Sun, Y.-P.; Franke, J.; Davidson, K.; Sievert, H.; Sacco, R.L.; Di Tullio, M.R. Patent foramen ovale. *Nat. Rev. Dis. Prim.* **2016**, *2*, 15087. [CrossRef] [PubMed]
107. Jensen, B.; Joyce, W.; Gregorovicova, M.; Sedmera, D.; Wang, T.; Christoffels, V.M. Low incidence of atrial septal defects in nonmammalian vertebrates. *Evol. Dev.* **2019**, *22*, 241–256. [CrossRef] [PubMed]

108. Anderson, R.H.; Brown, N.A. The anatomy of the heart revisited. *Anat. Rec. Adv. Integr. Anat. Evol. Biol.* **1996**, *246*, 1–7. [CrossRef]
109. Anderson, R.H.; Spicer, D.E.; Brown, N.A.; Mohun, T.J. The Development of Septation in the Four-Chambered Heart. *Anat. Rec. Adv. Integr. Anat. Evol. Biol.* **2014**, *297*, 1414–1429. [CrossRef]
110. Naqvi, N.; McCarthy, K.P.; Ho, S.Y. Anatomy of the atrial septum and interatrial communications. *J. Thorac. Dis.* **2018**, *10*, S2837–S2847. [CrossRef]
111. Wessels, A. *Inflow Tract Development, in Congenital Heart Diseases: The Broken Heart: Clinical Features, Human Genetics and Molecular Pathways*; Springer: Vienna, Austria, 2016; pp. 55–62.
112. Jensen, B.; Wang, T.; Moorman, A.F. Evolution and Development of the Atrial Septum. *Anat. Rec. Adv. Integr. Anat. Evol. Biol.* **2018**, *302*, 32–48. [CrossRef]
113. Sharratt, G.P.; Webb, S.; Anderson, R.H. The vestibular defect: An interatrial communication due to a deficiency in the atrial septal component derived from the vestibular spine. *Cardiol. Young* **2003**, *13*, 184–190. [CrossRef]
114. Snarr, B.S.; O'Neal, J.L.; Chintalapudi, M.R.; Wirrig, E.E.; Phelps, A.L.; Kubalak, S.W.; Wessels, A. Isl1 Expression at the Venous Pole Identifies a Novel Role for the Second Heart Field in Cardiac Development. *Circ. Res.* **2007**, *101*, 971–974. [CrossRef] [PubMed]
115. Mommersteeg, M.T. Two Distinct Pools of Mesenchyme Contribute to the Development of the Atrial Septum. *Circ. Res.* **2006**, *99*, 351–353. [CrossRef]
116. Loomba, R.S.; Tretter, J.T.; Mohun, T.J.; Anderson, R.H.; Kramer, S.; Spicer, D.E. Identification and Morphogenesis of Vestibular Atrial Septal Defects. *J. Cardiovasc. Dev. Dis.* **2020**, *7*, 35. [CrossRef] [PubMed]
117. Becker, A.E.; Anderson, R.H.; Durrer, D.; Wellens, H.J. The anatomical substrates of wolff-parkinson-white syndrome. A clinicopathologic correlation in seven patients. *Circulation* **1978**, *57*, 870–879. [CrossRef] [PubMed]
118. Anderson, R.H.; Becker, A.E.; Arnold, R.; Wilkinson, J.L. The Conducting Tissues in Congenitally Corrected Transposition. *Circulation* **1974**, *50*, 911–923. [CrossRef] [PubMed]
119. Piazza, N.; De Jaegere, P.; Schultz, C.; Becker, A.E.; Serruys, P.W.; Anderson, R.H. Anatomy of the Aortic Valvar Complex and Its Implications for Transcatheter Implantation of the Aortic Valve. *Circ. Cardiovasc. Interv.* **2008**, *1*, 74–81. [CrossRef]
120. Li, Y.; Chen, K.; Dai, Y.; Li, C.; Sun, Q.; Chen, R.; Gold, M.R.; Zhang, S. Left bundle branch pacing for symptomatic bradycardia: Implant success rate, safety, and pacing characteristics. *Hear. Rhythm.* **2019**, *16*, 1758–1765. [CrossRef]
121. Ali, N.; Shin, M.S.; Whinnett, Z. The Emerging Role of Cardiac Conduction System Pacing as a Treatment for Heart Failure. *Curr. Hear. Fail. Rep.* **2020**, *17*, 288–298. [CrossRef]
122. Sedmera, D.; Gourdie, R.G. Why do we have Purkinje fibers deep in our heart? *Physiol. Res.* **2014**, *63*, 9–18. [CrossRef]
123. Anderson, R.H.; Mori, S. Wilhelm His Junior and his bundle. *J. Electrocardiol.* **2016**, *49*, 637–643. [CrossRef]
124. De Almeida, M.C.; Sanchez-Quintana, D.; Anderson, R.H. Sunao Tawara: Further musings on his tribulations in providing the basis for the modern-day understanding of cardiac electrophysiology. *Anat. Sci. Int.* **2020**, *95*, 381–386. [CrossRef]
125. Sanders, E.; Groot, I.J.M.; Geerts, W.J.C.; De Jong, F.; A Van Horssen, A.; Los, J.A.; Moorman, A.F.M. The local expression of adult chicken heart myosins during development. *Brain Struct. Funct.* **1986**, *174*, 187–193. [CrossRef]
126. Gorza, L.; Schiaffino, S.; Vitadello, M. Heart conduction system: A neural crest derivative? *Brain Res.* **1988**, *457*, 360–366. [CrossRef]
127. Anderson, R.H.; Mori, S.; Spicer, D.E.; Sanchez-Quintana, D.; Jensen, B. The Anatomy, Development, and Evolution of the Atrioventricular Conduction Axis. *J. Cardiovasc. Dev. Dis.* **2018**, *5*, 44. [CrossRef] [PubMed]
128. Dobrzynski, H.; Anderson, R.H.; Atkinson, A.; Borbas, Z.; D'Souza, A.; Fraser, J.F.; Inada, S.; Logantha, S.J.; Monfredi, O.J.; Morris, G.M.; et al. Structure, function and clinical relevance of the cardiac conduction system, including the atrioventricular ring and outflow tract tissues. *Pharmacol. Ther.* **2013**, *139*, 260–288. [CrossRef]
129. Delorme, B.; Dahl, E.; Jarry-Guichard, T.; Marics, I.; Briand, J.-P.; Willecke, K.; Gros, D.; Théveniau-Ruissy, M. Developmental regulation of connexin 40 gene expression in mouse heart correlates with the differentiation of the conduction system. *Dev. Dyn.* **1995**, *204*, 358–371. [CrossRef] [PubMed]

130. Oosthoek, P.W.; Virágh, S.; Lamers, W.H.; Moorman, A.F. Immunohistochemical delineation of the conduction system. II: The atrioventricular node and Purkinje fibers. *Circ. Res.* **1993**, *73*, 482–491. [CrossRef]
131. Krogh, A. The progress of physiology. *Science* **1929**, *70*, 200–204. [CrossRef]
132. Mummery, C. Perspectives on the Use of Human Induced Pluripotent Stem Cell-Derived Cardiomyocytes in Biomedical Research. *Stem Cell Rep.* **2018**, *11*, 1306–1311. [CrossRef]
133. Bakkers, J. Zebrafish as a model to study cardiac development and human cardiac disease. *Cardiovasc. Res.* **2011**, *91*, 279–288. [CrossRef]
134. Kvon, E.Z.; Kamneva, O.K.; Melo, U.S.; Barozzi, I.; Osterwalder, M.; Mannion, B.J.; Tissières, V.; Pickle, C.S.; Plajzer-Frick, I.; Lee, E.A.; et al. Progressive Loss of Function in a Limb Enhancer during Snake Evolution. *Cell* **2016**, *167*, 633–642. [CrossRef]

Publisher's Note: MDPI stays neutral with regard to jurisdictional claims in published maps and institutional affiliations.



© 2020 by the authors. Licensee MDPI, Basel, Switzerland. This article is an open access article distributed under the terms and conditions of the Creative Commons Attribution (CC BY) license (<http://creativecommons.org/licenses/by/4.0/>).

Review

The Intrinsic Cardiac Nervous System and Its Role in Cardiac Pacemaking and Conduction

Laura Fedele * and Thomas Brand * 

Developmental Dynamics, National Heart and Lung Institute (NHLI), Imperial College, London W12 0NN, UK

* Correspondence: l.fedele@imperial.ac.uk (L.F.); t.brand@imperial.ac.uk (T.B.);

Tel.: +44-(0)-207-594-6531 (L.F.); +44-(0)-207-594-8744 (T.B.)

Received: 17 August 2020; Accepted: 20 November 2020; Published: 24 November 2020

Abstract: The cardiac autonomic nervous system (CANS) plays a key role for the regulation of cardiac activity with its dysregulation being involved in various heart diseases, such as cardiac arrhythmias. The CANS comprises the extrinsic and intrinsic innervation of the heart. The intrinsic cardiac nervous system (ICNS) includes the network of the intracardiac ganglia and interconnecting neurons. The cardiac ganglia contribute to the tight modulation of cardiac electrophysiology, working as a local hub integrating the inputs of the extrinsic innervation and the ICNS. A better understanding of the role of the ICNS for the modulation of the cardiac conduction system will be crucial for targeted therapies of various arrhythmias. We describe the embryonic development, anatomy, and physiology of the ICNS. By correlating the topography of the intracardiac neurons with what is known regarding their biophysical and neurochemical properties, we outline their physiological role in the control of pacemaker activity of the sinoatrial and atrioventricular nodes. We conclude by highlighting cardiac disorders with a putative involvement of the ICNS and outline open questions that need to be addressed in order to better understand the physiology and pathophysiology of the ICNS.

Keywords: nervous system; development; neural crest cells; innervation; ganglia; sympathetic neurons; parasympathetic neurons; neurotransmitter; neurocardiac junction

1. Introduction

The intrinsic cardiac nervous system (ICNS) is sometimes referred as the “little brain” of the heart [1]. It makes continuous adjustments of the cardiac mechanical and electrical activity and it consists of a network of neurons that communicate with each other and with neurons located in the extracardiac thoracic ganglia, all under the control of the central nervous system. The ICNS comprises afferent (sensory), interconnecting (local circuit), and cardio-motor (efferent sympathetic and parasympathetic) neurons [1,2]. The intrinsic cardiac neurons are mainly concentrated in intracardiac ganglia residing in specific regions of the heart, mostly in the atria, and each ganglion has a preferential region of action [2]. The activation of efferent neurons results in the modulation of the heart rate, atrio-ventricular node conduction as well as inotropism of atria and ventricles. Local circuit neurons (LCNs) work as inter- and intra-ganglionic connections, whilst afferent neurons transduce information of the cardiovascular milieu [1,3].

The control of the heart by the cardiac autonomic nervous system (CANS) is hierarchically organized and it can be subdivided into three levels (Figure 1). Level 1 is composed of the neurons in the medulla oblongata (brainstem) and spinal cord, which are controlled by higher cortical neurons (e.g., insular cortex, anterior cingulate cortex, medial prefrontal cortex, and amygdala) in the central nervous system [2,4,5]. Level 2 and 3 are in the periphery, level 2 comprises the intrathoracic extracardiac ganglia, and level 3 the ICNS [2]. Notably, the ICNS can modulate regional cardiac function in a beat-to-beat fashion and it can regulate heart function, even when disconnected from the higher levels [2]. Overall, the CANS plays a

fundamental role in modulating contractility (inotropy), relaxation (lusitropy), beating rate (chronotropy), conduction velocity (dromotropy), and myocyte cohesion (adhesiotropy), and therefore affects both the electrophysiology and hemodynamics of the heart [6]. Importantly, clinical studies have demonstrated an implication of the cardiac nervous system in atrial and ventricular arrhythmias [7].

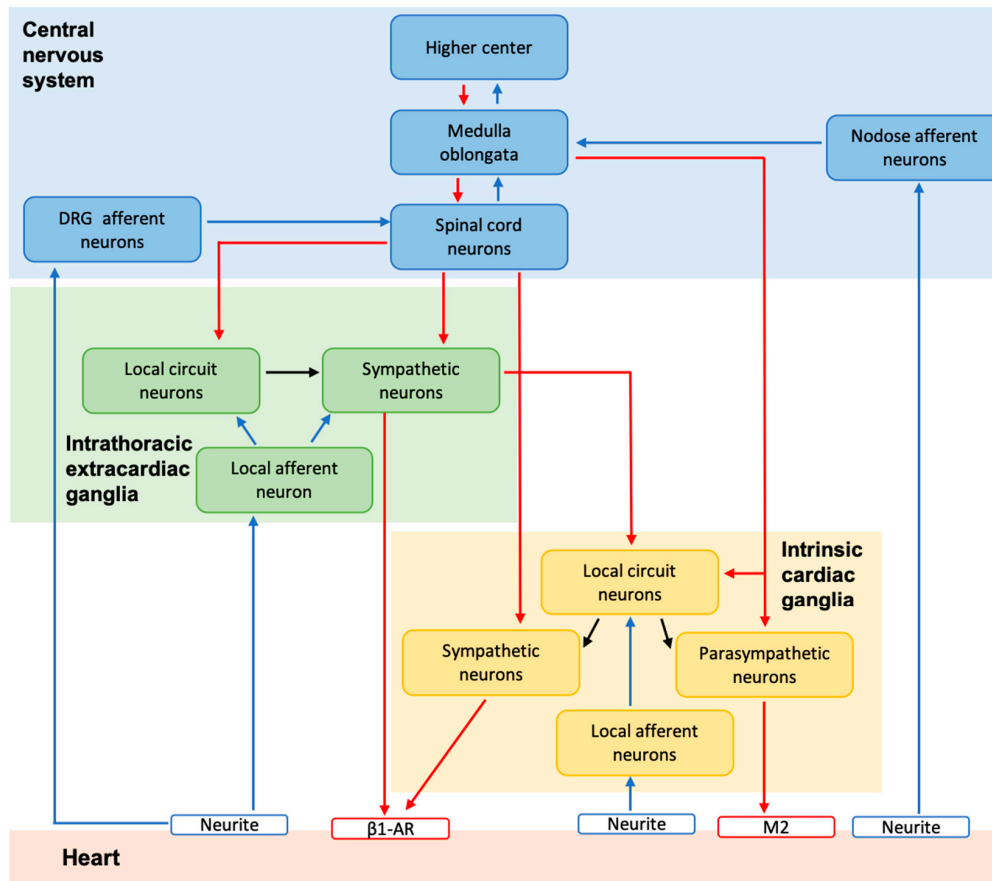


Figure 1. Model of the hierarchical control of the heart by the cardiac autonomic nervous system (CANS). The intrinsic cardiac nervous system (ICNS) contains efferent (parasympathetic and sympathetic) neurons, local afferent neurons and local circuit neurons. The intrathoracic extracardiac ganglia (stellate ganglia and middle cervical ganglia) contain sympathetic neurons, local afferent and local circuit neurons. The intrathoracic ganglia (intra- and extracardiac) work in close coordination as a nested loop, which is further tuned by the CNS (spinal cord, brainstem, hypothalamus, and forebrain) resulting in the regulation of cardiac function on a beat-to-beat basis. DRG: dorsal root ganglion; β 1AR: beta 1 adrenergic receptor, M2: muscarinic acetylcholine receptor type 2. Neurite: local afferent neurites embedded in the cardiac walls. Figure adapted from Ardell & Armour *J. Phys* published by Wiley 2016 [2].

Various cardiothoracic reflexes depend on the sensory transduction of the local afferent neurons (in the intrathoracic intra- and extracardiac ganglia) as well as the afferent neurons in the spinal cord, dorsal root, and nodose ganglia. Their transductions result in the initiation of the reflex both in the central and peripheral nervous system [2]. The afferent neurons can transduce mechanical (mechanosensory neurons) and chemical (chemosensory neurons) stimuli, with the majority of the intrinsic cardiac afferent neurons transducing both modalities [3].

Cardiomyocytes and coronary vessels are regulated by the efferent neurons, as well as by circulating hormones. The efferent cardiac neuronal outputs depend on both pre-ganglionic and post-ganglionic neurons [2,8]. The sympathetic branch comprehends the pre-sympathetic efferent neurons in the brainstem that project to the pre-ganglionic neurons in the spinal cord (intermediolateral column), which, in turn synapse to the post-ganglionic sympathetic neurons residing in the intrathoracic

ganglia (cervical and stellate ganglia) [2]. As depicted in Figure 1, some spinal cord neurons (although a small number) form synapses with sympathetic post-ganglionic neurons in the ICNS [2,8]. The parasympathetic pre-ganglionic neurons reside in the brainstem (mainly in the nucleus ambiguus), and project to post-ganglionic neurons that are located in the ICNS ganglia [2]. Both the sympathetic and parasympathetic efferent neurons in the ICNS are located in the major atrial and ventricular ganglia and regulate the electrical and mechanical activity of the heart [2,8].

The cardiac conduction system (CCS) plays an essential role in the initiation and coordination of the heart's electrophysiology. It is composed of the sinoatrial node (SAN), the atrioventricular node (AVN) and the His–Purkinje system. The SAN residing in the inflow tract of the right atrium, acts as the primary pacemaker initiating the cardiac action potential. The AVN retards the conduction of the action potential from the atria to the ventricles and works as a “back-up” pacemaker in the case of a failure of the SAN. The His-Purkinje system is composed of a common bundle (the bundle of His) branching into the left and right networks of Purkinje fibers and propagates the action potential throughout the ventricles to permit their simultaneous electrical activation [9].

In this review, we will describe the role of the ICNS for cardiac electrophysiology with a particular focus on its role in modulating the function of the CCS. We discuss the embryonic development of the ICNS, the anatomy and physiological role, and its interaction with the CCS. We conclude the review with some examples of heart disease that might also involve a disruption of the ICNS and highlighting gaps that we identified in the literature that need to be addressed in the future.

2. Development of the Innervation of the Heart

The development of the innervation of the heart is a tightly regulated process, both spatially and temporally, which occurs concurrently with the development of the cardiovascular system [10,11]. The ICNS originates from the neuroectoderm, whereas the heart is a mesoderm derivative [12]. Cardiac innervation starts during the fifth week of human development (E10-E11 in mice) and it is characterized by four developmental stages: (1) the migration of neural crest cells (NCCs) to the dorsal aorta; (2) their differentiation into neurons; (3) the formation of the paravertebral sympathetic chain and parasympathetic cardiac ganglia through migration and aggregation of neuronal precursors; and (4) patterning and differentiation of the neuronal projection in the heart [13]. The parasympathetic innervation of the heart becomes functional before sympathetic neurons start to differentiate. The developing heart is initially relying on intrinsic cardiac adrenergic (ICA) cells as a source of catecholamines [10]. Cholinesterase activity appears in cardiac neurons between the fourth and seventh month of gestation in humans and at postnatal day 4 (P4) in rats; while, acetylcholine appears at E19 in rats [14,15].

2.1. Intrinsic Cardiac Adrenergic Cells (ICA)

Catecholamines play a key role in cardiac embryonic development, even in the pre-innervation stages and before chromaffin cells of the adrenal glands can synthesize them (E15.5 in mice). Targeted disruption in mice of the genes encoding the enzymes that are involved in catecholamine biosynthesis, dopamine β -hydroxylase (DBH), and tyrosine hydroxylase (TH) are embryonic lethal [16,17]. In the early embryo (E8.5 in mice), the myocardium itself expresses the catecholamine synthesizing enzyme phenylethanolamine-*N*-methyltransferase (PNMT), with the ICA cells being the major source of catecholamine synthesis [18].

ICA cells are transiently found during development, their fate is not clear, and some might differentiate into pacemaker cells [13]. In accordance with this, in the mouse embryo, ICA cells are present in regions that are associated with the CCS, which suggests a specific role in its development [19,20]. Interestingly, some ICA cells persist in the adult ventricular myocardium, and they might act as a “backup” system when innervation is lost [21]. In fact, after denervation due to cardiac transplantation, the number of ICA cells increased along with the expression of TH, DBH, and PNMT. ICA cells might have a cardioprotective role, as they also express cardioprotective genes, e.g., calcitonin gene related peptide (CGRP) [22,23].

2.2. Migration of Neural Crest Cells

Neural crest cells (NCCs) migrate into the developing heart in the fifth week in humans (E8.5 in mice). Depending on their region of origin, they give rise to distinct cell types, among them the sympathetic, sensory, and parasympathetic neurons [10].

Sympathetic neurons originate from the trunk NCCs that migrate along the ventral pathway towards the dorsal aorta; they then migrate into rostral and caudal direction to form the paravertebral sympathetic chain. On their migratory route, the NCCs are guided by attracting and repelling factors, among them ephrins and semaphorins (SEMA) [13]. Ephrins orchestrate the direction of the migration along the ventral pathway: EphrinB, present in the posterior side of the somite, has a repulsive effect on NCCs, which express the EphB2 receptor [24]. The migration towards the dorsal aorta is directed by SEMA acting on its receptors (e.g., Neuropilin-1/2), which are expressed in NCCs. SEMA3C is expressed in the myocardial cuff cells in the outflow tract and it acts as an attractive cue for NCCs, contrasting to the action of the repelling SEMA6B and SEMA6B present in the dorsal neural tube. In accordance with the key role of SEMA in the migration of NCCs destined to form sympathetic neurons, *Nrp1* and *Sema3a* knock-out mice display a sinus bradycardia phenotype as a result of sympathetic ganglia dysfunction, e.g., ectopic sympathetic ganglia and malformed stellate ganglia [25].

The cardiac parasympathetic ganglia originate from the so-called “cardiac NCCs”, which is a subset of the vagal neural crest (Figure 2). In contrast to the sympathetic counterparts, they migrate either through or lateral to the somites, entering the heart and forming the cardiac ganglia from E12.5 onwards [26]. Interestingly, NCCs are not the only source of parasympathetic neurons, as they can also originate from the nodose placode. This was demonstrated by the ablation of the NCCs in quail to chick chimeras and by *Wnt1-Cre* lineage tracing in mice [26,27]. Further research is needed in order to elucidate the potential role of guidance cues in the migration of the parasympathetic neurons, as some factors have been proposed, purely based on their transient immunoreactivity during development, e.g., HNK1 (human natural killer-1/CD57) in regions with ingrowing parasympathetic fibers in the basal region of the heart [28].

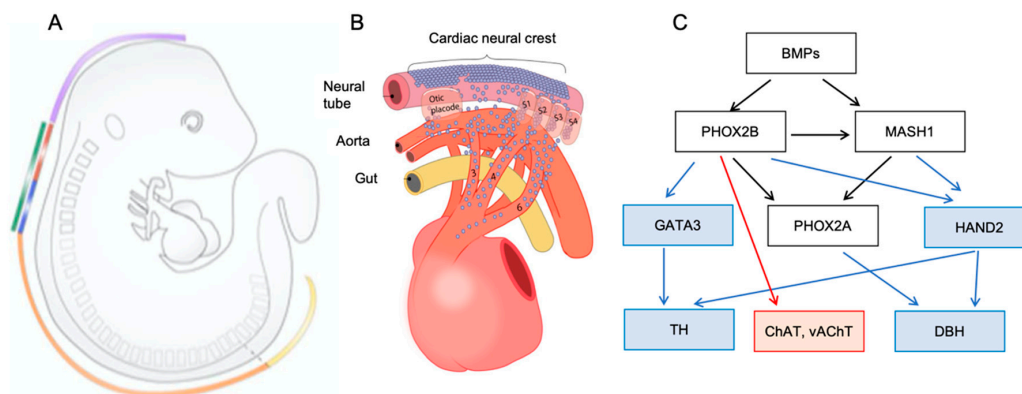


Figure 2. (A) Regionalization of the neural crest along the dorsal neural tube of the mouse embryo (E10.5): cranial (purple), vagal (green), trunk (orange), and sacral (yellow). Vagal neural crest cells (NCCs) are further subdivided into: cardiac (red) and enteric (blue) lineages. (B) Migration of cardiac NCCs through or lateral to the somites into the branchial arch arteries and further into the outflow tract. (C) Transcriptional network involved in the specification and differentiation of NCCs into sympathetic and parasympathetic neurons. White box: factors involved in both pathways; blue: factors involved in the differentiation of sympathetic neurons and red: of parasympathetic neurons. Abbreviations: BMPs- bone morphogenic proteins; ChAT- choline acetyltransferase; DBH- dopamine β -hydroxylase; GATA3- GATA binding protein 3; HAND2: heart and neural crest derivative expressed 2; MASH1- mammalian achaete-scute homologue; PHOX2 (A or B)- paired-like homeobox 2A or 2B; TH- tyrosine hydroxylase; vAChT- vesicular acetylcholine transporter. (A) reproduced with permission from Hutchins, E.J., et al. *Dev. Biol* published by Elsevier 2018 [29]; (B) reproduced with permission from Vég h A.M.D., et al. *JCDD* by MDPI 2016 [10]; (C) adapted from Vég h A.M.D., et al. *JCDD* by MDPI 2016 [10].

2.3. Differentiation of Neural Crest Cells

After NCCs have reached the dorsal aorta (E9.5) and the outflow tract (E10.5), they encounter various factors that are involved in their specification towards sympathetic or parasympathetic neuronal identity [10]. It has been suggested that sympathetic and parasympathetic neurons share a common precursor, with a potential role of bone morphogenetic protein (BMP)2 in their specification. In accordance with this, sympathetic neurons can transdifferentiate in vitro into parasympathetic neurons upon stimulation with low BMP2 levels [30]. High levels of BMP2 favors sympathetic differentiation, whilst low levels induce parasympathetic identity [10].

The initial steps in the differentiation process are similar between sympathetic and parasympathetic neurons (Figure 2). BMPs that are released by the epicardial and vascular cells elicit a transcriptional differentiation cascade, which is shared by both, sympathetic and parasympathetic neuronal precursors. The disruption of BMPs results in compromised differentiation into sympathetic neurons. For example, inhibition of BMP4-7 in avian embryos prevents sympathetic differentiation and sympathetic neuronal progenitors die after they have reached the dorsal aorta in *Alk3* (the type 1 BMP receptor) conditional knockout mice [31,32]. Regarding parasympathetic neurons, BMP5 and 7 are present in ciliary neurons [33]. In both sympathetic and parasympathetic neuronal differentiation, BMPs initiate the expression of paired-like homeobox 2b (PHOX2B) and the mammalian *achaete-scute* homolog (MASH1). Accordingly, *Phox2b* and *Mash1* knockout mice display a disruption of the development of all autonomic ganglia [34–36]. PHOX2B and MASH1 have a key role in the induction of the expression of the enzymes that are involved in catecholamine biosynthesis, TH, and DBH (Figure 2). The former through the action of PHOX2B via GATA3, whilst the latter through the action of PHOX2B and MASH1 via PHOX2A and heart and neural crest derivative expressed 2 (HAND2) [10]. *Gata3*^{-/-} and *Hand2*^{-/-} mice die in utero (E9.5-E11) and they both display a reduction of *Th* and *Dbh* expression [37–39]. Likewise, mice with a specific deletion of *Hand2* in NCCs also displayed an impaired formation of sympathetic neurons [37–39].

Studies using ciliary ganglia have reported that parasympathetic neurons do not express GATA3 and HAND2, nor do they synthesize catecholamine enzymes [33]. By contrast, they express the parasympathetic markers choline acetyltransferase (ChAT) and vesicular acetylcholine transporter (vAChT), possibly via a pathway downstream of PHOX2B through the action of the glial cell line-derived neurotrophic factor GDNF/Ret, as shown in cranial parasympathetic ganglia [10,40]. In accordance with a role of the signaling pathway downstream of GDNF and the involvement of the GDNF receptor Ret, E18 *Ret* knockout mice present a reduction in the volume of cardiac ganglia together with decreased innervation in the ventricular CCS [41].

The differentiation of cardiac parasympathetic neurons has not been extensively studied. The extrapolation or conclusions drawn from research done on ciliary and/or cranial parasympathetic ganglia might not be very accurate and, therefore, more research is needed in this regard.

2.4. Survival and Patterning

Once the target destinations have been reached, both sympathetic and parasympathetic neurons require various factors that are released by cardiomyocytes, vascular smooth muscle cells, and glial cells in order to ensure that the neurons are matched to their targets and to prevent apoptosis [10].

In the case of sympathetic neurons, nerve growth factor (NGF) and neurotrophin-3 (NT-3) are among the most important trophic factors [10]. NGF is secreted in its proform (proNGF) and extracellularly cleaved by neuron-specific matrix metalloproteinases, with the ratio of proNGF to NGF determining the cell fate [42,43]. ProNGF in fact, has a high affinity to the neurotrophin receptor p75 (NGFR), which triggers the apoptotic pathway with minimal activation of the survival pathway mediated by NTRK1 (TRKA). In contrast, NGF has a higher affinity to NTRK1, hence triggering the “survival” signaling [42]. The transient expression (E13.5–E15.5) of NGF from venous smooth muscle cells dictates the pattern of sympathetic growth. It directs the nerve growth along the subepicardial layer of the developing heart, establishing an epicardial-endocardial gradient [10]. NGF is not only

produced by vascular smooth muscle cells, but is also synthesized by cardiomyocytes. The expression of NGF is upregulated by endothelin-1 (ET-1), which plays a key role in sympathetic innervation. Accordingly, *Et1*^{-/-} mice display a significant reduction of NGF expression and a decrease in the number of stellate ganglia. The defects can be rescued by the forced expression of cardiac NGF [44]. The NGF levels decrease at birth (P0), but reach a second peak at P8 and a low level persists from P21 onwards (in rats) [10]. In addition to neuronal survival/patterning, NGF is also involved in the formation and strengthening of the neurocardiac varicosities between sympathetic neurons and cardiomyocytes [45,46]. These varicosities and neurocardiac junction will be addressed in more details in Section 5.

NT-3 is secreted from smooth muscle cells of blood vessels that are located adjacent to sympathetic ganglia. During sympathetic neuronal development in rats, there is a switch from the NT-3 to the NGF pathway. This is consistent with the developmental regulation of their respective receptors: NTRK3 (TRKC), which is expressed in early stages, whilst NTRK1 (which binds to NGF) from E15 [47]. *Nt3*^{-/-} and *Ntrk3*^{-/-} mice show similar cardiac defects, but *Nt3*^{-/-} mice present a more severe loss of sympathetic ganglia, indicating that other receptors might also be involved [48]. Interestingly, the sympathetic neuronal loss occurs at P0, and there are no differences in neuroblast numbers at E15 between the knockout and wild-type counterparts [49]. These results would suggest either a concomitant role of the two trophic factors; potential differences in developmental expression between rats and mice or other compensatory mechanisms should not be excluded.

The four glial cell-line-derived neurotrophic factor family of ligands (GFLs) and their receptors are involved in parasympathetic neuron survival. Despite their name, they are also expressed in cardiomyocytes [50]. GFLs are produced as preproGFL, followed by a cleavage of the signal sequence to generate proGFL. The activation of proGFL possibly requires another cleavage, but the specific proteases that are involved are yet to be identified [51]. The four ligands are called glial cell line derived neurotrophic factor, neurturin, artemin, and persephin and they act on their respective receptors: GFRa1, GFRa2, GFRa3, and GFRa4 [51]. The GFRas work as co-receptors of the receptor tyrosine kinase RET [51]. Ligand binding elicits the activation of downstream signaling, e.g., the inhibition of apoptosis and promotion of cell survival via the AKT signaling pathway [52]. Ret and GFRa2 are highly expressed in cardiac ganglia at E18 and P21 in rat hearts. The role of these signaling pathways in cardiac innervation is evident by studies using knock-out mice: neurturin knock-out (*Ntn*^{-/-}) mice exhibit cardiac innervation defects and *Gfra2*^{-/-} mice display reduced innervation in both ventricles (by 40%) and in the ventricular CCS (by 60%) [41,53,54].

Apart from the GDNF family, there is some evidence of the potential involvement of NGF in the survival of parasympathetic neurons. The NGF receptor NTRK1 was, in fact, identified in adult cholinergic cardiac ganglia, and both sympathetic and parasympathetic ganglia are lost in *Ngf*^{-/-} mice [55–57]. From a more functional perspective, it has been shown that in vivo application of NGF in mice potentiates the excitability of the parasympathetic neurons, it also decreases their cumulative afterhyperpolarization in vitro and increases their dendritic growth in vivo [58]. The effects of NGF on neurite growth were also shown while using dissociated parasympathetic ciliary ganglia [59].

3. Anatomy of the ICNS

Cardiac innervation was first studied in the myocardium of frogs and various large mammals (dogs, lambs, cats, monkey) while using bright field microscopy [60,61]. Methylene blue staining permitted the visualization of neurons, their ramification, and the identification of ganglionated plexi (GP) in the heart in various species, including humans [62]. GP are defined as a cluster of neuronal somata and nerve fibers [7]. The wider employment of electron microscopy allowed for the ultrastructural investigation of the neuronal organization of both atrial and ventricular walls [62–64] as well as providing the first evidence for a neuro-cardiac communication [65–67]. In the last 50 years, immunohistochemistry/immunofluorescence studies allowed for the characterization of the innervation

of the heart during development, their higher density in specific regions of the heart (e.g., CCS), the transmural pattern of innervation [68], and differences in health and disease [64,69,70].

These anatomical studies have elucidated the location of GP, the majority of them are located in supraventricular regions, either on the epicardium or embedded in fat pads on the surface of the heart hilum [7]. The distribution of GPs is different across species, they are more scattered in larger (e.g., sheep, pigs) [71,72] when compared to smaller mammals (e.g., mice and rats), with a lower density of innervation of the cell bodies in smaller mammals [7,73,74] (Figure 3). Moreover, intracardiac ganglia in the ventricles are only present in larger mammals, with innervation originating from atrial ganglia [7,73]. In larger mammals (e.g., rabbit, dog, sheep, and humans, the GP can be located in 5–7 subregions: dorsal right atrial, ventral right atrial, ventral left atrial, left dorsal, middle dorsal, right coronary, left coronary [7] (Figure 3). For a more detailed comparison across species of the intrinsic innervation of the heart, refer to Wake and Brack 2016 [7]. The left and right coronary GP emerge from the arterial regions, the dorsal right atrial GP from either the right caudal vein or the vena cava, the middle dorsal GP is located between the pulmonary veins with some contact with the left dorsal, and the ventral ganglia are positioned ventrally from the left pulmonary vein [7,11]. From an anatomical perspective, the SAN is innervated by post-ganglionic fibers from the ventral and dorsal right atrial, whilst the AVN from the middle dorsal and in part from the left dorsal [11].

Recent studies have established the isolated zebrafish heart as an alternative model for studying the autonomic modulation of the primary pacemaker of the zebrafish, which is a ring-like structure termed the sinoatrial ring (SAR), in order to address the limitations that are present in larger animals [75,76] (Figure 3). Using the zebrafish heart preparation with an intact intrinsic and extrinsic innervation, it has been shown that cardiac pacemaking can be modulated by both sympathetic and parasympathetic pathways. This work has also revealed that the zebrafish pacemaker cells express both muscarinic acetylcholine (M2) and β 2-adrenergic receptors [75]. Similar to mammals, most of the zebrafish intracardiac ganglia are located adjacent to the SAR and they are immunoreactive to ChAT, some to TH, together with other “non-classical” neurotransmitters (e.g., nitric oxide) [77]. These ganglia are innervated by the right and left vagus nerve. Moreover, neuronal somata in the ganglia projecting back to the central nervous system were observed, possibly acting as afferent neurons providing a link between the ICNS and central nervous system [78]. The zebrafish has been widely employed in cardiovascular research [79]. It has become a powerful model, as the human and zebrafish genomes are similar (70% of the protein-coding human genes are found in zebrafish and 84% of human disease genes have a zebrafish counterpart) [80]. Despite significant anatomical differences, the functional properties of the zebrafish heart (e.g., comparable heart rate, action potential morphology) are surprisingly similar to the human heart [79]. The zebrafish genome has been fully sequenced and it can be easily manipulated and, in addition, cardiac function can be examined *in vivo* [77].

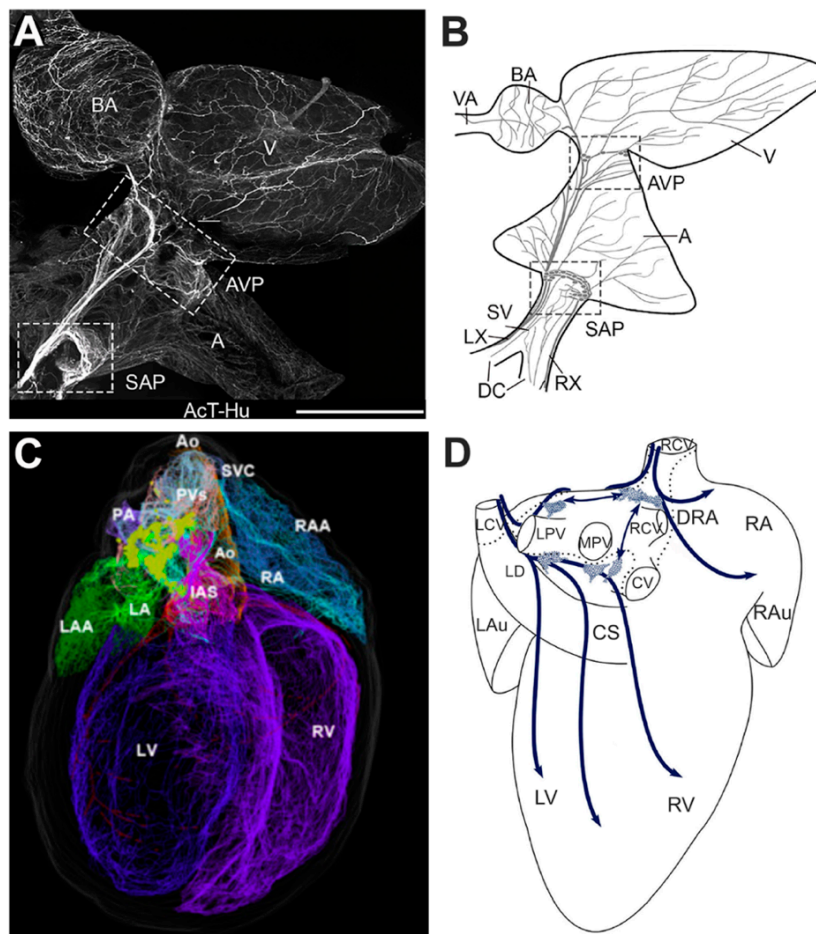


Figure 3. Intracardiac innervation of the zebrafish, rat and mouse hearts. (A) Whole mount immunostaining using antibodies directed against acetylated tubulin (AcT) and human neuronal protein (Hu) to label the ICNS of the zebrafish heart. (B) Schematic overview of the major elements of cardiac innervation. Boxed areas: sinoatrial plexus (SAP) and atrioventricular plexus (AVP). Abbreviations for A and B: A—atrium; AVP—atrioventricular plexus; BA—bulbus arteriosus; DC—ducts of Cuvier; LX and RX, left and right vagosympathetic trunks; SAP- sinoatrial plexus; SV—sinus venosus; V—ventricle; VA—ventral aorta (to the gills). (C) Posterior view of a 3D reconstructed male rat heart showing the context, extent, and distribution of the intrinsic cardiac neurons (yellow labelled), located on superior and posterior surfaces of the atria (D) Schematic overview of the intracardiac ganglia in the mouse heart, dorsal view. Dotted lines delineate the heart hilum, polygonal areas the main locations of the cardiac ganglia. Abbreviations for C and D: Ao- aorta; CS- coronary sinus veins; CV—caudal vein; DRA—dorsal right atrial; IAS—interatrial septum; LA—left atrium; LAA (or LAu)—left auricle; LCV—left cranial; LD—left dorsal; LPV—left pulmonary; LV—left ventricle; MPV—middle pulmonary veins; PA—pulmonary artery; PVs—pulmonary veins; RA—right atrium; RAA (or Rau) —right auricle; RCV—right cranial (superior caval) vein; RV—right ventricle; SVC—superior vena cava. Panel (A-B) reproduced with permission from Stoyek, M.R. et al., *J. Comp. Neurol.* Published by Wiley, 2015 [78]. (C) Reproduced with permission from Achanta, S. et al. *iScience* published by Elsevier, 2020 [81] (D) reproduced with permission from Rysevaite, K. et al., *Heart Rhythm* published by Elsevier, 2011 [74].

3.1. Morphology and Electrophysiological Properties of Cardiac Ganglia

Intracardiac ganglia are heterogeneous and they also include the small intensely fluorescent (SIF) cells that can have various functions: endocrine, chemoreceptive and interneuronal [82]. On the basis of their three-dimensional cell shape, size, and acetylcholinesterase (AChE) staining, Pauza and co-workers distinguished them into globular and plain ganglia. The former are more densely packed,

containing 100–200 neurons occupying 0.01–0.17 mm², whilst the latter present a more intense staining for AChE, neurons reside side-by-side and they contain no more than 50 cells [83]. The size of neuronal somata is similar to the ones in other autonomic ganglia: 15–30 μm in the short axis and 20–45 μm in the long axes [83] and they are classified into large (80%) and small neurons (20%) [84].

According to their morphological and electrophysiological features, intracardiac neurons have been classified into type I (or phasic, also known as somatic (S) cells) and type II (or tonic). Type II neurons are further subclassified into slow afterhyperpolarization (SAH) cells, and pacemaker (P) cells (Figure 4) [85–88]. S-cells receive local excitatory inputs; they have small somata and are monopolar; their action potentials have a phasic profile that is characterized by brief afterhyperpolarizations [85,86]. SAH and P cells are both defined by their prominent afterhyperpolarization. SAH cells are multipolar principal neurons; they receive strong efferent connections from the vagus and present a tonic profile [85]. P cells (or pacemaker cells) are neurons that present a pseudounipolar or bipolar morphology. They are named after their electrophysiological profile: they present an hyperpolarization-activated inward current that is similar to the one in cardiac pacemaker cells [85]. Interestingly, immunostaining with synaptophysin to visualize synaptic boutons revealed that P-cells were the only types that did not receive any synaptic inputs and may act as sensory neurons [86]. Using a working heart-brainstem preparation, McAllen and colleagues further reported that about 40% of intracardiac neurons received vagal inputs (principal cells) (Figure 4). The remaining were classified as quiescent, as they did not respond to vagal stimulation, supporting their role as interneurons or sensory neurons [89]. Contrasting to the above subdivision, Rimmer and Harper did not find any spontaneous rhythmic activity (i.e., in P-cells) and classified the intracardiac neurons on the basis of their excitatory post-synaptic potentials into phasic, multiply adapting, and tonic neurons [90].

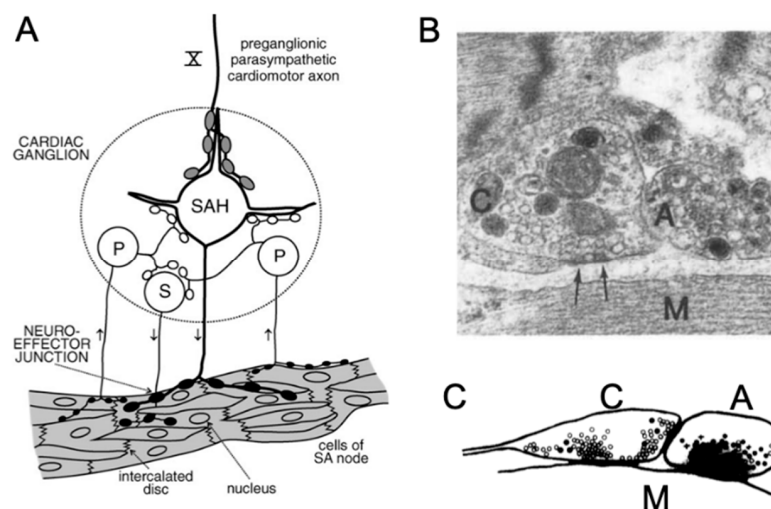


Figure 4. Neurocardiac transmission in the sinoatrial node (SAN). (A) Diagram illustrating the distinct cell types of the intracardiac ganglia and their putative roles: SAH (slow afterhyperpolarization) cells are the principal cells and the only ones receiving pre-ganglionic inputs. S (somatic) cells and some SAH cells can receive inputs from P (pacemaker) cells. P cells are putative sensory neurons. (B) Electron micrograph of the neurocardiac junction at the level of the sinus venosus of the toad. Cholinergic (C) and adrenergic (A) varicosities in contact with a cardiomyocyte (M). No membrane specializations are visible except for an electron dense area as indicated by the arrows. (C) Reconstruction of the neurocardiac junction depicted in (B). Cholinergic vesicles are present in the prejunctional membrane facing the cardiomyocyte and the adrenergic varicosity, respectively whilst adrenergic vesicles are mainly present in close opposition to the cardiomyocyte. The black area between the neuronal varicosity and the cardiomyocyte represents the cleft. Panel (A) reproduced with permission from Jänig, W., *J. Physiol.* published by Wiley, 2011 [91]. Panel (B,C) reproduced with permission from Klemm, M. et al., *J. Auton. Nerv. Syst.* published by Elsevier, 1992 [92].

3.2. Neurochemical Characteristics

Various immunohistochemical studies have reported the immunoreactivity of intracardiac ganglia to various neuromodulators and neurotransmitters, debunking the former belief that these were purely post-ganglionic parasympathetic efferent neurons [7]. They were found to stain positive for cholinergic (choline acetyltransferase, ChAT), adrenergic (TH), as well as putative sensory neuronal (substance P and CGRP) markers along with other co-transmitters, such as neuropeptide Y (NPY), neuronal nitric oxide synthase (nNOS), and vasoactive intestinal peptide (VIP) [7]. The functional relevance of these co-transmitters is discussed in more detail in Section 5.3. The majority of ganglia in various species (e.g., mouse, rat, guinea pig, human) were immunoreactive to ChAT [93–95]. It has been shown that cholinergic ganglia innervate both the sinoatrial and atrioventricular regions as well as the ventricles, supporting evidence for the parasympathetic regulation of the ventricles. TH immunoreactivity was found in both small intensely fluorescent cells as well as in larger neurons [96,97]. SIF cells are either present as small cell clusters in large ganglia or dispersed across the cardiac walls. There is some contrasting evidence on the percentage of ganglia positive to TH, with some studies reporting their absence in P neurons and presence in fibers [95], whilst others showing staining in larger neurons [98]. Notably, a study on human intrinsic cardiac ganglia reported a colocalization of TH and the vesicular monoamine transporter 2 (VMAT-2) [99]. VMAT-2 is usually required for catecholamine storage and release. This colocalization suggests the ability of a subset of the intrinsic cardiac neurons to synthesize, store, and release catecholamines [99]. Interestingly, several investigators have reported a group of neurons (10–20%) that are labelled with both ChAT and TH antibodies [94,100].

Contrasting to the atria with higher levels of ChAT immunoreactivity in the somata and fibers, the ventricles present a dominance of TH labelled fibers [97]. There is some variability across various studies on the proportion of nNOS immunoreactive cells, but mostly they are co-localized with ChAT neurons [7,95,99] consistent with the role of NO as co-transmitter in parasympathetic neurons [101]. A number of studies found VIP to be expressed mainly in neuronal fibers, with immunoreactivity in neuronal somata being absent or present in a low number of neurons [99,102,103]. NPY is co-released with norepinephrine (NE) in sympathetic neurons [104] and is found to co-localize in TH, nNOS, and ChAT immunoreactive neurons [7,95]. Substance P (SP) and CGRP are generally considered to be markers of afferent neurons, i.e., neurons that monitor the chemical and physical state of the myocardium, for example, giving feedback about the heart rate. They have a similar pattern, although SP is less abundant [94]. The number of SP or CGRP immunoreactive neuronal fibers is higher near the heart hilum with various bifurcations near the atrial regions and the roots of the pulmonary veins. SP-positive fibers were found to be around nNOS and ChAT immunoreactive somata, possibly suggesting an afferent role related to cholinergic and nitrogenous neurons [7]. Notably, the ICNS contain no or very little cell bodies that are immunoreactive to SP and CGRP. These findings suggest that the cell bodies of these immunoreactive afferent fibers reside either in the nodose or stellate ganglia [7], although one study identified SP and CGRP somata in the ICNS of the guinea pig [84]. On the basis of their molecular profile and spatial distribution, Achanta and coworkers have recently classified the intracardiac neurons in various clusters employing laser captured neuronal microdissection paired with RT-qPCR. Consistent with the previously reported immunohistochemical characteristics, in some neurons some genes were expressed in a pairwise fashion, e.g., neuropeptide Y and tyrosine hydroxylase [81]. However, the biophysical characteristics are yet to be correlated with the molecular profile of each class of neurons. This could be, for example, undertaken while using the Patch-seq technology [105] either in cultured cardiac neurons or from neurons patched from the intact atrial preparation. This technology would allow for the analyses of the neuronal biophysical profile using whole-cell patch clamp, followed by the aspiration of the somatic compartment for single-cell RNA seq analysis [105].

4. Physiological Role of Innervation in the CCS

The neurochemical heterogeneity of the intrinsic cardiac neurons that are mentioned in Section 3.2 provide evidence for different neuronal populations, suggesting the presence of efferent cholinergic and adrenergic neurons all in close vicinity to the afferent fibers [7,106]. In this section, we will discuss their function in the modulation of the conduction system, through their direct action, their interactions within the ICNS, or with the intrathoracic extracardiac neurons.

4.1. Direct Action of the Cardiac Ganglia on the CCS

A functional contribution of both sympathetic and parasympathetic intracardiac efferent neurons has been demonstrated, employing the decentralized and non-decentralized canine heart [107] and the Langendorff-perfused rabbit hearts [108]. Specific stimulation of selective loci in intracardiac ganglia (with nicotine) or with electrical stimulation elicited bradycardia, tachycardia, or bradycardia, followed by tachycardia. These effects depended on the activation of the intracardiac ganglia through nicotinic agonists and they were abolished in the presence of the hexamethonium [108]. The bradycardic effects were mediated by parasympathetic efferent neurons, as they were abolished in the presence of the muscarinic antagonist atropine. By contrast, the tachycardia was blocked by β -adrenergic antagonists (e.g., metoprolol and propranolol) in the presence of atropine. Moreover, a subset of intrinsic cardiac neurons was found to be responsive to NE *in vitro* through α -adrenergic receptors [108,109]. These data support a physiological relevance of both parasympathetic and sympathetic efferent neurons in the ICNS [107,108]. Some more specific studies have focused on the action of the intracardiac ganglia on the CCS. Zarzoso and coworkers reported a biphenotypic (adrenergic and cholinergic) action of the pulmonary vein ganglia on the SAN [100]. They employed a right atrial or a Langendorff-perfused heart preparation from mice, together with a combination of adrenergic and cholinergic antagonists (propranolol and atropine, respectively). The high frequency stimulation of the pulmonary vein ganglia evoked first a slowing of the heartbeat followed by an acceleration [100]. This biphasic response was explained by various factors: a delayed sympathetic response, the modulation of sympathetic neurons by parasympathetic neurons, and the faster breakdown of acetylcholine [100]. Employing a right atrial preparation and optical mapping, they further demonstrated that stimulation of the pulmonary vein ganglia evoked a downward shift of the leading pacemaker of the SAN in the majority of cases (68.2%) and an upward shift in the minority of cases (31.8%) [100]. These data are in accordance with a dominant parasympathetic response, consistent with other studies that reported either an inferior or superior shift of the leading pacemaker site, in response to the direct stimulation of cholinergic neurons or ACh [110–112]. Sampaio and coworkers investigated the effects of the stimulation of two clusters of intracardiac ganglia on the heart rate and atrioventricular conduction in rats. They reported that stimulating the SAN ganglion (the one located between the right atrium and superior vena cava) elicited a bradycardia, but had no effects on conduction; in contrast, the stimulation of the AVN ganglion (located between the pulmonary vein and the right atrium) did not affect heart rate, but slowed conduction [113]. Using subthreshold stimulation in the inferior node extension and compact atrioventricular area, Huckler and coworkers [114] showed that the effects on the AVN resulted from an involvement of both the parasympathetic and sympathetic branches, in contrast to other studies reporting that subthreshold stimulation elicited a purely vagal effect [115]. In contrast to the shifts in the leading pacemaker site in the SAN upon ganglia stimulation, in the rabbit atrial preparation, the location of the AVN pacemaker was found to be stable upon autonomic stimulation [114]. By contrast, a similar protocol resulted in a shift of the AVN pacemaker site in atrial preparations from failing human hearts, i.e., closer to the bundle of His [116].

Overall, these data on the modulation of the ICNS of the SAN and AVN by the ICNS are in accordance with the anatomical distribution of the cardiac ganglia. The dual action of the ganglia innervating the SAN and AVN is consistent with the observation of the presence of both adrenergic and cholinergic neurons in the same ganglia, as discussed in Section 3.2.

4.2. Interaction with Peripheral Nerves

The control of the heart by the CANS is hierarchically organized with high levels of interactions within and across the different levels, as mentioned in the introduction and summarized in Figure 1. Notably, using intracellular recordings (in vitro and in vivo) and microelectrode arrays, it was shown that around 40% of neurons in the ICNS receive pre-ganglionic inputs and are classified as principal cells or SAH cells (Figure 4) [85,89,117]. The synaptic transmission from the pre-ganglionic neurons to the post-ganglionic neurons (in the ICNS) has been classified based on the response of excitatory postsynaptic potentials (EPSPs) into three groups: weak (subthreshold), secure, and strong (generally suprathreshold) [90]. In vitro (using the right atrial preparation in conjunction with the vagus nerve), most of the synapses were classified as secure and strong across different developmental stages (neonatal, juvenile, and adult), with only a small proportion being weak [90]. By contrast, using the working heart-brainstem preparation, McAllen and co-workers reported that the synaptic transmission between the pre-ganglionic and post-ganglionic neurons is less than 1:1. A limited number of synapses were, in fact, classified as secure and the majority being strong or weak, some were silent synapses [89]. Notably, the cardiac neurons presenting spontaneous activity were excited by the cardiorespiratory stimuli that elicited bradycardic reflexes (e.g., peripheral chemoreceptors, arterial baroreceptors, and nasotrigeminal receptors). These results were consistent with their role as principal neurons and suggested a convergence of these reflexes on the cardiac ganglia [89]. The contrasting results across the two different preparations might be due to an ongoing synaptic activity in the working heart-brainstem that could have caused a frequency-dependent depression of transmission [89].

As shown in Figure 1, the interactions between the different levels of the CANS are not only between pre- and post-ganglionic neurons, but also through the LCNs. LCNs receive inputs from CNS neurons (e.g., from spinal cord or medulla oblongata), from sympathetic neurons, as well as local afferent neurons. They participate in the transduction of signals within the intrathoracic (intra- and extracardiac) ganglia; this constant communication also persists when chronically disconnected from the central nervous system [2]. LCNs are classified in three main subsets, depending on the cells from which they receive the inputs. The efferent-related LCNs receive inputs from the parasympathetic and sympathetic efferent neurons; the afferent-related transduce regional inputs from local afferent neurons. The third group consists of the convergent LCNs, which integrate information from central efferent (sympathetic and parasympathetic) projections as well as afferent inputs [2,117]. LCNs have also been found to play a role in the initiation and maintenance of tachyarrhythmias. For example, experiments in dogs have shown that the stimulation of mediastinal projections within the ICNS results in atrial fibrillations that can be reduced by selective inhibition of the LCNs [2,118]. In accordance, targeting these subsets of neurons has been suggested as a putative therapy for reducing the nervous system imbalance in cardiac arrhythmias [2].

Cardiac innervation from the stellate ganglia and the vagus nerve presents a high degree of anatomical and functional lateralization. Their lateralization is paired with the GP location in the right and left side of the heart, suggesting a contribution of the intracardiac ganglia in this context [89,119,120]. The right branches of the sympathetic and vagal nerves regulate the SAN, whilst the left branch mainly acts through the AVN influencing ventricular contractility and electrical conduction mainly on the left side [119–121]. The role of the GP as integration centers between the extrinsic and intrinsic cardiac nervous system was studied by various groups employing either selective ablation of the GP or via the selective inhibition of nicotinic receptors in the ganglia while using hexamethonium [122,123]. Consistent with the lateralization of the vagal and sympathetic branches, the SAN is controlled by the GP located in the right pulmonary vein, the right atrium, and the superior vena cava, whilst the AVN is regulated by the ones located between the inferior vena cava and the inferior left atrium [122,124,125]. The interactions between the sympathetic and parasympathetic branches are complex. It was reported that reduction in heart rate by vagal stimulation was greater under sympathetic tonic activation [126]. The term “accentuated antagonism” was later coined by Levy [127] to explain the enhanced parasympathetic effect under background sympathetic tone. This is not only

observed in case of the heart rate, but also affect the regulation of ventricular performance, intracellular Ca^{2+} levels and cardiac electrophysiology [126]. Various factors might contribute to this response. Muscarinic acetylcholine receptors at the sympathetic terminals inhibit NE release, but adrenergic receptors are not present on parasympathetic terminals [128]. Only under tonic sympathetic activation, the activation of postjunctional muscarinic M2 receptors by parasympathetic terminals results in the inhibition of cAMP production together with the upregulation of PDE2 activity, resulting in cAMP hydrolysis [129]. Apart from the effects at the neurocardiac junction, the accentuated antagonism by the parasympathetic branch can also be modulated at higher brain centers (e.g., cholinergic neurons in the medulla oblongata) [130].

4.3. Interaction within the ICNS

It was previously believed that individual GPs were purely responsible for the modulation of the neighboring regions, for example, the right atrial GP for the SAN [7]. However, there is now substantial evidence that the GP can innervate both neighboring regions but also form an intricate network [106,131,132]. Anatomical studies injecting fluorescent tracers in selected ganglia have demonstrated that multiple ganglia can innervate the same cardiac regions and that can also form an inter-ganglionic neuronal circuit [123].

It has been proposed that the short-latency (20–40 ms) reflexes are the results of the action of the neuronal somata in the ICNS located adjacent to cardiomyocytes and, thereby, regulating each cardiac cycle. By contrast longer latency reflexes (100–200 ms) are suggested to be dependent on polysynaptic transmission that involves LCNs modulating efferent neurons for the following cycles also upon stimulus removal [1,3]. Employing decentralized canine hearts, it has been demonstrated that ICNS neurons can work independently from the higher levels. The intrinsic neurons from atrial and ventricular GPs are able to transduce chemical and mechanical modifications: sensing mechanical stimuli from discrete cardiac regions and their spontaneous activity is correlated with the respiratory cycle. Moreover, their spontaneous activity is not modified when the extracardiac tissue is disconnected [133].

Hou and colleagues provided functional evidence for the role of the interplay between various GPs in the regulation of SAN and AVN function [131]. The ablation of selective GPs further demonstrated the collective role of the right atrial and posterior atrial plexi in heart rate regulation. The ones in the right atria directly regulate the heart, whilst the ones on the posterior side are involved in the interaction of the sympathetic and parasympathetic modulation of the heart rate [132].

5. Neurocardiac Communication

The foundations of the neuro-cardiac communication have been laid down in the second half of the 20th century employing ultrastructural examinations of heart sections and analyzing the relationship between axon varicosities and the cardiomyocytes [134]. The autonomic neuroeffector communication has long been described as a non-specialized junction that is characterized by a lack of any specific pre- and postjunctional membrane domains with a release of the neurotransmitter *en passage* upon neuronal stimulation [135,136]. However, various studies, especially on sympathetic neurotransmission, suggested a quasi-synaptic mode that is similar, at least to some extent, to the neuromuscular junction (NMJ) [68,137]. The measurement of the distance between the pre- and post-junctional membrane in various species (e.g., toad, guinea pig, mole, and mouse) resulted in the classification of the neurocardiac junction into three groups: intimate (<20 nm), close (20–100 nm), and separated (>100 nm) [67,92,138,139]. Many of these studies were undertaken using random sections; however, when the same varicosity was analyzed in serial sections, most of the varicosities that lost their Schwann cell coating revealed close or intimate contacts [67]. Analyzing serial sections of post-ganglionic varicosities, in the SAN region in amphibian and mammalian species, revealed that the majority of them formed specialized neurocardiac junction with a gap of less than 100 nm in both sympathetic and parasympathetic junctions [67,92]. These junctions presented a high density of

synaptic vesicles in the varicosities facing the effector cell and a lower population of vesicles in other parts, with the latter containing larger peptide vesicles, although no pre- or post-synaptic membrane specialization (e.g., thickening) was observed [67,92] (Figure 4).

5.1. The Sympathetic-Cardiac Junction

Sympathetic neurons release NE and, together with epinephrine released by the adrenal medulla, act on adrenergic receptors in the heart. β 1-, β 2-, and β 3- adrenergic receptors (ARs) are expressed in the heart, with higher overall levels of β 1ARs and they are all G protein-coupled receptors (GPCRs) [140]. The β ARs signaling cascade downstream of the β ARs is distinct: β 1AR couples to G_s , eliciting an increase in cAMP and inducing an activation of its downstream effector proteins. By contrast, β 2 and β 3ARs can act on both G_s and G_i , with the latter being involved in the attenuation of the cAMP signaling with β 2ARs able to modulate β 1AR signaling [140]. The activation of β 3ARs can also result into cGMP production via eNOS activation [140,141]. Another factor influencing their downstream effects is the microdomain localization with β 1ARs being widely distributed in the sarcolemma and β 2- and β 3ARs mostly confined to T-tubules in ventricular myocytes, with receptor redistribution occurring in disease, e.g., in heart failure [141,142]. Cardiomyocytes also express α 1-adrenoceptors (α 1a and α 1b), which are coupled to $G_{q/11}$. Their activation results in positive inotropic effects, and chronic stimulation induces hypertrophy [140].

As mentioned in Section 3.2, a subset of intrinsic cardiac neurons has been found to express the enzymes that are involved in catecholamine biosynthesis [99]. Moreover, as mentioned in Section 4.1 a subgroup of intrinsic neurons has been reported to elicit a tachycardia effect, which was blocked by β ARs antagonists further supporting their functional relevance [2,108]. The sympathetic neuro-cardiac communication has been mainly investigated in vitro using, as a model system, co-cultures of neonatal cardiomyocytes with sympathetic neurons that are isolated from superior cervical or stellate ganglia. It has been reported that sympathetic neurons in vitro can differentiate into cholinergic or adrenergic neurons [143]. Neurotrophic factors can alter their fate (e.g., BDNF induces cholinergic differentiation [144]) and that NGFs strengthen the excitatory transmission between sympathetic neuron and cardiomyocytes in culture [45,46]. Many groups that use NGF in the culture medium reported nearly exclusive catecholamine release from sympathetic neurons, recapitulating in vitro sympathetic innervation, and revealed the structure and function of the sympathetic neurocardiac junction [45,46,145,146]. In axons, which are in contact with cardiomyocytes, activity-dependent recycling of synaptic vesicles can be observed, together with the presence of markers for neuroexocytosis in the prejunctional region (e.g., synapsin 1, synaptosomal-associated protein 25 (SNAP25), and synaptotagmin) [145,146]. The post-junctional cardiomyocyte membrane is characterized by the presence of scaffolding proteins (e.g., synapse-associated protein 97 (SAP97), A kinase anchoring protein 79 (AKAP79), and ankyrin G) and molecular complexes potentially stabilizing cell-cell adhesion (e.g., cadherin and β -catenin) both in vitro and in vivo [145–147]. Moreover, the postjunctional membrane reorganization was also defined by the enrichment of specific channels (e.g., voltage gated sodium channel 1.5 ($Na_v1.5$) and the voltage activated K^+ channel subfamily Q member 1 (KCNQ1)) and receptors (e.g., β 1ARs), with the exclusion of caveolin-3 at contact sites and the removal of β 2ARs upon neuronal stimulation [145,147]. Interestingly, in accordance with a role of β 1ARs in the post-junctional membrane, the tachycardia that is induced in pacemaker cells by sympathetic neural stimulation is mostly blocked by a β 1AR-selective antagonist. In contrast, little inhibition is elicited by β 2ARs antagonists in a guinea pig atrial preparation in contiguity with the thoracic ganglia [148]. Evidence of distinct functional pools of adrenergic receptors at extra-junctional and post-junctional sites was also obtained using the toad atrial preparation and the catecholamine reuptake inhibitor desmethylimipramine (DMI) to allow for the escape of catecholamines from the junction [149].

In sympathetic neuron-cardiomyocytes co-cultures, NE release in the neurocardiac junction peaks at around 200 ms after neuronal stimulation and declines after 460 ms. The time-course of NE in the cleft is mainly determined by the NE reuptake transporter (NET) in the prejunctional membrane [150].

NET dysfunction has been reported in various cardiac diseases. Polymorphisms of the human gene encoding NET-1 (*SLC6A2*), which are often associated with a reduction of its function, have, for example, been associated with postural tachycardia syndrome and congestive heart failure [151]. In accordance with the release of NE in a “diffusion-restricted” manner, in sympathetic neuron-cardiomyocyte co-cultures, NE concentration was estimated to be around 100 nmol L⁻¹ in the cleft resulting in a spatially restricted increase of cAMP in the innervated cardiomyocyte [146]. Furthermore, the prejunctional membrane presents various receptors that are involved in the regulation of NE release, with β 2ARs facilitating and α 2-adrenergic receptors inhibiting the release [152–154]. Notably, in atrial preparations from mammals and amphibians, the adrenergic responses in the pacemaker cells elicited by stellate ganglia stimulation do not appear to be mediated by the cAMP-dependent pathways. However, catecholamines bath application, in the same preparation, elicited an increase in cAMP [148,149]. Interestingly, studies employing Förster resonance energy transfer (FRET) sensors in co-cultures of sympathetic neurons and cardiomyocytes revealed an increase of cAMP in cardiomyocytes, which were in direct contact with the stimulated neuron [146]. The rise in cAMP levels was faster and greater in the region of the cardiomyocyte proximal to the neuronal contact site when compared to distal regions [146]. These findings are consistent with the highly compartmentalized nature of cAMP signaling, which is characterized by changes in nanodomain signaling upon localized stimulation [142]. This could perhaps explain the absence of a cAMP response at the whole-cell level when pacemaker cells were recorded upon stellate ganglia stimulation. Further experiments are needed and employing for example FRET sensors targeted to distinct cellular microdomains [155]. However, a putative involvement of cAMP-independent pathways downstream of β -adrenergic stimulation should not be excluded. Accordingly, in rabbit cardiomyocytes, a direct effect of isoproterenol causes an enhancement of the Na⁺ current (I_{Na}) via a G_s-coupled pathway, which is independent of cAMP signaling [156].

Apart from the effects on pacemaker cells, sympathetic neurons also modulate the contractility of rodent cardiomyocytes [46,157,158] and induced pluripotent stem cells (iPSC)-derived cardiomyocytes [159,160]. Sympathetic innervation in the murine heart is more abundant in the epicardial layer and it diminishes towards the endocardium [161–163]. This transmural innervation gradient may be responsible for size difference of cardiomyocytes in the epicardial and endocardial layer. Accordingly, a trophic role of sympathetic neurons on cardiomyocytes has been reported [164]. Sympathetic innervation also plays a role in cardiac regeneration in neonatal mouse with sympathetic cardiac denervation completely inhibiting this process [165].

5.2. The Parasympathetic-Neurocardiac Junction

In the heart, acetylcholine that is released by nerve terminals acts on the metabotropic muscarinic acetylcholine receptors, which are classified into M1–5. M2 is highly expressed in cardiac tissue and is coupled to G_i, resulting into a decrease in cAMP signaling. There is also some evidence of the presence of M1 and M3 in the heart, which, in contrast to M2, are coupled to G_{q/11} and trigger the PLC signaling pathways [140]. Evidence for the formation of functional neurocardiac junctions between parasympathetic neurons and myocytes was obtained in neuron-myocytes co-cultures. Stimulation of the parasympathetic neurons (isolated from sacral cord explants or ciliary muscle or iPSC-derived) elicits a negative chronotropic effect in innervated cardiomyocytes (ventricular, sinoatrial node, or iPSC-derived) [160,166–168]. In neurocardiac co-cultures from either rat or chicken, the functional neuromodulation of cardiomyocytes develops after three days in culture. The mere vicinity between neurons and cardiomyocytes does not necessarily implicate the formation of functional contacts [167,168]. An increase in the expression levels of specific G_α subunits is concomitant with the enhancement of the muscarinic responsiveness of the cardiomyocytes only when co-cultured with neurons [168]. Similar to the sympathetic neurocardiac junction, changes in protein localization in the pre- and postjunctional membrane may occur upon parasympathetic neurocardiac junction formation and neuronal stimulation or triggered by molecules that are involved in cell–cell adhesion. Although this has not been investigated in the heart, various cadherins have been reported to be involved in

parasympathetic neuroeffector junction formation. Accordingly, the expression of *N*-cadherin in CHO cells induces a partial differentiation of presynaptic cholinergic terminals of brainstem neurons when cell–cell contact are established [169].

The parasympathetic neurocardiac junction at the level of the SAN has been studied by the Hirst group in an atrial preparation in contiguity with the vagus nerve using intracellular recordings of the sinoatrial pacemaker cells, in order to compare the effects of either ACh application or vagal stimulation [85,170,171]. Both treatments result in a decrease in action potential generation and beating rate. ACh also elicits membrane hyperpolarization, action potential shortening, and an increase in its peak potential, whilst vagus nerve stimulation induces membrane depolarization and has little or no effects on the peak potential and its duration [170–172]. Using pharmacological tools, e.g., cesium for blocking the funny current channels and Ba²⁺ for K⁺ current channels, they proposed the existence of post-junctional and extra-junctional muscarinic receptors, with both effects being inhibited by muscarinic antagonists. Vagal stimulation result in the reduction of the funny current (*i_f*) without an involvement of the K⁺ channels (i.e., I_{KACH}) downstream of a pool of muscarinic postjunctional receptors, whilst bath application of ACh activates also muscarinic extra-junctional receptors that are coupled to K⁺ channels [134,170–172]. The distinct effects of exogenous application of agonists compared to neuronal stimulation, debunked the idea that the exogenous application of agonist mimics physiological conditions [4]. Other groups assessing the beating rate of a mammalian atrial preparation using Ba²⁺ [173] or the diastolic tension in the preparation while using the selective I_{KACH} blocker tertiapin-Q [174] obtained different results. They described an involvement of the I_{KACH} downstream of the muscarinic receptor upon vagal stimulation. A contribution of I_{KACH} was also postulated by the reduction of cardiac autonomic regulation in a mouse mutant lacking Kir3.4 channels [175]. These results raise questions regarding the contribution of I_{KACH} in pacemaker cells upon vagal stimulation. Do these channels reside at the post-junctional membrane or are they activated by, for example, spillover ACh? The carefully executed experiments by the Hirst group should not be refuted without reproducing them [176]. When comparing the experimental results across different studies, it is also important to keep in mind the structural heterogeneity of SAN tissue with distinct densities of ion channels, innervation levels, and the expression of different connexin isoforms [177].

At the level of the parasympathetic neurocardiac junction, acetylcholine in the cleft is cleaved by AChE, which is a hydrolytic enzyme that is present at both pre- and postsynaptic membranes. Choline, which results from this enzymatic reaction, is readily transported back into the neuron by a high affinity choline uptake mechanism, ACh can then be re-synthesized by choline acetyltransferase and subsequently released again [135]. The AChE levels are higher surrounding the SAN when compared to atrial muscle and they are even lower in the ventricles [178]. The lower AChE levels in atrial tissue are probably the reason for the slower rate of recovery in atrial muscle after vagal nerve stimulation [179]. There is some evidence using the right atrial preparation that acetylcholine can inhibit its own release from parasympathetic terminals through its action on muscarinic autoreceptors. In accordance with this, the muscarinic receptor antagonist atropine strongly increases ACh release from the vagus nerve in the right atrial preparation [180].

Apart from the role of cholinergic neurons in action potential modulation, they have also been implicated in cardiac regeneration in both zebrafish and neonatal mice. Their pharmacological or genetic blockade prevents cardiac regeneration upon nerve injury, resulting in a decrease of cardiomyocyte proliferation paired with a decrease of cell cycle genes [181].

5.3. Co-Transmission

The idea according to which neurons could only release one neurotransmitter, known as “Dale’s principle”, was first challenged by Geoffrey Burnstock in 1976, who suggested that neurons of the same class could release more than one neurotransmitter [182]. Dales’ principle was hence rectified by Sir John Eccles into ‘at all the axonal branches of a neuron, there is liberation of the same transmitter substance or substances’ [183]. Sympathetic neurons, in addition to NE, can release neuropeptide

Y (NPY) and adenosine triphosphate (ATP), with distinct stimulation parameters favoring some neurotransmitters over others: e.g., low frequency favors ATP release, longer period NE, and high frequency with sporadic burst towards NPY [135]. In contrast, parasympathetic neurons can release, in addition to ACh, vasoactive intestinal peptide (VIP), ATP, and NO [135]. Figure 5 summarizes the co-transmitters released at the neurocardiac junction and the cross-talks between the sympathetic and parasympathetic varicosities at the level of the sinoatrial node.

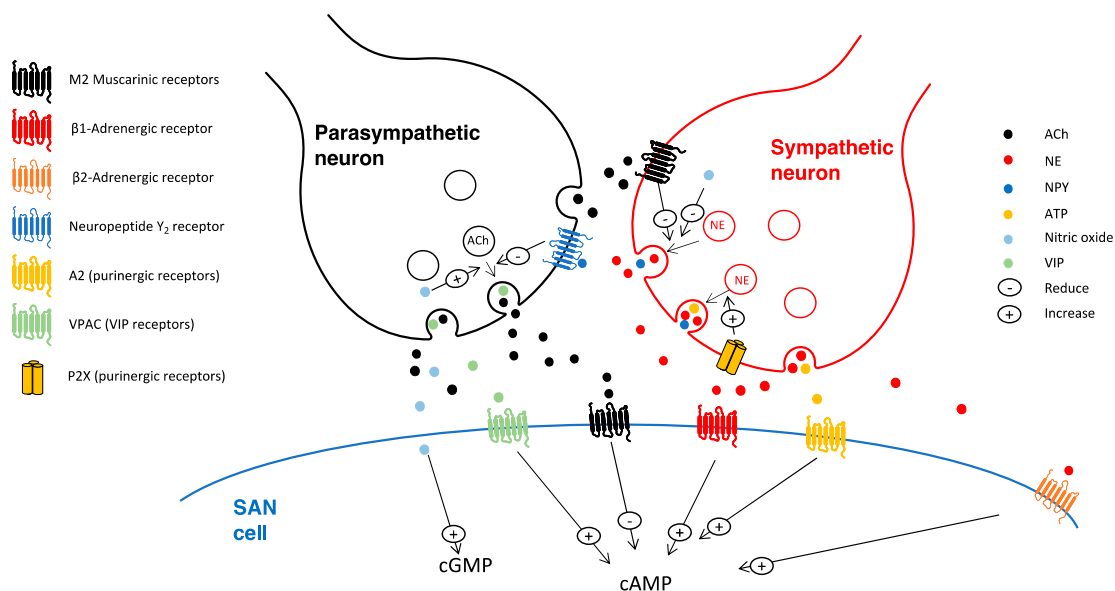


Figure 5. Diagram illustrating the crosstalk by the sympathetic and parasympathetic varicosities at the level of a sinoatrial node myocyte. The parasympathetic neuron can release acetylcholine, nitric oxide and vasoactive intestinal peptide, whilst the sympathetic neuron norepinephrine, ATP and neuropeptide Y. This figure was created using images from Servier Medical Art Commons Attribution 3.0 Unported License (<http://smart.servier.com>). Servier Medical Art by Servier is licensed under a Creative Commons Attribution 3.0 Unported License.

NPY can be released together with NE and it can inhibit cholinergic release [183]. The analyses of the perfusate from the atrial preparation in vitro and the coronary sinus blood in vivo demonstrated that electrical stimulation protocols of sympathetic neurons (e.g., stellate ganglia), known to inhibit the vagal bradycardia, result in the release of NPY [183,184]. NPY acts on GPCRs that are coupled to the $G_{i/o}$ pathway. Y_1 , Y_2 and Y_5 receptors are expressed in the heart and neuropeptide Y detected in the CCS, atria and coronary vessels [185]. NPY receptors have been reported to be present both at presynaptic sites inhibiting neurotransmitter release as well as postjunctional sites enhancing the NE effects [185]. In the heart, the full action of NPY is not clear, with inconsistent changes in heart rates [186]. Y_1 receptors are found in ventricular cardiomyocyte and they enhance the response of NE [183,184]. In contrast, Y_2 receptors are expressed in prejunctional cholinergic terminals (e.g., from intrinsic cardiac neurons as shown in the guinea pig atrial preparation) and upon activation they inhibit ACh release via a PKC-dependent pathway [104,183,184]. Y_2 receptors in these terminals have been shown to be functionally active, as NPY application in the atrial preparation in conjunction with the right vagal nerve reduced the heart rate response to vagal stimulation and decreased acetylcholine release [104,184]. Moreover, these effects were blocked by Y_2 antagonists or through genetic ablation [183,184].

Some intrinsic cardiac somata and fibers in the guinea pig atria are found to be reactive to quinacrine, which is a marker of high ATP content in vesicles containing neuropeptides. These findings suggested that these neurons could release ATP [187]. Purinergic receptors binding ATP are classified into P1 (A_1 , A_{2A} , A_{2B} and A_3) and P2 receptors. P2 receptors are sub-categorized into P2X ($P2X_{1-7}$) and P2Y ($P2Y_{1,2,4,6,11,12,13,14}$). P1 is most sensitive to adenosine, which results from ATP breakdown,

whilst P2 to ATP. P2X receptors are inotropic (ligand-gated ion channel) receptors, whereas P1 and P2Y GPCRs [135]. A₁ and A₃ receptors are coupled to G_i and G_{q/11} pathways mimicking downstream effects that are similar to muscarinic M₂ receptors, whilst A₂ receptors are coupled to G_s; the sinoatrial node expresses A₁ receptors [186]. Adenosine and ATP reduce the pacemaker activity of the SAN, the conduction of the AVN, and the automaticity of the His bundle and Purkinje fibers. In human patients, intravenous administration of ATP produces AV block via P1 receptors. In patients with paroxysmal supraventricular tachycardia, bolus injection of adenosine (Adenocard) is employed in order to reduce the conduction time of the AVN [187]. In the heart, the P2 receptor has a distinct spatial distribution with P2X_{1/3/4/5/6} being expressed in the ventricles, whilst P2X₁₋₆ in the atria [188]. P2X activation and the resulting increase of intracellular cations (e.g., Na⁺) elicits cardiomyocyte contractility [189]. P2X receptors are also found in the prejunctional regions of cardiac sympathetic neurons, and their activation promotes NE release [190]. Studies of sympathetic neuro-effector junctions of smooth muscle cells have reported that, when ATP is co-released with NE, the action of ATP on the effector cell is faster due to the faster P2X receptor response as compared to the slower effects of NE via GPCRs [146,150].

A subset of intracardiac neurons present P2Y₂ receptors and they are sensitive to ATP application and, to a lesser extent, to ADP (but not to AMP or adenosine) [187], although there is some evidence of a putative role of P1 receptors in prejunctional regions [191].

The application of ATP elicits distinct effects on intrinsic cardiac neurons via P2Y receptors, resulting in three different responses. In the first group of cells, it elicits a rapid transient depolarization; in the second group, the depolarization is followed by an hyperpolarization and a slow prolonged depolarization; in the third subset, ATP induces a slow depolarization [187,192]. These results suggest that some intrinsic cardiac neurons are local afferent neurons, playing a role in the regional cardiac reflexes, in accordance with this, nodose afferent neurons can be activated by ATP and adenosine [187,192].

VIP-positive fibers are present in high density around the SAN of all mammals [193]. Despite being released from parasympathetic terminals, VIP has the opposite effects of ACh i.e., it increases the synthesis of cAMP, which results in the enhancement of the heart rate. It has been suggested to be involved in postvagal tachycardia, as its removal from the neuroeffector junction is slower when compared to ACh [175]. Vagal nerve stimulation in the presence of muscarinic and adrenergic antagonist results in an increase in heart rate. This effect was found to be mediated by VIP receptors, as their antagonists prevented it and it was mimicked by VIP application [193]. VIP acts on two receptor types (VPAC1 and VPAC2), both being expressed in the heart; they are both G_s-coupled GPCRs. In SAN, AVN, and Purkinje fibers, VIP application results in a positive shift in the funny current activation curve, resulting in a chronotropic effect [175,186]. VIP receptor distribution is affected in various diseases (e.g., heart failure and hypertension) also affecting their responsiveness to agonists [186].

Nitric oxide (NO) is a fundamental intra/intercellular signaling molecule that can act in an autocrine/paracrine manner [101,194]. NO is tonically released and it can reach 1–3 μM during diastole. NO has a dual action on its modulation of heart rate. Its action on prejunctional receptors facilitates ACh release and decreasing heart rate, whilst its postjunctional action on I_f can increase heart rate [101]. NO can modulate neurotransmitter release from autonomic neurons: it inhibits NE and facilitates ACh release [101]. It can facilitate the cholinergic suppression of βARs signaling in cardiomyocytes, although there is some debate on its physiological action [194]. It is produced from L-arginine by nitric oxide synthases. There are three isoforms of this enzyme with distinct cellular expression: eNOS (in endothelium and plasma membrane of cardiomyocytes), nNOS (neurons and sarcoplasmic reticulum of cardiomyocytes), and iNOS expressed during inflammation [140]. NO increases the intracellular cGMP production by binding to the soluble form of guanylyl cyclase, which, in turn, activates various signaling partners e.g., PKG and PDEs modulating heart rate, for example, by reducing I_{CaL} in the SAN [186]. There is some controversy regarding the functional effects of nNOS on heart rate regulation of parasympathetic neurons [101]. It has been reported that nNOS levels vary across development

with an increase of nNOS in older animals, which might explain the discrepancy of the data in the literature [101]. In accordance to changes across developmental stages, Herring and coworkers have shown that the inhibition of nNOS and guanylyl cyclase significantly reduces the heart rate response of vagal stimulation on the atrial preparation in older guinea pigs, but not in younger ones [195]. It seems that the effects of NO on heart rate, are mainly through its action on prejunctional receptors. Sodium nitroprusside (the nitric oxide donor) increases ³H-ACh release, the application of NO activators in the presence of carbamylcholine (the stable analogue of ACh), and NOS and guanylyl cyclase inhibitors do not result in any changes in heart rate [101].

6. Cardiac Innervation and Heart Disease

Disruption in cardiac innervation has been implicated in various disorders (as summarized in Table 1), for example, dysautonomia (i.e., diseases arising from disrupted autonomic interactions), as well as in cardiac arrhythmia (e.g., in atrial fibrillation). In other cases, for example, after heart transplantation, the cardiac afferent and efferent neurons (to and from the extrinsic cardiac nervous system) are completely removed. This results in the loss of the functional interaction with the stellate ganglia and vagus nerve and, ultimately, causes a depletion of the modulation by the higher brain centers.

Table 1. Summary of the contribution of the ICNS in some cardiac diseases.

Disease	Involvement of the ICNS
Ageing	General reduction of parasympathetic and sympathetic function in aged animals [196,197]
Dysautonomia	General reduction of NE synthesis. Specific contribution of the ICNS not known [198].
Atrial fibrillation	Stimulation of GPs can elicit whilst their ablation can prevent atrial fibrillation [199,200], evidence of neuronal remodeling [7]
Conduction disorders	Expression of some “cardiac” proteins associated with the disease pathology in the ICNS [201]. Evidence of pathology secondary to increased autonomic activity [202,203].
Heart transplantation	Loss of the extrinsic innervation (efferent and afferent) to/from the heart [204]; changes in ICNS membrane properties [205]

Anatomical studies of the human heart have shown age-dependent changes of innervation. It has been reported that, during infancy, there is a dominance of sympathetic innervation of the CCS. There is a codominance of sympathetic and parasympathetic innervation during adulthood and an overall reduction of innervation in the elderly, with a specific reduction of parasympathetic function [196]. Moreover, anatomical and functional studies using aged mice reported a reduction in sympathetic heart rate regulation in the atria and ventricles of aged animals, which was the result of a reduction in ventricular sympathetic innervation and atrial β -adrenergic responsiveness [197].

The most common forms of dysautonomia are the familial ones. Patients with familial dysautonomia express low levels of dopamine-beta-hydroxylase resulting in a reduction of NE synthesis. This syndrome has been associated with mutations in the inhibitor of kappa light polypeptide gene enhancer in B-cells, kinase complex-associated protein (*IKBKAP*) gene. Individuals with familial dysautonomia have an abnormal heart rate, cardiac tone, and blood pressure together with higher risk of sudden death [198,206,207]. Another disease that is associated with abnormal development of the autonomic nervous system, possibly due to delayed maturation, is sudden infant death syndrome (SIDS), which is characterized by a reduction of the cardiac sympathovagal balance and anomalies in sleeping pattern [198].

Atrial fibrillation arises from multiple factors, among them: elevated vagal tone and ectopic firing in the region that surrounds the pulmonary vein. This region contains various intrinsic cardiac

ganglia and myocytes with specific electrophysiological properties making them more susceptible to arrhythmogenesis [200,208]. Moreover, the stimulation of GP in the left atrial fat pad lowers the threshold for atrial fibrillation, whilst their ablation can prevent it [199,200]. However, because of the intricately GP network, their role in physiological regulation of the CCS, innervation, and modulation of ventricles, ablation procedures can have serious side-effects, among them ventricular fibrillation [209]. Furthermore, neuronal remodeling (e.g., an increased presence of sympathetic neurons) has been reported in atrial fibrillation, which could have an effect on the outcome of ablation therapy [7].

Some studies investigating the pathophysiology of sick sinus syndrome in patients reported that the disease phenotype was mainly the result of an intrinsic abnormality of the SAN. Nonetheless, in some cases it was secondary to increased autonomic activity, in fact, autonomic blockade restored normal heart rate [202,203]. From the patient pathological phenotypes, it was difficult to distinguish whether the SAN bradycardia was the result of SAN or autonomic nervous system dysfunction [202]. It is also important to note that, some ion channels, which have been associated with cardiac arrhythmogenic disorders, are expressed not only in cardiomyocytes, but also in intracardiac ganglia. One example is the sodium channel $Na_v1.5$, whose functional expression has been reported in canine intracardiac ganglia implying a potential role of the ICNS in the pathophysiology of various disorders [201]. In accordance with this, mutations in its gene (*SCN5A*) have been associated with various cardiac arrhythmic disorders, e.g., long QT syndrome 3 (LQT3), Brugada syndrome and progressive conduction disease [201]. LQT3 is often linked to SAN dysfunction (e.g., sinus bradycardia and pauses), together with atrial standstill [201]. A number of studies on the dysfunction of the CCS have focused on ion channels, transmembrane and membrane-associated proteins in the SAN e.g., ankyrin B [111], $Ca_v1.3$, $Ca_v3.1$ [210], GIRK [211], POPDC1 [212], POPDC2 [213], or studied the effects of muscarinic or β AR agonists and/or antagonists on SAN excitability [111,210]. However, little work has been undertaken so far on the putative contribution of the ICNS in these diseases. There are some preliminary data on a potential role of the cAMP-binding transmembrane protein POPDC1 in the ICNS (unpublished data). Mutations in the *POPDC1* gene have been associated with skeletal muscle and cardiac disorders, specifically causing a disruption of CCS function e.g., atrioventricular block in patients and zebrafish mutants and a stress-induced sinus bradycardia in mutant mice [212,214]. Interestingly, *popdc1* expression has recently been detected in the ICNS of the zebrafish (unpublished data). The recessive *POPDC1*^{S201F} missense mutation causes a second-degree atrio-ventricular block in patients [214]. A subset of zebrafish mutants carrying the homologous mutation (*popdc1*^{S191F}) showed electrocardiogram (ECG) changes at baseline (atrioventricular block) [214]; isoproterenol and neuronal stimulation elicited arrhythmia, including sinus pauses (unpublished data). Notably, fishes with the most severe abnormalities also presented dysfunctions at the level of the ICNS. Significantly, the phenotype was rescued by cholinergic agonist suggesting a role of POPDC1 for the proper ICNS function (unpublished data). Interestingly, Mangoni and coworkers undertook extensive research on mouse models with SAN and AVN dysfunction and reported a rescue of the pathological phenotype after either pharmacological blockade or genetic ablation of the IK_{ACh} channel (GIRK4), which acts downstream of the muscarinic receptors [210,215]. These data suggest distinct pathophysiological mechanisms that are involved in conduction disorders with a beneficial role of either muscarinic agonist or antagonist, depending on the underlying disease mechanisms. Until now, the question of the role of the ICNS or the cardiac nervous system, in general, in heart rhythm disorders has not been sufficiently experimentally addressed. Further studies involving, for example, the conditional ablation of genes in neurons and SAN myocytes could reveal the potential contribution of the ICNS in these disorders.

Heart transplantation is characterized by the surgical interruption of the extrinsic efferent and afferent neurons to and from the heart (e.g., vagal input, extrinsic cardiac ganglia) leading to axonal degeneration and impairments of the cardiac reflexes [204]. Abnormal afferent-efferent communications have also been reported in various diseases, for example, in ischemic ventricles resulting in an increased susceptibility of sudden cardiac death [2].

Because of the allograft denervation, abnormal cardiac function at rest and during exercise, e.g., higher heart rate, slower changes in heart rate, and abnormal cardiac output, have been

reported [204]. After heart transplantation, it has been reported that the intracardiac neurons preserve synaptic neurotransmission, but they undergo changes in membrane properties, e.g., reducing their afterhyperpolarization current, hence increasing the proportion of phasic neurons, and possibly increasing their excitability [205]. Interestingly, in 40–70% patients, partial restoration of the innervation after heart transplantation has been reported, but is sometimes defined as partial or patchy reinnervation, with some patients presenting little or no innervation after 10 years [204]. The sympathetic branch can arise after six months and the parasympathetic after 1–3 years following sympathetic innervation [204]. The delay in the parasympathetic reinnervation can result into unbalanced autonomic innervation causing abnormal heart rate and response to stimuli [204]. Sympathetic ventricular innervation was reported to be time-dependent starting from the base towards the apex, whilst innervation of the sinoatrial node was more variable [204]. Another factor affecting adrenergic-cholinergic balance is the upregulation of the neural-crest derived ICA cells, which, however, has only been reported so far in mice [22]. Given the partial innervation after heart transplantation and the resulting abnormal sympathetic-parasympathetic balance, promoting cardiac innervation opens up a research scope for tissue engineering, e.g., triggering neo-innervation before heart transplantation or prior to implantation [216].

7. Conclusions

There is increasing appreciation of the important function of the ICNS in the modulation of heart function through its regulation of the CCS. However, the full degree of its physiological action and how it is affected in various cardiovascular disorders remains to be properly studied. There are still many open questions that need to be addressed.

The cardiac parasympathetic innervation as compared to sympathetic innervation is generally understudied. For example, during development, some information has been extrapolated from ciliary ganglia and, therefore, might not be fully correct. Various animal models could be employed in order to address this question; one could, for example, take advantage of the transparency of the zebrafish embryo, as the zebrafish has recently been established as a novel model for studying the ICNS [78].

Despite evidence of a neurocardiac junction similar to the sympathetic branch, less work has been undertaken for the parasympathetic junction. Moreover, the protocols often used to study the effect of sympathetic and parasympathetic innervation involved bath application of agonists/antagonists, which does not recapitulate the physiological condition. It is important to keep in mind the role of co-transmitters and the structure of the neurocardiac junction with a differential distribution of channels and receptors at post-junctional versus extra-junctional membrane domains. The neurocardiac junction could be further studied, for example, employing FRET sensors localized to distinct cellular microdomains in neuron-cardiomyocyte co-cultures. Moreover, co-cultures of iPSC-derived neurons and cardiomyocytes form functional neurocardiac junctions and may also permit modelling various neurocardiac diseases while using patient-derived cells.

Despite the advances in the classification of neurons of intracardiac ganglia based on their molecular profile, their biophysical profile is yet to be paired to their neurochemical characteristics. This could be achieved, for example, using Patch-seq, as already mentioned in Section 3.2. Elucidating the transcriptome of ICNS neurons could reveal whether some genes that are known to be involved in the pathophysiology of cardiovascular diseases (e.g., *SCN5A* in Brugada syndrome) are also expressed in the ICNS. Further insights in their molecular expression profile in combination with the generation of animal models with neuron or cardiomyocyte-specific ablation of genes will allow for the assessment of the contribution of different cell types in the disease pathology possibly resulting in the identification of novel drug targets. Further research is also needed in order to study the role of the ICNS in atrial fibrillation. Tissue engineering approaches may help to restore cardiac innervation after heart transplantation.

Research on the ICNS has long been a neglected area in cardiac biology. However, with the recent development of single-cell sequencing and the availability of marker genes for cell sorting, it is likely that we will soon have deeper insight into the makeup of the ICNS and its role in health and disease.

Funding: Research in the authors' laboratory is funded through the British Heart Foundation (BHF) (PG//19/13/34247).

Conflicts of Interest: The authors declare no conflict of interest. The funders had no role in the design of the study; in the collection, analyses, or interpretation of data; in the writing of the manuscript, or in the decision to publish the results.

Abbreviations

β1AR	beta1 adrenergic receptor
β2AR	beta2 adrenergic receptor
ACh	acetylcholine
AChE	acetylcholinesterase
ATP	adenosine triphosphate
AVN	atrioventricular node
BMP	bone morphogenetic protein
CANS	cardiac autonomic nervous system
CCS	cardiac conduction system
CGRP	calcitonin gene related peptide
ChAT	choline acetyltransferase
DBH	dopamine β-hydroxylase
ECG	electrocardiogram
ET-1	endothelin-1
FRET	Förster Resonance Energy Transfer
GATA3	GATA binding protein 3
GDNF	glial cells neurotrophic factors
GFL	Glial cell-line derived neurotrophic factor family of ligands
GP	ganglionated plexi
GPCRs	G-protein coupled receptors
HAND2	heart and neural crest derivative expressed 2
ICA	intrinsic cardiac adrenergic
ICNS	intrinsic cardiac nervous system
IPSCs	induced-pluripotent stem cells
IKBKA	kinase complex-associated protein
LCNs	local circuit neurons
MASH1	mammalian achaete-scute homolog
M2	muscarinic acetylcholine receptors type 2
NCCs	neural crest cells
NE	norepinephrine
NET	norepinephrine reuptake transporter
NGF	nerve growth factor
nNOS	neuronal nitric oxide synthase
NO	nitric oxide
NOS	nitric oxide synthase
NPY	neuropeptide Y
PHOX2A	paired- like homeobox 2a
PHOX2B	paired- like homeobox 2b
PNMT	phenylethanolamine- <i>N</i> -methyltransferase
SAN	sinoatrial node
SAR	sinoatrial ring
SIF	small intensely fluorescent cells
SP	substance P
TH	tyrosine hydroxylase
vAChT	vesicular acetylcholine transporter
VMAT-2	vesicular monoamine transporter 2
VIP	vasoactive intestinal peptide

References

1. Armour, J.A. Potential clinical relevance of the ‘little brain’ on the mammalian heart. *Exp. Physiol.* **2008**, *93*, 165–176. [CrossRef]
2. Ardell, J.L.; Armour, J.A. Neurocardiology: Structure-Based Function. In *Comprehensive Physiology*; Wiley: Hoboken, NJ, USA, 2016; pp. 1635–1653.
3. Armour, J.A. Cardiac neuronal hierarchy in health and disease. *Am. J. Physiol.* **2004**, *287*, R262–R271. [CrossRef]
4. Jaenig, W. Neurocardiology: A neurobiologist’s perspective. *J. Physiol.* **2016**, *594*, 3955–3962. [CrossRef] [PubMed]
5. Shivkumar, K.; Ajjjola, O.A.; Anand, I.; Armour, J.A.; Chen, P.-S.; Esler, M.; De Ferrari, G.M.; Fishbein, M.C.; Goldberger, J.J.; Harper, R.M.; et al. Clinical neurocardiology defining the value of neuroscience-based cardiovascular therapeutics. *J. Physiol.* **2016**, *594*, 3911–3954. [CrossRef]
6. Zipes, D.P.; Jalife, J.; Stevenson, W.G. *Cardiac Electrophysiology: From Cell to Bedside*, 7th ed.; Elsevier: Philadelphia, PA, USA, 2018; ISBN 978-0-323-44733-1.
7. Wake, E.; Brack, K. Characterization of the intrinsic cardiac nervous system. *Auton. Neurosci.* **2016**, *199*, 3–16. [CrossRef] [PubMed]
8. Ardell, J.L.; Andresen, M.C.; Armour, J.A.; Billman, G.E.; Chen, P.; Foreman, R.D.; Herring, N.; O’Leary, D.S.; Sabbah, H.N.; Schultz, H.D.; et al. Translational neurocardiology: Preclinical models and cardioneural integrative aspects. *J. Physiol.* **2016**, *594*, 3877–3909. [CrossRef] [PubMed]
9. Boyett, M. ‘And the beat goes on’ The cardiac conduction system: The wiring system of the heart. *Exp. Physiol.* **2009**, *94*, 1035–1049. [CrossRef] [PubMed]
10. Végh, A.M.D.; Duim, S.N.; Smits, A.M.; Poelmann, R.E.; Harkel, A.D.J.T.; DeRuiter, M.C.; Goumans, M.J.; Jongbloed, M.R.M. Part and Parcel of the Cardiac Autonomic Nerve System: Unravelling Its Cellular Building Blocks during Development. *J. Cardiovasc. Dev. Dis.* **2016**, *3*, 28. [CrossRef] [PubMed]
11. Campos, I.D.; Pinto, V.; Sousa, N.; Pereira, V.H. A brain within the heart: A review on the intracardiac nervous system. *J. Mol. Cell. Cardiol.* **2018**, *119*, 1–9. [CrossRef]
12. Coskun, V.; Lombardo, D.M. Studying the pathophysiologic connection between cardiovascular and nervous systems using stem cells. *J. Neurosci. Res.* **2016**, *94*, 1499–1510. [CrossRef]
13. Hasan, W. Autonomic cardiac innervation. *Organogenesis* **2013**, *9*, 176–193. [CrossRef] [PubMed]
14. Marvin, W.J.; Hermsmeyer, K.; McDonald, R.I.; Roskoski, L.M.; Roskoski, R. Ontogenesis of cholinergic innervation in the rat heart. *Circ. Res.* **1980**, *46*, 690–695. [CrossRef] [PubMed]
15. Navaratnam, V. The ontogenesis of cholinesterase activity within the heart and cardiac ganglia in man, rat, rabbit and guinea-pig. *J. Anat.* **1965**, *99*, 459–467.
16. Zhou, Q.-Y.; Quaife, C.J.; Palmiter, R.D. Targeted disruption of the tyrosine hydroxylase gene reveals that catecholamines are required for mouse fetal development. *Nat. Cell Biol.* **1995**, *374*, 640–643. [CrossRef] [PubMed]
17. Thomas, S.A.; Matsumoto, A.M.; Palmiter, R.D. Noradrenaline is essential for mouse fetal development. *Nat. Cell Biol.* **1995**, *374*, 643–646. [CrossRef] [PubMed]
18. Ebert, S. Expression of phenylethanolamine n-methyltransferase in the embryonic rat heart. *J. Mol. Cell. Cardiol.* **1996**, *28*, 1653–1658. [CrossRef]
19. Ebert, S.N.; Thompson, R.P. Embryonic epinephrine synthesis in the rat heart before innervation. *Circ. Res.* **2001**, *88*, 117–124. [CrossRef]
20. Ebert, S.N.; Rong, Q.; Boe, S.; Thompson, R.P.; Grinberg, A.; Pfeifer, K. Targeted insertion of the Cre-recombinase gene at the phenylethanolamine n-methyltransferase locus: A new model for studying the developmental distribution of adrenergic cells. *Dev. Dyn.* **2004**, *231*, 849–858. [CrossRef]
21. Owji, A.; Varudkar, N.; Ebert, S.N. Therapeutic potential of Pnmt+ primer cells for neuro/myocardial regeneration. *Am. J. Stem Cells* **2013**, *2*, 137–154.
22. Tamura, Y.; Sano, M.; Nakamura, H.; Ito, K.; Sato, Y.; Shinmura, K.; Ieda, M.; Fujita, J.; Kurosawa, H.; Ogawa, S.; et al. Neural crest-derived resident cardiac cells contribute to the restoration of adrenergic function of transplanted heart in rodent. *Cardiovasc. Res.* **2015**, *109*, 350–357. [CrossRef]

23. Huang, M.H.; Nguyen, V.; Wu, Y.; Rastogi, S.; Lui, C.Y.; Birnbaum, Y.; Wang, H.-Q.; Ware, D.L.; Chauhan, M.; Garg, N.; et al. Reducing ischaemia/reperfusion injury through delta-opioid-regulated intrinsic cardiac adrenergic cells: Adrenoceptor-mediated co-signalling. *Cardiovasc. Res.* **2009**, *84*, 452–460. [CrossRef] [PubMed]
24. Kasemeier-Kulesa, J.C.; Bradley, R.; Pasquale, E.B.; Lefcort, F.; Kulesa, P.M. Eph/ephrins and N-cadherin coordinate to control the pattern of sympathetic ganglia. *Development* **2006**, *133*, 4839–4847. [CrossRef] [PubMed]
25. Ieda, M.; Kanazawa, H.; Kimura, K.; Hattori, F.; Ieda, Y.; Taniguchi, M.; Lee, J.-K.; Matsumura, K.; Tomita, Y.; Miyoshi, S.; et al. *Sema3a* maintains normal heart rhythm through sympathetic innervation patterning. *Nat. Med.* **2007**, *13*, 604–612. [CrossRef] [PubMed]
26. Hildreth, V.; Webb, S.; Bradshaw, L.; Brown, N.A.; Anderson, R.H.; Henderson, D.J. Cells migrating from the neural crest contribute to the innervation of the venous pole of the heart. *J. Anat.* **2007**, *212*, 1–11. [CrossRef] [PubMed]
27. Kirby, M.L. Nodose placode contributes autonomic neurons to the heart in the absence of cardiac neural crest. *J. Neurosci.* **1988**, *8*, 1089–1095. [CrossRef] [PubMed]
28. Verberne, M.E.; Groot, A.C.G.-D.; Poelmann, R.E. Distribution of antigen epitopes shared by nerves and the myocardium of the embryonic chick heart using different neuronal markers. *Anat. Rec. Adv. Integr. Anat. Evol. Biol.* **2000**, *260*, 335–350. [CrossRef]
29. Hutchins, E.J.; Kunttas, E.; Piacentino, M.L.; Howard, A.G.; Bronner, M.E.; Uribe, R.A. Migration and diversification of the vagal neural crest. *Dev. Biol.* **2018**, *444*, S98–S109. [CrossRef]
30. White, P.M.; Morrison, S.J.; Orimoto, K.; Kubu, C.J.; Verdi, J.M.; Anderson, D.J. Neural crest stem cells undergo cell-intrinsic developmental changes in sensitivity to instructive differentiation signals. *Neuron* **2001**, *29*, 57–71. [CrossRef]
31. Morikawa, Y.; Zehir, A.; Maska, E.; Deng, C.; Schneider, M.D.; Mishina, Y.; Cserjesi, P. BMP signaling regulates sympathetic nervous system development through Smad4-dependent and -independent pathways. *Development* **2009**, *136*, 3575–3584. [CrossRef]
32. Schneider, C.; Wicht, H.; Enderich, J.; Wegner, M.; Rohrer, H. Bone morphogenetic proteins are required in vivo for the generation of sympathetic neurons. *Neuron* **1999**, *24*, 861–870. [CrossRef]
33. Müller, F. Molecular control of ciliary neuron development: BMPs and downstream transcriptional control in the parasympathetic lineage. *Development* **2002**, *129*, 5707–5717. [CrossRef] [PubMed]
34. Pattyn, A.; Morin, X.; Cremer, H.; Goridis, C.; Brunet, J.-F. The homeobox gene *Phox2b* is essential for the development of autonomic neural crest derivatives. *Nat. Cell Biol.* **1999**, *399*, 366–370. [CrossRef]
35. Pattyn, A.; Guillemot, F.; Brunet, J.-F. Delays in neuronal differentiation in *Mash1/Ascl1* mutants. *Dev. Biol.* **2006**, *295*, 67–75. [CrossRef]
36. Guillemot, F.; Lo, L.-C.; Johnson, J.E.; Auerbach, A.; Anderson, D.J.; Joyner, A.L. Mammalian achaete-scute homolog 1 is required for the early development of olfactory and autonomic neurons. *Cell* **1993**, *75*, 463–476. [CrossRef]
37. Lim, K.-C.; Lakshmanan, G.; Crawford, S.E.; Gu, Y.; Grosveld, F.; Engel, J.D. *Gata3* loss leads to embryonic lethality due to noradrenaline deficiency of the sympathetic nervous system. *Nat. Genet.* **2000**, *25*, 209–212. [CrossRef] [PubMed]
38. Hendershot, T.J.; Liu, H.; Clouthier, D.E.; Shepherd, I.T.; Coppola, E.; Studer, M.; Firulli, A.B.; Pittman, D.L.; Howard, M.J. Conditional deletion of *Hand2* reveals critical functions in neurogenesis and cell type-specific gene expression for development of neural crest-derived noradrenergic sympathetic ganglion neurons. *Dev. Biol.* **2008**, *319*, 179–191. [CrossRef] [PubMed]
39. Morikawa, Y.; D’Autréaux, F.; Gershon, M.D.; Cserjesi, P. *Hand2* determines the noradrenergic phenotype in the mouse sympathetic nervous system. *Dev. Biol.* **2007**, *307*, 114–126. [CrossRef]
40. Enomoto, H.; Heuckeroth, R.O.; Golden, J.P.; Johnson, E.M.; Milbrandt, J. Development of cranial parasympathetic ganglia requires sequential actions of GDNF and neurturin. *Development* **2000**, *127*, 4877–4889.
41. Hiltunen, J.O.; Laurikainen, A.; Airaksinen, M.S.; Saarna, M. GDNF family receptors in the embryonic and postnatal rat heart and reduced cholinergic innervation in mice hearts lacking *Ret* or *GFRalpha2*. *Dev. Dyn.* **2000**, *219*, 28–39. [CrossRef]
42. Lee, R.; Kermani, P.; Teng, K.K.; Hempstead, B.L. Regulation of cell survival by secreted proneurotrophins. *Science* **2001**, *294*, 1945–1948. [CrossRef]

43. Bruno, M.A.; Cuello, A.C. Activity-dependent release of precursor nerve growth factor, conversion to mature nerve growth factor, and its degradation by a protease cascade. *Proc. Natl. Acad. Sci. USA* **2006**, *103*, 6735–6740. [CrossRef] [PubMed]
44. Ieda, M.; Fukuda, K.; Hisaka, Y.; Kimura, K.; Kawaguchi, H.; Fujita, J.; Shimoda, K.; Takeshita, E.; Okano, H.; Kurihara, Y.; et al. Endothelin-1 regulates cardiac sympathetic innervation in the rodent heart by controlling nerve growth factor expression. *J. Clin. Investig.* **2004**, *113*, 876–884. [CrossRef] [PubMed]
45. Lockhart, S.T.; Mead, J.N.; Pisano, J.M.; Slonimsky, J.D.; Birren, S.J. Nerve growth factor collaborates with myocyte-derived factors to promote development of presynaptic sites in cultured sympathetic neurons. *J. Neurobiol.* **2000**, *42*, 460–476. [CrossRef]
46. Lockhart, S.T.; Turrigiano, G.G.; Birren, S.J. Nerve growth factor modulates synaptic transmission between sympathetic neurons and cardiac myocytes. *J. Neurosci.* **1997**, *17*, 9573–9582. [CrossRef] [PubMed]
47. Birren, S.J.; Lo, L.; Anderson, D.J. Sympathetic neuroblasts undergo a developmental switch in trophic dependence. *Development* **1993**, *119*, 597–610. [PubMed]
48. Tessarollo, L.; Tsoulfas, P.; Donovan, M.J.; Palko, M.E.; Blair-Flynn, J.; Hempstead, B.L.; Parada, L.F. Targeted deletion of all isoforms of the *trkC* gene suggests the use of alternate receptors by its ligand neurotrophin-3 in neuronal development and implicates *trkC* in normal cardiogenesis. *Proc. Natl. Acad. Sci. USA* **1997**, *94*, 14776–14781. [CrossRef]
49. Francis, N.; Fariñas, I.; Brennan, C.; Rivas-Plata, K.; Backus, C.; Reichardt, L.; Landis, S. NT-3, like NGF, is required for survival of sympathetic neurons, but not their precursors. *Dev. Biol.* **1999**, *210*, 411–427. [CrossRef]
50. Martinelli, P.M.; Camargos, E.R.S.; Morel, G.; Tavares, C.A.P.; Nagib, P.R.A.; Machado, C.R. Rat heart GDNF: Effect of chemical sympathectomy. *Histochem. Cell Biol.* **2002**, *118*, 337–343. [CrossRef]
51. Airaksinen, M.S.; Saarma, M. The GDNF family: Signalling, biological functions and therapeutic value. *Nat. Rev. Neurosci.* **2002**, *3*, 383–394. [CrossRef]
52. Garcia-Lavandeira, M.; Diaz-Rodriguez, E.; García-Rendueles, M.E.; Rodrigues, J.S.; Perez-Romero, S.; Bravo, S.; Alvarez, C.V. Functional role of the RET dependence receptor, GFRA co-receptors and ligands in the pituitary. *Front. Horm. Res.* **2010**, *38*, 127–138. [CrossRef]
53. Rossi, J.; Luukko, K.; Poteryaev, D.; Laurikainen, A.; Sun, Y.F.; Laakso, T.; Eerikäinen, S.; Tuominen, R.; Lakso, M.; Rauvala, H.; et al. Retarded growth and deficits in the enteric and parasympathetic nervous system in mice lacking GFR $\alpha 2$, a functional neurturin receptor. *Neuron* **1999**, *22*, 243–252. [CrossRef]
54. Heuckeroth, R.O.; Enomoto, H.; Grider, J.R.; Golden, J.P.; Hanke, J.A.; Jackman, A.; Molliver, D.; Bardgett, M.E.; Snider, W.D.; Johnson, E.M.; et al. Gene targeting reveals a critical role for neurturin in the development and maintenance of enteric, sensory, and parasympathetic neurons. *Neuron* **1999**, *22*, 253–263. [CrossRef]
55. Hoard, J.L.; Hoover, D.B.; Mabe, A.M.; Blakely, R.D.; Feng, N.; Paolocci, N. Cholinergic neurons of mouse intrinsic cardiac ganglia contain noradrenergic enzymes, norepinephrine transporters, and the neurotrophin receptors tropomyosin-related kinase A and p75. *Neuroscience* **2008**, *156*, 129–142. [CrossRef] [PubMed]
56. Levi-Montalcini, R.; Booker, B. Destruction of the sympathetic ganglia in mammals by an antiserum to a nerve-growth protein. *Proc. Natl. Acad. Sci. USA* **1960**, *46*, 384–391. [CrossRef] [PubMed]
57. Chen, K.S.; Nishimura, M.C.; Armanini, M.P.; Crowley, C.; Spencer, S.D.; Phillips, H.S. Disruption of a Single Allele of the Nerve Growth Factor Gene Results in Atrophy of Basal Forebrain Cholinergic Neurons and Memory Deficits. *J. Neurosci.* **1997**, *17*, 7288–7296. [CrossRef] [PubMed]
58. Hazari, M.S.; Pan, J.H.; Myers, A.C. Nerve growth factor acutely potentiates synaptic transmission in vitro and induces dendritic growth in vivo on adult neurons in airway parasympathetic ganglia. *Am. J. Physiol.* **2007**, *292*, L992–L1001. [CrossRef] [PubMed]
59. Collins, F.; Dawson, A. An effect of nerve growth factor on parasympathetic neurite outgrowth. *Proc. Natl. Acad. Sci. USA* **1983**, *80*, 2091–2094. [CrossRef]
60. Miller, M.R.; Kasahara, M. Studies on the nerve endings in the heart. *Am. J. Anat.* **1964**, *115*, 217–233. [CrossRef]
61. Woollard, H.H. The innervation of the heart. *J. Anat.* **1926**, *60*, 345–373.
62. Armour, J.A.; Murphy, D.A.; Yuan, B.-X.; Macdonald, S.; Hopkins, D.A. Gross and microscopic anatomy of the human intrinsic cardiac nervous system. *Anat. Rec. Adv. Integr. Anat. Evol. Biol.* **1997**, *247*, 289–298. [CrossRef]

63. Pauziene, N.; Pauza, D.H.; Stropus, R. Morphology of human intracardiac nerves: An electron microscope study. *J. Anat.* **2000**, *197*, 437–459. [CrossRef] [PubMed]
64. Pauziene, N.; Rysevaite-Kyguoliene, K.; Alaburda, P.; Pauza, A.G.; Skukauskaite, M.; Masaityte, A.; Laucaityte, G.; Saburkina, I.; Inokaitis, H.; Plisiene, J.; et al. Neuroanatomy of the Pig Cardiac Ventricles. A Stereomicroscopic, Confocal and Electron Microscope Study. *Anat. Rec. Adv. Integr. Anat. Evol. Biol.* **2017**, *300*, 1756–1780. [CrossRef] [PubMed]
65. Fawcett, D.W.; Selby, C.C. Observations on the Fine Structure of the Turtle Atrium. *J. Cell Biol.* **1958**, *4*, 63–72. [CrossRef] [PubMed]
66. Price, Z.; Eide, B.; Printzmetal, M.; Carpenter, C. Ultrastructure of the Dog Cardiac Muscle Cell. *Circ. Res.* **1959**, *7*, 858–865. [CrossRef]
67. Choate, J.K.; Klemm, M.; Hirst, G. Sympathetic and parasympathetic neuromuscular junctions in the guinea-pig sino-atrial node. *J. Auton. Nerv. Syst.* **1993**, *44*, 1–15. [CrossRef]
68. Di Bona, A.; Vita, V.; Costantini, I.; Zaglia, T. Towards a clearer view of sympathetic innervation of cardiac and skeletal muscles. *Prog. Biophys. Mol. Biol.* **2020**, *154*, 80–93. [CrossRef]
69. Kimura, K.; Ieda, M.; Fukuda, K. Development, maturation, and transdifferentiation of cardiac sympathetic nerves. *Circ. Res.* **2012**, *110*, 325–336. [CrossRef]
70. Franzoso, M.; Zaglia, T.; Mongillo, M. Putting together the clues of the everlasting neuro-cardiac liaison. *Biochim. Biophys. Acta* **2016**, *1863*, 1904–1915. [CrossRef]
71. Saburkina, I.; Rysevaite, K.; Pauziene, N.; Mischke, K.; Schauerte, P.; Jalife, J.; Pauza, D.H. Epicardial neural ganglionated plexus of ovine heart: Anatomic basis for experimental cardiac electrophysiology and nerve protective cardiac surgery. *Heart Rhythm.* **2010**, *7*, 942–950. [CrossRef]
72. Batulevicius, D.; Skripka, V.; Pauziene, N.; Pauza, D.H. Topography of the porcine epicardial nerve plexus as revealed by histochemistry for acetylcholinesterase. *Auton. Neurosci.* **2008**, *138*, 64–75. [CrossRef]
73. Batulevicius, D.; Pauziene, N.; Pauza, D.H. Topographic morphology and age-related analysis of the neuronal number of the rat intracardiac nerve plexus. *Ann. Anat.* **2003**, *185*, 449–459. [CrossRef]
74. Rysevaite, K.; Saburkina, I.; Pauziene, N.; Noujaim, S.F.; Jalife, J.; Pauza, D.H. Morphologic pattern of the intrinsic ganglionated nerve plexus in mouse heart. *Heart Rhythm.* **2011**, *8*, 448–454. [CrossRef]
75. Stoyek, M.R.; Quinn, T.A.; Croll, R.P.; Smith, F.M. Zebrafish heart as a model to study the integrative autonomic control of pacemaker function. *Am. J. Physiol.* **2016**, *311*, H676–H688. [CrossRef] [PubMed]
76. Poon, K.-L.; Liebling, M.; Kondrychyn, I.; Brand, T.; Korzh, V. Development of the cardiac conduction system in zebrafish. *Gene Expr. Patterns* **2016**, *21*, 89–96. [CrossRef] [PubMed]
77. Macdonald, E.A.; Stoyek, M.R.; Rose, R.A.; Quinn, T.A. Intrinsic regulation of sinoatrial node function and the zebrafish as a model of stretch effects on pacemaking. *Prog. Biophys. Mol. Biol.* **2017**, *130*, 198–211. [CrossRef]
78. Stoyek, M.R.; Croll, R.P.; Smith, F.M. Intrinsic and extrinsic innervation of the heart in zebrafish (*Danio rerio*). *J. Comp. Neurol.* **2015**, *523*, 1683–1700. [CrossRef]
79. Poon, K.L.; Brand, T. The zebrafish model system in cardiovascular research: A tiny fish with mighty prospects. *Glob. Cardiol. Sci. Pr.* **2013**, *2013*, 9–28. [CrossRef]
80. Howe, K.; Clark, M.D.; Torroja, C.F.; Torrance, J.; Berthelot, C.; Muffato, M.; Collins, J.E.; Humphray, S.; McLaren, K.; Matthews, L.; et al. The zebrafish reference genome sequence and its relationship to the human genome. *Nature* **2013**, *496*, 498–503. [CrossRef]
81. Achanta, S.; Gorky, J.; Leung, C.; Moss, A.; Robbins, S.; Eisenman, L.; Chen, J.; Tappan, S.; Heal, M.; Farahani, N.; et al. A Comprehensive Integrated Anatomical and Molecular Atlas of Rat Intrinsic Cardiac Nervous System. *iScience* **2020**, *23*, 101140. [CrossRef]
82. Kuder, T.; Nowak, E. Autonomic cardiac nerves: Literature review. *Folia Morphol.* **2015**, *74*, 1–8. [CrossRef]
83. Pauza, D.H.; Pauziene, N.; Pakeltyte, G.; Stropus, R. Comparative quantitative study of the intrinsic cardiac ganglia and neurons in the rat, guinea pig, dog and human as revealed by histochemical staining for acetylcholinesterase. *Ann. Anat.* **2002**, *184*, 125–136. [CrossRef]
84. Horackova, M.; Armour, J.A.; Byczko, Z. Distribution of intrinsic cardiac neurons in whole-mount guinea pig atria identified by multiple neurochemical coding. *Cell Tissue Res.* **1999**, *297*, 409–421. [CrossRef] [PubMed]
85. Edwards, F.R.; Hirst, G.D.; Klemm, M.F.; Steele, P.A. Different types of ganglion cell in the cardiac plexus of guinea-pigs. *J. Physiol.* **1995**, *486*, 453–471. [CrossRef] [PubMed]

86. Klemm, M.F.; Wallace, D.J.; Hirst, G. Distribution of synaptic boutons around identified neurones lying in the cardiac plexus of the guinea-pig. *J. Auton. Nerv. Syst.* **1997**, *66*, 201–207. [CrossRef]
87. Selyanko, A. Membrane properties and firing characteristics of rat cardiac neurones in vitro. *J. Auton. Nerv. Syst.* **1992**, *39*, 181–189. [CrossRef]
88. Dyavanapalli, J.; Rimmer, K.; Harper, A.A. The action of high K⁺ and aglycaemia on the electrical properties and synaptic transmission in rat intracardiac ganglion neurones in vitro. *Exp. Physiol.* **2008**, *94*, 201–212. [CrossRef] [PubMed]
89. McAllen, R.M.; Salo, L.M.; Paton, J.F.R.; Pickering, A.E. Processing of central and reflex vagal drives by rat cardiac ganglion neurones: An intracellular analysis. *J. Physiol.* **2011**, *589*, 5801–5818. [CrossRef]
90. Rimmer, K.; Harper, A.A. Developmental Changes in Electrophysiological Properties and Synaptic Transmission in Rat Intracardiac Ganglion Neurons. *J. Neurophysiol.* **2006**, *95*, 3543–3552. [CrossRef]
91. Jaenig, W. Transmission of impulses in the parasympathetic cardiomotor pathway to the sino-atrial node. *J. Physiol.* **2011**, *589*, 5911–5913. [CrossRef]
92. Klemm, M.; Hirst, G.; Campbell, G. Structure of autonomic neuromuscular junctions in the sinus venosus of the toad. *J. Auton. Nerv. Syst.* **1992**, *39*, 139–150. [CrossRef]
93. Hoard, J.L.; Hoover, D.B.; Wondergem, R. Phenotypic properties of adult mouse intrinsic cardiac neurons maintained in culture. *Am. J. Physiol.* **2007**, *293*, C1875–C1883. [CrossRef] [PubMed]
94. Rysevaite, K.; Saburkina, I.; Pauziene, N.; Vaitkevicius, R.; Noujaim, S.F.; Jalife, J.; Pauza, D.H. Immunohistochemical characterization of the intrinsic cardiac neural plexus in whole-mount mouse heart preparations. *Heart Rhythm.* **2011**, *8*, 731–738. [CrossRef] [PubMed]
95. Richardson, R.J.; Grkovic, I.; Anderson, C.R. Immunohistochemical analysis of intracardiac ganglia of the rat heart. *Cell Tissue Res.* **2003**, *314*, 337–350. [CrossRef] [PubMed]
96. Coote, J. Myths and realities of the cardiac vagus. *J. Physiol.* **2013**, *591*, 4073–4085. [CrossRef]
97. Pauziene, N.; Alaburda, P.; Rysevaite-Kyguoliene, K.; Pauza, A.G.; Inokaitis, H.; Masaityte, A.; Rudokaite, G.; Saburkina, I.; Plisiene, J.; Pauza, D.H. Innervation of the rabbit cardiac ventricles. *J. Anat.* **2015**, *228*, 26–46. [CrossRef] [PubMed]
98. Horackova, M.; Slavikova, J.; Byczko, Z. Postnatal development of the rat intrinsic cardiac nervous system: A confocal laser scanning microscopy study in whole-mount atria. *Tissue Cell* **2000**, *32*, 377–388. [CrossRef]
99. Hoover, D.B.; Isaacs, E.; Jacques, F.; Hoard, J.; Pagé, P.; Armour, J. Localization of multiple neurotransmitters in surgically derived specimens of human atrial ganglia. *Neuroscience* **2009**, *164*, 1170–1179. [CrossRef] [PubMed]
100. Zarzoso, M.; Rysevaite, K.; Milstein, M.L.; Calvo, C.J.; Kean, A.C.; Atienza, F.; Pauza, D.H.; Jalife, J.; Noujaim, S.F. Nerves projecting from the intrinsic cardiac ganglia of the pulmonary veins modulate sinoatrial node pacemaker function. *Cardiovasc. Res.* **2013**, *99*, 566–575. [CrossRef]
101. Paterson, D.J. Nitric oxide and the autonomic regulation of cardiac excitability. *Exp. Physiol.* **2001**, *86*, 1–12. [CrossRef] [PubMed]
102. Steele, P.A.; Gibbins, I.L.; Morris, J.L. Projections of intrinsic cardiac neurons to different targets in the guinea-pig heart. *J. Auton. Nerv. Syst.* **1996**, *56*, 191–200. [CrossRef]
103. Parsons, R.L.; Locknar, S.A.; Young, B.A.; Hoard, J.L.; Hoover, D.B. Presence and co-localization of vasoactive intestinal polypeptide with neuronal nitric oxide synthase in cells and nerve fibers within guinea pig intrinsic cardiac ganglia and cardiac tissue. *Cell Tissue Res.* **2005**, *323*, 197–209. [CrossRef] [PubMed]
104. Herring, N.; Lokale, M.N.; Danson, E.J.; Heaton, D.A.; Paterson, D.J. Neuropeptide Y reduces acetylcholine release and vagal bradycardia via a Y2 receptor-mediated, protein kinase C-dependent pathway. *J. Mol. Cell. Cardiol.* **2008**, *44*, 477–485. [CrossRef]
105. Fuzik, J.; Zeisel, A.; Máté, Z.; Calvigioni, D.; Yanagawa, Y.; Szabó, G.; Linnarsson, S.; Harkany, T. Integration of electrophysiological recordings with single-cell RNA-seq data identifies neuronal subtypes. *Nat. Biotechnol.* **2016**, *34*, 175–183. [CrossRef] [PubMed]
106. Ripplinger, C.M.; Noujaim, S.F.; Linz, D. The nervous heart. *Prog. Biophys. Mol. Biol.* **2016**, *120*, 199–209. [CrossRef]
107. Yuan, B.-X.; Ardell, J.L.; Hopkins, D.A.; Armour, J.A. Differential cardiac responses induced by nicotine sensitive canine atrial and ventricular neurones. *Cardiovasc. Res.* **1993**, *27*, 760–769. [CrossRef] [PubMed]

108. Allen, E.; Coote, J.H.; Grubb, B.D.; Batten, T.F.; Pauza, D.H.; Ng, G.A.; Brack, K.E. Electrophysiological effects of nicotinic and electrical stimulation of intrinsic cardiac ganglia in the absence of extrinsic autonomic nerves in the rabbit heart. *Heart Rhythm*. **2018**, *15*, 1698–1707. [CrossRef] [PubMed]
109. Xu, Z.J.; Adams, D.J. Alpha-adrenergic modulation of ionic currents in cultured parasympathetic neurons from rat intracardiac ganglia. *J. Neurophysiol.* **1993**, *69*, 1060–1070. [CrossRef]
110. Fedorov, V.V.; Hucker, W.J.; Dobrzynski, H.; Rosenshtraukh, L.V.; Efimov, I.R. Postganglionic nerve stimulation induces temporal inhibition of excitability in rabbit sinoatrial node. *Am. J. Physiol.* **2006**, *291*, H612–H623. [CrossRef]
111. Glukhov, A.V.; Fedorov, V.V.; Anderson, M.E.; Mohler, P.J.; Efimov, I.R. Functional anatomy of the murine sinus node: High-resolution optical mapping of ankyrin-B heterozygous mice. *Am. J. Physiol.* **2010**, *299*, H482–H491. [CrossRef]
112. Shibata, N.; Inada, S.; Mitsui, K.; Honjo, H.; Yamamoto, M.; Niwa, R.; Boyett, M.; Kodama, I. Pacemaker shift in the rabbit sinoatrial node in response to vagal nerve stimulation. *Exp. Physiol.* **2001**, *86*, 177–184. [CrossRef]
113. Sampaio, K.N.; Mauad, H.; Spyer, K.M.; Ford, T.W. Differential chronotropic and dromotropic responses to focal stimulation of cardiac vagal ganglia in the rat. *Exp. Physiol.* **2003**, *88*, 315–327. [CrossRef] [PubMed]
114. Hucker, W.J.; Nikolski, V.P.; Efimov, I.R. Autonomic control and innervation of the atrioventricular junctional pacemaker. *Heart Rhythm*. **2007**, *4*, 1326–1335. [CrossRef] [PubMed]
115. Mazgalev, T.N.; Garrigue, S.; Mowrey, K.A.; Yamanouchi, Y.; Tchou, P.J. Autonomic modification of the atrioventricular node during atrial fibrillation. *Circulation* **1999**, *99*, 2806–2814. [CrossRef]
116. Fedorov, V.V.; Ambrosi, C.M.; Kosteki, G.; Hucker, W.J.; Glukhov, A.V.; Wuskell, J.P.; Loew, L.M.; Moazami, N.; Efimov, I.R. Anatomic localization and autonomic modulation of atrioventricular junctional rhythm in failing human hearts. *Circ. Arrhythm. Electrophysiol.* **2011**, *4*, 515–525. [CrossRef] [PubMed]
117. Beaumont, E.; Salavatan, S.; Southerland, E.M.; Vinet, A.; Jacquemet, V.; Armour, J.A.; Ardell, J.L. Network interactions within the canine intrinsic cardiac nervous system: Implications for reflex control of regional cardiac function. *J. Physiol.* **2013**, *591*, 4515–4533. [CrossRef]
118. Gibbons, D.D.; Southerland, E.M.; Hoover, N.B.; Beaumont, E.; Armour, J.A.; Ardell, J.L. Neuromodulation targets intrinsic cardiac neurons to attenuate neuronally mediated atrial arrhythmias. *Am. J. Physiol.* **2012**, *302*, R357–R364. [CrossRef]
119. Ng, G.A.; Brack, K.E.; Coote, J.H. Effects of direct sympathetic and vagus nerve stimulation on the physiology of the whole heart—A novel model of isolated Langendorff perfused rabbit heart with intact dual autonomic innervation. *Exp. Physiol.* **2001**, *86*, 319–329. [CrossRef]
120. Winter, J.; Tanko, A.S.; Brack, K.E.; Coote, J.H.; Ng, G.A. Differential cardiac responses to unilateral sympathetic nerve stimulation in the isolated innervated rabbit heart. *Auton. Neurosci.* **2012**, *166*, 4–14. [CrossRef]
121. Brack, K.E. The heart's 'little brain' controlling cardiac function in the rabbit. *Exp. Physiol.* **2014**, *100*, 348–353. [CrossRef]
122. Hou, Y.; Scherlag, B.J.; Lin, J.; Zhang, Y.; Lu, Z.; Truong, K.; Patterson, E.; Lazzara, R.; Jackman, W.M.; Po, S.S. Ganglionated plexi modulate extrinsic cardiac autonomic nerve input. *J. Am. Coll. Cardiol.* **2007**, *50*, 61–68. [CrossRef]
123. Gray, A.L.; Johnson, T.A.; Ardell, J.L.; Massari, V.J. Parasympathetic control of the heart. II. A novel interganglionic intrinsic cardiac circuit mediates neural control of heart rate. *J. Appl. Physiol.* **2004**, *96*, 2273–2278. [CrossRef] [PubMed]
124. Gatti, P.J.; Johnson, T.A.; Phan, P.; Jordan, I.; Coleman, W.; Massari, V.; Iii, I.J. The physiological and anatomical demonstration of functionally selective parasympathetic ganglia located in discrete fat pads on the feline myocardium. *J. Auton. Nerv. Syst.* **1995**, *51*, 255–259. [CrossRef]
125. Dickerson, L.W.; Rodak, D.J.; Fleming, T.J.; Gatti, P.J.; Massari, V.J.; McKenzie, J.C.; Gillis, R.A. Parasympathetic neurons in the cranial medial ventricular fat pad on the dog heart selectively decrease ventricular contractility. *J. Auton. Nerv. Syst.* **1998**, *70*, 129–141. [CrossRef]
126. Shen, M.J.; Zipes, D.P. Role of the autonomic nervous system in modulating cardiac arrhythmias. *Circ. Res.* **2014**, *114*, 1004–1021. [CrossRef]
127. Levy, M.N. Brief reviews: Sympathetic-parasympathetic interactions in the heart. *Circ. Res.* **1971**, *29*, 437–445. [CrossRef] [PubMed]

128. Kubista, H.; Boehm, S. Molecular mechanisms underlying the modulation of exocytotic noradrenaline release via presynaptic receptors. *Pharmacol. Ther.* **2006**, *112*, 213–242. [CrossRef]
129. Sasaki, S.; Daitoku, K.; Iwasa, A.; Motomura, S. NO is involved in MCh-induced accentuated antagonism via type II PDE in the canine blood-perfused SA node. *Am. J. Physiol.* **2000**, *279*, H2509–H2518. [CrossRef] [PubMed]
130. Rajendran, P.S.; Challis, R.C.; Fowlkes, C.C.; Hanna, P.; Tompkins, J.D.; Jordan, M.C.; Hiyari, S.; Gabris-Weber, B.A.; Greenbaum, A.; Chan, K.Y.; et al. Identification of peripheral neural circuits that regulate heart rate using optogenetic and viral vector strategies. *Nat. Commun.* **2019**, *10*, 1–13. [CrossRef] [PubMed]
131. Hou, Y.; Scherlag, B.J.; Lin, J.; Zhou, J.; Song, J.; Zhang, Y.; Patterson, E.; Lazzara, R.; Jackman, W.M.; Po, S.S. Interactive atrial neural network: Determining the connections between ganglionated plexi. *Heart Rhythm.* **2007**, *4*, 56–63. [CrossRef] [PubMed]
132. Randall, D.C.; Brown, D.R.; McQuirt, A.S.; Thompson, G.W.; Armour, J.A.; Ardell, J.L. Interactions within the intrinsic cardiac nervous system contribute to chronotropic regulation. *Am. J. Physiol.* **2003**, *285*, R1066–R1075. [CrossRef]
133. Ardell, J.L.; Butler, C.K.; Smith, F.M.; Hopkins, D.A.; Armour, J.A. Activity of in vivo atrial and ventricular neurons in chronically decentralized canine hearts. *Am. J. Physiol.* **1991**, *260*, H713–H721. [CrossRef] [PubMed]
134. Hirst, G.; Choate, J.; Cousins, H.; Edwards, F.; Klemm, M. Transmission by post-ganglionic axons of the autonomic nervous system: The importance of the specialized neuroeffector junction. *Neurosci.* **1996**, *73*, 7–23. [CrossRef]
135. Burnstock, G. Autonomic Neurotransmission: 60 Years since Sir Henry Dale. *Annu. Rev. Pharmacol. Toxicol.* **2009**, *49*, 1–30. [CrossRef] [PubMed]
136. Burnstock, G. Non-synaptic transmission at autonomic neuroeffector junctions. *Neurochem. Int.* **2008**, *52*, 14–25. [CrossRef]
137. Zaglia, T.; Mongillo, M. Cardiac sympathetic innervation, from a different point of (re)view. *J. Physiol.* **2017**, *595*, 3919–3930. [CrossRef]
138. Kikuchi, S. The structure and innervation of the sinu-atrial node of the mole heart. *Cell Tissue Res.* **1976**, *172*, 345–356. [CrossRef]
139. Thaemert, J.C. Atrioventricular node innervation in ultrastructural three dimensions. *Am. J. Anat.* **1970**, *128*, 239–263. [CrossRef]
140. Finlay, M.C.; Harmer, S.C.; Tinker, A. The control of cardiac ventricular excitability by autonomic pathways. *Pharmacol. Ther.* **2017**, *174*, 97–111. [CrossRef]
141. Schobesberger, S.; Wright, P.T.; Poulet, C.; Mardones, J.L.S.A.; Mansfield, C.; Friebe, A.; Harding, S.E.; Balligand, J.-L.; Nikolaev, V.O.; Gorelik, J. β 3-Adrenoceptor redistribution impairs NO/cGMP/PDE2 signalling in failing cardiomyocytes. *eLife* **2020**, *9*. [CrossRef]
142. Nikolaev, V.O.; Moshkov, A.; Lyon, A.R.; Miragoli, M.; Novak, P.; Paur, H.; Lohse, M.J.; Korchev, Y.E.; Harding, S.E.; Gorelik, J. Beta2-adrenergic receptor redistribution in heart failure changes cAMP compartmentation. *Science* **2010**, *327*, 1653–1657. [CrossRef]
143. Furshpan, E.J.; MacLeish, P.R.; O’Lague, P.H.; Potter, D.D. Chemical transmission between rat sympathetic neurons and cardiac myocytes developing in microcultures: Evidence for cholinergic, adrenergic, and dual-function neurons. *Proc. Natl. Acad. Sci. USA* **1976**, *73*, 4225–4229. [CrossRef] [PubMed]
144. Yang, B.; Slonimsky, J.D.; Birren, S.J. A rapid switch in sympathetic neurotransmitter release properties mediated by the p75 receptor. *Nat. Neurosci.* **2002**, *5*, 539–545. [CrossRef] [PubMed]
145. Shcherbakova, O.G.; Hurt, C.M.; Xiang, Y.; Dell’Acqua, M.L.; Zhang, Q.; Tsien, R.W.; Kobilka, B.K. Organization of β -adrenoceptor signaling compartments by sympathetic innervation of cardiac myocytes. *J. Cell Biol.* **2007**, *176*, 521–533. [CrossRef] [PubMed]
146. Prando, V.; Da Broi, F.; Franzoso, M.; Plazzo, A.P.; Pianca, N.; Francolini, M.; Basso, C.; Kay, M.W.; Zaglia, T.; Mongillo, M. Dynamics of neuroeffector coupling at cardiac sympathetic synapses. *J. Physiol.* **2018**, *596*, 2055–2075. [CrossRef]
147. Shcherbakova, O.G. Localization of Ankyrin G, Na_v and KCNQ1 channels to neuro-cardiac junctions. *BioRxiv* **2019**. [CrossRef]

148. Choate, J.K.; Edwards, F.R.; Hirst, G.D.; O'Shea, J.E. Effects of sympathetic nerve stimulation on the sino-atrial node of the guinea-pig. *J. Physiol.* **1993**, *471*, 707–727. [CrossRef]
149. Bramich, N.J.; Brock, J.A.; Edwards, F.R.; Hirst, G.D. Responses to sympathetic nerve stimulation of the sinus venosus of the toad. *J. Physiol.* **1993**, *461*, 403–430. [CrossRef]
150. Gonon, F.; Msgghina, M.; Stjärne, L. Kinetics of noradrenaline released by sympathetic nerves. *Neuroscience* **1993**, *56*, 535–538. [CrossRef]
151. Schroeder, C.; Jordan, J. Norepinephrine transporter function and human cardiovascular disease. *Am. J. Physiol.* **2012**, *303*, H1273–H1282. [CrossRef]
152. Abadie, C.; Foucart, S.; Pagé, P.; Nadeau, R. Modulation of noradrenaline release from isolated human atrial appendages. *J. Auton. Nerv. Syst.* **1996**, *61*, 269–276. [CrossRef]
153. Rump, L.C.; Riera-Knorrenschild, G.; Schwertfeger, E.; Bohmann, C.; Spillner, G.; Schollmeyer, P. Dopaminergic and α -adrenergic control of neurotransmission in human right atrium. *J. Cardiovasc. Pharmacol.* **1995**, *26*, 462–470. [CrossRef]
154. Bardsley, E.N.; Paterson, D.J. Neurocardiac regulation: From cardiac mechanisms to novel therapeutic approaches. *J. Physiol.* **2020**, *598*, 2957–2976. [CrossRef] [PubMed]
155. Surdo, N.C.; Berrera, M.; Koschinski, A.; Brescia, M.; Machado, M.R.; Carr, C.; Wright, P.; Gorelik, J.; Morotti, S.; Grandi, E.; et al. FRET biosensor uncovers cAMP nano-domains at β -adrenergic targets that dictate precise tuning of cardiac contractility. *Nat. Commun.* **2017**, *8*, 15031. [CrossRef] [PubMed]
156. Matsuda, J.J.; Lee, H.; Shibata, E.F. Enhancement of rabbit cardiac sodium channels by beta-adrenergic stimulation. *Circ. Res.* **1992**, *70*, 199–207. [CrossRef] [PubMed]
157. Lloyd, T.R. Sympathetic innervation improves the contractile performance of neonatal cardiac ventricular myocytes in culture. *J. Mol. Cell. Cardiol.* **1990**, *22*, 333–342. [CrossRef]
158. Zaika, O.; Zhang, J.; Shapiro, M.S. Functional role of M-type (KCNQ) K⁺ channels in adrenergic control of cardiomyocyte contraction rate by sympathetic neurons. *J. Physiol.* **2011**, *589*, 2559–2568. [CrossRef]
159. Winbo, A.; Ramanan, S.; Eugster, E.; Jovinge, S.; Skinner, J.R.; Montgomery, J.M. Functional coculture of sympathetic neurons and cardiomyocytes derived from human induced pluripotent stem cells. *Am. J. Physiol.* **2020**, *319*, H927–H937. [CrossRef]
160. Takayama, Y.; Kushige, H.; Akagi, Y.; Suzuki, Y.; Kumagai, Y.; Kida, Y.S. Selective induction of human autonomic neurons enables precise control of cardiomyocyte beating. *Sci. Rep.* **2020**, *10*, 1–13. [CrossRef]
161. Zaglia, T.; Milan, G.; Franzoso, M.; Bertaggia, E.; Pianca, N.; Piasentini, E.; Voltarelli, V.A.; Chiavegato, D.; Brum, P.C.; Glass, D.J.; et al. Cardiac sympathetic neurons provide trophic signal to the heart via β 2-adrenoceptor-dependent regulation of proteolysis. *Cardiovasc. Res.* **2013**, *97*, 240–250. [CrossRef]
162. Atkins, D.L.; Rosenthal, J.K.; Krumm, P.A.; Marvin, W.J. Application of stereological analysis of cell volume to isolated myocytes in culture with and without adrenergic innervation. *Anat. Rec.* **1991**, *231*, 209–217. [CrossRef]
163. Kreipke, R.E.; Birren, S.J. Innervating sympathetic neurons regulate heart size and the timing of cardiomyocyte cell cycle withdrawal. *J. Physiol.* **2015**, *593*, 5057–5073. [CrossRef] [PubMed]
164. Pianca, N.; Di Bona, A.; Lazzeri, E.; Costantini, I.; Franzoso, M.; Prando, V.; Armani, A.; Rizzo, S.; Fedrigo, M.; Angelini, A.; et al. Cardiac sympathetic innervation network shapes the myocardium by locally controlling cardiomyocyte size through the cellular proteolytic machinery. *J. Physiol.* **2019**, *597*, 3639–3656. [CrossRef] [PubMed]
165. White, I.A.; Gordon, J.; Balkan, W.; Hare, J.M. Sympathetic Reinnervation Is Required for Mammalian Cardiac Regeneration. *Circ. Res.* **2015**, *117*, 990–994. [CrossRef] [PubMed]
166. Atkins, D.L.; Marvin, W.J. Chronotropic responsiveness of developing sinoatrial and ventricular rat myocytes to autonomic agonists following adrenergic and cholinergic innervation in vitro. *Circ. Res.* **1989**, *64*, 1051–1062. [CrossRef]
167. Marvin, W.J.; Atkins, D.L.; Chittick, V.L.; Lund, D.D.; Hermsmeyer, K. In vitro adrenergic and cholinergic innervation of the developing rat myocyte. *Circ. Res.* **1984**, *55*, 49–58. [CrossRef]
168. Barnett, J.V.; Taniuchi, M.; Yang, M.B.; Galper, J.B. Co-culture of embryonic chick heart cells and ciliary ganglia induces parasympathetic responsiveness in embryonic chick heart cells. *Biochem. J.* **1993**, *292*, 395–399. [CrossRef]
169. Flannery, R.J.; Brusés, J.L. N-cadherin induces partial differentiation of cholinergic presynaptic terminals in heterologous cultures of brainstem neurons and CHO cells. *Front. Synaptic Neurosci.* **2012**, *4*, 6. [CrossRef]

170. Bywater, R.A.; Campbell, G.; Edwards, F.R.; Hirst, G.D.; O'Shea, J.E. The effects of vagal stimulation and applied acetylcholine on the sinus venosus of the toad. *J. Physiol.* **1989**, *415*, 35–56. [CrossRef]
171. Campbell, G.D.; Edwards, F.R.; Hirst, G.D.; O'Shea, J.E. Effects of vagal stimulation and applied acetylcholine on pacemaker potentials in the guinea-pig heart. *J. Physiol.* **1989**, *415*, 57–68. [CrossRef]
172. Hartzell, H.C. Distribution of muscarinic acetylcholine receptors and presynaptic nerve terminals in amphibian heart. *J. Cell Biol.* **1980**, *86*, 6–20. [CrossRef]
173. Choate, J.K.; Feldman, R. Neuronal control of heart rate in isolated mouse atria. *Am. J. Physiol.* **2003**, *285*, H1340–H1346. [CrossRef] [PubMed]
174. Han, S.Y.; Bolter, C.P. The muscarinic-activated potassium channel always participates in vagal slowing of the guinea-pig sinoatrial pacemaker. *Auton. Neurosci.* **2011**, *164*, 96–100. [CrossRef] [PubMed]
175. Mangoni, M.E.; Nargeot, J. Genesis and regulation of the heart automaticity. *Physiol. Rev.* **2008**, *88*, 919–982. [CrossRef]
176. Jaenig, W. Reply to the Letter of Otto Hutter 'The vagus and the heart: Revisiting an early contribution to a still on-going dispute'. *J. Physiol.* **2012**, *590*, 2537. [CrossRef]
177. Boyett, M.R.; Honjo, H.; Kodama, I. The sinoatrial node, a heterogeneous pacemaker structure. *Cardiovasc. Res.* **2000**, *47*, 658–687. [CrossRef]
178. Löffelholz, K.; Pappano, A.J. The parasympathetic neuroeffector junction of the heart. *Pharmacol. Rev.* **1985**, *37*, 1–24.
179. Kodama, I.; Boyett, M.; Suzuki, R.; Honjo, H.; Toyama, J. Regional differences in the response of the isolated sino-atrial node of the rabbit to vagal stimulation. *J. Physiol.* **1996**, *495*, 785–801. [CrossRef]
180. Manabe, N.; Foldes, F.; Töröcsik, A.; Nagashima, H.; Goldiner, P.; Vizi, E. Presynaptic interaction between vagal and sympathetic innervation in the heart: Modulation of acetylcholine and noradrenaline release. *J. Auton. Nerv. Syst.* **1991**, *32*, 233–242. [CrossRef]
181. Mahmoud, A.I.; O'Meara, C.C.; Gemberling, M.; Zhao, L.; Bryant, D.M.; Zheng, R.; Gannon, J.B.; Cai, L.; Choi, W.-Y.; Egnaczyk, G.F.; et al. Nerves regulate cardiomyocyte proliferation and heart regeneration. *Dev. Cell* **2015**, *34*, 387–399. [CrossRef]
182. Burnstock, G. Do some nerve cells release more than one transmitter? *Neuroscience* **1976**, *1*, 239–248. [CrossRef]
183. Herring, N. Autonomic control of the heart: Going beyond the classical neurotransmitters. *Exp. Physiol.* **2014**, *100*, 354–358. [CrossRef] [PubMed]
184. Herring, N.; Cranley, J.; Lokale, M.N.; Li, D.; Shanks, J.; Alston, E.N.; Girard, B.M.; Carter, E.; Parsons, R.L.; Habecker, B.A.; et al. The cardiac sympathetic co-transmitter galanin reduces acetylcholine release and vagal bradycardia: Implications for neural control of cardiac excitability. *J. Mol. Cell. Cardiol.* **2012**, *52*, 667–676. [CrossRef] [PubMed]
185. Beaulieu, P. Peptidic regulation of heart rate and interactions with the autonomic nervous system. *Cardiovasc. Res.* **1998**, *37*, 578–585. [CrossRef]
186. Macdonald, E.A.; Rose, R.A.; Quinn, T.A. Neurohumoral control of sinoatrial node activity and heart rate: Insight from experimental models and findings from humans. *Front. Physiol.* **2020**, *11*, 170. [CrossRef]
187. Burnstock, G. Purinergic signaling in the cardiovascular system. *Circ. Res.* **2017**, *120*, 207–228. [CrossRef]
188. Burnstock, G. Introduction and perspective, historical note. *Front. Cell. Neurosci.* **2013**, *7*, 7. [CrossRef]
189. Shen, J.-B.; Yang, R.; Pappano, A.; Liang, B.T. Cardiac P2X purinergic receptors as a new pathway for increasing Na⁺ entry in cardiac myocytes. *Am. J. Physiol.* **2014**, *307*, H1469–H1477. [CrossRef]
190. Ralevic, V. P2X receptors in the cardiovascular system. *WIREs Membr. Transp. Signal.* **2012**, *1*, 663–674. [CrossRef]
191. Horackova, M.; Huang, M.H.; Armour, J.A. Purinergic modulation of adult guinea pig cardiomyocytes in long term cultures and co-cultures with extracardiac or intrinsic cardiac neurones. *Cardiovasc. Res.* **1994**, *28*, 673–679. [CrossRef]
192. Burnstock, G.; Pelleg, A. Cardiac purinergic signalling in health and disease. *Purinergic Signal.* **2015**, *11*, 1–46. [CrossRef]
193. Henning, R.J. Vasoactive intestinal peptide: Cardiovascular effects. *Cardiovasc. Res.* **2001**, *49*, 27–37. [CrossRef]
194. Schultz, H.D. Nitric oxide regulation of autonomic function in heart failure. *Curr. Heart Fail. Rep.* **2009**, *6*, 71–80. [CrossRef] [PubMed]

195. Herring, N.; Golding, S.; Paterson, D.J. Pre-synaptic NO-cGMP Pathway Modulates Vagal Control of Heart Rate in Isolated Adult Guinea Pig Atria. *J. Mol. Cell. Cardiol.* **2000**, *32*, 1795–1804. [CrossRef] [PubMed]
196. Chow, L.T.C.; Chow, S.S.M.; Anderson, R.H.; Gosling, J.A. Autonomic innervation of the human cardiac conduction system: Changes from infancy to senility—an immunohistochemical and histochemical analysis. *Anat. Rec.* **2001**, *264*, 169–182. [CrossRef] [PubMed]
197. Stuart, S.D.F.; Wang, L.; Woodard, W.R.; Ng, G.A.; Habecker, B.A.; Ripplinger, C.M. Age-related changes in cardiac electrophysiology and calcium handling in response to sympathetic nerve stimulation. *J. Physiol.* **2018**, *596*, 3977–3991. [CrossRef]
198. Hildreth, V.; Anderson, R.H.; Henderson, D.J. Autonomic innervation of the developing heart: Origins and function. *Clin. Anat.* **2009**, *22*, 36–46. [CrossRef] [PubMed]
199. Scherlag, B.J.; Nakagawa, H.; Jackman, W.M.; Yamanashi, W.S.; Patterson, E.; Po, S.; Lazzara, R. Electrical Stimulation to Identify Neural Elements on the Heart: Their Role in Atrial Fibrillation. *J. Interv. Card. Electrophysiol.* **2005**, *13*, 37–42. [CrossRef]
200. Herring, N.; Kalla, M.; Paterson, D.J. The autonomic nervous system and cardiac arrhythmias: Current concepts and emerging therapies. *Nat. Rev. Cardiol.* **2019**, *16*, 707–726. [CrossRef]
201. Scornik, F.S.; Desai, M.; Brugada, R.; Guerschicoff, A.; Pollevick, G.D.; Antzelevitch, C.; Pérez, G.J. Functional expression of “cardiac-type” Nav1.5 sodium channel in canine intracardiac ganglia. *Heart Rhythm.* **2006**, *3*, 842–850. [CrossRef]
202. Kang, P.S.; Gomes, J.A.; Kelen, G.; El-Sherif, N. Role of autonomic regulatory mechanism in sinoatrial conduction and sinus node automaticity in sick sinus syndrome. *Circulation* **1981**, *64*, 832–838. [CrossRef]
203. Jordan, J.L.; Yamaguchi, I.; Mandel, W.J. Studies on the mechanism of sinus node dysfunction in the sick sinus syndrome. *Circulation* **1978**, *57*, 217–223. [CrossRef] [PubMed]
204. Awad, M.; Czer, L.S.C.; Hou, M.; Golshani, S.S.; Goltche, M.; De Robertis, M.; Kittleson, M.; Patel, J.; Azarbal, B.; Kransdorf, E.; et al. Early Denervation and Later Reinnervation of the Heart Following Cardiac Transplantation: A Review. *J. Am. Heart Assoc.* **2016**, *5*, e004070. [CrossRef] [PubMed]
205. Smith, F.; McGuirt, A.S.; Leger, J.; Armour, J.A.; Ardell, J.L. Effects of chronic cardiac decentralization on functional properties of canine intracardiac neurons in vitro. *Am. J. Physiol.* **2001**, *281*, R1474–R1482. [CrossRef] [PubMed]
206. Close, P.; Hawkes, N.; Cornez, I.; Creppe, C.; Lambert, C.A.; Rogister, B.; Siebenlist, U.; Merville, M.-P.; Slaugenhaupt, S.A.; Bours, V.; et al. Transcription Impairment and Cell Migration Defects in Elongator-Depleted Cells: Implication for Familial Dysautonomia. *Mol. Cell* **2006**, *22*, 521–531. [CrossRef] [PubMed]
207. Anderson, S.L.; Coli, R.; Daly, I.W.; Kichula, E.A.; Rork, M.J.; Volpi, S.A.; Ekstein, J.; Rubin, B.Y. Familial Dysautonomia Is Caused by Mutations of the IKAP Gene. *Am. J. Hum. Genet.* **2001**, *68*, 753–758. [CrossRef] [PubMed]
208. Egorov, Y.V.; Kuz’Min, V.S.; Glukhov, A.V.; Rosenshtraukh, L.V. Electrophysiological Characteristics, Rhythm, Disturbances and Conduction Discontinuities under Autonomic Stimulation in the Rat Pulmonary Vein Myocardium. *J. Cardiovasc. Electrophysiol.* **2015**, *26*, 1130–1139. [CrossRef]
209. Ashton, J.L.; Burton, R.A.B.; Bub, G.; Smail, B.H.; Montgomery, J.M. Synaptic Plasticity in Cardiac Innervation and Its Potential Role in Atrial Fibrillation. *Front. Physiol.* **2018**, *9*, 240. [CrossRef]
210. Mesirca, P.; Bidaud, I.; Mangoni, M.E. Rescuing cardiac automaticity in L-type Cav1.3 channelopathies and beyond. *J. Physiol.* **2016**, *594*, 5869–5879. [CrossRef]
211. Kuß, J.; Stallmeyer, B.; Goldstein, M.; Rinné, S.; Pees, C.; Zumhagen, S.; Seebohm, G.; Decher, N.; Pott, L.; Kienitz, M.-C.; et al. Familial Sinus Node Disease Caused by a Gain of GIRK (G-Protein Activated Inwardly Rectifying K⁺ Channel) Channel Function. *Circ. Genom. Precis. Med.* **2019**, *12*. [CrossRef]
212. Froese, A.; Breher, S.S.; Waldeyer, C.; Schindler, R.F.; Nikolaev, V.O.; Rinné, S.; Wischmeyer, E.; Schlueter, J.; Becher, J.; Simrick, S.; et al. Popeye domain containing proteins are essential for stress-mediated modulation of cardiac pacemaking in mice. *J. Clin. Investig.* **2012**, *122*, 1119–1130. [CrossRef]
213. Rinné, S.; Ortiz-Bonnin, B.; Stallmeyer, B.; Kiper, A.K.; Fortmüller, L.; Schindler, R.F.; Herbort-Brand, U.; Kabir, N.S.; Dittmann, S.; Friedrich, C.; et al. POPDC2 a novel susceptibility gene for conduction disorders. *J. Mol. Cell. Cardiol.* **2020**, *145*, 74–83. [CrossRef] [PubMed]

214. Schindler, R.F.; Scotton, C.; Zhang, J.; Passarelli, C.; Ortiz-Bonnin, B.; Simrick, S.; Schwerte, T.; Poon, K.-L.; Fang, M.; Rinné, S.; et al. POPDC1S201F causes muscular dystrophy and arrhythmia by affecting protein trafficking. *J. Clin. Investig.* **2015**, *126*, 239–253. [CrossRef] [PubMed]
215. Bidaud, I.; Chong, A.C.Y.; Carcouet, A.; De Waard, S.; Charpentier, F.; Ronjat, M.; De Waard, M.; Isbrandt, D.; Wickman, K.; Vincent, A.; et al. Inhibition of G protein-gated K⁺ channels by tertiapin-Q rescues sinus node dysfunction and atrioventricular conduction in mouse models of primary bradycardia. *Sci. Rep.* **2020**, *10*, 1–13. [CrossRef] [PubMed]
216. Das, S.; Gordián-Vélez, W.J.; Ledebur, H.C.; Mourkioti, F.; Rompolas, P.; Chen, H.I.; Serruya, M.D.; Cullen, D.K. Innervation: The missing link for biofabricated tissues and organs. *NPJ Regen. Med.* **2020**, *5*, 1–19. [CrossRef]

Publisher’s Note: MDPI stays neutral with regard to jurisdictional claims in published maps and institutional affiliations.



© 2020 by the authors. Licensee MDPI, Basel, Switzerland. This article is an open access article distributed under the terms and conditions of the Creative Commons Attribution (CC BY) license (<http://creativecommons.org/licenses/by/4.0/>).



Review

Critical Assessment of the Concepts and Misconceptions of the Cardiac Conduction System over the Last 100 Years: The Personal Quest of Robert H. Anderson

Eduardo Back Sternick ^{1,*} and Damián Sánchez-Quintana ²

¹ Electrophysiology Unit, Biocor Instituto, Nova Lima 34006083, Minas Gerais, Brazil

² Department of Anatomy and Cell Biology, Universidad de Extremadura, 06071 Badajoz, Spain; sanchezquintana55@gmail.com

* Correspondence: eduardosternick@gmail.com

Abstract: Anatomical concepts regarding the conduction system of the heart have been a matter of debate since pioneering work done at the beginning of the 20th century. Robert H. Anderson was actively involved in this field for half a century. We aimed to investigate how his own concepts evolved over time. We have assessed anatomical concepts relating to the cardiac conduction system appearing since the key contributions made in the initial decade of the 20th century, analyzing them from the perspective of Robert H. Anderson, particularly focusing on the anatomical aspects of structures such as accessory atrioventricular pathways, including the so-called Mahaim-type fibers, connections between the atrioventricular node and the atrial myocardium, and so-called “specialized” internodal atrial tracts. To accomplish this task, we have taken as our starting point the initial concepts published in the first decade of the century, along with those subsequently reported up to 1976, and assessing them in the light of our most recently published works. The concepts put forward by Robert Anderson with regard to atrioventricular nodal bypass tracts, atrioventricular nodal inputs, decrementally conducting accessory pathways, and “tracts” for internodal atrial conduction, have remained consistent along the time frame of half a century.

Keywords: conduction system of the heart; atrio-his connection; atriofascicular pathway; fasciculo-ventricular pathway

Citation: Sternick, E.B.; Sánchez-Quintana, D. Critical Assessment of the Concepts and Misconceptions of the Cardiac Conduction System over the Last 100 Years: The Personal Quest of Robert H. Anderson. *J. Cardiovasc. Dev. Dis.* **2021**, *8*, 5. <https://doi.org/10.3390/jcdd8010005>

Received: 3 January 2021

Accepted: 16 January 2021

Published: 19 January 2021

Publisher’s Note: MDPI stays neutral with regard to jurisdictional claims in published maps and institutional affiliations.



Copyright: © 2021 by the authors. Licensee MDPI, Basel, Switzerland. This article is an open access article distributed under the terms and conditions of the Creative Commons Attribution (CC BY) license (<https://creativecommons.org/licenses/by/4.0/>).

1. Introduction

Robert H. Anderson was a West Point graduate, born in 1835, who served as a brigadier general in the army of the Confederate States during the American civil war. In spite of pursuing combat and potential victory on the battlefield, he subsequently played an important role with the efforts for reunification after the war. A different Robert H. Anderson, a British national, has dedicated most of his time to the research of the normal and congenitally malformed heart. Based initially at the Royal Brompton Hospital, supported by the British Heart Foundation, and known to his friends and colleagues as Bob, he has enjoyed a long, ongoing, and very productive career, with 1200 manuscripts and collaborative interaction with scientists all over the world. Like his namesake, who became famous at seeking reunification, Bob has worked together with other scientists and physicians to translate concepts of anatomy and embryology into relevant clinical and surgical information. Even his “enforced retirement” in 2007 did not diminish his impetus and drive to study. He is currently working at the Institute for Genetic Medicine, Newcastle University, Newcastle upon Tyne, and at Birmingham Children’s Hospital in the United Kingdom, but also collaborates extensively with colleagues based in the United States of America.

It has been an honor and joy for us to work with him in a number of projects, all designed to improve our understanding of cardiac arrhythmias and their anatomic–functional

relationships. This current review is dedicated to his work in the field of cardiac arrhythmias, with emphasis on a particular set of sub-structures. In his early formative years, Professor Anderson spent a remarkably productive year at the University of Amsterdam, where he collaborated with pathologists and electrophysiologists, in particular with Giel Janse, Anton Becker, and Hein Wellens, with their studies at that time providing the basis for important subsequent contributions. In this review, we reappraise some of the concepts reported back in the 1970s in the light of current knowledge, mostly accumulated by himself.

2. Methods

We assessed anatomical concepts relating to the cardiac conduction system appearing since the key contributions made in the initial decade of the 20th century, analyzing them from the perspective of Robert H. Anderson, who has now been actively involved for half a century in understanding the anatomical aspects of structures such as accessory atrioventricular pathways, including the Mahaim-type fibers, connections between the atrioventricular node and the atrial myocardium, and so-called “specialized” internodal atrial tracts. To accomplish this task, we have taken as our starting point the initial concepts published in the first decade of the century [1–4], along with those subsequently reported up to 1976 [5–7], and assessing them in the light of our most recently published works.

In addition, we have taken advantage of a series of e-mails exchanged directly with Bob, aiming to unravel details not possible to discern from the published manuscripts themselves. References [5,6] are chapters from a book released in 1976 by Stenfert Kroese BV. The monograph had its genesis in a workshop on the cardiac conduction system held in the spring of 1975. It took place at the Department of Cardiology, Wilhelmina Gasthuis, Amsterdam, The Netherlands. The reference is important, since this was the home ground of one of the most outstanding electrocardiologists of the time, Dirk Dürrer, who made several important contributions to modern cardiac electrophysiology, and was the initial mentor of Robert H. Anderson. He created an amazing institute, where investigators in various disciplines cooperated in the study and treatment of cardiac disease. The book was dedicated to him by three of his outstanding pupils, Hein Wellens, KI Lie, and Michiel Janse. As we have already stated, Bob, early in his career, had spent a formative year training in the Netherlands. His special interest in the cardiac conduction system was nurtured at that point in time, thanks to the interactions with these luminaries of cardiac electrophysiology and pathology.

We will include in our reappraisal the concepts of atrioventricular nodal bypass tracts, as alleged to exist by James and Brechenmacher [8–10], the pathways described initially by Ivan Mahaim, and the controversies that still surround the presence of tracts within the atrial walls.

Concerning the technical aspects of examination of the conduction system, Bob has stated that his approach in the 1970s, and even now, was no different from that used by Tawara [1], namely the careful assessment of serial sectioned histological material. As Bob stated in one of his recent e-mails, “I have been fortunate throughout my career to have been able to work with people able to produce excellent histological material. The recent work done with Damian, who initially studied with me in London, investigating the myocardial architecture in tetralogy of Fallot, has served greatly to increase my knowledge. I also now have a much better understanding of the development of the heart. From the earliest times, however, I have always thought it was necessary to stress the differences between the species. Only now, however, am I in a position to emphasize the significant differences! The work we have done together over the past two to three years has served to bring everything together”.

3. Results

3.1. Atrioventricular Nodal Bypass Tracts

As Bob stated in 1976, the concept of nodal bypass tracts was introduced by James [8] on the basis of morphological studies carried out to provide an explanation of some abnormalities of atrioventricular conduction, which might then be distinguished electrophysiologically. He warned at that time that it was dangerous to directly extrapolate morphological findings to function. He pointed out the considerable variation to be found in the manner in which the transitional or nodal approach, cardiomyocytes, make contact with the compact node. He considered it preferable to return to the initial definition provided by Tawara [1], and to recognize the boundary between the compact node and the penetrating bundle as the point at which the atrial cardiomyocytes cease to make contact with the atrioventricular conduction axis. On this basis, the penetrating bundle can be considered to represent the final common pathway for normal atrioventricular conduction.

Using this definition, a morphological by-pass tract, without implying any functional significance, will be represented as any aggregation of atrial cardiomyocytes that make contact with the nodal-bundle axis distal to the point of origin of the penetrating bundle, in other words, inserting into the final common pathway distal to the compact atrioventricular node. Such a tract had allegedly been described by Brechenmacher and his colleagues [9,10] in a patient known to have exhibited electrophysiological abnormalities. In the experience of Bob, the last atrial cardiomyocytes to make contact with the compact node could be derived either from superficial overlay myocardium, or from the deep left side of the atrial septum. The anterior overlay cardiomyocytes were known to originate directly from the antero-inferior buttress of the atrial septum, and then to make contact with the compact node.

Bob had been unable to identify any aggregated cardiomyocytes coursing from the posteroinferior part of the atrial septum, as had allegedly been described by James. In Bob's opinion, if the variations described by James were considered to be significant to nodal function, they should be interpreted as variations in nodal structure, and hence representing intranodal pathways, rather than considering them as by-pass tracts. If such pathways are, indeed, of functional significance, which is yet to be proven, then account must also be taken of the arrangement of the inferior extensions of the compact node. Variations in these pathways self-evidently can influence the route taken to the final common pathway. In this regard, we now know that the connection between the leftward inferior extension of the compact node and the left side of the atrial septum and the mitral vestibular myocardium is particularly noteworthy. As Scherf and Cohen [11] pointed out long since, the node is an interatrial structure, and not a right atrial structure.

Now, in 2020, 54 years later, Bob and his colleagues, including ourselves, have reassessed the structure of the atrioventricular node and its atrial connections [12]. We achieved this by studying 20 human hearts, assessing serial histological sections that covered the entirety of the triangle of Koch and the cavotricuspid isthmus. We were able to determine the location of the atrioventricular conduction axis, and the connections between the specialized cardiomyocytes of the conduction axis and the adjacent working atrial cardiomyocytes. As expected, the atrioventricular node was found towards the apex of the triangle of Koch (Figure 1A), with insulation of the conduction axis by the fibrous components of the atrioventricular junction providing the criterion for distinction of the bundle of His (Figure 1B). We found marked variation in the inferior extensions of the node, the shape of the node, the presence or absence of a connecting bridge with the myocardium of the atrial septum, the presence of transitional cardiomyocytes, and in particular, the last connection between the working atrial myocardium and the conduction axis before it became the bundle of His. In the majority of datasets, the last input came from the central part of the atrial septum (Figure 2A), and was composed of working atrial cardiomyocytes. In some instances, nonetheless, it was found to arise from the left-side of the septum (Figure 2B). The observed variations in the extent of the inferior extensions, combined with the arrangement of the last connections between the atrial myocardium and

the conduction axis prior to its insulation as the bundle of His, now provide compelling evidence to support the concept for atrioventricular nodal re-entry as previously advanced by Katritsis, working with Anton Becker [13].

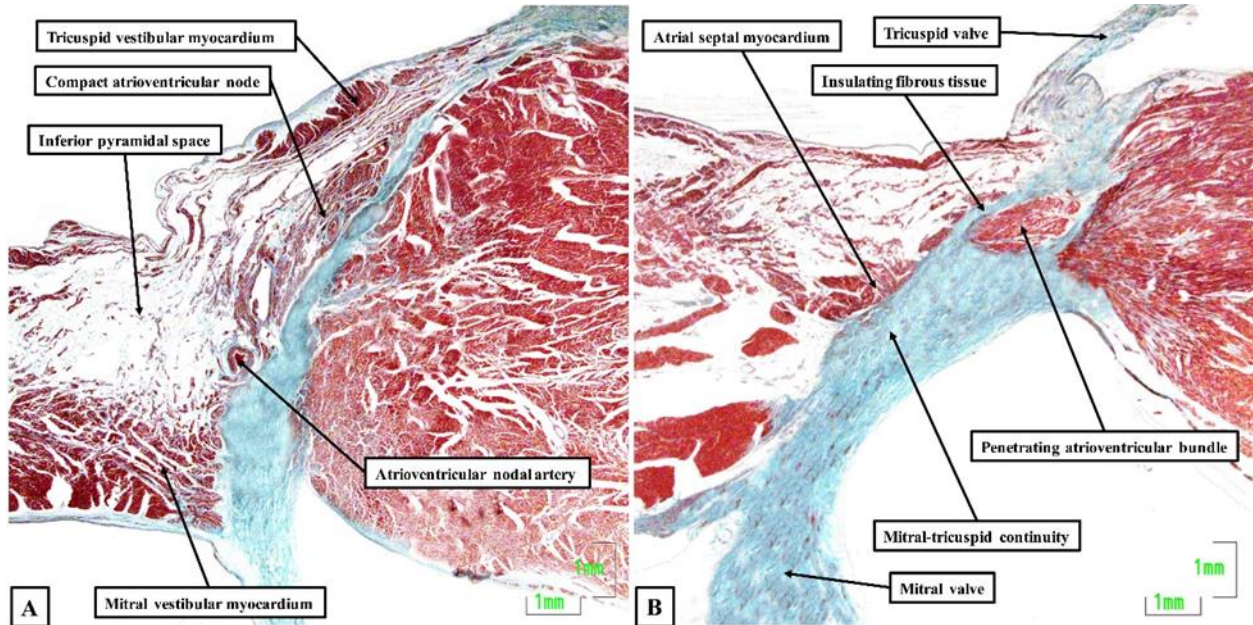


Figure 1. Atrioventricular node and penetrating bundle: The histological sections, stained using the trichrome technique, show the features of the atrioventricular node (A) and the insulation provided to produce the penetrating atrioventricular bundle (B). The sections were made using an adult human heart.

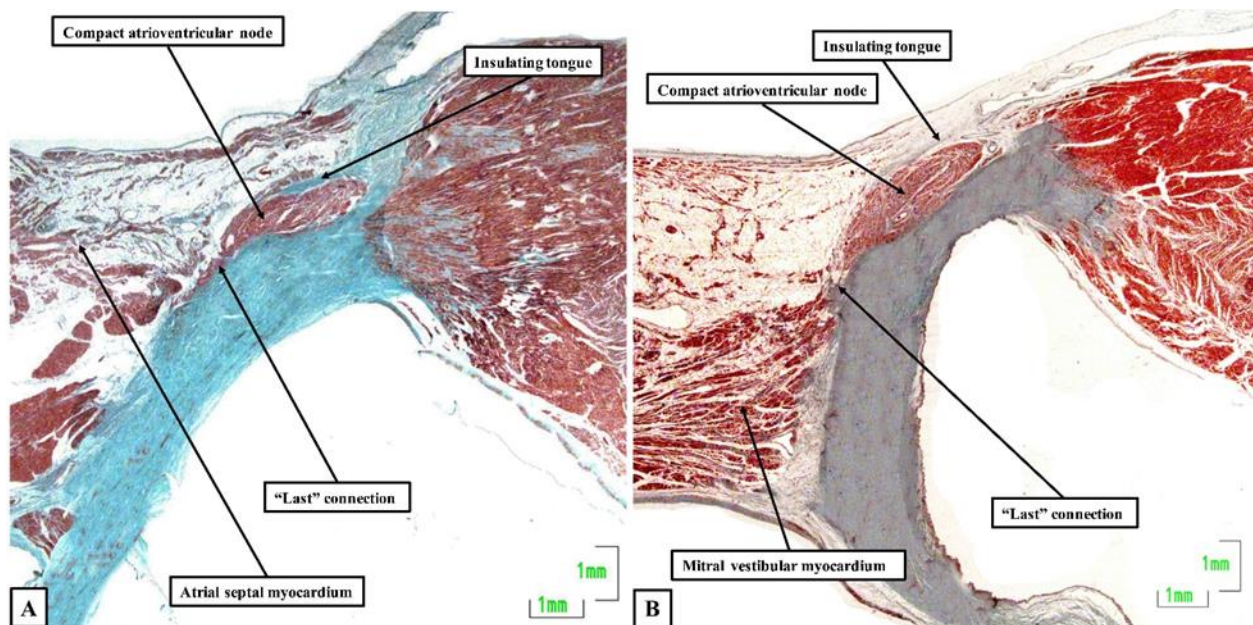


Figure 2. The compact node and the last connection: The sections, again stained using the trichrome technique, show the last connections to the atrioventricular node from the central part of the atrial septum (A) as opposed to the mitral vestibule (B). The section shown in Panel A is from the same series of sections as shown for the atrioventricular node and penetrating bundle in Figure 1. Both sections are taken from adult human hearts.

3.2. The Pathways Described by Ivan Mahaim

3.2.1. Fasciculo-Ventricular and Nodo-Ventricular Pathways

It was in the early 1940s that Ivan Mahaim, a Belgian cardiologist working in Switzerland, described the presence of “*fines hautes connexions*”, translated as delicate proximal connections, and also called paraspecific pathways, which connected the central part of the atrioventricular node and the penetrating bundle directly to the crest of the ventricular septum [14,15]. These entities were considered to be remnants of the embryonic anlagen of the conducting tissues. Indeed, such remnants are readily identifiable in infant, childhood, adolescent, and adult hearts, although in decreasing frequencies. Mahaim had concluded that these structures might serve as septal conduction pathways, providing alternative pathways to the bundle branches and their ramifications, but with a wide spectrum of variability in dimensions and locations. He attempted to demonstrate their functional role by showing experimentally that sequential cutting of these connections modified the surface electrocardiogram.

Bob, along with Janse and Becker, studied a fetal human heart in which multiple atrioventricular connections, as described by Mahaim, were shown to be present. During electrical stimulation of the atrium, however, atrioventricular conduction occurred only through the normal pathways for atrioventricular conduction [16]. In 1971, Wellens [17] reported the electrophysiologic findings in a young boy having paroxysmal tachycardia caused by an accessory pathway with decremental properties. That finding subsequently rekindled interest in the anatomic–functional relationship of the so-called Mahaim connections.

A few years thereafter, Anderson and his colleagues [5] suggested separating the pathways described by Mahaim into nodo-ventricular connections, which took their origin from the compact atrioventricular node (Figure 3A), and fasciculo-ventricular connections, which originated more distally from the atrioventricular conduction axis (Figure 3B).

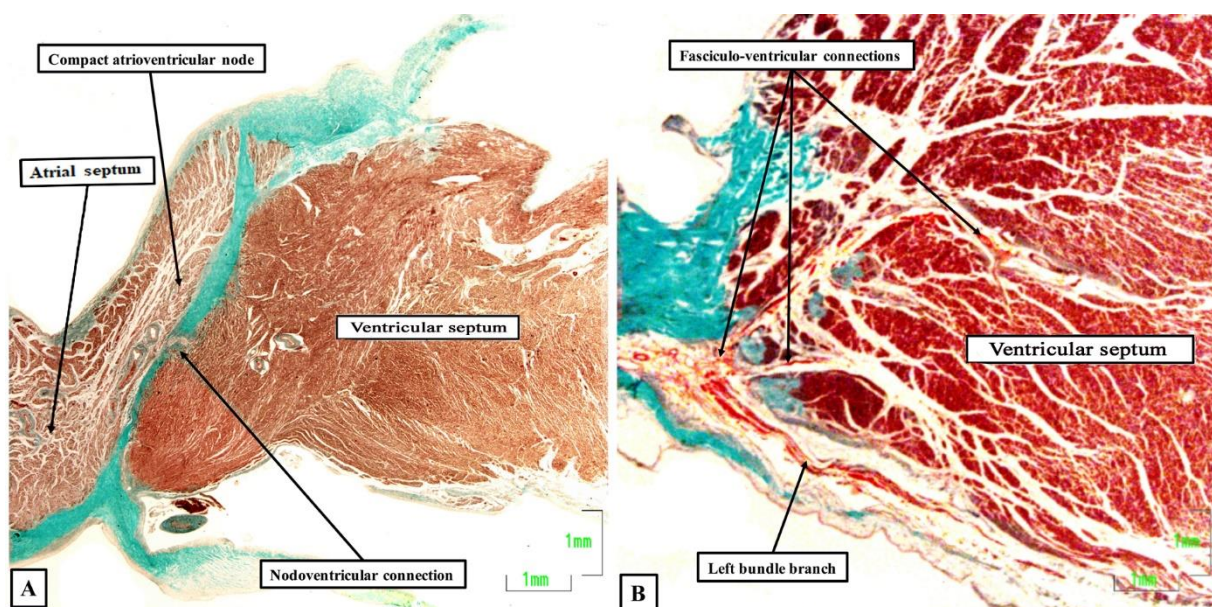


Figure 3. Nodo-ventricular and fasciculo-ventricular pathways: The sections are again stained using the trichrome technique. (A) shows a nodo-ventricular connection in an infant human heart, while (B) shows multiple fasciculo-ventricular connections in an adult human heart.

It was then Becker working with Gmeiner and colleagues, who were the first to document the anatomical existence of a functional nodo-ventricular pathway. This pathway was found in an eleven-year-old boy with a previous history of paroxysmal recurrent tachycardia, who had suffered a cardiac arrest while tobogganing. He was found in ven-

tricular fibrillation, was resuscitated, but developed a persistent vegetative state for three years, and eventually died [18]. At autopsy, Becker removed the complete atrioventricular junction, including the left and right parietal zones as well as the septal junctional zone, for serial histological examination. On examination of the sections, he found a discrete tract of specialized cardiomyocytes, which extended obliquely from the base of the compact atrioventricular node, crossed the fibrous plane of atrioventricular insulation, and inserted into the crest of the muscular ventricular septum. Such nodo-ventricular connections have subsequently been shown to be ubiquitous in the setting of Ebstein’s malformation. Thus, Bob, again working with one of us and our clinical colleagues, [19] reported the findings in six autopsied hearts from patients known to have had Ebstein’s malformation. The lesion was fully developed in four, but was of a so-called “micro-Ebstein” form in two. All hearts had been studied subsequent to serial histological sectioning of the full extent of the atrioventricular conduction axis, along with limited sectioning of the right atrioventricular junction supporting the inferior and antero-superior leaflets of the deformed tricuspid valve. In all of the hearts, overt nodo-ventricular connections were identified (Figure 4A). In two of the five, fasciculo-ventricular pathways were also present (Figure 4B).

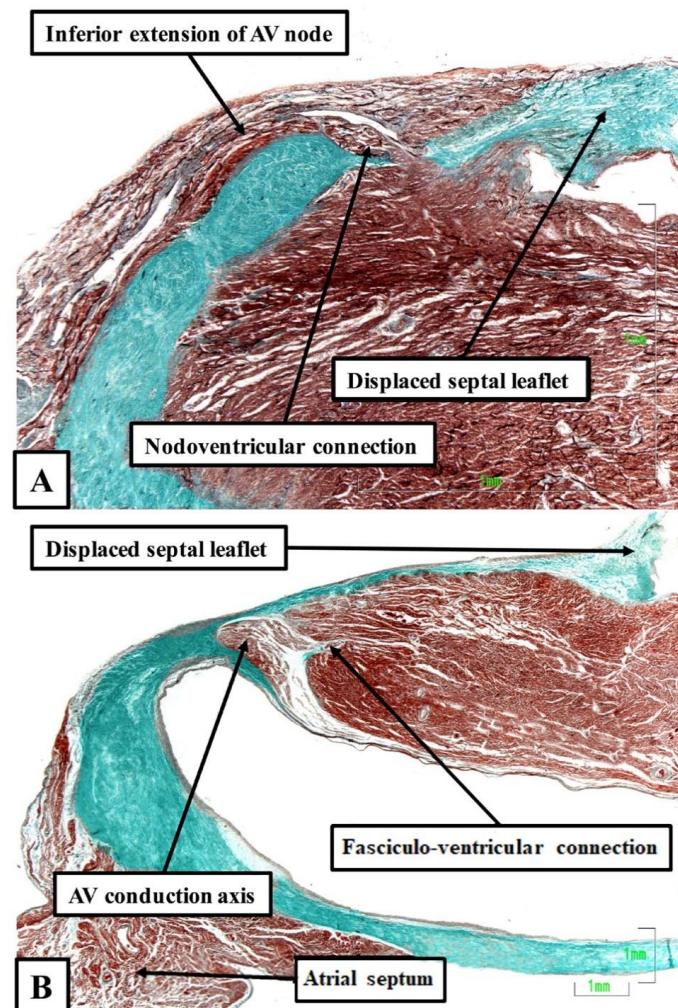


Figure 4. Nodo-ventricular and fasciculo-ventricular pathways: Both sections were taken from human hearts shown at autopsy to exhibit Ebstein’s malformation. (A) shows a direct nodoventricular connection between the inferior rightward extension of the atrioventricular (AV) node and the crest of the ventricular septum, while (B) shows a fasciculo-ventricular connection given off from the conduction axis prior to the origin of the right bundle branch. The sections were stained using the trichrome technique.

Clinical correlations: fasciculo-ventricular pathways have not been reported to play an active role in re-entrant circuits, but they may be used as bystander structures. The nodo-ventricular pathway may be part of a re-entry circuit, and have a role as the retrograde limb or as the anterograde limb, giving rise to orthodromic or antidromic tachycardias, like in the case reported by Gmeiner and colleagues [18].

3.2.2. Accessory Atrioventricular Node or Atriofascicular Pathway

Becker in 1978, working with Dürer, Hein Wellens, and Bob [20] sought to establish whether the hearts also exhibited so-called “atriofascicular tracts”. In this investigation, which was focused on elucidating the pathways present in patients who had presented with Wolff-Parkinson-White syndrome, an accessory atrioventricular node was identified that gave rise to an insulated tract of specialized cardiomyocytes. The tract pierced the insulating pathways of the atrioventricular junction, and extended into the right ventricle, thus producing a second atrioventricular conduction system located on the lateral part of the tricuspid annulus. Due to the lack of specific structure–function correlation, their finding did not serve to challenge the prevailing concept that the structure responsible for so-called Mahaim conduction was, indeed, produced by nodo-ventricular connections, as described by Mahaim himself, and endorsed by the findings of Gmeiner and associates [18]. It was not until the early 1980s that it became clear that the pathway for the majority of instances of “Mahaim conduction” was instead mediated through accessory atrioventricular nodes. We are now well aware that these nodes themselves represent remnants of so-called atrioventricular ring tissue, shown to exist in the human heart by Bob, working along with Anton Becker and the late Michael Davies. We now describe these right sided and parietal pathways as being “atriofascicular”, recognizing that their ventricular termination can be with the right bundle branch [21,22].

The atriofascicular pathways, are usually the antegrade limb of the circuit of an antidromic tachycardia, while the retrograde limb is the atrioventricular conduction axis, or a second accessory atrioventricular pathway. It may also be a bystander structure when the patient has an additional accessory pathway or dual atrioventricular pathways and atrioventricular node re-entrant tachycardia.

3.3. Specialized Tracts for Internodal Atrial Conduction

The pathways for conduction between the atrioventricular and sinus nodes [1–3], themselves newly described at the time, had been hotly debated by the end of the first decade of the 20th century. To resolve this conflict, a session of the meeting of the German Pathological Society held in 1910 at Erlangen was allocated to discuss the proposal made by Thorel that internodal conduction occurred through a specialized tract [20]. The session was attended by JG Mönckeberg, Ludwig Aschoff, Thorel himself, Walter Koch, James Mackenzie, and Thomas Lewis, among other luminaries. The key points emerging from the meeting were summarized by Aschoff and Mönckeberg [3,4]. They provided criteria for conduction tracts based on the identification of the right bundle branch, which they pointed out could be traced from section to section in histological material and was distinguishable from the adjacent myocardium on the basis of its histological appearance, and these features were insulated by a fibrous sheath (Figure 5). It was the last feature that was identified as the significant criterion for a conducting tract. All agreed that, on this basis, no such insulated tracts were to be found within the atrial walls separating the sinus and atrioventricular nodes. In 1910, therefore, the concept as advanced by Thorel was summarily dismissed. Throughout the subsequent decades of the 20th century, others made claims for the existence of the alleged pathways, but were always seemingly ignorant of the criteria proposed by Mönckeberg and Aschoff [3,4]. It was Thomas N. James, however, who subsequently brought the alleged pathways to the attention of cardiologists, such that they are currently depicted on the cover of “Heart Rhythm”. James, too, had also ignored the conclusion of the Erlangen meeting. Instead, he argued that the existence of such tracts had been proven on the basis of clinical findings, and hence his task was

simply to illustrate their location [23]. In 2001, reviewing his anatomical investigations, he stressed that his original report on internodal pathways had been based on examinations of 69 human hearts [24]. Since then, he explained that he had examined more than 1100 additional human hearts, 89 dogs, 7 sperm whales, 9 cows, 7 horses, 12 rabbits, 6 cats, and a few rats, pigs, monkeys, nutria, chipmunks, and chickens. In each heart, he had studied two blocks of myocardium, which contained, on the one hand, the sinus node and on the other hand, the atrioventricular junctional tissues. He had examined each block on the basis of serial histological sectioning. There can be no question that he was a meticulous histologist, and the leading American cardiologist investigating the conduction system of the heart. It is self-evident, nonetheless, that his technique made it impossible to examine the entirety of the atrial walls so as to identify insulated pathways paralleling the insulation provided for by the right bundle branch (Figure 6).

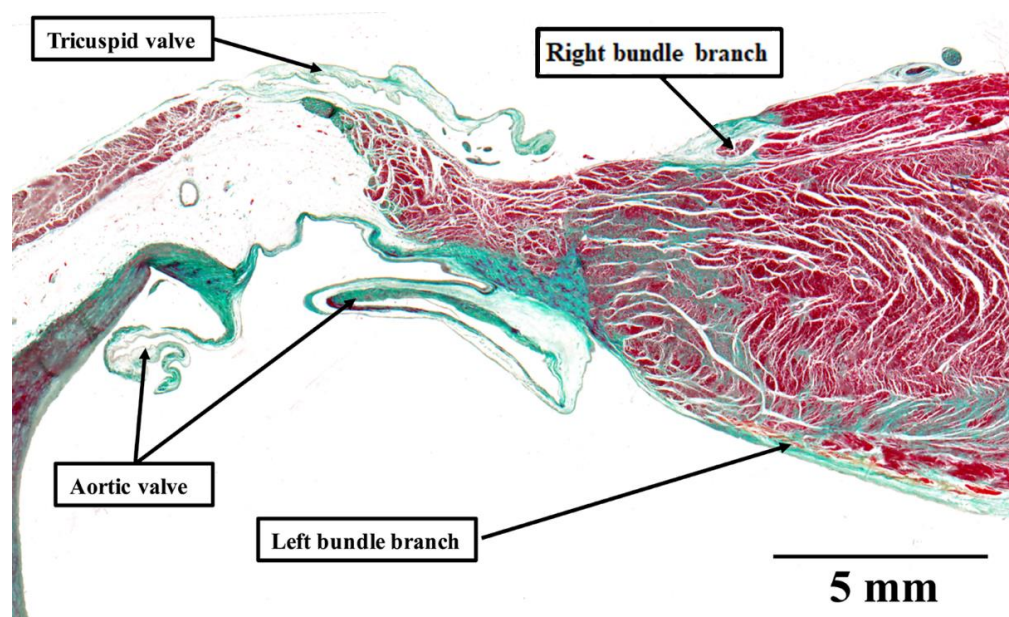


Figure 5. Mönckeberg and Aschoff’s criteria for a conducting tract: The histological section shows the crest of the ventricular septum in a human heart stained using the trichrome technique. The right bundle branch is insulated by a sheath of fibrous tissue, colored green. This makes it possible to distinguish the bundle from the adjacent myocardium, and follow the bundle in serial sections. Thus, the structure satisfies all of the criteria established by Mönckeberg and Aschoff [3,4] for recognition as a conducting tract.

His initial findings, published in 1963, furthermore, had already been challenged by the Dutch school represented by Dürrer, who had been unable to find electrophysiological evidence of such “specialized” tracts [25]. Becker and Anderson, who had examined the entirety of the atrial walls, pointed out that no anatomical evidence, when assessed on the criteria propounded in Erlangen [3,4], existed to support the presence of the tracts alleged to exist by James [23]. Janse, again working with Bob, subsequently emphasized that the walls of the right atrium were arranged around several “holes”, represented by the orifices of the caval veins, the coronary sinus, and the surrounds of the oval fossa. As they pointed out, when considering the anatomy delineated by these holes, four distinct pathways are present between the site of the sinus node and the atrioventricular junctional area [26]. These areas are rightly considered to be preferential pathways, but none of them contain “tracts” comparable to the insulated right bundle branch (Figure 5). As they emphasized, the mere presence of so-called “Purkinje” cells is not, by itself, a criterion for the existence of a tract specialized for conduction. Indeed, Spach and his colleagues [27] later showed that anisotropic conduction was more than enough to explain the preferential conduction through the atrial walls, which existed in the absence of insulated tracts.

Thomas Naum James, nonetheless, along with other anatomists, continued to ignore the definition provided by Mönckeberg and Aschoff [3,4], supporting his hypothesis for the rest of his life.

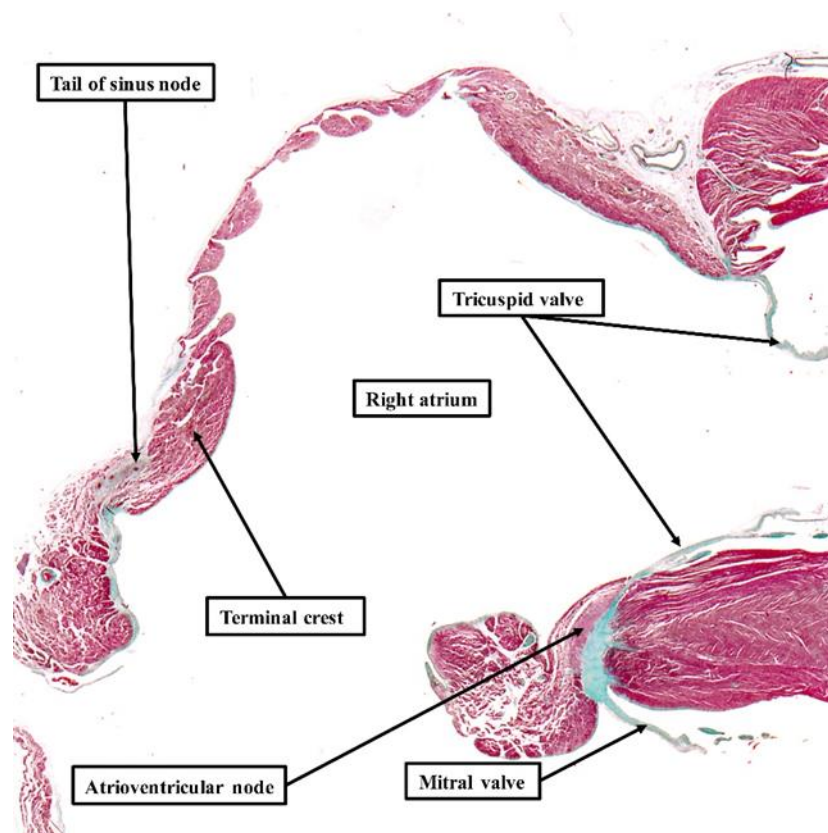


Figure 6. Absence of specialized tracts within atrial walls: The section is taken from a human of 35 weeks. It shows the entirety of the walls of the right atrium, with the section again stained using the trichrome technique. Even at the low power of magnification used to show the features of the right atrium, it is possible to recognize the tail of the sinus node and the atrioventricular node. The atrial walls, however, do not contain any insulated tracts comparable to the right bundle branch (see Figure 5). Only when assessing the entirety of the atrial myocardium in this fashion, using serial histological sections, is it justifiable to draw any conclusions regarding the presence or absence of “specialized” tracts responsible for conduction. When using the criteria established by Mönckeberg and Aschoff [3,4], which retain their validity for histological studies, examination of serial sections shows that there are no such tracts.

4. Discussion

It is noteworthy that the views of Bob Anderson with regard to structures such as the inputs and extensions of the atrioventricular node, atrio-nodal, and atrio-His connections, the so-called “specialized” internodal tracts, and the pathways responsible for Mahaim conduction, have not changed over the period of half a century. On the contrary, Bob remembers that “when proposing the arrangements, we did not really have the evidence to back up the concepts. Much of the evidence needed came from the collaborative work with Damián, who is now able to “capture” the images as seen through the microscope, and make direct measurements [19,28–30]. He combines the gross photographs of the specimens with selected photographs of the serial sections, and prepares them in powerpoint presentations, sharing them with all of us. I can then choose selected images, crop or expand them to show the salient features. In this way, Damian has now shared datasets from over 70 adult hearts, 10 plus fetal hearts, a series of infant hearts with Ebstein’s malformation and controls, and examples of canine, porcine, and murine hearts. It is the ability to analyse this material “at a distance” on the basis of my prior knowledge that has enhanced my current understanding.

It has been these spectacular and detailed datasets that have provided the much-needed evidence, particularly regarding the “atrioHisian” connections. I was dubious about these alleged pathways from the outset. And we have subsequently validated our skepticism concerning the publications of James! Our updated knowledge of development has also helped a lot”.

We are now in a position to assess the functional significance of these recent endorsements. With regard to the alleged atrioventricular nodal bypass tracts, it is certainly feasible that the last connection between the atrial cardiomyocytes and the atrioventricular node prior to its insulation as the bundle of His can provide potential pathways for the exit of proposed re-entry circuits for atrioventricular nodal reentrant tachycardia. It is likely that these last connections were previously misinterpreted as “atrio-Hisian connections” [9,10]. In reality, we now know that these connections are ubiquitous. As we showed in our collaborative study, their connection with the compact node just prior to its insulation as the bundle of His involves a minimal, if any, layer of interposing transitional cardiomyocytes. This paucity of nodal tissue can explain the absence of decremental conduction, as well as the lack of response to adenosine in the retrogradely conducting “fast” nodal pathway.

The entities were described initially by Mahaim, Bob, and his colleagues in 1975 and were separated into fasciculo-ventricular and nodo-ventricular connections [5]. This distinction still holds good. In the study revealing the connections of the atrioventricular node, we found one fasciculo-ventricular connection in the 20 hearts examined [12]. In an ongoing more extensive study, however, using datasets that contain more extensive parts of the ventricular components of the atrioventricular axis, and are as yet unpublished, we discovered fasciculo-ventricular pathways in one-third of the datasets (Figure 6). These findings are consistent with a survey of electrocardiographic screenings recently carried out in asymptomatic Japanese first- and seventh-grade children. This revealed two-thirds of 30 children with pre-excitation to have a fasciculo-ventricular pathway as the anatomic substrate [31]. Taken together with our histological findings, this raises the possibility that fasciculo-ventricular pathways may be the most common substrate for ventricular pre-excitation.

The concept that decrementally conducting accessory pathways might be related to the remnants of the atrioventricular ring, already reported in 1974, was revisited in 2009. The more detailed investigation included the reporting of the retroaortic node [32]. Although not associated with the variants of pre-excitation, Bob and his colleagues, again including one of us, proposed it to be a potential substrate for a variety of adenosine-sensitive atrial tachycardias [33].

Bob has also commented with regard to what is likely to be the very first histologically recognized atriofascicular pathway, which they had identified in 1978 [20]: “With regard to the accessory atrioventricular node, we had already discovered the atrioventricular ring tissues, and had shown that remnants could be found in all normal human hearts [34]. I had shown the presence of the “rings” in experimental animals using staining for choline esterase, again employing serial sections. Hein Wellens had studied the ECGs of all the patients, but the individual with the accessory node had multiple pathways, along with Ebstein’s malformation. The heart was huge, and it was an amazing undertaking simply to analyse the entirety of the atrioventricular junctions. We had to cut serial sections through 20 or more individual blocks, and then try to put the pieces back like a jigsaw puzzle! Becker’s histology technician was the real star!”.

If we conclude by returning to the so-called “specialized” atrial pathways, in Bob’s own words: “This topic was debated at length in 1910, and perfect definitions for insulated tracts were provided by Aschoff and Mönckeberg. Those definitions retain their validity. It is a simple fact that there are no insulated pathways extending between the sinus and atrioventricular nodes. The preferential conduction is well explained on the basis of the manner of aggregation of the individual cardiomyocytes. The claims for “specialization” on the basis of immunocytochemistry have never provided evidence of conduction ahead of that adjacent to the alleged “pathways”. With regard to Bachmann’s bundle, if you read his

original account you will find that he explains that is the alignment of the cardiomyocytes in the anterior interatrial wall that is responsible for the preferential conduction! He was well ahead of his time!!”

5. Conclusions

Thus, we are able to conclude that the concepts put forward by Bob with regard to atrioventricular nodal bypass tracts, atrioventricular nodal inputs, decrementally conducting accessory pathways, and “tracts” for internodal atrial conduction, have remained consistent along the time frame of half a century. This is very unusual, given that the addition of new technologic tools, combined with critical reappraisal by other investigators, very often allows for a new perspective on a myriad of issues. There can be no question that his concepts have passed the test of time.

Funding: This research received no external funding.

Institutional Review Board Statement: Not applicable.

Informed Consent Statement: Not applicable.

Conflicts of Interest: The authors declare no conflict of interest.

References

1. Tawara, S. *Das Reizleitungssystem Des Säugetierherzens: Eine Anatomisch Histologische Studie Über Das Atrioventrikularbündel und Die Purkinjeschen Fäden*; Gustav Fischer: Jena, Germany, 1906; pp. 135–136.
2. Keith, A.; Flack, M. The form and nature of the muscular connections between the primary divisions of the vertebrate heart. *J. Anat. Physiol.* **1907**, *41*, 172–189. [PubMed]
3. Aschoff, L. Bericht über die Untersuchungen des Herrn Dr. Tawara, die Brückenfasern betreffend, und Demonstration der zugehörigen mikroskopischen Präparate. *Zentralbl. Physiol.* **1905**, *19*, 298–301.
4. Mönckeberg, J.G. Beiträge zur normalen und pathologischen Anatomie des Herzens. *Verh. Dtsch. Pathol. Ges* **1910**, *14*, 64–71.
5. Anderson, R.H.; Becker, A.E.; Brechenmacher, C.; Davies, M.J.; Rossi, L. Ventricular pre-excitation. A proposed nomenclature for its substrates. *Eur. J. Cardiol.* **1975**, *3*, 27–36. [PubMed]
6. Anderson, R.H.; Becker, A.E.; Wenink, A.C.G.; Janse, M.J. The development of the cardiac specialized tissue. In *The Conduction System of the Heart—Structure, Function and Clinical Implications*; Wellens, H.J.J., Lie, K., Janse, M.J., Eds.; HE Stenfert Kroese B.V.: Leiden, The Netherlands, 1976; pp. 3–28.
7. Becker, A.E.; Anderson, R.H. Morphology of the human atrioventricular junctional area. In *The Conduction System of the Heart—Structure, Function and Clinical Implications*; Wellens, H.J.J., Lie, K., Janse, M.J., Eds.; HE Stenfert Kroese B.V.: Leiden, The Netherlands, 1976; pp. 263–286.
8. James, T. Morphology of the human atrioventricular node, with remarks pertinent to its electrophysiology. *Am. Heart. J.* **1961**, *62*, 756. [CrossRef]
9. Brechenmacher, C.; Laham, J.; Iris, L.; Gerbaux, A.; Lenegre, J. Histological study of abnormal conduction pathways in the Wolff-Parkinson-White syndrome and Lown-Ganong-Levine syndrome. *Arch. Mal. Coeur. Vaiss.* **1974**, *67*, 507–519.
10. Brechenmacher, C. Atrio-His bundle tracts. *Br. Heart J.* **1975**, *37*, 853–855. [CrossRef]
11. Scherf, D.; Cohen, J. *The Atrioventricular Node and Selected Cardiac Arrhythmias*; Grune & Straton: New York, NY, USA, 1964; pp. 1–466.
12. Anderson, R.H.; Sanchez-Quintana, D.; Mori, S.; Cabrera, J.A.; Back Sternick, E. Re-evaluation of the structure of the atrioventricular node and its connections with the atrium. *Europace* **2020**, *22*, 821–830. [CrossRef]
13. Katričis, D.G.; Becker, A. The circuit of atrioventricular nodal reentrant tachycardia: A proposal. *Heart Rhythm* **2007**, *4*, 1354–1360. [CrossRef]
14. Mahaim, I.; Benatt, A. Nouvelles recherches sur les connexions supérieures de la branche gauche du faisceau de His-Tawara avec cloison interventriculaire. *Cardiologia* **1938**, *1*, 61–76. [CrossRef]
15. Mahaim, I. Kent’s fibers and the A-V paraspecific conduction through the upper connections of the bundle of His-Tawara. *Am. Heart J.* **1947**, *33*, 6553. [CrossRef]
16. Anderson, R.H.; Bouton, J.; Burrow, C.T.; Smith, A. Sudden death in infancy: A study of the cardiac specialized tissue. *Br. Med. J.* **1974**, *2*, 135–139. [CrossRef] [PubMed]
17. Wellens, H.J.J. *Electrical Stimulation of the Heart in the Study and Treatment of Tachycardias*; University Park Press: Baltimore, MD, USA, 1971; pp. 97–109. [CrossRef]
18. Gmeiner, R.; Keung, C.; Hammer, I.; Becker, A.E. Tachycardia caused by an accessory nodoventricular tract: A clinico-pathologic correlation. *Eur. Heart J.* **1984**, *5*, 233–242. [CrossRef] [PubMed]

19. Sánchez-Quintana, D.; Cabrera, J.A.; Picazo-Angelin, B.; Cabrera, A.; Anderson, R.H. Histological examination of the potential arrhythmic substrates in the setting of Ebstein's malformation. *J. Anat.* **2020**, *237*, 155–165. [CrossRef]
20. Becker, A.E.; Anderson, R.H.; Durrer, D.; Wellens, H.J.J. The anatomical substrates of Wolff Parkinson White Syndrome. A clinicopathologic correlation in seven patients. *Circulation* **1978**, *57*, 870–879. [CrossRef]
21. Gillette, P.C.; Garson, A.; Cooley, D.A.; McNamara, D.G. Prolonged and decremental anterograde conduction properties in right anterior accessory connections: Wide QRS antidromic tachycardia of left bundle branch block pattern without Wolff-Parkinson-White configuration in sinus rhythm. *Am. Heart J.* **1982**, *103*, 66–74. [CrossRef]
22. Klein, G.J.; Guiraudon, G.M.; Kerr, C.R.; Sharma, A.D.; Yee, R.; Szabo, T.; Wah, J.A. "Nodoventricular" accessory pathway: Evidence for a distinct accessory atrioventricular pathway with atrioventricular node-like properties. *J. Am. Coll. Cardiol.* **1988**, *11*, 1035–1040. [CrossRef]
23. James, T.N. The connecting pathways between the sinus node and A-V node and between the right and left atrium in the human heart. *Am. Heart J.* **1963**, *66*, 498–508. [CrossRef]
24. James, T.N. The internodal pathways of the human heart. *Prog. Cardiovasc. Dis.* **2001**, *43*, 495–535. [CrossRef]
25. Dürrer, D.; van Dam, R.T.; Freud, G.E.; Janse, M.J.; Meijler, F.L.; Arzbaeher, R.C. Total excitation of the isolated human heart. *Circulation* **1970**, *61*, 899–912. [CrossRef]
26. Janse, M.J.; Anderson, R.H. Specialized internodal atrial pathways- fact or fiction? *Eur. J. Cardiol.* **1974**, *2*, 117–136.
27. Spach, M.S. Anisotropy of cardiac tissue: A major determinant of conduction? *J. Cardiovasc. Electrophysiol.* **1999**, *10*, 887–890. [CrossRef] [PubMed]
28. Anderson, R.H.; Sanchez-Quintana, D.; Mori, S.; Lokhandwala, Y.; Correa, F.S.; Wellens, H.J.J.; Back Sternick, E. Unusual variants of pre-excitation: From anatomy to ablation: Part I—Understanding the anatomy of the variants of ventricular pre-excitation. *J. Cardiovasc. Electrophysiol.* **2019**, *30*, 2170–2180. [CrossRef] [PubMed]
29. Correa, F.S.; Lokhandwala, Y.; Filho, F.C.; Sánchez-Quintana, D.; Mori, S.; Anderson, R.H.; Wellens, H.J.J.; Back Sternick, E. Unusual variants of pre-excitation; Part II—Clinical presentation, electrophysiologic characteristics, and when and how to ablate atriofascicular pathways and long and short decrementally conducting accessory pathways. *J. Cardiovasc. Electrophysiol.* **2019**, *30*, 3079–3096. [CrossRef]
30. Correa, F.S.; Lokhandwala, Y.; Filho, F.C.; Sánchez-Quintana, D.; Mori, S.; Anderson, R.H.; Wellens, H.J.J.; Back Sternick, E. Unusual variants of pre-excitation: From anatomy to ablation: Part III—Clinical presentation, electrophysiologic characteristics, when and how to ablate nodoventricular, nodofascicular, fasciculoventricular pathways, along with considerations of permanent junctional reciprocating tachycardia. *J. Cardiovasc. Electrophysiol.* **2019**, *30*, 3097–3115. [CrossRef]
31. Suzuki, T.; Nakamura, Y.; Yoshida, S.; Yoshida, Y.; Shintaku, H. Differentiating fasciculoventricular pathway from Wolff-Parkinson-White syndrome by electrocardiography. *Heart Rhythm* **2014**, *11*, 686–690. [CrossRef]
32. Yanni, J.; Boyett, M.R.; Anderson, R.H.; Dobrzynski, H. The extent of the specialized atrioventricular ring tissues. *Heart Rhythm* **2009**, *6*, 672–680. [CrossRef]
33. Bohora, S.; Lokhandwala, Y.; Back Sternick, E.; Anderson, R.H.; Wellens, H.J.J. Reappraisal and new observations on atrial tachycardia ablated from the non-coronary aortic sinus of Valsalva. *Europace* **2018**, *20*, 124–133. [CrossRef]
34. Anderson, R.H.; Davies, M.J.; Becker, A.E. Atrioventricular ring specialized tissue in the human heart. *Eur. J. Cardiol.* **1974**, *2*, 219–230.



Review

The Mesenchymal Cap of the Atrial Septum and Atrial and Atrioventricular Septation

Ray Deepe ^{1,†}, Emily Fitzgerald ^{1,†}, Renélyn Wolters ^{1,†}, Jenna Drummond ^{1,†},
Karen De Guzman ¹, Maurice J. B. van den Hoff ² and Andy Wessels ^{1,*}

¹ Department of Regenerative Medicine and Cell Biology, Medical University of South Carolina, 173 Ashley Avenue, Charleston, SC 29425, USA; deepe@musc.edu (R.D.); emilyfitz15@gmail.com (E.F.); woltersr@musc.edu (R.W.); drummonj@musc.edu (J.D.); kadeguz@g.clemson.edu (K.D.G.)

² Amsterdam UMC, Academic Medical Center, Department of Medical Biology, Meibergdreef 15, 1105AZ Amsterdam, The Netherlands; m.j.vandenhoff@amsterdamumc.nl

* Correspondence: wesselsa@musc.edu; Tel.: +1-843-792-8183

† These authors contributed equally to this work.

Received: 9 October 2020; Accepted: 2 November 2020; Published: 4 November 2020

Abstract: In this publication, dedicated to Professor Robert H. Anderson and his contributions to the field of cardiac development, anatomy, and congenital heart disease, we will review some of our earlier collaborative studies. The focus of this paper is on our work on the development of the atrioventricular mesenchymal complex, studies in which Professor Anderson has played a significant role. We will revisit a number of events relevant to atrial and atrioventricular septation and present new data on the development of the mesenchymal cap of the atrial septum, a component of the atrioventricular mesenchymal complex which, thus far, has received only moderate attention.

Keywords: atrial septum; valve; dorsal mesenchymal protrusion; cushion; mesenchymal cap

1. Introduction

The development of a fully septated four-chambered heart is a complex process that involves the contribution of multiple cell populations with distinct embryonic origins, a myriad of regulatory pathways, and a series of complicated spatiotemporal remodeling events. It is crucial to the proper function of the heart after birth that valves and septa form correctly to ensure that the oxygenated and deoxygenated blood are properly separated within the heart. This guarantees that during each cardiac cycle, the blood is propagated unidirectionally through its respective components. Separating the oxygen-rich and oxygen-depleted blood is achieved by the dividing walls between the left and right parts of the heart. The septum between the left and right atrium is the atrial septum, while the septum between the two ventricles is the ventricular septum. The unidirectional flow of blood is controlled by one-way atrioventricular (AV) valves that allow antegrade flow from atria to ventricles but prevent retrograde flow from ventricles into the atria. The process in which septa and valves are formed is commonly referred to as valvuloseptal morphogenesis. In earlier papers, we have described how the AV mesenchymal complex plays a central and critical role in this process [1–5]. The AV mesenchymal complex consists of the AV cushions, the dorsal mesenchymal protrusion (DMP), and the mesenchymal cap on the leading edge of the primary atrial septum (pAS) [4]. While the development of the AV cushions and DMP has been described in detail over the years, the mesenchymal cap has not received much attention.

2. Early Heart Development

In their studies on the initial stages of the development of the heart, Rawles [6] and Rosenquist and DeHaan [7] illustrated that one of the first steps in this process is the formation of two bilateral heart-forming fields of embryonic mesoderm during gastrulation. This population of “precardiac mesoderm” is now known as the First Heart Field (FHF). The two heart-forming fields eventually fuse at the embryonic midline to form the primary heart tube. After its formation, this heart tube consists of an outer layer of myocardial cells and an inner layer of endocardial cells. An acellular, extracellular matrix-rich substance, commonly referred to as the cardiac jelly, is located between these two cell layers. Roughly 20 years ago, a series of studies revealed the contribution of a second wave of mesodermally derived cardiac precursors to the developing heart. This population of cells is known as the Second Heart Field (SHF) [8–12]. Cell fate tracing studies have established that each heart field contributes to specific compartments of the heart. The left ventricle (LV) and both atria (LA and RA, respectively) are mainly derived from the FHF. Initial studies on the contribution of the SHF to the developing heart mainly focused on its importance for the expansion of the arterial pole, showing that the anterior SHF (aSHF) primarily contributes to the outflow tract, right ventricle, and ventricular septum [9,12,13]. Subsequent studies demonstrated that the posterior SHF (pSHF) plays a role in the development of the venous pole by contributing to the DMP and its derivatives [4,14], the pAS [15], and to the atrial myocardium (Figure 1), although the extent to which the pSHF contributes to the atrial myocardial tissues is still a matter of debate [16].

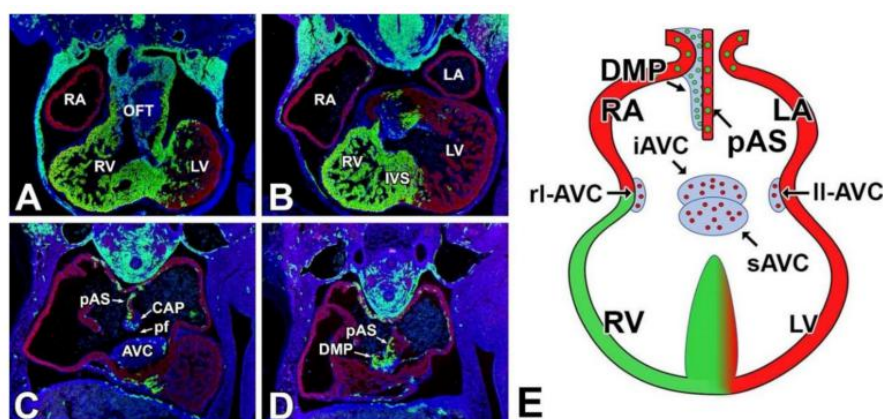


Figure 1. Contribution of First and Second Heart Field to the Developing Heart. Panels (A–D) show serial sections of an 11ED *Mef2c*-AHF-cre; *ROSA*^{mt/mG} mouse heart. All myocardial structures express cardiac Actin (red); the Second Heart Field derived tissues are labeled in green. DAPI staining (blue) was used to identify all nuclei. Panel (E) is a schematic representation of an embryonic heart around this stage. Note that the complex three-dimensional structure cannot be properly depicted. DMP—dorsal mesenchymal protrusion; iAVC—inferior atrioventricular cushion; pAS—primary atrial septum; pASD—primum atrial septal defect; pf—primary foramen; LA—left atrium; ll-AVC—left lateral atrioventricular cushion; LV—left ventricle; OFT—outflow tract; rl-AVC—right lateral atrioventricular cushions; RA—right atrium; RV—right ventricle; sAVC—superior atrioventricular cushion; VSD—ventricular septal defect; sAS—secondary atrial septum.

3. Cardiac Mesenchyme and Its Contribution to Cardiac Septation

As described above, the myocardium and endocardium are the first cardiac cell lineages to appear as the primary heart tube develops. Subsequent events in heart development, including cardiac septation, critically rely on the contribution of various populations of mesenchymal cells. Below, we have summarized the most relevant information regarding the origin of these cells as it relates to septation.

3.1. Endocardially Derived Mesenchyme

The first mesenchymal cells to appear in the developing heart derive from the endocardium. As the primary heart tube is growing and begins to loop [17,18], the extracellular matrix starts to accumulate in the cardiac jelly underneath the endocardium. This takes place in the outflow tract (OFT) and AV junction. In the OFT, this results in the formation of two endocardial ridges, whereas in the AV junction, it leads to the development of, initially, two AV cushions [19]. Subsequent to the development of these structures, the endocardium lining them goes through a process of endocardial-to-mesenchymal transformation (endMT), in which a subset of the endocardial cells differentiate within the endocardial lining and eventually, bud as endocardially derived mesenchymal cells (ENDCs) which migrate into the underlying ECM-rich space, where they eventually become valve interstitial cells (VICs) [20,21]. This process of endMT has been studied in detail for years and has been demonstrated to be controlled by multiple gene regulatory pathways including the TGFbeta, BMP, Notch, and Hippo signaling pathways [22–26]. Slightly later in development, two additional small AV cushions develop on the lateral walls of the AV canal [19,27]. These lateral AV cushions will also become populated by ENDCs as a result of endMT. It is interesting to note that very little work has been done on the question of how the spatiotemporal development of these two sets of cushions is regulated. In addition to being the source of mesenchymal cells in the developing AV cushions and OFT ridges, the endocardium also gives rise to cells that are found in the mesenchymal cap [4,28–30]. Compared to the significant body of work published on the mechanisms that control the development of the AV cushions and OFT ridges, very little is known about the mechanisms that regulate the formation of the mesenchymal cap, about the specific characteristics of the cells that comprise the mesenchymal cap, and about the role of the mesenchymal cap in atrial/atrioventricular septation. Below, we will address the mesenchymal cap in more detail.

3.2. Cardiac Neural Crest-Derived Mesenchyme

The neural crest plays a very important part in embryonic development [31]. Cells that derive from the segment of the neural crest located between the mid-otic placode and the third somite are particularly important for heart formation. The work on these so-called “cardiac neural crest-derived cells” (CNDCs) was pioneered by Dr. Margaret Kirby and colleagues. Their studies demonstrated how CNDCs contribute to the developing OFT. Moreover, they showed how perturbation of cardiac neural crest development can lead to the kind of OFT abnormalities seen in patients with congenital heart disease (CHD) [32–38]. As, to the best of our knowledge, the CNDCs do not play a discernable role in atrial septation, they will not be further discussed in the remainder of this contribution.

3.3. Epicardially Derived Mesenchyme

The epicardium is an epithelium located on the surface of the heart. The formation of the epicardium is initiated when cells from the proepicardium attach to the myocardial surface of the looping heart and spread out to form an epicardial sheet. The proepicardium is a conglomerate of mesothelially derived cells that form a cauliflower-shaped structure at the interface between liver and sinus venosus [39–43]. A subset of epicardial cells will undergo an epicardial-to-mesenchymal transformation (epiMT), leading to the formation of epicardially derived cells (EPDCs) [44]. These EPDCs migrate into the subepicardial space located between the epicardium and myocardium in a process similar to that of endMT in the AV cushions (see above). However, unlike the ENDCs, which typically do not migrate into the myocardium, EPDCs have the ability to enter the myocardial walls of the developing heart where they differentiate to interstitial fibroblasts, pericytes, coronary smooth muscle cells, and coronary endothelium [44–49]. EPDCs also play an important role in the formation of the annulus fibrosis, separating the working myocardium of atria and ventricles, and contribute significantly to the formation of leaflets of the AV valves where they eventually, just like the endocardially derived cells, turn into VICs [48,50,51]. Like CNDCs (see above), EPDCs do not seem to have an active role in atrial septation.

3.4. Second Heart Field-Derived Cells

Cell fate tracing using the SHF-specific Mef2c-AHF-cre mouse [12], as well as staining for the expression of ISL1, a transcription factor characteristically expressed in cells of the SHF [11], have convincingly demonstrated that the mesenchyme of the DMP, an important component of the atrioventricular mesenchymal complex, is derived from the pSHF [4,14]. The DMP develops between ED9.5 and ED10.5 when the pSHF cell population located between the venous pole of the heart (sinus venosus/common atrium) and the foregut expands as a result of proliferation and, using the dorsal mesocardium as a portal of entry, protrudes into the common atrium [1,3]. It is important to point out that there has been some discussion regarding the nomenclature of the structure that we call the DMP. In his studies on the anatomy of human embryos in 1880, the Swiss-born German embryologist Wilhelm His described a “fibrous/mesenchymal” structure within the heart as the “spina vestibuli” [52,53]. Given the original description by His, it is possible that the tissue that we have dubbed the DMP was indeed part of this “spina”. The histological and microscopical techniques at the end of the 19th century were obviously not as advanced as they are today and did not allow for the discrimination between the mesenchymal cells of the DMP, the AV cushions, and the mesenchymal cap. We and others have shown, using molecular and cell fate mapping techniques, that there are in fact distinct differences between the origin and fate of the DMP and the other mesenchymal structures in the atrioventricular region [14,28,54,55]. We therefore believe that the term DMP more accurately reflects the fact that this SHF-derived structure is a unique entity that plays its own, and very specific, role in atrial and AV septation. With that being said, we acknowledge that, for all intents and purposes, the term “spina vestibuli” or “vestibular spine” has been correctly used in the literature over the last 20 years to describe the DMP, for instance, in a number of studies on the relation of the DMP/vestibular spine and congenital heart defects [56,57].

4. Atrioventricular Septal Defects—The AV Cushions and the DMP

The mesenchymal tissues described above all play their own specific role in the events that lead to the development of a four-chambered heart with functional AV and OFT valves and properly formed septa. In our contribution to this Special Issue, we will focus on the remodeling events at the AV junction. A number of years ago, the mechanisms that lead to the formation of the AV septal complex gained renewed attention as a result of the emerging insight into the contribution of the DMP to the AV mesenchymal complex and the notion that the DMP could be involved in the pathogenesis of atrioventricular septal defects (AVSDs). AVSDs are serious congenital heart defects found in approximately 5% of all persons born with congenital heart disease (CHD) and a common component of genetic disorders such as Down Syndrome (DS), CHARGE Syndrome (CS), Di George Syndrome [58], and Heterotaxy Syndrome (HS) [59–61]. It is important to note that both major forms of AVSDs, i.e., partial AVSD (pAVSDs, Figure 2B) and complete AVSD (cAVSD, Figure 2C), are characterized by the presence of a primary atrial septal defect (pASD or ASD-I), also known as a “ostium primum” defect [52], and a common AV valve (cAVV). In addition, in a cAVSD, a ventricular septal defect (VSD) is also found (Figure 2).

For many years, it was generally believed that AVSDs were exclusively the result of failure of the proper development of the AV cushions. This belief led to the introduction of the term “endocardial cushion defect” [62–65]. This terminology is still widely used in the medical field as well as in websites that are designed to provide information to the general public about congenital heart disease. Several years ago, however, based on the growing insight into the anatomical, cellular, and molecular mechanisms controlling heart development, it became increasingly clear that mere failure of normal AV cushion development could not account for the complex malformations observed in patients with AVSDs [66]. In particular, abnormal AV cushion formation and/or fusion of the cushions did not seem to satisfactorily explain the pathogenesis of pASD and the presence of cAVV. Among the factors that led to the reconsideration of the role of the endocardial cushions in AVSD pathogenesis was a paper on BMP signaling in valvuloseptal morphogenesis by Jiao and colleagues [67].

In this paper, the importance of BMP4 in heart formation was investigated using a mouse model carrying a hypomorphic BMP4 allele. Analysis of the offspring revealed the presence of heart defects, including AVSDs. Given the prevailing model for the pathogenesis of these defects, it was suggested that the presence of AVSDs was likely the result of perturbation of AV cushion development. However, when we conducted a study in our lab designed to determine the role of BMP signaling in the formation of the AV mesenchymal complex, our *in situ* hybridization experiments did not show significant levels of BMP4 mRNA in the AV cushions or in the myocardium adjacent to the cushions, but instead we found significant expression of BMP4 mRNA in the mesocardial reflections of the dorsal mesocardium which flank the DMP during its expansion into the common atrium [3]. This observation strongly suggested to us that the role of BMP4 in regulating AV cushion development was likely very limited and that the observed AVSDs in the BMP4 hypomorphic model should likely be attributed to perturbation of the development of other components of the AV mesenchymal complex [3]. Combined, these observations led to the hypothesis that BMP signaling might be an important mechanism controlling the formation of the DMP [3]. To test this hypothesis, the BMP receptor BMPR1A/ALK3 was deleted from the SHF. This approach led to inhibition of the expansion of the pSHF as a result of reduced proliferation, perturbation of DMP development, and eventually resulted in pASVDs [2,3]. Using similar approaches, the importance for Hedgehog signaling in SHF and DMP development was established [1,68–70], while other studies showed the importance of Wnt signaling in the development of the DMP [71]. Combined, these results have led to a significant paradigm shift in our understanding of the pathogenesis of AVSDs. While the AV cushions can still be involved in certain aspects of AVSD pathogenesis, the fact that perturbation of SHF development, systematically leads to pASDs with cAVV (i.e., the common defects in all forms of AVSDs) shows that the SHF-derived DMP is a critical component of the AV septal complex and that perturbation of its development is associated with AVSD pathogenesis [72].

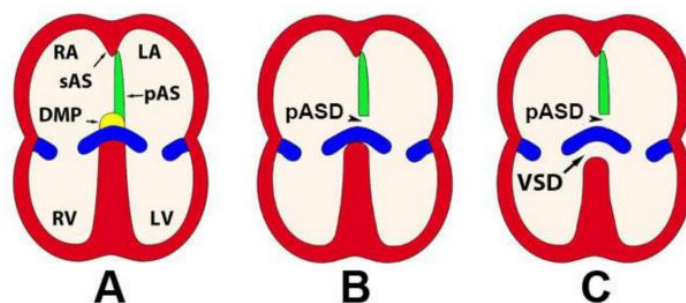


Figure 2. Atrioventricular Septal Defects (AVSDs). Panels (A–C) show cartoons of a normal heart (A), a heart with a partial AVSD (B), and a heart with a complete AVSD (C). DMP—dorsal mesenchymal protrusion; pAS—primary atrial septum; pASD—primum atrial septal defect; LA—left atrium; LV—left ventricle; RA—right atrium; RV—right ventricle; VSD—ventricular septal defect; sAS—secondary atrial septum.

5. The Mesenchymal Cap

While the AV cushions and the DMP have been studied in detail in the context of AV septation, the third component of the AV mesenchymal complex, the mesenchymal cap, has thus far by and large been ignored. In particular, whether mesenchymal cap development plays any role in the context of the pathogenesis of congenital malformations involving the atrial septum and/or the AV junctional complex has not received any serious attention. In fact, the mesenchymal cap is typically only mentioned as functioning as the “glue” that allows the descending primary atrial septum to attach to the AV cushions in the process in which the primary foramen is closed (see below). As we have previously shown [14], the mesenchymal cap and the mesenchyme of the DMP are in continuity with each other. This is also clearly demonstrated in Figure 3. Taking the above into consideration, and given the fact that there are a number of papers that suggest that the mesenchymal cap seems to be abnormal in appearance

in the mouse models studied, we have started to develop an interest in investigating the role of the mesenchymal cap in atrial septation. This is done in an attempt to determine whether, and if so how, the cap might play a role in the pathogenesis of defects involving the AV mesenchymal complex. The information on the developing cap in this contribution is not meant to give a comprehensive description, but rather provide a framework for upcoming studies. We will restrict ourselves to a descriptive narrative of some of the features of the cap as they may be relevant in the context of future studies of atrial septation.

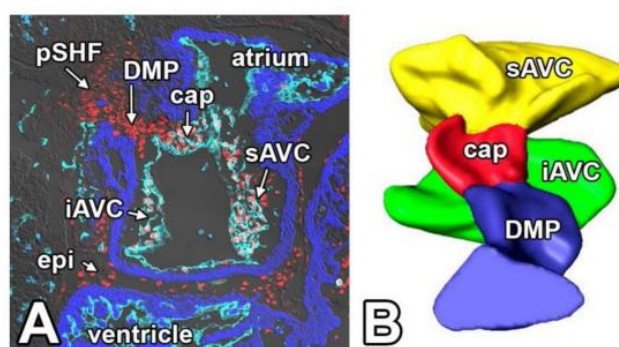


Figure 3. The spatial relationship of the components of the Atrioventricular Mesenchymal Complex at ED11.5. Panel (A) shows a sagittal section of an 11.5ED *Nfatc1-cre; ROSA^{mT/mG}* mouse heart. The endocardial/endocardially derived cells are shown in light turquoise, the myocardial tissues in dark blue, and the expression of the transcription factor SOX9 in red. The image clearly shows how the mesenchyme of the SHF-derived DMP is contiguous with the mesenchymal cap and the inferior AV cushion. In panel (B), this situation is schematically depicted. This reconstruction was made in 2007 before we had established that the DMP was derived from the SHF. cap—mesenchymal cap; DMP—dorsal mesenchymal protrusion; epi—epicardium; iAVC—inferior atrioventricular cushion; sAVC—superior atrioventricular cushion; pSHF—posterior second heart field.

6. Atrial Septation

Atrial septation is the process in which the embryonic common atrium becomes physically and functionally divided into a left and right atrium. In this process, a number of different tissues are involved, and several remodeling events take place at the same time. As a result, any description of the complex spatiotemporal process of septation is inherently an oversimplification. In this paper, we will focus on the development of the atrial septum as it is observed in the developing heart of the mouse. It is important to point out that this process in mice is very similar to that seen in humans [28]. Atrial septation (Figures 4 and 5) starts with the formation of the primary atrial septum (pAS—or septum primum). In the mouse, the pAS emerges from the roof of the common atrium between embryonic day 9.5 (ED9.5) (Figure 4A,A') and ED 10.5 (Figure 4B,B'), in the human at around 4–5 weeks of development [28]. The accumulation of ECM material on the midline of the atrial roof indicates the initial stages of formation of the mesenchymal cap. As the pAS starts to grow, the mesenchymal cap becomes clearly visible on its leading edge. The pAS then subsequently grows down (in a posterior-to-anterior direction) as a myocardial sheath from the atrial roof toward the midline of the common AV canal where the two major AV cushions are located (Figure 4C,C',D,D' and Figure 5). Fusion of the two major AV cushions results in the separation of the common AV canal into the left AV orifice (in which the mitral valve will develop) and the right AV orifice (in which the tricuspid valve will develop) [19]. The open window between left and right atrium, situated in between the cap on the leading edge and the cushions, is known as the primary (inter) atrial foramen (or foramen primum), which allows for free communication between the left and right atrium (Figure 5A). Fusion of the mesenchymal cap with the (fused) AV cushions will eventually lead to the closure of the primary atrial foramen (Figure 4E,E'). The merging of the cap and the AV cushions results in the formation of a central mass of endocardially derived mesenchyme in which the derivatives of the individual

components, at least based on our current knowledge, cannot be distinguished anymore. As the primary foramen is closing, fenestrations start to appear in the (myocardial) upper part of the pAS (Figure 5B). These fenestrations eventually coalesce and form the secondary interatrial foramen (or foramen secundum) [28,52,73]. At this point, the communication between left and right atrium occurs through the secondary foramen. During this process, the secondary atrial septum (sAS or septum secundum) develops within the roof of the right atrium. As this septum (which develops as a thick myocardial ridge) grows into the right atrium, it will start to cover the secondary foramen (Figure 5C,D) without physically fusing with the (lower) part of the primary septum to facilitate the embryonic blood circulation (i.e., before the pulmonary circulation becomes established after birth). After birth, the two septa will typically fuse, a process which has been described to take place in mice around 1–3 months after birth [74]. This fusion also take place in humans. However, in roughly one-third of the human population, the two septa will not fuse, leading to a condition known as patent foramen ovale (PFO), a condition which is sometimes linked to stroke. Failure of the sAS to completely cover the secondary interatrial foramen can lead to a more serious secondary atrial septal defect (sASD or ASD-II), also known as “septum secundum” defect.

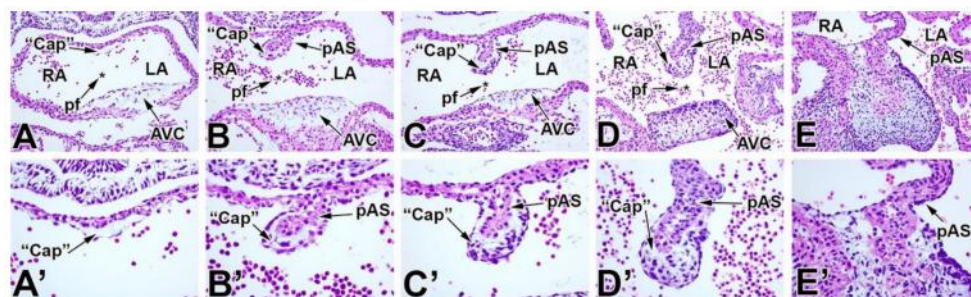


Figure 4. The development of the primary atrial septum and its associated mesenchymal cap in the mouse. The primary atrial septum (pAS) emerges between ED9.5 (A,A') and ED10.5 (B,B'). A virtual acellular cap (Cap) can be observed at ED9.5 (A,A'). As the pAS continues to grow between ED11.5 (C,C') and ED12.5 (D,D'), the mesenchymal cap also increases in size and the number of mesenchymal cells within the mesenchymal cap is increasing accordingly. At ED 13.5 (E,E') the Cap has fused with the other mesenchymal tissues. FO—foramen ovale; IVS—interventricular septum; LA—left atrium; pAS—primary atrial septum; RA—right atrium; RV—right ventricle.

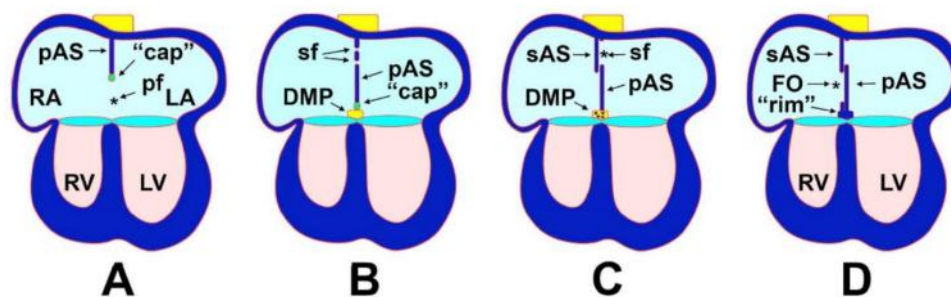


Figure 5. Atrial septation. These simplified diagrams show the critical stages in atrial septation. A detailed explanation is provided in the text. The yellow box in the back of the heart represents the posterior Second Heart Field giving rise to the DMP which in turn develops into the base of the atrial septal complex and becomes muscularized to form the muscular rim (B–D). The asterisk in (A) marks the primary foramen; the asterisk in (C) marks the secondary foramen. cap—mesenchymal cap; DMP—dorsal mesenchymal protrusion; FO—foramen ovale; IVS—interventricular septum; LA—left atrium; LV—left ventricle; pAS—primary atrial septum; pf—primary foramen; RA—right atrium; RV—right ventricle; rim—myocardial rim at base of atrial septum; sAS—secondary atrial septum; sf—secondary foramen (from: Burns et al., *J. Cardiovasc. Dev. Dis.* 2016) [72].

7. Development of the Mesenchymal Cap and Primary Atrial Septum

The embryological origins of tissues found in the mouse are nowadays typically studied using cre-lox technology with mouse models that express cre-recombinase under the regulation of tissue-specific promoters. To determine the origin of the tissues of the pASD and mesenchymal cap, we used the Tie2-cre and Nfatc-cre mice (each allowing tracing of the fate of endocardial cells) (Figure 6), and the Mef2c-AHF-cre mouse (to determine the fate of SHF-derived cells). These cre-models were used in combination with the ROSA26^{mT/mG} reporter mouse, in which cre-mediated events lead to the expression of green fluorescent protein (EGFP) (Figures 1, 3 and 6). The results of this study show that the endocardial lining of the cap, as well as the mesenchymal cells within the cap, express EGFP in the Tie2-cre, ROSA26^{mT/mG} and Nfatc-cre, and ROSA26^{mT/mG} mice, indicating that the cap mesenchyme is endocardially derived [5,55] (Figure 6A,B). Furthermore, Mef2c-AHF-cre and ROSA26^{mT/mG} lineage tracing shows that the majority of these cells do not express EGFP, indicating that they are not SHF-derived. It needs to be noted that, based on the presence of some scattered EGFP positive cells, it cannot be excluded that some SHF-derived cells find their way into the mesenchymal cap. Given the fact that the mesenchyme of the DMP and that of the cap are contiguous, this is not too difficult to imagine. The Mef2c-AHF-cre and ROSA26^{mT/mG} lineage tracing experiments also show that, at least part of, the myocardial component of the pAS is derived from the pSHF (Figure 6C). As previously reported, the development of the pAS is intrinsically related to the development of the DMP [14,28,30,70], a structure which, itself, is derived from the pSHF. Taking this into consideration and assuming that, as is the case for the development of the AV cushions, the development of the mesenchymal cap is (at least partly) regulated by myocardially expressed genes, a complex partly pSHF-dependent mechanism for the regulation of the development of the mesenchymal cap should be considered.

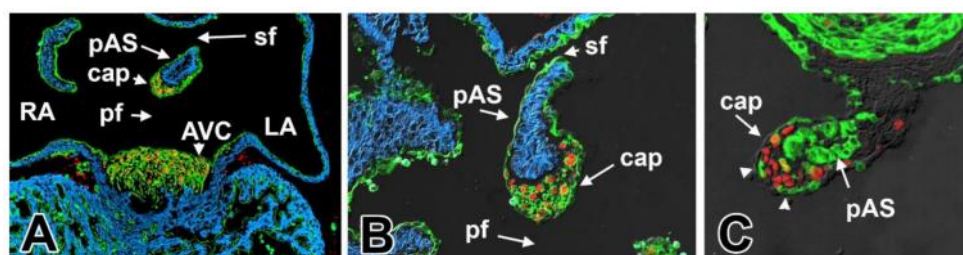


Figure 6. Tissue origin of the mesenchymal cap and primary atrial septum. This figure shows sections of Tie2-cre and ROSA26^{mT/mG} (A,B) and Mef2c-AHF-cre and ROSA26^{mT/mG} (C) hearts at 11.5ED. Cre-induced expression of GFP is shown in green (A–C), expression of cardiac myosin is visualized in blue (A,B), and expression of the transcription factor SOX9 is shown in red (A–C). AVC—atrioventricular cushion; cap—mesenchymal cap; LA—left atrium; pAS—primary atrial septum; pf—primary foramen; RA—right atrium; sf—secondary foramen.

8. Regulatory Mechanisms Associated with the Development of the Mesenchymal Cap

Insight into the molecular mechanisms involved in the regulation of the development of the various mesenchymal tissues at the AV junction, such as the AV cushions, the DMP, and the epicardium, has significantly evolved over the last 20 years. In particular, the complex regulatory networks that govern the development of the AV cushions have received much attention. It is well established that members of the TGFbeta superfamily of growth factors play a major role in endMT in the cushions [24,75–78]. The importance of the extracellular matrix (ECM) [79–83] is also well-established, as is the significance of various transcription factors [25,84–87]. One of the advantages of the study of AV cushion development is that the tissues involved (i.e., AV junctional myocardium and the associated developing cushion material) are relatively easy to isolate and that the cellular behavior of these tissues can be experimentally manipulated using well-established in vitro assays [88–90]. Given its size and location, this is unfortunately not the case for this mesenchymal cap. As a result, we rely, at least at

this point, mainly on identifying which genes and pathways are associated with the developing cap. With this knowledge, we aim to develop an understanding of how its growth in normal development is regulated and how it might be affected in pathological conditions.

8.1. Growth Factors and the Development of the Mesenchymal Cap—TGFbeta and BMP Signaling

To determine whether growth factor-mediated endMT mechanisms, which have been found to be important in the AV cushions, may also play a role in controlling endMT in the mesenchymal cap, we started by surveying the literature. Given the fact that the mesenchymal cap has received very little recognition as a separate entity and is often (irrespective of what it would have been called) not identified as such, it was not surprising that we were not able to find published papers that specifically focus on the role of growth factor signaling, or any other regulatory mechanisms for that matter, involved in cap development. What we did find, and share in this paper, comes from looking for information in the related literature. In 2002, Gaussin and colleagues published a paper on the role of the BMP receptor ALK3/BMPRI1A in heart development [91]. In this paper, images of 10.5–11.5ED mouse hearts are shown that are stained for the presence of multiple genes of interest, including TGFbeta2 and BMP2. While the resolution of these images is limited, the respective panels indicate that both these growth factors, which are also expressed in the AV junctional myocardium, are expressed in the pAS, suggesting that they may be involved in the regulation of endMT in the mesenchymal cap. In a paper on the role of TGFbeta2 in heart development, Bartram and colleagues report on the phenotype of the TGFbeta2 knock-out mouse [92]. They describe how the TGFbeta2 knockout mouse develops a spectrum of different heart defects. In all but one of the 24 inspected mutant mice, the atrial septum had developed properly. In one specimen, however, the pAS had not fused with the AV cushion tissues (which had not developed properly either) but a mesenchymal cap could be seen on its leading edge. In a paper from 2006, Jiao and colleagues investigated the role of TGFbetaR2 in the endocardium by specifically deleting this receptor using the Tie2-cre mouse. While not specifically commenting on the mesenchymal cap, the data presented suggest that deleting this receptor from the endocardium does not have a major impact (if at all) on the initial development of the mesenchymal cap. Revisiting a series of in situ hybridization experiments which we previously published in our 2013 paper on the role of BMP signaling in the pSHF [3], we noted that at ED9.5, BMP2 is expressed in the myocardium adjacent to the developing cap at a stage in which the pAS proper still has to emerge (Figure 7). Following up on the above, and to determine the possible role of TGFbeta and BMP signaling in the development of the cap, we stained for the presence of pSmad2 (indicative for active TGFbeta signaling) and pSmad1,5,8 (indicative for active BMP signaling) (Figure 8). This experiment demonstrated the presence of both sets of signaling intermediates. Combined, these data strongly suggest that TGFbeta and BMP signaling both play a role in the formation of the mesenchymal cap.

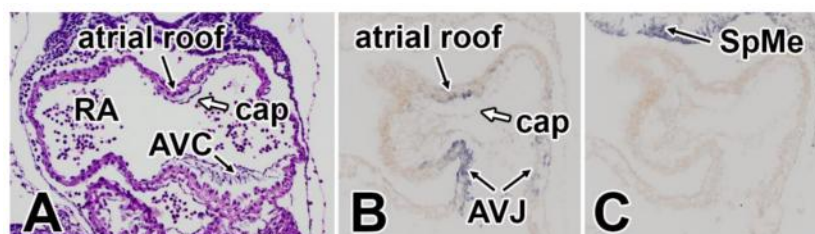


Figure 7. Expression of BMP2 and BMP4. Panel (A) shows a H/E staining of a heart at ED9.5. Panel (B) shows the expression of BMP2 mRNA in the AV junction and in the myocardial roof of the common atrium adjacent to the developing cap indicated that this growth factor might be involved in the regulation of cap development. Panel (C) shows the expression of BMP4, demonstrating the absence of this BMP isoform in AV junction and atrial roof. AVC—atrioventricular cushion; AVJ—atrioventricular junction; cap—mesenchymal cap; RA—right atrium; SpMe—splanchnic mesoderm.

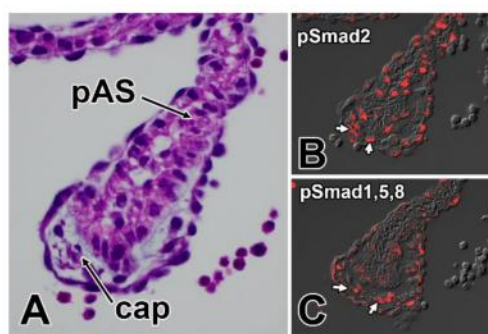


Figure 8. Presence of pSmad2 and pSmad1,5,8 in the mesenchymal cap indicates active signaling through the TGFbeta and BMP pathways. Panel (A) shows an H/E staining of the primary atrial septum and mesenchymal cap at ED11.5. The mesenchyme of the cap at this stage stains for pSmad2 (B) and pSmad1,5,8 (C) indicating active TGFbeta and BMP signaling. cap—mesenchymal cap; pAS—primary atrial septum.

8.2. Extracellular Matrix and the Mesenchymal Cap—Versican, Link Protein, and Hyaluronan

It is well-established that the ECM plays a significant role in the development of the AV cushions [93,94]. Among the ECM components identified as being critically important in this process are versican (CSPG2) [82,83,95], Cartilage Link Protein 1 (CRTL1 or HAPLN1) [83], and Hyaluronan (HA) [79–81]. In particular, CSPG2 and HA (synthesized by Hyaluron synthase 2, HAS2) have been described to be involved in the early stages of cushion formation. While the spatiotemporal expression of these genes in the developing AV cushions is well-documented [83,95], with the exception of CSPG2 [96], little is known about the expression of these genes in the mesenchymal cap. To obtain a better insight into the expression of these ECM members in the developing cap, we stained immunofluorescently and found that CRTL1, CSPG2, and HA (not shown) are expressed in a pattern similar to what has been described in the AV cushions (Figure 9). Whether, and if so how, the development of the cap is affected in any of the knockout models of these ECM components has not been investigated.

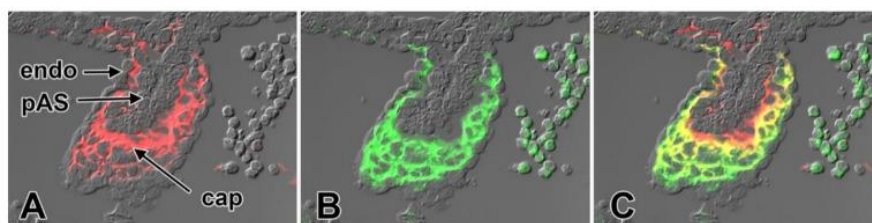


Figure 9. Expression of versican and cartilage link protein 1 in the cap. Immunofluorescent staining for cartilage link protein (CRTL1/HAPLN1) (A) and versican (CSPG2) (B) show that these ECM proteins are expressed in the mesenchyme of the cap but not in the endocardial lining or in the myocardial part of the pAS. In panel (C), the images of A and B are merged. Endo—endocardium; pAS—primary atrial septum.

8.3. Transcription Factors and the Development of the Primary Atrial Septum and the Mesenchymal Cap

Atrial septal defects (ASDs) are relatively common congenital heart malformations, observed in approximately 10% of all patients born with congenital heart disease (CHD). An increasing number of genetic mutations have been identified as being associated with these defects. However, not much is known about the specific mechanisms that lead to ASDs. Among the genes found to be associated with ASDs are sarcomeric cardiac alpha-myosin heavy chain protein (MYH6 [97]) and a growing number of transcription factors, including TBX5 [70,98,99], TBX20 [100], SOX9 [101], GATA4 [102–105], GATA6 [106], and NKX2.5 [102,103]. Additionally, gene deletions in a number of other genes in mice, including members of the Forkhead box transcription factors (FOXF1 and FOXF2) [15] and SOX9 [84,107,108] have been reported to cause ASDs in knockout mouse models. It is important to

mention that in humans, mutations in these genes typically lead to sASD (or ASD-II) [98,109,110]. Interestingly, the septal defects seen in mouse models that carry mutations for these genes are often pASDs [70,84,107,108] or not well-defined [111]. This suggests that there may be common components in the pathogenic mechanisms leading to the respective types of ASDs. In an effort to obtain a better insight into how some of these transcription factors might be involved in ASD pathogenesis, we decided to begin with documenting the expression patterns of these candidate genes in pAS and the mesenchymal cap. Some information on the expression of these transcription factors in the atrial septal complex is available in the literature. For instance, the expression of TBX5 in the pAS is well-documented [70,99], as is the expression of some other transcription factors such as NKX2.5 and GATA4 [112]. However, detailed information on the expression of these genes as it relates to the mesenchymal cap is still by and large lacking. To establish how the “ASD-candidate genes” (as well as a few other genes involved in heart development) are expressed in the pAS and the mesenchymal cap, we conducted a series of immunofluorescent studies on mouse embryos at 9.5–11.5ED. We do not claim that the data presented in Figures 10 and 11 are all novel or provide a comprehensive picture of all there is to know about transcription factor expression and pAS/cap development. In future papers, we will build on these data as we explore the roles of selected genes in the pathogenesis of atrial/atrioventricular septal defects, specifically as it relates to the mesenchymal cap. Below, we will describe our findings as they relate to the mesenchymal cap at 11.5ED.

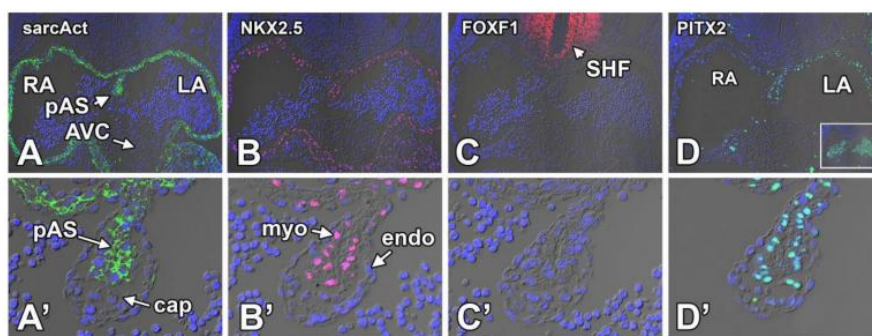


Figure 10. Expression of sarcomeric actin (A,A'), NKX2.5 (B,B'), FOXF1 (C,C'), and PITX2 (D,D') in the primary atrial septum and mesenchymal cap at ED11.5. Specifics regarding the observed expression patterns are discussed in the body of the text. AVC—atrioventricular cushion; cap—mesenchymal cap; LA—left atrium; pAS—primary atrial septum; RA—right atrium; myo—myocardial part of the pAS; endo—endocardium.

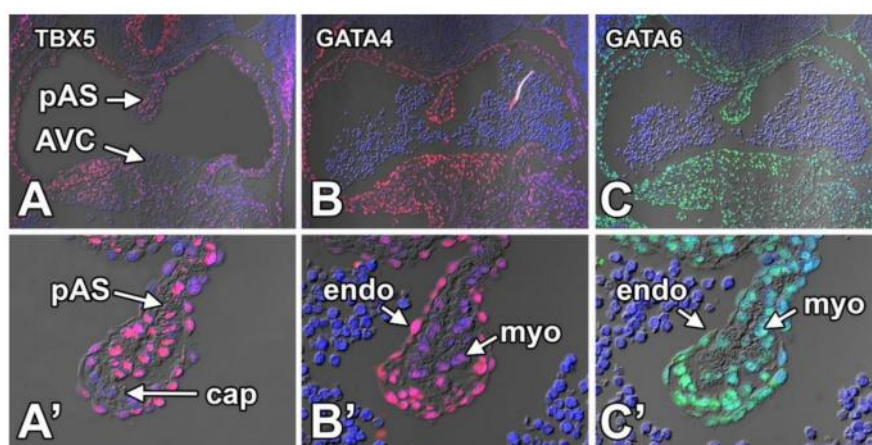


Figure 11. Expression of TBX5 (A,A'), GATA4 (B,B'), and GATA6 (C,C') in the primary atrial septum and mesenchymal cap at ED11.5. Specifics regarding the observed expression patterns are discussed in the body of the text. AVC—atrioventricular cushion; cap—mesenchymal cap; LA—left atrium; pAS—primary atrial septum; RA—right atrium; myo—myocardial part of the pAS; endo—endocardium.

8.3.1. Sarcomeric Actin

The staining shown in Figure 10A,A' is shown as a reference to demonstrate the delineation between the myocardial component of the pAS and the non-myocardial mesenchymal cap and endocardial lining.

8.3.2. NKX2.5

The association between mutations in NKX2.5 and congenital heart disease has been known for over 20 years [113,114]. Mutations in NKX2.5 are linked to sASD, Tetralogy of Fallot (TOF), and conduction abnormalities. Staining performed on ED11.5 mouse hearts shows that NKX2.5 is expressed in virtually all cardiomyocytes, but not in the mesenchyme of the AV cushions, cap, or DMP (Figure 10B,B'). As described in a paper we published in 2007, when the mesenchyme of the DMP undergoes a myocardial differentiation, eventually forming the inferior muscular rim of the atrial septum, the SHF-derived cells from the DMP start to express NKX2.5 [115]. Note that NKX2.5 is not expressed in the pSHF at this stage.

8.3.3. FOXF1

Forkhead box transcription factors have been implicated in the regulation of AV septation by interacting with TBX5 and the Hedgehog signaling pathway [15]. Compound haploinsufficiency for FOXF1a and FOXF2, as well as endothelial-specific knockouts for FOXF1, develop AVSDs [15,116]. Immunostaining for FOXF1 at ED11.5 showed that while FOXF1 is expressed in the SHF (Figure 10C), it is not detected in any myocardial structures, the endocardium, or the mesenchymal cap (Figure 10C,C'). Interestingly, the size of the mesenchymal cap in FOXF1A/FOXF2 compound knockout mice was found to be enlarged when compared to control specimens.

8.3.4. PITX2

The homeobox gene PITX2c plays a crucial role in heart development and septation. In mice that lack PITX2c, the normal left/right laterality patterning is disturbed. PITX2c knockout mice develop right atrial isomerism (RAI), a condition in which the left side of the heart develops right-sided characteristics [117]. An AVSD is typically part of the spectrum of cardiac defects observed in mice and humans with RAI. Immunolabeling with an antibody for PITX2 shows expression of PITX2 in the left atrium and in the myocardium of the pAS. PITX2 is not expressed in the mesenchymal cap or the pSHF.

8.3.5. TBX5

Mutations in the T-box transcription factor TBX5 cause Holt–Oram Syndrome (HOS) [98,118], a syndrome characterized by multiple developmental abnormalities. Cardiac defects found in patients with HOS include VSDs, pASDs, and sASDs [119]. In our expression study, focusing on the tissues involved in atrial septation, we found TBX5, as previously reported, predominantly expressed in the pSHF, the atrial myocardium, and the myocardial pAS (Figure 11A,A'). While the vast majority of the mesenchymal cells in the cap do not express TBX5, a few isolated TBX5-positive cells are occasionally observed. TBX5-positive cells are also detected in the endocardial lining of the pAS and mesenchymal cap. As the pSHF also expresses TBX5 and, as shown in Figure 3, the pSHF-derived DMP and the mesenchymal cap are contiguous, it is possible that TBX5 positive cells in the cap are of a pSHF origin.

8.3.6. GATA4

Patients with mutations in GATA4 can develop a number of different congenital heart defects including VSDs and sASDs [105]. GATA4 is strongly expressed throughout the mesenchyme of the cap (Figure 11B,B') and AV cushions with weaker staining being observed in the myocardium of the pAS and other myocardial structures.

8.3.7. GATA6

The staining observed with the antibody against GATA6 shows very strong expression in the mesenchyme of the cap and AVC. Strong expression is also observed in the myocardium of the pAS and other myocardial structures (Figure 11C,C'). Expression is also observed in the endocardium, but the staining is slightly less intense suggesting a lower level of expression.

8.3.8. SOX9

The significance of the High Mobility Group (HMG) transcription factor SOX9 (SRY-type box 9) in heart development is well-documented. SOX9 is found in the AV cushion mesenchyme where it regulates endMT and the proliferation of the endocardially derived mesenchyme [84,107,108]. Mice in which SOX9 is knocked out develop pASDs [84,107]. Staining for SOX9 shows strong expression in the pSHF and the cap mesenchyme. SOX9 is also expressed in the AV cushions and DMP (not shown in this figure) (Figure 12A,A'). SOX9 is also expressed in epicardial cells at the AV junction and epicardial cells scattered elsewhere on the myocardial surface. No SOX9 expression is seen in the myocardium of the pAS or in any other myocardial structures in the atrium. SOX9 is also not seen in the endocardium.

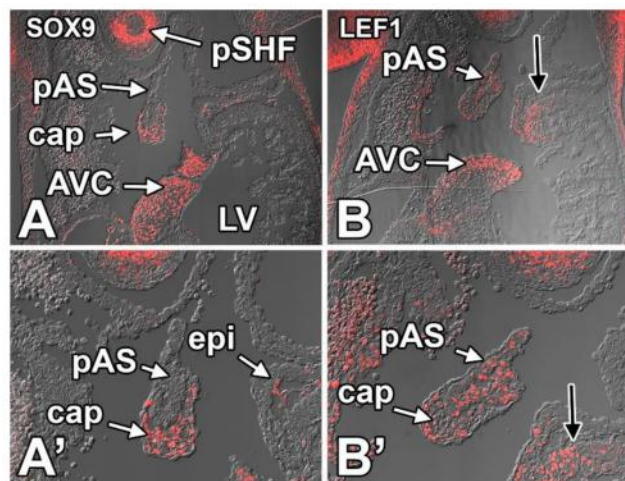


Figure 12. Expression of SOX9 (A,A') and LEF1 (B,B') in the primary atrial septum and mesenchymal cap at ED11.5. Specifics regarding the observed expression patterns are discussed in the body of the text. AVC—atrioventricular cushion; cap—mesenchymal cap; LA—left atrium; pAS—primary atrial septum; pSHF—posterior second heart field; LV—left ventricle; epi—epicardium.

8.3.9. LEF1

Lymphoid enhancer binding factor (LEF1) is a downstream target of WNT/beta-catenin signaling and its expression in cells indicates activation of this signaling pathway. LEF1 expression was observed, albeit scattered, in the pSHF, the pAS, and the mesenchymal cap, suggesting that WNT/beta-catenin signaling is playing a role in the development of all these structures. LEF1 expression is also observed in the myocardial “shoulders” of the left and right ventricles (black arrows) (Figure 12B,B').

8.4. Conclusions

The pAS and the associated mesenchymal cap express a variety of genes that are known to be expressed and involved in the development of other components of the atrioventricular septal complex. Whether the development of the cap is regulated in ways similar to that described for the AV cushions and the DMP remains to be elucidated. Retrospective studies (where possible) on the consequences of knockout models for candidate genes here described and other genes of interest as well as new studies focusing on the development of the mesenchymal cap may provide new insights into whether perturbation of cap formation may be a factor in the pathogenesis of congenital heart defects.

9. Discussion and Future Directions

For many years, proper development of the AV cushions was seen as the most critical event in AV valvuloseptal morphogenesis and considered crucial for correct formation of the septal structures at the AV junction. Cushions hypoplasia and/or failure of the cushions to fuse was for decades seen as the primary mechanism leading to AVSDs. Because of that, these congenital defects were (and still are) typically referred to as “endocardial cushion defects”. However, as pointed out by Professor Anderson in a paper from 2010 [66], AVSDs can be found in animal models in which the cushions are actually larger than normal and in settings where the cushions actually have fused. Studies conducted over the last 10 years have demonstrated that interfering with the development of the SHF-derived DMP, without affecting the initial development of the AV cushions, can generate AVSDs. This led to a paradigm shift in the understanding of the pathogenesis of AVSD as it showed that the development of the DMP, rather than that of the AV cushions, could be the most critical step in AV septal development. The work presented in this paper focuses on the third, by and large historically ignored, component of the AV mesenchymal complex, i.e., the mesenchymal cap on the leading edge of the primary atrial septum. Compared to what is known about the AV valves and the DMP, understanding of the mechanisms that drive the development of the mesenchymal cap and an appreciation of its role in AV septation are still in their infancy. In this contribution, we have presented data on how the cap develops and showed results of studies that provide insight on how a number of signaling mechanisms, transcription factors, and extracellular matrix components might be involved in controlling the development of the cap. In ongoing studies, we are building on these (preliminary) results by specifically focusing on cap development in mouse models in which candidate genes believed to be important for the development of the AV mesenchymal complex are deleted in a tissue-specific manner. These studies will provide more information of how the cap is forming, but also on its specific role in AV septation; we believe that they will reveal that the cap is playing a significant role in AV septation.

10. Methods

10.1. Mice

Generation and use of the cre-recombinase mouse models used for cell fate tracing (Mef2c-AHF-cre, Tie2-cre, and Nfatc1-cre) have been described previously [3,12,120,121]. The cre-mice were used in combination with the B6.129(Cg)-Gt(ROSA)26Sor^{tm4(ACTB-tdTomato,dTomatoLuo)/J} (R26^{mT/mG} reporter mouse (Jackson Laboratory; stock no 007676). Staging and hematoxylin/eosin staining were performed as previously described [122]. All experiments using animals were approved by the MUSC Institutional Animal Care and Use Committee (IACUC) and complied with federal and institutional guidelines. Tissue processing and hematoxylin/eosin staining was performed as previously described.

10.2. Immunolabeling

Primary antibodies: Myosin Heavy Chain (MF20; DSHB), Sarcomeric Actin (Sigma #A2172), pSMAD1,5,8 (Cell Signaling #13820), pSMAD2 (Cell Signaling #3108), VERSICAN, CRTL1/HAPLN1 (DSHB #9/30/8-A-4-c), GATA4 (Santa Cruz #sc-1237), GATA6 (R&D #AF1700), TBX5 (R&D #AF5918), NKX2.5 (R&D #AF2444), SOX9 (Novus #NBP1-8555), FoxF1 (R&D #AF4798), and EGFP (Aves Labs Inc. #GFP-1020). Secondary antibodies were obtained from Jackson ImmunoResearch and Invitrogen. Nuclei were detected using DAPI (Invitrogen, Carlsbad, CA, USA; Slowfade Gold Antifade Reagent with DAPI; catnr S36938). Fluorescent staining was visualized using a Zeiss AxioImager II microscope.

Author Contributions: R.D. and A.W. designed the experiments. R.D., E.F., R.W., J.D. and K.D.G. conducted the majority of the experiments. R.D., M.J.v.d.H., A.W. created the manuscript. All authors have read and agreed to the published version of the manuscript.

Funding: This research was funded by the National Institutes of Health (NIH) grant R01HL122906 (R.D., A.W.) and a Research Grant from the CHARGE Syndrome Foundation (A.W.). The contents are solely the responsibility of the authors.

Conflicts of Interest: The authors declare no conflict of interest.

References

1. Briggs, L.E.; Burns, T.A.; Lockhart, M.M.; Phelps, A.L.; Van den Hoff, M.J.; Wessels, A. Wnt/beta-catenin and sonic hedgehog pathways interact in the regulation of the development of the dorsal mesenchymal protrusion. *Dev. Dyn.* **2016**, *245*, 103–113. [CrossRef]
2. Briggs, L.E.; Kakarla, J.; Wessels, A. The pathogenesis of atrial and atrioventricular septal defects with special emphasis on the role of the dorsal mesenchymal protrusion. *Differentiation* **2012**, *84*, 117–130. [CrossRef] [PubMed]
3. Briggs, L.E.; Phelps, A.L.; Brown, E.; Kakarla, J.; Anderson, R.H.; van den Hoff, M.J.; Wessels, A. Expression of the bmp receptor alk3 in the second heart field is essential for development of the dorsal mesenchymal protrusion and atrioventricular septation. *Circ. Res.* **2013**, *112*, 1420–1432. [CrossRef] [PubMed]
4. Snarr, B.S.; Kern, C.B.; Wessels, A. Origin and fate of cardiac mesenchyme. *Dev. Dyn.* **2008**, *237*, 2804–2819. [CrossRef] [PubMed]
5. Snarr, B.S.; Wirrig, E.E.; Phelps, A.L.; Trusk, T.C.; Wessels, A. A spatiotemporal evaluation of the contribution of the dorsal mesenchymal protrusion to cardiac development. *Dev. Dyn.* **2007**, *236*, 1287–1294. [CrossRef] [PubMed]
6. Rawles, M.E. The heart-forming areas of the early chick blastoderm. *Physiol. Zool.* **1943**, *16*, 22–44. [CrossRef]
7. Rosenquist, G.C.; DeHaan, R.L. Migration of precardiac cells in the chick embryo: A radiographic study. *Carnegie Inst. Wash. Contrib. Embryol.* **1966**, *38*, 111–121.
8. Dyer, L.A.; Kirby, M.L. The role of secondary heart field in cardiac development. *Dev. Biol.* **2009**, *336*, 137–144. [CrossRef]
9. Mjaatvedt, C.H.; Nakaoka, T.; Moreno-Rodriguez, R.; Norris, R.A.; Kern, M.J.; Eisenberg, C.A.; Turner, D.; Markwald, R.R. The outflow tract of the heart is recruited from a novel heart-forming field. *Dev. Biol.* **2001**, *238*, 97–109. [CrossRef]
10. Kelly, R.G.; Buckingham, M.E. The anterior heart-forming field: Voyage to the arterial pole of the heart. *Trends Genet.* **2002**, *18*, 210–216. [CrossRef]
11. Cai, C.L.; Liang, X.; Shi, Y.; Chu, P.H.; Pfaff, S.L.; Chen, J.; Evans, S. Isl1 identifies a cardiac progenitor population that proliferates prior to differentiation and contributes a majority of cells to the heart. *Dev. Cell* **2003**, *5*, 877–889. [CrossRef]
12. Verzi, M.P.; McCulley, D.J.; De Val, S.; Dodou, E.; Black, B.L. The right ventricle, outflow tract, and ventricular septum comprise a restricted expression domain within the secondary/anterior heart field. *Dev. Biol.* **2005**, *287*, 134–145. [CrossRef] [PubMed]
13. Waldo, K.L.; Kumiski, D.H.; Wallis, K.T.; Stadt, H.A.; Hutson, M.R.; Platt, D.H.; Kirby, M.L. Conotruncal myocardium arises from a secondary heart field. *Development* **2001**, *128*, 3179–3188. [PubMed]
14. Snarr, J. Risk, benefits and complications of epidural steroid injections: A case report. *Aana J.* **2007**, *75*, 183–188. [PubMed]
15. Hoffmann, A.D.; Yang, X.H.; Burnicka-Turek, O.; Bosman, J.D.; Ren, X.; Steimle, J.D.; Vokes, S.A.; McMahon, A.P.; Kalinichenko, V.V.; Moskowitz, I.P. Foxf genes integrate tbx5 and hedgehog pathways in the second heart field for cardiac septation. *PLoS Genet.* **2014**, *10*, e1004604. [CrossRef] [PubMed]
16. Stefanovic, S.; Laforest, B.; Desvignes, J.P.; Lescroart, F.; Argiro, L.; Maurel-Zaffran, C.; Salgado, D.; Plainedoux, E.; De Bono, C.; Pazur, K.; et al. Hox-dependent coordination of mouse cardiac progenitor cell patterning and differentiation. *Elife* **2020**, *9*, e55124. [CrossRef] [PubMed]
17. Manner, J. Cardiac looping in the chick embryo: A morphological review with special reference to terminological and biomechanical aspects of the looping process. *Anat. Rec.* **2000**, *259*, 248–262. [CrossRef]
18. Manner, J. The anatomy of cardiac looping: A step towards the understanding of the morphogenesis of several forms of congenital cardiac malformations. *Clin. Anat.* **2009**, *22*, 21–35. [CrossRef]

19. Wessels, A.; Sedmera, D. Developmental anatomy of the heart: A tale of mice and man. *Physiol. Genom.* **2003**, *15*, 165–176. [CrossRef]
20. Bolender, D.L.; Markwald, R.R. Epithelial-mesenchymal transformation in chick atrioventricular cushion morphogenesis. *Scan. Electron Microsc.* **1979**, 313–321.
21. Markwald, R.; Eisenberg, C.; Eisenberg, L.; Trusk, T.; Sugi, Y. Epithelial-mesenchymal transformations in early avian heart development. *Acta Anat.* **1996**, *156*, 173–186. [CrossRef] [PubMed]
22. Zhang, H.; von Gise, A.; Liu, Q.; Hu, T.; Tian, X.; He, L.; Pu, W.; Huang, X.; He, L.; Cai, C.L.; et al. Yap1 is required for endothelial to mesenchymal transition of the atrioventricular cushion. *J. Biol. Chem.* **2014**, *289*, 18681–18692. [CrossRef]
23. Brown, C.B.; Boyer, A.S.; Runyan, R.B.; Barnett, J.V. Requirement of type iii tgf-beta receptor for endocardial cell transformation in the heart. *Science* **1999**, *283*, 2080–2082. [CrossRef] [PubMed]
24. Sugi, Y.; Yamamura, H.; Okagawa, H.; Markwald, R.R. Bone morphogenetic protein-2 can mediate myocardial regulation of atrioventricular cushion mesenchymal cell formation in mice. *Dev. Biol.* **2004**, *269*, 505–518. [CrossRef]
25. Timmerman, L.A.; Grego-Bessa, J.; Raya, A.; Bertran, E.; Perez-Pomares, J.M.; Diez, J.; Aranda, S.; Palomo, S.; McCormick, F.; Izpisua-Belmonte, J.C.; et al. Notch promotes epithelial-mesenchymal transition during cardiac development and oncogenic transformation. *Genes Dev.* **2004**, *18*, 99–115. [CrossRef] [PubMed]
26. Luna-Zurita, L.; Prados, B.; Grego-Bessa, J.; Luxan, G.; del Monte, G.; Benguria, A.; Adams, R.H.; Perez-Pomares, J.M.; de la Pompa, J.L. Integration of a notch-dependent mesenchymal gene program and bmp2-driven cell invasiveness regulates murine cardiac valve formation. *J. Clin. Investig.* **2010**, *120*, 3493–3507. [CrossRef] [PubMed]
27. Wessels, A.; Markman, M.W.; Vermeulen, J.L.; Anderson, R.H.; Moorman, A.F.; Lamers, W.H. The development of the atrioventricular junction in the human heart. *Circ. Res.* **1996**, *78*, 110–117. [CrossRef]
28. Wessels, A.; Anderson, R.H.; Markwald, R.R.; Webb, S.; Brown, N.A.; Viragh, S.; Moorman, A.F.; Lamers, W.H. Atrial development in the human heart: An immunohistochemical study with emphasis on the role of mesenchymal tissues. *Anat. Rec.* **2000**, *259*, 288–300. [CrossRef]
29. Anderson, R.H.; Brown, N.A.; Webb, S. Development and structure of the atrial septum. *Heart* **2002**, *88*, 104–110. [CrossRef]
30. Jensen, B.; Wang, T.; Moorman, A.F.M. Evolution and development of the atrial septum. *Anat. Rec. (Hoboken)* **2019**, *302*, 32–48. [CrossRef]
31. Le Douarin, N.M.; Dupin, E. The “beginnings” of the neural crest. *Dev. Biol.* **2018**, *444*, S3–S13. [CrossRef]
32. Hutson, M.R.; Kirby, M.L. Neural crest and cardiovascular development: A 20-year perspective. *Birth Defects Res. C Embryo Today* **2003**, *69*, 2–13. [CrossRef]
33. Kirby, M.L.; Gale, T.F.; Stewart, D.E. Neural crest cells contribute to normal aorticopulmonary septation. *Science* **1983**, *220*, 1059–1061. [CrossRef]
34. Kirby, M.L.; Hutson, M.R. Factors controlling cardiac neural crest cell migration. *Cell Adh. Migr.* **2010**, *4*, 609–621. [CrossRef]
35. Phillips, M.T.; Kirby, M.L.; Forbes, G. Analysis of cranial neural crest distribution in the developing heart using quail-chick chimeras. *Circ. Res.* **1987**, *60*, 27–30. [CrossRef]
36. Waldo, K.; Zdanowicz, M.; Burch, J.; Kumiski, D.H.; Stadt, H.A.; Godt, R.E.; Creazzo, T.L.; Kirby, M.L. A novel role for cardiac neural crest in heart development. *J. Clin. Investig.* **1999**, *103*, 1499–1507. [CrossRef] [PubMed]
37. Hutson, M.R.; Kirby, M.L. Model systems for the study of heart development and disease. Cardiac neural crest and conotruncal malformations. *Semin. Cell Dev. Biol.* **2007**, *18*, 101–110. [CrossRef]
38. Kirby, M.L.; Waldo, K.L. Neural crest and cardiovascular patterning. *Circ. Res.* **1995**, *77*, 211–215. [CrossRef]
39. Hiriart, E.; Deepe, R.; Wessels, A. Mesothelium and malignant mesothelioma. *J. Dev. Biol.* **2019**, *7*, 7. [CrossRef] [PubMed]
40. Perez-Pomares, J.M.; Phelps, A.; Sedmerova, M.; Carmona, R.; Gonzalez-Iriarte, M.; Munoz-Chapuli, R.; Wessels, A. Experimental studies on the spatiotemporal expression of wt1 and raldh2 in the embryonic avian heart: A model for the regulation of myocardial and valvuloseptal development by epicardially derived cells (epdcs). *Dev. Biol.* **2002**, *247*, 307–326. [CrossRef]

41. Wessels, A.; Perez-Pomares, J.M. The epicardium and epicardially derived cells (epdcs) as cardiac stem cells. *Anat. Rec. A Discov. Mol. Cell. Evol. Biol.* **2004**, *276*, 43–57. [CrossRef]
42. Viragh, S.; Challice, C.E. The origin of the epicardium and the embryonic myocardial circulation in the mouse. *Anat. Rec.* **1981**, *201*, 157–168. [CrossRef]
43. Vrancken Peeters, M.P.; Mentink, M.M.; Poelmann, R.E.; Gittenberger-de Groot, A.C. Cytokeratins as a marker for epicardial formation in the quail embryo. *Anat. Embryol.* **1995**, *191*, 503–508.
44. Gittenberger-de Groot, A.; Vrancken Peeters, M.; Mentink, M.; Gourdie, R.; Poelmann, R. Epicardium-derived cells contribute a novel population to the myocardial wall and the atrioventricular cushions. *Circ. Res.* **1998**, *82*, 1043–1052. [CrossRef]
45. Perez-Pomares, J.M.; Macias, D.; Garcia-Garrido, L.; Munoz-Chapuli, R. Contribution of the primitive epicardium to the subepicardial mesenchyme in hamster and chick embryos. *Dev. Dyn.* **1997**, *210*, 96–105. [CrossRef]
46. Perez-Pomares, J.M.; Macias, D.; Garcia-Garrido, L.; Munoz-Chapuli, R. The origin of the subepicardial mesenchyme in the avian embryo: An immunohistochemical and quail-chick chimera study. *Dev. Biol.* **1998**, *200*, 57–68. [CrossRef]
47. Dettman, R.W.; Denetclaw, W., Jr.; Ordahl, C.P.; Bristow, J. Common epicardial origin of coronary vascular smooth muscle, perivascular fibroblasts, and intermyocardial fibroblasts in the avian heart. *Dev. Biol.* **1998**, *193*, 169–181. [CrossRef]
48. Wessels, A.; van den Hoff, M.J.; Adamo, R.F.; Phelps, A.L.; Lockhart, M.M.; Sauls, K.; Briggs, L.E.; Norris, R.A.; van Wijk, B.; Perez-Pomares, J.M.; et al. Epicardially derived fibroblasts preferentially contribute to the parietal leaflets of the atrioventricular valves in the murine heart. *Dev. Biol.* **2012**, *366*, 111–124. [CrossRef] [PubMed]
49. Manner, J. Does the subepicardial mesenchyme contribute myocardioblasts to the myocardium of the chick embryo heart? A quail-chick chimera study tracing the fate of the epicardial primordium. *Anat. Rec.* **1999**, *255*, 212–226. [CrossRef]
50. Zhou, B.; von Gise, A.; Ma, Q.; Hu, Y.; Pu, W. Genetic fate mapping demonstrates contribution of epicardium-derived cells to the annulus fibrosis of the mammalian heart. *Dev. Biol.* **2010**, *338*, 251–261. [CrossRef]
51. Lockhart, M.M.; Phelps, A.L.; van den Hoff, M.J.; Wessels, A. The epicardium and the development of the atrioventricular junction in the murine heart. *J. Dev. Biol.* **2014**, *2*, 1–17. [CrossRef]
52. Anderson, R.H.; Mohun, T.J.; Brown, N.A. Clarifying the morphology of the ostium primum defect. *J. Anat.* **2015**, *226*, 244–257. [CrossRef]
53. His, W. Die area interposita, die eustachi'sche klappe und die spina vestibuli. *Anat. Menschl. Embryonen* **1880**, *149*, 52.
54. Kim, J.S.; Viragh, S.; Moorman, A.F.; Anderson, R.H.; Lamers, W.H. Development of the myocardium of the atrioventricular canal and the vestibular spine in the human heart. *Circ. Res.* **2001**, *88*, 395–402. [CrossRef]
55. Mommersteeg, M.T.; Soufan, A.T.; de Lange, F.J.; van den Hoff, M.J.; Anderson, R.H.; Christoffels, V.M.; Moorman, A.F. Two distinct pools of mesenchyme contribute to the development of the atrial septum. *Circ. Res.* **2006**, *99*, 351–353. [CrossRef]
56. Blom, N.A.; Ottenkamp, J.; Wenink, A.G.; Gittenberger-de Groot, A.C. Deficiency of the vestibular spine in atrioventricular septal defects in human fetuses with down syndrome. *Am. J. Cardiol.* **2003**, *91*, 180–184. [CrossRef]
57. Sharratt, G.P.; Webb, S.; Anderson, R.H. The vestibular defect: An interatrial communication due to a deficiency in the atrial septal component derived from the vestibular spine. *Cardiol. Young* **2003**, *13*, 184–190. [CrossRef]
58. De Bono, C.; Thellier, C.; Bertrand, N.; Sturny, R.; Jullian, E.; Cortes, C.; Stefanovic, S.; Zaffran, S.; Theveniau-Ruissy, M.; Kelly, R.G. T-box genes and retinoic acid signaling regulate the segregation of arterial and venous pole progenitor cells in the murine second heart field. *Hum. Mol. Genet.* **2018**, *27*, 3747–3760. [CrossRef] [PubMed]
59. Al-Hay, A.A.; MacNeill, S.J.; Yacoub, M.; Shore, D.F.; Shinebourne, E.A. Complete atrioventricular septal defect, down syndrome, and surgical outcome: Risk factors. *Ann. Thorac. Surg.* **2003**, *75*, 412–421. [CrossRef]
60. Dickinson, D.F.; Arnold, R.; Wilkinson, J.L. Congenital heart disease among 160 480 liveborn children in liverpool 1960 to 1969. Implications for surgical treatment. *Br. Heart J.* **1981**, *46*, 55–62. [CrossRef]
61. Corsten-Janssen, N.; Kerstjens-Frederikse, W.S.; du Marchie Sarvaas, G.J.; Baardman, M.E.; Bakker, M.K.; Bergman, J.E.; Hove, H.D.; Heimdal, K.R.; Rustad, C.F.; Hennekam, R.C.; et al. The cardiac phenotype in patients with a chd7 mutation. *Circ. Cardiovasc. Genet.* **2013**, *6*, 248–254. [CrossRef]
62. McCullough, A. Further examples of endocardial cushion defect in production of a cardiac anomaly complex; a presentation of three cases from autopsy reports. *J. Pediatr.* **1953**, *43*, 429–433. [CrossRef]

63. Campbell, M.; Missen, G.A. Endocardial cushion defects; common atrio-ventricular canal and ostium primum. *Br. Heart J.* **1957**, *19*, 403–418. [CrossRef]
64. Van Mierop, L.H.S.; Alley, R.D.; Kausel, H.W.; Stranahan, A. The anatomy and embryology of endocardial cushion defects. *J. Thorac. Cardio. Surg.* **1962**, *43*, 71. [CrossRef]
65. Carmi, R.; Boughman, J.A.; Ferencz, C. Endocardial cushion defect: Further studies of “isolated” versus “syndromic” occurrence. *Am. J. Med. Genet.* **1992**, *43*, 569–575. [CrossRef]
66. Anderson, R.H.; Wessels, A.; Vettukattil, J.J. Morphology and morphogenesis of atrioventricular septal defect with common atrioventricular junction. *World J. Pediatr. Congenit. Heart Surg.* **2010**, *1*, 59–67. [CrossRef] [PubMed]
67. Jiao, K.; Kulesa, H.; Tompkins, K.; Zhou, Y.; Batts, L.; Baldwin, H.S.; Hogan, B.L. An essential role of bmp4 in the atrioventricular septation of the mouse heart. *Genes Dev.* **2003**, *17*, 2362–2367. [CrossRef] [PubMed]
68. Goddeeris, M.M.; Rho, S.; Petiet, A.; Davenport, C.L.; Johnson, G.A.; Meyers, E.N.; Klingensmith, J. Intracardiac septation requires hedgehog-dependent cellular contributions from outside the heart. *Development* **2008**, *135*, 1887–1895. [CrossRef]
69. Hoffmann, A.D.; Peterson, M.A.; Friedland-Little, J.M.; Anderson, S.A.; Moskowitz, I.P. Sonic hedgehog is required in pulmonary endoderm for atrial septation. *Development* **2009**, *136*, 1761–1770. [CrossRef]
70. Xie, L.; Hoffmann, A.D.; Burnicka-Turek, O.; Friedland-Little, J.M.; Zhang, K.; Moskowitz, I.P. Tbx5-hedgehog molecular networks are essential in the second heart field for atrial septation. *Dev. Cell* **2012**, *23*, 280–291. [CrossRef]
71. Tian, Y.; Yuan, L.; Goss, A.M.; Wang, T.; Yang, J.; Lepore, J.J.; Zhou, D.; Schwartz, R.J.; Patel, V.; Cohen, E.D.; et al. Characterization and in vivo pharmacological rescue of a wnt2-gata6 pathway required for cardiac inflow tract development. *Dev. Cell* **2010**, *18*, 275–287. [CrossRef]
72. Burns, T.; Yang, Y.; Hiriart, E.; Wessels, A. The dorsal mesenchymal protrusion and the pathogenesis of atrioventricular septal defects. *J. Cardiovasc. Dev. Dis.* **2016**, *3*, 29. [CrossRef]
73. Terada, R.; Warren, S.; Lu, J.T.; Chien, K.R.; Wessels, A.; Kasahara, H. Ablation of nkx2-5 at mid-embryonic stage results in premature lethality and cardiac malformation. *Cardiovasc. Res.* **2011**, *91*, 289–299. [CrossRef] [PubMed]
74. Cole-Jeffrey, C.T.; Terada, R.; Neth, M.R.; Wessels, A.; Kasahara, H. Progressive anatomical closure of foramen ovale in normal neonatal mouse hearts. *Anat. Rec. (Hoboken)* **2012**, *295*, 764–768. [CrossRef]
75. Brown, C.B.; Boyer, A.S.; Runyan, R.B.; Barnett, J.V. Antibodies to the type ii tgfbeta receptor block cell activation and migration during atrioventricular cushion transformation in the heart. *Dev. Biol.* **1996**, *174*, 248–257. [CrossRef]
76. Camenisch, T.D.; Molin, D.G.; Person, A.; Runyan, R.B.; Gittenberger-de Groot, A.C.; McDonald, J.A.; Klewer, S.E. Temporal and distinct tgfbeta ligand requirements during mouse and avian endocardial cushion morphogenesis. *Dev. Biol.* **2002**, *248*, 170–181. [CrossRef]
77. Inai, K.; Norris, R.A.; Hoffman, S.; Markwald, R.R.; Sugi, Y. Bmp-2 induces cell migration and periostin expression during atrioventricular valvulogenesis. *Dev. Biol.* **2008**, *315*, 383–396. [CrossRef] [PubMed]
78. Saxon, J.G.; Baer, D.R.; Barton, J.A.; Hawkins, T.; Wu, B.; Trusk, T.C.; Harris, S.E.; Zhou, B.; Mishina, Y.; Sugi, Y. Bmp2 expression in the endocardial lineage is required for av endocardial cushion maturation and remodeling. *Dev. Biol.* **2017**, *430*, 113–128. [CrossRef]
79. Camenisch, T.D.; Runyan, R.B.; Markwald, R.R. *Molecular Regulation of Cushion Morphogenesis*; Elsevier: Cambridge, MA, USA, 2010.
80. Camenisch, T.D.; Schroeder, J.A.; Bradley, J.; Klewer, S.E.; McDonald, J.A. Heart-valve mesenchyme formation is dependent on hyaluronan-augmented activation of erbb2-erbb3 receptors. *Nat. Med.* **2002**, *8*, 850–855. [CrossRef]
81. Camenisch, T.D.; Spicer, A.P.; Brehm-Gibson, T.; Biesterfeldt, J.; Augustine, M.L.; Calabro, A., Jr.; Kubalak, S.; Klewer, S.E.; McDonald, J.A. Disruption of hyaluronan synthase-2 abrogates normal cardiac morphogenesis and hyaluronan-mediated transformation of epithelium to mesenchyme. *J. Clin. Investig.* **2000**, *106*, 349–360. [CrossRef]
82. Mjaatvedt, C.H.; Yamamura, H.; Capehart, A.A.; Turner, D.; Markwald, R.R. The cspg2 gene, disrupted in the hdf mutant, is required for right cardiac chamber and endocardial cushion formation. *Dev. Biol.* **1998**, *202*, 56–66. [CrossRef] [PubMed]
83. Wirrig, E.E.; Snarr, B.S.; Chintalapudi, M.R.; O’Neal, J.L.; Phelps, A.L.; Barth, J.L.; Fresco, V.M.; Kern, C.B.; Mjaatvedt, C.H.; Toole, B.P.; et al. Cartilage link protein 1 (crtl1), an extracellular matrix component playing an important role in heart development. *Dev. Biol.* **2007**, *310*, 291–303. [CrossRef] [PubMed]

84. Lincoln, J.; Kist, R.; Scherer, G.; Yutzey, K. Sox9 is required for precursor cell expansion and extracellular matrix organization during mouse heart valve development. *Dev. Biol.* **2007**, *305*, 120–132. [CrossRef]
85. Tao, G.; Levay, A.K.; Gridley, T.; Lincoln, J. Mmp15 is a direct target of snail during endothelial to mesenchymal transformation and endocardial cushion development. *Dev. Biol.* **2011**, *359*, 209–221. [CrossRef]
86. de la Pompa, J.L.; Timmerman, L.A.; Takimoto, H.; Yoshida, H.; Elia, A.J.; Samper, E.; Potter, J.; Wakeham, A.; Marengere, L.; Langille, B.L.; et al. Role of the nf-atc transcription factor in morphogenesis of cardiac valves and septum. *Nature* **1998**, *392*, 182–186. [CrossRef] [PubMed]
87. Torregrosa-Carrion, R.; Luna-Zurita, L.; Garcia-Marques, F.; D'Amato, G.; Pineiro-Sabaris, R.; Bonzon-Kulichenko, E.; Vazquez, J.; de la Pompa, J.L. Notch activation promotes valve formation by regulating the endocardial secretome. *Mol. Cell Proteom.* **2019**, *18*, 1782–1795. [CrossRef]
88. Bernanke, D.H.; Markwald, R.R. Effects of hyaluronic acid on cardiac cushion tissue cells in collagen matrix cultures. *Tex. Rep. Biol. Med.* **1979**, *39*, 271–285.
89. Bernanke, D.H.; Markwald, R.R. Migratory behavior of cardiac cushion tissue cells in a collagen-lattice culture system. *Dev. Biol.* **1982**, *91*, 235–245. [CrossRef]
90. Runyan, R.B.; Markwald, R.R. Invasion of mesenchyme into three-dimensional collagen gels: A regional and temporal analysis of interaction in embryonic heart tissue. *Dev. Biol.* **1983**, *95*, 108–114. [CrossRef]
91. Gaussin, V.; Van de Putte, T.; Mishina, Y.; Hanks, M.C.; Zwijsen, A.; Huylebroeck, D.; Behringer, R.R.; Schneider, M.D. Endocardial cushion and myocardial defects after cardiac myocyte-specific conditional deletion of the bone morphogenetic protein receptor alk3. *Proc. Natl. Acad. Sci. USA* **2002**, *99*, 2878–2883. [CrossRef]
92. Bartram, U.; Molin, D.G.; Wisse, L.J.; Mohamad, A.; Sanford, L.P.; Doetschman, T.; Speer, C.P.; Poelmann, R.E.; Gittenberger-de Groot, A.C. Double-outlet right ventricle and overriding tricuspid valve reflect disturbances of looping, myocardialization, endocardial cushion differentiation, and apoptosis in tgf-beta(2)-knockout mice. *Circulation* **2001**, *103*, 2745–2752. [CrossRef]
93. Krug, E.L.; Mjaatvedt, C.H.; Markwald, R.R. Extracellular matrix from embryonic myocardium elicits an early morphogenetic event in cardiac endothelial differentiation. *Dev. Biol.* **1987**, *120*, 348–355. [CrossRef]
94. Bouchev, D.; Argraves, W.S.; Little, C.D. Fibulin-1, vitronectin, and fibronectin expression during avian cardiac valve and septa development. *Anat. Rec.* **1996**, *244*, 540–551. [CrossRef]
95. Kern, C.B.; Twal, W.O.; Mjaatvedt, C.H.; Fairey, S.E.; Toole, B.P.; Iruela-Arispe, M.L.; Argraves, W.S. Proteolytic cleavage of versican during cardiac cushion morphogenesis. *Dev. Dyn.* **2006**, *235*, 2238–2247. [CrossRef] [PubMed]
96. Henderson, D.J.; Copp, A.J. Versican expression is associated with chamber specification, septation, and valvulogenesis in the developing mouse heart. *Circ. Res.* **1998**, *83*, 523–532. [CrossRef]
97. Posch, M.G.; Waldmuller, S.; Muller, M.; Scheffold, T.; Fournier, D.; Andrade-Navarro, M.A.; De Geeter, B.; Guillaumont, S.; Dauphin, C.; Youssef, D.; et al. Cardiac alpha-myosin (myh6) is the predominant sarcomeric disease gene for familial atrial septal defects. *PLoS ONE* **2011**, *6*, e28872. [CrossRef]
98. Basson, C.T.; Bachinsky, D.R.; Lin, R.C.; Levi, T.; Elkins, J.A.; Soultis, J.; Grayzel, D.; Kroumpouzou, E.; Traill, T.A.; Leblanc-Straceski, J.; et al. Mutations in human cause limb and cardiac malformation in holt-oram syndrome. *Nat. Genet.* **1997**, *15*, 30–35. [CrossRef]
99. Bruneau, B.G.; Logan, M.; Davis, N.; Levi, T.; Tabin, C.J.; Seidman, J.G.; Seidman, C.E. Chamber-specific cardiac expression of tbx5 and heart defects in holt-oram syndrome. *Dev. Biol.* **1999**, *211*, 100–108. [CrossRef] [PubMed]
100. Posch, M.G.; Gramlich, M.; Sunde, M.; Schmitt, K.R.; Lee, S.H.; Richter, S.; Kersten, A.; Perrot, A.; Panek, A.N.; Al Khatib, I.H.; et al. A gain-of-function tbx20 mutation causes congenital atrial septal defects, patent foramen ovale and cardiac valve defects. *J. Med. Genet.* **2010**, *47*, 230–235. [CrossRef] [PubMed]
101. Kim, H.Y.; Yoon, C.H.; Kim, G.H.; Yoo, H.W.; Lee, B.S.; Kim, K.S.; Kim, E.A. A case of campomelic dysplasia without sex reversal. *J. Korean Med. Sci.* **2011**, *26*, 143–145. [CrossRef]
102. Posch, M.G.; Perrot, A.; Schmitt, K.; Mittelhaus, S.; Esenwein, E.M.; Stiller, B.; Geier, C.; Dietz, R.; Gessner, R.; Ozcelik, C.; et al. Mutations in gata4, nkx2.5, creld1, and bmp4 are infrequently found in patients with congenital cardiac septal defects. *Am. J. Med. Genet. A* **2008**, *146A*, 251–253. [CrossRef]
103. Hirayama-Yamada, K.; Kamisago, M.; Akimoto, K.; Aotsuka, H.; Nakamura, Y.; Tomita, H.; Furutani, M.; Imamura, S.; Takao, A.; Nakazawa, M.; et al. Phenotypes with gata4 or nkx2.5 mutations in familial atrial septal defect. *Am. J. Med. Genet. A* **2005**, *135*, 47–52. [CrossRef] [PubMed]

104. Garg, V.; Kathiriya, I.S.; Barnes, R.; Schluterman, M.K.; King, I.N.; Butler, C.A.; Rothrock, C.R.; Eapen, R.S.; Hirayama-Yamada, K.; Joo, K.; et al. Gata4 mutations cause human congenital heart defects and reveal an interaction with tbx5. *Nature* **2003**, *424*, 443–447. [CrossRef]
105. Tomita-Mitchell, A.; Maslen, C.L.; Morris, C.D.; Garg, V.; Goldmuntz, E. Gata4 sequence variants in patients with congenital heart disease. *J. Med. Genet.* **2007**, *44*, 779–783. [CrossRef]
106. Lin, X.; Huo, Z.; Liu, X.; Zhang, Y.; Li, L.; Zhao, H.; Yan, B.; Liu, Y.; Yang, Y.; Chen, Y.H. A novel gata6 mutation in patients with tetralogy of fallot or atrial septal defect. *J. Hum. Genet.* **2010**, *55*, 662–667. [CrossRef]
107. Akiyama, H.; Chaboissier, M.C.; Behringer, R.R.; Rowitch, D.H.; Schedl, A.; Epstein, J.A.; de Crombrughe, B. Essential role of sox9 in the pathway that controls formation of cardiac valves and septa. *Proc. Natl. Acad. Sci. USA* **2004**, *101*, 6502–6507. [CrossRef]
108. Garside, V.C.; Cullum, R.; Alder, O.; Lu, D.Y.; Vander Werff, R.; Bilenky, M.; Zhao, Y.; Jones, S.J.; Marra, M.A.; Underhill, T.M.; et al. Sox9 modulates the expression of key transcription factors required for heart valve development. *Development* **2015**, *142*, 4340–4350. [CrossRef] [PubMed]
109. Prall, O.W.; Menon, M.K.; Solloway, M.J.; Watanabe, Y.; Zaffran, S.; Bajolle, F.; Biben, C.; McBride, J.J.; Robertson, B.R.; Chaulet, H.; et al. An nkx2-5/bmp2/smad1 negative feedback loop controls heart progenitor specification and proliferation. *Cell* **2007**, *128*, 947–959. [CrossRef]
110. Reamon-Buettner, S.M.; Borlak, J. Nkx2-5: An update on this hypermutable homeodomain protein and its role in human congenital heart disease (chd). *Hum. Mutat.* **2010**, *31*, 1185–1194. [CrossRef]
111. Furtado, M.B.; Wilmanns, J.C.; Chandran, A.; Perera, J.; Hon, O.; Biben, C.; Willow, T.J.; Nim, H.T.; Kaur, G.; Simonds, S.; et al. Point mutations in murine nkx2-5 phenocopy human congenital heart disease and induce pathogenic wnt signaling. *JCI Insight* **2017**, *2*, e88271. [CrossRef]
112. Nadeau, M.; Georges, R.O.; Laforest, B.; Yamak, A.; Lefebvre, C.; Beaugard, J.; Paradis, P.; Bruneau, B.G.; Andelfinger, G.; Nemer, M. An endocardial pathway involving tbx5, gata4, and nos3 required for atrial septum formation. *Proc. Natl. Acad. Sci. USA* **2010**, *107*, 19356–19361. [CrossRef]
113. Benson, D.W.; Silberbach, G.M.; Kavanaugh-McHugh, A.; Cottrill, C.; Zhang, Y.; Riggs, S.; Smalls, O.; Johnson, M.C.; Watson, M.S.; Seidman, J.G.; et al. Mutations in the cardiac transcription factor nkx2.5 affect diverse cardiac developmental pathways. *J. Clin. Investig.* **1999**, *104*, 1567–1573. [CrossRef]
114. Schott, J.J.; Benson, D.W.; Basson, C.T.; Pease, W.; Silberbach, G.M.; Moak, J.P.; Maron, B.J.; Seidman, C.E.; Seidman, J.G. Congenital heart disease caused by mutations in the transcription factor nkx2-5. *Science* **1998**, *281*, 108–111. [CrossRef] [PubMed]
115. Snarr, B.S.; O’Neal, J.L.; Chintalapudi, M.R.; Wirrig, E.E.; Phelps, A.L.; Kubalak, S.W.; Wessels, A. Isl1 expression at the venous pole identifies a novel role for the second heart field in cardiac development. *Circ. Res.* **2007**, *101*, 971–974. [CrossRef]
116. Ren, X.; Ustiyani, V.; Pradhan, A.; Cai, Y.; Havrilak, J.A.; Bolte, C.S.; Shannon, J.M.; Kalin, T.V.; Kalinichenko, V.V. Foxf1 transcription factor is required for formation of embryonic vasculature by regulating vegf signaling in endothelial cells. *Circ. Res.* **2014**, *115*, 709–720. [CrossRef]
117. Franco, D.; Campione, M. The role of pitx2 during cardiac development. Linking left-right signaling and congenital heart diseases. *Trends Cardiovasc. Med.* **2003**, *13*, 157–163. [CrossRef]
118. Li, Q.Y.; Newbury-Ecob, R.A.; Terrett, J.A.; Wilson, D.I.; Curtis, A.R.; Yi, C.H.; Gebuhr, T.; Bullen, P.J.; Robson, S.C.; Strachan, T.; et al. Holt-oram syndrome is caused by mutations in tbx5, a member of the brachyury (t) gene family. *Nat. Genet.* **1997**, *15*, 21–29. [CrossRef]
119. Basson, C.T.; Cowley, G.S.; Solomon, S.D.; Weissman, B.; Poznanski, A.K.; Traill, T.A.; Seidman, J.G.; Seidman, C.E. The clinical and genetic spectrum of the holt-oram syndrome (heart-hand syndrome). *N. Engl. J. Med.* **1994**, *330*, 885–891. [CrossRef]
120. Kisanuki, Y.Y.; Hammer, R.E.; Miyazaki, J.; Williams, S.C.; Richardson, J.A.; Yanagisawa, M. Tie2-cre transgenic mice: A new model for endothelial cell-lineage analysis in vivo. *Dev. Biol.* **2001**, *230*, 230–242. [CrossRef]
121. Zhou, B.; Wu, B.; Tompkins, K.L.; Boyer, K.L.; Grindley, J.C.; Baldwin, H.S. Characterization of nfatc1 regulation identifies an enhancer required for gene expression that is specific to pro-valve endocardial cells in the developing heart. *Development* **2005**, *132*, 1137–1146. [CrossRef]

122. Waller, B.R., 3rd; Wessels, A. Cardiac morphogenesis and dysmorphogenesis. An immunohistochemical approach. *Methods Mol. Biol.* **2000**, *135*, 151–161. [PubMed]



Publisher's Note: MDPI stays neutral with regard to jurisdictional claims in published maps and institutional affiliations.



© 2020 by the authors. Licensee MDPI, Basel, Switzerland. This article is an open access article distributed under the terms and conditions of the Creative Commons Attribution (CC BY) license (<http://creativecommons.org/licenses/by/4.0/>).

Review

Muscularization of the Mesenchymal Outlet Septum during Cardiac Development

Maurice J. B. van den Hoff ^{1,*}  and Andy Wessels ² ¹ Department of Medical Biology, AmsterdamUMC, Location AMC, 1105AZ Amsterdam, The Netherlands² Department of Regenerative Medicine and Cell Biology, Medical University of South Carolina, Charleston, SC 29425, USA; wesselsa@musc.com

* Correspondence: m.j.vandenhoff@amsterdamumc.nl; Tel.: +1-3120-5665-405

Received: 1 October 2020; Accepted: 2 November 2020; Published: 4 November 2020

Abstract: After the formation of the linear heart tube, it becomes divided into right and left components by the process of septation. Relatively late during this process, within the developing outflow tract, the initially mesenchymal outlet septum becomes muscularized as the result of myocardialization. Myocardialization is defined as the process in which existing cardiomyocytes migrate into flanking mesenchyme. Studies using genetically modified mice, as well as experimental approaches using in vitro models, demonstrate that Wnt and TGF β signaling play an essential role in the regulation of myocardialization. They also show the significance of the interaction between cardiomyocytes, endocardial derived cells, neural crest cells, and the extracellular matrix. Interestingly, Wnt-mediated non-canonical planar cell polarity signaling was found to be a crucial regulator of myocardialization in the outlet septum and Wnt-mediated canonical β -catenin signaling is an essential regulator of the expansion of mesenchymal cells populating the outflow tract cushions.

Keywords: myocardialization; muscularization; differentiation; Wnt signaling; outflow tract

1. Introduction

In the western world, approximately 3% of live-born children have a congenital abnormality. Of these children, a third have a cardiac defect, and of these children, again, a third have an arterial pole malformation. Over the past few decades, significant progress has been made in the understanding of the formation of the arterial pole. Professor Anderson has contributed nearly 200 publications to this effort. In this review, we will focus on one specific aspect of arterial pole formation, being the muscularization of the initially mesenchymal outlet septum. First, we will discuss the formation of the arterial pole to set the stage and then focus on myocardialization (for reviews of heart development, see [1,2]).

The arterial pole of the adult heart comprises (1) the intrapericardial portion of the aorta and pulmonary trunk, (2) the valves and the surrounding myocardium, and (3) the subvalvular ventricular outlets [3–6] (Figure 1). The formation of the arterial pole of the heart starts at the end of the fourth week of human development (Carnegie Stage (CS) 10), embryonic day (E) 8 in mice, and Hamburger and Hamilton stage (HH) 11 in chickens. At this stage, the outflow tract (OFT) can be discriminated as a smooth-walled, myocardial, tube-like structure in between the site of the forming ventricular trabeculae and the border of the pericardial cavity [7,8]. At the outer surface of the heart, the proximal side of the OFT is marked by the ventriculoarterial groove and the distal side by the pericardial reflection. Up to CS15 in human, E11 in mouse, and HH23 in chicken, the OFT elongates by the addition of cardiomyocytes at its distal end. This population of cardiomyocytes is derived from the so-called second heart field (SHF) resulting from de novo differentiation of mesodermal cells into cardiomyocytes [9–13]. During this process, the distal myocardial border of the OFT remains at the pericardial reflection and the pericardial cavity increases in size. At the same time, the cardiomyocytes at the proximal

side of the OFT differentiate into ventricular cardiomyocytes, contributing to the right ventricle and interventricular septum [14,15]. Intriguingly, at the outer surface of the heart, the ventriculoarterial groove still marks the proximal site of the OFT, suggesting that the cells that form this groove are constantly changing. With the formation of the right ventricle, also the interventricular groove on the outer surface of the heart becomes apparent, marking the position of the forming interventricular septum. With development of the right ventricle, the distance between the ventriculoarterial and interventricular grooves increases in size. After CS15 (sixth week of human development, HH23 in chicken, and E11 in mouse), the OFT increases further in length due to the addition of non-myocytes to its distal border. As a consequence, the distal myocardial border of the heart is no longer found at the level of the pericardial reflection. This non-myocardial portion is referred to as the non-myocardial OFT and will become the intrapericardial portion of the aorta and pulmonary trunk. With further development, the non-myocardial OFT increases in length and the myocardial OFT becomes (relatively) shorter. Although most of the OFT myocardium differentiates into the right ventricular myocardium, a portion remains as OFT myocardium, supporting the semilunar valves and the smooth-walled subvalvular myocardium [14,16,17].

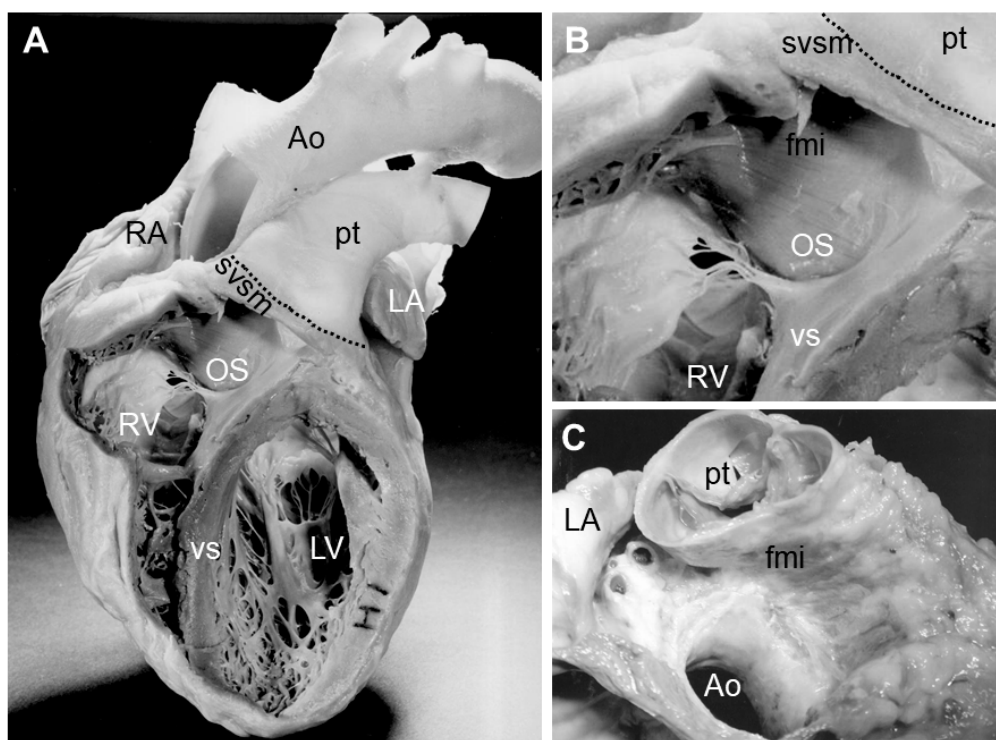


Figure 1. Images showing the distal myocardial border in the adult human heart. (A) shows an adult human heart in which windows were cut from the right and left ventricles to expose the interior structures. The dotted line indicates the distal myocardial border on the pulmonary trunk. (B) shows a detail of the windowed right ventricle focusing on the area of the outlet septum. (C) shows the relation of the large vessels leaving the heart. Note the difference in the level of the semilunar valves and the myocardial sleeve on the pulmonary trunk. The large vessels are cut at the distal myocardial border, showing the level of the myocardial border in relation to the semilunar valves. Abbreviations: Ao: aorta; fmi: freestanding muscular infundibulum; LA: left atrium; LV: left ventricle; OS: outlet septum; pt: pulmonary trunk; RA: right atrium; RV: right ventricle; svsm: semilunar valve supporting myocardium; vs: ventricular septum.

2. Septation of the Arterial Pole

The OFT comprises not only cardiomyocytes but also an inner layer of endocardial cells. The myocardium and endocardium are separated by a layer of extracellular matrix (ECM), referred to

as a cardiac jelly. Prior to the onset of the formation of the non-myocardial OFT, the cardiac jelly of the OFT forms two major spiraling cushions, the parietal and septal OFT cushions (also referred to as OFT ridges). The cushions swell and fuse midway, separating the left and right bloodstreams. The fusion of the cushions starts from the distal side and proceeds proximally, i.e., in the direction of the ventricles. During this phase of development, the non-myocardial OFT forms (as described above) and it is important to note that no cardiac jelly is found in between the endocardium and the wall of the non-myocardial OFT. The lumen of the non-myocardial OFT connects the OFT lumen with the lumen of the aortic sac and the pharyngeal arch arteries that are located outside the pericardial cavity. The pharyngeal arch artery system shows extensive remodeling, which we will not discuss as it is beyond the scope of this review. Of relevance for this review is, however, that the left fourth pharyngeal arch artery will contribute to the aorta, and the left and right sixth pharyngeal artery to the left and right pulmonary artery, respectively. From the dorsal wall of the aortic sac, in between the origins of the fourth and the sixth pharyngeal arch arteries, the roof bulges into the lumen of the aortic sac at CS16 to form the aorticopulmonary septum (APS). The APS then expands in the direction of the fused OFT cushions. With its lengthening and the eventual fusion of its tip with the distal border of the fused OFT cushions, the aortic and pulmonary bloodstreams are separated [4,5,18].

During subsequent development, the non-myocardial OFT is separated into the intrapericardial portion of the aorta and pulmonary trunk. As a consequence, the APS is no longer recognized as a septum, but materially contributes to the facing walls of the intrapericardial portion of the aorta and pulmonary trunk. The separation of the arterial pole continues in the direction of the ventricles. The septation of the distal portion of the OFT results in completing the myocardial cuffs that support the forming semilunar valves. At this stage of development, the coronary orifices are still embedded within the myocardium. With ongoing development, the distal myocardial border further decreases to a level below the coronary orifices, approximately halfway the semilunar cusps. The disappearance of this last section of the myocardium is not only due to differentiation of the OFT myocardium into the ventricular myocardium but also due to apoptosis [14,19,20]. The extent of this process is different in the aortic and pulmonary segment, which is probably responsible for the fact that the primordia of the valves and, eventually, the formed aortic and pulmonary valves are no longer found at the same level but rather tilted with respect to each other. As a consequence of these changes, the myocardial cuff of the pulmonary outlet facing the aorta is now recognized as the freestanding muscular infundibulum. Thus, this free-standing muscular infundibulum is simply a myocardial sleeve supporting the leaflets of the pulmonary valve. It is only below the level of the aortic semilunar valves and distally of the membranous septum that a muscular septum persists.

3. Myocardialization of the Outlet Septum

Prior to the onset of fusion of the OFT cushions, they become populated by mesenchymal cells. In the proximal part of the OFT, the cushions, the mesenchymal cells are mainly derived from the endocardium, as a result of endocardial to mesenchymal transition (endMT) [21]. In the distal as well as the middle part of the OFT, the cushions are primarily populated by mesenchymal cells that originate from the cardiac neural crest. These cardiac neural crest cells form a condensed pillar in both cushions located in the middle part of the OFT and become dispersed and intermingle with the endocardially-derived mesenchymal cells in the cushions of the proximal part of the OFT [16,22–24]. When the cushions in the proximal OFT are fused, the dispersed neural crest cells enter into apoptosis and the cardiomyocytes of the initially smooth-walled myocardium start to form protrusions into the flanking mesenchyme [16,20,25,26] (Figure 2). While invading the mesenchyme, they never lose their contact with the flanking OFT myocardium [16,27–29]. This process is referred to as myocardialization and continues until the entire outlet septum is myocardial. In the mouse, myocardialization takes place between E11 and E15 [30], in chicken between HH28 and HH38 [28], and in human between CS17 and CS23 [17].

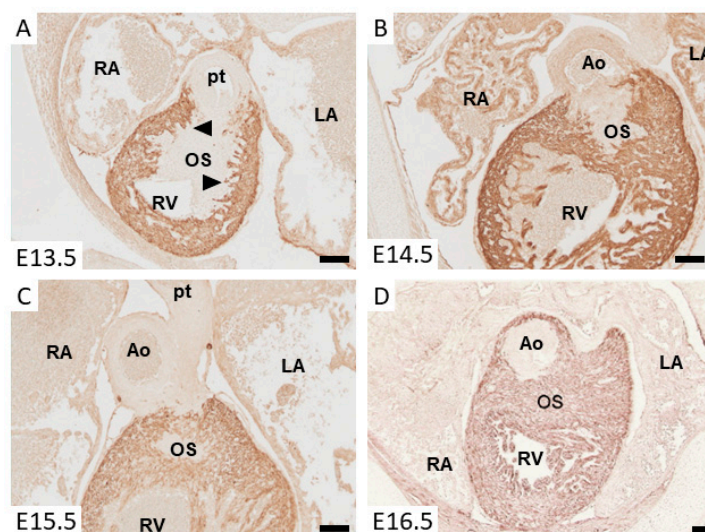


Figure 2. Micrographs of immunohistochemically stained sections of mouse embryos at the level of the outlet septum. The cardiomyocytes expressing ventricular myosin heavy chain are identified by their brown/red staining. (A) shows a section of the arterial pole at embryonic day (E) 13.5. Note the cardiomyocytes that protrude from the OFT myocardium into the mesenchyme of the outlet septum (arrow heads), being a hallmark of the onset of myocardialization. At E14.5 (B), the mesenchymal outlet septum is muscularized and becomes smaller. At E15.5 (C), only a small part of the mesenchymal outlet septum is found, and at E16.5 (D), the entire outlet septum is muscularized. The bar indicates a length of 100 μ m. Abbreviations: Ao: aorta; LA: left atrium; OS: outlet septum; pt: pulmonary trunk; RA: right atrium; RV: right ventricle.

4. Congenital Cardiac Abnormalities and Absence of Myocardialization

Now that we have described the process of myocardialization, there are two (related) questions that need to be addressed: What would be the consequence of failure of myocardialization to take place? Are there congenital cardiac malformations that could be attributed to abnormal myocardialization of the proximal OFT?

If cardiac formation was normal and only myocardialization was absent, one would expect to find a fibrous continuity between the leaflets of the aortic and pulmonary semilunar valves, which are positioned at the same level, and a mesenchymal outlet septum in the formed heart. A congenital cardiac abnormality resembling these features is the doubly committed ventricular septal defect (VSD), the rarest form of VSD. In this situation, there is a fibrous continuity between the aortic and pulmonary semilunar valves and a VSD situated immediately below both the aortic and pulmonary semilunar valves, i.e., in the position of the outlet septum. In this situation, the position of the pulmonary and aortic outlets can be normal, or one or both can override the ventricular septum. In case the VSD is committed to either the aortic or the pulmonary outlet, the muscular freestanding infundibulum is formed. Another situation to be considered is the double outlet right ventricle (DORV). DORV is a very heterogeneous group, which has in common the fact that both the aorta and pulmonary trunk emanate from the right ventricle. In addition, there is an obligatory communication between the left and right ventricle, of which a small portion has a doubly committed VSD. In case of a transposition of the great arteries, the connection of the aorta and pulmonary trunk is discordant with respect to the ventricles, but the muscular freestanding infundibulum and muscular outlet septum are formed. In case the OFT is not septated at all, as is the case in a common arterial trunk (CAT), it is evident that the freestanding muscular infundibulum and the muscular outlet septum are not formed. In CAT, absence of myocardialization is most probably secondary [3,31,32].

5. Mechanism of Cardiac Muscle Formation in the Outlet Septum: Muscularization vs. Differentiation

The mechanism by which the outlet septum changes from a mesenchymal into a myocardial structure is still contentious. Initially, we have described muscularization of the outlet septum as the result of migration of existing proximal OFT cardiomyocytes into the flanking mesenchyme, a process that we named “myocardialization” [28]. Migration was proposed based on the following *in vivo* and *in vitro* observations. (i) Prior to the onset of myocardialization *in vivo*, the myocardial wall flanking the cushion mesenchyme is smooth. The first signs of myocardialization are the appearance of protrusions from the proximal OFT myocardium into the flanking cushion mesenchyme. With ongoing development, the cardiomyocytes that intermingle with the cushion mesenchyme remain slender and show projections. (ii) Culturing chicken or mouse OFT explants (of stages that do show myocardialization *in vivo*) on a thick 3D collagen lattice showed spontaneous 3D network formation of cardiomyocytes below and surrounding the explant in the collagen lattice. OFT explants prepared of stages prior to myocardialization *in vivo*, distal OFT explants, or ventricular explants of any developmental stage did not show network formation when tested in this assay. When OFT explants prepared of stages prior to myocardialization *in vivo* were cultured in medium conditioned by OFT explants that do form a myocardial network in the collagen, they can be induced to do so. This conditioned medium was not able to induce myocardialization in ventricular or distal OFT explants. Moreover, medium conditioned by ventricular explants did not induce myocardial network formation of young OFTs [28,30]. These findings support the hypothesis that the myocardialization-inducing substance is a factor secreted by cells of the OFT at stages when myocardialization is observed *in vivo*.

In an attempt to further characterize myocardialization, proximal OFT cushion mesenchyme was cultured in the myocardialization assay. Cushion mesenchyme did not form cardiomyocytes or networks. However, when proximal OFT cushion mesenchyme was cultured in medium conditioned by OFT explants that do form myocardial networks *in vivo*, cardiomyocytes were formed. This effect was found to be specific for the proximal OFT cushion mesenchyme, because explants of the non-myocardial OFT were not able to do so [30]. Both *in vitro* and *in vivo*, the expression of myosin heavy chain in the cells forming the myocardial network is preceded by alpha smooth muscle actin [17,33,34] or calponin [35] expression, being suggestive of a differentiation process. It should, however, be noted that smooth muscle actin expression has also been used as a marker for migration [36]. Taken together, these findings suggest that muscularization of the outlet septum might not only be the result of myocardialization but that differentiation of the proximal OFT cushion mesenchyme may also contribute.

If cardiomyocytes are indeed newly formed as a result of differentiation, one needs to consider the origin of the differentiating cells. The mesenchyme of the outlet septum is derived from the endocardium, cardiac neural crest [23,24], and the epicardium (unpublished observations). The epicardially derived mesenchyme seems to be an unlikely cell source for myocardial differentiation in the context of myocardialization of the OFT as epicardially derived cells arrive after the onset of muscularization in the outlet septum. Neural crest-derived mesenchyme can also be excluded because these cells undergo apoptosis prior to the onset of the muscularization [16,25,37]. Furthermore, the non-myocardial OFT, which is largely derived from cardiac neural crest cells, is not able to form myocardial networks in the *in vitro* 3D collagen assay [28]. Taken together, this points to the endocardially derived mesenchyme as a possible source of newly differentiated cardiomyocytes. This idea is supported by the observations that (i) the endocardial derived cells are abundantly present at the proper time and location and (ii) that endocardial cells are derived from the cardiogenic mesoderm [15,38–40]. Importantly, however, genetically tracing the endocardial cell lineage using the Tie2-Cre; ROSA26 model does not identify cardiomyocytes that are of endocardial origin. The latter finding suggests that if any muscularizing cells in the outlet septum have formed as a result of a process of myocardial differentiation, it is not as a result of differentiation of any cell type in the OFT that we know of to date.

6. Molecular Regulation of Myocardium Formation in the Outlet Septum

The *in vitro* experiments with conditioned medium discussed above suggest that muscularization of the outlet septum might be induced by a secreted soluble factor. Efforts to identify the nature of this factor from conditioned medium have not yet been successful. In a candidate gene approach, a large set of growth factors was tested for their ability to induce myocardial network formation in early OFT explants. These experiments showed that, when tested individually, activin A, angiotensin II, BMP2, BMP4, cardiotrophin, endothelin-1, -2, -3, FGF2, IGF-II, neurotrophin-3, osteopontin, or TGF β 1 were not able to induce myocardial network formation. However, TGF β 2 and TGF β 3 were, in a concentration-dependent manner, able to induce the formation of myocardial networks [41]. In studies analyzing mesenchyme formation in atrioventricular explants, TGF β 2 or TGF β 3 have been identified as important regulators of endMT and to regulate the migration of the mesenchymal cells into the acellular cushions (for review, see [42]). *In vitro* analyses also uncovered a role for the TGF β receptors in the regulation of endEMT (for review, see [43]). A difference in the spatiotemporal expression pattern of the TGF β receptors might underlie the difference in the effect of TGF β 2 and TGF β 3 in myocardialization. However, this idea has, to the best of our knowledge, not been pursued. In mice, deletion of TGF β 2 [44,45] was found to affect the development of the OFT to different degrees. In several of the TGF β 2 knockout embryos, the cushions in the proximal OFT were underdeveloped, had not fused, and were not muscularized. When OFT explants of wildtype and TGF β 2 knockout mice were studied in the 3D collagen myocardialization assay, no difference in myocardial network formation was found [46]. These results suggest that aberrant myocardialization is not a direct effect of the absence of TGF β 2, but rather a secondary effect related to mesenchyme formation in the cushions. Although, in the first report describing TGF β 3 knockout mice, cardiac defects were not reported [47], a recent study reported a small fraction of TGF β 3 knockout embryos in which the OFT cushions were not fused or myocardialized [48].

The abundance of mesenchymal cells in the OFT cushions seems to be of relevance in the regulation of myocardialization, because the level of dysregulation of endMT in the TGF β 2 and TGF β 3 knockout models is different. Another example of a mouse model with abnormal cushion development and failure of muscularization is the neurofibromin 1 (Nf1) knockout mouse in which the OFT cushions are hyperplastic and are not muscularized [49]. Interestingly, in the friend-of-GATA 2 (Fog2) knockout mouse, the proximal parts of the OFT cushions are hyperplastic and muscularization does take place [50]. The major difference between these latter two mouse models seems to be the extent of apoptosis of mesenchyme in the proximal part of the OFT. During normal development, the dispersed neural crest cells in the proximal part of the OFT cushions enter into apoptosis prior to myocardialization. In the Fog2 knockout mouse, the level of apoptosis appears normal, perhaps even elevated, whereas in the Nf1 knockout mouse, the level is significantly decreased. Further analysis of the Nf1 knockout mouse showed that the OFT cushions are enlarged due to expansion of the endocardially derived cell population, which seems to hamper the invasion of neural crest cells [49]. Thus, the absence of apoptosis in the Nf1 knockout mice is due to the absence of the neural crest cells rather than a dysregulation of apoptosis. The presence of the dispersed neural crest cells and their subsequent apoptosis seems to be an important aspect in the regulation of myocardialization.

Deletion of semaphorin-3c (Sema3c) from the neural crest cells or absence of its receptor neuropilin-1 (Nrp1) interferes with the invasion of the neural crest cells. In this model, the mesenchymal cells in the cushions in the proximal part of the OFT are disorganized and myocardialization is absent. Interestingly, the cardiac muscle cells in these mutant mice show the phenotypic characteristics of myocardialization in the distal portion of the OFT [51]. Ectopic myocardialization in the distal OFT was also found in the Trisomy 16 mouse [52]. In this study, ectopic myocardialization was suggested to be associated with the location of the invading cardiac neural crest cells. In connexin 43 (Cx43) knockout mice, which display OFT and right ventricular abnormalities, a reduction in the number of invading cardiac neural crest cells was observed [53]. In a detailed analysis, myocardialization was found to be affected, as the cardiomyocytes of the proximal part of the OFT were found to form relatively late and

only a few projections into the cushion mesenchyme were observed. Furthermore, the myofibrillar structure in these cardiomyocytes was disorganized [54]. A similar defect was observed in the loop-tail mouse. In a series of manuscripts by the Henderson group, it was established that in these mice, Vangl2, expressed in the cardiomyocytes, was mutated. Vangl2 is a component of the Wnt-planar cell polarity (Wnt/PCP) signaling pathway [55]. Downstream of Vangl2, RhoA and Rock1 were found to be required for the polarization and movement of the cardiomyocytes into the OFT cushions [56–58]. Disrupting the interaction of Prickle1 with Vangl2 was found to lead to similar abnormalities [59]. Interestingly, Cx43 expression also seems to be linked to the Wnt/PCP pathway through Rock1, which is downregulated in Cx43 KO mice [60].

It has not yet been established which Wnt ligand activates the Vangl2-mediated signaling pathway. Based on the analysis of genetically modified mice, Wnt5a and Wnt11 are candidates. In Wnt11 knockout mice, transposition of the great arteries (TGA) is observed. An in-depth analysis revealed that the freestanding muscular infundibulum and muscular outlet septum were not formed [61,62] due to altered polarity of the cardiomyocytes of the proximal part of the OFT [62]. Wnt11 expression is regulated through the cooperative action of Pitx2 and β -catenin on its proximal promoter in cardiomyocytes. Wnt11, in turn, activated TGF β 2 through JNK and ATF2 [62], pointing to an indirect effect on endEMT. Wnt5a knockout mice show a large array of abnormalities, including common arterial trunk (CAT). Expression of Wnt5A in the mesodermal cells of the pharyngeal arches and in the myocardium of the OFT [63] was found to regulate the migration of cardiac neural crest cell into the OFT. The myocardial expression of Ror 1 and Ror 2 receptors [64], which propagate Wnt5a mediated PCP signaling [65], is suggestive of a role in the regulation of myocardialization. This idea is underscored by the observations that Ror1/Ror2 double knockout mice display TGA and a membranous VSD, whereas Ror1 knockout mice have a normal heart and Ror2 knockout mice have a membranous VSD [66,67].

Wnt5a was also found to activate Wnt/ β -catenin-mediated signaling through Frizzled-4 [68]. Interestingly, a mutation screen identified Frizzled-4 in a mouse line showing a large VSD in the region of the outlet septum. Further analysis of this mouse line showed that the VSD was due to aberrant migration of the cardiac neural crest cells into the OFT [69]. In Dishevelled-2 (Dvl2) knockout mice, perturbed neural crest migration into the OFT was observed, resulting in CAT and DORV [70]. This observation should be interpreted with caution as in mouse and human, three homologous Dvl genes are found that are expressed abundantly. Knockout analysis has shown that they have complementary and unique functions. Dvl was found to activate both Wnt/ β -catenin and Wnt/PCP signaling pathways. The specificity of the signaling is regulated through different domains in the Dvl protein and interacting partners and as such affect different biological effects [55].

Conditional removal of focal adhesion kinase (FAK), which is also a component of Wnt/ β -catenin-mediated signaling, from the cardiomyocytes using Nkx2.5-Cre results in an overriding aorta or DORV. In this model, cardiomyocytes do not invade the proximal OFT cushions, and in *in vitro* assays, it was observed that cardiomyocytes isolated from homozygous FAK knockout mice were not able to migrate. Further analysis of the underlying signaling pathways identified FAK-dependent CAS (Crk-associated substrate) activation as an essential regulator of polarized myocyte movement [71].

The involvement of FAK-dependent CAS in the regulation of myocardialization links Wnt/ β -catenin-mediated signaling with integrin-mediated signaling. Integrins are the main receptors transferring extracellular matrix (ECM) information into the cells. Thus far, altered integrin expression has not been considered in the context of myocardialization. The ECM is not only of importance for the migration of cardiomyocytes into the OFT cushions, but also for the population of the cushions by mesenchymal cells. The mesenchymal cells of the proximal OFT cushions might not only directly but also indirectly affect myocardialization through ECM modulation. In this respect, it is interesting to note that both *in vitro* and *in vivo* analyses showed that low levels of fibronectin are required for intermingling of cardiomyocytes and mesenchymal cells, whereas high levels of fibronectin inhibit their intermingling [72]. Moreover, altering the relative abundance of splice variants of the chondroitin

sulfate proteoglycan versican was observed to result in underdeveloped OFT cushions and absence of myocardialization [73]. These findings point to a role of the ECM in supporting or regulating myocardialization and warrant further analysis.

Taken together, the regulation of muscularization of the cushions in the proximal OFT is a complex process in which Wnt and TGF β signaling play essential roles and where the interaction between cardiomyocytes, endocardial derived cells, neural crest cells, and the extracellular matrix seems to be essential.

7. Muscularization of the Dorsal Mesenchymal Protrusion

Although this review primarily deals with the process of muscularization of the outflow tract, it seems appropriate to also briefly pay attention to one other part of the developing heart where a mesenchymal structure eventually becomes muscularized. This structure is the dorsal mesenchymal protrusion (DMP), which plays a crucial role in atrioventricular septation together with two other mesenchymal structures: the AV cushions and the mesenchymal cap on the leading edge of the primary atrial septum (for review, see [74]). The DMP, which is sometimes also referred to as the spina vestibula or the vestibular spine, is a second heart field-derived structure [75,76]. In the early stages of atrioventricular septation (in the mouse between E9.5 and E10.5), the DMP protrudes into the common atrium, using the dorsal mesocardium as its portal of entry. It will eventually fuse with the other mesenchymal component and, as part of the AV mesenchymal complex, sits on top of the fused AV cushions, forming the base of the atrial septal complex. It is not until E13 in the mouse that the DMP becomes muscularized and becomes the inferior muscular rim of the atrial septum. Muscularization of the DMP was initially considered to take place by myocardialization [29,30,77]. However, more recent work from us and others shows that the DMP becomes muscularized as a result of a mesenchymal-to-myocardial differentiation of SHF-derived mesenchyme [75,78–82].

8. Concluding Remarks

During cardiac septation, a mesenchymal outlet septum is formed in the outflow tract by the fusion of the OFT cushions. During subsequent development, this mesenchymal outlet septum becomes muscularized by the process of myocardialization, which is defined as the migration of existing cardiomyocytes into flanking mesenchyme. Detailed analyses of myocardialization using genetically modified mice and in vitro assays suggest that the relative contribution of each cell population and the interaction between endocardially derived mesenchymal cells, cardiac neural crest-derived mesenchymal cells, and cardiomyocytes in the outlet septum is essential for the correct orchestration of the transition of the cardiomyocytes into a migratory phenotype and their migration into the adjacent cushion mesenchyme. The migration of cardiomyocytes into the mesenchyme is mediated by the Wnt non-canonical planar cell polarity signaling and the expansion of the mesenchymal cells in the OFT cushions by Wnt-mediated canonical β -catenin signaling. In addition, the TGF β signaling pathway seems to be important in the regulation of myocardialization by affecting the mesenchymal cell population of the cushions.

While the importance of muscularization/myocardialization for proper heart development is evident, it is tempting to speculate about the importance of this mechanism in a broader context. A myocardial infarction results in loss of cardiomyocytes and subsequent replacement by fibrous scar tissue. The limited inherent regenerative capacity of the adult cardiomyocytes prevents the repopulation of the scar (for review, see [83]). As a therapeutic approach to repopulating the fibrous scar and, hence, preserving cardiac function, insight into the mechanisms that regulate myocardialization in the embryonic heart may also be of relevance in designing strategies to induce healthy cardiomyocytes from the border zone of the infarct to migrate into the scar and improve cardiac function.

Author Contributions: M.J.B.v.d.H. and A.W. have been together involved in the conceptualization, writing—original draft preparation, review and editing. Both authors have read and agreed to the published version of the manuscript.

Funding: Work presented in this contribution was partly supported by the Netherlands Heart Foundation through the Molecular Cardiology Program on Heart Failure (MvdH) and the National Institutes of Health (NIH) grant R01HL122906 (AW).

Conflicts of Interest: The authors declare no conflict of interest.

References

1. Sylva, M.; van den Hoff, M.J.B.; Moorman, A.F.M. Development of the human heart. *Am. J. Med. Genet. Part A* **2014**, *164A*, 1347–1371. [CrossRef] [PubMed]
2. Buijtendijk, M.F.J.; Barnett, P.; van den Hoff, M.J.B. Development of the human heart. *Am. J. Med. Genet. Part C Semin. Med. Genet.* **2020**, *184*, 7–22. [CrossRef] [PubMed]
3. Anderson, R.H.; Freedom, R.M. Normal and abnormal structure of the ventriculo-arterial junctions. *Cardiol. Young* **2005**, *15* (Suppl. 1), 3–16. [CrossRef]
4. Anderson, R.H.; Brown, N.A.; Webb, S.; Chaudhry, B.; Henderson, D.; Moorman, A.F.M. Morphology of the Developing Cardiac Outflow Tract. In *Shaping the Heart in Development and Disease*; Mikhailov, A.T., Torrado, M., Eds.; Transworld Research Network: Kerala, India, 2010.
5. Anderson, R.H.; Chaudhry, B.; Mohun, T.J.; Bamforth, S.D.; Hoyland, D.; Phillips, H.M.; Webb, S.; Moorman, A.F.; Brown, N.A.; Henderson, D.J. Normal and Abnormal Development of the Intrapericardial Arterial Trunks in Man and Mouse. *Cardiovasc. Res.* **2012**, *95*, 108–115. [CrossRef] [PubMed]
6. Anderson, R.H.; Mori, S.; Spicer, D.E.; Brown, N.A.; Mohun, T.J. Development and Morphology of the Ventricular Outflow Tracts. *World J. Pediatr. Congenit. Hear. Surg.* **2016**, *7*, 561–577. [CrossRef] [PubMed]
7. Moorman, A.F.M.; Anderson, R.H.; Christoffels, V.M. The ballooning model for formation of the cardiac chambers. In *Heart Development and Regeneration*; Harvey, R.P., Rosenthal, N., Eds.; Academic Press: San Diego, CA, USA, 2007.
8. Moorman, A.F.M.; Christoffels, V.M. Cardiac chamber formation: Development, genes and evolution. *Physiol. Rev.* **2003**, *83*, 1223–1267. [CrossRef] [PubMed]
9. Kelly, R.G.; Brown, N.A.; Buckingham, M.E. The arterial pole of the mouse heart forms from Fgf10-expressing cells in pharyngeal mesoderm. *Dev. Cell* **2001**, *1*, 435–440. [CrossRef]
10. Mjaatvedt, C.H.; Nakaoka, T.; Moreno-Rodriguez, R.A.; Norris, R.A.; Kern, M.J.; Eisenberg, C.A.; Turner, D.; Markwald, R.R. The outflow of the heart is recruited from a novel heart forming field. *Dev. Biol.* **2001**, *238*, 97–109. [CrossRef]
11. Waldo, K.L.; Kumiski, D.H.; Wallis, K.T.; Stadt, H.A.; Hutson, M.R.; Platt, D.H.; Kirby, M.L. Conotruncal myocardium arises from a secondary heart field. *Development* **2001**, *128*, 3179–3188. [PubMed]
12. Buckingham, M.; Meilhac, S.; Zaffran, S. Building the mammalian heart from two sources of myocardial cells. *Nat. Rev. Genet.* **2005**, *6*, 826–837. [CrossRef]
13. Moorman, A.F.M.; Christoffels, V.M.; Anderson, R.H.; van den Hoff, M.J.B. The heart-forming fields: One or multiple? *Philos. Trans. R. Soc. B* **2007**, *362*, 1257–1265. [CrossRef]
14. Rana, M.S.; Horsten, N.C.A.; Tesink-Taekema, S.; Lamers, W.H.; Moorman, A.F.M.; van den Hoff, M.J.B. Trabeculated right ventricular free wall in the chicken heart forms by ventricularization of the myocardium initially forming the outflow tract. *Circ. Res.* **2007**, *100*, 1000–1007. [CrossRef]
15. Verzi, M.P.; McCulley, D.J.; De, V.S.; Dodou, E.; Black, B.L. The right ventricle, outflow tract, and ventricular septum comprise a restricted expression domain within the secondary/anterior heart field. *Dev. Biol.* **2005**, *287*, 134–145. [CrossRef] [PubMed]
16. Ya, J.; van den Hoff, M.J.; de Boer, P.A.; Tesink-Taekema, S.; Franco, D.; Moorman, A.F.; Lamers, W.H. Normal development of the outflow tract in the rat. *Circ. Res.* **1998**, *82*, 464–472. [CrossRef] [PubMed]
17. Sizarov, A.; Lamers, W.H.; Mohun, T.J.; Brown, N.A.; Anderson, R.H.; Moorman, A.F. Three-dimensional and molecular analysis of the arterial pole of the developing human heart. *J. Anat.* **2012**, *220*, 336–349. [CrossRef]
18. Rana, M.S.; Sizarov, A.; Christoffels, V.M.; Moorman, A.F. Development of the Human Aortic Arch System Captured in an Interactive Three-Dimensional Reference Model. *Am. J. Med. Genet. A* **2014**, *164*, 1372–1383. [CrossRef] [PubMed]
19. Watanabe, M.; Choudry, A.; Berlan, M.; Singal, A.; Siwik, E.; Mohr, S.; Fisher, S.A. Developmental remodeling and shortening of the cardiac outflow tract involves programmed cell death. *Development* **1998**, *125*, 3809–3820.

20. van den Hoff, M.J.B.; van den Eijnde, S.M.; Virágh, S.; Moorman, A.F.M. Programmed cell death in the developing heart. *Cardiovasc. Res.* **2000**, *45*, 603–620. [CrossRef]
21. Wirrig, E.E.; Snarr, B.S.; Chintalapudi, M.R.; O’Neal, J.L.; Phelps, A.L.; Barth, J.L.; Fresco, V.M.; Kern, C.B.; Mjaatvedt, C.H.; Toole, B.P.; et al. Cartilage link protein 1 (Crtl1), an extracellular matrix component playing an important role in heart development. *Dev. Biol.* **2007**, *310*, 291–303. [CrossRef]
22. Waldo, K.; Miyagawa-Tomita, S.; Kumiski, D.; Kirby, M.L. Cardiac neural crest cells provide new insight into septation of the cardiac outflow tract: Aortic sac to ventricular septal closure. *Dev. Biol.* **1998**, *196*, 129–144. [CrossRef]
23. de Lange, F.J.; Moorman, A.F.M.; Anderson, R.H.; Manner, J.; Soufan, A.T.; de Gier-de Vries, C.; Schneider, M.D.; Webb, S.; van den Hoff, M.J.B.; Christoffels, V.M. Lineage and morphogenetic analysis of the cardiac valves. *Circ. Res* **2004**, *95*, 645–654. [CrossRef]
24. Jiang, X.; Rowitch, D.H.; Soriano, P.; McMahon, A.P.; Sucov, H.M. Fate of the mammalian cardiac neural crest. *Development* **2000**, *127*, 1607–1616.
25. Cheng, G.; Wessels, A.; Gourdie, R.G.; Thompson, R.P. Spatiotemporal and tissue specific distribution of apoptosis in the developing chick heart. *Dev. Dyn.* **2002**, *223*, 119–133. [CrossRef] [PubMed]
26. Poelmann, R.E.; Gittenberger-de Groot, A.C. Apoptosis as an instrument in cardiovascular development. *Birth Defects Res. C Embryo Today.* **2005**, *75*, 305–313. [CrossRef]
27. Lamers, W.H.; Wessels, A.; Verbeek, F.J.; Moorman, A.F.M.; Virágh, S.; Wenink, A.C.G.; Gittenberger-de Groot, A.C.; Anderson, R.H. New findings concerning ventricular septation in the human heart. Implications for maldevelopment. *Circulation* **1992**, *86*, 1194–1205. [CrossRef]
28. van den Hoff, M.J.B.; Moorman, A.F.M.; Ruijter, J.M.; Lamers, W.H.; Bennington, R.W.; Markwald, R.R.; Wessels, A. Myocardialization of the cardiac outflow tract. *Dev. Biol.* **1999**, *212*, 477–490. [CrossRef]
29. Kruithof, B.P.T.; van den Hoff, M.J.B.; Wessels, A.; Moorman, A.F.M. Cardiac muscle cell formation after development of the linear heart tube. *Dev. Dyn.* **2003**, *227*, 1–13. [CrossRef] [PubMed]
30. van den Hoff, M.J.B.; Kruithof, B.P.T.; Moorman, A.F.M.; Markwald, R.R.; Wessels, A. Formation of myocardium after the initial development of the linear heart tube. *Dev. Biol.* **2001**, *240*, 61–76. [CrossRef] [PubMed]
31. Anderson, R.H.; Ho, S.Y.; Wilcox, B.R. The surgical anatomy of ventricular septal defect part IV: Double outlet ventricle. *J. Card. Surg.* **1996**, *11*, 2–11. [CrossRef]
32. McCarthy, K.P.; Ching Leung, P.K.; Ho, S.Y. Perimembranous and muscular ventricular septal defects—Morphology revisited in the era of device closure. *J. Interv. Cardiol.* **2005**, *18*, 507–513. [CrossRef]
33. Colas, J.F.; Lawson, A.; Schoenwolf, G.C. Evidence that translation of smooth muscle alpha-actin mRNA is delayed in the chick promyocardium until fusion of the bilateral heart-forming regions. *Dev. Dyn.* **2000**, *218*, 316–330. [CrossRef]
34. Kruithof, B.P.T.; van den Hoff, M.J.B.; Tesink-Taekema, S.; Moorman, A.F.M. Recruitment of intra- and extracardiac cells into the myocardial lineage during mouse development. *Anat. Rec. Adv. Integr. Anat. Evol. Biol.* **2003**, *271*, 303–314. [CrossRef]
35. Moralez, I.; Phelps, A.; Riley, B.; Raines, M.; Wirrig, E.; Snarr, B.; Jin, J.-P.; van den Hoff, M.J.B.; Hoffman, S.; Wessels, A. Muscularizing tissues in the endocardial cushions of the avian heart are characterized by the expression of h1-calponin. *Dev. Dyn.* **2006**, *235*, 1648–1658. [CrossRef]
36. Okagawa, H.; Markwald, R.R.; Sugi, Y. Functional BMP receptor in endocardial cells is required in atrioventricular cushion mesenchymal cell formation in chick. *Dev. Biol.* **2007**, *306*, 179–192. [CrossRef]
37. Poelmann, R.E.; Mikawa, T.; Gittenberger-de Groot, A.C. Neural crest cells in outflow tract septation of the embryonic chicken heart: Differentiation and apoptosis. *Dev. Dyn.* **1998**, *212*, 373–384. [CrossRef]
38. Sun, Y.; Liang, X.; Najafi, N.; Cass, M.; Lin, L.; Cai, C.L.; Chen, J.; Evans, S.M. Islet 1 is expressed in distinct cardiovascular lineages, including pacemaker and coronary vascular cells. *Dev. Biol.* **2007**, *304*, 286–296. [CrossRef]
39. Cai, C.L.; Liang, X.; Shi, Y.; Chu, P.H.; Pfaff, S.L.; Chen, J.; Evans, S. Isl1 identifies a cardiac progenitor population that proliferates prior to differentiation and contributes a majority of cells to the heart. *Dev. Cell* **2003**, *5*, 877–889. [CrossRef]
40. Stanley, E.G.; Biben, C.; Elefanty, A.; Barnett, L.; Koentgen, F.; Robb, L.; Harvey, R.P. Efficient Cre-mediated deletion in cardiac progenitor cells conferred by a 3’UTR-ires-Cre allele of the homeobox gene Nkx2-5. *Int. J. Dev. Biol.* **2002**, *46*, 431–439.

41. van den Hoff, M.J.B.; Kruithof, B.P.T.; Wessels, A.; Markwald, R.R.; Moorman, A.F.M. Regulation of myocardium formation after the initial development of the linear heart tube. In *Cardiovascular Development and Congenital Malformations; Molecular and Genetic Mechanisms*; Artman, M., Benson, D.W., Srivastava, D., Nakazawa, M., Eds.; Blackwell Publishing, Inc.: Malden, MA, USA, 2005; pp. 37–40.
42. Mercado-Pimentel, M.E.; Runyan, R.B. Multiple transforming growth factor-beta isoforms and receptors function during epithelial-mesenchymal cell transformation in the embryonic heart. *Cells Tissues Organs* **2007**, *185*, 146–156. [CrossRef]
43. Doetschman, T.; Barnett, J.V.; Runyan, R.B.; Camenisch, T.D.; Heimark, R.L.; Granzier, H.L.; Conway, S.J.; Azhar, M. Transforming growth factor beta signaling in adult cardiovascular diseases and repair. *Cell Tissue Res.* **2012**, *347*, 203–223. [CrossRef]
44. Sanford, L.P.; Ormsby, I.; Gittenberger-de Groot, A.C.; Sariola, H.; Friedman, R.; Boivin, G.P.; Cardell, E.L.; Doetschman, T. TGF β 2 knockout mice have multiple developmental defects that are non-overlapping with other TGF β knockout phenotypes. *Development* **1997**, *124*, 2659–2670. [PubMed]
45. Bartram, U.; Molin, D.G.; Wisse, L.J.; Mohamad, A.; Sanford, L.P.; Doetschman, T.; Speer, C.P.; Poelmann, R.E.; Gittenberger-de Groot, A.C. Double-outlet right ventricle and overriding tricuspid valve reflect disturbances of looping, myocardialization, endocardial cushion differentiation, and apoptosis in TGF- β 2-knockout mice. *Circulation* **2001**, *103*, 2745–2752. [CrossRef] [PubMed]
46. Kruithof, B.P.T. Myocardium Formation after the Initial Development of the Linear Heart Tube. Ph.D. Thesis, University of Amsterdam, Amsterdam, The Netherlands, 2003.
47. Proetzel, G.; Pawlowski, S.A.; Wiles, M.V.; Yin, M.; Boivin, G.P.; Howles, P.N.; Ding, J.; Ferguson, M.W.; Doetschman, T. Transforming growth factor-beta 3 is required for secondary palate fusion. *Nat. Genet.* **1995**, *11*, 409–414. [CrossRef]
48. Chakrabarti, M.; Al-Sammarraie, N.; Gebere, M.G.; Bhattacharya, A.; Chopra, S.; Johnson, J.; Pena, E.A.; Eberth, J.F.; Poelmann, R.E.; Gittenberger-de Groot, A.C.; et al. Transforming Growth Factor Beta3 is Required for Cardiovascular Development. *J. Cardiovasc. Dev. Dis.* **2020**, *7*, 19. [CrossRef]
49. Lakkis, M.M.; Epstein, J.A. Neurofibromin modulation of ras activity is required for normal endocardial-mesenchymal transformation in the developing heart. *Development* **1998**, *125*, 4359–4367.
50. Flagg, A.E.; Earley, J.U.; Svensson, E.C. FOG-2 attenuates endothelial-to-mesenchymal transformation in the endocardial cushions of the developing heart. *Dev. Biol.* **2007**, *304*, 308–316. [CrossRef]
51. Plein, A.; Calmont, A.; Fantin, A.; Denti, L.; Anderson, N.A.; Scambler, P.J.; Ruhrberg, C. Neural crest-derived SEMA3C activates endothelial NRP1 for cardiac outflow tract septation. *J. Clin. Inv.* **2015**, *125*, 2661–2676. [CrossRef]
52. Waller, B.R.; McQuinn, T.; Phelps, A.; Markwald, R.R.; Lo, C.W.; Thompson, R.P.; Wessels, A. Conotruncal anomalies in the trisomy 16 mouse: An immunohistochemical analysis with emphasis on the involvement of the neural crest. *Anat. Rec.* **2000**, *260*, 279–293. [CrossRef]
53. Huang, G.Y.; Wessels, A.; Smith, B.R.; Linask, K.K.; Ewart, J.L.; Lo, C.W. Alteration in connexin 43 gap junction gene dosage impairs conotruncal heart development. *Dev. Biol.* **1998**, *198*, 32–44. [CrossRef]
54. Rhee, D.Y.; Zhao, X.Q.; Francis, R.J.; Huang, G.Y.; Mably, J.D.; Lo, C.W. Connexin 43 regulates epicardial cell polarity and migration in coronary vascular development. *Development* **2009**, *136*, 3185–3193. [CrossRef] [PubMed]
55. Ruiz-Villalba, A.; Hoppler, S.; van den Hoff, M.J. Wnt signaling in the heart fields: Variations on a common theme. *Dev. Dyn.* **2015**. [CrossRef] [PubMed]
56. Phillips, H.M.; Hildreth, V.; Peat, J.D.; Murdoch, J.N.; Kobayashi, K.; Chaudhry, B.; Henderson, D.J. Non-cell-autonomous roles for the planar cell polarity gene Vangl2 in development of the coronary circulation. *Circ. Res.* **2008**, *102*, 615–623. [CrossRef]
57. Phillips, H.M.; Murdoch, J.N.; Chaudhry, B.; Copp, A.J.; Henderson, D.J. Vangl2 Acts via RhoA Signaling to Regulate Polarized Cell Movements During Development of the Proximal Outflow Tract. *Circ. Res.* **2005**, *96*, 292–299. [CrossRef]
58. Henderson, D.J.; Phillips, H.M.; Chaudhry, B. Vang-like 2 and noncanonical Wnt signaling in outflow tract development. *Trends Cardiovasc. Med.* **2006**, *16*, 38–45. [CrossRef]
59. Gibbs, B.C.; Damerla, R.R.; Vladar, E.K.; Chatterjee, B.; Wan, Y.; Liu, X.; Cui, C.; Gabriel, G.C.; Zahid, M.; Yagi, H.; et al. Prickle1 mutation causes planar cell polarity and directional cell migration defects associated with cardiac outflow tract anomalies and other structural birth defects. *Biol. Open* **2016**, *5*, 323–335. [CrossRef]

60. Qi, C.H.; Zhao, X.Q.; Ma, D.; Ma, X.J.; Zhou, G.M.; Huang, G.Y. Downregulation of Rho associated coiled-coil forming protein kinase 1 in the process of delayed myocardialization of cardiac proximal outflow tract septum in connexin 43 knockout mice embryo. *Chin. Med. J.* **2011**, *124*, 2021–2027.
61. Nagy, I.I.; Railo, A.; Rapila, R.; Hast, T.; Sormunen, R.; Tavi, P.; Rasanen, J.; Vainio, S.J. Wnt-11 signalling controls ventricular myocardium development by patterning N-cadherin and beta-catenin expression. *Cardiovasc. Res.* **2010**, *85*, 100–109. [CrossRef]
62. Zhou, W.; Lin, L.; Majumdar, A.; Li, X.; Zhang, X.; Liu, W.; Etheridge, L.; Shi, Y.; Martin, J.; Van de Ven, W.; et al. Modulation of morphogenesis by noncanonical Wnt signaling requires ATF/CREB family-mediated transcriptional activation of TGFbeta2. *Nat. Genet.* **2007**, *39*, 1225–1234. [CrossRef]
63. Schleiffarth, J.R.; Person, A.D.; Martinsen, B.J.; Sukovich, D.J.; Neumann, A.; Baker, C.V.; Lohr, J.L.; Cornfield, D.N.; Ekker, S.C.; Petryk, A. Wnt5a is required for cardiac outflow tract septation in mice. *Pediatr. Res.* **2007**, *61*, 386–391. [CrossRef]
64. Matsuda, T.; Nomi, M.; Ikeya, M.; Kani, S.; Oishi, I.; Terashima, T.; Takada, S.; Minami, Y. Expression of the receptor tyrosine kinase genes, Ror1 and Ror2, during mouse development. *Mech. Dev.* **2001**, *105*, 153–156. [CrossRef]
65. Yuan, Y.; Niu, C.C.; Deng, G.; Li, Z.Q.; Pan, J.; Zhao, C.; Yang, Z.L.; Si, W.K. The Wnt5a/Ror2 noncanonical signaling pathway inhibits canonical Wnt signaling in K562 cells. *Int. J. Mol. Med.* **2011**, *27*, 63–69. [CrossRef]
66. Takeuchi, S.; Takeda, K.; Oishi, I.; Nomi, M.; Ikeya, M.; Itoh, K.; Tamura, S.; Ueda, T.; Hatta, T.; Otani, H.; et al. Mouse Ror2 receptor tyrosine kinase is required for the heart development and limb formation. *Genes Cells* **2000**, *5*, 71–78. [CrossRef]
67. Nomi, M.; Oishi, I.; Kani, S.; Suzuki, H.; Matsuda, T.; Yoda, A.; Kitamura, M.; Itoh, K.; Takeuchi, S.; Takeda, K.; et al. Loss of mRor1 enhances the heart and skeletal abnormalities in mRor2-deficient mice: Redundant and pleiotropic functions of mRor1 and mRor2 receptor tyrosine kinases. *Mol. Cell Biol.* **2001**, *21*, 8329–8335. [CrossRef]
68. Verkaar, F.; Zaman, G.J. A model for signaling specificity of Wnt/Frizzled combinations through co-receptor recruitment. *FEBS Lett.* **2010**, *584*, 3850–3854. [CrossRef] [PubMed]
69. DeRossi, C.; Laiosa, M.D.; Silverstone, A.E.; Holdener, B.C. Mouse fzd4 maps within a region of chromosome 7 important for thymus and cardiac development. *Genesis* **2000**, *27*, 64–75. [CrossRef]
70. Hamblet, N.S.; Lijam, N.; Ruiz-Lozano, P.; Wang, J.; Yang, Y.; Luo, Z.; Mei, L.; Chien, K.R.; Sussman, D.J.; Wynshaw-Boris, A. Dishevelled 2 is essential for cardiac outflow tract development, somite segmentation and neural tube closure. *Development* **2002**, *129*, 5827–5838. [CrossRef] [PubMed]
71. Hakim, Z.S.; DiMichele, L.A.; Doherty, J.T.; Homeister, J.W.; Beggs, H.E.; Reichardt, L.F.; Schwartz, R.J.; Brackhan, J.; Smithies, O.; Mack, C.P.; et al. Conditional deletion of focal adhesion kinase leads to defects in ventricular septation and outflow tract alignment. *Mol. Cell. Biol.* **2007**, *27*, 5352–5364. [CrossRef]
72. Armstrong, P.B.; Armstrong, M.T. Intercellular invasion and the organizational stability of tissues: A role for fibronectin. *Biochim. Biophys. Acta* **2000**, *1470*, O9–O20. [CrossRef]
73. Burns, T.A.; Dours-Zimmermann, M.T.; Zimmermann, D.R.; Krug, E.L.; Comte-Walters, S.; Reyes, L.; Davis, M.A.; Schey, K.L.; Schwacke, J.H.; Kern, C.B.; et al. Imbalanced expression of Vcan mRNA splice form proteins alters heart morphology and cellular protein profiles. *PLoS ONE* **2014**, *9*, e89133. [CrossRef]
74. Burns, T.; Yang, Y.; Hiriart, E.; Wessels, A. The Dorsal Mesenchymal Protrusion and the Pathogenesis of Atrioventricular Septal Defects. *J. Cardiovasc. Dev. Dis.* **2016**, *3*, 29. [CrossRef]
75. Snarr, B.S.; O’Neal, J.L.; Chintalapudi, M.R.; Wirrig, E.E.; Phelps, A.L.; Kubalak, S.W.; Wessels, A. Isl1 Expression at the Venous Pole Identifies a Novel Role for the Second Heart Field in Cardiac Development. *Circ. Res.* **2007**, *101*, 971–974. [CrossRef]
76. Snarr, B.S.; Wirrig, E.E.; Phelps, A.L.; Trusk, T.C.; Wessels, A. A spatiotemporal evaluation of the contribution of the dorsal mesenchymal protrusion to cardiac development. *Dev. Dyn.* **2007**, *236*, 1287–1294. [CrossRef]
77. Kim, J.S.; Virágh, S.; Moorman, A.F.M.; Anderson, R.H.; Lamers, W.H. Development of the myocardium of the atrioventricular canal and the vestibular spine in the human heart. *Circ. Res.* **2001**, *88*, 395–402. [CrossRef] [PubMed]
78. Tian, Y.; Yuan, L.; Goss, A.M.; Wang, T.; Yang, J.; Lepore, J.J.; Zhou, D.; Schwartz, R.J.; Patel, V.; Cohen, E.D.; et al. Characterization and in vivo pharmacological rescue of a Wnt2-Gata6 pathway required for cardiac inflow tract development. *Dev. Cell* **2010**, *18*, 275–287. [CrossRef]

79. Briggs, L.E.; Phelps, A.L.; Brown, E.; Kakarla, J.; Anderson, R.H.; van den Hoff, M.J.; Wessels, A. Expression of the BMP Receptor Alk3 in the Second Heart Field is Essential for Development of the Dorsal Mesenchymal Protrusion and Atrioventricular Septation. *Circ. Res.* **2013**, *112*, 1420–4132. [CrossRef]
80. Briggs, L.E.; Burns, T.A.; Lockhart, M.M.; Phelps, A.L.; van den Hoff, M.J.; Wessels, A. The Wnt/beta-catenin and Sonic Hedgehog pathways interact in the regulation of the development of the Dorsal Mesenchymal Protrusion. *Dev. Dyn.* **2016**, *245*, 103–113. [CrossRef]
81. van Vliet, P.P.; Lin, L.; Boogerd, C.J.; Martin, J.F.; Andelfinger, G.; Grossfeld, P.D.; Evans, S.M. Tissue specific requirements for WNT11 in developing outflow tract and dorsal mesenchymal protrusion. *Dev. Biol.* **2017**, *429*, 249–259. [CrossRef]
82. Li, D.; Angermeier, A.; Wang, J. Planar cell polarity signaling regulates polarized second heart field morphogenesis to promote both arterial and venous pole septation. *Development* **2019**, *146*, dev181719. [CrossRef]
83. Gunthel, M.; Barnett, P.; Christoffels, V.M. Development, Proliferation, and Growth of the Mammalian Heart. *Mol. Ther.* **2018**, *26*, 1599–1609. [CrossRef]

Publisher’s Note: MDPI stays neutral with regard to jurisdictional claims in published maps and institutional affiliations.



© 2020 by the authors. Licensee MDPI, Basel, Switzerland. This article is an open access article distributed under the terms and conditions of the Creative Commons Attribution (CC BY) license (<http://creativecommons.org/licenses/by/4.0/>).

Review

New Concepts in the Development and Malformation of the Arterial Valves

Deborah J. Henderson *, Lorraine Eley and Bill Chaudhry

Biosciences Institute, Newcastle University, Newcastle upon Tyne NE1 3BZ, UK; lorraine.eley@ncl.ac.uk (L.E.); bill.chaudhry@ncl.ac.uk (B.C.)

* Correspondence: deborah.henderson@ncl.ac.uk

Received: 28 August 2020; Accepted: 23 September 2020; Published: 24 September 2020

Abstract: Although in many ways the arterial and atrioventricular valves are similar, both being derived for the most part from endocardial cushions, we now know that the arterial valves and their surrounding structures are uniquely dependent on progenitors from both the second heart field (SHF) and neural crest cells (NCC). Here, we will review aspects of arterial valve development, highlighting how our appreciation of NCC and the discovery of the SHF have altered our developmental models. We will highlight areas of research that have been particularly instructive for understanding how the leaflets form and remodel, as well as those with limited or conflicting results. With this background, we will explore how this developmental knowledge can help us to understand human valve malformations, particularly those of the bicuspid aortic valve (BAV). Controversies and the current state of valve genomics will be indicated.

Keywords: arterial valve; semilunar; outflow cushion; leaflet; EndMT; second heart field; neural crest cells; signalling; bicuspid aortic valve

1. Anatomy, Histology and Nomenclature of the Mature Arterial (Semilunar) Valves

The aortic and pulmonary valves, which sit within the arterial roots between the myocardium of the left and right ventricular outflow tracts and the aorta and pulmonary trunk, respectively, are structurally similar to one another, and are closely comparable in humans and mice [1–3]. Thus, in the mature heart both the aortic and pulmonary valves have three superficially similar leaflets that form the moving parts of the valve. The right (R) and left (L) sinuses of the aortic valve each host the ostium of a coronary artery, whilst the third non coronary/non-facing/posterior (N) and the three pulmonary valve sinuses are almost never associated with a coronary artery—even in congenitally malformed hearts. However, we now recognise the valve complexes to include more than just the three moving leaflets, with additional components including: the hinges, the attachment points of the leaflets to the wall; the commissures, the points of apposition of the leaflets close to the wall; the sinuses, pockets that form between the leaflets and the wall; and the interleaflet triangles, the regions of the wall that lie upstream (on the ventricular side) of the hinges, but are distal to the base of the sinuses that are found on the arterial side (Figure 1). The nomenclature used to describe the arterial roots is controversial. For example, the outflow tract has been divided by some authors into a proximal conus and a distal truncus, although this terminology is falling out of practice and three rather than two components are increasingly recognised. In this nomenclature, the distal component represents the intra-pericardial arterial trunks and the proximal component comprises the ventricular outflow tracts, with the valve complex appearing in the intermediate part [2]. In other contexts, anatomically artificial “rings” are described for clinically important measurements, although some publications have highlighted the misuse of these descriptions for developmental and anatomical purposes [4,5]. Thus, the development of this highly complex area remains the topic of speculation and controversy.

One longstanding conundrum is, what are the similarities and differences between arterial and atrioventricular valve development, particularly those that relate to their pathology? How does the valve achieve an undulating crown-like attachment, crossing the arterial–myocardial boundary? How do the outflow cushions remodel to form the sculpted valve leaflets? Overall, the question of how aortic valve malformations relate to other cardiovascular malformations, both congenital and apparently acquired, has not been answered. The answer to all these puzzles may lie with the progenitor cells that form the arterial roots. Thus, a re-evaluation of arterial valve development focusing on the second heart field (SHF) and neural crest cells (NCC) may explain the relationships between these different elements and make sense of abnormalities in transgenic animal models and human malformations.

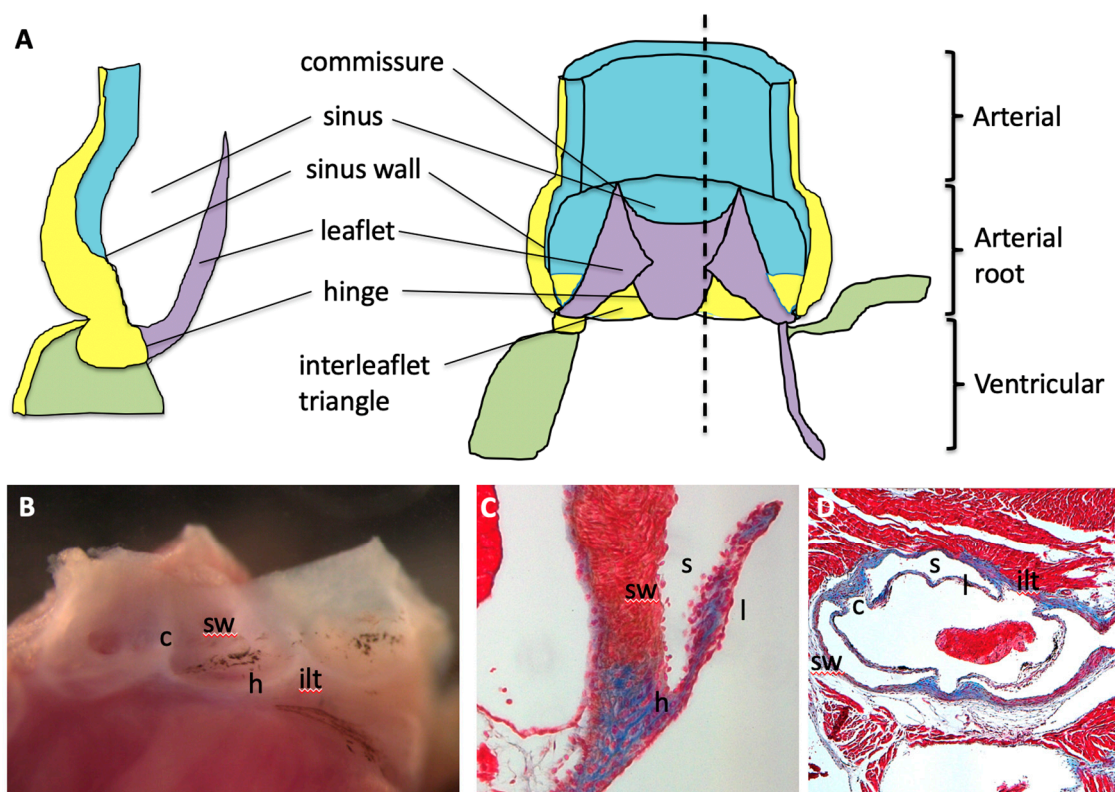


Figure 1. Anatomy of the arterial roots. (A) The arterial valve complex is made up of: three moving leaflets; the hinges, the attachment points of the leaflets to the wall; the commissures, the points of apposition of the leaflets close to the wall; the sinuses, pockets that form between the leaflets and the wall; and the interleaflet triangles, the regions of the wall that lie upstream (on the ventricular side) of the hinges, but are distal to the base of the sinuses that are found on the arterial side. Green = cardiomyocytes, blue = smooth muscle cells, yellow = fibrous tissue, purple = valve leaflet. The dotted line represents the position of the cross section through the valve complex. (B) Wholemout view of the adult mouse aortic root. The leaflets have been removed to allow the view of the other structures of the valve complex. (C,D) Masson’s trichrome images of the mouse aortic root at P21 in longitudinal and transverse planes. Red staining is muscle tissue, blue staining is fibrous tissue. c = commissure, h = hinge, ilt = interleaflet triangle, l = leaflet, s = sinus, sw = sinus wall.

Cre-lox-based lineage tracing technology in the developing mouse has indicated how cells originating in the SHF and NCC are involved in the development of the outflow wall, as well as septal and valve structures. It is clear that the hinges and the leaflets have contributions from both SHF-derived cells and NCC [3,6]. Similarly, above the undulating leaflet hinge, the sinus wall is made up of vascular smooth muscle cells (SMC) that also derive from NCC and SHF. Within the roots, SHF-derived cells predominate, whilst more distally the entire tunica media is of NCC lineage.

In the transition, these progenitors maintain separation as a thinning inner layer of NCC-derived SMC, and a thickening outer layer of SHF-derived SMC [3,7,8]. Proximal to the root, the myocardium is also derived from the SHF. Thus, the supporting structures for the leaflets, the hinge attachments and the interleaflet triangles, the fibroblasts and SMC at the base of the sinus and the subaortic and sub pulmonary myocardium, all arise from SHF progenitors and NCC to a greater or lesser extent. The question of the undulating attachment of the leaflets must be expanded to ask, how do the SHF-derived cells on the arterial side of the hinge become SMC whilst those on the ventricular side become myocardial? Moreover, how do the interleaflet triangles that are found on the ventricular side of the hinge attachments become fibrous, whilst apparently originating from the same SHF progenitors as the SMC within the sinus? Although these questions remain unresolved, it seems likely that local signalling events, rather than patterning within primitive fields of progenitors, are responsible for defining the precise characteristics of specific structures and tissues within the arterial roots.

2. Positioning of the Arterial Valves

The left and right leaflets of the aortic and pulmonary valves, as well as the septal leaflets of the mitral and tricuspid valves, are known to be derived from endocardial cushions. The main aspects of initial formation and positioning are similar for all these cushions, particularly those relating to cellular invasion through the endocardial to mesenchymal transition (EndMT) [9–11]. These endocardial cushions initially appear as expansions of pre-existing extracellular matrix (ECM; cardiac jelly) between the outer myocardium and inner endocardial layer, at approximately embryonic day (E) 9.5 in the mouse embryo (Carnegie stage (CS) 10–11 in the human embryo). In both the outflow tract and atrioventricular canal, the initial positioning of the cushions is regulated by local Bmp signalling and a complex interaction between several T-box transcription factors and Notch signalling (reviewed recently [11]). The expanded cardiac jelly of the outflow cushions is also in continuity with the much thinner layer of ECM that extends proximally towards the ventricular chambers. This can, at least in theory, allow for the movement of the cellular component of the forming cushions relative to the overlying myocardial wall. This slippage may allow for repositioning of the three valve primordia in each arterial root relative to each other and could also provide an explanation of how the undulating line of hinge attachment can later span both myocardial and arterial aspects of the roots.

Whilst Bmp signalling determines the positioning of the forming cushions within the myocardial part of the outflow tract, little is known about how the original circumferential deposition of ECM becomes two longitudinal cushions in the superior–inferior opposition. Our previous studies have suggested that the aggregation of NCC within the outflow tract cushions affects where the discrete outflow cushions will form in the initially circumferential cardiac jelly [12]. It is possible that this localised NCC aggregation could be directed by signals from the surrounding myocardium or endothelium, however, it seems more likely that this is dictated by the physical properties of vortical blood flow through the looping, but as yet unseptated, heart tube. Indeed, it has been shown that shear stress is asymmetrically localised in the outflow wall as the cushions are beginning to cellularise [13]; this could help to position and/or stabilise the cellularising cushions within the circumference of the outflow tract ([12]; Figure 2A). Later, the fusion of these spiralling cushions leads to placing of the root of the aorta to the left of the pulmonary trunk. The deletion of the heparan sulphate proteoglycan perlecan is associated with hyperplastic and malpositioned outflow cushions that ultimately result in transposition of the great arteries in a high proportion of mutant embryos [14]. In this model, the excessive numbers of mesenchymal cells (probably of NCC origin) do not form well defined “ridges” within the cardiac jelly. It can be imagined that this failure to form discrete aggregates of cells within the circumferential cardiac jelly will lead to aberrant positioning of the aorta and pulmonary trunk after septation.

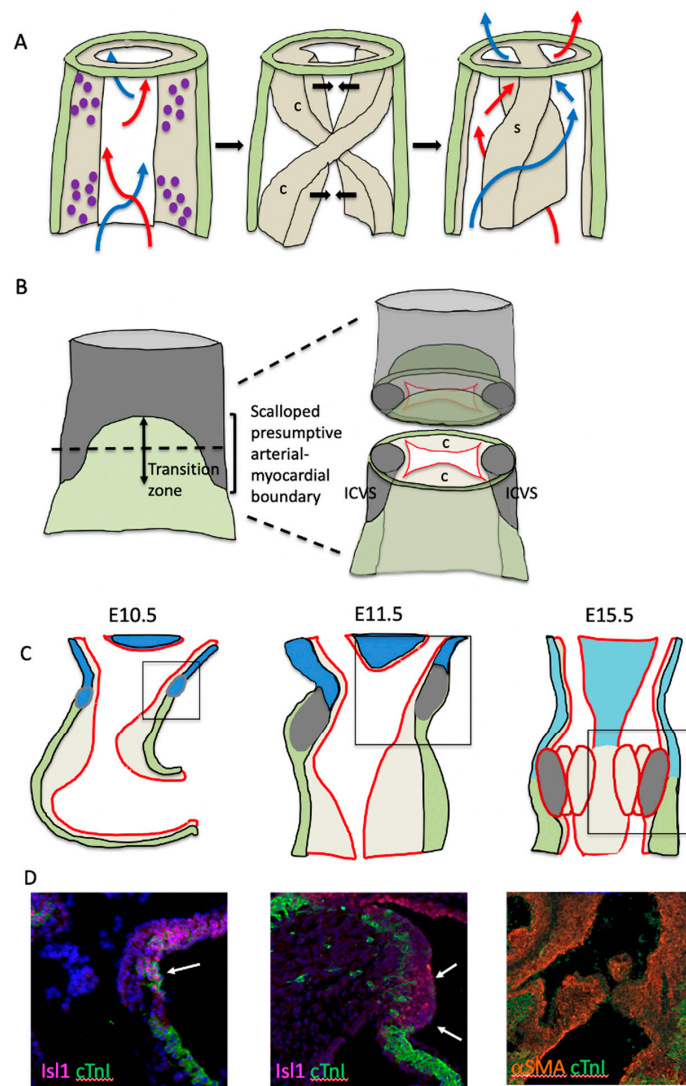


Figure 2. Early outflow tract development. (A) Model representing how flow of blood through the unseptated outflow tract may lead to formation of the spiralling outflow septum. Vortical flow of blood through the outflow tract as the cushions are beginning to cellularise leads to aggregation of these cells (purple dots) in columns that prefigure the spiralling cushions (c). This positions and/or stabilises the cellularising cushions within the circumference of the outflow tract. The ensuing fusion of these cushions leads to formation of a spiralling septum (s) that places the root of the aorta to the left of the pulmonary trunk. (B) The boundary between myocardial and non-myocardial fate is first apparent at 10.5 in the mouse as the transition zone. The cells in this region are transitioning from a progenitor (grey) to a cardiomyocyte (green) fate. However, not all the undifferentiated SHF cells within this boundary region become cardiomyocytes. Two tongues of undifferentiated SHF cells can be seen to extend laterally into the myocardial outflow tract and these form the intercalated valve swellings (ICVS) that are the primordia of the posterior (non-coronary) and anterior intercalated leaflets of the aortic and pulmonary valves. (C,D) The myocardial-non-myocardial boundary is labelled by *Isl1* (pink) and *cTnl* (green) at E10.5, with the cells in the transition zone labelled by both markers (arrow). By E11.5 the ICVS can clearly be seen in the outflow wall, as it continues to express *Isl1* (arrows). By E15.5 the myocardial (green)-SMC (red) boundary at the level of the valve complex is well defined.

3. The Transition Zone and the Arterial-Myocardial Boundary

Initially, the main outflow cushions are completely contained within the SHF-derived myocardial part of the outflow tract [15]. However, at E10.5, SHF cells continue to add to the outflow tract

and, although they initially remain undifferentiated, will later form SMC [3,15,16]. This produces a histologically defined arterial–myocardial junction within the aortic root. Thus, the defining process in the formation and positioning of the aortic root may be the switch from differentiation of the SHF progenitors to cardiomyocytes proximal to the boundary, to SMC distal to the boundary (Figure 2B–D). This boundary between myocardial and non-myocardial fate is first apparent at E10.5 in mice, as a region we named the transition zone [17]. The transition zone does not have an anatomical identity but is identified as a region with cells that express the SHF-specific transcription factor *Isl1*, but at the same time co-express differentiated cardiomyocyte markers. Thus, cells in this region are transitioning from a progenitor to a cardiomyocyte fate. Above the transition zone, the SHF progenitors are in continuity with similar cells in the dorsal pericardial wall and will later downregulate *Isl1* expression; the majority of these will go on to form the arterial SMC of the aorta and pulmonary trunk. However, not all the undifferentiated SHF cells within this boundary region become cardiomyocytes. At E10.5 (CS12 or around 28 dpc in human), two tongues of undifferentiated SHF cells can be seen to extend laterally into the otherwise myocardial outflow tract ([15,18]; Figure 2B). By E11.5, these non-myocardial extensions, surrounded laterally by cardiomyocytes, form the intercalated valve swellings (ICVS; sometimes erroneously called the intercalated cushions—see later) and are the primordia of the posterior (P) aortic (non-coronary) and anterior (A) pulmonary intercalated leaflets [1,19,20]. The origin and remodelling of these ICVS to valve leaflets will be discussed in more detail later, but it is important to emphasise that their localisation within the wall, at the boundary between the myocardial and presumptive-arterial parts of the outflow tract, is unlikely to be coincidental to the remodelling of the main outflow cushions and may play an important role in defining the position of the arterial valve complex.

4. EndMT and Cushion Formation

The process of endocardial cushion mesenchyme formation has been reviewed extensively [10,11,21–23]. There is evidence from numerous sources that the outflow endocardium is derived from the second heart field (SHF). Thus, in lineage tracing studies utilising the “SHF-specific” *Isl1-Cre* and *Mef2c-AHF-Cre* mouse lines, outflow cushion endocardium and mesenchyme is labelled [24,25]. This contrasts with the atrioventricular endocardium where only a few cells are labelled by these SHF-specific Cre lines [6]. It remains to be seen whether there are significant implications of this different origin or whether, in practice, origin is of less importance than specification to undergo EndMT. EndMT initially occurs in the proximal outflow cushions, with only limited EndMT-derived mesenchyme observed within the distal cushions until after E11.5 [26,27]. Thus, EndMT-derived cells are not initially found in the region of the outflow cushions where the valves will form. The endocardium overlying the valve primordia expresses *Nfatc1*, which is important for valve development [28–30]. There appears to be two roles for *Nfatc1* in valve formation, playing an early role in initiating EndMT and then a later role in valve remodelling [30]. Cells labelled by *Nfatc1-Cre* (in which the *Nfatc1* has ever been active) remain in the endocardium and do not undergo EndMT [27]. Targeted deletion of *Nfatc1* in the endocardium results in an over-abundance of EndMT-derived cushion mesenchyme in the proximal outflow tract cushions at E10.5, and an extension of these cells into the distal region [27], perhaps indicating that EndMT continues unchecked in the absence of *Nfatc1*. The observation that the arterial valve leaflets later appear under-developed in the mutant embryos [28–30] seems counter-intuitive, but it may be that appropriate interactions between EndMT-derived cells and NCC are essential for leaflet remodelling, and that if this balance is disrupted, underdeveloped leaflets result. Many other signals that induce or repress EndMT of endocardial cells have now been described, including the Notch, BMP and TGF β signalling pathways [31–34]. For example, the Nf1/Ras pathway has also been implicated in repressing EndMT in the outflow and atrioventricular cushions [35–37], with exacerbated Ras signalling leading to hyperplastic cushions.

Although EndMT-derived cells are not initially found in the distal outflow cushions, by E12.5 they are abundant in the forming leaflets [12,26,38] and are maintained in the postnatal valves (Figure 3A,B). These endocardial-derived cells (EDC) seem to play a crucial role in regulating the growth and

remodelling of the cushion. There seems to be a functional difference between early endocardium and the *Nfatc1*-expressing late valve endocardium regarding Notch signalling. The loss of Notch signalling from the endocardium before EndMT results in grossly hypoplastic cushions and early death. However, if this stage is bypassed, perhaps by using *Nfatc1-enCre* (valve endocardium-specific [27]) rather than *Tie2-Cre* (all endocardium and endothelium [39]), or by deleting a Notch ligand that is only active in the endocardium after EndMT (e.g., [40]), then thickened arterial valve leaflets are the usual result. Recently, it has been suggested that some macrophages in the late foetal and postnatal valve mesenchyme are derivatives of the endocardium [41]. However, it remains unclear whether other EndMT-derived cells in the interstitium play specific roles within the adult valve.

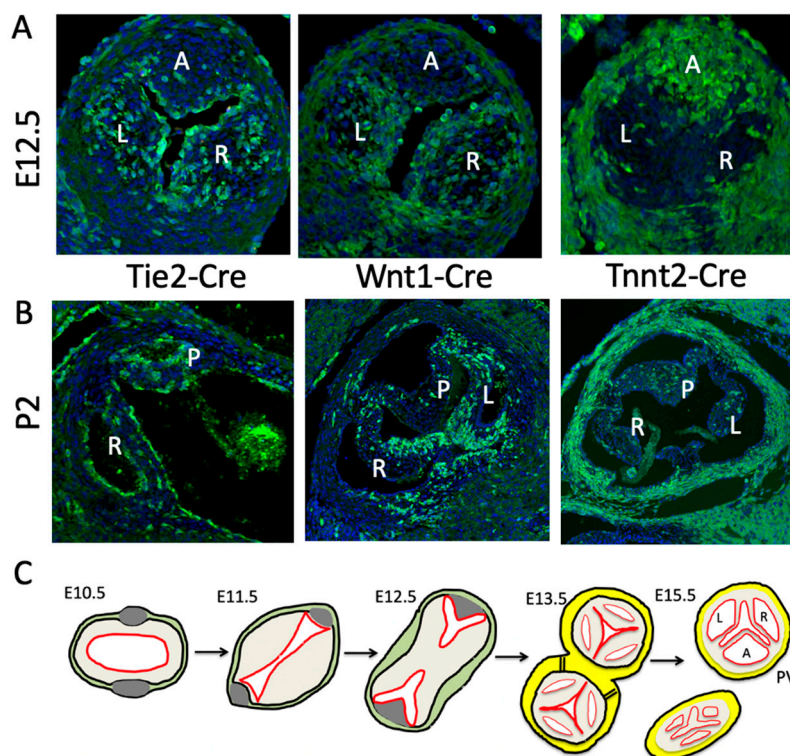


Figure 3. Lineage tracing of cells in the foetal and neonatal arterial valves. (A) At E12.5, *Tie2-Cre* labelled endocardial-derived cells, *Wnt1-Cre*-labelled NCC and *Tnnt2-Cre* labelled cells derived directly from the SHF, via the outflow wall, are found within the pulmonary valve leaflet primordia. Whilst *Tie2-Cre* and *Wnt1-Cre*-labelled cells are most abundant in the left (L) and right (R) leaflets, the *Tnnt2-Cre* labelled cells are the most abundant in the anterior (A) leaflet derived from the ICVS. Similar observations are made for the aortic valve (not shown). (B) At P2, each of the three lineages of cells are maintained within the leaflets of the aortic valve. As at E12.5, *Wnt1-Cre* and *Tie2-Cre* labelled cells are most abundant in the L and R leaflets, whilst *Tnnt2-Cre* labelled cells are most abundant in the posterior (P) leaflet derived from the ICVS. Similar observations are made for the pulmonary valve (not shown). (C) Cartoon illustrating how arterial valve leaflet formation is intimately linked to outflow tract septation. At E10.5, the forming endocardial cushions (buff coloured) are circumferential within the outflow vessel and the ICVS (grey) can first be seen within the outflow wall (green). By E11.5 the endocardial cushions (buff) have expanded and are coming together to fuse in the midline. Fusion of these cushions separates the outflow tract and gives rise to the L and R valve primordia. The ICVS give rise to the A and P valve primordia. By E13.5 the aortic and pulmonary valve are distinct, and the sinuses are beginning to appear. At E15.5, valve sculpting is almost complete, and the aorta and pulmonary valves are offset. Green = myocardium, yellow = SMC, red = endocardium.

5. Neural Crest Cells, Outflow Tract Septation and Valve Development

Outflow tract septation is intimately involved in arterial valve formation through shared cells, cushions and timing of events. Analysing human embryos, Kramer [19] showed that the fusion of the main outflow cushions (at around CS 12–13 or ~30 dpc in human embryos, corresponding to E11.5 in the mouse embryo) produces the precursors of the right and left leaflets of the forming arterial valves, with the parietal main outflow cushion contributing to the left leaflets of the aortic and pulmonary valve, and the septal leaflet contributing to the right leaflets (see Figure 3C). The fusion of the main cushions separates the channels of the aorta and pulmonary trunk and subsequent separation of the aorta from the pulmonary trunk in a plane perpendicular to the line of cushion fusion, results in the formation of two, free-standing arterial trunks with their distinct valves. This corresponds well with what is seen in the mouse embryo (Figure 3; [12]). This septation is dependent on NCC and cannot occur if there are significantly reduced numbers within the outflow cushions [42].

A great deal is known about NCC and their developmental roles outside the heart. NCC are a population of progenitor cells that arise in the dorsal neural tube and migrate throughout the body to contribute to a variety of cell types and organ systems, including the heart [43]. There is an extensive literature reviewing the processes of NCC induction, migration and differentiation (for example [44–46]) and these will not be considered further here. In contrast, although there have been many studies that have shown that NCC are critically required for outflow tract septation, their roles in heart development are relatively poorly understood and there have been only limited studies in recent years (reviewed in [47–49]). NCC migrate through the pharyngeal arches and first appear in the cardiac jelly of the distal outflow cushions early on E10 of mouse development (CS11 in human). At this stage, the distal outflow cushions are acellular, as although EndMT is initiating in the outflow cushions, this occurs in the proximal region. NCC that remain in the pharyngeal region rapidly differentiate into SMC and in doing so stabilise the nascent endocardial tubes that will become the pharyngeal arch arteries [50–52]. In contrast, the NCC entering the outflow cushions initially remain relatively undifferentiated (do not express for example α SMA or SM22 α ; [3]) and retain their expression of early NCC markers including *PlexinA2* and *Ap2 α* [53,54]. The main function of these NCC appears to be to provide bulk to the distal cushions, causing them to come into sustained contact, and permitting fusion, with each other and the dorsal wall of the aortic sac [15]. This fusion event initiates outflow tract septation and separates the systemic (aortic) and pulmonary circulations. Once septation is complete, the majority of the NCC in the proximal cushions die by apoptosis [55] and are replaced by ingrowth of myocardial cells to form the muscular subpulmonary infundibulum [56,57]. It has been suggested that the NCC might be involved in defining the position of the arterial valves, as at E11.5, NCC are restricted to the distal cushions and appear to form a boundary with the EndMT-derived mesenchymal population in the proximal region [27]. However, this is a transient boundary, as by E12.5, NCC are found throughout the outflow cushions, apart from their most proximal tips [15,52]. Whilst the role of NCC in the proximal outflow tract appears to be a transient one, the NCC make a permanent contribution to the arterial valve complex, contributing to the fibroblast-like cells found within the commissures, interleaflet triangles and the leaflets of the valves (Figure 3A,B; [3]). How the NCC-derived cells in these different components of the valves differ from one another remains unclear, and they may have more similarities than differences. Unfortunately, there is no mechanism currently to specifically disrupt the NCC that contribute to the valve leaflets, leaving those that are involved in other structures within the arterial roots, or those required for septation, intact. Thus, we do not know for certain if loss of these cells, in the setting of normal outflow septation, would disrupt valve formation and/or remodelling.

6. Direct Differentiation of SHF Progenitors into Valve Mesenchyme

The intercalated leaflet valve swellings (ICVS), the precursors of the anterior/posterior leaflets, were first noted by Kramer [19] and are seen clearly in cross sections through the outflow tract as lateral bulges within the outflow wall ([20]; Figures 3 and 4). Importantly, although they are overlaid by a thin layer of ECM, the bulk of these structures is completely distinct from the main endocardial

cushions and, at their first appearance at E10.5, they do not contain ECM or form by EndMT. Nor do they contain significant numbers of NCC [12,20,58,59]. Lineage tracing studies have shown that the majority of the cells contained within the ICVS are derived from the SHF [20,59], with much smaller contributions from EndMT or NCC than are seen for the main endocardial cushions [12,20,58,59]. Although in some ways they have similarities to the lateral cushions that form the mural leaflets of the mitral and tricuspid valve [20], they do not contain cells derived from the epicardium. Thus, they are distinct from other valve-forming structures within the developing heart. Although the ICVS are continuous with the outflow wall at E10.5–E11.5, they do not label with cardiomyocyte markers and are instead immuno-labelled with antibodies specific to Isl1. Whilst maintaining this progenitor-phenotype, they begin to express Sox9, a characteristic marker of cushion mesenchymal cells [60], and thus differentiate to this fate without passing through the endocardial lineage during EndMT. The conclusion from this is that the ICVS are not endocardial cushions and that the cells within them differentiate directly from the SHF [20]. The confusion arises because although these ICVS arise from the outflow wall and their early formation is entirely distinct from the main outflow cushions [20,58], they rapidly take on the superficial appearance of endocardial cushions by generating large amounts of ECM and expressing typical cushion markers such as Sox9 [20]. Hence, by E12.5 they are almost indistinguishable from other cellularised valve primordia originating from endocardial cushions. Thus, after septation it is reasonable to call them “intercalated cushions”. However, subtle differences remain, for example, the ICVS are more cell-dense and express tropoelastin which the primordia derived from the main cushions do not (Eley, Chaudhry, Henderson; unpublished data). As well as having distinct origins, the ICVS also appear more distally than the right and left cushions, although later remodelling places all the leaflets within each root on their own orthogonal planes. Despite these later similarities, the undifferentiated SHF cells that form the ICVS can still be recognised as they are labelled by the “myocardial-specific” *Tnnt2-Cre* transgenic marker ([20,58,61]; Figure 3A,B). Despite this they are not transdifferentiated cardiomyocytes (they never at any point express markers of differentiated cardiomyocytes) but at a very early stage activated the promoter used to produce the *Tnnt2-Cre* transgene. Whilst the *Tnnt2-Cre* line is therefore extremely useful for following the ICVS cells, it is important to recognise that if it is used to drive Cre in the myocardium, there could also be direct effects on arterial valve development.

Although the mechanisms underpinning the formation of the ICVS have only recently been elucidated, we do have some ideas about the molecular mechanisms that are likely to be involved as there are several mouse mutants where the non-coronary leaflet is missing or hypoplastic. This includes mice null for *Tbx1* [62], *Alk2* [63], *Robo1/2* [64] and when *Vangl2* is knocked out specifically in the developing SHF [20]. Of particular interest, Notch1-ICD and Jag1/2 are localised within the ICVS during its formation at E10.5–E11.5 [20], in a pattern that suggests that Notch signalling may play an important role during their development. Although it is clear that Notch signalling is important in valve development in general, there is also specific evidence that it is important in the developing ICVS. Knockout of *Jag1* and *Jag2* in the developing ICVS using *Tnnt2-Cre* results in defects in the formation of the ICVS that result in a dysplastic or missing non-coronary leaflet of the aortic valve (and to a lesser extent the posterior leaflet of the pulmonary valve; [20]). Thus, there appears to be a specific signalling network acting within the ICVS to bring about direct differentiation of SHF cells to valve mesenchyme; this network utilises Notch signalling.

In summary, it seems that NCC and SHF-derived cells (both via direct differentiation and transitory passage through the endocardial state) are crucial to the formation of arterial valve primordia, although their roles in these processes may be complimentary rather than overlapping. Further work will be needed to better define these specific requirements and roles.

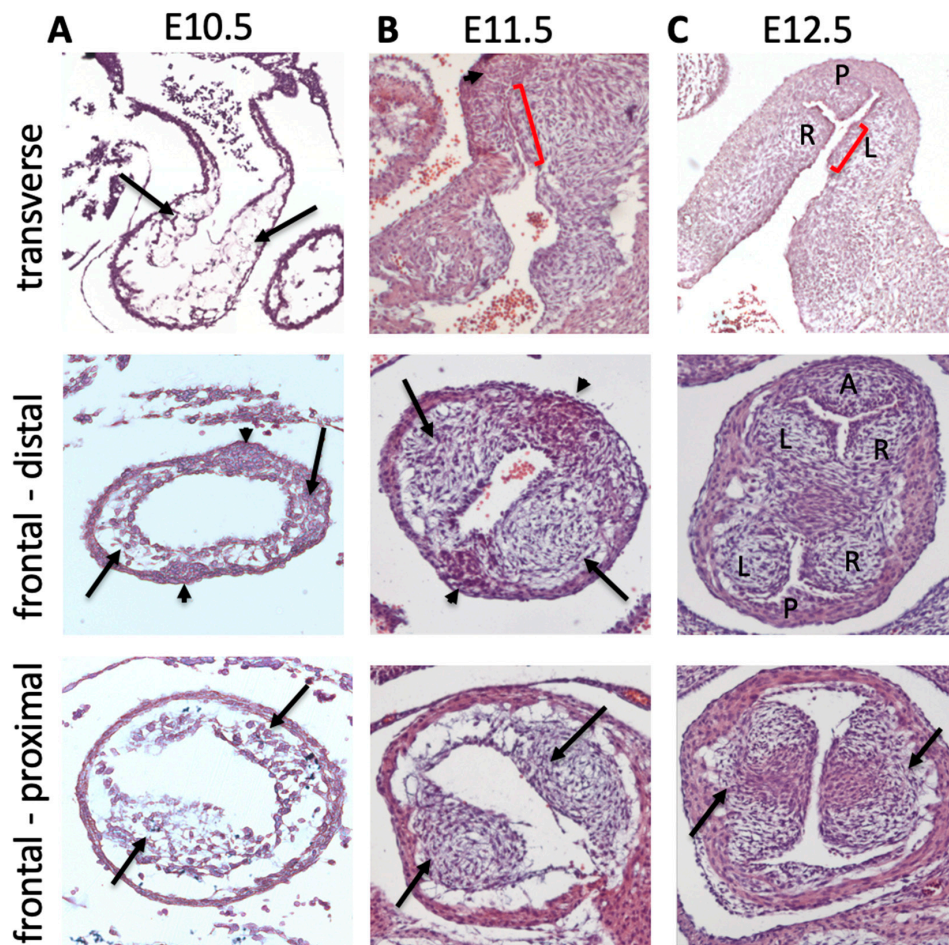


Figure 4. Contributions of the cushions and ICVS to the arterial valve primordia. Histological sections of mouse hearts stained with H&E. (A) At E10.5 the outflow is unseptated. The cushions (arrows) are forming and can be seen to extend along the length of the outflow tract in transverse view and to be circumferential in both the distal and proximal regions, in frontal view. The ICVS cannot be seen in transverse sections at this stage, but in frontal sections can be seen distally as cell dense regions within the outflow wall (arrowheads). (B) By E11.5, the cushions are more cell dense and in transverse sections the valve forming part (red bar) can be seen to be distinct from the proximal part of the cushions that will form the sub-pulmonary infundibulum in transverse sections. The ICVS (arrowhead) can now be seen adjacent to the valve-forming parts of the cushions. In frontal sections the main cushions (arrows) are coming together towards the midline of the outflow tract in the distal region. The ICVS (arrowheads) have expanded but are still continuous with the outflow wall. More proximally, the cushions (arrows) are still widely separated. (C) By E12.5 the outflow tract has septated and the primordia of all three leaflets are apparent in transverse and frontal views. The proximal region of the outflow tract remains unseptated at this time point, although the cushions (arrows) are beginning to come together. A = anterior leaflet; L=left leaflet; P = posterior leaflet; R = right leaflet.

7. Cushion Expansion to Form Arterial Valve Primordia

The period between E10.5 and E12.5 is crucial for the appearance of discrete arterial valve primordia that remodel at the distal end of the outflow cushions, distinct from the septal components that form from the proximal cushions (Figure 4). Although the factors that regulate this process remain unclear, the presence of the transitional tissues at the myocardial–arterial boundary, or indeed the formation of the ICVS adjacent to the main cushions, may be significant. Thus, it is possible that unique factors within the boundary region influence the development of the adjacent cushion tissue to

become valve-like, whilst the more distant proximal cushion acquires a septal phenotype, becoming muscularised by cardiomyocytes migrating from the enveloping myocardial outflow wall [56,57]. The resolution of this point will require further investigation.

Once the relevant progenitor lineages have contributed cells to the mesenchyme by late on E10.5, they undergo a period of proliferation that results in rapid cushion growth. A number of molecules are implicated in this process, most of which affect both the atrioventricular and outflow regions. These include *Vegf* and FGFs (particularly FGF4) which are major drivers of cushion mesenchyme proliferation [65–68]. Other genes negatively regulate cushion mesenchyme proliferation, for example, EGF plays an important role in limiting proliferation in the cushion mesenchyme, with mice hypomorphic for the EGF receptor having increased mesenchymal cell numbers and enlarged arterial valve leaflets [69]. Similarly, *Jag1*, a Notch ligand, also appears to limit cushion mesenchyme proliferation [40]. Thus, too much [35–37,70], or too little (for example [71,72]) cell division is associated with defects in the leaflets as development proceeds.

As well as increasing cell numbers, the ECM matures and increases in complexity as the cushions expand. Knockout of the ECM components found in the remodelling cushions, such as versican, frequently result in acellular cushions (e.g., [73,74]) as these molecules are required for cushion formation as well as remodelling. Thus, it will take more nuanced approaches to reveal the specific roles for these molecules in the latter stages of cushion development and maturation. However, mouse embryos lacking *Adams5*, which is required for versican cleavage, have grossly hyperplastic arterial valves (interestingly the pulmonary valves are most affected) due to the accumulation of uncleaved versican that, as well as increasing the ECM component, also results in increased mesenchymal cell numbers, with abnormalities seen as early as E12.5 [75]. Thus, along with its early role in supporting EndMT, versican also appears to be important for remodelling of the cushion/valve mesenchyme.

Recently, there has been much interest in the potential role of cilia in the development and maintenance of valve leaflets, largely because of the association between mutations in cilia-associated genes and valve defects (e.g., [76]). Primary cilia are small projections of membrane with a microtubule core that are implicated in cell signalling and mechano-sensation [77]. There is considerable evidence to show that the presence of cilia is temporally and spatially regulated during valve formation, and that although they are rarely found on the surface of endocardial cells, they are found on almost all cushion mesenchyme cells at mid gestation [78]. Cilia numbers decrease on the cushion mesenchyme from E11.5 onwards, declining to around 15% of adult VIC [78]. Although the reasons for this decline are not clear, it may be related to differentiation, as in a variety of cell types, cilia are required for this process [79]. The loss of cilia from the EndMT-derived component of the cushion mesenchyme (using *Nfatc1-Cre* to delete *Ift88*) resulted in dysplastic aortic valves, with an enlargement of the hinge region between the leaflets suggestive of BAV, and over-expression of ECM molecules including versican and collagen I [78]. Although it is unclear when or how the BAV arose, this suggests that cilia regulate ECM production or turnover in the developing valves and may play a similar role in the adult. This is supported by other studies that have shown that defects in cilia can lead to mitral valve prolapse, a disease where myxomatous degeneration is a characteristic feature [76]. It is not clear whether a specific subset of VIC retain a cilium in the adult valve, although it is interesting to speculate that these cells are the ones that are activated in response to stress. Absence from the valve endocardium suggests that their role is unlikely to be related to the detection of shear stress.

8. Valve Sculpting

Over the remaining days of foetal and early postnatal life, the bulky, primitive valve precursors are sculpted into thin fibrous leaflets, connected to the vessel wall by hinges that delineate the sinuses (Figure 1). These sculpting stages of arterial valve development remain the least well understood but may be the most relevant to human disease. Recent studies generally refer to a process of valve elongation or lengthening that is required to produce well-functioning and coapted leaflets [11,80–82]. However, by E11.5 in the mouse heart, before the outflow tract has septated and the cushions have

remodelled to form distinct valve primordia, the outflow cushions cyclically occlude the outflow tract [83], allowing only unidirectional flow of blood. Thus, the valve leaflets do not need to lengthen in order to coapt (and thus function efficiently) when the valve is closed. This suggests that lengthening of valves may not be necessary, but that maintaining the overall proportions of valves during growth and enlargement of this area may be more important. The molecular mechanism(s) underpinning sculpting of the arterial valve leaflets have not been described in detail although there are some hypotheses, with varying amounts of supporting data. One hypothesis suggests that cushion mesenchyme is removed close to the wall, by a process of cell death. High levels of apoptotic cell death have been reported in the developing outflow cushions [84–88] and removal of cushion tissue by cell death in order to refine their shape continues to be an attractive model for leaflet sculpting (Figure 5). However, apoptosis has not been described in the sculpting arterial valve leaflets, although detailed studies are lacking. In contrast to cell death, phagocytosis (cell engulfment), carried out by macrophages derived from the endocardium, plays an essential role in remodelling the mature leaflets and in their absence, the leaflets become dysplastic [41]. Thus, the targeted removal of cushion mesenchyme and/or turnover of mature interstitial cells may be an important component of leaflet sculpting and homeostasis. Alternative mechanisms of leaflet sculpting have been suggested. Early investigations, before the era of molecular biology, utilised electron microscopy to show that there is ingrowth of a thickened endocardium into the outflow cushion mesenchyme in both chicken and mouse embryos (from approximately E12.5; [89,90]). Furthermore, it was suggested that this ingrowth is associated with cell death of endocardial cells, although the data to support this was minimal. The valve endocardium expresses a number of signalling molecules including Fgfs, Wnts and Hh [68,91,92] and similarities have been drawn with the apical ectodermal ridge that acts as a signalling centre for limb bud outgrowth [22]. These signalling molecules may modify proliferation, differentiation and/or cell death within the underlying cushion mesenchyme, thereby regulating the process of valve leaflet formation and sculpting. Although there have been no detailed studies of how the valve sinuses form since those of Hurler, 40 years ago [89,90], it seems possible that their formation is intimately linked with leaflet sculpting, as the cavity of the sinus takes up much of the space previously occupied by cushion tissue (Figure 5). Whatever the cellular mechanism, high resolution electron microscopy (HREM) has revealed that the first indications of cushion excavation to form the sinuses are apparent late on E12.5 of mouse development [2], and that the part of the valve primordium closest to the muscular walls of the arterial root excavates, whilst the part closest to the lumen is retained as the valve leaflet. As the gradual excavation of the sinus simultaneously results in the free (lumenal) edge of the valve leaflet getting longer, this may explain why the valve has been interpreted as lengthening as it remodels (Figure 5).

Although the precise mechanisms are unclear, evidence from the zebrafish and chicken embryo suggest that haemodynamic forces play an important part in the morphogenesis [93] and remodelling of cushions to form sculpted valve leaflets [94–97]. In the absence of normal blood flow through the heart, either as a result of reduced contractility, disturbed flow resulting from anatomical alterations, or the absence of molecules that sense the flow and send signals that lead to a change in cell/tissue behaviour, the cushions remain bulky, are malpositioned and the leaflets do not remodel properly. Although a detailed discussion of this topic is beyond the scope of this manuscript, there have been several excellent reviews published recently (for example, [98,99]). These have highlighted the importance of shear stress in sculpting the leaflets and have shown that mechanosensors in the valve endocardium activate the transcription *Klf2*, which brings about the cellular changes involved in valve sculpting via a Wnt signalling cascade [94,100]. For example, *Piezo1*, a mechanosensor, has been implicated in valve sculpting [101]. In the absence of this mechanosensory signalling cascade, the cushions fail to remodel appropriately resulting in dysplastic leaflets. It should be noted that as the mechanisms underpinning valve sculpting remain unclear, the details of how shear stress brings about this remodelling are correspondingly poorly defined.

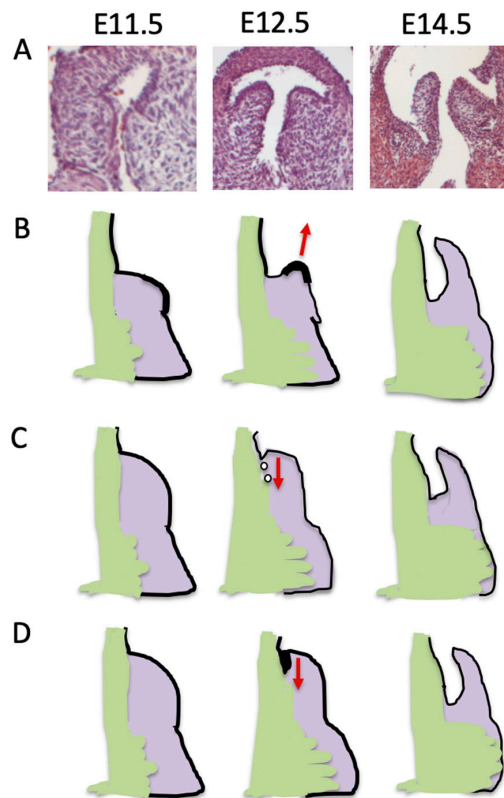


Figure 5. Models of valve sculpting. (A) Histological images showing how the leaflet sculpts from a bulky cushion at E11.5, to a well-defined leaflet by E14.5. (B) The leaflet elongation model proposes that under the influence of factors secreted by the thickened valve endocardium, the leaflet actively elongates to acquire its sculpted form. (C) In the second model a process of cell death removes cushion tissue at the boundary with the outflow wall and in this way excavates the sinus, leading to freeing of the leaflet. (D) In the final model, the endocardium bends into the cushion tissue and in so doing creates the sinus, again freeing the leaflet. Experimental evidence is minimal for each of the three models and further work is needed to determine which, if any, are accurate.

9. Maturation of the Arterial Valve Leaflets

Mature valve leaflets contain valvular interstitial cells (VIC) that are derivatives of the cushion mesenchyme. These VIC form three cellular layers, characterized by distinct ECM profiles: the fibrosa (on the arterial side of the leaflet) composed mostly of collagens; the spongiosa made up mostly of proteoglycans; and the ventricularis, which contain elastin fibres. The leaflets are also covered by a specialised endocardial layer (valve endocardial cells; VEC) [80]. This stratification of the valve into its three layers occurs relatively late, first becoming apparent at approximately E16.5 of mouse development [80], at the end of the first trimester in human embryos. Initially, collagens and proteoglycans, including versican, hyaluronan and perlecan [14,102,103] are widespread in the developing cushions. Elastin, in contrast, is found only at low levels in the valve leaflets before birth in the mouse heart (Henderson; unpublished data), although it has been shown to be present by Hamburger and Hamilton stage 30 in the chicken embryo ([104]; equivalent to approximately E13.5 in the mouse) and as early as 7 weeks of gestation in developing human arterial valves [105]. However, after birth, elastin is markedly upregulated in mammalian valves and it is well recognized that remodelling of the ECM continues into postnatal life [80]. Recently, the relationship between the three layers of extracellular proteins and subgroups of VIC has begun to be elucidated [106]. Thus, subpopulations of VIC that express high levels of fibrillar collagen, as well as other genes known to be involved in fibril organisation and ECM maturation have been identified at postnatal day 7 in the

mouse heart. Similarly, VIC expressing high levels of glycosaminoglycan-containing proteins including versican, fibulin-2 and lumican, have been identified at the same stage [106]. Surprisingly, elastin was expressed by both subgroups, but a specific elastin-rich subgroup of VIC was not identified. Indeed, there is a disconnection between the initial lineage of VIC and those in mature valves. Whilst mouse studies have shown that the distinct embryonic lineages that give rise to VIC are differentially localised within the foetal and postnatal valves [3,12,107], this has not yet been mapped in the adult valve and it remains unknown how the subgroups of VIC identified on the basis of their transcriptome [106] correspond to the different lineages, or to different disease states. It is possible that distinct embryonic lineages may predispose to disease and this is supported by the observation that when only one of the three leaflets is thickened, it is usually the non-coronary [108], suggesting that its different origin may predispose it to disease in some scenarios. However, studies where the three valve leaflets are examined separately are rare. Current evidence leads us to believe that there are distinct groups of VIC (potentially with distinct origins) with differing roles and susceptibilities to disease, but there may be a significant degree of overlap between these factors. Whilst all three lineages (EndMT-derived, NCC and directly differentiated SHF-derived cells) are retained into postnatal life [12,20,39,43,109], cells derived from the bone marrow—largely macrophages and dendritic cells—are mostly found in the valve leaflets postnatally, expanding to make up almost 20% of cells in the valve mesenchyme by a few weeks after birth [110–112]. Other studies have suggested that some macrophages in the valve interstitium are derivatives of the endocardium and that these cells appear to be more phagocytic than those derived from the bone marrow [41]. In healthy, mature valve leaflets, the VIC are generally quiescent with only a low level of cell turnover. These cells maintain normal valve structure and function and express a variety of markers that place them within the phenotypic spectrum of fibroblasts (although they are distinct from fibroblasts in other tissues). Similarly, the endocardial and immune cells found in the arterial valves appear to change little in the first few weeks of postnatal life. However, in response to disease or injury, a subpopulation of these apparently quiescent VIC can be activated to take on features of myofibroblasts. This activation occurs in response to signalling factors such as TGF β which rapidly results in the formation of stress fibres and alignment, leading to increased contractility and increased mechanical stress. This may be the first step in a pathway that ultimately leads to gross remodelling of the valve matrix and valve disease. In diseased valves, some VIC begin to differentiate into osteoblasts to promote calcification of the leaflets. The transcriptional and signalling factors underlying this transition have been reviewed in detail [80,113]. However, the lineage of these VIC has not yet been determined. It is equally possible that different lineages have specific functions, or conversely, that there are no functional differences between them, with each are as likely as any other to remain in the mature valves.

10. Mechanisms Underpinning BAV

Congenital malformations of arterial valves include valve leaflet dysplasia, in which the leaflets are typically thickened and/or shortened, and valves with abnormal numbers of leaflets, including unicuspid, bicuspid and quadricuspid variants [114,115]. In all cases, the valves are predisposed to stenosis and/or regurgitation and degeneration in later life. Clinical series from the U.S. and Europe have suggested a common left-right leaflet (LR) occurs in about 85% of non-syndromic BAV cases [116,117]. However, studies from South Korea and Japan suggest that the LR pattern may be found in less than 60% of Asian patients [118,119]. Common left/non-coronary (LN) leaflets are rare in any population. Recent studies have suggested that genetic syndromes can be associated with different patterns of leaflet fusion. For example, Down's syndrome is associated with a common RN leaflet, whilst Turner and DiGeorge syndrome with a common LR leaflet [120]. Together, all this evidence suggests that there is likely to be a strong genetic element to leaflet patterning. A well-recognised feature of bicuspid valves is the presence or absence of a raphe, presumed to represent a fusion seam, which in some cases is associated with a notch or an asymmetry suggesting a third leaflet formed

during development, but fused with one of the others. Although it is commonly stated that 85–90% of BAV have a raphe [116,117], recent studies suggest as many as 25% may have no raphe [121].

Numerous mechanisms to explain development of BAV have been proposed (Figure 6A) over the last century [122–127]. These include excessive cushion/leaflet fusion, failure to form the main cushions, abnormal outflow tract septation, and the absence of one of the leaflet primordia, primarily the ICVS that will form the non-coronary leaflet. Although many of these suggestions were made decades before developmental molecular genetics existed, these potential mechanisms remain and there is evidence for each of them as potential mechanisms for BAV in the literature today.

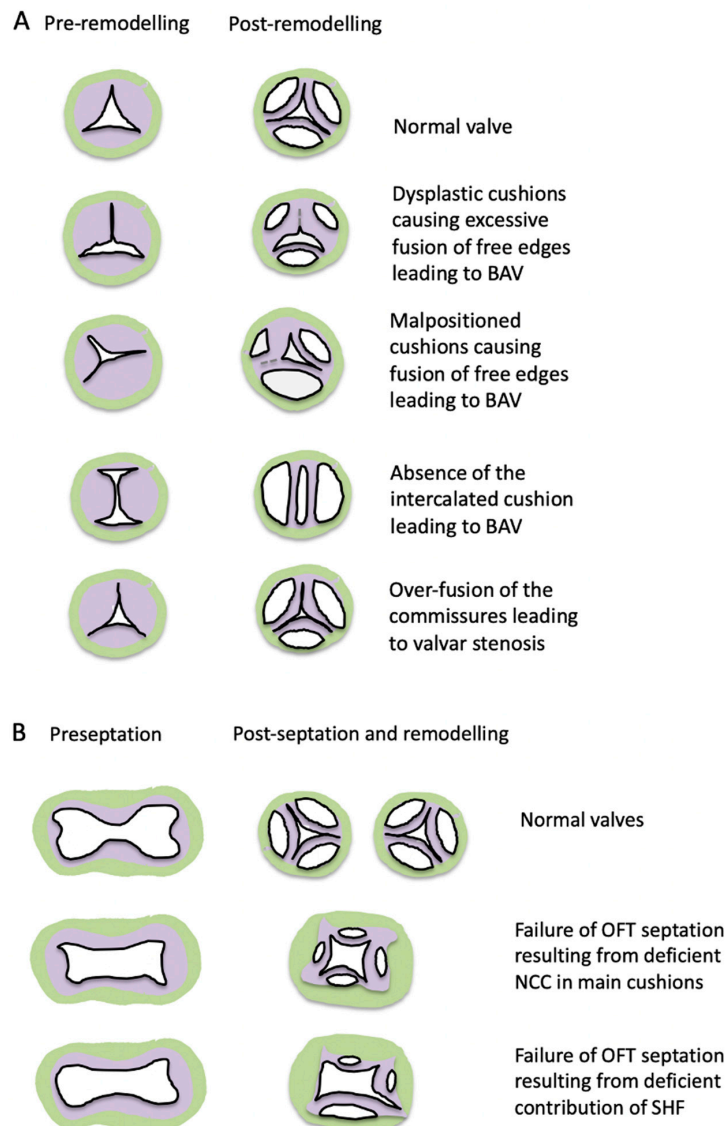


Figure 6. Possible mechanisms underlying THE bicuspid aortic valve BAV. **(A)** Cartoon illustrating several possible mechanisms underlying BAV in the situation of outflow tract septation. These can result in different numbers of sinuses and raphe and can occur early in development (as shown) or later in development as a consequence of pathological processes. Valvar stenosis could also be caused by over fusion of the cushions, at the commissures. **(B)** Cartoon illustrating possible valve outcomes when outflow septation fails. In the case of the proposed situation where the SHF is deficient, the numbers of leaflets can be highly variable, possibly depending on the extent of deficiency.

11. Hyperplastic Cushions/Leaflets and Excessive Fusion

Whilst we now know that severe disruption of EndMT results in acellular or severely hypoplastic cushions and embryonic death in mid development (e.g., [128]), it remains possible that more subtle defects, for instance those that prevent appropriate resolution of EndMT, might disrupt cushion positioning or lead to hyperplastic cushions and leaflets that are forced into apposition and thus are more likely to fuse. There is accumulating evidence to support the idea that cushion or leaflet fusion may be a cause of BAV. BAV resulting from excessive fusion of the main outflow cushions has been described in the Syrian hamster, leading to LR fusions. This includes BAV and more rarely bicuspid pulmonary valves (BPV; [126,129,130]) as well as quadricuspid leaflets, all in the same colony of animals [130,131]. An investigation of the developmental defects underlying the abnormal leaflet fusion suggest that hyperplasia of the main cushions shortly after outflow septation pushes the cushions into apposition and this leads to fusion; a fusion seam can sometimes but not always be seen later in gestation in these animals [126,132]. Interestingly, in an inbred colony of the hamsters, even those animals determined to have a tricuspid valve frequently had excessive fusion of the left and right leaflets [132] suggesting that the affected gene (currently unknown) shows variable expressivity, or that other non-genetic factors affect the phenotype. Quadricuspid aortic valves in the outbred colony appear to result from splitting of one of the cushions (usually the right) into two relatively undeveloped cushions [133]; how this relates to the BAV remains unclear.

Recently, another well-described example of leaflet fusion, but this time later in gestation, has been described. In this case *Krox20*, a transcriptional regulator, was analysed during heart development revealing that the loss of *Krox20* in NCC (and more rarely when removed from EDC) can lead to BAV [134,135]. Interestingly, the loss of *Krox20* increased the numbers of NCC whilst the numbers of the EDC population remained normal. Excessive numbers of NCC, particularly in the non-coronary leaflet, led to malpositioned and hyperplastic leaflets that fused by late gestation [135]; a raphe could clearly be seen in these cases of BAV. These studies thus confirm that fusions between the cushions or leaflets, at different stages of development, can lead to BAV.

12. Displaced Cushions

A novel mechanism for the development of BAV has been suggested based on anatomical examination of a series of human embryos [136]. These authors observed that in some embryos the aortic ICVS was displaced proximally, with the developing valve tissue first appearing external to the myocardium. The valve then appeared to develop without this displaced ICVS, giving rise to a bicuspid phenotype. Interestingly, this did not appear to occur in the developing pulmonary valve, suggesting that there may be some subtle differences between the formation of the aortic and pulmonary valves [20,136]. The abnormal positioning of the outflow cushions in early development has been suggested to cause BAV in *eNOS* mutants [137]. In this case, the endocardial cushions were found to be misplaced and the main cushions were fused with the ICVS. More recently, this has been suggested to result from relatively small changes in the contributions of SHF and NCC to the forming cushions [59]. These authors also suggested that the BAV in the *eNOS* null mice might arise from a distinct mechanism, where the precursor of the anterior/posterior leaflet fails to separate from the main cushions. However, this implies that the ICVS does not exist as a separate entity, and thus is at odds to what we have described earlier, and what seems to be the generally accepted view [2,12,18–20,58]. Interestingly, it has been shown that *Krox20* can regulate *eNOS* expression, and that mice heterozygous for mutations in *Krox20* and *eNOS* develop BAV, whereas single heterozygous mutants do not [138], supporting the genetic interaction between these two genes. Similarly, abnormal cushion positioning in mice expressing a dominant-negative form of Rho kinase (ROCK; a modifier of the cytoskeleton) in the NCC lineage results in their fusion. In this case, the abnormal positioning of the cushions appears to result from disrupted aggregation of NCC within the forming cushions [12].

13. Bicuspid Valve without Raphe and the Absent Leaflet

Although the majority of human BAV present with a raphe [115,116] some studies suggest that BAV without raphe is more common than generally reported. For example, Koenraadt et al. [120] suggested that absence of raphe was represented in 25% of Dutch patients with BAV. Moreover, in cases of BPV, the majority also had BAV without raphe, suggesting that whatever process causes bicuspid valves without raphe, it affects both valves at the same time [139]. However, it should be remembered that a raphe might be present initially and then disappear later, particularly if the fusion event occurred very early in development [125]. When the complete absence of a leaflet is considered, the non-coronary leaflet is usually suggested to be the missing one [20,62,63,140]. As the non-coronary leaflet has a distinct origin from the main cushions (although the SHF is crucial to all; [20,59]) it can readily be seen how formation of this leaflet could be disrupted whilst leaving the right and left leaflets intact and with no evidence of raphe. Interestingly, there appears to be an over-representation of this type of BAV (absent non-coronary leaflet) within the mouse literature, suggesting that this mechanism may be common, at least in this species.

14. Abnormal Leaflet Numbers in the Setting of Defects in Outflow Tract Septation

Abnormalities in outflow tract septation, for example, common arterial trunk, are accompanied by defects in the arterial valves, with dysplasia and abnormal numbers of leaflets seen in the common truncal valve. However, the number of leaflets observed varies, with 3 or 4 leaflets being most common. It seems probable that the number of leaflets varies according to the cause of the common trunk, with abnormalities in cushion fusion, as is seen in the setting of NCC deficiency, usually resulting in four leaflets, (for example the *Splotch (Pax3)* mutant; [141]), as might be expected if the two main cushions do not fuse and separate (Figure 6B). In contrast, three leaflets are more commonly seen in the setting of single trunk associated with pulmonary atresia, as has been suggested in the *Tbx1* mouse mutant [61], and are likely to result from loss of the SHF-derived tissue that would normally form the pulmonary trunk. However, there is considerable variation in the numbers of leaflets found in the setting of common arterial trunk, even those where the lineage origin of the defect is clear, showing that there is not a straightforward relationship between abnormalities of particular cell types and valve phenotype.

15. Bicuspid Valves and Congenital Heart Malformations

BAV is frequently found in combination with other left ventricular outflow tract malformations, including coarctation of the aorta (which is particularly common in Turner syndrome) ventricular septal defects and hypoplastic left heart syndrome (reviewed in [116]). It is reasonable to suggest that when malformations frequently occur together, they share a common aetiology. This could be due to the disruption of specific genes or signalling pathways, or to disruption of related developmental processes. For example, it has been speculated that defects in NCC could lead to a range of defects that include BAV, coarctation of the aorta, common arterial trunk and VSD [142–145]. As all the affected areas have major contributions from NCC, this seems a reasonable conclusion.

Alternatively, some groupings of malformations could be sequences rather than syndromes, meaning that a primary abnormality leads to secondary consequences that are not directly linked to the primary insult. An example of this might be some sub-types of HLHS, where it is speculated that the primary defect specifically affects the mitral valve, with all of the other defects (ventricular hypoplasia, aortic stenosis/atresia and aortic hypoplasia) being secondary consequences of this that result from disrupted blood flow (the “no flow no grow” hypothesis (reviewed in [6])). It remains to be seen whether the association of left-sided ventricular outflow tract (LVOT) anomalies, that includes BAV, aortic stenosis, VSD and coarctation of the aorta and HLHS, is linked to a genetic defect that disrupts all of the affected areas of the heart, with variable expressivity. BAV has also been linked to atherosclerotic vascular disease as well as aortopathy and linked syndromes, e.g., Marfan, (reviewed in [116]). In all

these cases it will be important to determine whether there is a common genetic pathway or progenitor cell linking the conditions or whether they are linked by physiological disturbance.

In contrast to BAV, isolated bicuspid pulmonary valve (BPV) is extremely rare, except in patients with tetralogy of Fallot, where it affects half to 2/3 of patients [146]. Surprisingly, the morphology of these valves has not been systematically described, probably because it has no bearing on the immediate surgical issues. However, as during surgical repair the transannular patch is placed on the accessible anterior aspect of the pulmonary trunk, it is possible that the anterior intercalated leaflet is missing in the majority of cases. Anecdotally, it has been suggested that raphes are not seen in these BPV. Clearly, an analysis of the morphology of BPV is needed. If the anterior intercalated leaflet is missing, this would support the notion that tetralogy of Fallot is due to an abnormality of the SHF. This is important since it was assumed for many years that the outflow defects seen in DiGeorge syndrome—most commonly tetralogy of Fallot or common arterial trunk—were due to a defect in NCC [147,148]. However, since the identification of *TBX1* as the main cardiovascular gene linked to DiGeorge syndrome, it has become clear that this is an indirect effect on NCC, as *TBX1* is not expressed in NCC, but it influences their migration (reviewed in [149–151]). Furthermore, three of the characteristic malformations found in tetralogy of Fallot (pulmonary atresia, deviation of the outlet septum and ventricular septal defect) can be linked to defects in the SHF [61,151,152], whilst the fourth, right ventricular hypertrophy does not manifest until after birth and may be secondary to the other defects.

16. The Genomics of BAV

Genomic analyses of congenital heart disease have been successful in discovering a small number of variants in the small percentage of patients with syndromic conditions [153–156]. However, the genetic basis of common conditions such as BAV, even when appearing to affect families, has remained elusive. A number of genes including *NOTCH1*, *GATA 4*, *5* and *6*, and have been previously implicated in CHD from mouse models [157–166]. Thus, there is obviously good reason to consider these genes as candidates for human BAV. However, knockout of most of these genes results in severe, complex cardiovascular defects, rather than simply BAV, and modelling of human variants of these genes is limited and often disappointing. This is particularly so with *NOTCH1*. Variants are readily reported in genomic studies, but mouse knock out studies do not recapitulate the BAV (see [127]). Some of this may relate to incomplete penetrance where the mice carry a variant but are not subject to malformation (as is commonly seen in BAV families) or variable expressivity where variations of phenotype are seen. If so, this questions the utility of functional assays in preclinical models, and also preventative treatment or preconceptual counselling for families. Alternatively, some variants may not be in themselves pathological in isolation but may interact with the individual's developmental genetic landscape to make abnormalities more likely. If there is a specific modifier gene, we might call this oligogenic inheritance, but a range of modifiers may equally contribute. Again, in this scenario, it is very difficult to perform functional assays. There is also a problem regarding what functional assays to perform. The most popular functional assay for BAV variants is an EndMT assay. However, the failure of EndMT results in hypoplasia of the cushions (e.g., [167]) and this causes severe septal as well as valve defects (e.g., [168]). Hence, there is no experimental evidence to indicate a failure of EndMT could cause isolated BAV. Furthermore, EndMT is only one discrete process in valve development—much of which we still do not mechanistically understand. Another example of a suggested BAV-causing gene is *GATA4* (e.g., [163,169,170]). Patient variants in *GATA4* have been shown to disrupt EndMT in induced pluripotent stem cells [163] and *Gata4* has been shown to be required for EndMT to form the endocardial cushions in the mouse heart [26]; indeed, mice lacking functional *Gata4* have severe heart defects. Unfortunately, to our knowledge, BAV has not been reported in any mouse models of *Gata4* insufficiency (e.g., [171–173]). In contrast, *GATA6* seems more likely to be relevant to BAV. *GATA6* variants have been reported in patients with BAV [161,174,175] and these have been at least partially validated, in some cases by in vitro assays (showing that patient variants had reduced transcriptional activity; [174]) and

importantly by knocking out *Gata6* in mice and showing that BAV results [161]. Of relevance to this review, it was also shown that knockout of *Gata6* solely in SHF progenitors was enough to recapitulate the BAV seen in total knockouts [161], highlighting the importance of this lineage in the development of the arterial valve leaflets. Studies using zebrafish have also been able to validate the importance of BAV variants for cardiovascular development (e.g., [100]), although these have the disadvantage of not being able to recapitulate the BAV phenotype itself, as zebrafish ordinarily have a bicuspid aortic valve. The best validated BAV gene currently is *ROBO4* [166]. A potential disease-causing variant in this gene was originally identified by whole exome sequencing in a family with BAV, although in the presence of thoracic aortic aneurysm. Further variants were then identified in another small family and in sporadic cases with a mixture of RL and RN fusions. The relevance of *ROBO4* for BAV was confirmed in a variety of ways. This included in vitro studies that showed that *ROBO4* variant alleles disrupt endothelial barrier function, a mouse knockout for *Robo4* that developed BAV and aortic aneurysm, and most impressively, a mouse knock-in of the specific variant that was identified in the original family, which also developed BAV and aortic aneurysm [166]. This comprehensively validates the *ROBO4* gene as a cause of BAV in the setting of aortopathy. Although this sets a “gold standard” for such studies it is again remarkable that a gene has been fully validated for a syndromic/familial condition rather than in sporadic cases. Finally, it may be time to re-evaluate the mechanisms by which sporadic developmental defects occur as arguably, the sum of experience to date suggests that the simple concept of the disease-causing gene variant is not valid. Other modes of disturbing genetic cascades such as alternative splicing or stochastic mechanisms may need to be explored.

17. Final Conclusions

In this review, we have indicated the major roles performed by NCC and the SHF in forming the arterial valves elucidated using animal models. In contrast the recent attempts to interpret the causes of human malformations through genomic approaches have been limited. It is clear that objective and detailed analysis of the arterial valve phenotypes in human aortic and pulmonary valve malformations has not been historically performed and this is especially relevant in bicuspid aortic and pulmonary valves. Similarly, in developmental studies there are areas of valve development, such as sculpting and sinus formation, that have received little attention so far, but are essential to understand if variants invoked in human disease conditions are to be correctly interpreted. Finally, the homeostatic biology of the valves is of great relevance for the aging human heart and in particular it will be essential to know whether developmental populations such as SHF and NCC, or indeed later additions from bone marrow-derived cells, have specific roles, or alternatively, the differentiated identity, regardless of origin, is what matters.

Funding: The authors were funded by British Heart Foundation Programme Grant RG/19/2/34256.

Conflicts of Interest: The authors declare no conflict of interest. The funders had no role in the design of the study; in the collection, analyses, or interpretation of data; in the writing of the manuscript, or in the decision to publish the results.

References

1. Webb, S.; Qayyum, S.R.; Anderson, R.H.; Lamers, W.H.; Richardson, M.K. Septation and separation within the outflow tract of the developing heart. *J. Anat.* **2003**, *202*, 327–342. [CrossRef]
2. Anderson, R.H.; Mori, S.; Spicer, D.E.; Brown, N.A.; Mohun, T.J. Development and Morphology of the Ventricular Outflow Tracts. *World J. Pediatr. Congenit. Hear. Surg.* **2016**, *7*, 561–577. [CrossRef]
3. Richardson, R.; Eley, L.; Donald-Wilson, C.; Davis, J.; Curley, N.; Alqahtani, A.; Murphy, L.; Anderson, R.H.; Henderson, D.J.; Chaudhry, B. Development and maturation of the fibrous components of the arterial roots in the mouse heart. *J. Anat.* **2017**, *232*, 554–567. [CrossRef]

4. Sievers, H.H.; Hemmer, W.; Beyersdorf, F.; Moritz, A.; Moosdorf, R.; Lichtenberg, A.; Misfeld, M.; Charitos, E.I.; Working Group for Aortic Valve Surgery of German Society of Thoracic and Cardiovascular Surgery. The everyday used nomenclature of the aortic root components: The tower of Babel? *Eur. J. Cardiothorac. Surg.* **2012**, *41*, 478–482. [CrossRef]
5. Anderson, R.H.; Devine, W.A.; Ho, S.Y.; Smith, A.; McKay, R. The myth of the aortic annulus: The anatomy of the subaortic outflow tract. *Ann. Thorac. Surg.* **1991**, *52*, 640–646. [CrossRef]
6. Crucean, A.; Alqahtani, A.; Barron, D.J.; Brawn, W.J.; Richardson, R.V.; O’Sullivan, J.; Anderson, R.H.; Henderson, D.J.; Chaudhry, B. Re-evaluation of hypoplastic left heart syndrome from a developmental and morphological perspective. *Orphanet J. Rare Dis.* **2017**, *12*, 1–10. [CrossRef]
7. Choudhary, B.; Zhou, J.; Li, P.; Thomas, S.; Kaartinen, V.; Sucov, H.M. Absence of TGF β signaling in embryonic vascular smooth muscle leads to reduced lysyl oxidase expression, impaired elastogenesis, and aneurysm. *Genesis* **2009**, *47*, 115–121. [CrossRef]
8. Harmon, A.; Nakano, A. Nkx2-5 lineage tracing visualizes the distribution of second heart field-derived aortic smooth muscle. *Genesis* **2013**, *51*, 862–869. [CrossRef]
9. Von Gise, A.; Pu, W.T. Endocardial and epicardial epithelial to mesenchymal transitions in heart development and disease. *Circ. Res.* **2012**, *110*, 1628–1645. [CrossRef]
10. MacGrogan, D.; Luxán, G.; Driessen-Mol, A.; Bouten, C.V.; Baaijens, F.; De La Pompa, J.L. How to Make a Heart Valve: From Embryonic Development to Bioengineering of Living Valve Substitutes. *Cold Spring Harb. Perspect. Med.* **2014**, *4*, a013912. [CrossRef]
11. O’Donnell, A.; Yutzey, K.E. Mechanisms of heart valve development and disease. *Development* **2020**, *147*, dev183020. [CrossRef]
12. Phillips, H.M.; Mahendran, P.; Singh, E.; Anderson, R.H.; Chaudhry, B.; Henderson, D.J. Neural crest cells are required for correct positioning of the developing outflow cushions and pattern the arterial valve leaflets. *Cardiovasc. Res.* **2013**, *99*, 452–460. [CrossRef]
13. Courchaine, K.; Gray, M.J.; Beel, K.; Thornburg, K.L.; Rugonyi, S. 4-D Computational Modeling of Cardiac Outflow Tract Hemodynamics over Looping Developmental Stages in Chicken Embryos. *J. Cardiovasc. Dev. Dis.* **2019**, *6*, 11. [CrossRef]
14. Costell, M.; Carmona, R.; Gustafsson, E.; González-Iriarte, M.; Faessler, R.; Muñoz-Chápuli, R. Hyperplastic conotruncal endocardial cushions and transposition of great arteries in perlecan-null mice. *Circ. Res.* **2002**, *91*, 158–164. [CrossRef]
15. Anderson, R.H.; Chaudhry, B.; Mohun, T.J.; Bamforth, S.D.; Hoyland, D.; Phillips, H.M.; Webb, S.; Moorman, A.F.; Brown, N.A.; Henderson, D.J. Normal and abnormal development of the intrapericardial arterial trunks in humans and mice. *Cardiovasc. Res.* **2012**, *95*, 108–115. [CrossRef]
16. Waldo, K.L.; Hutson, M.R.; Ward, C.C.; Zdanowicz, M.; Stadt, H.A.; Kumiski, D.; Abu-Issa, R.; Kirby, M.L. Secondary heart field contributes myocardium and smooth muscle to the arterial pole of the developing heart. *Dev. Biol.* **2005**, *281*, 78–90. [CrossRef]
17. Ramsbottom, S.A.; Sharma, V.; Rhee, H.J.; Eley, L.; Phillips, H.M.; Rigby, H.F.; Dean, C.; Chaudhry, B.; Henderson, D.J. Vangl2-Regulated Polarisation of Second Heart Field-Derived Cells is Required for Outflow Tract Lengthening during Cardiac Development. *PLoS Genet.* **2014**, *10*, e1004871. [CrossRef]
18. Sizarov, A.; Lamers, W.H.; Mohun, T.J.; Brown, N.A.; Anderson, R.H.; Moorman, A.F. Three-dimensional and molecular analysis of the arterial pole of the developing human heart. *J. Anat.* **2012**, *220*, 336–349. [CrossRef]
19. Kramer, T.C. The partitioning of the truncus and conus and the formation of the membranous portion of the interventricular septum in the human heart. *Am. J. Anat.* **1942**, *71*, 343–370. [CrossRef]
20. Eley, L.; Alqahtani, A.; MacGrogan, D.; Richardson, R.V.; Murphy, L.; Salguero-Jiménez, A.; Pedro, M.S.R.S.; Tiurma, S.; McCutcheon, L.; Gilmore, A.; et al. A novel source of arterial valve cells linked to bicuspid aortic valve without raphe in mice. *eLife* **2018**, *7*, e34110. [CrossRef]
21. Combs, M.D.; Yutzey, K.E. Heart Valve Development. *Circ. Res.* **2009**, *105*, 408–421. [CrossRef]
22. De Vlaming, A.; Sauls, K.; Hajdu, Z.; Visconti, R.P.; Mehesz, A.N.; Levine, R.A.; Slaughter, S.A.; Hagege, A.; Chester, A.H.; Markwald, R.R.; et al. Atrioventricular valve development: New perspectives on an old theme. *Differentiation* **2012**, *84*, 103–116. [CrossRef]
23. Puceat, M. Embryological origin of the endocardium and derived valve progenitor cells: From developmental biology to stem cell-based valve repair. *Biochim. Biophys. Acta* **2013**, *1833*, 917–922. [CrossRef]

24. Cai, C.-L.; Liang, X.; Shi, Y.; Chu, P.-H.; Pfaff, S.L.; Chen, J.; Evans, S. Isl1 Identifies a Cardiac Progenitor Population that Proliferates Prior to Differentiation and Contributes a Majority of Cells to the Heart. *Dev. Cell* **2003**, *5*, 877–889. [CrossRef]
25. Verzi, M.P.; McCulley, D.J.; De Val, S.; Dodou, E.; Black, B.L. The right ventricle, outflow tract, and ventricular septum comprise a restricted expression domain within the secondary/anterior heart field. *Dev. Biol.* **2005**, *287*, 134–145. [CrossRef]
26. Rivera-Feliciano, J.; Lee, K.-H.; Kong, S.W.; Rajagopal, S.; Ma, Q.; Springer, Z.; Izumo, S.; Tabin, C.J.; Pu, W.T. Development of heart valves requires Gata4 expression in endothelial-derived cells. *Development* **2006**, *133*, 3607–3618. [CrossRef]
27. Wu, B.; Wang, Y.; Lui, W.; Langworthy, M.; Tompkins, K.L.; Hatzopoulos, A.K.; Baldwin, H.S.; Zhou, B. Nfatc1 Coordinates Valve Endocardial Cell Lineage Development Required for Heart Valve Formation. *Circ. Res.* **2011**, *109*, 183–192. [CrossRef]
28. De La Pompa, J.L.; Timmerman, L.A.; Takimoto, H.; Yoshida, H.; Elia, A.J.; Samper, E.; Potter, J.; Wakeham, A.; Marengere, L.; Langille, B.L.; et al. Role of the NF-ATc transcription factor in morphogenesis of cardiac valves and septum. *Nature* **1998**, *392*, 182–186. [CrossRef]
29. Ranger, A.M.; Grusby, M.J.; Hodge, M.R.; Gravalles, E.M.; De La Brousse, F.C.; Hoey, T.; Mickanin, C.; Baldwin, H.S.; Glimcher, L.H. The transcription factor NF-ATc is essential for cardiac valve formation. *Nature* **1998**, *392*, 186–190. [CrossRef]
30. Chang, C.-P.; Neilson, J.R.; Bayle, J.; Gestwicki, J.E.; Kuo, A.; Stankunas, K.; Graef, I.A.; Crabtree, G.R. A Field of Myocardial-Endocardial NFAT Signaling Underlies Heart Valve Morphogenesis. *Cell* **2004**, *118*, 649–663. [CrossRef]
31. Timmerman, L.A.; Grego-Bessa, J.; Raya, A.; Bertran, E.; Pérez-Pomares, J.; Díez, J.; Aranda, S.; Palomo-Ponce, S.; McCormick, F.; Izpisua-Belmonte, J.C.; et al. Notch promotes epithelial-mesenchymal transition during cardiac development and oncogenic transformation. *Genes Dev.* **2004**, *18*, 99–115. [CrossRef]
32. Luna-Zurita, L.; Prados, B.; Grego-Bessa, J.; Luxán, G.; Del Monte, G.; Benguria, A.; Adams, R.H.; Pérez-Pomares, J.; De La Pompa, J.L. Integration of a Notch-dependent mesenchymal gene program and Bmp2-driven cell invasiveness regulates murine cardiac valve formation. *J. Clin. Investig.* **2010**, *120*, 3493–3507. [CrossRef]
33. Ma, L.; Lu, M.-F.; Schwartz, R.J.; Martin, J.F. Bmp2 is essential for cardiac cushion epithelial-mesenchymal transition and myocardial patterning. *Development* **2005**, *132*, 5601–5611. [CrossRef]
34. Kokudo, T.; Suzuki, Y.; Yoshimatsu, Y.; Yamazaki, T.; Watabe, T.; Miyazono, K. Snail is required for TGFbeta-induced endothelial-mesenchymal transition of embryonic stem cell-derived endothelial cells. *J. Cell Sci.* **2008**, *121 Pt 20*, 3317–3324. [CrossRef]
35. Lakkis, M.M.; Epstein, J.A. Neurofibromin modulation of ras activity is required for normal endocardial-mesenchymal transformation in the developing heart. *Development* **1998**, *125*, 4359–4367.
36. Gitler, A.D.; Zhu, Y.; Ismat, F.A.; Lu, M.M.; Yamauchi, Y.; Parada, L.F.; Epstein, J.A. Nf1 has an essential role in endothelial cells. *Nat. Genet.* **2002**, *33*, 75–79. [CrossRef]
37. Araki, T.; Chan, G.; Newbigging, S.; Morikawa, L.; Bronson, R.T.; Neel, B.G. Noonan syndrome cardiac defects are caused by PTPN11 acting in endocardium to enhance endocardial-mesenchymal transformation. *Proc. Natl. Acad. Sci. USA* **2009**, *106*, 4736–4741. [CrossRef]
38. Lincoln, J.; Alfieri, C.M.; Yutzey, K.E. Development of heart valve leaflets and supporting apparatus in chicken and mouse embryos. *Dev. Dyn.* **2004**, *230*, 239–250. [CrossRef]
39. Kisanuki, Y.Y.; Ehammerbc, R.; Miyazaki, J.; Williamsba, S.C.; Arichardsonef, J.; Yanagisawabea, M. Tie2-Cre Transgenic Mice: A New Model for Endothelial Cell-Lineage Analysis In Vivo. *Dev. Biol.* **2001**, *230*, 230–242. [CrossRef]
40. MacGrogan, D.; D’Amato, G.; Travisano, S.; Martínez-Poveda, B.; Luxán, G.; Del Monte-Nieto, G.; Papoutsis, T.; Sbroggiò, M.; Bou, V.; Arco, P.G.-D.; et al. Sequential Ligand-Dependent Notch Signaling Activation Regulates Valve Primordium Formation and Morphogenesis. *Circ. Res.* **2016**, *118*, 1480–1497. [CrossRef]
41. Shigeta, A.; Huang, V.; Zuo, J.; Besada, R.; Nakashima, Y.; Lu, Y.; Ding, Y.; Pellegrini, M.; Kulkarni, R.P.; Hsiai, T.; et al. Endocardially Derived Macrophages are Essential for Valvular Remodeling. *Dev. Cell* **2019**, *48*, 617–630. [CrossRef]
42. Kirby, M.L.; Gale, T.F.; Stewart, D.E. Neural crest cells contribute to normal aorticopulmonary septation. *Science* **1983**, *220*, 1059–1061. [CrossRef]

43. Jiang, X.; Rowitch, D.H.; Soriano, P.; McMahon, A.P.; Sucov, H.M. Fate of the mammalian cardiac neural crest. *Development* **2000**, *127*, 1607–1616.
44. Simões-Costa, M.; Bronner, M.E. Establishing neural crest identity: A gene regulatory recipe. *Development* **2015**, *142*, 242–257. [CrossRef]
45. Leonard, C.E.; Taneyhill, L.A. The road best traveled: Neural crest migration upon the extracellular matrix. *Semin. Cell Dev. Biol.* **2020**, *100*, 177–185. [CrossRef]
46. Dupin, E.; Calloni, G.W.; Coelho-Aguiar, J.D.M.; Le Douarin, N.M. The issue of the multipotency of the neural crest cells. *Dev. Biol.* **2018**, *444*, S47–S59. [CrossRef]
47. Scholl, A.M.; Kirby, M.L.; Reinhold, A.M. Signals controlling neural crest contributions to the heart. *Wiley Interdiscip. Rev. Syst. Biol. Med.* **2009**, *1*, 220–227. [CrossRef]
48. Keyte, A.L.; Alonzo-Johnsen, M.; Hutson, M.R. Evolutionary and developmental origins of the cardiac neural crest: Building a divided outflow tract. *Birth Defects Res. C Embryo Today* **2014**, *102*, 309–323. [CrossRef]
49. Plein, A.; Fantin, A.; Ruhrberg, C. Neural Crest Cells in Cardiovascular Development. *Mech. Regen.* **2015**, *111*, 183–200. [CrossRef]
50. Bockman, D.E.; Redmond, M.E.; Kirby, M.L. Alteration of early vascular development after ablation of cranial neural crest. *Anat. Rec. Adv. Integr. Anat. Evol. Biol.* **1989**, *225*, 209–217. [CrossRef]
51. Bockman, D.E.; Redmond, M.E.; Kirby, M.L. Altered Development of Pharyngeal Arch Vessels after Neural Crest Ablation. *Ann. N. Y. Acad. Sci.* **1990**, *588*, 296–304. [CrossRef]
52. Bradshaw, L.; Chaudhry, B.; Hildreth, V.; Webb, S.; Henderson, D.J. Dual role for neural crest cells during outflow tract septation in the neural crest-deficient mutant *Splotch2H*. *J. Anat.* **2009**, *214*, 245–257. [CrossRef] [PubMed]
53. Brown, C.B.; Feiner, L.; Lu, M.M.; Li, J.; Ma, X.; Webber, A.L.; Jia, L.; Raper, J.A.; Epstein, J.A. PlexinA2 and semaphorin signaling during cardiac neural crest development. *Development* **2001**, *128*, 3071–3080. [PubMed]
54. Luo, T.; Lee, Y.-H.; Saint-Jeannet, J.-P.; Sargent, T.D. Induction of neural crest in *Xenopus* by transcription factor AP2. *Proc. Natl. Acad. Sci. USA* **2003**, *100*, 532–537. [CrossRef] [PubMed]
55. Poelmann, R.; Groot, A.G.-D. A Subpopulation of Apoptosis-Prone Cardiac Neural Crest Cells Targets to the Venous Pole: Multiple Functions in Heart Development? *Dev. Biol.* **1999**, *207*, 271–286. [CrossRef] [PubMed]
56. Hoff, M.J.V.D.; Moorman, A.F.; Ruijter, J.M.; Lamers, W.H.; Bennington, R.W.; Markwald, R.R.; Wessels, A. Myocardialization of the Cardiac Outflow Tract. *Dev. Biol.* **1999**, *212*, 477–490. [CrossRef]
57. Hoff, M.J.V.D.; Kruihof, B.P.; Moorman, A.F.; Markwald, R.R.; Wessels, A. Formation of Myocardium after the Initial Development of the Linear Heart Tube. *Dev. Biol.* **2001**, *240*, 61–76. [CrossRef]
58. Mifflin, J.J.; Dupuis, L.E.; Alcalá, N.E.; Russell, L.G.; Kern, C.B. Intercalated cushion cells within the cardiac outflow tract are derived from the myocardial troponin T type 2 (*Tnnt2*) Cre lineage. *Dev. Dyn.* **2018**, *247*, 1005–1017. [CrossRef]
59. Peterson, J.C.; Chughtai, M.; Wisse, L.J.; Groot, A.C.G.-D.; Feng, Q.; Goumans, M.-J.; VanMunsteren, J.C.; Jongbloed, M.R.M.; DeRuiter, M.C. Bicuspid aortic valve formation: *Nos3* mutation leads to abnormal lineage patterning of neural crest cells and the second heart field. *Dis. Model. Mech.* **2018**, *11*, dmm034637. [CrossRef]
60. Akiyama, H.; Chaboissier, M.-C.; Behringer, R.R.; Rowitch, D.H.; Schedl, A.; Epstein, J.A.; De Crombrughe, B. Essential role of *Sox9* in the pathway that controls formation of cardiac valves and septa. *Proc. Natl. Acad. Sci. USA* **2004**, *101*, 6502–6507. [CrossRef]
61. Jiao, K.; Kulesha, H.; Tompkins, K.; Zhou, Y.; Batts, L.; Baldwin, H.S.; Hogan, B. An essential role of *Bmp4* in the atrioventricular septation of the mouse heart. *Genes Dev.* **2003**, *17*, 2362–2367. [CrossRef]
62. Théveniau-Ruissy, M.; Dandonneau, M.; Mesbah, K.; Ghez, O.; Mattei, M.; Miquerol, L.; Kelly, R.G. The *del22q11.2* Candidate Gene *Tbx1* Controls Regional Outflow Tract Identity and Coronary Artery Patterning. *Circ. Res.* **2008**, *103*, 142–148. [CrossRef]
63. Thomas, P.S.; Sridurongrit, S.; Ruiz-Lozano, P.; Kaartinen, V. Deficient Signaling via *Alk2* (*Acvr1*) Leads to Bicuspid Aortic Valve Development. *PLoS ONE* **2012**, *7*, e35539. [CrossRef]
64. Mommersteeg, M.T.; Yeh, M.L.; Parnavelas, J.G.; Andrews, W.D. Disrupted Slit-Robo signalling results in membranous ventricular septum defects and bicuspid aortic valves. *Cardiovasc. Res.* **2015**, *106*, 55–66. [CrossRef]
65. Miquerol, L.; Langille, B.L.; Nagy, A. Embryonic development is disrupted by modest increases in vascularendothelial growth factor gene expression. *Development* **2000**, *127*, 3941–3946.

66. Dor, Y.; Camenisch, T.D.; Itin, A.I.; Fishman, G.; McDonald, J.A.; Carmeliet, P.; Keshet, E. A novel role for VEGF in endocardial cushion formation and its potential contribution to congenital heart defects. *Development* **2001**, *128*, 1531–1538.
67. Lee, Y.M.; Cope, J.J.; Ackermann, G.E.; Goishi, K.; Armstrong, E.J.; Paw, B.H.; Bischoff, J. Vascular endothelial growth factor receptor signaling is required for cardiac valve formation in zebrafish. *Dev. Dyn.* **2006**, *235*, 29–37. [CrossRef]
68. Sugi, Y.; Ito, N.; Szebenyi, G.; Myers, K.; Fallon, J.F.; Mikawa, T.; Markwald, R.R. Fibroblast growth factor (FGF)-4 can induce proliferation of cardiac cushion mesenchymal cells during early valve leaflet formation. *Dev. Biol.* **2003**, *258*, 252–263. [CrossRef]
69. Chen, B.; Bronson, R.T.; Klaman, L.D.; Hampton, T.G.; Wang, J.-F.; Green, P.J.; Magnuson, T.; Douglas, P.S.; Morgan, J.P.; Neel, B.G. Mice mutant for *Egfr* and *Shp2* have defective cardiac semilunar valvulogenesis. *Nat. Genet.* **2000**, *24*, 296–299. [CrossRef]
70. Chen, Y.-H.; Ishii, M.; Sun, J.; Sucov, H.M.; Maxson, R.E.; Maxson, R.E. *Msx1* and *Msx2* regulate survival of secondary heart field precursors and post-migratory proliferation of cardiac neural crest in the outflow tract. *Dev. Biol.* **2007**, *308*, 421–437. [CrossRef]
71. Srinivasan, D.K.; Dheen, S.T.; Tay, S.S.-W. Maternal diabetes induces congenital heart defects in mice by altering the expression of genes involved in cardiovascular development. *Cardiovasc. Diabetol.* **2007**, *6*, 34. [CrossRef]
72. Zhang, H.; Von Gise, A.; Liu, Q.; Hu, T.; Tian, X.; He, L.; Pu, W.; Huang, X.; He, L.; Cai, C.-L.; et al. *Yap1* is Required for Endothelial to Mesenchymal Transition of the Atrioventricular Cushion. *J. Biol. Chem.* **2014**, *289*, 18681–18692. [CrossRef] [PubMed]
73. Mjaatvedt, C.; Yamamura, H.; Capehart, A.; Turner, D.; Markwald, R. The *Cspg2* Gene, Disrupted in the *hdf* Mutant, is Required for Right Cardiac Chamber and Endocardial Cushion Formation. *Dev. Biol.* **1998**, *202*, 56–66. [CrossRef] [PubMed]
74. Camenisch, T.D.; Spicer, A.P.; Brehm-Gibson, T.; Biesterfeldt, J.; Augustine, M.L.; Calabro, A.; Kubalak, S.; Klewer, S.E.; McDonald, J.A. Disruption of hyaluronan synthase-2 abrogates normal cardiac morphogenesis and hyaluronan-mediated transformation of epithelium to mesenchyme. *J. Clin. Investig.* **2000**, *106*, 349–360. [CrossRef]
75. Dupuis, L.E.; McCulloch, D.R.; McGarity, J.D.; Bahan, A.; Wessels, A.; Weber, D.; Diminich, A.M.; Nelson, C.M.; Apte, S.S.; Kern, C.B. Altered versican cleavage in *ADAMTS5* deficient mice; a novel etiology of myxomatous valve disease. *Dev. Biol.* **2011**, *357*, 152–164. [CrossRef]
76. Durst, R.; Sauls, K.; Peal, D.S.; DeVlaming, A.; Toomer, K.; Leyne, M.; Salani, M.; Talkowski, M.E.; Brand, H.; Perrocheau, M.; et al. Mutations in *DCHS1* cause mitral valve prolapse. *Nature* **2015**, *525*, 109–113. [CrossRef]
77. Anvarian, Z.; Mykytyn, K.; Mukhopadhyay, S.; Pedersen, L.B.; Christensen, S.T. Cellular signalling by primary cilia in development, organ function and disease. *Nat. Rev. Nephrol.* **2019**, *15*, 199–219. [CrossRef]
78. Toomer, K.A.; Fulmer, D.; Guo, L.; Drohan, A.; Peterson, N.; Swanson, P.; Brooks, B.; Mukherjee, R.; Body, S.; Lipschutz, J.H.; et al. A role for primary cilia in aortic valve development and disease. *Dev. Dyn.* **2017**, *246*, 625–634. [CrossRef]
79. Irigoín, F.; Badano, J.L. Keeping the Balance Between Proliferation and Differentiation: The Primary Cilium. *Curr. Genom.* **2011**, *12*, 285–297. [CrossRef]
80. Hinton, R.B.; Lincoln, J.; Deutsch, G.H.; Osinska, H.; Manning, P.B.; Benson, D.W.; Yutzey, K.E. Extracellular Matrix Remodeling and Organization in Developing and Diseased Aortic Valves. *Circ. Res.* **2006**, *98*, 1431–1438. [CrossRef]
81. Lin, C.-J.; Chen, C.-H.; Zhou, B.; Chang, C.-P. Partitioning the heart: Mechanisms of cardiac septation and valve development. *Development* **2012**, *139*, 3277–3299. [CrossRef]
82. Wu, B.; Baldwin, H.S.; Zhou, B. *Nfatc1* directs the endocardial progenitor cells to make heart valve primordium. *Trends Cardiovasc. Med.* **2013**, *23*, 294–300. [CrossRef]
83. Nomura-Kitabayashi, A.; Phoon, C.K.; Kishigami, S.; Rosenthal, J.; Yamauchi, Y.; Abe, K.; Yamamura, K.-I.; Samtani, R.; Lo, C.W.; Mishina, Y. Outflow tract cushions perform a critical valve-like function in the early embryonic heart requiring BMPRIA-mediated signaling in cardiac neural crest. *Am. J. Physiol. Circ. Physiol.* **2009**, *297*, H1617–H1628. [CrossRef]
84. Keyes, W.M.; Sanders, E.J. Regulation of apoptosis in the endocardial cushions of the developing chick heart. *Am. J. Physiol. Physiol.* **2002**, *282*, C1348–C1360. [CrossRef]

85. Cheng, G.; Wessels, A.; Gourdie, R.G.; Thompson, R.P. Spatiotemporal and tissue specific distribution of apoptosis in the developing chick heart. *Dev. Dyn.* **2002**, *223*, 119–133. [CrossRef]
86. Abdelwahid, E.; Rice, D.P.; Pelliniemi, L.J.; Jokinen, E. Overlapping and differential localization of Bmp-2, Bmp-4, Msx-2 and apoptosis in the endocardial cushion and adjacent tissues of the developing mouse heart. *Cell Tissue Res.* **2001**, *305*, 67–78. [CrossRef]
87. Zhao, Z.; Rivkees, S.A. Programmed cell death in the developing heart: Regulation by BMP4 and FGF2. *Dev. Dyn.* **2000**, *217*, 388–400. [CrossRef]
88. Sharma, P.R.; Anderson, R.H.; Copp, A.J.; Henderson, D.J. Spatiotemporal analysis of programmed cell death during mouse cardiac septation. *Anat. Rec. Adv. Integr. Anat. Evol. Biol.* **2004**, *277*, 355–369. [CrossRef]
89. Hurle, J.; Blanco, A.M. Development of mouse semilunar valves. *Brain Struct. Funct.* **1980**, *160*, 83–91. [CrossRef]
90. Hurle, J. Scanning and light microscope studies of the development of the chick embryo semilunar heart valves. *Brain Struct. Funct.* **1979**, *157*, 69–80. [CrossRef]
91. Alfieri, C.M.; Cheek, J.; Chakraborty, S.; Yutzey, K.E. Wnt signaling in heart valve development and osteogenic gene induction. *Dev. Biol.* **2010**, *338*, 127–135. [CrossRef]
92. Bitgood, M.J.; McMahon, A.P. Hedgehog and Bmp genes are coexpressed at many diverse sites of cell-cell interaction in the mouse embryo. *Dev. Biol.* **1995**, *172*, 126–138. [CrossRef]
93. Biechler, S.V.; Junor, L.; Evans, A.N.; Eberth, J.F.; Price, R.L.; Potts, J.D.; Yost, M.J.; Goodwin, R.L. The impact of flow-induced forces on the morphogenesis of the outflow tract. *Front. Physiol.* **2014**, *5*. [CrossRef]
94. Goddard, L.M.; Duchemin, A.-L.; Ramalingan, H.; Wu, B.; Chen, M.; Bamezai, S.; Yang, J.; Li, L.; Morley, M.P.; Wang, T.; et al. Hemodynamic Forces Sculpt Developing Heart Valves through a KLF2-WNT9B Paracrine Signaling Axis. *Dev. Cell* **2017**, *43*, 274–289. [CrossRef]
95. Hsu, J.J.; Vedula, V.; Baek, K.I.; Chen, C.; Chen, J.; Chou, M.I.; Lam, J.; Subhedar, S.; Wang, J.; Ding, Y.; et al. Contractile and hemodynamic forces coordinate Notch1b-mediated outflow tract valve formation. *JCI Insight* **2019**, *5*. [CrossRef]
96. Menon, V.; Eberth, J.F.; Goodwin, R.L.; Potts, J.D. Altered Hemodynamics in the Embryonic Heart Affects Outflow Valve Development. *J. Cardiovasc. Dev. Dis.* **2015**, *2*, 108–124. [CrossRef]
97. Menon, V.; Eberth, J.F.; Junor, L.; Potts, A.J.; Belhaj, M.; DiPette, N.J.; Jenkins, M.W.; Potts, J.D. Removing vessel constriction on the embryonic heart results in changes in valve gene expression, morphology, and hemodynamics. *Dev. Dyn.* **2017**, *247*, 531–541. [CrossRef]
98. Steed, E.; Boselli, F.; Vermot, J. Hemodynamics driven cardiac valve morphogenesis. *Biochim. Biophys. Acta* **2016**, *1863*, 1760–1766. [CrossRef] [PubMed]
99. Poelmann, R.E.; Groot, A.C.G.-D. Hemodynamics in Cardiac Development. *J. Cardiovasc. Dev. Dis.* **2018**, *5*, 54. [CrossRef] [PubMed]
100. Heckel, E.; Boselli, F.; Roth, S.; Krudewig, A.; Belting, H.-G.; Charvin, G.; Vermot, J. Oscillatory Flow Modulates Mechanosensitive *klf2a* Expression through *trpv4* and *trpp2* during Heart Valve Development. *Curr. Biol.* **2015**, *25*, 1354–1361. [CrossRef]
101. Faucherre, A.; Maati, H.M.O.; Nasr, N.; Pinard, A.; Theron, A.; Odelin, G.; Desvignes, J.-P.; Salgado, D.; Collod-Bérout, G.; Avierinos, J.-F.; et al. Piezo1 is required for outflow tract and aortic valve development. *J. Mol. Cell. Cardiol.* **2020**, *143*, 51–62. [CrossRef]
102. Henderson, D.J.; Copp, A.J. Versican expression is associated with chamber specification, septation, and valvulogenesis in the developing mouse heart. *Circ. Res.* **1998**, *83*, 523–532. [CrossRef]
103. Fenderson, B.A.; Stamenkovic, I.; Aruffo, A. Localization of hyaluronan in mouse embryos during implantation, gastrulation and organogenesis. *Differentiation* **1993**, *54*, 85–98. [CrossRef]
104. Hurle, J.; Kitten, G.; Sakai, L.Y.; Volpin, D.; Solursh, M. Elastic extracellular matrix of the embryonic chick heart: An immunohistological study using laser confocal microscopy. *Dev. Dyn.* **1994**, *200*, 321–332. [CrossRef] [PubMed]
105. Votteler, M.; Berrio, D.A.C.; Horke, A.; Sabatier, L.; Reinhardt, D.P.; Nsair, A.; Aikawa, E.; Schenke-Layland, K. Elastogenesis at the onset of human cardiac valve development. *Development* **2013**, *140*, 2345–2353. [CrossRef] [PubMed]
106. Hulin, A.; Hortells, L.; Gomez-Stallons, M.V.; O'Donnell, A.; Chetal, K.; Adam, M.; Lancellotti, P.; Oury, C.; Potter, S.S.; Salomonis, N.; et al. Maturation of heart valve cell populations during postnatal remodeling. *Development* **2019**, *146*, dev173047. [CrossRef]

107. Wu, B.; Wang, Y.; Xiao, F.; Butcher, J.T.; Yutzey, K.E.; Zhou, B. Developmental Mechanisms of Aortic Valve Malformation and Disease. *Annu. Rev. Physiol.* **2017**, *79*, 21–41. [CrossRef]
108. Cujec, B.; Pollick, C. Isolated Thickening of One Aortic Cusp: Preferential Thickening of the Noncoronary Cusp. *J. Am. Soc. Echocardiogr.* **1988**, *1*, 430–432. [CrossRef]
109. Nakamura, T.; Colbert, M.C.; Robbins, J. Neural Crest Cells Retain Multipotential Characteristics in the Developing Valves and Label the Cardiac Conduction System. *Circ. Res.* **2006**, *98*, 1547–1554. [CrossRef]
110. Anstine, L.J.; Horne, T.E.; Horwitz, E.M.; Lincoln, J. Contribution of Extra-Cardiac Cells in Murine Heart Valves is Age-Dependent. *J. Am. Hear. Assoc.* **2017**, *6*. [CrossRef]
111. Hulin, A.; Anstine, L.J.; Kim, A.J.; Potter, S.J.; DeFalco, T.J.; Lincoln, J.; Yutzey, K.E. Macrophage Transitions in Heart Valve Development and Myxomatous Valve Disease. *Arter. Thromb. Vasc. Biol.* **2018**, *38*, 636–644. [CrossRef] [PubMed]
112. Deb, A.; Wang, S.H.; Skelding, K.; Miller, D.; Simper, D.; Caplice, N. Bone marrow-derived myofibroblasts are present in adult human heart valves. *J. Hear. Valve Dis.* **2005**, *14*, 674–678.
113. Tao, G.; Kotick, J.D.; Lincoln, J. Heart Valve Development, Maintenance, and Disease. *Mech. Regen.* **2012**, *100*, 203–232. [CrossRef]
114. Krepp, J.M.; Roman, M.J.; Devereux, R.B.; Bruce, A.; Prakash, S.K.; Morris, S.A.; Milewicz, D.M.; Holmes, K.W.; Ravekes, W.; Shohet, R.V.; et al. Bicuspid and unicuspid aortic valves: Different phenotypes of the same disease? Insight from the GenTAC Registry. *Congenit. Hear. Dis.* **2017**, *12*, 740–745. [CrossRef]
115. Lopez, A.; Fernández, M.C.; Durán, A.C.; Sans-Coma, V.; Fernández, B. Quadricuspid aortic valves in Syrian hamsters and their formation according to current knowledge on valvulogenesis. *Jpn. J. Veter. Res.* **2015**, *63*, 37–43.
116. Sievers, H.-H.; Schmidtke, C. A classification system for the bicuspid aortic valve from 304 surgical specimens. *J. Thorac. Cardiovasc. Surg.* **2007**, *133*, 1226–1233. [CrossRef]
117. Urena, M.; Doyle, D.; Dumont, É.; Ribeiro, H.B.; Bilodeau, S.; Rodés-Cabau, J. Transcatheter Aortic Valve Replacement with a Balloon-expandable Valve for the Treatment of Noncalcified Bicuspid Aortic Valve Disease. *Rev. Española Cardiol.* **2014**, *67*, 327–329. [CrossRef]
118. Kinoshita, T.; Naito, S.; Tomoaki, S.; Asai, T. Valve Phenotype and Risk Factors of Aortic Dilatation After Aortic Valve Replacement in Japanese Patients With Bicuspid Aortic Valve. *Circ. J.* **2016**, *80*, 1356–1361. [CrossRef]
119. Sun, B.J.; Jin, X.; Song, J.-K.; Lee, S.; Lee, J.H.; Park, J.-B.; Lee, S.-P.; Kim, D.-H.; Park, S.-J.; Kim, Y.-J.; et al. Clinical Characteristics of Korean Patients with Bicuspid Aortic Valve Who Underwent Aortic Valve Surgery. *Korean Circ. J.* **2018**, *48*, 48. [CrossRef]
120. Niaz, T.; Poterucha, J.T.; Olson, T.M.; Johnson, J.N.; Craviari, C.; Nienaber, T.; Palfreeman, J.; Cetta, F.; Hagler, D.J. Characteristic Morphologies of the Bicuspid Aortic Valve in Patients with Genetic Syndromes. *J. Am. Soc. Echocardiogr.* **2017**, *31*, 194–200. [CrossRef]
121. Koenraadt, W.M.C.; Grewal, N.; Gaidoukevitch, O.Y.; DeRuiter, M.C.; Groot, A.C.G.-D.; Bartelings, M.M.; Holman, E.R.; Klautz, R.J.M.; Schalij, M.J.; Jongbloed, M.R. The extent of the raphe in bicuspid aortic valves is associated with aortic regurgitation and aortic root dilatation. *Neth. Hear. J.* **2016**, *24*, 127–133. [CrossRef] [PubMed]
122. De Vries, W.M. Ueber Abweichungen in der Zahl der Semilunar-klappen. *Beitr. Pathol. Anat.* **1918**, *64*, 39–54.
123. Simonds, J.P. Congenital Malformations of the Aortic and Pulmonary Valves. *Am. J. Med Sci.* **1923**, *166*, 584–595. [CrossRef]
124. Koletsky, S. Congenital bicuspid pulmonary valves. *Arch. Pathol.* **1941**, *31*, 338–353.
125. Shaner, R.F. Abnormal pulmonary and aortic semilunar valves in embryos. *Anat. Rec. Adv. Integr. Anat. Evol. Biol.* **1963**, *147*, 5–13. [CrossRef]
126. Sans-Coma, V.; Fernández, B.; Durán, A.C.; Thiene, G.; Arqué, J.M.; Muñoz-Chápuli, R.; Cardo, M. Fusion of valve cushions as a key factor in the formation of congenital bicuspid aortic valves in Syrian hamsters. *Anat. Rec.* **1996**, *244*, 490–498. [CrossRef]
127. Soto-Navarrete, M.T.; López-Unzu, M.Á.; Durán, A.C.; Fernandez, B. Embryonic development of bicuspid aortic valves. *Prog. Cardiovasc. Dis.* **2020**, *25*. [CrossRef]
128. Luxán, G.; D’Amato, G.; MacGrogan, D.; De La Pompa, J.L. Endocardial Notch Signaling in Cardiac Development and Disease. *Circ. Res.* **2016**, *118*. [CrossRef]

129. Sans-Coma, V.; Cardo, M.; Thiene, G.; Fernández, B.; Arqué, J.M.; Durán, A.C. Bicuspid aortic and pulmonary valves in the Syrian hamster. *Int. J. Cardiol.* **1992**, *34*, 249–254. [CrossRef]
130. Fernández, B.; Fernandez, M.C.; Durán, A.C.; Lopez, D.; Martire, A.; Sans-Coma, V. Anatomy and formation of congenital bicuspid and quadricuspid pulmonary valves in Syrian hamsters. *Anat. Rec. Adv. Integr. Anat. Evol. Biol.* **1998**, *250*, 70–79. [CrossRef]
131. Fernández, B.; Durán, A.C.; Thiene, G.; Cardo, M.; Arqué, J.M.; Sans-Coma, V. Embryological evidence for the formation of a quadricuspid aortic valve in the Syrian hamster. *Cardiovasc. Pathol.* **1994**, *3*, 287–291. [CrossRef]
132. Sans-Coma, V.; Fernandez, M.C.; Fernández, B.; Durán, A.C.; Anderson, R.H.; Arqué, J.M. Genetically alike Syrian hamsters display both bifoliate and trifoliate aortic valves. *J. Anat.* **2011**, *220*, 92–101. [CrossRef]
133. Fernandez, B.; Durán, A.; Martire, A.; López, D.; Sans-Coma, V. New Embryological Evidence for the Formation of Quadricuspid Aortic Valves in the Syrian Hamster (*Mesocricetus auratus*). *J. Comp. Pathol.* **1999**, *121*, 89–94. [CrossRef]
134. Odelin, G.; Faure, E.; Kober, F.; Maurel-Zaffran, C.; Theron, A.; Coulpier, F.; Guillet, B.; Bernard, M.; Avierinos, J.-F.; Charnay, P.; et al. Loss of Krox20 results in aortic valve regurgitation and impaired transcriptional activation of fibrillar collagen genes. *Cardiovasc. Res.* **2014**, *104*, 443–455. [CrossRef]
135. Odelin, G.; Faure, E.; Coulpier, F.; Di Bonito, M.; Bajolle, F.; Studer, M.; Avierinos, J.-F.; Charnay, P.; Topilko, P.; Zaffran, S. Krox20 defines a subpopulation of cardiac neural crest cells contributing to arterial valves and bicuspid aortic valve. *Development* **2017**, *145*, dev151944. [CrossRef] [PubMed]
136. Milos, N.C.; Nordstrom, D.B.; Ongaro, I.; Chow, A.K. Variations in structure of the outflow tract of the human embryonic heart: A new hypothesis for generating bicuspid aortic semilunar valves. *Ann. Anat. Anat. Anz.* **2017**, *211*, 88–103. [CrossRef] [PubMed]
137. Fernandez, B.; Durán, A.C.; Fernández-Gallego, T.; Fernandez, M.C.; Such, M.; Arqué, J.M.; Sans-Coma, V. Bicuspid Aortic Valves With Different Spatial Orientations of the Leaflets Are Distinct Etiological Entities. *J. Am. Coll. Cardiol.* **2009**, *54*, 2312–2318. [CrossRef]
138. Odelin, G.; Faure, E.; Maurel-Zaffran, C.; Zaffran, S. Krox20 Regulates Endothelial Nitric Oxide Signaling in Aortic Valve Development and Disease. *J. Cardiovasc. Dev. Dis.* **2019**, *6*, 39. [CrossRef]
139. Koenraad, W.M.C.; Bartelings, M.M.; Groot, A.C.G.-D.; Bökenkamp, R.; DeRuiter, M.C.; Schalij, M.J.; Jongbloed, M.R. Pulmonary Valve Morphology in Patients with Bicuspid Aortic Valves. *Pediatr. Cardiol.* **2018**, *39*, 690–694. [CrossRef] [PubMed]
140. Laforest, B.; Andelfinger, G.; Nemer, M. Loss of Gata5 in mice leads to bicuspid aortic valve. *J. Clin. Investig.* **2011**, *121*, 2876–2887. [CrossRef]
141. Franz, T. Persistent truncus arteriosus in the Splotch mutant mouse. *Brain Struct. Funct.* **1989**, *180*, 457–464. [CrossRef] [PubMed]
142. Sundeen, J.T.; Bloom, S. Sinus of valsalva aneurysm associated with multiple conotruncal congenital malformations. *Hum. Pathol.* **1987**, *18*, 96–99. [CrossRef]
143. Kappetein, A.; Groot, A.G.-D.; Zwinderman, A.; Rohmer, J.; Poelmann, R.; Huysmans, H. The neural crest as a possible pathogenetic factor in coarctation of the aorta and bicuspid aortic valve. *J. Thorac. Cardiovasc. Surg.* **1991**, *102*, 830–836. [CrossRef]
144. Jain, R.; Engleka, K.A.; Rentschler, S.L.; Manderfield, L.J.; Li, L.; Yuan, L.; Epstein, J.A. Cardiac neural crest orchestrates remodeling and functional maturation of mouse semilunar valves. *J. Clin. Investig.* **2011**, *121*, 422–430. [CrossRef]
145. Komiyama, M. Cardio-cephalic neural crest syndrome: A novel hypothesis of vascular neurocristopathy. *Interv. Neuroradiol.* **2017**, *23*, 572–576. [CrossRef]
146. Quintessenza, J.A. Tetralogy of Fallot: Management of the Pulmonary Valve. In *Surgery of Conotruncal Anomalies*; Lacour-Gayet, F., Bove, E.L., Hruska, V., Morell, V.O., Spray, T.L., Eds.; Springer International Publishing: Cham, Switzerland, 2016; pp. 139–147.
147. Lammer, E.J.; Opitz, J.M.; Reynolds, J.F. The DiGeorge anomaly as a developmental field defect. *Am. J. Med. Genet.* **1986**, *25*, 113–127. [CrossRef]
148. Van Mierop, L.H.; Kutsche, L.M. Cardiovascular anomalies in digeorge syndrome and importance of neural crest as a possible pathogenetic factor. *Am. J. Cardiol.* **1986**, *58*, 133–137. [CrossRef]
149. Keyte, A.; Hutson, M.R. The neural crest in cardiac congenital anomalies. *Differentiation* **2012**, *84*, 25–40. [CrossRef]

150. Parisot, P.; Mesbah, K.; Théveniau-Ruissy, M.; Kelly, R.G. Tbx1, subpulmonary myocardium and conotruncal congenital heart defects. *Birth Defects Res. Part A Clin. Mol. Teratol.* **2011**, *91*, 477–484. [CrossRef]
151. Hasten, E.; McDonald-McGinn, D.M.; Crowley, T.B.; Zackai, E.; Emanuel, B.S.; Morrow, B.E.; Racedo, S.E. Dysregulation of TBX1 dosage in the anterior heart field results in congenital heart disease resembling the 22q11.2 duplication syndrome. *Hum. Mol. Genet.* **2018**, *27*, 1847–1857. [CrossRef]
152. Zhou, Z.; Wang, J.; Guo, C.; Chang, W.; Zhuang, J.; Zhu, P.; Li, X. Temporally Distinct Six2-Positive Second Heart Field Progenitors Regulate Mammalian Heart Development and Disease. *Cell Rep.* **2017**, *18*, 1019–1032. [CrossRef] [PubMed]
153. Zaidi, S.; Choi, M.; Wakimoto, H.; Ma, L.; Jiang, J.; Overton, J.D.; Romano-Adesman, A.; Bjornson, R.D.; Breitbart, R.E.; Brown, K.K.; et al. De novo mutations in histone-modifying genes in congenital heart disease. *Nature* **2013**, *498*, 220–223. [CrossRef] [PubMed]
154. Homsy, J.; Zaidi, S.; Shen, Y.; Ware, J.S.; Samocha, K.E.; Karczewski, J.; DePalma, S.R.; Mckean, D.; Wakimoto, H.; Gorham, J.; et al. De novo mutations in congenital heart disease with neurodevelopmental and other congenital anomalies. *Science* **2015**, *350*, 1262–1266. [CrossRef] [PubMed]
155. Glessner, J.T.; Bick, A.G.; Ito, K.; Homsy, J.G.; Rodriguez-Murillo, L.; Fromer, M.; Mazaika, E.; Vardarajan, B.; Italia, M.; Leipzig, J.; et al. Increased Frequency of De Novo Copy Number Variants in Congenital Heart Disease by Integrative Analysis of Single Nucleotide Polymorphism Array and Exome Sequence Data. *Circ. Res.* **2014**, *115*, 884–896. [CrossRef] [PubMed]
156. Sifrim, A.; Hitz, M.-P.; Wilsdon, A.; Breckpot, J.; Al Turki, S.H.; Thienpont, B.; McRae, J.; Fitzgerald, T.W.; Singh, T.; Swaminathan, G.J.; et al. Distinct genetic architectures for syndromic and nonsyndromic congenital heart defects identified by exome sequencing. *Nat. Genet.* **2016**, *48*, 1060–1065. [CrossRef] [PubMed]
157. Wooten, E.C.; Iyer, L.K.; Montefusco, M.C.; Hedgepeth, A.K.; Payne, D.D.; Kapur, N.K.; Housman, D.E.; Mendelsohn, M.E.; Huggins, G.S. Application of gene network analysis techniques identifies AXIN1/PDIA2 and endoglin haplotypes associated with bicuspid aortic valve. *PLoS ONE* **2010**, *5*, e8830. [CrossRef] [PubMed]
158. Martin, L.J.; Pilipenko, V.; Kaufman, K.M.; Cripe, L.H.; Kottyan, L.; Keddache, M.; Dexheimer, P.; Weirauch, M.T.; Benson, D.W. Whole Exome Sequencing for Familial Bicuspid Aortic Valve Identifies Putative Variants. *Circ. Cardiovasc. Genet.* **2014**, *7*, 677–683. [CrossRef] [PubMed]
159. Bonachea, E.M.; Zender, G.; White, P.; Corsmeier, D.J.; Newsom, D.; Fitzgerald-Butt, S.; Garg, V.; McBride, K.L. Use of a targeted, combinatorial next-generation sequencing approach for the study of bicuspid aortic valve. *BMC Med. Genom.* **2014**, *7*, 56. [CrossRef]
160. Dargis, N.; Lamontagne, M.; Gaudreault, N.; Sbarra, L.; Henry, C.; Pibarot, P.; Mathieu, P.; Bossé, Y. Identification of Gender-Specific Genetic Variants in Patients With Bicuspid Aortic Valve. *Am. J. Cardiol.* **2016**, *117*, 420–426. [CrossRef]
161. Gharibeh, L.; Komati, H.; Bossé, Y.; Boodhwani, M.; Heydarpour, M.; Fortier, M.; Hassanzadeh, R.; Ngu, J.; Mathieu, P.; Body, S.; et al. GATA6 Regulates Aortic Valve Remodeling, and Its Haploinsufficiency Leads to Right-Left Type Bicuspid Aortic Valve. *Circulation* **2018**, *138*, 1025–1038. [CrossRef] [PubMed]
162. Giusti, B.; Sticchi, E.; De Carlo, R.; Magi, A.; Nistri, S.; Pepe, G. Genetic Bases of Bicuspid Aortic Valve: The Contribution of Traditional and High-Throughput Sequencing Approaches on Research and Diagnosis. *Front. Physiol.* **2017**, *8*. [CrossRef] [PubMed]
163. Yang, B.; Zhou, W.; Jiao, J.; Nielsen, J.B.; Mathis, M.R.; Heydarpour, M.; Lettre, G.; Folkersen, L.; Prakash, S.; Schurmann, C.; et al. Protein-altering and regulatory genetic variants near GATA4 implicated in bicuspid aortic valve. *Nat. Commun.* **2017**, *8*, 15481. [CrossRef] [PubMed]
164. McKellar, S.H.; Tester, D.J.; Yagubyan, M.; Majumdar, R.; Ackerman, M.J.; Sundt, T.M. Novel NOTCH1 mutations in patients with bicuspid aortic valve disease and thoracic aortic aneurysms. *J. Thorac. Cardiovasc. Surg.* **2007**, *134*, 290–296. [CrossRef] [PubMed]
165. Mohamed, S.A.; Aherrahrou, Z.; Liptau, H.; Erasmi, A.W.; Hagemann, C.; Wrobel, S.; Borzym, K.; Schunkert, H.; Sievers, H.-H.; Erdmann, J. Novel missense mutations (p.T596M and p.P1797H) in NOTCH1 in patients with bicuspid aortic valve. *Biochem. Biophys. Res. Commun.* **2006**, *345*, 1460–1465. [CrossRef]
166. Gould, R.A.; Genomics, B.-H.C.F.M.; Aziz, H.; Woods, C.E.; Seman-Senderos, M.A.; Sparks, E.; Preuss, C.; Wünnemann, F.; Bedja, D.; Moats, C.R.; et al. ROBO4 variants predispose individuals to bicuspid aortic valve and thoracic aortic aneurysm. *Nat. Genet.* **2018**, *51*, 42–50. [CrossRef]

167. Wang, Y.; Wu, B.; Chamberlain, A.A.; Lui, W.; Koirala, P.; Susztak, K.; Klein, D.; Taylor, V.; Zhou, B. Endocardial to Myocardial Notch-Wnt-Bmp Axis Regulates Early Heart Valve Development. *PLoS ONE* **2013**, *8*, e60244. [CrossRef]
168. Koenig, S.N.; Bosse, K.; Majumdar, U.; Bonachea, E.M.; Radtke, F.; Garg, V. Endothelial Notch1 is Required for Proper Development of the Semilunar Valves and Cardiac Outflow Tract. *J. Am. Hear. Assoc.* **2016**, *5*. [CrossRef]
169. Li, R.-G.; Xu, Y.; Wang, J.; Liu, X.-Y.; Yuan, F.; Huang, R.-T.; Xue, S.; Li, L.; Liu, H.; Li, Y.-J.; et al. GATA4 Loss-of-Function Mutation and the Congenitally Bicuspid Aortic Valve. *Am. J. Cardiol.* **2018**, *121*, 469–474. [CrossRef]
170. Musfee, F.I.; Guo, D.; Pinard, A.C.; Hostetler, E.M.; Blue, E.E.; Nickerson, D.A.; Bamshad, M.J.; Milewicz, D.M.; Prakash, S.K. Rare deleterious variants of NOTCH1, GATA4, SMAD6, and ROBO4 are enriched in BAV with early onset complications but not in BAV with heritable thoracic aortic disease. *Mol. Genet. Genom. Med.* **2020**, e1406. [CrossRef]
171. Moskowitz, I.P.; Wang, J.; Peterson, M.A.; Pu, W.T.; MacKinnon, A.C.; Oxburgh, L.; Chu, G.C.; Sarkar, M.; Berul, C.; Smoot, L.; et al. Transcription factor genes Smad4 and Gata4 cooperatively regulate cardiac valve development. *Proc. Natl. Acad. Sci. USA* **2011**, *108*, 4006–4011. [CrossRef]
172. Misra, C.; Chang, S.-W.; Basu, M.; Huang, N.; Garg, V. Disruption of myocardial Gata4 and Tbx5 results in defects in cardiomyocyte proliferation and atrioventricular septation. *Hum. Mol. Genet.* **2014**, *23*, 5025–5035. [CrossRef] [PubMed]
173. Zhou, L.; Liu, J.; Xiang, M.; Olson, P.; Guzzetta, A.; Zhang, K.; Moskowitz, I.P.; Xie, L. Gata4 potentiates second heart field proliferation and Hedgehog signaling for cardiac septation. *Proc. Natl. Acad. Sci. USA* **2017**, *114*, E1422–E1431. [CrossRef] [PubMed]
174. Xu, Y.; Di, R.-M.; Qiao, Q.; Li, X.-M.; Huang, R.-T.; Xue, S.; Liu, X.-Y.; Wang, J.; Yang, Y.-Q. GATA6 loss-of-function mutation contributes to congenital bicuspid aortic valve. *Gene* **2018**, *663*, 115–120. [CrossRef] [PubMed]
175. Montes, C.A.; Martín, M.; Arias, L.M.; Coto, E.; Naves-Díaz, M.; Moris, C.; Andía, J.B.C.; Rodríguez, I. Variants in cardiac GATA genes associated with bicuspid aortic valve. *Eur. J. Clin. Investig.* **2018**, *48*, e13027. [CrossRef]



© 2020 by the authors. Licensee MDPI, Basel, Switzerland. This article is an open access article distributed under the terms and conditions of the Creative Commons Attribution (CC BY) license (<http://creativecommons.org/licenses/by/4.0/>).



Review

A Rare Presentation of Common Arterial Trunk with Intact Ventricular Septum

Diane E. Spicer^{1,2,*} and Thora S. Steffensen¹

¹ Department of Pathology, Tampa General Hospital, Tampa, FL 33594, USA; Thora.Steffensen@gmail.com

² Division of Pediatric Cardiology, University of Florida, Gainesville, FL 32611, USA

* Correspondence: spicerpath@hotmail.com; Tel.: +1-813-966-4346

Received: 31 August 2020; Accepted: 10 October 2020; Published: 12 October 2020

Abstract: Common arterial trunk is a rare anomaly on its own, but with an intact ventricular septum it is extremely rare. An unexpected finding at autopsy prompted a review of the literature and a review of the developmental considerations associated with the outflow tracts. The case presented was an intrauterine fetal death at 37 weeks gestation. At autopsy, the only anatomic abnormalities were pulmonary dominant common arterial trunk with an intact ventricular septum, ventriculo-arterial septal defect, coarctation and widely patent arterial duct. A review of the literature and the developmental concepts related to the outflow tracts of the developing heart demonstrate the rare nature of this particular variation of common arterial trunk.

Keywords: common arterial trunk; intact ventricular septum; ventriculo-arterial septal defect; outflow tract development

1. Introduction

Utilizing pure descriptive terms proves to be the most sufficient method in defining the anatomy of a common arterial trunk. The initial classification put forth by Collett and Edwards [1], and subsequently modified by Van Praagh and Van Praagh [2], leaves gray zones within the alpha-numeric classifications, although Van Praagh and Van Praagh did recognize that a common arterial trunk could co-exist with an intact ventricular septum. Several anatomic variations have subsequently been presented in the literature. The cases presented by Carr et al. [3], McElhinney et al. [4], Garg et al. [5] and Ajami et al. [6] have anatomy that is similar to the case being presented. The case presented by Carr and colleagues appears to have a very small ventricular septal defect with the dysplastic valvar leaflets overriding the edges of the defect, but not forming dual orifices. The common arterial trunk in each of the remaining cases had an intact ventricular septum with a plane of tissue arising from the crest of the muscular ventricular septum and separating the pulmonary and aortic components of the valve. The anatomy of the valves showed some variation, with the majority having a dysplastic appearance. All of the cases had right and left ventricles of relatively equal size with marked hypertrophy. Zeevi et al. [7], in contrast, presented a case with a hypoplastic right ventricle, intact ventricular septum, and a common arterial trunk arising exclusively from the left ventricle. This case also demonstrated a patent, stenotic right atrioventricular connection, and coronary arterial fistulous connections with the right ventricle. The case presented by Alves and Ferrari [8] showed a common arterial trunk arising exclusively from the right ventricle, with a hypoplastic left ventricle and an absent left atrioventricular connection. An interrupted aortic arch, atrial septal defect, and tricuspid valvar dysplasia were also described. A most interesting arrangement is described by Tsang et al. [9]. Their patient had a ventriculo-arterial septal defect, with separate aortic and pulmonary valves, but with a common ventriculo-arterial junction.

The cases listed above represent rare variations of a congenital cardiac malformation, namely common arterial trunk, that is a rare malformation in and of itself. This sets the stage for a discussion of the developmental considerations associated with the outflow tracts, often considered 'cono-truncal' malformations, and the differences between common arterial trunk, aortopulmonary window, and the juxtaarterial ventricular septal defect. Our case is differentiated from aortopulmonary window because there is a common intrapericardial arterial trunk, along with a common ventriculo-arterial junction. It does not show two separate arterial valves guarding separate ventriculo-arterial junctions. Although developmentally similar to those hearts with juxtaarterial ventricular septal defects, where there is hypoplasia of the proximal outflow cushions, our case demonstrates hypoplasia of the proximal outflow tract, but with an intact ventricular septum. Probably the most interesting observation is the presence of a pulmonary component and an aortic component on either side of the fibrous partition that is in direct communication with the crest of the ventricular septum. The anatomic characteristics of the aortic and pulmonary components, however, have a very different appearance, and are somewhat different from what has been previously described. This feature also distinguishes our case, in a small way, from those described earlier. The essentially common valves in the previously described cases all had three or four leaflets, with variation in the leaflets bridging the fibrous partition to form a valvar structure shared between the right and left ventricular outlets. In our case the subpulmonary infundibulum was represented, and although hypoplastic, it demonstrates the developmental independence of the proximal component from the intermediate and distal components of the outflow tract. The intermediate component demonstrates its own independence with separate aortic and pulmonary valvar components arising on either side of the fibrous partition at the common ventriculo-arterial junction. This leaves the door open to look even deeper into the way in which the outflow tracts develop, and presents yet another variation in this group of exceedingly rare lesions. Comparisons between a common ventriculo-arterial junction and a common atrioventricular junction will be drawn.

2. Case Report

The intrauterine fetal death occurred at 37 weeks of gestation, with the fetus born to a 31 year old mother who had received adequate prenatal care. The finding of a common arterial trunk, particularly with an intact ventricular septum, was an unexpected finding at autopsy. Petechial hemorrhages were noted over the lungs and the anterior surface of the right ventricle, with hemorrhage in the fat within the atrioventricular grooves. Initial examination revealed an enlarged heart with a common arterial trunk arising from the base of the heart. (Figure 1)

The common arterial trunk was pulmonary dominant, with the right and left pulmonary arteries branching separately from its posterior lateral aspect. The aortic arch was hypoplastic, with the hypoplastic segment extending from the brachiocephalic trunk to the isthmus at its junction with a widely patent arterial duct. The brachiocephalic arteries had a normal branching pattern, with the left subclavian artery arising in juxtaductal position. The aortic arch extended leftward. The left brachiocephalic vein was normal, and the superior and inferior caval veins connected with the right atrium in the usual fashion. The pulmonary venous drainage was normal. The oval foramen was probe patent, and the coronary sinus was of normal caliber. Concordant atrioventricular connections were observed, with hypertrophy of the atrial and ventricular chambers secondary to the severe stenosis at the ventricular outlets. The heart weighed 37.6 g, with the normal expected weight being 16 g. The myocardium throughout both ventricles was pale. The interventricular septum was intact, and there was a common ventriculo-arterial junction. The truncal valve was divided into right and left orifices by a partition of fibrous tissue that arose from the crest of the ventricular septum and separated the pulmonary and aortic components. The partition of fibrous tissue was up to 0.4 cm in length from the crest of the muscular ventricular septum to the valvar components. The pulmonary component (Figure 2, left panel) was committed to the right ventricle, and the aortic component (Figure 2, right panel) to the left ventricle.

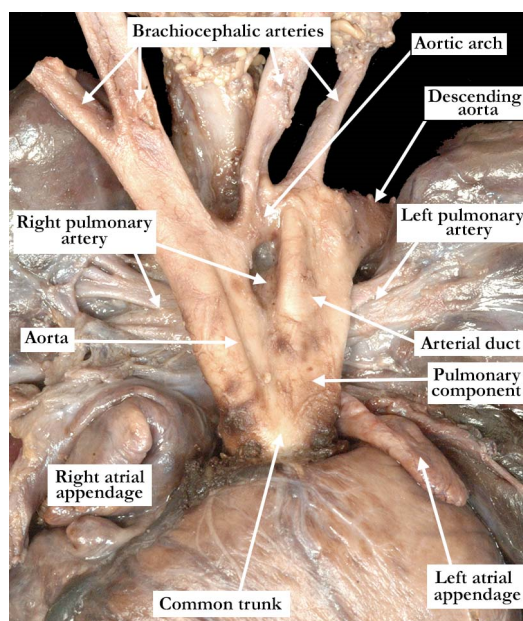


Figure 1. This anterior view demonstrates the common arterial trunk arising from the ventricular mass. The right and left pulmonary arteries arise separately from the posterior lateral aspects of the trunk, and there is a widely patent arterial duct. The aortic arch is hypoplastic, with the left subclavian artery arising in juxtaductal position.

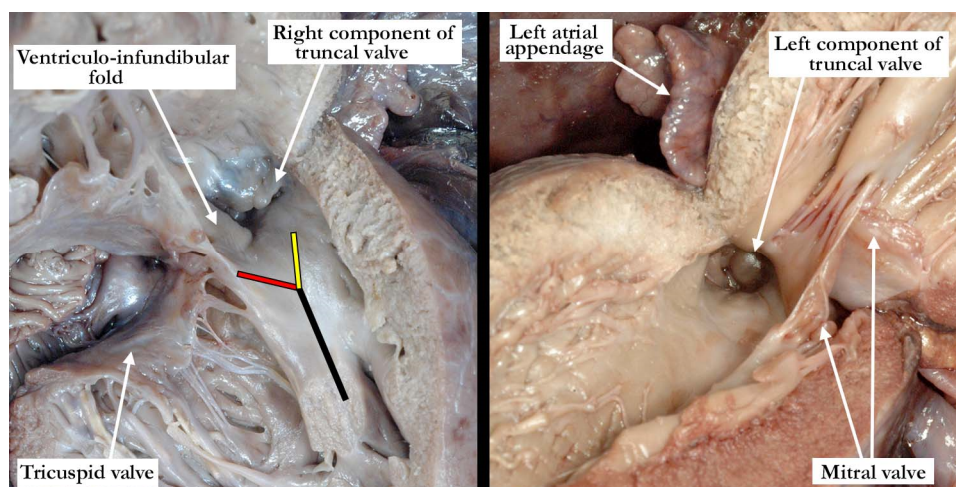


Figure 2. The left panel shows the right ventricle opened in clam-shell fashion with the tricuspid valve guarding the inlet and the stenotic valve at the outlet. Note the somewhat broad septal band (black line) that gives rise to the caudal (red line) and cephalic (yellow line) arms. The ventriculo-infundibular fold is hypoplastic, and inserts into the ‘Y’ of the septal band. The right panel shows the left ventricular outflow tract with the stenotic, dysplastic valve guarding the outlet. Note the hypertrophy within both the right and left ventricles.

The pulmonary component of the valve was stenotic and composed of multiple dysplastic nodules of valvar tissue dispersed in roughly annular fashion at the ventriculo-arterial junction. This arrangement is reminiscent of the valvar tissue typical for those cases that have so-called “absent pulmonary valve”. The aortic component of the valve was markedly stenotic and dysplastic. It was bicuspid, one of the sinuses being shallow and elongated, with an evident raphe or incomplete interleaflet triangle at its base. The raphe was between the right anterior leaflet and the posterior-most leaflet. The other

sinus was short and quite deep. The right coronary orifice arose from the right anterior-most leaflet, and was unobstructed. This right anterior-most leaflet was adjacent to the fibrous tissue that divided the aortic and pulmonary valvar components, the leaflet partially riding on the fibrous partition (Figure 3, left panel). The leaflet associated with the short, deep, leftward sinus did not override the fibrous partition, with one well-formed interleaflet triangle between it and the posterior-most leaflet, along with an apparent commissure immediately adjacent to the fibrous partition. There were two nodular structures, very similar to the remainder of the aortic component of the valve, that lay in left anterior lateral position. One of these overrode the fibrous partition, while the other impinged on the pulmonary component. There was no valvar sinus associated with these nodular structures, although distal to the fibrous partition there was an area reminiscent of a broad commissure. The left coronary arterial orifice arose immediately adjacent to the commissure between the posterior-most and leftward sinuses. It is noteworthy that both coronary orifices arose from the aortic component of the common truncal valve. On the left side of the fibrous partition, there was an adherent and single dysplastic nodule of valvar tissue that had no associated valvar sinus (Figure 3, right panel).

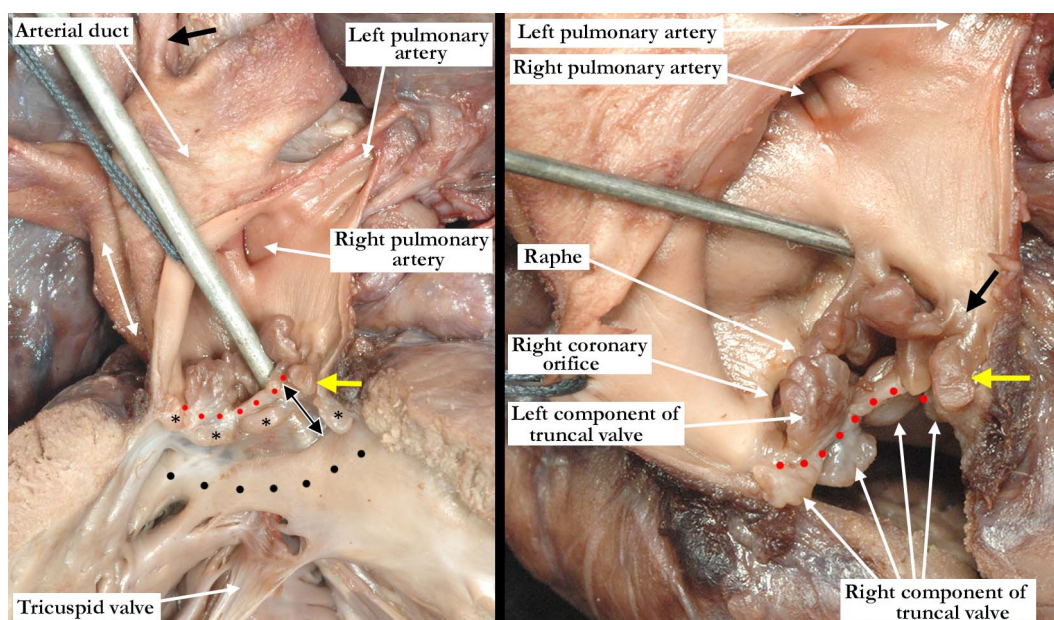


Figure 3. In the left panel, the anterior view of the common trunk is viewed through the opened, right component of the valve, demonstrating the separate right and left pulmonary arteries and the ascending aortic component of the trunk (double headed white arrow). The patent arterial duct is large, with the left subclavian arising in juxtaductal position (black arrow). The probe is within the left ventricular outflow tract and can be seen through the fibrous partition that lies between the valvar components and the crest of the ventricular septum (double headed black arrow). The red dots mark the upper margin of the fibrous partition. The subvalvar infundibulum (black dots) within the right ventricle is hypoplastic. The nodular valvar tissue surrounding the right ventricular outlet to the right side of the fibrous partition is marked with black asterisks. The right panel is an anterior superior view of the truncal valve with the fibrous partition marked with red dots. The nodular right component lies inferior to the dysplastic left component. The right coronary arterial orifice lies midway between the attachment of the anterior-most leaflet to the fibrous partition and the incomplete interleaflet triangle or raphe. The probe is within the left coronary arterial orifice, which lies adjacent to the well-formed interleaflet triangle between the posterior most and leftward leaflets. The black arrow marks the area reminiscent of a broad commissure, this area directly above the fibrous partition. The yellow arrow marks the dysplastic nodule that overrides into the right ventricular component. Note the elliptical nodule on the left side of the partition. Both components of the valve are stenotic, most marked on the left.

In the normal situation the arterial valves are supported within separate arterial roots. It is important to understand that the right and left halves of the valve in the reported case are supported within a common arterial root. Although separated into right and left components, however, they cannot be considered to be 'normal'. The fibrous partition represents hypoplasia of the proximal outflow cushions and effectively divides the right and left ventricular outflow tracts. The ventricular septum is intact, with no shunting possible at the ventricular level, but is not normal. This particular arrangement at the ventriculo-arterial junction can be directly compared to defects at the atrioventricular junction. A subsequent discussion will be provided.

The study was conducted in accordance with the declaration of Helsinki. An autopsy permit was appropriately signed.

3. Discussion

During embryonic development of all structures throughout the body, there are certainly many small deficiencies or abnormal pathways occurring to give us what we refer to as 'variation of normal', but do not significantly affect the function of the organ or organ system. Recent study of the 'normal' heart is revealing many anatomic variations that are not considered, at this point in time, as being abnormal or causing abnormal function. This is especially important with regard to the cardiac valves, with minor variations potentially affecting assessment of the mortality and morbidity of certain interventional procedures. That being said, the cases of common arterial trunk in the setting of an intact ventricular septum represent the opposite end of the developmental spectrum, where development takes an extreme deviation from normal.

Developmentally, as in the postnatal heart, it is optimal to describe the outflow tracts in a tripartite fashion, noting the proximal, intermediate and distal segments, all of which are intrapericardial. In the past, the development of the outflow tracts was described with relationship to the 'truncus' and the 'conus', but with little agreement on what represents these entities [10]. Thus, within the current 'conotruncal' classification, the development of the arterial valves is ignored. The valves develop within the intermediate segment, or the middle, of the developing outflow tract. This obvious fact raises the question as to why abnormalities of the arterial valves are not considered to be 'conotruncal' malformations? Developmentally, the arterial roots, made up of the valvar leaflets and their supporting sinuses, make up the intermediate segment of the outflow tract. It is the proximal segment that forms the ventricular outflow tracts, while the distal segment becomes the intrapericardial arterial trunks.

In the recent past, the study of mouse embryos using episcopic datasets has provided new insight on cardiac development, including the arterial valves [11–14]. It has been shown that ingrowth of nonmyocardial components, coupled with migration of neural crest cells, plays an important part in the formation of the intrapericardial arterial trunks and the arterial valves. The distal separation of the aorta and pulmonary trunk commences with growth of nonmyocardial tissue into the pericardial cavity, which will form the parietal walls of the two arterial trunks. The aortopulmonary septum, when first seen, originates as a ventral protrusion from the dorsal wall of the aortic sac. It will grow in a caudal direction, extending toward the cushions that have developed at the same time within the component of the outflow tract that retains its myocardial walls. The protrusion will eventually fuse with the distal outflow cushions, thus obliterating the embryonic aortopulmonary foramen. With obliteration of the foramen, the intrapericardial outflow tract becomes separated into the aorta and pulmonary trunk. Closure of the embryonic aortopulmonary foramen is also dependent on the appropriate migration of cells derived from the neural crest. It is abnormal formation of the aortopulmonary septum that will underscore the known variations of aortopulmonary window, along with the intrapericardial pathways found in the setting of common arterial trunk. The intrapericardial pathways refer to the portion of the developing outflow tract that is distal to the sinutubular junction, but which remains within the confines of the pericardial cavity.

During the process of obliteration of the aortopulmonary foramen, however, the distal cushions have themselves fused in what is now the intermediate portion of the outflow tract, along with

appearance of the intercalated valvar swellings. The intercalated swellings are located parietally within the intermediate part of the outflow tract, which retains its myocardial walls. They are offset, with one located more cranially than the other. Cavitation commences at the distal margin of the fused major cushions, along with the intercalated swellings, thus forming the primordiums of the aortic and pulmonary valves. If the major outflow cushions within the intermediate portion of the outflow tract fail to fuse, this results in a common arterial valve. The variation in the number of leaflets seen in those hearts with common arterial trunk are dependent either on the failure of fusion, or hypoplasia, of the cushions and swellings found within the intermediate portion. As emphasized, the myocardial walls of the intermediate portion, at this point, are retained. As cavitation continues, nonetheless, there is continuing ingrowth of nonmyocardial tissue from the second heart field. The cushions and swellings will remodel as cavitation continues, becoming the valvar leaflets. The added non-myocardial tissue from the second heart field then forms the sinuses of the arterial roots. As development continues, the central component of the fused cushions, initially derived from neural crest cells, undergoes apoptosis to result in separation of the aortic from the pulmonary root. At this point, the shell of the cushion mass is also undergoing myocardialisation.

As development progresses, the proximal outflow cushions will also fuse with one another, and with the crest of the ventricular septum. This process creates a shelf within the roof of the right ventricle, placing the aortic root in continuity with the cavity of the left ventricle. The shelf will eventually become the subpulmonary infundibulum, and will lift the pulmonary valve above the aortic root. The central core of these cushions is also populated with neural crest cells that will undergo apoptosis, thus creating the extracavitary space between the muscularized subpulmonary infundibulum and the sinuses of the aortic root. Maldevelopment or hypoplasia of the proximal outflow cushions results, most commonly, in the retention of the juxtaarterial ventricular septal defect. The proximal cushions, of course, themselves usually fail to fuse in the setting of common arterial trunk.

Indeed, the fact that failure of fusion of the outflow cushions was the reason for persistence of the common arterial trunk was demonstrated in an animal model, as long ago as 1978 by Van Mierop and his colleagues studying Keeshond dogs [15]. Most recently, the study of episcopic data sets in the mouse have shown similar models to clarify many of the developmental pathways. The knowledge of embryologic development of many different congenital cardiac malformations has significantly increased with the availability of the 3-dimensional models, but they fail to replicate many of the variants that are seen in the clinical setting. With advances in molecular biology and genetics, however, it is likely that the clinical variations can be explored with greater specificity in the animal models knowing the anatomical variations that can occur.

Our case, however, represents a variant of common arterial trunk with an intact ventricular septum that differs from the cases previously noted in the literature. As described in all of the similar cases, there was a fibrous partition that separated the right from the left components of the outflow tracts. This fibrous partition is reminiscent of the fibrous raphe that is often appreciated between the conjoined leaflets, and is to be found in the roof of the doubly committed and juxtaarterial ventricular septal defect. The raphe, and the fibrous partition described in our case, are most likely derived from the proximal cushions which have failed to muscularise. On either side of this fibrous partition, our case showed valvar components that had a significantly different appearance from one another. The tissue to the right is very reminiscent of the valvar tissue observed in those cases described as having absent pulmonary valve. The nodular remnants of valve tissue encircled the right ventricular outflow in annular fashion and did not bridge the fibrous partition. There was, furthermore, formation of a muscular infundibulum. The aortic component, on the other hand, had a very dysplastic appearance, with recognizable leaflets and valvar sinuses. As would be expected, the subvalvar infundibulum within the right ventricle is hypoplastic. It is interesting to note that the right component of the valve was actually slightly inferior to the left component (see Figure 3, right panel). This is consistent with hypoplasia of the proximal outflow cushions.

Common arterial trunk is frequently associated with DiGeorge Syndrome (del 22q11.2), but the chromosomal microarray in our case revealed a chromosomally normal female. Our case, therefore, is an example of isolated congenital heart disease with no other associated abnormalities. As previously stated, common arterial trunk is a rare anomaly, comprising no more than 1% of all occurrences of congenital heart disease. Nearly half of all patients with common arterial trunk, however, present with some associated genetic abnormality, a syndrome, or other noncardiac abnormality.

4. Conclusions

Straightforward descriptive analysis is the best path to follow when describing complex cardiac abnormalities such as the one presented here. This also applies to the developmental processes, allowing embryonic development and pre- or postnatal anatomy to be correlated in simple fashion. For those not familiar with a ventriculo-arterial septal defect, it may better be understood by comparing it to a so-called 'ostium primum' type of atrioventricular septal defect, where the bridging leaflets are attached to one another across the crest of the ventricular septum and effectively dividing the common atrioventricular junction into separate right and left atrioventricular orifices, as proposed in the previous description of Garg and colleagues. They draw comparison between the ventral protrusion from the dorsal wall of the aortic sac, which will form the aortopulmonary septum, and the vestibular spine, which occurs at the venous pole, and is responsible for separating the atrioventricular junction into tricuspid and mitral valves. A direct comparison can be drawn between the types of shunting that can occur with a common atrioventricular junction (Figure 4), and those hearts with a ventriculo-arterial septal defect and common ventriculo-arterial junction (Figure 5).

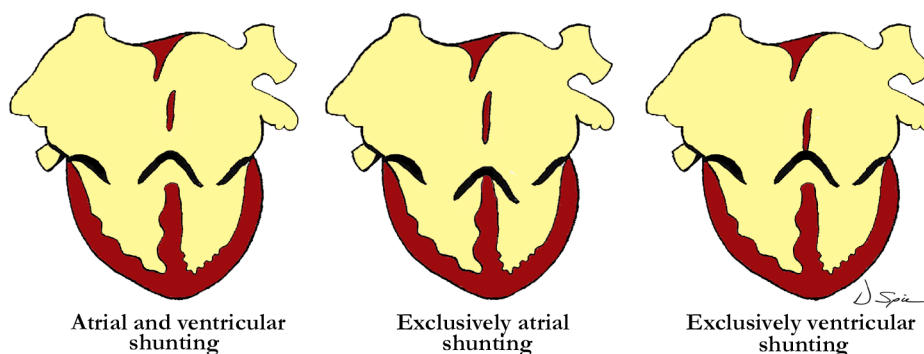


Figure 4. The illustration demonstrates the levels of shunting associated with the valvar arrangements in those hearts with atrioventricular septal defect. The left image shows both atrial and ventricular shunting, in the center there is exclusively atrial shunting, and to the right, exclusively ventricular shunting.

The case presented shows similarity to some of those presented in the literature in that the ventriculo-arterial junction was common, there was an associated common arterial trunk, and the ventricular septum was intact. Our case has a discrete subpulmonary infundibulum, and although hypoplastic, it was indeed present. Presence of an infundibulum is proof that the proximal cushions fused and muscularized, thus the formation of separate ventricular outflow tracts, along with an intact ventricular septum. The valvar components on either side of the fibrous partition, dividing the right and left components of the outlet, are what differs most significantly between our case and the others. The other cases had three to four dysplastic leaflets shared between the outlets, and bridging, to varying degrees, over the fibrous partition. The outflow cushions within the intermediate portion of the developing outflow tract failed to fuse in all cases with incomplete remodeling of the valves and sinuses to varying degrees. Even though our case had distinctive pulmonary and aortic components, it has a common ventriculo-arterial junction which differentiates it from the two, entirely separate arterial valves associated with aortopulmonary window (Figure 6). Even though some aortopulmonary windows can be quite large, the three developmental components are typically well represented

with failure of the embryonic aortopulmonary foramen to close, allowing for the defect between the intrapericardial arterial trunks. Hearts that have an aortopulmonary window most often have an intact ventricular septum.

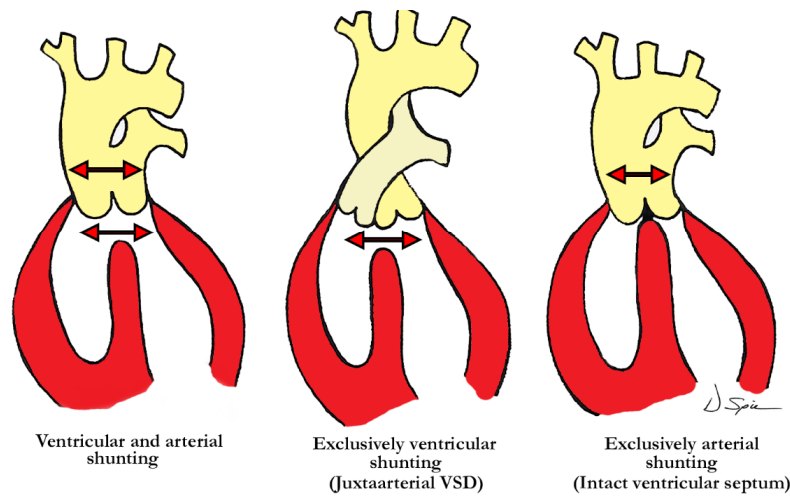


Figure 5. The illustration demonstrates the level of shunting in hearts with ventriculo-arterial septal defect with common ventriculo-arterial junction. The left image shows shunting at both ventricular and arterial levels, in the center there is exclusively ventricular shunting (juxtaarterial ventricular septal defect), and to the right, exclusively arterial shunting as demonstrated in our case with common arterial trunk and intact ventricular septum.

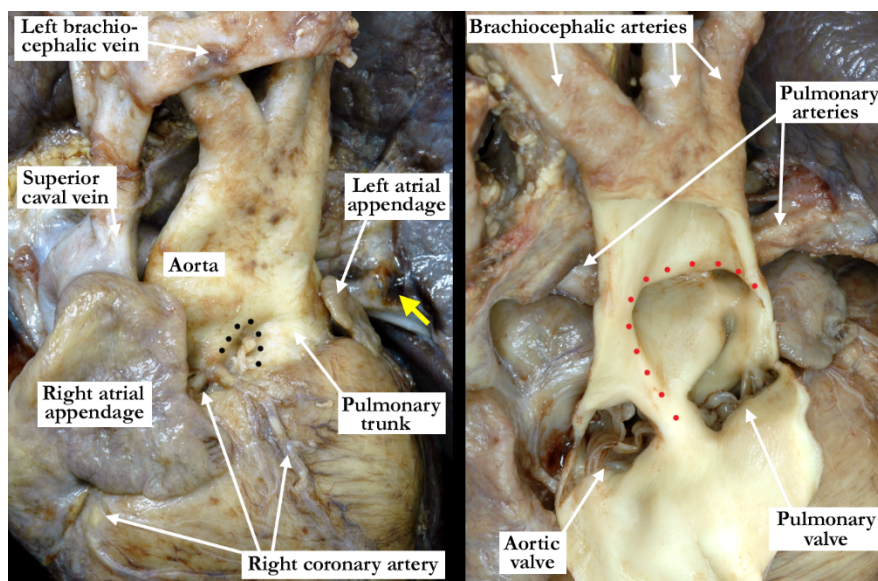


Figure 6. The left panel is an anterior superior view of the intrapericardial arterial trunks in a heart with an aortopulmonary window. The black dots demonstrate the separate aortic and pulmonary roots as the arterial trunks arise from the ventricular mass. (Yellow arrow—Left pulmonary artery) The right panel is from the same heart shown in the left panel. It demonstrates the large aortopulmonary window with the anterior aspect of the arterial trunks incised and folded forward. The borders of the window are marked with red dots. Note the entirely separate aortic and pulmonary valves.

One of the typical anatomic findings occurring with a common arterial trunk is a subarterial ventricular septal defect allowing for shunting at both the ventricular and arterial levels. This is directly comparable to those cases with a common atrioventricular junction and a common atrioventricular valve

where shunting is permitted at the atrial and ventricular levels. A common ventriculo-arterial junction with an intact septum can also be directly compared to a common atrioventricular junction with shunting permitted only at the atrial level, as in the so-called 'ostium primum' defect (Figure 7, left panel). In this situation the atrial vestibules can be discrete just as our outflow tracts are discrete. The superior and inferior bridging leaflets are adherent to one another across the crest of the ventricular septum and analogous to what we see in those hearts with common ventriculo-arterial junction and intact ventricular septum. Not only did our case have a subpulmonary infundibulum marking the presence of separate or discrete ventricular outflow tracts, the common valve also had different characteristics on either aspect of the fibrous partition that divided the common ventriculo-arterial junction. Those hearts with a doubly committed and juxtaarterial ventricular septal defect allow shunting only at the ventricular level with developmental hypoplasia of the proximal most component of the outflow tract. The intermediate and distal components are well developed in this situation with two separate arterial valves, that are in fibrous continuity with one another, and two separate intrapericardial arterial trunks (Figure 7, right panel).

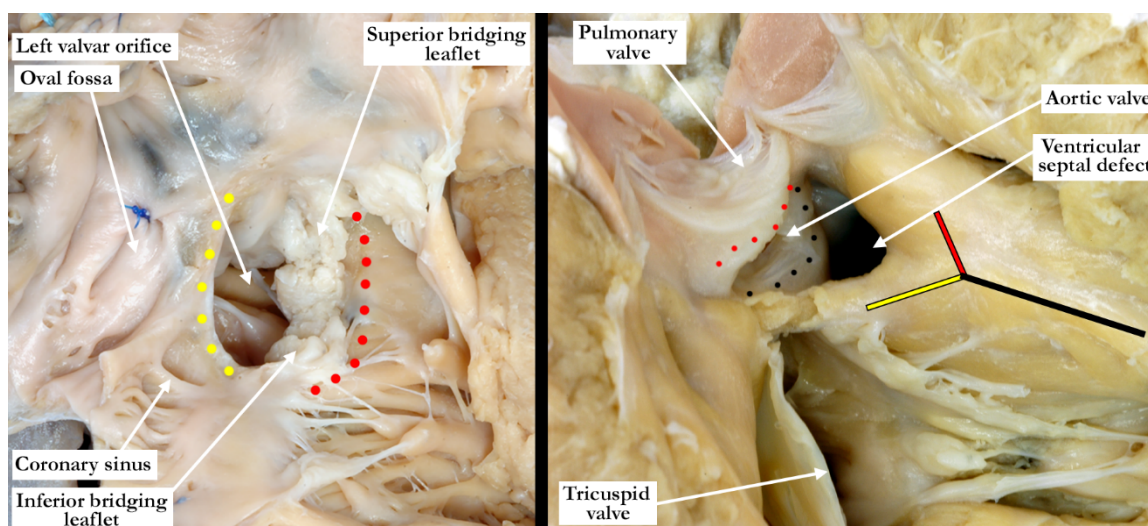


Figure 7. The left panel shows the opened right atrioventricular junction in this heart with a common atrioventricular junction. The superior and inferior bridging leaflets are adherent to one another and to the crest of the ventricular septum (red dots) effectively dividing the common junction into separate right and left orifices. Shunting can only take place at the atrial level. The yellow dots mark the leading edge of the atrial septum. The right panel shows the right ventricular outflow with a doubly committed, subarterial ventricular septal defect. The black line marks the body of the septal band, the red line, the cephalic arm and the yellow line the caudal arm which maintains its connection with the inner heart curvature, and thus will protect the conduction tissue. The pulmonary and aortic (black dots) valves are separate structures, and are in fibrous continuity (red dots) at the roof of the defect. Shunting can only occur at the ventricular level.

The case presented shows how all three components of the outflow tract develop with great independence. Abnormalities, inhibiting the migration of the extracardiac components, which include those from the second heart field along with the neural crest cells can significantly affect the anatomy of each of the three components of the developing outflow tracts. Our case demonstrates significant differentiation at the common ventriculo-arterial junction that has not yet been reported.

Funding: This research received no external funding.

Conflicts of Interest: The authors declare no conflict of interest.

References

1. Collett, R.W.; Edwards, J.E. Persistent truncus arteriosus: A classification according to anatomic types. *Surg. Clin. N. Am.* **1949**, *29*, 1245–1270. [CrossRef]
2. Van Praagh, R.; Van Praagh, S. The anatomy of common aorticopulmonary trunk (truncus arteriosus communis) and its embryologic implications. A study of 57 necropsy cases. *Am. J. Cardiol.* **1965**, *16*, 406–425. [CrossRef]
3. Carr, I.; Bharati, S.; Kusnoor, V.S.; Lev, M. Truncus arteriosus communis with intact ventricular septum. *Br. Heart J.* **1979**, *42*, 97–102. [CrossRef] [PubMed]
4. McElhinney, D.B.; Reddy, V.M.; Brook, M.M.; Hanley, F.L. Repair of truncus arteriosus with intact ventricular septum (Van Praagh type B2) in a neonate. *J. Thorac. Cardiovasc. Surg.* **2011**, *141*, 645–653. [CrossRef]
5. Garg, P.; Mishra, A.; Shah, R.; Parmar, D.; Anderson, R.H. Neonatal repair of common arterial trunk with intact ventricular septum. *World J. Ped. Cong. Heart Surg.* **2015**, *6*, 93–97. [CrossRef] [PubMed]
6. Ajami, G.; Amirghofran, A.A.; Amoozgar, H.; Borzouee, M. Persistent truncus arteriosus with intact ventricular septum: Clinical, hemodynamic and short-term outcome. *Iran. J. Pediatr.* **2015**, *25*, e2081. [CrossRef] [PubMed]
7. Zeevi, B.; Dembo, L.; Berant, M. Rare variant of truncus arteriosus with intact ventricular septum and hypoplastic right ventricle. *Br. Heart J.* **1992**, *68*, 214–215. [CrossRef] [PubMed]
8. Alves, P.M.; Ferrari, A.H. Common arterial trunk arising exclusively from the right ventricle with hypoplastic left ventricle and intact ventricular septum. *Int. J. Cardiol.* **1987**, *16*, 99–102. [CrossRef]
9. Tsang, V.T.; Kang, N.; Sullivan, I.; Marek, J.; Anderson, R.H. Ventriculoarterial septal defect with separate aortic and pulmonary valves, but common ventriculoarterial junction. *J. Thorac. Cardiovasc. Surg.* **2008**, *135*, 222–223. [CrossRef] [PubMed]
10. Kramer, T.C. The partitioning of the truncus and conus and formation of the membranous portion of the interventricular septum in the human heart. *Anat. Rec.* **1942**, *71*, 343–370. [CrossRef]
11. Anderson, R.H.; Chaudhry, B.; Mohun, T.J.; Bamforth, S.D.; Hoyland, D.; Phillips, H.M.; Webb, S.; Moorman, A.F.M.; Brown, N.A.; Henderson, D.J. Normal and abnormal development of the intrapericardial arterial trunks in humans and mice. *Cardiovasc. Res.* **2012**, *95*, 108–115. [CrossRef] [PubMed]
12. Spicer, D.E.; Bridgeman, J.M.; Brown, N.A.; Mohun, T.J.; Anderson, R.H. Anatomy and development of the cardiac valves. *Cardiol. Young* **2014**, *24*, 1008–1022. [CrossRef] [PubMed]
13. Anderson, R.H.; Mohun, T.J.; Spicer, D.E.; Bamforth, S.D.; Brown, N.A.; Chaudhry, B.; Henderson, D.J. Myths and realities relating to the development of the arterial valves. *J. Cardiovasc. Dev. Dis.* **2014**, *1*, 177–200. [CrossRef]
14. Tretter, J.T.; Steffensen, T.S.; Westover, T.; Anderson, R.H.; Spicer, D.E. Developmental considerations with regard to so-called absence of the leaflets of the arterial valves. *Cardiol. Young* **2016**, *27*, 302–311. [CrossRef]
15. Van Mierop, L.H.; Patterson, D.F.; Schnarr, W.R. Pathogenesis of persistent truncus arteriosus in light of observations made in a dog embryo with the anomaly. *Am. J. Cardiol* **1978**, *41*, 755–762. [CrossRef]



© 2020 by the authors. Licensee MDPI, Basel, Switzerland. This article is an open access article distributed under the terms and conditions of the Creative Commons Attribution (CC BY) license (<http://creativecommons.org/licenses/by/4.0/>).



Review

Atrioventricular Septal Defect: What Is in a Name?

Michael Rigby

MD FRCP FRCPC, Royal Brompton Hospital, London SW3 6NP, UK; M.Rigby@rbht.nhs.uk

Abstract: Robert Anderson has made a huge contribution to almost all aspects of morphology and understanding of congenital cardiac malformations, none more so than the group of anomalies that many of those in the practice of paediatric cardiology and adult congenital heart disease now call 'Atrioventricular Septal Defect' (AVSD). In 1982, with Anton Becker working in Amsterdam, their hallmark 'What's in a name?' editorial was published in the *Journal of Thoracic and Cardiovascular Surgery*. At that time most described the group of lesions as 'atrioventricular canal malformation' or 'endocardial cushion defect'. Perhaps more significantly, the so-called ostium primum defect was thought to represent a partial variant. It was also universally thought, at that time, that the left atrioventricular valve was no more than a mitral valve with a cleft in the aortic leaflet. In addition to this, lesions such as isolated cleft of the mitral valve, large ventricular septal defects opening to the inlet of the right and hearts with straddling or overriding tricuspid valve were variations of the atrioventricular canal malformation. Anderson and Becker emphasised the differences between the atrioventricular junction in the normal heart and those with a common junction for which they recommended the generic name, 'atrioventricular septal defect'. As I will discuss, over many years, they continued to work with clinical cardiologists and cardiac surgeons to refine diagnostic criteria and transform the classification and understanding of this complex group of anomalies. Their emphasis was always on accurate diagnosis and communication, which is conveyed in this review.

Keywords: atrioventricular septal defect; AVSD; atrioventricular junction; bridging leaflets; nomenclature; classification

Citation: Rigby, M. Atrioventricular Septal Defect: What Is in a Name?. *J. Cardiovasc. Dev. Dis.* **2021**, *8*, 19. <https://doi.org/10.3390/jcdd8020019>

Received: 13 January 2021
Accepted: 9 February 2021
Published: 15 February 2021

Publisher's Note: MDPI stays neutral with regard to jurisdictional claims in published maps and institutional affiliations.



Copyright: © 2021 by the author. Licensee MDPI, Basel, Switzerland. This article is an open access article distributed under the terms and conditions of the Creative Commons Attribution (CC BY) license (<https://creativecommons.org/licenses/by/4.0/>).

1. Introduction

Robert Anderson has made a huge contribution to almost all aspects of morphology and understanding of congenital cardiac malformations, none more so than the group of anomalies that many of those in the practice of paediatric cardiology and adult congenital heart disease now call 'Atrioventricular Septal Defect' (AVSD). In 1982, with Anton Becker working in Amsterdam, their hallmark 'What's in a name?' editorial was published in the *Journal of Thoracic and Cardiovascular Surgery* [1].

Prior to that groundbreaking publication, it was already recognised that a group of malformations had comparable morphology comprising abnormal atrioventricular valves. Blieden and colleagues [2] had previously described disproportion between the inlet and outlet dimensions of the ventricles, readily demonstrated by the left ventricular 'goose-neck' on angiography, as the key to diagnosis. At that stage most described the group of lesions as 'atrioventricular canal malformation' or 'endocardial cushion defect' [3,4]. Perhaps more significantly, the so-called ostium primum defect was thought to represent a partial variant. It was also universally thought, at that time, that the left atrioventricular valve was no more than a mitral valve with a cleft in the aortic leaflet. In addition to this, lesions such as isolated cleft of the mitral valve, large ventricular septal defects opening to the inlet of the right and hearts with straddling or overriding tricuspid valve were considered variations of the atrioventricular canal malformation.

There were two extremely important events contributing to the breakthrough in understanding. The first was when Anderson and Becker, working with heart specimens in Amsterdam, stripped away completely from the atrioventricular junction, the leaflets of

the atrioventricular valves. Having removed the valve leaflets, it was realised that in any individual heart with this group of anomalies, it was impossible to know whether, initially, the specimen had represented a so-called 'partial', 'intermediate' or 'complete' example of the anatomy, because each of the hearts had a common atrioventricular junction completely different from the normal heart. The second important event was when cardiologists, using their newly acquired skills in cross-sectional echocardiography, were able to produce exquisite moving images of these hearts, representing cross-sectional anatomic sections. I recall Bob Anderson being 'blown away' by what he was seeing at our regular weekly meetings and immediately our understanding began to reach completion. With morphological sections of the heart [5], he simulated echocardiographic sections in four chamber and short axis of the atrioventricular junction, confirming, at a stroke, these provided almost all of the information for accurate diagnosis apart from demonstrating the ventricular outflows.

By coincidence, in 1982 we were both guests of the Brazilian Society of Pediatric Cardiology in Porto Alegre around the time of publication. During this, my first visit to South America (Figure 1) it was no coincidence that some of the academic sessions revolved around the potentially controversial topic of AVSD, the subject of the 'What's in a name' publication. Anderson and Becker had advocated dismissing the terms 'endocardial cushion defect' and 'atrioventricular canal defect' on the basis they were morphologically unsound and inaccurate despite them being in common usage. By that time, I had found their arguments persuasive and, using the 'new' nomenclature, together we demonstrated heart specimens and moving echocardiographic images of the heart painstakingly recorded and edited onto high quality video tape. The presentations and recommendations were received enthusiastically by the large international faculty and many delegates. So began a new era of understanding, crucial to improvements in surgical outcome. However, although it was the intention of Becker and Anderson to provide a precise and accurate way of describing hearts with AVSD, the term has continued to be used imprecisely by many cardiologists and surgeons, as I will outline later.

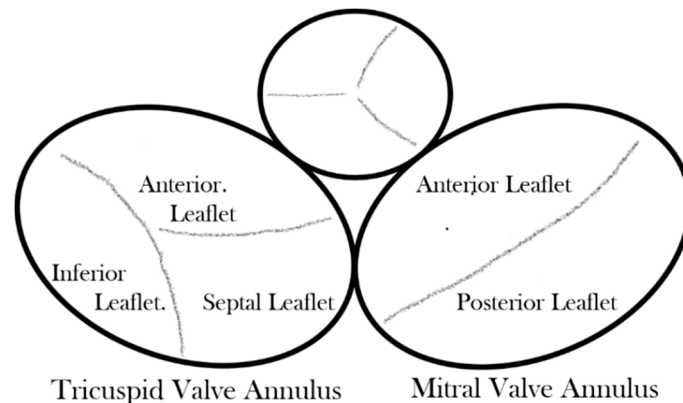


Figure 1. Invited faculty, Brazilian Congress of Pediatric Cardiology, Porto Alegre, 1982.

2. Consideration of the Atrioventricular Junction and Valve Leaflets

Considering first the normal atrioventricular junction [6], it is divided into discrete right and left components that surround the orifices of the mitral and tricuspid valves,

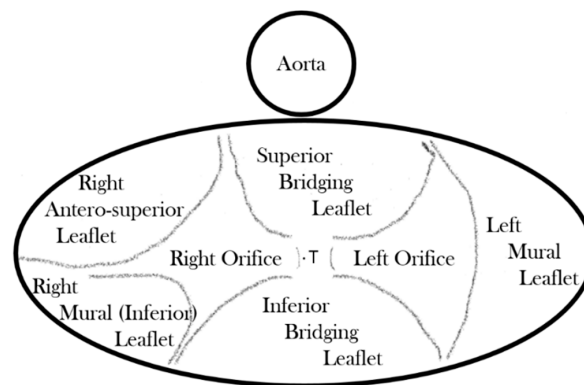
respectively (Figure 2). The two junctions are themselves contiguous only over a very short area, which is that of the muscular atrioventricular septum anterior, and superior to this short area, the subaortic outflow tract of the left ventricle interposes between the mitral valve and the muscular ventricular septum and the fibrous membranous septum. At all other points around the atrioventricular junctions, the fibrofatty tissue of the atrioventricular grooves interposes between atrial and ventricular myocardium and becomes contiguous with the fibrous leaflets of mitral and tricuspid valves while the aortic valve is wedged anteriorly between the mitral and tricuspid valves.



The normal atrioventricular junction viewed from above
Figure 2. Drawing of the normal atrioventricular junction.

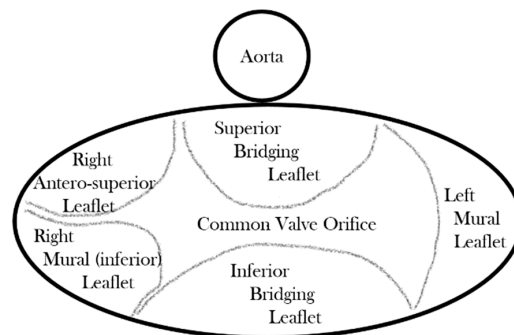
In essence, Anderson and Becker had proposed the term ‘atrioventricular septal defect’ as a generic name for a group of anomalies characterised by absence of atrioventricular septal structures and consequently possessing a common atrioventricular junction guarded by a common atrioventricular valve and therefore completely different from the atrioventricular junction of the normal heart [7]. There is not only a grossly abnormal atrioventricular junction morphology but also of necessity an abnormally positioned conduction axis as well as the subaortic outflow no longer being able to interpose between the left and right sides of the junction.

In almost every form, the common atrioventricular valve is composed of five leaflets of which only the superior and inferior bridging leaflets are found within both the left and right ventricles, whereas the left mural leaflet is confined to the left ventricle and the right (inferior) mural and right anterosuperior leaflets are located inferiorly and anterosuperiorly, respectively, in the right ventricle. The zone of apposition of the inferior and superior bridging leaflets is the most frequent site of valve insufficiency. This common valve will have a single (‘common’) orifice or will be divided into two orifices by a tongue of valve tissue joining the bridging leaflets; this provides the basis for a broad classification of all cases (Figure 3a,b). Irrespective of common or separate orifices the left ventricular component of the common valve has a trileaflet arrangement that cannot be compared with the normal mitral valve, an appellation that should be avoided. The right ventricular component of the common valve similarly should not be called ‘tricuspid’ [6]. It is also important to be aware that ‘AVSD’ on its own is not a diagnosis and should not be used alone to describe any of the various forms of this group of anomalies because it lacks any specificity whatsoever.



Atrioventricular junction in AVSD with 2 valve orifices

(a)



Atrioventricular Junction in AVSD with Common (single) valve orifice

(b)

Figure 3. (a) Drawing of the atrioventricular junction in Atrioventricular Septal Defect (AVSD) with two valve orifices. (b) Drawing of the atrioventricular junction in AVSD with common valve orifice.

With two valve orifices the most frequent form is the isolated primum defect, which is also commonly described as ‘partial AVSD’, although there is nothing partial about the common atrioventricular junction, which is just as complete as that seen in patients with common valve orifice. Other variations include an isolated interventricular defect or combined primum interatrial defect and interventricular component; both forms can also be described as ‘intermediate’, but qualifying additional description is required in diagnosis to distinguish the two forms. Rarely are completely intact septal structures found, an AVSD without interatrial or interventricular communication. With common orifice the main variation is found in the degree of bridging of the superior bridging leaflet, but there is almost always an interatrial and interventricular communication. Whatever the type of AVSD, the left ventricular outflow is sometimes longer than that of the normal heart [8], and the value of the inlet/outlet dimensions ratio was significantly less in hearts with atrioventricular septal defects, with $p < 0.001$ in Table III of that publication. So, it seems to me that it could indeed be a diagnostic criterion on its own.

3. Variations from Usual Forms of AVSD

Quite independent of these various types, associated anomalies can include left or right ventricular inflow obstruction, dual orifice left ventricular atrioventricular valve leaflets, atrioventricular valve regurgitation, left or right ventricular outflow tract obstruction in various forms, and right or left ventricular hypoplasia (‘ventricular imbalance’). Left ventricular outflow obstruction can be particularly complex. The subaortic outflow is frequently elongated and relatively narrow in all forms of AVSD. The causes of obstruction include anomalous tissue tags, anomalous chords to the ventricular septum, discrete fibro-

muscular stenosis and tunnel-like narrowing. Another variation to be aware of is double outlet right atrium, in which inevitably blood flows directly from right atrium to left ventricle, causing unexplained systemic arterial desaturation. There is also a well-recognised association of AVSD with Trisomy 21, atrial isomerism, total anomalous pulmonary venous connection and Tetralogy of Fallot and, rarely, even with common arterial trunk.

The key to the diagnosis of AVSD and, to a major extent, appropriate and effective surgical management lies in the structure of the atrioventricular valve leaflets found in the left ventricle [9,10]. When the left atrioventricular component of the common junction is considered in isolation, the mural leaflet forms less than one-third of the circumference of the orifice, the remainder being formed of components of the superior and inferior bridging leaflets, which together form a zone of apposition that some still and incorrectly describe as 'a cleft'. Even if a surgeon were to suture together completely this zone of apposition, such a manoeuvre would not restore the morphology to that of a normal mitral valve. There is not complete agreement as to whether or not at the time of operation the surgeon should suture together, partially or completely, the zone of apposition, particularly in the absence of preoperative valve insufficiency.

There is a potentially complicating aspect when the left ventricular valve leaflets lack the usual morphology found in an AVSD, and this also has major surgical significance [11,12]. The classical distortion is found in parachute malformations. In such cases all the valve chords attach to a single papillary muscle, usually because the mural leaflet is extremely small or absent. The valve orifice is then represented only by the zone of apposition between the bridging leaflets, and the key point of surgical significance is it cannot be sutured, even in the presence of significant valve insufficiency, because stenosis will almost inevitably be the outcome. However, the parachute malformation of the left AV valve in AVSD may not be caused by an absent mural leaflet. It could be the reverse in that, if there is a single papillary muscle, then the mural leaflet is by necessity absent. In the study by Oosthoek PW et al. [13], the anomaly of the papillary muscles was considered the primary event leading to parachute valve. Other deviations from the usual valve morphology include leaflet dysplasia, a small or miniaturized orifice, short superior bridging leaflet, extremely short valve chords or dual orifice produced by an anomalous bridge of valve tissue between any two of the leaflets.

It is important briefly to discuss a rare form of deficient atrioventricular septation with separate left and right atrioventricular junctions. The patients with deficiency of the fibrous atrioventricular septum, although properly described as atrioventricular septal defects, do not have a common atrioventricular junction. It was the view of Anderson that it was more convenient to describe them as 'Gerbode' defects while recognising their affinity with hearts with perimembranous VSD combined with the potential for ventriculo-atrial shunting because of a deficiency in the commissure between the septal and anterior leaflets of the tricuspid valve.

4. Diagnostic Considerations

The diagnosis of any form of AVSD is almost always made by cross-sectional echocardiography, which provides exquisite imaging and a precise diagnosis in most cases, particularly in early life [5,7]; magnetic resonance imaging, rarely required in primary diagnosis, can also be helpful and carries the advantage of being able to demonstrate the atrial and ventricular components en face more reliably than transthoracic three-dimensional echocardiography in older patients. In practice, because primary diagnosis is made in infancy, the resolution of 3D echocardiography makes it of limited value in presurgical work up. But cardiac ultrasound does allow a complete morphological diagnosis in most cases, and colour flow Doppler is complementary because it shows the sites of intracardiac shunting and the location and direction of any atrioventricular valve regurgitation. There is frequently a curtain of regurgitant blood flow between the bridging leaflets, and although exact quantification of valve insufficiency is often difficult, it can broadly be classified into trivial, mild, moderate or severe. Atrioventricular septal defects may be

encountered when there is atrial isomerism, and for this reason the accurate determination of atrial arrangement, atrioventricular and ventricular relationships, ventricular topology, great artery relationships and systemic and pulmonary venous drainage is also important. The various forms of AVSD are now readily diagnosed antenatally by the fetal cardiologist; an accurate description and complete diagnosis also provides important information regarding postnatal prognosis.

There are some basic rules of cross-sectional echocardiography that are fundamental to the diagnosis [5,7]. The subcostal short axis section can always demonstrate a common atrioventricular junction guarded by a common atrioventricular valve with the aortic valve in an anterior and 'unwedged' position (Figures 4 and 5). These features can also be demonstrated by 3D echocardiography (Figures 6 and 7). This seems to be a consistent and diagnostic echocardiographic feature of all atrioventricular septal defects that can be equally well seen with magnetic resonance imaging. In many instances both imaging techniques potentially allow the differentiation of each of the five leaflets of the common atrioventricular valve. In general terms echocardiographic four chamber sections allow the immediate recognition of an atrioventricular septal defect. It is important to be aware, however, that it is the subcostal four chamber section used expertly that best defines the inferior bridging leaflet (Figure 8), clearly inferior to the more anterior, superior bridging leaflet (7). When scanning from the horizontal subdiaphragmatic sections to the paracardiac section of the atrioventricular junction, it is the inferior leaflet that is imaged first. The apical and parasternal four chamber sections allow visualisation of the more anterior, superior bridging leaflet (Figure 9). The subcostal long axis section will show the left ventricular outflow tract formed medially by the superior bridging leaflet and laterally by the wall of the left ventricle. The trileaflet left atrioventricular valve will be evident on subcostal and parasternal short axis sections of the left ventricle. This is again a very consistent finding in atrioventricular septal defects and is particularly useful in unusual examples when standard four chamber sections are not diagnostic. The trileaflet valve is composed of the left mural leaflet and the left ventricular components of the superior and inferior bridging leaflets. The commissure between the bridging leaflets that points towards the ventricular septum is still often described incorrectly as a 'cleft'.

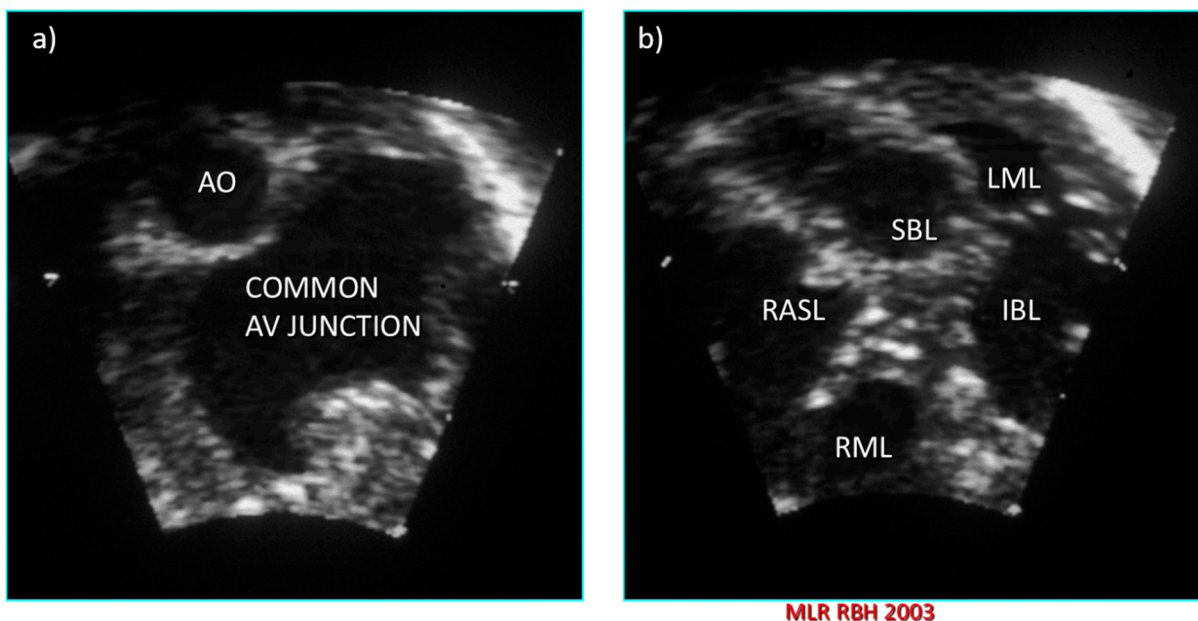


Figure 4. Subcostal left oblique short axis echocardiographic sections of the AV junction showing (a) the common atrioventricular junction and (b) the five leaflets of the common atrioventricular valve.

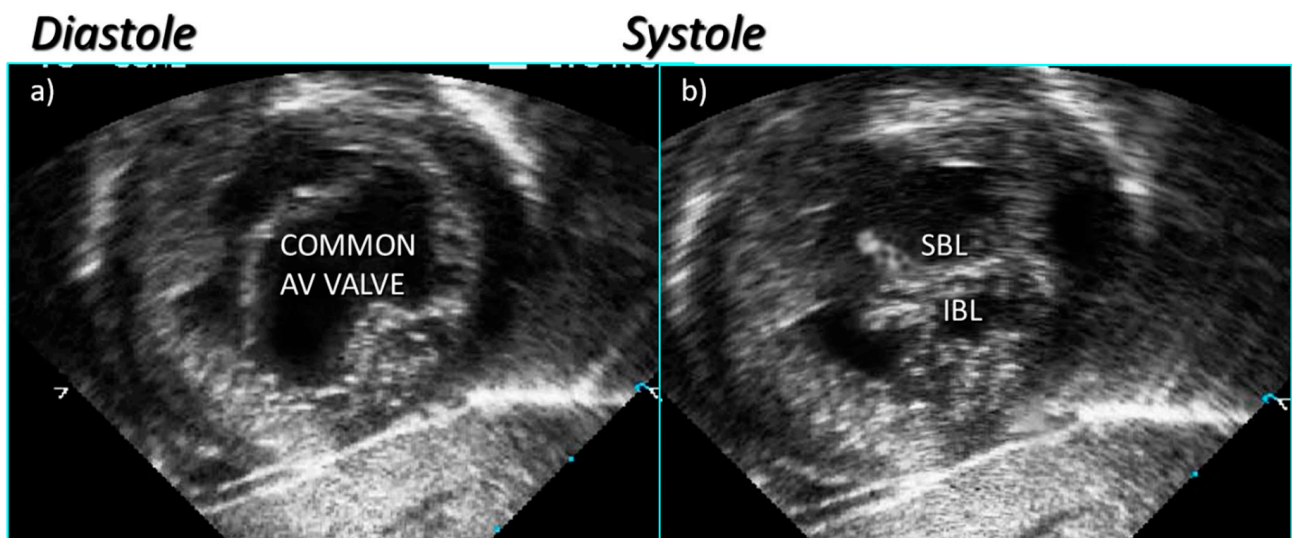


Figure 5. Subcostal left oblique short axis echocardiographic section of AV junction at level of AV valve leaflets showing (a) common atrioventricular valve during atrial systole and (b) the zone of apposition of the superior and inferior bridging leaflets.

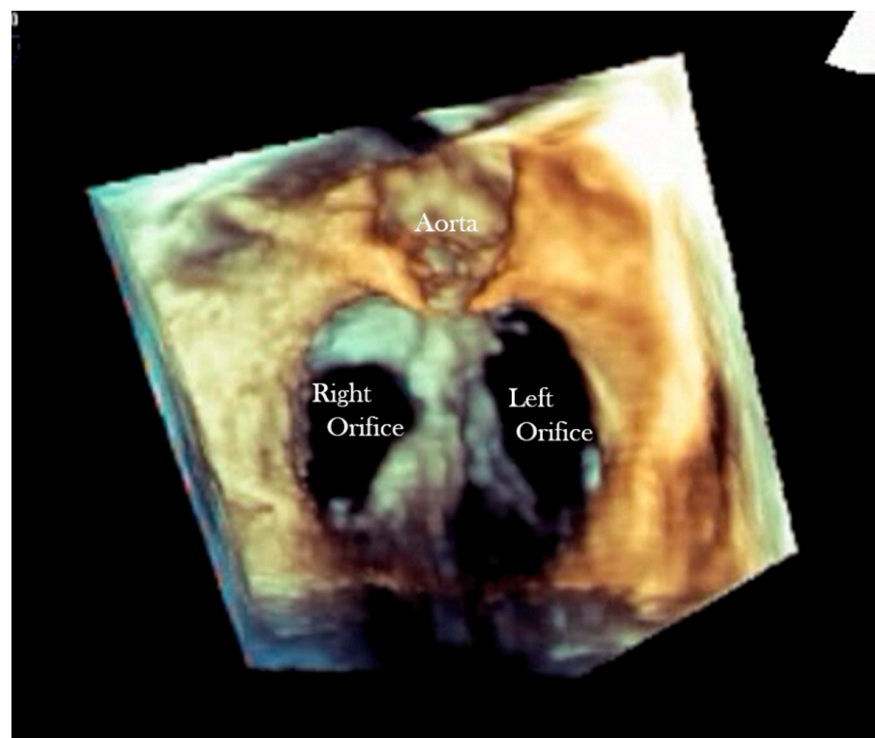


Figure 6. Short axis 3D echocardiographic section in a heart with AVSD and two valve orifices.

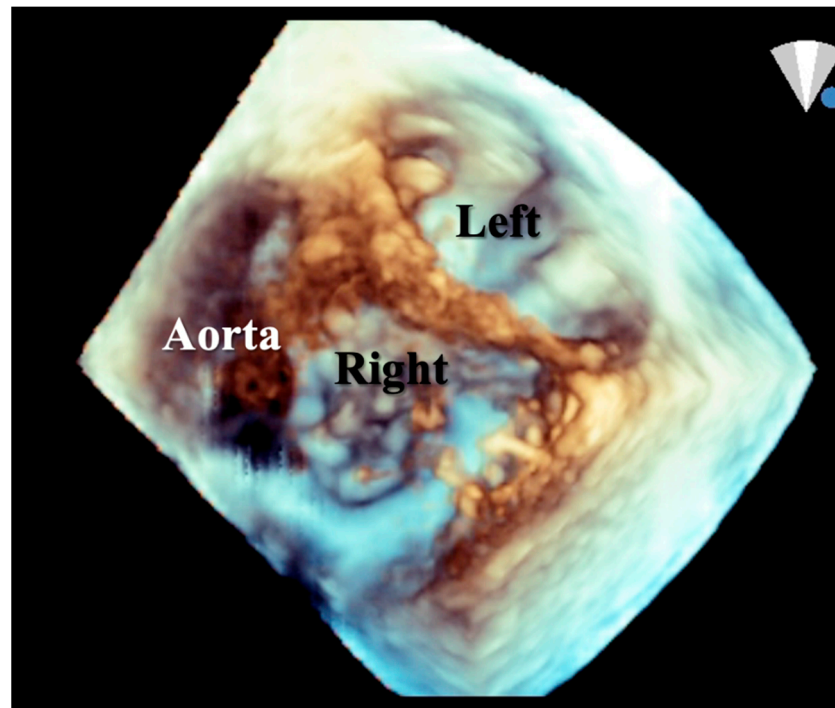


Figure 7. Short axis 3-D echocardiographic section in a heart with partial AVSD with left and right valve orifices. Part of the ventricular septum can be seen between these orifices.

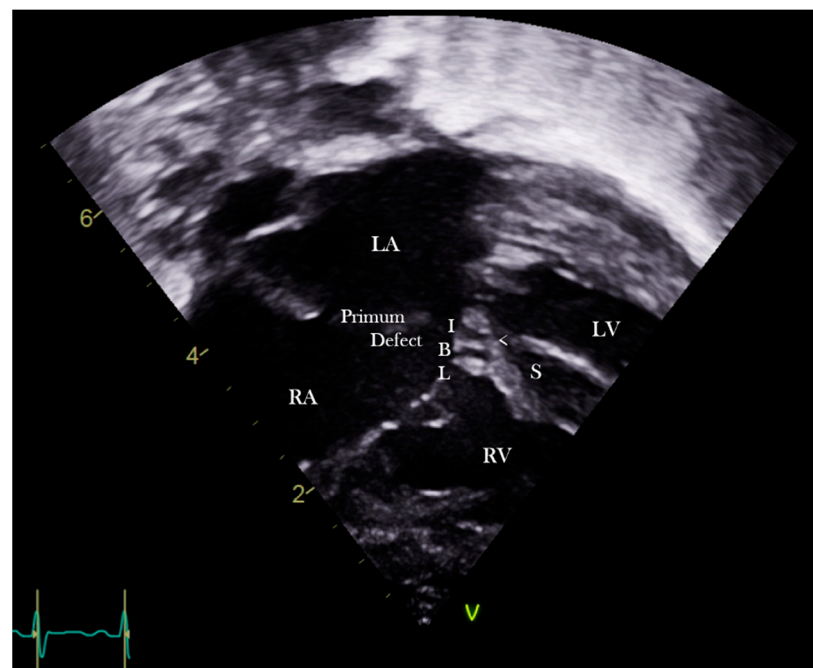


Figure 8. Subcostal echocardiographic four chamber section showing the inferior bridging leaflet.

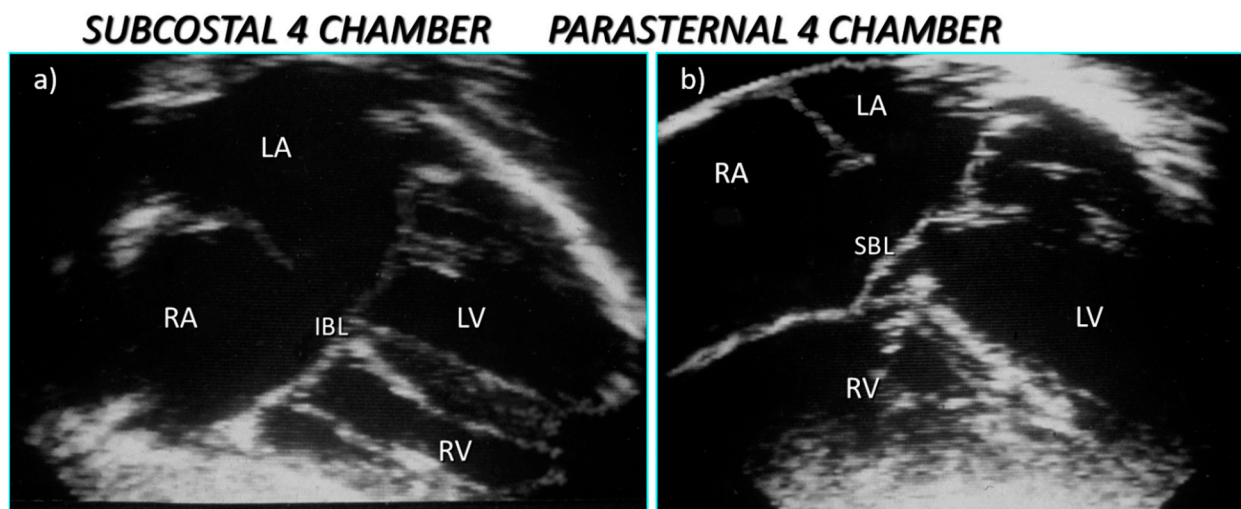


Figure 9. Echocardiography sections from a partial atrioventricular septal defect showing (a) the primum defect and inferior bridging leaflet in the subcostal section and (b) the anterior and bridging leaflet in the apical section with an obvious recess beneath the superior bridging leaflet.

It is important to be aware that the typical trileaflet appearance of the left ventricular valve is distorted when there is a dual orifice or severe leaflet dysplasia [10]. A two-leaflet valve will be found when the left mural leaflet is absent, and this can result in problems in diagnosis of an AVSD, particularly in cases with an isolated interventricular defect or intact septal structures. However, the bileaflet valve is still quite distinct from the normal mitral valve. Absence of the left mural leaflet frequently causes the left-sided AV valve to be small and or potentially stenotic. As I described earlier, a parachute abnormality is also associated with a bileaflet valve, and short axis echocardiographic sections of the left ventricle will usually reveal a single papillary muscle.

The mainstay of diagnosis remains cross-sectional echocardiography [5,7]. The most frequently observed form of an atrioventricular septal defect with two valve orifices is an isolated primum defect ('partial AVSD') between the lower edge of the atrial septum and the atrioventricular valve leaflets (Figure 9). In four chamber sections there appear to be two atrioventricular valves, each attached to the crest of the ventricular septum and in continuity through the bridging leaflets, so that there is absence of the normal offsetting. The commonly observed recess, directly below the superior bridging leaflet, attached to the ventricular septum should not be described as an interventricular communication or VSD. Less common variants with two valve orifices include complete absence of a primum defect ('intermediate AVSD'), with an interventricular communication masquerading as a perimembranous inlet ventricular septal defect (Figure 10a,b); the diagnosis relies on the finding of a trileaflet left atrioventricular valve (Figure 10b) and a common atrioventricular junction. Alternatively, both a primum defect and an interventricular component can be seen in parasternal four chamber sections. The ventricular component is then usually relatively small, and this variation has also been called an 'intermediate' form. Rarely, an isolated trileaflet left atrioventricular valve may be associated with intact septal structures, although in a number of cases spontaneous closure of a small interventricular component will have occurred postnatally. Nevertheless, it is important to be aware that an atrioventricular septal defect can occasionally exist in the absence of any atrial septal defect or interventricular communication. We have encountered such cases presenting with severe left atrioventricular valve regurgitation, but it was usually possible for the valve to be repaired at surgery. These cases also need to be distinguished from the isolated cleft of the anterior leaflet of the mitral valve, which is directed towards the outlet of the left ventricle rather than towards the septum.

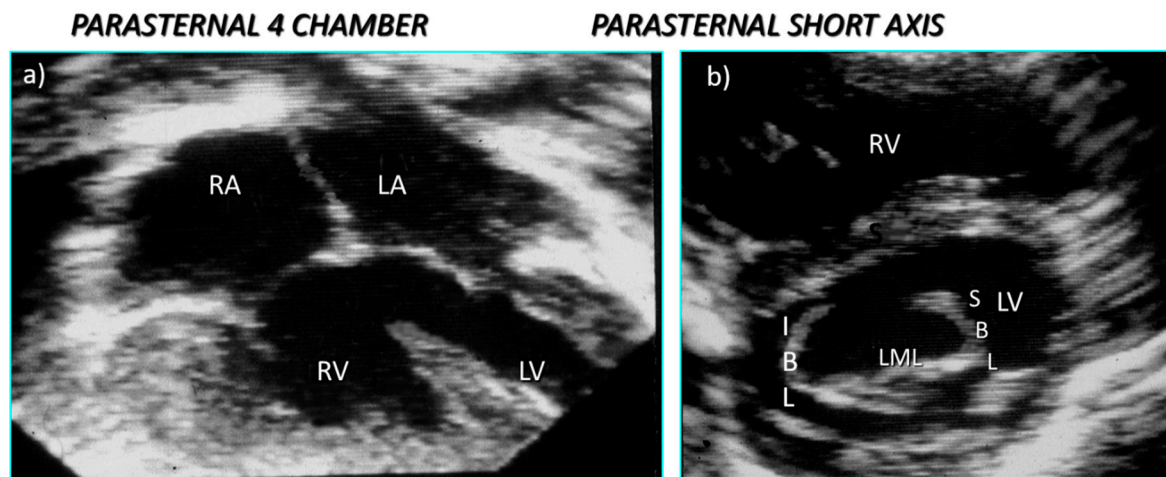


Figure 10. Echocardiographic sections from a heart with the form of AVSD in which (a) the parasternal four chamber section reveals the isolated interventricular communication and (b) the parasternal short axis section reveals the trileaflet left atrioventricular valve.

The typical features of the so-called ‘complete’ AVSD are also best identified in four chamber sections and include a primum interatrial defect, common atrioventricular valve orifice and an interventricular communication that can be more or less extensive, depending on the attachment of bridging leaflets (Figure 11). The inferior bridging leaflet is frequently attached by a mid-line raphe to the septal crest so that there is no additional defect posteriorly, but it may be free-floating so that the defect extends beneath this leaflet. Most variation in the size of the ventricular septal component, however, is found anteriorly beneath the superior bridging leaflet and is evident on parasternal four chamber sections. There is considerable variation in the amount of bridging of the superior leaflet, which may be more or less extensive. Extreme bridging is more likely to be encountered in those cases associated with Tetralogy of Fallot or double outlet right ventricle.

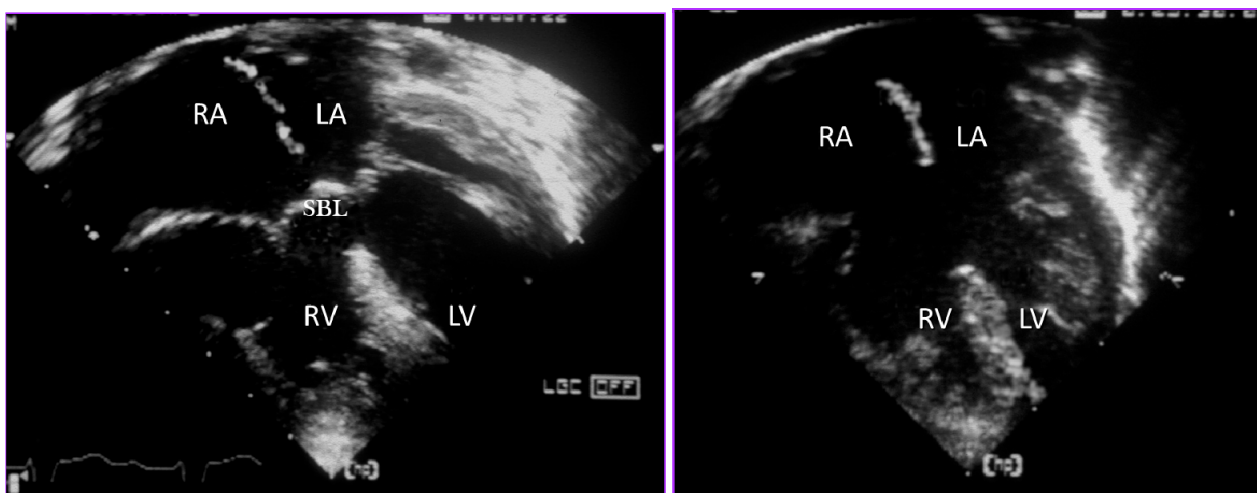


Figure 11. Echocardiographic sections from a heart with complete AVSD (a) during ventricular systole with the valve closed and (b) during diastole with the valve open.

5. What Is in a Name?

So, what is in a name when today’s cardiovascular imaging is so good? In many situations, the exquisite detail provided by echocardiography cannot be described in a single word or phrase, although in most cases there is a primary diagnosis that alerts physicians and surgeons to the basic abnormality [14]. Considering first the simplest form

of atrioventricular septal defect, the commonly used term ‘primum atrial septal defect’ or ‘partial AVSD’ is clearly preferable to ‘atrioventricular septal defect with two valve orifices and an isolated interatrial defect’, if only because the former is shorter and more precise and everyone knows what it means. Anderson and Becker understandably disliked the term ‘partial’ because there is a complete common atrioventricular junction. Of course, there may be the additional abnormalities I referred to earlier as well as atrioventricular valve regurgitation or left ventricular outflow tract obstruction, but these can be included as supplementary lines in the diagnosis, enabling a full description of the heart to emerge.

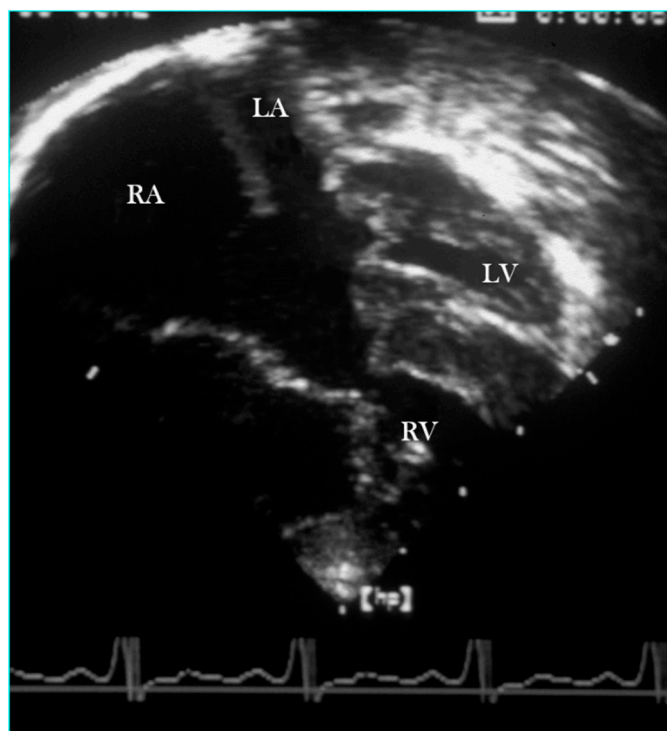
But what of hearts with a common atrioventricular junction and common orifice (‘complete AVSD’)? Such examples are often called ‘atrioventricular septal defect’ as the primary diagnosis. This is clearly an unsatisfactory state of affairs taking into account that this is the selected generic name for all types, but the terms ‘complete atrioventricular septal defect’ or even ‘complete atrioventricular canal defect’, although imperfect, are still better able to convey a diagnosis that everyone understands. To my mind ‘atrioventricular septal defect with common valve orifice’ is too much of a mouthful. Any additional abnormalities such as left or right ventricular hypoplasia (‘ventricular imbalance’) can be recorded as additional secondary diagnoses.

So, what should we call the various types of AVSD? Always, the underlying principle is precise and accurate communication. I would suggest ‘complete AVSD’ is a term understood and accepted as referring to hearts with a common valve orifice and primum and interventricular defects. I would also advocate that the terms ‘partial’ or ‘incomplete’ refer to all types of AVSD with two valve orifices and isolated primum defect while ‘intermediate’ refers to any AVSD with two valve orifices and an interventricular communication. However, in the nomenclature of CHD (congenital heart disease) recently designed by the ISNPCHD for the ICD-11 [15], the term ‘intermediate AVSD’ (and its synonym ‘transitional AVSD’) has a very different meaning. It refers to an “Atrioventricular septal defect with communication at atrial level and restrictive communication at ventricular level”, when there is complete absence of a primum defect (‘intermediate AVSD’) corresponding in ICD-11 to an “Atrioventricular septal defect with communication at the ventricular level only”, with the synonym “atrioventricular septal defect with isolated ventricular component”. It is therefore better to be more specific and use the following terms:

- ‘Isolated primum ASD’ or ‘partial AVSD’,
- ‘AVSD with two valve orifices and isolated ventricular component’ or ‘AVSD with isolated VSD’,
- ‘AVSD with two valve orifices, primum ASD and small ventricular component’ or ‘intermediate AVSD with primum ASD and VSD’,
- ‘Complete AVSD’,
- ‘AVSD with intact septal structures’.

This basic classification can be used when there are deviations from the usual forms, such as ventricular hypoplasia [12,14–16].

Problems in nomenclature can also arise in some hearts with AVSD because there is a profound departure from the usual morphology. For example, with usual atrial arrangement, if the atrioventricular connection is discordant, then the ventriculo-arterial connection is almost always discordant or double outlet right ventricle. The diagnosis requires the accurate recognition and description of ventricular morphology and ventricular topology, but the unifying feature will remain a common atrioventricular junction albeit with the right side of the common valve having a trileaflet structure instead of the left. Similar ventricular relationships may be encountered with atrial isomerism and atrioventricular septal defect in Figure 12 [16]. When there are abnormalities of atrioventricular connection, the essential role of imaging is a sequential segmental approach to diagnosis in order to fully describe such hearts. In such a situation a name is unimportant, but describing the way the atria connect to the ventricles and the morphology of the atrioventricular valve together with details of the type and mode of ventriculo-arterial connection is crucial to accurate diagnosis and surgical planning.



MLR RBH 2003

Figure 12. Echocardiographic four chamber section from a heart with partial AVSD, hypoplastic left ventricle and miniaturised left atrioventricular valve orifice.

6. Other Examples of Absence of the Atrioventricular Septum

At the outset I explained that according to Anderson and Becker one of the hallmarks of an AVSD was absence of the atrioventricular septum. Yet they would accept that this will be absent in other situations such as tricuspid atresia, double inlet left ventricle with two atrioventricular valves and even some posterior ‘inlet’ perimembranous ventricular septal defects. These malformations, however, fail to satisfy a second criterion for inclusion, a common atrioventricular junction. But there is a close cousin, which, although characterised by absence of the atrioventricular septum and a common atrioventricular junction, is not necessarily an atrioventricular septal defect. In some cases of double inlet ventricle, a common atrioventricular valve neither straddles nor overrides the ventricular septum and is committed entirely to one ventricle. Such hearts are not examples, therefore, of an atrioventricular septal defect with ventricular imbalance but clear examples of a univentricular atrioventricular connection with double inlet. Even those who might argue the case for using the term unbalanced AVSD when there is a dominant left or right ventricle could not continue the argument in the presence of double inlet connection to a solitary indeterminate ventricle. It is, however, morphologically correct to describe the connection as double inlet when 75% or more of the common atrioventricular valve is committed to one ventricle in the presence of a second hypoplastic and rudimentary contralateral ventricular chamber (Figures 13 and 14). I recall Anderson informing me “we have thus far been unable to discern any consistent difference in the characteristics of the common valve in double inlet and atrioventricular septal defect although in the former the common valve sometimes consists of four rather than five leaflets”.

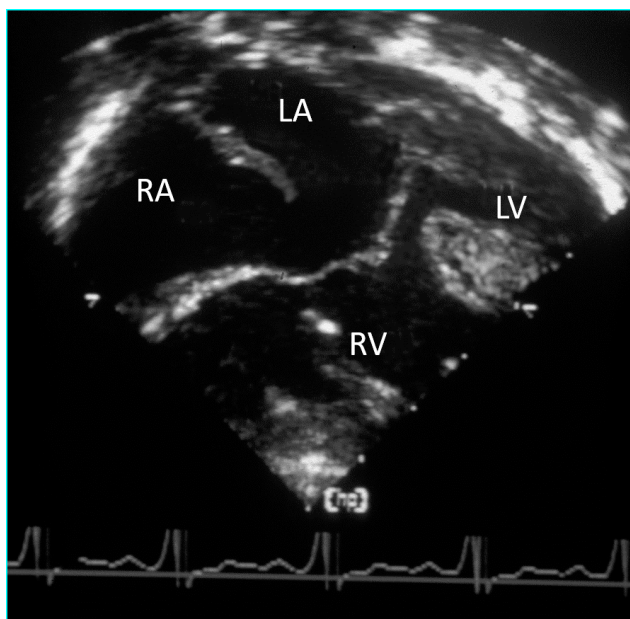


Figure 13. Echocardiographic four chamber section from a heart with complete AVSD, hypoplastic left ventricle and the morphological criteria for the double inlet right ventricle.

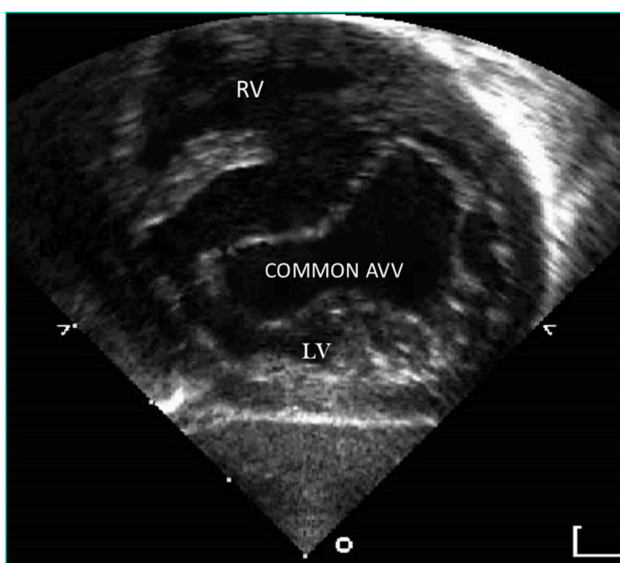


Figure 14. Subcostal left oblique echocardiographic section at the level of the atrioventricular junction showing the common atrioventricular valve committed entirely to the left ventricle.

7. Some Implications of Names and Classification

Finally, I will put forth the question, ‘What is in a name, particularly when today’s imaging techniques show everything?’ The fundamental reason for allocating names to congenital heart malformations is to allow communication between those working in the field. Names are also essential to research and audit. Surgeons must be able to investigate the results of radical repair of hearts with the various morphological features of an atrioventricular septal defect and identify any incremental risk factors for poor outcome. Retrospective review can only be made possible by an adequate system of nomenclature and classification.

Learning to be a paediatric cardiologist or cardiac surgeon is extremely complex. For example, to the less experienced, echocardiographic, angiographic, CT or resonance images of the heart appear at first as a meaningless blur. Gradually, however, our brains are able

to connect together the findings on clinical examination of the patient with the images that we see. For example, even without allocating a name, an echocardiographic four chamber section from a patient with a primum atrial septal defect will immediately trigger a variety of complex thoughts ranging from expectations of clinical findings, symptoms, natural history and likely outcome of repair. The surgeon will imagine the appearance of the heart in the operating room while the morphologist will be aware of what the heart would be like held in the hand and examined in the laboratory. For the individual expert, names have potentially become irrelevant. For those of us involved in managing patients with congenital heart disease it is often unwise to rely entirely on individual names for particular conditions because of the presence of unusual features or associated anomalies.

Consider the hypothetical situation of a paediatric cardiologist who, on the basis of a cross-sectional echocardiogram, informs a cardiac surgeon about a patient with a primum atrial septal defect that requires routine repair, and the surgeon takes the patient to the operating room without carefully reviewing and discussing any investigations. For a simple primum defect, no doubt the outcome would be very good because, simply on the basis of the name, the surgeon would anticipate correctly the operative findings. But just imagine the likely consequence if in addition to the primum defect there had been double outlet right atrium, a small and restrictive primum defect with left atrial hypertension, double orifice left atrioventricular valve and left ventricular outflow tract obstruction (Figure 15) caused by anomalous chords from the superior bridging leaflet to the ventricular septum. The patient would have been much more likely to survive the operation or have a perfect outcome of repair had the surgeon undertaken a complete review of all the investigations and completely understood the data. But giving the cardiac malformation a 'label' is unlikely materially to improve outcome further if the cardiac surgeon was unable to interpret echocardiographic or magnetic resonance images and relied entirely on verbal or written descriptions of any anomalies and observations at the time of surgery.

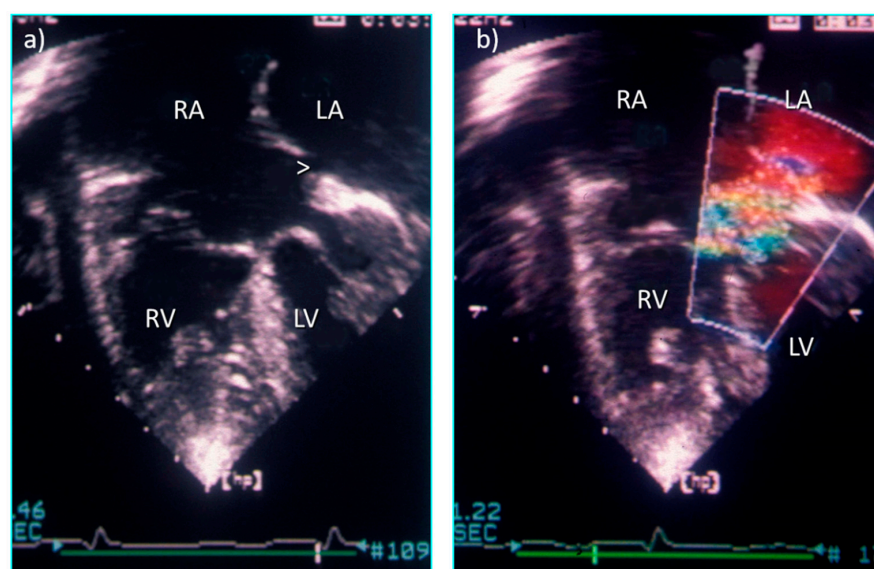


Figure 15. Four chamber echocardiographic sections from a heart with double outlet right atrium and restrictive primum defect (ASD) (a) without colour flow Doppler and (b) with turbulence across the restrictive ASD.

Consider also another hypothetical situation of a four-month-old infant with isolated primum defect, mild to moderate left atrioventricular valve regurgitation with unexpected congestive heart failure and failure to thrive. The cardiologist was unable to be present when the case was shown to colleagues and surgeons, and an echocardiogram was interpreted as a straightforward 'partial AVSD' requiring early surgical repair and

the management was agreed upon quickly. At operation the surgeons found an atypical left atrioventricular valve and could not achieve a complete operation. In a retrospective review, the outpatient report from the referring cardiologist was discovered.

‘Partial Atrioventricular Septal Defect (Isolated primum ASD)

Bileaflet left atrioventricular—deficient left mural leaflet

Parachute deformity of left AV valve

Small/potentially stenotic left-sided valve orifice

Short chords of left-sided valve orifice

(Repair of left ventricular AV valve may be impossible)’

This is an example of a case where access to the complete diagnosis at the multidisciplinary team meeting and a more careful review of the clinical history and the echocardiogram at the time would have alerted everyone to potential difficulties and possibly changed the clinical management and surgical approach and timing.

Given the precision and quality of cardiovascular imaging now available and the ability to transmit digital images with great speed virtually anywhere, it is difficult to avoid the conclusion that names are less important than they were. We must not forget, however, that words, names and language are the essential prerequisites of communication, audit and teaching. Good practice in the management of congenital heart disease cannot be achieved without accurate communication! A complete and accurate description in the diagnosis will also alert the surgeon to potential difficulties that will be encountered during surgery, and, as I have tried to convey, there can be a complex constellation of deviations from the usual morphology. Indeed, I have also attempted to emphasise both the clinical (surgical) and scientific importance of preciseness. Preciseness, no matter how impractical it may be in contemporary ‘fast-track’ life and medicine, implies a deep understanding, which is a hallmark of the Anderson and Becker school of morphology. The marvellous contribution of Bob Anderson and his many collaborators to the understanding of congenital heart malformations has in part been made possible by the emphasis on nomenclature and precise communication. However, it is regrettable that his message seems not yet to have reached everyone.

Funding: This research received no external funding.

Institutional Review Board Statement: Ethical approval or informed consent was not required.

Data Availability Statement: Not available.

Acknowledgments: I acknowledge the help, advice and influence of my colleagues at the Royal Brompton Hospital, particularly S Y Ho, Karen McCarthy and Wei Li.

Conflicts of Interest: There were no conflicts of interest in writing this review.

Abbreviations

RA	right atrium
LA	left atrium
RV	right ventricle
LV	left ventricle
S	ventricular septum
LML	left mural leaflet
SBL	superior bridging leaflet
RASL	right antero-superior leaflet
RML	right mural leaflet
IBL	inferior bridging leaflet
T	Connecting Tongue of valve tissue
AVV	atrioventricular valve
Ao	Aorta

References

1. Becher, A.E.; Anderson, R.H. Atrioventricular septal defects. What's in a name? *J. Thorac. Cardiovasc. Surg.* **1982**, *83*, 461–469. [CrossRef]
2. Blieden, L.C.; Randall, P.A.; Castaneda, A.R.; Lucas, R.V., Jr.; Edwards, J.E. The 'goose neck' of the endocardial cushion defect: Anatomical basis. *Chest* **1974**, *65*, 13–17. [CrossRef]
3. Rastelli, G.; Kirklin, J.W.; Titus, J.L. Anatomic observations on complete form of persistent common atrioventricular canal with special reference to atrioventricular valves. *Mayo Clin. Proc.* **1966**, *41*, 296–308. [PubMed]
4. Van Mierop, L.H.S.; Alley, R.D.; Kausel, H.W.; Stranahan, A. The anatomy and embryology of endocardial cushion defects. *J. Thorac. Cardiovasc. Surg.* **1962**, *43*, 71–83. [CrossRef]
5. Smallhorn, J.F.; Tommasini, G.; Anderson, R.H.; Macartney, F.J. Assessment of atrioventricular septal defects by two-dimensional echocardiography. *Br. Heart J.* **1982**, *30*, 446–457.
6. Anderson, R.H.; Ho, S.Y.; Becker, A.E. Anatomy of the human atrioventricular junctions revisited. *Anat. Rec. Adv. Integr. Anat. Evol. Biol.* **2000**, *260*, 81–91. [CrossRef]
7. Silverman, N.H.; Zuberbuhler, J.R.; Anderson, R.H. Atrioventricular septal defects: Cross-sectional echocardiographic and morphologic comparisons. *Int. J. Cardiol.* **1986**, *13*, 309–331. [CrossRef]
8. Penkoske, P.A.; Neches, W.H.; Anderson, R.H.; Zuberbuhler, J.R. Further observations on the morphology of atrioventricular septal defects. *J. Thorac. Cardiovasc. Surg.* **1985**, *90*, 611–622. [CrossRef]
9. Anderson, R.H.; Ho, S.Y.; Falcao, S.; Daliendo, L.; Rigby, M.L. The diagnostic features of atrioventricular septal defect with common atrioventricular junction. *Cardiol. Young* **1998**, *8*, 33–49. [CrossRef] [PubMed]
10. Akiba, T.; Becker, A.E.; Neirotti, R.; Tatsuno, K. Valve morphology in complete atrioventricular septal defect: Variability relevant to operation. *Ann. Thorac. Surg.* **1993**, *56*, 295–299. [CrossRef]
11. Piccoli, G.P.; Ho, S.Y.; Wilkinson, J.L.; Macartney, F.J.; Gerlis, L.M.; Anderson, R.H. Left-sided obstructive lesions in atrioventricular septal defects. *J. Thorac. Cardiovasc. Surg.* **1982**, *83*, 453–460. [CrossRef]
12. Ebels, T.; Anderson, R.H.; Devine, W.A.; Debich, D.E.; Penkoske, P.A.; Zuberbuhler, J.R. Anomalies of the left atrioventricular valve and related ventricular septal morphology in atrioventricular septal defects. *J. Thorac. Cardiovasc. Surg.* **1990**, *99*, 299–307. [CrossRef]
13. Oosthoek, P.W.; Wenink, A.C.; Macedo, A.J.; Groot, A.C.G.-D. The parachute-like asymmetric mitral valve and its two papillary muscles. *J. Thorac. Cardiovasc. Surg.* **1997**, *114*, 9–15. [CrossRef]
14. Mahle, W.T.; Shirali, G.S.; Anderson, R.H. Echo-morphological correlates in patients with atrioventricular septal defect and common atrioventricular junction. *Cardiol. Young* **2006**, *16*, 43–51. [CrossRef] [PubMed]
15. Franklin, R.C.G.; Béland, M.J.; Colan, S.D.; Walters, H.L.; Aiello, V.D.; Anderson, R.H.; Bailliard, F.; Boris, J.R.; Cohen, M.S.; Gaynor, J.W.; et al. Nomenclature for congenital and paediatric cardiac disease: The International Paediatric and Congenital Cardiac Code (IPCCC) and the Eleventh Iteration of the International Classification of Diseases (ICD-11). *Cardiol. Young* **2017**, *27*, 1872–1938. [CrossRef] [PubMed]
16. Carvalho, J.S.; Rigby, M.L.; Shinebourne, E.A.; Anderson, R.H. Cross sectional echocardiography for recognition of ventricular topology in atrioventricular septal defect. *Br. Heart J.* **1989**, *61*, 285–288. [CrossRef] [PubMed]



Article

Congenitally Malformed Hearts: Aspects of Teaching and Research Involving Medical Students

Catherine C. Pickin ^{1,†}, James Castle ^{1,†}, Vibha Shaji ^{1,†}, Adeolu Banjoko ^{1,†}, Aimee-Louise Chambault ^{1,†}, Anna N. Seale ^{2,3}, Anthony Lander ⁴, Chetan Mehta ² and Adrian Crucean ^{5,*}

- ¹ Department of Anatomy, College of Medical and Dental Sciences, University of Birmingham, Birmingham B15 2GW, UK; catherine.pickin@nhs.net (C.C.P.); james.castle@nhs.net (J.C.); vibha.shaji@nhs.net (V.S.); adeolu.banjoko@nhs.net (A.B.); aimee-louise.chambault@nhs.net (A.-L.C.)
- ² Department of Paediatric Cardiology, Birmingham Women's and Children's Hospital, Birmingham B4 6NH, UK; annaseale@nhs.net (A.N.S.); chetan.mehta1@nhs.net (C.M.)
- ³ Institute of Cardiovascular Sciences, University of Birmingham, Birmingham B15 2TT, UK
- ⁴ Department of Paediatric Surgery, Birmingham Women's and Children's Hospital, Birmingham B4 6NH, UK; t.lander@nhs.net
- ⁵ Department of Paediatric Cardiac Surgery, Birmingham Women's and Children's Hospital, Birmingham B4 6NH, UK
- * Correspondence: adrian.crucean@nhs.net; Tel.: +44-1213339999
- † These authors contributed equally to this work.

Citation: Pickin, C.C.; Castle, J.; Shaji, V.; Banjoko, A.; Chambault, A.-L.; Seale, A.N.; Lander, A.; Mehta, C.; Crucean, A. Congenitally Malformed Hearts: Aspects of Teaching and Research Involving Medical Students. *J. Cardiovasc. Dev. Dis.* **2021**, *8*, 34. <https://doi.org/10.3390/jcdd8040034>

Academic Editors:
Deborah Henderson and Nigel Brown

Received: 17 February 2021
Accepted: 25 March 2021
Published: 28 March 2021

Publisher's Note: MDPI stays neutral with regard to jurisdictional claims in published maps and institutional affiliations.



Copyright: © 2021 by the authors. Licensee MDPI, Basel, Switzerland. This article is an open access article distributed under the terms and conditions of the Creative Commons Attribution (CC BY) license (<https://creativecommons.org/licenses/by/4.0/>).

Abstract: To appreciate congenital heart disease fully, a detailed understanding of the anatomical presentation, as well as the physiology, is required. This is often introduced at an advanced stage of training. Professor Anderson has been influential in the Clinical Anatomy Intercalated BSc programme at the University of Birmingham, in particular in his teaching on Sequential Segmental Analysis. This article describes the experiences of the latest cohort of students on this programme, who undertook varying research projects using the Birmingham Cardiac Archive, with the guidance of Professor Anderson. The projects outlined include various aspects of isomerism, encompassing both the cardiac and abdominal manifestations, as well as details of congenitally corrected transposition of the great arteries and prenatally diagnosed right aortic arch and double arch. These studies all aimed to increase the knowledge base of their respective cardiac malformations and provide a basis for further research.

Keywords: congenital heart defects; congenitally corrected transposition of the great arteries; right isomerism of the atrial appendages; left isomerism of the atrial appendages; right aortic arch; double aortic arch; abdominal heterotaxy

1. Introduction

The study of congenital heart disease was considered to require a substantial layer of anatomy and physiology enriched with a solid knowledge of clinical cardiology and multiple elements of general surgery, cardiac surgery and intensive care. Hence, it is still the case that most medical professionals start this advanced specialisation once they have completed their training in areas such as paediatrics, cardio-thoracic surgery and cardiology. It may seem counterintuitive to propose such complex topics to medical students still early in their careers.

We would like to share here the experience with our latest cohort of year 3 and 4 students in BSc Intercalation in Clinical Anatomy at the University of Birmingham who completed their degree projects in congenital heart disease. This brings to light several important roles that Professor Robert H. Anderson generously undertook in the past 8 years in relation to the Birmingham Cardiac Archive.

Professor Anderson while allegedly retired, visited the Birmingham Children's Hospital on numerous occasions since 2013 in order to classify a significant and vast archive of

more than 2000 preserved malformed hearts. He painstakingly contributed to catalogue the specimens based on the updated nomenclature, delivered numerous high quality teaching sessions, participated in numerous clinical discussions of complex patients, mentored the current curator of the archive, and advised for a robust governance process for the archive committee including a novel digital database for the systematic documentation of the hearts examined. He also contributed to initiate the Intercalation Programme with the University of Birmingham, an optional one-year programme taken between third and fourth or fourth and fifth years during the MBChB programme. Professor Anderson understood very early on that a dedicated clinical and academic team would be able to overcome any obstacles raised against achieving excellent results with such a programme. He has taught countless students on the programme the intricacies of Sequential Segmental Analysis to properly understand the anatomy of congenitally malformed hearts. The University of Birmingham is now running the 5th such programme and the results have been nothing short of very satisfactory: all students achieved first class honours following an external examination at the end of the intercalation year, some students were able to publish in high quality journals in our specialty and presented to highly ranked international conferences such as EACTS (European Association of Cardio-Thoracic Surgery) meeting or ESC (European Society of Cardiology) Development meeting, and some students became enthused with the paediatric cardiac specialty and are now following it as a medical career. Nevertheless, the most important achievement was to witness their transformation during the academic year: their unleashed curiosity blended with hard work and youthful passion which eroded any barriers to understanding even of the most complex aspects of cardiac anatomy in malformed hearts.

This is just another aspect of the multiple pronged legacies that Professor Anderson created during his considerably long career as a pioneer in a domain that will continue to marvel and attract generations of healthcare professionals, academic researchers and teachers in the decades to come. To his credit we describe a few projects collated from the latest academic year in a student format. In these projects, hearts with atrial appendage isomerism and congenitally corrected transposition of the great arteries (ccTGA) were identified in the Birmingham Cardiac Archive. The complex cardiac morphology was analysed and documented according to Sequential Segmental Analysis. Care has been taken to present only partial results as the separate detailed papers will contain the complete data for each separate project. We are thankful to the students and their supervisors who agreed to share their work for this special article.

2. Left Isomerism of the Atrial Appendages—Catherine Pickin

Atrial appendage isomerism is a rare form of congenital heart disease characterised by mirror imaged appendages of the heart [1]. It is associated with a heterogenous spectrum of cardiac morphology, extracardiac associations, presentation, management and outcomes [1–4].

This heterogeneity has led to controversy over the diagnosis and classification of this condition, which has also been known as ‘heterotaxy’ and ‘bodily isomerism’, particularly with regard to its left and right subtypes [5,6]. Professor Anderson and colleagues have consistently shown in post-mortem morphological studies that hearts with atrial appendage isomerism can and should be classified according to their most constant morphological component: the extent of the pectinate muscles within the appendages of the heart [1,7]. Left atrial appendage isomerism is defined by the presence of bilateral morphologic left atrial appendages, themselves defined by the pectinate muscle being confined to the appendage, not extending to the crux of the heart [1].

Seven hearts with left atrial appendage isomerism were analysed. We particularly noted the variation in external shape of the appendages of the same heart, when the extent of the pectinate muscle in both indicated left atrial appendage isomerism (Figure 1). One heart had juxtaposed appendages, meaning assessment of the pectinate muscle was difficult

(Figure 2). These highlighted the difficulty in assessing the morphological diagnosis of hearts with atrial appendage isomerism.

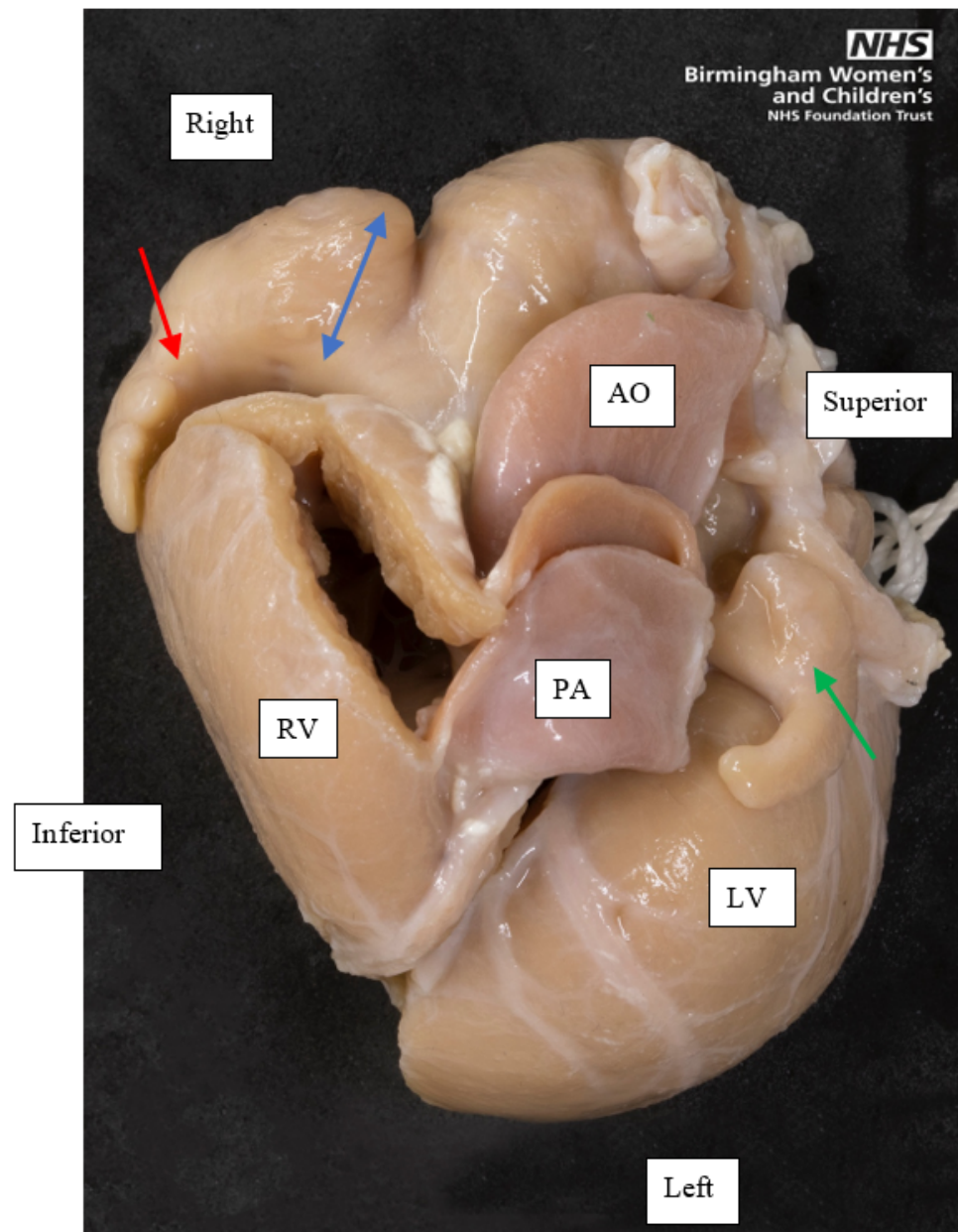


Figure 1. A superior view of the base of a heart with left atrial appendage isomerism, showing the external appearance of both appendages. The left-sided appendage, indicated by the green single-headed arrow, is small and tubular. The right-sided appendage, indicated by the red single-headed arrow, is tubular at its distal parts, but its proximal part is broad based, shown by the blue double-headed arrow. The pectinate muscle of both appendages was confined to the appendage (not shown in this image), confirming this as a heart with left atrial appendage isomerism. Orientation points displayed in an attitudinally correct fashion. AO, Aorta; PA, Pulmonary artery; RV, Right ventricle; LV, Left ventricle.

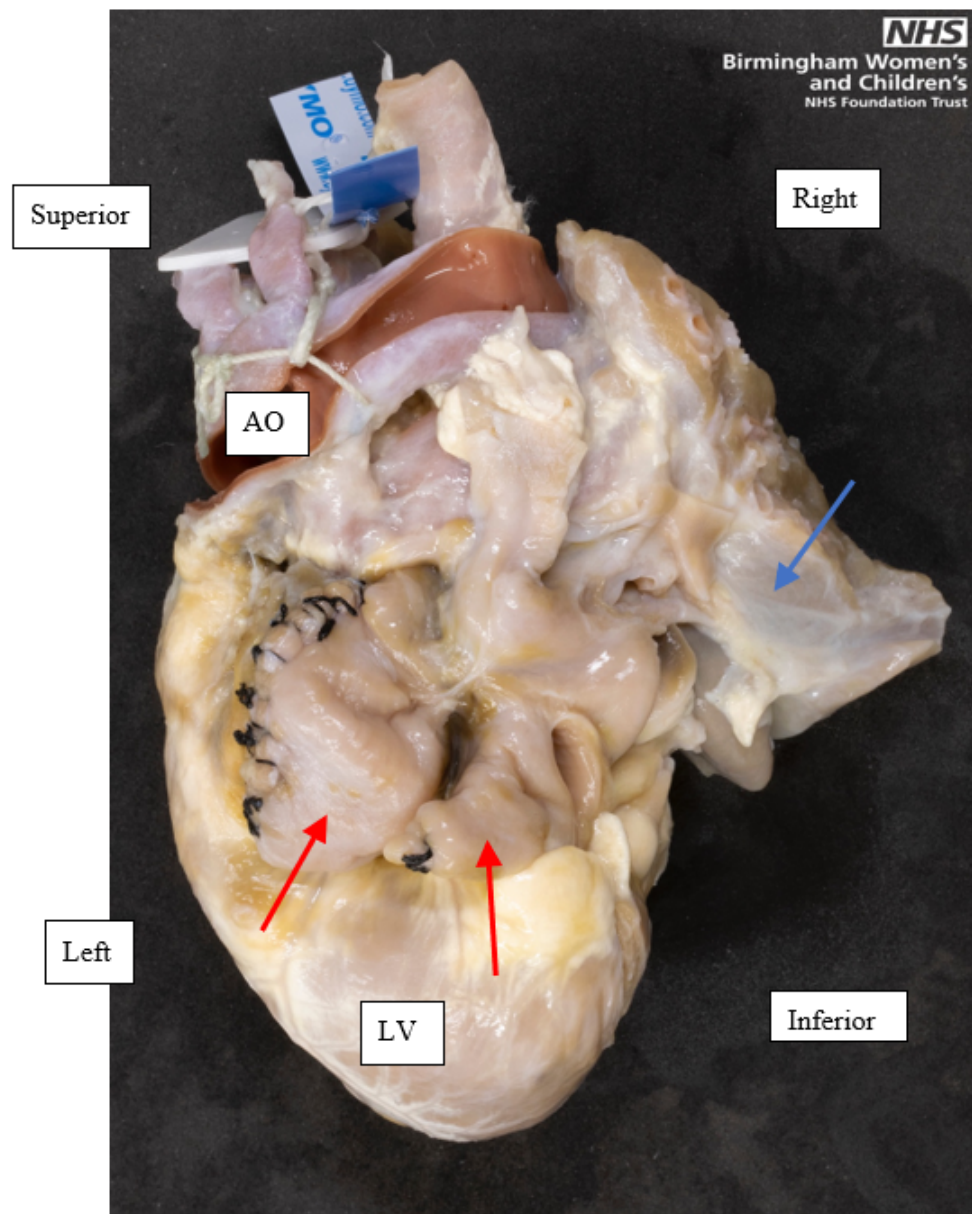


Figure 2. A left posterior view of a heart with left atrial isomerism, showing the juxtapsed morphologic left atrial appendages, indicated by the red single-headed arrows. Both appendages are tubular and had a narrow base to the atrium. Parts of the lungs, indicated by the blue single-headed arrow, have been moved to the right and superiorly to expose the appendages. This heart had been operated on in life, indicated by the black stitches in both appendages. Orientation points displayed in an attitudinally correct fashion. AO, Aorta; LV, Left ventricle.

We found atrial septum anomalies (Figure 3) in all seven hearts, consistent with the landmark study by Professor Anderson and colleagues in which they found the atrial septum was rarely properly formed in left atrial appendage isomerism [1]. We also found incidences of common atrioventricular (AV) valve (5/7, 71%) and common AV junction (6/7, 86%) similar to those found by Anderson [1], indicating the importance of using consistent diagnostic criteria so studies are able to be accurately compared.

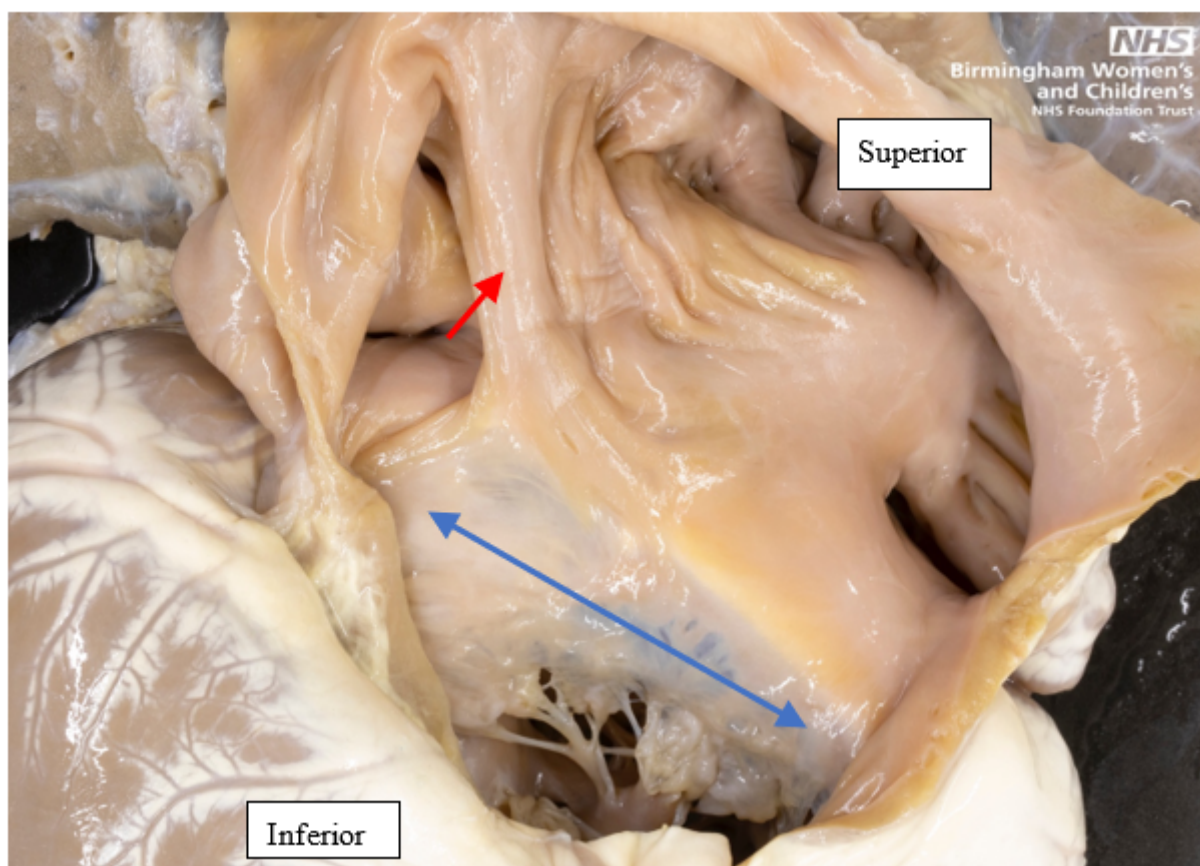


Figure 3. Antero-superior view of the internal aspect of the common atrium and the common AV valve of a heart with left atrial appendage isomerism. The anterior wall of the atrium has been dissected and reflected superiorly and laterally. A septal strand on the posterior wall of the atrium is shown by the red single-headed arrow. The common AV valve, within the common AV junction, is shown by the double headed blue arrow.

This research, instigated by Professor Anderson, continues the much needed exploration into the cardiac morphology and associations in the heterogeneous condition of left atrial appendage isomerism.

In parallel we also conducted a large 20-year retrospective cohort study of cardiac morphology and clinical outcomes in right and left atrial appendage isomerism at Birmingham Women's and Children's NHS Foundation Trust (BWCH). We found 138 patients with atrial appendage isomerism of whom 59% (81/138) had left atrial appendage isomerism.

3. Right Isomerism of the Atrial Appendages—James Castle

Right atrial appendage isomerism is defined by the presence of bilateral morphologic right atrial appendages, themselves defined by pectinate muscle extending around the atrioventricular junction.

21 hearts with right atrial appendage isomerism were identified. In addition, a descriptive study examining the patient factors, treatments and outcomes of patients with RAI treated by the Cardiology and Cardiac Surgery departments at BWCH was carried out. Through automated key term searches followed by manual validation, the retrospective analysis of the cardiology departmental records identified 57 patients with RAI.

The greatest utility for the archive with respect to cardiac morphology is the unsurpassed detail with which specimens can be examined compared with *in vivo* imaging techniques. It has been shown in the literature that although extremely accurate, modern imaging systems are not perfect, having particular issues with valvular morphology and anomalous venous connections [8]. Given that these features are common in hearts with

RAI, the importance of physical specimens is perhaps even greater than for simpler cardiac malformations. In addition, working with a physical specimen allows a greater understanding of the three-dimensional relationship of features within the malformed heart which cannot be fully appreciated with two-dimensional imaging or even computerised reconstructions.

4. Abdominal Heterotaxy and Cardiac Isomerism–Vibha Shaji

Isomerism of the atrial appendages (AAI) only describes isomerism within the heart. However, it is associated with numerous extracardiac manifestations encompassing malformations of the stomach, spleen, liver, gallbladder, pancreas and intestines; this is acknowledged by the currently prevalent terms ‘heterotaxy’, ‘heterotaxy syndrome’ and ‘atrial isomerism’, which are used as synonyms for situs ambiguous, asplenia or polysplenia syndromes. When discussing the abnormalities of situs in the abdomen, ‘heterotaxy syndrome’ was deemed appropriate as the term atrial isomerism cannot apply in the way it is applied to the heart since paired structures are being discussed [9]. Moreover, the abdomen demonstrates inconsistent features in comparison to the isomeric atrial appendages.

Sequential segmental analysis enables a thorough analysis of cardiac morphology to understand the patient’s condition better. There is often agreement that any abdominal surgery should be undertaken after cardiac palliation [10] due to the higher underlying risk of mortality associated with particular cardiac lesions. For this reason, it has made sense in the past to focus on developing a descriptive manner to characterise cardiac morphology. Recently, however, given that patients are surviving for long enough to exhibit signs of abdominal abnormalities [11], it seems rational to foster a similar method of analysis of the abdomen to allow for better guided patient care.

To this end, the literature was reviewed and showed that most studies address the need for exploring the arrangement of abdominal organs in greater detail, with some even stating that they will give the “precise arrangement” of these viscera [12]. However, these very papers frequently provide no more detail than the organ laterality [13,14]. Moreover, while most document the side of these organs, as this can be beneficial to a surgical approach, very few relate these to their clinical significance [15–17].

Therefore, a retrospective observational study of all patients with AAI who had malrotation was designed at BWCH using more imaging modalities than all other previous studies to allow for a more profound analysis of the anatomy of the 23 patients included. A systematic approach to describing the abdominal viscera was also created, the details of which are to be described in a future manuscript.

All patients included within the study displayed unique anatomical morphology, emphasising the importance of appropriate description to guide clinical management. However, none had a complete anatomical description available. Given the clinical implications of these varied presentations, this should be obtained as a standardised aspect of management, especially given the increased life span of these patients [11]. The newly proposed systematic approach would facilitate this, providing several key additional benefits. These include the standardisation of reporting of the morphology present and complete visualisation and description of the viscera, ensuring that all relevant anatomical information is collated.

5. Prenatally Diagnosed Right Aortic Arch and Double Arch: Incidence, Associations and Outcomes–Aimee-Louise Chambault

Right aortic arch (RAA) and double aortic arch (DAA) abnormalities can form structures called vascular rings (VR) [18]. VR can encircle the trachea and oesophagus and cause compression, which consequently produces symptoms [19]. There is limited literature regarding the incidence, associations and outcomes of both RAA and DAA abnormalities in a prenatally diagnosed cohort. Therefore, this subject was explored further as part of this dissertation project, via a retrospective observational study conducted at BWCH. This was in addition to the production of a treatment pathway for these patients within

this institution. This study provided pilot data for a nationwide collaborative study on this lesion.

This project reviewed patients who received a prenatal diagnosis of a RAA or DAA following referral to BWCH. The primary inclusion criterion for this project was that patients must have had a prenatal diagnosis of a RAA/DAA. Exclusion criteria for this project included cases that were only postnatally diagnosed with a RAA/DAA. Additionally, patients with a prenatal diagnosis of concurrent major congenital heart disease were also excluded. The final cohort of patients included 160 in the prenatal cohort and 123 patients in the postnatal cohort. Some of the key outcomes explored included genetic testing results, additional cardiac/extracardiac abnormalities, as well as surgical outcomes for those patients who underwent surgery.

Results of this project found that the incidence of an isolated RAA and DAA was 9.1 and 1.3 per 10,000 women undergoing fetal second trimester anomaly screening, respectively. Since the introduction of the three-vessel and trachea view into the second trimester fetal anomaly scan in 2015, the BWCH fetal medicine department was referred approximately 45 cases per annum of isolated RAA/DAA; previously this had been less than 3. Postnatally, 14 patients had genetic abnormalities, 19.2% (14/73), of 73 patients with known genetic test results. Extracardiac abnormalities were found in 13.0% (16/123) of patients in the postnatal cohort. In total, 17.1% (21/123) of patients underwent surgery, and the anatomy of these patients was either a DAA, 52.4% (11/21) or a RAA with an aberrant left subclavian artery, 47.6% (10/21).

For this project, it was important to understand the embryological origins of the aortic arch, and the subsequent formation of RAA and DAA abnormalities. This was achieved using articles and books authored by Professor Anderson, as well as the embryology lectures that he delivered as part of the wider clinical anatomy course [18,20,21]. These helped shed light on a relatively complicated developmental lesion, as well as aid in understanding of some of the more complex anatomical presentations of RAA abnormalities in particular.

In conclusion, the results of this project were able to establish the incidence, associations and outcomes of patients with a prenatally diagnosed RAA/DAA referred to BWCH for diagnosis. These preliminary results have provided valuable data at a local level, and data collected will also be utilised in a nationwide project on the same subject matter. All of these factors will help to better establish a way forward, particularly in terms of management, for patients with this anatomical abnormality.

6. Congenitally Corrected Transposition–Adeolu Banjoko

Congenitally corrected transposition of the great arteries (ccTGA) is a rare congenital cardiac malformation impacting 0.5% of those born with congenital heart disease [22]. ccTGA has both atrioventricular and ventriculoarterial discordant connections, as described by Sequential Segmental Analysis [23,24]. There are four key malformations that are commonly associated with ccTGA. These include a ventricular septal defect, obstruction of the right ventricular outflow tract, Ebsteinoid's malformation of the tricuspid valve, and morphological right ventricular (mRV) hypoplasia [18]. While ccTGA is coined a "corrected transposition" due to having a relatively normal circulation, these associated malformations often have immediate impact on function and survival in ccTGA patients [18].

This project aimed to describe the associations between prenatal and postnatal morphology and clinical outcomes in a cohort of prenatally diagnosed ccTGA patients at BWCH. An analysis of 22 archived ccTGA hearts was used to supplement clinical images and descriptions, to better understand the morphology of these patients.

The 22 specimens in the BWCH archive were analysed as part of this project. The examination protocol was according to the blood flow, with variables collected to support the clinical data and build upon the current morphological knowledge of ccTGA in the literature. One innovative inclusion in our examination protocol was the assessment of ventricular septal defect (VSD) topography from the mRV. This is in continuation from a recent publication by Arribard et al. [25], in which they identify the mRV septum of ccTGA

to be an identical mirror image of that in normal hearts. Accordingly, VSD assessment should be standardised to the mRV because this allows for the use of the criteria widely agreed in isolated VSD. When capturing these VSD, specialised mirrors were used to make the mRV appear right sided.

All four associated anomalies were represented in the archive cohort (Figure 4). Of particular interest was capturing the unique “side by side” ventricular positioning of the ventricles in ccTGA. The clinical data found mRV hypoplasia was overly suspected prenatally. A contributor to this clinical finding could be the unusual positioning of the ventricles in ccTGA. When assessed in the limited echocardiographic cross sections available prenatally, this unique positioning of the ventricles can result in underestimation of the size of the mRV [26]. An awareness of this morphology, provided by this analysis in the archive, can help clinicians improve their fetal morphological assessment in ccTGA patients.

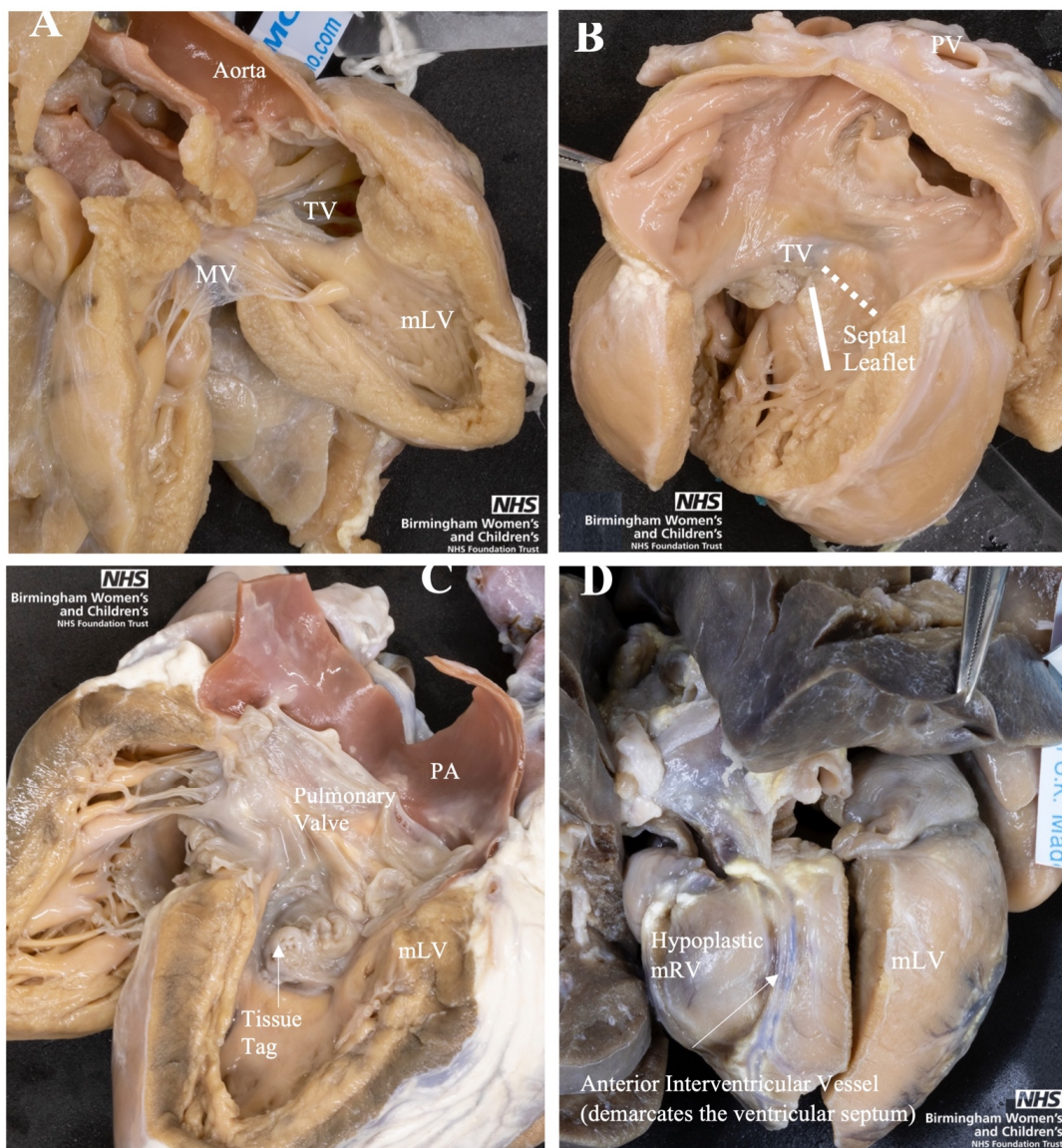


Figure 4. Four Associated Anomalies of ccTGA. (A) Peri-membranous VSD with aorta overriding and tricuspid valve straddling, from the morphological left ventricle (mLV). (B) Septal leaflet is plastered to septum of morphological right ventricle (mRV). Dashed line shows normal atrioventricular junction and solid line shows apical displacement of septal leaflet. (C) Subpulmonary obstruction due to tissue tag of septal leaflet of tricuspid valve. (D) Ventricular hypoplasia of the mRV. MV, Mitral Valve; PV, Pulmonary Vein; TV, Tricuspid Valve; mLV, morphological left ventricle; mRV, morphological right ventricle; mLA: morphological left atrium.

Furthermore, all the ccTGA hearts with VSD had their topography assessed from the mRV. Three of these hearts had their VSD photographed from the mRV using a mirror, to represent the VSD appearing right-sided, similar to concordant atrioventricular connections (Figure 5). We found the VSD in the archive has more diverse topographies when comparing to Arribard et al. [25]. While the majority of their ccTGA hearts had an outlet perimembranous VSD upon assessment from the mRV, our archive had a mix of 2 central, 6 inlet, 1 inlet to outlet, and 4 outlet perimembranous VSD [25].

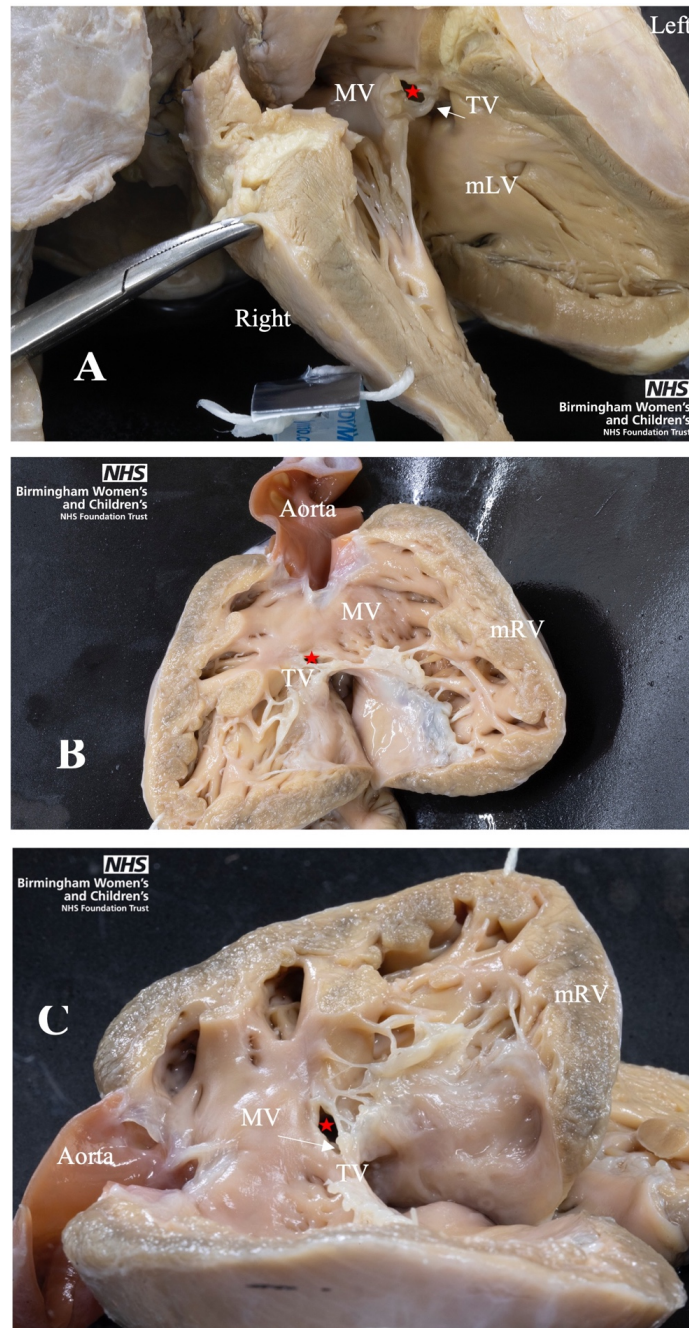


Figure 5. Four Associated Anomalies of ccTGA. (A) Photo from mLV showing Peri-membranous VSD. (B) Photo from mRV showing Peri-membranous VSD. (C) Photo from mRV using mirror so the ventricle appears right sided. Geographies of VSD assessed as central. Star: VSD; MV, Mitral Valve; TV, Tricuspid Valve; mLV, morphological left ventricle; mRV, morphological right ventricle.

This project described the morphology of both clinical patients and archive specimens with ccTGA. These specimens also contribute to current literature by assessing the VSD from the mRV, using a mirror to appear right sided. This exploration of the morphology helps improve understanding of the morphological spectrum of ccTGA patients.

7. Conclusions

This article attempted to provide an example of the extensive depth and breadth of Professor Anderson's contribution to the field of congenital heart disease. In an age of continuous super-specialisation, a polymath-like figure like him has been able not only to cross boundaries in terms of various clinical specialties but also to unite different levels of expertise such as students and beginners in the medical field, with world-renowned developmental or imaging scientists, archive curators and basic science researchers. Professor Anderson continues to inspire and guide new generations of young medical students in the quest for a better understanding of congenital heart disease.

Author Contributions: Conceptualization, A.B., C.C.P., J.C., V.S., A.-L.C., A.C., A.N.S., A.L., C.M.; Methodology, A.B., C.C.P., J.C., V.S., A.-L.C., A.C.; Validation, A.C.; Investigation, A.B., C.C.P., J.C., V.S., A.C.; Resources, A.C.; Writing—Original Draft Preparation, A.B., C.C.P., J.C., V.S., A.-L.C.; Writing—Review and Editing, A.B., C.C.P., J.C., V.S., A.-L.C., A.C., A.N.S., A.L., C.M.; Visualization, A.B., C.C.P., J.C., V.S.; Supervision, A.C., A.N.S., A.L., C.M.; Project Administration, A.C., A.N.S. All authors have read and agreed to the published version of the manuscript.

Funding: This research received no external funding.

Institutional Review Board Statement: Not applicable.

Informed Consent Statement: The BCH Cardiac Archive Committee approved the use of cardiac specimens for this project. The Curator (A.C.) maintains the registered filed approval.

Data Availability Statement: The data presented in this study are available on request from the corresponding author. The data are not publicly available due to separate submissions being prepared for individual papers and also data being part of multicentre studies.

Acknowledgments: The authors would like to acknowledge the generosity of the patients and families that donated hearts to the Birmingham Women's and Children's Hospital NHS Trust Archive. They thank Clinical Photography at the Birmingham Women's and Children's NHS Foundation Trust for making the original images of selected hearts from the archive for which they retain the copyright. A.B. and C.C.P. would also like to acknowledge the support of the Topham bursary from the College of Medical and Dental Sciences, University of Birmingham.

Conflicts of Interest: The authors declare no conflict of interest.

References

1. Tremblay, C.; Loomba, R.S.; Frommelt, P.C.; Perrin, D.; Spicer, D.E.; Backer, C.; Anderson, R.H. Segregating bodily isomerism or heterotaxy: Potential echocardiographic correlations of morphological findings. *Cardiol. Young* **2017**, *27*, 1470–1480. [CrossRef] [PubMed]
2. Loomba, R.S.; Nijhawan, K.; Anderson, R. Impact of Era, Type of Isomerism, and Ventricular Morphology on Survival in Heterotaxy: Implications for Therapeutic Management. *World J. Pediatr. Congenit. Heart Surg.* **2016**, *7*, 54–62. [CrossRef] [PubMed]
3. Loomba, R.S.; Geddes, G.C.; Basel, D.; Benson, D.W.; Leuthner, S.R.; Hehir, D.A.; Ghanayem, N.; Shillingford, A.J. Bacteremia in Patients with Heterotaxy: A Review and Implications for Management. *Congenit. Heart Dis.* **2016**, *11*, 537–547. [CrossRef]
4. Loomba, R.S.; Willes, R.J.; Kovach, J.R.; Anderson, R.H. Chronic Arrhythmias in the Setting of Heterotaxy: Differences between Right and Left Isomerism. *Congenit. Heart Dis.* **2016**, *11*, 7–18. [CrossRef] [PubMed]
5. Van Praagh, R.; Van Praagh, S. Atrial isomerism in the heterotaxy syndromes with asplenia, or polysplenia, or normally formed spleen: An erroneous concept. *Am. J. Cardiol.* **1990**, *66*, 1504–1506. [CrossRef]
6. Yim, D.; Nagata, H.; Lam, C.Z.; Grosse-Wortmann, L.; Seed, M.; Jaeggi, E.; Yoo, S.-J. Disharmonious Patterns of Heterotaxy and Isomerism: How Often Are the Classic Patterns Breached? *Circ. Cardiovasc. Imaging* **2018**, *11*, e006917. [CrossRef]
7. Uemura, H.; Ho, S.Y.; Devine, W.A.; Kilpatrick, L.L.; Anderson, R.H. Atrial appendages and venoatrial connections in hearts from patients with visceral heterotaxy. *Ann. Thorac. Surg.* **1995**, *60*, 561–569. [CrossRef]
8. Li, A.; Peng, Z.; Zhang, C. Comparison of echocardiography and 64-multislice spiral computed tomography for the diagnosis of pediatric congenital heart disease. *Med. Sci. Monit.* **2017**, *23*, 2258–2266. [CrossRef] [PubMed]

9. Anderson, R.H.; Spicer, D.E.; Loomba, R. Is an Appreciation of Isomerism the Key to Unlocking the Mysteries of the Cardiac Findings in Heterotaxy? *J. Cardiovasc. Dev. Dis.* **2018**, *5*, 11. [CrossRef]
10. Newman, B.; Koppolu, R.; Murphy, D.; Sylvester, K. Heterotaxy syndromes and abnormal bowel rotation. *Pediatr. Radiol.* **2014**, *44*, 542–551. [CrossRef]
11. Nakada, K.; Kawaguchi, F.; Wakisaka, M.; Nakada, M.; Enami, T.; Yamate, N. Digestive tract disorders associated with asplenia/polysplenia syndrome. *J. Pediatr. Surg.* **1997**, *32*, 91–94. [CrossRef]
12. Mori, S.; Anderson, R.H.; Nishii, T.; Matsumoto, K.; Loomba, R.S. Isomerism in the setting of the so-called “heterotaxy”: The usefulness of computed tomographic analysis. *Ann. Pediatr. Cardiol.* **2017**, *10*, 175–186. [CrossRef]
13. Loomba, R.S.; Ahmed, M.M.; Spicer, D.E.; Backer, C.L.; Anderson, R.H. Manifestations of bodily isomerism. *Cardiovasc. Pathol.* **2016**, *25*, 173–180. [CrossRef]
14. Burton, E.C.; Olson, M.; Rooper, L. Defects in Laterality with Emphasis on Heterotaxy Syndromes with Asplenia and Polysplenia: An Autopsy Case Series at a Single Institution. *Pediatr. Dev. Pathol.* **2014**, *17*, 250–264. [CrossRef]
15. Tawfik, A.M.; Batouty, N.M.; Zaky, M.M.; Eladalany, M.A.; Elmokadem, A.H. Polysplenia syndrome: A review of the relationship with viscerocardiac situs and the spectrum of extra-cardiac anomalies. *Surg. Radiol. Anat.* **2013**, *35*, 647–653. [CrossRef]
16. Mishra, S. Cardiac and Non-Cardiac Abnormalities in Heterotaxy Syndrome. *Indian J. Pediatr.* **2015**, *82*, 1135–1146. [CrossRef]
17. Lee, S.E.; Kim, H.Y.; Jung, S.E.; Lee, S.C.; Park, K.W.; Kim, W.K. Situs anomalies and gastrointestinal abnormalities. *J. Pediatr. Surg.* **2006**, *41*, 1237–1242. [CrossRef] [PubMed]
18. Wernovsky, G.; Anderson, R.H.; Robert, H.; Kumar, K.; Mussaton, K.; Redington, A.N.; Tweddell, J.S. *Anderson’s Pediatric Cardiology*; Wernovsky, G., Anderson, R.H., Robert, H., Kumar, K., Mussato, K., Redington, A.N., Tweddell, J.S., Tretter, J., Eds.; Elsevier: Amsterdam, The Netherlands, 2019; ISBN 9780702076084.
19. Backer, C.L.; Mongé, M.C.; Popescu, A.R.; Eltayeb, O.M.; Rastatter, J.C.; Rigsby, C.K. Vascular rings. *Semin. Pediatr. Surg.* **2016**, *25*, 165–175. [CrossRef] [PubMed]
20. Anderson, R.H.; Mori, S.; Spicer, D.E.; Brown, N.A.; Mohun, T.J. Development and Morphology of the Ventricular Outflow Tracts. *World J. Pediatr. Congenit. Heart Surg.* **2016**, *7*, 561–577. [CrossRef]
21. Anderson, R.H.; Brown, N.; Bamforth, S.; Chaudhry, B.; Henderson, D.; Mohun, T. *The ESC Textbook of Cardiovascular Development*; Pérez-Pomares, J., Kelly, R., Eds.; Oxford University Press: Oxford, UK, 2018.
22. Šamánek, M.; Voříšková, M. Congenital heart disease among 815,569 children born between 1980 and 1990 and their 15-year survival: A prospective Bohemia survival study. *Pediatr. Cardiol.* **1999**, *20*, 411–417. [CrossRef] [PubMed]
23. Wilkinson, J.L.; Anderson, R.H. Anatomy of Discordant Atrioventricular Connections. *World J. Pediatr. Congenit. Heart Surg.* **2011**, *2*, 43–53. [CrossRef] [PubMed]
24. Anderson, R.H.; Shirali, G. Sequential segmental analysis. *Ann. Pediatr. Cardiol.* **2009**, *2*, 24–35. [CrossRef]
25. Arribard, N.; Mostefa Kara, M.; Hascoët, S.; Bessières, B.; Bonnet, D.; Houyel, L. Congenitally corrected transposition of the great arteries: Is it really a transposition? An anatomical study of the right ventricular septal surface. *J. Anat.* **2020**, *236*, 325–333. [CrossRef] [PubMed]
26. Hunter, L.E.; Seale, A.N. Educational series in congenital heart disease: Prenatal diagnosis of congenital heart disease. *Echo Res. Pract.* **2018**, *5*, R81–R100. [CrossRef] [PubMed]

Communication

Sudden Death in Congenital Heart Disease: The Role of the Autopsy in Determining the Actual Cause

Mary N. Sheppard

CRY Unit of Cardiovascular Pathology, Molecular and Clinical Sciences Research Institute,
St. George's Medical School, St. George's University of London, London SW17 0RE, UK; m.sheppard@sgul.ac.uk

Received: 19 October 2020; Accepted: 14 December 2020; Published: 16 December 2020

Abstract: Congenital heart defects (CHDs) have undergone a large change in epidemiology due to prenatal screening and improved outcomes with surgery and percutaneous procedures. In patients with complex CHD there is an increased risk of sudden cardiac death (SCD) and up to 11% of all SCDs in the young occur in people with CHD. It is essential for clinicians to be aware of the risk factors, and for all patients to be followed up in specialised centres. When an SCD occurs, it is important that an autopsy is done and for the pathologist to have an in-depth knowledge of the particular defect and the corrective surgical techniques employed, as well as any complications due to these procedures. Both pathologist and cardiologist should work closely together to explain the cause of death to the family. A terminal cardiac arrhythmia explains many of the SCD cases, often with underlying cardiac fibrosis due to previous procedures. SCD may also be the first presentation of CHD, so great care is required when examining such cases and referral for a detailed expert opinion is recommended in all CHD-SCD cases.

Keywords: autopsy; cardiac arrhythmia; congenital heart disease; cardiac fibrosis; cardiac histology; cardiac surgery; surgical complications; pulmonary hypertension; sudden cardiac death

1. Introduction

Congenital heart defects (CHDs) are the most common birth defects, affecting approximately 1% of newborns [1]. In the past 50 years there has been a dramatic increase in the survival of patients with congenital heart disease, and they are more likely to survive into adulthood following corrective surgery [2]. The adult congenital heart diseases population is now exceeding the pediatric congenital heart diseases population and is annually increasing. There are approximately three million patients older than 18 years old with CHD in the United States and Europe. However, corrective surgery does not mean that the heart will return to normal. By the age of 50, adults with CHD are at a greater than 10% risk of cardiac arrhythmias and 4% experience sudden cardiac death (SCD) [3].

SCD is described as a sudden, natural, unexpected death; in witnessed cases, as an acute change in cardiovascular status with time to death being <1 h and, in unwitnessed cases, as a person last seen alive <24 h before being found dead. In CHD it is referred to as CHD-SCD.

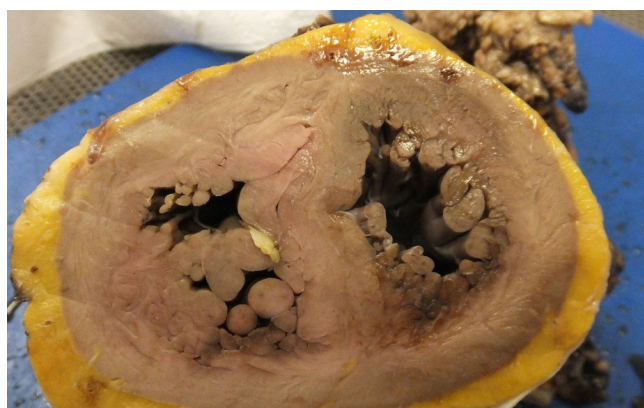
Clinical Challenges in CHD-SCD

When dealing with both children and adults with CHD, a major challenge for the cardiologist is risk stratifying the individual patients to the risk of SCD. As this population is growing, the risk also increases. Cardiologists who treat both children and adults with CHD are aware of the need for risk stratification, particularly as this population is increasing with long-term haemodynamic changes increasing the risk of SCD [4]. With increasing experience, electrocardiographic abnormalities are becoming more useful in determining the risk of SCD in this population [5]. Cardiac imaging with ECHO and MRI is increasingly applied—particularly to determine cardiac remodelling and

fibrosis which puts the patients at increased risk of SCD [6]. Patients with congenital heart disease develop atrial and ventricular arrhythmias, and implantable defibrillators are used for high risk of SCD [7,8]. Antiarrhythmic drugs are first line treatment, but surgical and catheter-based interventions for structural abnormalities and catheter ablation for recurrent ventricular arrhythmias are more widely applied today. The use of implantable defibrillators (ICDS) for CHD is now widely applied, but risk stratification remains poorly defined in many cases and there is also the risk of inappropriate shocks and infections—so great care is needed in their use, as ICDS are not a panacea and do not prevent SCD [9] (otherwise we might all have them implanted for immortality).

In a recent Danish study, there were 809 SCDs in young people between the ages of 0–35 years between 2000 and 2009, of which 90 (11%) had congenital heart disease. This gives a rate of 4.4 per hundred thousand person years. Out of the 90, 64 had autopsies of which 37 (50%) were not diagnosed prior to death. Most had been diagnosed during life, but the Danish study emphasizes that in total 41% of the SCD-CHD cases were not diagnosed with CHD before their sudden death, which highlights the importance of the autopsy in determining the exact cause of the SCD with CHD being important especially in young patients. The most frequent diagnosis was coarctation of aorta, transposition of the great arteries and univentricular heart. The mode of death was rupture of an aortic aneurysm in 13% of cases, while death was presumed arrhythmic in the remaining 87% of cases [10]. This study emphasises that at autopsy there are usually not specific direct findings that will explain the sudden death and interpretation of the findings is important. One must consider that the congenital lesion is incidental and that the true cause of death is sudden arrhythmic death syndrome [11]. In this situation the possibility of electrical abnormalities called ion channelopathies must be considered. These can occur in children as well as adults and they are genetic diseases with mutations in ion channels including sodium, potassium and calcium. In a recent study from our centre of 302 cases of sudden arrhythmogenic deaths syndrome (SADS) with a mean age of 24 years, the main aetiologies were catecholamine polymorphic ventricular tachycardia (CPVT), which is common in children, and the long Q-T syndrome [12]. The taking of genetic material at autopsy is important in establishing the mutations responsible for these electrical abnormalities, and this is known as the molecular autopsy. At present the genetic yield is low at approximately 13% but will increase as more mutations are discovered. We have shown that over half of sudden deaths in young people are due to SADS so it is an important cause of death in young people [13]. It is also important to get a specialist opinion from an expert cardiac pathologist in establishing the cause of death in children when a cardiac cause is being considered, be it congenital heart disease, cardiomyopathies or SADS [14,15].

In untreated CHD, there are long-term effects on the myocardium leading to cardiac hypertrophy with replacement fibrosis, and finally cardiac failure with a dilated thin walled ventricle with increased risk of lethal cardiac arrhythmias (Figure 1a,b). In treated CHDs, the interventions may cause further myocardial damage which can also acts as a focus for a cardiac arrhythmia and SCD (Figure 2).



(a)

Figure 1. *Cont.*

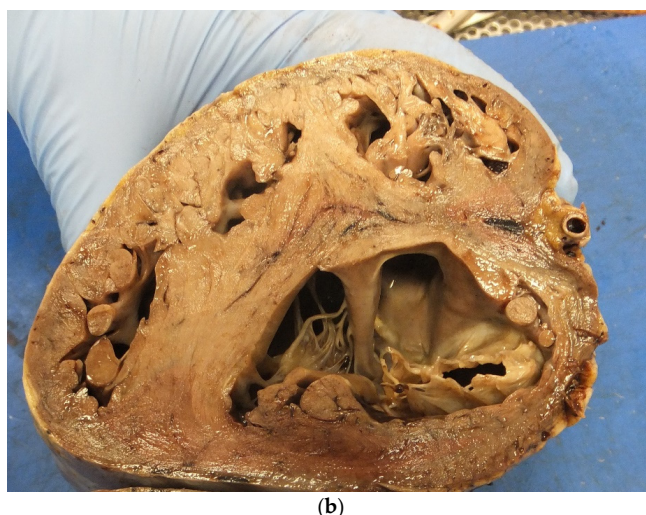


Figure 1. (a) A short axis view of a patient with tetralogy of Fallot in which there is marked right ventricular hypertrophy. (b) A short axis view of a patient with a thin walled left ventricle and markedly hypertrophied right ventricle in the case of Eisenmenger syndrome with VSD.

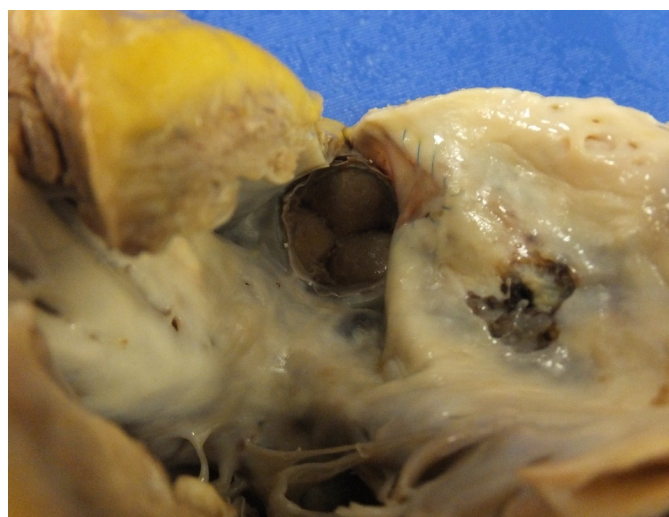


Figure 2. A corrected tetralogy of Fallot in which there is a pericardial patch to open up the right ventricular outflow tract. Note the calcification and ulceration and fibrosis in the areas of patching which can be a substrate for cardiac arrhythmia. Note also the biprosthetic valve in the pulmonary position.

2. Value of the Autopsy in CHD

The autopsy is valuable in paediatric cardiology. In an autopsy series in the 1990s on 150 post-operative congenital cases, in 8.5% the autopsy detected unexpected findings which if known prior to death, could have altered therapy [16]. Autopsy can be a very challenging procedure in CHD patients, especially if corrective surgery is carried out with several procedures over a prolonged period of time. The approach and protocol to be used may vary depending on whether the pathologist is facing unoperated cases or previously corrected CHD. Interventions for the same condition have evolved over many decades, as has perioperative myocardial preservations and postoperative care. Careful clinicopathological correlation is required to assist the pathologist in performing the autopsy and reaching a diagnosis regarding the cause of death. Recent guidelines from the European Association of Cardiovascular Pathology describe the most common types of CHDs and include a description of the various types of surgical and percutaneous procedures and major pathological complications. This is a valuable guide to pathologists facing such an autopsy [17]. Small autopsy studies in the forensic area

relate to SCD cases with known CHD in the majority but this study also showed that five cases had no diagnosis prior to autopsy, highlighting that the first presentation of CHD can be SCD like in the Danish study [15].

3. Surgical Correction and SCD

In a study we did in 2006, six cases of surgically corrected complex congenital heart diseases died suddenly, the majority many years after the surgery and there was no indication of clinical deterioration before the sudden death. At autopsy, apart from the surgical corrections and congenital anomalies, there were no specific new findings to explain the sudden death and the death was presumed due to a terminal cardiac arrhythmia, which may be difficult for the family to accept but provides the only explanation in these situations. Why the death occurs at a particular time is unexplained in most cases [13]. In a later study, 21 congenitally malformed hearts were in the same database with and without corrective surgery. High risk lesions were Eisenmenger syndrome, transposition of the great arteries (atrial switch or congenitally corrected) and Fontan circulation. The direct causes of death were attributed to ventricular myocardial fibrosis (11 cases) (Figure 3), pulmonary hypertension (3 cases) and perioperative haemorrhage (2 cases). Again, there were four cases with no explanation for the SCD [18]. Eisenmenger's syndrome is considered as high/moderate risk for SCD (Figure 4) and is related to age, history of cardiac arrhythmias, heart block, impaired ventricular function and pacemaker insertion and pulmonary hypertension [19,20].



Figure 3. A short axis section of the left ventricle showing replacement pale areas of fibrosis in a case of aortic stenosis.

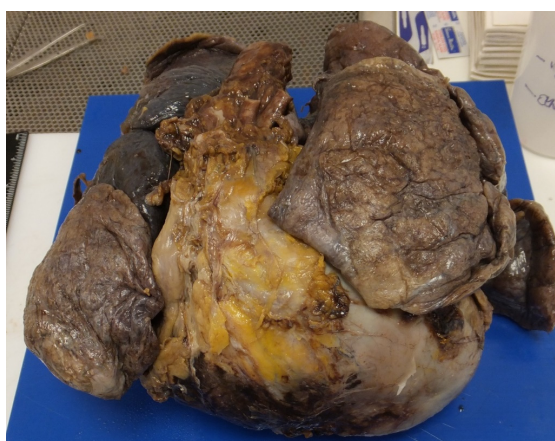


Figure 4. Heart and lungs from the thorax. Note the heart is enlarged and boot shaped extending well beyond the lungs giving the classic appearance of Eisenmenger's syndrome with biventricular hypertrophy due to a large VSD.

4. Pulmonary Hypertension and SCD

Pulmonary hypertension is linked to SCD as already stated. The timing of corrective surgery is important in preventing this, and it can persist despite surgery—especially in older patients. The presence of pulmonary hypertension especially with Eisenmenger syndrome contributes to mortality with right sided heart failure and SCD. Patients with congenital heart disease and pulmonary hypertension are at increased risk of cardiac arrhythmias and arrhythmias are strong predictor of death [21] In a series of 502 Eisenmenger cases, right heart failure is the most common cause of death (29.7%), followed by hemoptysis (18.9%), SCD (16.2%), and pulmonary hypertensive crisis (10.8%) [22]. We did a study of 44 SCD cases with pulmonary hypertensive changes in the lungs at autopsy. In total, 27 cases (61%) had CHD with undiagnosed septal defects and 7 patients were pregnant [23]. This study highlights that many cases can be undiagnosed prior to death and that pregnancy increases the risk of SCD. It is important that clinicians and pathologists be aware of the risk of SCD in asymptomatic patients with pulmonary hypertension, especially in those with congenital heart disease, after cardiac surgery or during pregnancy. Look for the changes with atheroma in the pulmonary arteries at autopsy and extensive sampling of the lungs is essential (Figures 5 and 6). Older procedures such as the Waterston shunt directly between the aorta and pulmonary artery can lead to pulmonary hypertension, in which case death is due to ruptured pulmonary aneurysms in adult life [24] Pulmonary hypertension leads to right ventricular hypertrophy and right-sided arrhythmias and right sided heart failure. In a recent study from China looking at 507 cases of congenital heart disease with pulmonary hypertension, mortality was highest in patients with small defects, less so after correction of the defect and Eisenmenger syndrome, while there were no deaths in patients with pulmonary to systemic shunts. The mode of death in the 37 cases was heart failure (11) haemoptysis (7), pulmonary hypertensive crisis (4) and sudden cardiac death (6) This study emphasises that the causes of the death can be variable but sudden cardiac death is important [22]. It is in these cases that an autopsy needs to be carried out to eliminate direct causes and study the lungs and heart to establish if there is a substrate explaining the terminal cardiac arrhythmia.

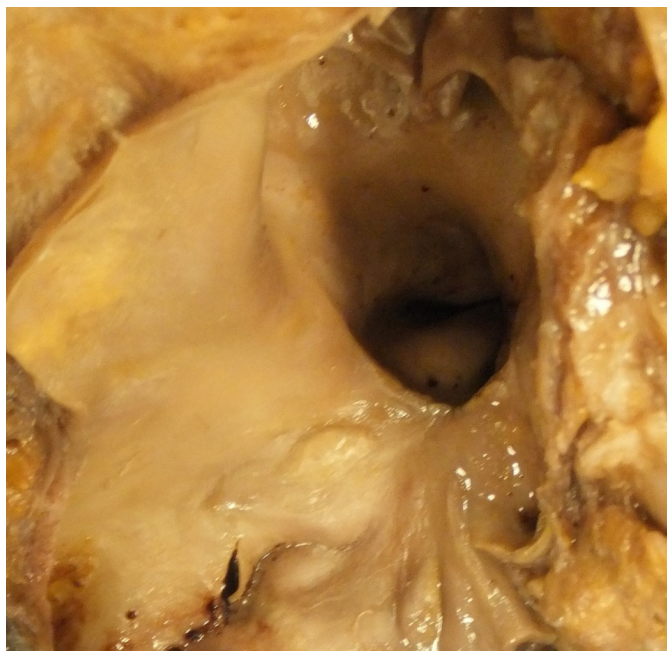


Figure 5. This shows an open pulmonary artery in the case of Eisenmenger syndrome in which there are raised intimal plaques of atheroma present indicating pulmonary hypertension.

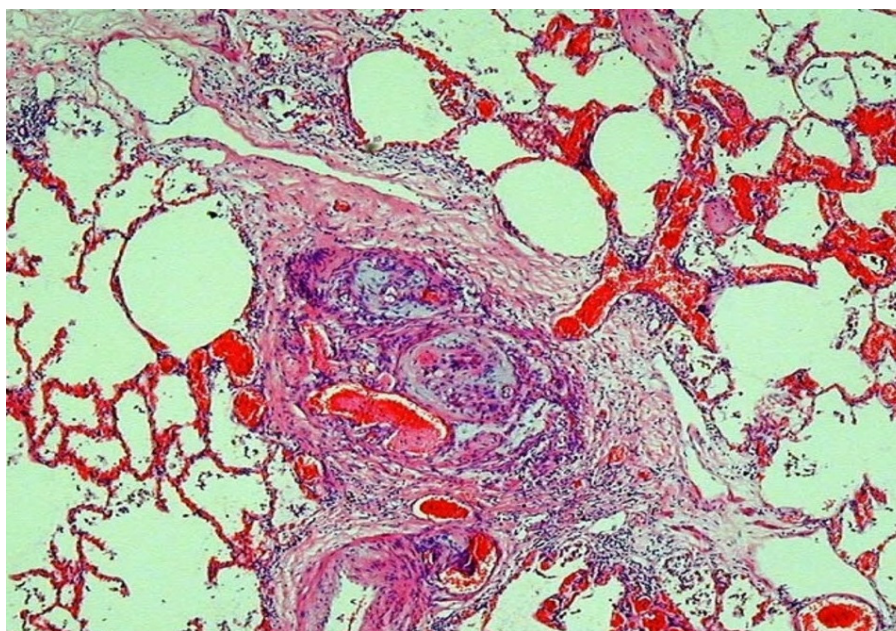


Figure 6. This shows a plexiform lesion in the lung of a case of pulmonary hypertension secondary to congenital heart disease.

5. CHD and Pregnancy and SCD

Pregnancy leads to increased demands on the myocardium in CHD and mortality is highest in those with pulmonary arterial hypertension [25]. Two out of 80 of maternal SCDs in our database were due to CHD and both had Eisenmenger's syndrome with pulmonary hypertension [26].

6. Coronary Artery Anomalies

Congenital coronary artery anomalies are of major significance in clinical cardiology due to their association with myocardial ischaemia and sudden death. Such anomalies are detectable by imaging modalities and their prevalence ranges from 0.21% to 5.79% in angiographic studies. A recent consensus document from the Development, Anatomy and Pathology Working Group of the European Society of Cardiology gives a wide spectrum of coronary artery anomalies [27]. Differentiating benign anomalies from lethal anomalies is obviously important for the pathologist. The proportion of SCDs caused by coronary anomalies has been variably reported ranging from 0% to 4% in the young general population and up to 20% among athletes [28]. Origin from the wrong sinus with interarterial course as well as anomalous origin from the pulmonary artery [29] are the most fatal variants recognized at postmortem of SCDs (Figure 7). It is a rare cause of SCD, but they cause 5% of SCD in sport in our database in the UK [30] Physical exercise is encouraged towards prevention of cardiovascular disease and improvement of ventricular function in congenital heart disease. However, in some congenital heart disease subtypes, especially coronary artery anomalies, physical activity transiently increases the risk of SCD. This is because during exercise there is increased pressure within the great vessels squeezing the anomalous vessels and causing ischaemia. However, ischaemia cannot be detected histologically at autopsy in many cases, and the death is attributed to arrhythmias as a result of the ischaemia [31]. Cardiac arrhythmias causing sudden death is likely in the 50% of cases without overt myocardial damage [31,32]. ICD implantation can act as a secondary prevention of sudden death as reported with ALCAPA [33].

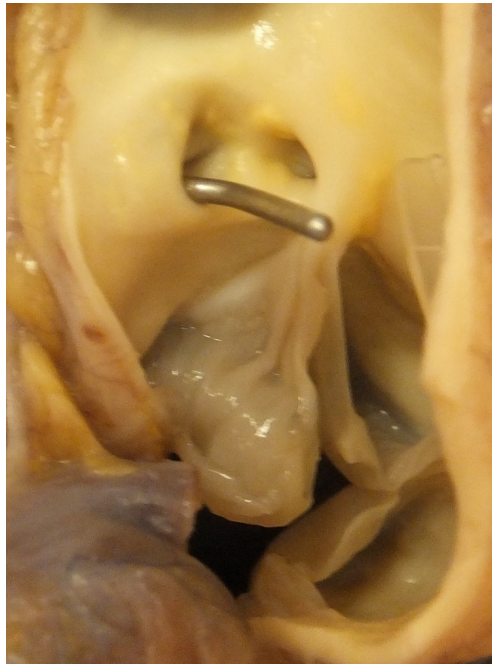


Figure 7. This shows the aortic sinuses and aortic valve. Note a probe is in the ostium of anomalous left coronary artery originating from the right coronary sinus, close to the origin of the right coronary artery.

7. Valve Disease and SCD

Congenital bicuspid valve with calcification and stenosis can lead to SCD (Figure 8) [13]. There are also the complications of endocarditis, regurgitation and aortic dilatation with dissection [34], as well as coarctation. In our recent review of hearts examined at the CRY Centre for Cardiovascular Pathology over a 5-year period, congenital heart valve defects were found in 5% of cases. The most frequent were abnormalities of the heart valves—mitral valve prolapse and bicuspid aortic valve with calcific stenosis. The immediate causes of death are malignant arrhythmias due to significant haemodynamic alterations. Patients with Ebstein’s anomaly of the tricuspid valve often have ventricular pre-excitation which is a risk factor for SCD.

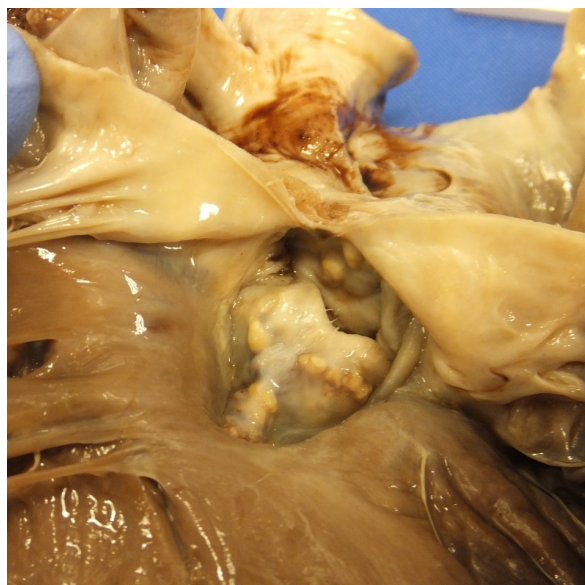
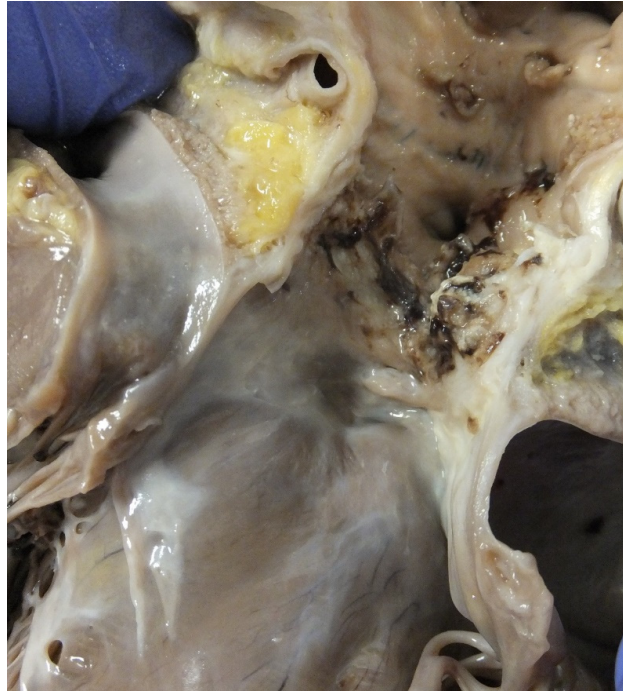


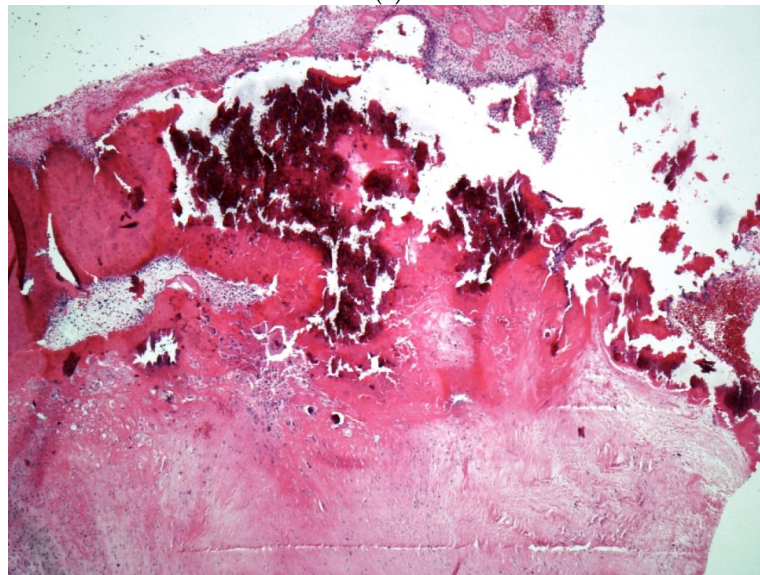
Figure 8. A view of the aorta from the ventricular aspect showing a stenotic calcified bicuspid aortic valve.

8. Endocarditis and CHD and SCD

Infective endocarditis (IE) is associated with significant morbidity and mortality in patients with adult congenital heart disease [35] In a recent study we published on 30 cases, of IE and SCD, the main lesion was a bicuspid aortic valve. SCD is due to perforation of the valve leaflets or embolization into the coronary circulation [36] IE can occur in CHD especially with interventions and valve replacements (Figure 9a,b) [37,38].



(a)



(b)

Figure 9. (a) A homograft valve in the pulmonary position in a case of repaired tetralogy of Fallot. Note that the valve leaflets have being destroyed by large haemorrhagic vegetations. (b) A haematoxylin and eosin-stained section of a valve vegetation with calcification admixed with bacterial colonies as well as acute inflammation and fibrin destroying the valve tissue.

9. Coarctation of the Aorta

This can present a challenge to the pathologist as many cases are missed, as pathologists may attribute left ventricular hypertrophy to perhaps hypertension and they fail to examine the aorta and many of these cases have hypertension. Pathologists may also find a dissection of the aorta and miss that the cause is linked to coarctation with narrowing beyond the left subclavian. Even treated patients are at increased risk of death compared to normal people. A recent study of 834 surgically or endovascular stented patients followed up over a long period showed 38 late deaths and the overall mortality was higher compared to controls. Sixty per cent developed hypertension, which is a risk factor for both aortic rupture and left ventricular hypertrophy [39].

10. CHD in Our SCD Database

We have published extensively on SCD, and in a recent analysis of 2653 cases of SCD referred to our pathology unit between 2015 and 2020, 114 (4%) were diagnosed with CHD of which 54% were male and 46% female. The median age was 33 years in both male and female. The most common lesion identified was mitral valve prolapse in 15 cases (13.2%), congenital aortic stenosis in 12 cases (10.5%), anomaly of coronary arteries (9) (7.8%) and pulmonary stenosis 9 (7.89%), tetralogy of Fallot in 8 hearts (7.0%), ventricular septal defect in 6 cases (5.3%), aortopathy with dissection associated either with Williams, Turner or Ehlers–Danlos syndrome in 6 (4.4%) cases and congenitally corrected transposition of the great arteries in 5 cases (4.4%). Isolated large atrial septal defect was found in 4 (3.5%) hearts, in another 3 (2.6%) hearts, atrioventricular septal defect was identified, 3 (2.6%) SCD cases were associated with single-ventricle circulation. Ebstein's anomaly as well as congenital mitral valve stenosis were identified in 1 heart (1.0%). Fibrosis in the heart was microscopically described in 70 hearts (61%). This study is interesting in that valve lesions are prominent, both mitral valve prolapse and congenital aortic stenosis followed by anomalous coronary arteries while myocardial fibrosis was seen in the majority of cases which could explain the sudden death. It emphasises that sampling of the myocardium will be important at autopsy in any congenital cardiac lesion.

In a recent Spanish study of over 3000 CHD patients, the accumulative sudden cardiac death incidence of 5, 10, 20 years was 0.7, 1.8 and 3.1 respectively. This study emphasises wide differences across specific lesions with high risk cases being Rastelli, severe coronary anomalies, cyanotic heart disease, complex TOF, moderate risk were non-complex TOF, Senning and Mustard cases, Fontan, congenitally corrected transposition of the great vessels (CCTGA), and Ebstein's anomaly, while coarctation and left heart lesions were low risk. Very low risk cases were left to right shunts and right ventricular outflow tract lesions. This study also used a predictive model indicating that those with a greater than 5% risk as five years follow-up should have an ICD inserted while those with a lower risk of 0.1% should avoid these strategies as ICD can have significant complications [40].

In a recent study from Australia of 2068 patients with CHD 341 died, which is a mortality rate of 11% and this was mainly in complex cases. Non-cardiac causes of death predominated in patients with simple lesions [41]. This highlights that the pathologist should not attribute death simply to the lesion if it is small and insignificant with no remodelling of the heart or lungs. It is important for pathologists to know what are high-risk and low-risk lesions, so that they can make a judgement at autopsy as to whether a congenital lesion found in the heart has actually caused the death of the patient. If a case is only an incidental congenital defect such as a small ASD or VSD, and slight variation of normal coronary anatomy, then the death case should not be attributed to the lesion. Additionally, surgically corrected conditions in which there are no surgical complications, no hypertrophy, dilatation, or fibrosis in the ventricles, should also not have the sudden death attributed to the underlying condition. Coarctation without dilatation and rupture of the aorta or hypertrophy of the left ventricle should also be listed as an incidental finding.

11. Summary

SCD is an important cause of mortality in congenital heart disease. Urgent referral for medical treatment of arrhythmias, catheter ablation of arrhythmias and use of implantable cardioverter-defibrillators (ICDs) has improved survival but will not prevent all SCD [7,42,43]. In any case of SCD in CHD it is imperative to carry out an autopsy to clarify the exact cause of death, which helps both the family and the cardiologist in coming to terms with the condition and leading to improvements in monitoring and survival in the future.

Funding: This research was funded by UK Charity Cardiac Risk in the Young (CRY-UK) www.c-r-y.org.uk.

Conflicts of Interest: The authors declare no conflict of interest.

References

1. Fanaroff, A. Birth Prevalence of Congenital Heart Disease Worldwide: A Systematic Review and Meta-Analysis. *Yearb. Neonatal Périnat. Med.* **2012**, *2012*, 101–103. [CrossRef]
2. Bildirici, I. Faculty Opinions recommendation of 20-year survival of children born with congenital anomalies: A population-based study. In *Faculty Opinions—Post-Publication Peer Review of the Biomedical Literature*; Faculty Opinions Ltd.: London, UK, 2010; Volume 375, pp. 649–656.
3. Henning, R.J. Diagnosis and treatment of adults with congenital heart disease. *Future Cardiol.* **2020**, *16*, 317–342. [CrossRef] [PubMed]
4. Brida, M.; Gatzoulis, M.A. Adult congenital heart disease: Past, present and future. *Acta Paediatr.* **2019**, *108*, 1757–1764. [CrossRef] [PubMed]
5. Vehmeijer, J.T.; Koyak, Z.; Bokma, J.P.; Budts, W.; Harris, L.; Mulder, B.J.; De Groot, J.R. Sudden cardiac death in adults with congenital heart disease: Does QRS-complex fragmentation discriminate in structurally abnormal hearts? *Europace* **2017**, *20*, f122–f128. [CrossRef] [PubMed]
6. Di Salvo, G.; Miller, O.; Narayan, S.B.; Li, W.; Budts, W.; Buechel, E.R.V.; Frigiola, A.; Bosch, A.E.V.D.; Bonello, B.; Mertens, L.; et al. Imaging the adult with congenital heart disease: A multimodality imaging approach—position paper from the EACVI. *Eur. Heart J. Cardiovasc. Imaging* **2018**, *19*, 1077–1098. [CrossRef] [PubMed]
7. Khairy, P. Arrhythmias in Adults with Congenital Heart Disease: What the Practicing Cardiologist Needs to Know. *Can. J. Cardiol.* **2019**, *35*, 1698–1707. [CrossRef]
8. Moore, J.P.; Khairy, P. Adults with Congenital Heart Disease and Arrhythmia Management. *Cardiol. Clin.* **2020**, *38*, 417–434. [CrossRef]
9. Moore, B.M.; Cao, J.; Cordina, R.L.; McGuire, M.A.; Celermajer, D. Defibrillators in adult congenital heart disease: Long-term risk of appropriate shocks, inappropriate shocks, and complications. *Pacing Clin. Electrophysiol.* **2020**, *43*, 746–753. [CrossRef]
10. Lyngé, T.H.; Jeppesen, A.G.; Winkel, B.G.; Glinge, C.; Schmidt, M.R.; Søndergaard, L.; Risgaard, B.; Tfelt-Hansen, J. Nationwide Study of Sudden Cardiac Death in People with Congenital Heart Defects Aged 0 to 35 Years. *Circ. Arrhythmia Electrophysiol.* **2018**, *11*, e005757. [CrossRef]
11. Mellor, G.; Raju, H.; De Noronha, S.V.; Papadakis, M.; Sharma, S.; Behr, E.R.; Sheppard, M. Clinical Characteristics and Circumstances of Death in the Sudden Arrhythmic Death Syndrome. *Circ. Arrhythmia Electrophysiol.* **2014**, *7*, 1078–1083. [CrossRef]
12. Lahrouchi, N.; Raju, H.; Lodder, E.M.; Papatheodorou, E.; Ware, J.S.; Papadakis, M.; Tadros, R.; Cole, D.; Skinner, J.R.; Crawford, J.; et al. Utility of Post-Mortem Genetic Testing in Cases of Sudden Arrhythmic Death Syndrome. *J. Am. Coll. Cardiol.* **2017**, *69*, 2134–2145. [CrossRef] [PubMed]
13. Fabre, A. Sudden adult death syndrome and other non-ischæmic causes of sudden cardiac death. *Heart* **2005**, *92*, 316–320. [CrossRef] [PubMed]
14. De Noronha, S.V.; Behr, E.R.; Papadakis, M.; Ohta-Ogo, K.; Banya, W.; Wells, J.; Cox, S.; Cox, A.; Sharma, S.; Sheppard, M. The importance of specialist cardiac histopathological examination in the investigation of young sudden cardiac deaths. *Europace* **2013**, *16*, 899–907. [CrossRef] [PubMed]

15. Gitto, L.; Serinelli, S.; Arunkumar, P.; White, S.M. Sudden Cardiac Deaths in Adults with Congenital Heart Disease with Structural Abnormalities: A Retrospective Review of Cases in the Cook County Medical Examiner's Office. *J. Forensic. Sci.* **2020**, *65*, 117–127. [CrossRef]
16. Gatzoulis, M.A.; Sheppard, M.N.; Ho, S.Y. Value and impact of necropsy in paediatric cardiology. *Heart* **1996**, *75*, 626–631. [CrossRef]
17. Angelini, A.; di Gioia, C.; Doran, H.; Fedrigo, M.; de Gouveia, R.H.; Ho, S.Y.; Leone, O.; Sheppard, M.N.; Thiene, G.; Dimopoulos, K.; et al. Association for European Cardiovascular P: Autopsy in adults with congenital heart disease (ACHD). *Virchows Arch.* **2020**, *476*, 797–820. [CrossRef]
18. Westaby, J.D.; Cooper, S.T.; Edwards, K.A.; Anderson, R.H.; Sheppard, M.N. Insights from examination of hearts from adults dying suddenly to the understanding of congenital cardiac malformations. *Clin. Anat.* **2019**, *33*, 394–404. [CrossRef]
19. Lee, M.-C.; Wu, M.-H.; Lin, M.-T.; Chen, H.-C.; Kao, F.-Y.; Huang, S.-K. Incidence and Postnatal Profile of Fontan Patients by Adolescence from a Nationwide Birth Cohort. *Acta Cardiol Sin.* **2020**, *36*, 367–374.
20. Chiriac, A.; Riley, D.C.; Russell, M.; Moore, J.P.; Padmanabhan, D.; Hodge, D.O.; Spiegel, M.R.; Vargas, E.R.; Phillips, S.D.; Ammass, N.M.; et al. Determinants of Sudden Cardiac Death in Adult Patients with Eisenmenger Syndrome. *J. Am. Heart Assoc.* **2020**, *9*, e014554. [CrossRef]
21. Drakopoulou, M.; Nashat, H.; Kempny, A.; Alonso-González, R.; Swan, L.; Wort, S.J.; Price, L.C.; McCabe, C.; Wong, T.A.; Gatzoulis, M.; et al. Arrhythmias in adult patients with congenital heart disease and pulmonary arterial hypertension. *Heart* **2018**, *104*, 1963–1969. [CrossRef]
22. Xu, Z.Y.; Li, Q.Q.; Zhang, C.; Zhang, H.S.; Gu, H. [Risk factors for death and the clinical features of different subtypes of patients with pulmonary arterial hypertension related to congenital heart disease]. *Zhonghua Xin Xue Guan Bing Za Zhi* **2020**, *48*, 315–322. [PubMed]
23. Krexi, D.; Sheppard, M. Pulmonary hypertensive vascular changes in lungs of patients with sudden unexpected death. Emphasis on congenital heart disease, Eisenmenger syndrome, postoperative deaths and death during pregnancy and postpartum. *J. Clin. Pathol.* **2014**, *68*, 18–21. [CrossRef] [PubMed]
24. Hull, D.A.; Shinebourne, E.; Gerlis, L.; Nicholson, A.G.; Sheppard, M.N. Rupture of pulmonary aneurysms in association with long-standing Waterston shunts. *Cardiol. Young* **2001**, *11*, 123–127. [CrossRef]
25. Roos-Hesselink, J.; Baris, L.; Johnson, M.; De Backer, J.; Otto, C.; Marelli, A.; Jondeau, G.; Budts, W.; Grewal, J.; Sliwa, K.; et al. Pregnancy outcomes in women with cardiovascular disease: Evolving trends over 10 years in the ESC Registry of Pregnancy And Cardiac disease (ROPAC). *Eur. Heart J.* **2019**, *40*, 3848–3855. [CrossRef]
26. Krexi, D.; Sheppard, M. Cardiovascular causes of maternal sudden death. Sudden Arrhythmic Death Syndrome is leading cause in UK. *Eur. J. Obstet. Gynecol. Reprod. Biol.* **2017**, *216*, 261. [CrossRef] [PubMed]
27. Pérez-Pomares, J.M.; De La Pompa, J.L.; Franco, D.; Henderson, D.; Ho, S.Y.; Houyel, L.; Kelly, R.G.; Sedmera, D.; Sheppard, M.; Sperling, S.; et al. Congenital coronary artery anomalies: A bridge from embryology to anatomy and pathophysiology—A position statement of the development, anatomy, and pathology ESC Working Group. *Cardiovasc. Res.* **2016**, *109*, 204–216. [CrossRef] [PubMed]
28. Hill, S.F.; Sheppard, M.N. A silent cause of sudden cardiac death especially in sport: Congenital coronary artery anomalies. *Br. J. Sports Med.* **2014**, *48*, 1151–1156. [CrossRef]
29. Krexi, L.; Sheppard, M.N. Anomalous origin of the left coronary artery from the pulmonary artery (ALCAPA), a forgotten congenital cause of sudden death in the adult. *Cardiovasc. Pathol.* **2013**, *22*, 294–297. [CrossRef]
30. Finocchiaro, G.; Papadakis, M.; Robertus, J.L.; Dhutia, H.; Steriotis, A.K.; Tome, M.; Mellor, G.; Merghani, A.; Malhotra, A.; Behr, E.; et al. Etiology of Sudden Death in Sports: Insights from a United Kingdom Regional Registry. *J. Am. Coll. Cardiol.* **2016**, *67*, 2108–2115. [CrossRef]
31. Finocchiaro, G.; Behr, E.R.; Tanzarella, G.; Papadakis, M.; Malhotra, A.; Dhutia, H.; Miles, C.; Diemberger, I.; Sharma, S.; Sheppard, M.N. Anomalous Coronary Artery Origin and Sudden Cardiac Death: Clinical and Pathological Insights from a National Pathology Registry. *JACC Clin. Electrophysiol.* **2019**, *5*, 516–522. [CrossRef]
32. Hill, S.F.; Sheppard, M.N. Non-atherosclerotic coronary artery disease associated with sudden cardiac death. *Heart* **2010**, *96*, 1119–1125. [CrossRef] [PubMed]
33. Dilaveris, P.; Koutagiar, I.; Alexopoulos, N.; Tsiachris, D.; Gatzoulis, K. Secondary prevention of sudden cardiac death in a 65 year untreated ALCAPA patient. *Int. J. Cardiol.* **2014**, *176*, e73–e74. [CrossRef] [PubMed]

34. Subramaniam, K.; Sheppard, M. Thoracic aortic dissection. Death may not always be due to rupture with haemorrhage. Unusual complications which can be missed at autopsy. *J. Forensic Leg. Med.* **2018**, *54*, 127–129. [CrossRef]
35. Tutarel, O.; Alonso-Gonzalez, R.; Montanaro, C.; Schiff, R.; Uribarri, A.; Kempny, A.; Grübler, M.R.; Uebing, A.; Swan, L.; Diller, G.-P.; et al. Infective endocarditis in adults with congenital heart disease remains a lethal disease. *Heart* **2017**, *104*, 161–165. [CrossRef] [PubMed]
36. Cooper, S.T.; Westaby, J.D.; Griffin, K.J.; Sheppard, M. The role of endocarditis in sudden cardiac death: Highlighting the value of the autopsy, pathological features and cardiac complications. *Cardiovasc. Pathol.* **2020**, *50*, 107292. [CrossRef] [PubMed]
37. Wijesekera, N.T.; Sheppard, M.N.; Mullen, M.J. Candida endocarditis with mycotic pulmonary emboli following re-do Rastelli operation. *Heart* **2004**, *90*, e34. [CrossRef] [PubMed]
38. Moore, B.; Cao, J.; Kotchetkova, I.; Celermajer, D.S. Incidence, predictors and outcomes of infective endocarditis in a contemporary adult congenital heart disease population. *Int. J. Cardiol.* **2017**, *249*, 161–165. [CrossRef]
39. Lee, M.G.Y.; Babu-Narayan, S.V.; Kempny, A.; Uebing, A.; Montanaro, C.; Shore, D.F.; D’Udekem, Y.A.; Gatzoulis, M. Long-term mortality and cardiovascular burden for adult survivors of coarctation of the aorta. *Heart* **2019**, *105*, 1190–1196. [CrossRef]
40. Oliver, J.M.; Gallego, P.; Gonzalez, A.E.; Avila, P.; Alonso, A.; Garcia-Hamilton, D.; Peinado, R.; Dos-Subirà, L.; Pijuan-Domenech, A.; Rueda, J.; et al. Predicting sudden cardiac death in adults with congenital heart disease. *Heart* **2020**, *107*, 67–75. [CrossRef]
41. Yu, C.; Moore, B.M.; Kotchetkova, I.; Cordina, R.L.; Celermajer, D.S. Causes of death in a contemporary adult congenital heart disease cohort. *Heart* **2018**, *104*, 1678–1682. [CrossRef]
42. Baumgartner, H.; De De Backer, J.; Babu-Narayan, S.V.; Budts, W.; Chessa, M.; Diller, G.-P.; Lung, B.; Kluin, J.; Lang, I.M.; Meijboom, F.; et al. 2020 ESC Guidelines for the management of adult congenital heart disease. *Eur. Heart J.* **2020**. [CrossRef] [PubMed]
43. Vehmeijer, J.T.; Koyak, Z.; Zwinderman, A.H.; Harris, L.; Peinado, R.; Oechslin, E.N.; Silversides, C.K.; Bouma, B.J.; Budts, W.; Van Gelder, I.C.; et al. PREVENTION-ACHD: PRospEctIVE study on implaNTable cardioverter-defibrillator therapy and suddEN cardiac death in Adults with Congenital Heart Disease; Rationale and Design. *Neth. Heart J.* **2019**, *27*, 474–479. [CrossRef] [PubMed]

Publisher’s Note: MDPI stays neutral with regard to jurisdictional claims in published maps and institutional affiliations.



© 2020 by the author. Licensee MDPI, Basel, Switzerland. This article is an open access article distributed under the terms and conditions of the Creative Commons Attribution (CC BY) license (<http://creativecommons.org/licenses/by/4.0/>).

MDPI
St. Alban-Anlage 66
4052 Basel
Switzerland
Tel. +41 61 683 77 34
Fax +41 61 302 89 18
www.mdpi.com

Journal of Cardiovascular Development and Disease Editorial Office

E-mail: jcdd@mdpi.com
www.mdpi.com/journal/jcdd



MDPI
St. Alban-Anlage 66
4052 Basel
Switzerland
Tel: +41 61 683 77 34
www.mdpi.com



ISBN 978-3-0365-6025-0